ELASTO-PLASTIC DYNAMIC BUCKLING OF STIFFENED PLATE

by

Wai-Wing LAU

A Thesis submitted for the Degree of Doctor of Philosophy of the University of London, and for the Diploma of Imperial College

Department of Aeronautics
Imperial College of Science & Technology

1981

SUMMARY

The elastic plastic dynamic buckling of a stiffened panel has been investigated. A Finite Element model which includes non-linearities due to large deformation and material property changes has been developed. The buckling behaviour of the structure under static loading has been studied extensively. The computed results agree very closely with the existing analytical results for static loading. The analysis is then extended to study the dynamic buckling behaviour of the structure under various loads for a given loading/unloading sequence. Due to the non-linearities involved, an explicit step-by-step time integration technique is employed to allow for the geometry and material changes. As the critical time step size often changes during plastic deformation, the analysis is kept stable by adjusting the time step. The stage-by-stage analyses give an accurate prediction of the overall dynamic buckling load. This load is found to be much lower than the static buckling load which shows the significance of the inertia effect. When this load is reached, the stresses on the upper flanges of some stiffeners are found to have exceeded their crippling stress level. The results also suggest that significant amounts of plastic deformation have taken place when the collapse load is reached.

The Finite Element package which was developed especially for the present investigation has been coded for B.A.C. who sponsored this project.

ACKNOWLEDGEMENT

I wish to express my gratitude to my supervisor, Dr. P.F. Kilty, Dept. of Aeronautics, Imperial College, for his continuous guidance and encouragement throughout the project. I also wish to thank Mr. H.P. Hitch of British Aerospace Corporation who financially supported this project. My sincere thanks are due to :
Dr. G.A.O. Davis for helping me to obtain a sponsorship for this project without which I would not have been able to continue my studies, and Dr. A.S.L. Chan whose advice during the early stage of this project is also much appreciated. My special thanks also go to Mrs. J. Coats for her help in the typing of this thesis and Babcock Power Ltd. for their permission to use the typing facilities. Finally, I would like to let my wife Ka-Wai know that her patience during my writing up period will be remembered forever.

CONTENTS

		PAGE NO.
1.	INTRODUCTION	1
2.	SMALL DISPLACEMENT AND LINEAR STRESS-STRAIN RELATION	7
	2.1 GENERAL OUTLINE OF THE F.E. APPROACH	7
	2.2 FORMULATION FO THE PLATE ELEMENT STIFFNESS MATRIX	8
	2.2.1 THE MEMBRANE CONSIDERATION	8
	2.2.2 THE BENDING CONSIDERATION	10
	2.3 FORMULATION OF THE BEAM ELEMENT STIFFNESS MATRIX	16
	2.4 SOLVING THE EQUATION OF EQUILIBRIUM	18
	2.5 LINEAR STATIC ANALYSIS	18
	2.5.1 PLATE ELEMENT	18
	2.5.2 BAR ELEMENT	21
3.	GEOMETRIC NON-LINEARITY	22
	3.1 FORMULATION OF LARGE DEFLECTION EQUATION	24
	3.1.1 FINITE ELEMENT FORMULATION OF THE PLATE ELEMENT STIFFNESS MATRIX	31
	3.1.2 FINITE ELEMENT FORMULATION OF THE BEAM ELEMENT STIFFNESS MATRIX	38
	3.2 LARGE DEFLECTION STATIC LOADING ANALYSIS	42
	3.2.1 NON-LINEAR DEFLECTION OF PLATE WITHOUT STIFFENERS	43
	3.3 NUMERICAL INTEGRATION OF THE TANGENTIAL STIFFNESS MATRIX	45
	3.4 THE INCREMENTAL LOAD PROCEDURE	48

CONTENTS

		PAGE NO.
4.	BUCKLING ANALYSIS	55
	4.1 EVALUATION OF THE BUCKLING LOADS	55
	4.2 BUCKLING ANALYSIS ON THE SIMPLE PLATE AND BEAM ELEMENT	58
	4.2.1 LINEAR BUCKLING OF PLATE WITHOUT STIFFENERS USING INCREMENTAL LOAD METHOD	58
	4.2.2 LINEAR BUCKLING OF BEAM ELEMENT WITH VARIOUS INITIAL DISPLACEMENTS USING INCREMENTAL LOAD METHOD	58
	4.2.3 LINEAR BUCKLING OF A BEAM WITH VARIOUS OFF-SETS FROM ITS LOCAL NEUTRAL AXIS	59
	4.2.4 NON-LINEAR BUCKLING OF THE PLATE WITHOUT STIFFENERS	60
	4.3 BUCKLING OF A STIFFENED PLATE	61
	4.3.1 BRIEF HISTORICAL REVIEW	61
	4.3.2 ANALYTICAL SOLUTION FOR BUCKLING OF STIFFENED PLATE AND STUDY OF THE ANALYTICAL AND F.E. RESULTS	62
	4.3.2.1 PLATE WITH STIFFENERS LOCATED ON ONE SIDE OF THE PLATE	64
	4.3.2.2 EXAMPLE STUDY	66
5.	MATERIAL NON-LINEARITY	69
	5.1 BASIC ASSUMPTION AND CONSTITUTIVE RELATION FOR AN ELASTIC PLASTIC MATERIAL	70
	5.2 F.E. FORMULATION OF MATERIAL CONSTITUTIVE EQUATION	80
	5.3 TRANSFORMATION OF CO-ORDINATE SYSTEM	81
	5.4 REDUCTION TO PLANE STRESS	82
	5.5 TOTAL STRAIN INCREMENT	84

CONTENTS

		PAGE NO.
5.6	PLASTIC STRAIN INCREMENT EVALUATION	85
5.7	EVALUATION OF PLASTICITY WITHIN A LOADING STEP	86
5.8	METHOD OF SOLUTION	88
5.8.1	INCREMENTAL STRESS APPROACH	88
5.8.2	INCREMENTAL STRAIN APPROACH	89
5.9	CRITERION FOR PLASTIC UNLOADING	92
5.10	CONVERGENCE	94
5.11	MATERIAL NON-LINEARITY ANALYSES	94
5.11.1	ELASTIC PLASTIC LOADING/UNLOADING OF A SIMPLE PLATE	95
6.	DYNAMIC LOADING ANALYSIS	97
6.1	MODAL SUPER POSITION SCHEME	97
6.2	NUMERICAL TIME INTEGRATION SCHEME	99
6.2.1	NEWMARK - β METHOD	99
6.2.2	CENTRAL DIFFERENCE METHOD	100
6.3	TREATMENT OF A NON-DIAGONAL DAMPING MATRIX WHEN USING A LUMPED MASS MATRIX	106
6.4	EVALUATION OF THE MAXIMUM EIGEN VALUE OF THE SYSTEM	108
6.5	SOLUTION PROCEDURE	109
6.6	DYNAMIC RESPONSE ANALYSIS TEST (COMPARISON BETWEEN NEWMARK - β AND CENTRAL DIFFERENCE METHOD	113

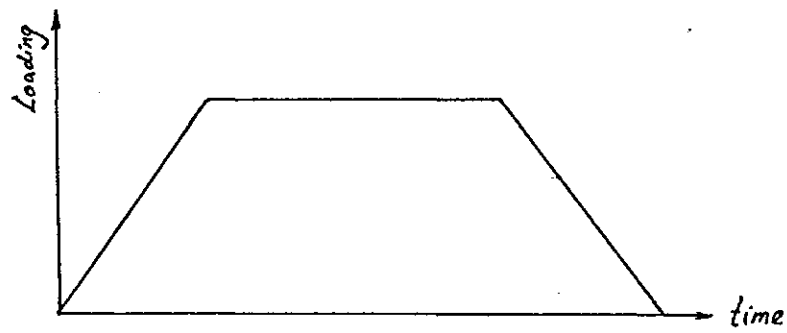
CONTENTS

		PAGE NO.
7.	FULL ANALYSIS (STATIC AND DYNAMIC LOADINGS) ON THE B.A.C. DESIGNED STIFFENED PANEL	119
	7.1 STATIC BUCKLING OF THE STIFFENED PLATE WITH B.A.C. DESIGN CRITERION	121
	7.1.1 ELASTIC BUCKLING OF THE STIFFENED PLATE	123
	7.1.2 ELASTIC PLASTIC BUCKLING OF THE STIFFENED PLATE	125
	7.2 DYNAMIC BUCKLING ANALYSIS	128
	7.2.1 ELASTIC RESPONSE OF THE STIFFENED PLATE SUBJECT TO DYNAMIC LOADING	133
	7.2.2 ELASTO-PLASTIC RESPONSES OF THE STIFFENED PLATE WHEN SUBJECT TO DYNAMIC LOADING	141
	7.3 DISCUSSIONS	155
8.	CONCLUSION	156
	REFERENCES	161
	APPENDIX 1	168
	APPENDIX 2	171
	TABLES AND FIGURES	179- 311

1. INTRODUCTION

Buckling of stiffened plates and cylindrical plates loaded in axial compression has been the subject of many analytical and experimental studies (1-17). In recent years Finite element method has also been used extensively in such investigation. However, none have been concerned with the elasto-plastic buckling of a stiffened plate subject to dynamic load. It is therefore the object of this thesis to examine the non-linear response of a stiffened panel and hence assess the buckling behaviour of the panel under various types of dynamic load. The problem arose after investigation studies, carried out by British Aerospace Corporation on some of their own design models, have found signs of buckling at the fuselage near the undercarriages. The structure also showed signs of material going through plastic buckling.

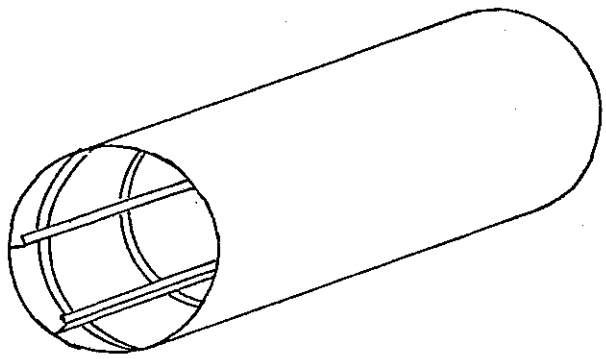
The primary loading expected in an aircraft landing is a suddenly and repeatedly applied axial compression and bending of a short to medium time duration. Such loading can be simulated as below:-



Early papers dealing with the danger of failure of a column subjected suddenly to an axial compression load which is suddenly removed after a finite time interval of action were published by Taub (18). The results showed that a sudden applied load can cause collapse even if it is smaller than the Euler load. At the same time, the column need not be damaged by a suddenly applied load greater than the Euler load, if the load is removed after a sufficiently short time.

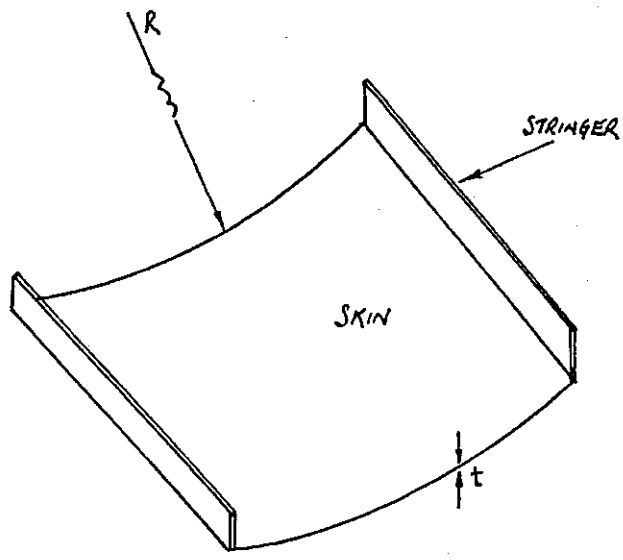
The analysis presented in this thesis follows the following sequences.

The basic structural element of an aircraft fuselage is assumed to be a thin cylindrical shell, internally stiffened by both stringers and rings (see diagrams below):-



The following assumptions were made to permit and simplify the mathematical and finite element model of the fuselage and are also intended to reflect, with sufficient accuracy, its physical behaviour under such loading.

1) The particular sections of the structure where buckling occurred can be represented by a rectangular element with stiffeners built along the edges.



2) Since t/R << 0.01, the element can be assumed to be a rectangular flat plate element.

3) Plane section before buckling remains plane after buckling.

4) The stiffeners are represented by the beam elements, having 3 degrees of freedom at each node.

6) The effect of rivet spacing and of rivet flexibility are ignored from the analysis.

7) The stiffeners are assumed to have zero flexural stiffness for bending parallel to the plane of the plate.

The effect of the torsional displacement and the out-of-plane bending from the Z-stringers will be ignored.

The modelling of the stiffened plate employs:- a) the rectangular plate element which has 6 degrees of freedom per node; 2 in-plane movements, 1 out-of-plane movement and 3 out-of-plane rotations, b) the beam element which has 3 degrees of freedom per node; 1 in-plane movement; 1 out-of-plane movement and 1 out-of-plane rotation. The rectangular plate elements are used to model the 'skin' sections and the beam elements are used to model the stringers.

The off-set of the stiffeners on one side of the plates is modelled by transforming the properties of the stiffener from the mid-plane of the plates to the mid-plane of the stiffeners themselves.

The analyses shown in this thesis can mainly be divided into two stages. In the first stage, the linear-elastic behaviour of the structure is being closely examined. In this first stage analysis, we also look into the behaviour of the structure when loadings are applied both statically and dynamically. The static analysis consists of the following:-

1) Comparing the bending behaviours of both a flat plate and a stiffened plate with some existing results.

2) Evaluation of the first mode of buckling using incremental load method and check the results against some existing results.

3)Evaluation of the modes of buckling and their corresponding critical stresses using Eigen-value method. The results are then used to check against those evaluated by the incremental load method.

In the dynamic analysis, it is found that the modal superposition method (i.e. using a frequency domain analysis) will not give a reliable solution to the problem. This is because when buckling occurs, the fundamental modes often change quite considerably, hence, giving a very poor modal correlations between the modes obtained before buckling occurs and those obtained afterwards. Therefore, much effort is devoted to choosing a suitable time integration algorithm. The prime criterion is the computation efficiency and reliability of the algorithm. Various time integration schemes have been examined here. It is found that the Central Difference Method coupled with a Lumped Mass Matrix is most suitable and computationally more efficient than other methods, for example the Newmark-β method.

In the second stage analysis, the non-linear behaviour of the structure is extended to include the large displacement effect as well as the non-linear material effect. The Lagrangian (fixed coordinates) system is adopted in all the large displacement analyses. Von-Mises yield criterion using Prandtl-Reuss flow theory is used to formulate the elasto-plastic equations. The organisation of this thesis follows the sequence of steps involved in the formulation of the finite element procedure with consideration given to:-

1) The formulation of the tangential stiffness matrix. This matrix consists of 3 sub-matrices; small displacement stiffness matrix $\underset{\sim}{K}e$; geometric stiffness matrix $\underset{\sim}{K}_G$ and the large displacement stiffness matrix $\underset{\sim}{K}_L$. While the load-softening effect in most instability problems is produced by the geometric stiffness matrix $\underset{\sim}{K}_G$, the

stiffening effect due to excessive out-of-plane bending is produced by the large displacement stiffness matrix $\underset{\sim}{K}_1$.

2)The Constitutive law which expresses the non-linear relation between stress and strain. Here, the Prandtl-Reuss flow theory, which assumes the increment of plastic strains to be proportional to the corresponding deviatoric stress components, is adopted because it seems the most consistent concept both mathematically and physically.

A volumetric approach is used in computing the plate element stiffness matrix and the stiffener stiffness matrix. This implies that during the formulation, the plate element stiffnesses are evaluated numerically using 2 x 2 Gaussian points across the plate area, while the stiffener element stiffnesses are evaluated numerically using 2 Gaussian points along the stiffener length. The integration across the thicknesses of the elements (whether it is the plate element or the stiffener element) employs the Simpson's integration scheme using 3 sampling points (one on each surface of the element and the other on the mid-plane of the element). This is because yielding normally occurs at the extreme surfaces of the elements and the Simpsons integrating points allow any surface yielding to be detected.

The equations of equilibrium used in the static loading analyses are solved by an incremental tangential stiffness procedure (also known as the incremental load method). This approach is selected in preference to the other methods (e.g. the 'initial stress' or 'initial strain' method) because of its general reliability and its compatibility with the incremental flow theory of plasticity. A modified Newton-Raphson iteration technique is also used to ensure convergency during the step-by-step loading procedure especially when the structure has entered into the plastic zone. The accuracy of the analyses is demonstrated by a series of examples which are then compared with the existing results and those obtained using the Engineering Data Sheets.

As described previously, the dynamic benaviour of the structure is calculated using the Central Difference Integration Scheme coupling

with the Diagonal Mass Matrix. This scheme allows the tangential stiffness-matrix of the structure to be evaluated at the end of each time step so that any change due to excessive displacement and stress-strain relationship can be accounted for. The disadvantage of this explicit integration scheme is its conditional stability. Thus, a suitable time step size has to be calculated before the analysis commences. When large displacements and plasticity develope, the time step sizes have also to be evaluated continuously so that the time integrations can be kept within the numerical stability requirement. In most analyses, this is done by a trial and error method. In our present analysis, however, we compare the change of the maximum eigen value of the system when large deformation takes place and adjust the time step size accordingly. Excellent results are obtained in this way.

The total number of time steps required throughout a complete loading/unloading history is around 5,000 which means that the tangential stiffness matrix has to be updated some 5,000 times.Attempts have also been made to see if the tangential stiffness matrix can be updated at a fixed time interval (say every 40 time steps)without affecting the response behaviour and the convergency of the analyses. Some interesting results are observed. External Damping is applied to the structure at the end of the unloading period to eliminate oscillations of the structure so that any permanent deformation caused by the occurrence of plasticity can be observed.

Having set up an accurate and reliable Finite Element mathematical model which can be used to study the behaviour of a stiffened plate under dynamic loadings, the analysis is then extended to predict the dynamic collapse load of a given structure.

Most results are expressed in a series of plots. A 3-dimensional plotting package is also employed in the post-processing of the results so that the deformation mode shapes can be illustrated.

2. SMALL DISPLACEMENT AND LINEAR STRESS-STRAIN RELATIONSHIP

2.1 General Outline of the Finite Element Approach

For a set of external applied nodal forces $\underset{\sim}{P}$ and internal set of stresses $\underset{\sim}{\sigma}$, and a system of displacement $\underset{\sim}{\rho}$ and strains $\underset{\sim}{\varepsilon}$, the principle of virtual work states that:-

$$\underset{\sim}{\rho}^t \cdot \underset{\sim}{P} = \int_v \underset{\sim}{\varepsilon}^t \cdot \underset{\sim}{\sigma} \cdot dV \qquad \text{----(2.1)}$$

In the case of linear strain and small displacement, the strain is assumed to be a known function of displacements in the form of:-

$$\underset{\sim}{\varepsilon} = \underset{\sim}{B} \cdot \underset{\sim}{\rho} \qquad \text{----(2.2)}$$

where $\underset{\sim}{B}$ is known as the displacement function and is based upon the undeformed geometry of the elements.

In most small displacement analysis, the stress-strain relationship is also assumed to be linear. Hence, the stresses can be written as:-

$$\underset{\sim}{\sigma} = \underset{\sim}{D} \cdot \underset{\sim}{\varepsilon} \qquad \text{----(2.3)}$$

where $\underset{\sim}{D}$ is known as the Constitutive equation for the material concerned.

Sub. equation (2.1) & (2.3) into (2.1); we have:-

$$\underset{\sim}{\rho}^t \cdot \underset{\sim}{P} = \int_v \underset{\sim}{\rho}^t \cdot \underset{\sim}{B}^t \cdot \underset{\sim}{D} \cdot \underset{\sim}{B} \cdot \underset{\sim}{\rho} \cdot dV \qquad \text{----(2.4)}$$

Equation (2.4) becomes:-

$$\underset{\sim}{P} = \left[\int_v \underset{\sim}{B}^t \cdot \underset{\sim}{D} \cdot \underset{\sim}{B} \cdot dV\right] \underset{\sim}{\rho} \qquad \text{----(2.5)}$$

The 1st term in R.H.S. of equation (2.5) is known as the generalised coordinate element stiffness $\underset{\sim}{K_i}$

2.2 Formulation of the Plate Element Stiffness Matrix

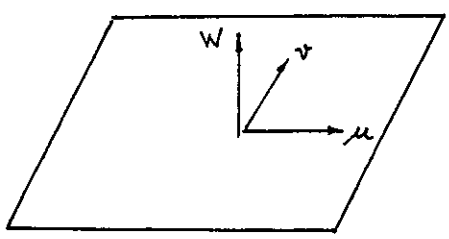
The plate element employed in the present analysis is a 4 noded rectangular element with 6 degrees of freedom per node. These consist of 2 membrane displacements (u, v), 1 out-of-plane displacement (w), 2 first order rotational displacements ($\partial w/\partial x$, $\partial w/\partial y$) and 1 second order rotational displacement ($\partial^2 w/\partial x \partial y$). Since the plate element considered here is reasonably thin, coupling between the bending and the membrane displacement can be neglected at this stage. (This will not be the case when out-of-plane bendings become excessive).

Let the global displacements be represented by $\underset{\sim}{U}$ and

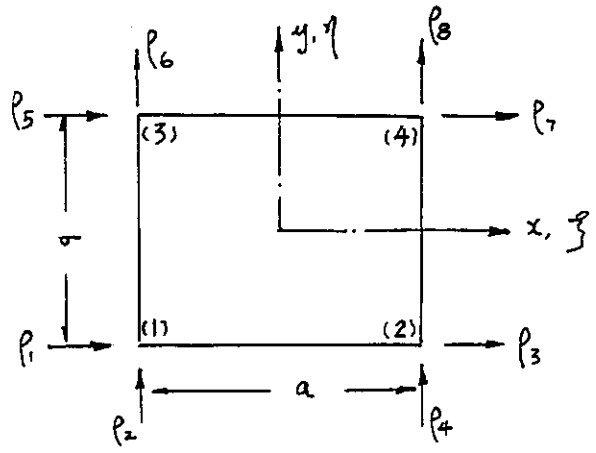
$$\underset{\sim}{U} = \begin{bmatrix} u \\ v \\ W \end{bmatrix}$$

where u, v are the global in-plane displacements in the horizontal plane.

W is the global out-of-plane displacements in the vertical plane.



2.2.1 The membrane consideration



Let the generalised displacements in the global in-plane directions be u & v . If linear strain is assumed to vary between the adjacent nodes, the relationship between the nodal displacements (i.e. $\rho_1, \rho_2, \ldots\ldots, \rho_8$) to the global displacements can be written as:-

$$\begin{bmatrix} u \\ v \end{bmatrix} = \frac{1}{4}\begin{bmatrix} (1-\xi)(1-\eta) & 0 & (1+\xi)(1-\eta) & 0 & (1-\xi)(1+\eta) & 0 & (1+\xi)(1+\eta) & 0 \\ 0 & (1-\xi)(1-\eta) & 0 & (1+\xi)(1-\eta) & 0 & (1-\xi)(1+\eta) & 0 & (1+\xi)(1+\eta) \end{bmatrix} \quad \text{----(2.6)}$$

The strain can be written as:-

$$\underset{\sim}{\varepsilon} = \begin{bmatrix} \varepsilon_x \\ \varepsilon_y \\ \varepsilon_{xy} \end{bmatrix} = \begin{bmatrix} \frac{\partial u}{\partial x} \\ \frac{\partial v}{\partial y} \\ \frac{\partial u}{\partial y} + \frac{\partial v}{\partial x} \end{bmatrix} = \begin{bmatrix} \frac{\partial}{\partial x} & 0 \\ 0 & \frac{\partial}{\partial y} \\ \frac{\partial}{\partial y} & \frac{\partial}{\partial x} \end{bmatrix} \begin{bmatrix} u \\ v \end{bmatrix} \quad \text{----(2.7)}$$

For the generalised coordinates:-

$$\xi = x/a_2 = 2x/a$$

$$\eta = y/b_2 = 2y/b \quad \text{----(2.8)}$$

Furthermore:-

$$\frac{\partial \xi}{\partial x} = \frac{2}{a} \Longrightarrow \frac{1}{dx} = \frac{2}{a} \cdot \frac{1}{d\xi}$$

$$\frac{\partial \eta}{\partial y} = \frac{2}{b} \Longrightarrow \frac{1}{dy} \quad \frac{2}{b} \frac{1}{d\eta} \quad \text{----(2.9)}$$

Sub (2.9) into (2.7) & (2.6); the $\underset{\sim}{B}$ matrix in equation (2.2) becomes:-

$$\underset{\sim}{B}_m = \begin{bmatrix} \frac{\eta-1}{2a} & 0 & \frac{1-\eta}{2a} & 0 & \frac{-(1+\eta)}{2a} & 0 & \frac{(1+\eta)}{2a} & 0 \\ 0 & \frac{\xi-1}{2b} & 0 & \frac{-(1+\xi)}{2b} & 0 & \frac{(1-\xi)}{2b} & 0 & \frac{(1+\xi)}{2b} \\ \frac{\xi-1}{2b} & \frac{\eta-1}{2a} & \frac{-(1+\xi)}{2b} & \frac{1-\eta}{2a} & \frac{1-\xi}{2b} & \frac{-(1+\eta)}{2a} & \frac{1+\xi}{2b} & \frac{1+\eta}{2a} \end{bmatrix} \qquad \text{----(2.10)}$$

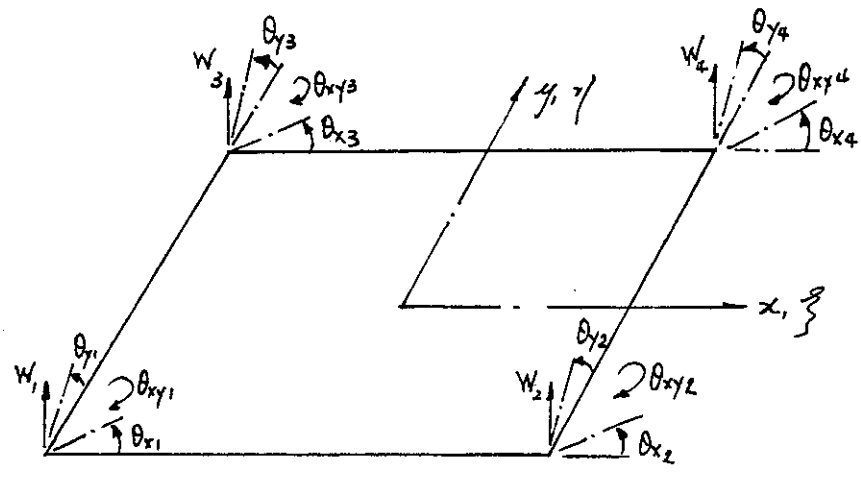
Hence the membrane stiffness of the plate can be written as:-

$$\underset{\sim}{K}_m = \frac{a \cdot b}{4} \cdot \int_{-t/2}^{t/2} \cdot \int_{-1}^{1} \cdot \int_{-1}^{1} \cdot \underset{\sim}{B}_m^t \cdot \underset{\sim}{D} \cdot \underset{\sim}{B}_m \cdot d\xi \cdot d\eta \cdot dz \qquad \text{----(2.11)}$$

Where $\underset{\sim}{D}$ is the stress-strain relationship of the material and can be written as:-

$$\underset{\sim}{D} = \frac{E}{1-\nu^2} \begin{bmatrix} 1 & \nu & 0 \\ \nu & 1 & 0 \\ 0 & 0 & \frac{1-\nu}{2} \end{bmatrix} \qquad \text{for plane stress assumption} \qquad \text{----(2.12)}$$

2.2.2 <u>The bending consideration</u>



The displacement function employed to describe the nodal displacements to the global displacement is a polynomial expression using 16 parameters. This in fact is one of the first few plate bending elements derived when Finite Element method was first developed (19, 20).

The polynomial can be expressed as:-

$$\left.\begin{aligned} W = {} & C_1 + C_2x + C_3y + C_4x^2 + C_5xy + C_6y^2 + C_7x^3 \\ & + C_8x^2y + C_9xy^2 + C_{10}y^3 + C_{11}x^3y + C_{12}x^2y^2 + C_{13}xy^3 \\ & + C_{14}x^3y^2 + C_{15}x^2y^3 + C_{16}x^3y^3 \end{aligned}\right\} \text{----(2.13)}$$

$$\left.\begin{aligned} \theta_x = \frac{\partial W}{\partial x} = {} & 0 + C_2 + 0 + 2C_4x + C_5y + 0 + 3C_7x^2 \\ & + 2C_8xy + C_9y^2 + 0 + 3C_{11}x^2y + 2C_{12}xy^2 \\ & + C_{13}y^3 + 3C_{14}x^2y^2 + 2C_{15}xy^3 + 3C_{16}x^2y^3 \end{aligned}\right\} \text{----(2.14)}$$

$$\left.\begin{aligned} \theta_y = \frac{\partial W}{\partial y} = {} & 0 + 0 + C_3 + 0 + C_5x + 2C_6y + 0 \\ & + C_8x^2 + 2C_9xy + 3C_{10}y^2 + C_{11}x^3 \\ & + 2C_{12}x^2y + 3C_{13}xy^2 + 2C_{14}x^3y + 3C_{15}x^2y^2 \\ & + 3C_{16}x^3y^2 \end{aligned}\right\} \text{----(2.15)}$$

$$\left.\begin{aligned} \theta_{xy} = \frac{\partial^2 W}{\partial x \partial y} = {} & 0 + 0 + 0 + 0 + C_5 + 0 + 0 + 2C_8x \\ & + 2C_9y + 0 + 3C_{11}x^2 + 4C_{12}xy \\ & + 3C_{13}y^2 + 6C_{14}x^2y + 6C_{15}xy^2 + 9C_{16}x^2y^2 \end{aligned}\right\} \text{----(2.16)}$$

Knowing the co-ordinates and further substituting them into equations (2.15) to (2.16) for each of the 4 nodes, then, we will have 16 sets of equations with 16 unknowns $C_1, C_2, C_3, \cdots\cdots C_{16}$ which can be expressed as:-

$$\underset{\sim}{P} = \begin{bmatrix} w_1 \\ \theta_{x1} \\ \theta_{y1} \\ \theta_{xy1} \\ w_2 \\ \theta_{x2} \\ \theta_{y2} \\ \theta_{xy2} \\ w_3 \\ \theta_{x3} \\ \theta_{y3} \\ \theta_{xy3} \\ w_4 \\ \theta_{x4} \\ \theta_{y4} \\ \theta_{xy4} \end{bmatrix} \begin{bmatrix} 1 & x_1 & y_1 & x_1^2 & x_1y_1 & y_1^2 & \cdots & x_1^3y_1^3 \\ 0 & 1 & 0 & 2x_1 & y_1 & 0 & \cdots & 3x_1^2y_1^3 \\ 0 & 0 & 1 & 0 & x_1 & 2y_1 & \cdots & 3x_1^3y_1^2 \\ 0 & 0 & 0 & 0 & 1 & 0 & \cdots & 9x_1^2y_1^2 \\ 1 & x_2 & y_2 & x_2^2 & x_2y_2 & y_2^2 & \cdots & x_2^3y_2^3 \\ 0 & - & - & - & - & - & - & - \\ 0 & - & - & - & - & - & - & - \\ 0 & - & - & - & - & - & - & - \\ 1 & - & - & - & - & - & - & - \\ 0 & - & - & - & - & - & - & - \\ 0 & - & - & - & - & - & - & - \\ 0 & - & - & - & - & - & - & - \\ 1 & x_4 & y_4 & x_4^2 & x_4y_4 & y_4^2 & \cdots & x_4^3y_4^3 \\ 0 & - & - & - & - & - & - & - \\ 0 & - & - & - & - & - & - & - \\ 0 & 0 & 0 & 0 & 1 & 0 & \cdots & 9x_4^2y_4^2 \end{bmatrix} = \underset{\sim}{N} \cdot \underset{\sim}{C} \quad \cdots\cdots (2.17)$$

where the value of $x_1 \cdots x_4$, $y_1 \cdots\cdots y_4$ are known.
Hence $\underset{\sim}{C} = \underset{\sim}{N}^{-1} \cdot \underset{\sim}{P}$ where $\underset{\sim}{N}^{-1}$ is the inversion of a 16x16 matrix.

From equation (2.13), the out-of-plane displacement of any point on the plate can be expressed as:-

$$W = (1, x, y, x^2, xy, y^2, x^3, x^2y, xy^2, y^3, x^3y, x^2y^2, xy^3, x^3y^2, x^2y^3, x^3y^3) \times \underset{\sim}{C}$$

$$= \underset{\sim}{P} \cdot \underset{\sim}{\varepsilon} \qquad = \underset{\sim}{P} \cdot \underset{\sim}{N}^{-1} \cdot f \qquad \text{----(2.18)}$$

From equation (2.7):-

$$\underset{\sim}{\varepsilon} = \begin{bmatrix} \varepsilon_x \\ \varepsilon_y \\ \varepsilon_{xy} \end{bmatrix} = \begin{bmatrix} \frac{\partial u}{\partial x} \\ \frac{\partial v}{\partial y} \\ \frac{\partial u}{\partial y} + \frac{\partial v}{\partial x} \end{bmatrix}$$

From Engineering theory of Bending for plane sections remain plane after bending, we have:-

$$\underset{\sim}{\varepsilon} = \begin{bmatrix} \frac{\partial u}{\partial x} \\ \frac{\partial v}{\partial y} \\ \frac{\partial v}{\partial x} + \frac{\partial u}{\partial y} \end{bmatrix} = \begin{bmatrix} -z \cdot \frac{\partial^2 w}{\partial x^2} \\ -z \cdot \frac{\partial^2 w}{\partial y^2} \\ -2 \cdot z \cdot \frac{\partial^2 w}{\partial x \cdot \partial y} \end{bmatrix} \qquad \text{----(2.19)}$$

Substitute (2.9) into (2.19), we have:-

$$\underset{\sim}{\varepsilon} = \begin{bmatrix} -z \frac{4}{a^2} \cdot \frac{\partial^2}{\partial \xi^2} \\ -z \cdot \frac{4}{b^2} \cdot \frac{\partial^2}{\partial \eta^2} \\ -z \cdot \frac{8}{a \cdot b} \cdot \frac{\partial^2}{\partial \xi \cdot \partial \eta} \end{bmatrix} \cdot w \qquad \text{----(2.20)}$$

Substitute (2.18) into (2.20), we have:-

$$\underset{\sim}{\varepsilon} = \begin{bmatrix} -z\cdot\frac{4}{a^2}\cdot\frac{\partial^2}{\partial\xi^2} \\ -z\cdot\frac{4}{b^2}\cdot\frac{\partial^2}{\partial\eta^2} \\ -z\cdot\frac{8}{a\cdot b}\cdot\frac{\partial^2}{\partial\xi\cdot\partial\eta} \end{bmatrix} \cdot \underset{\sim}{P}\cdot\underset{\sim}{N}^{-1} f = \underset{\sim}{\alpha}\cdot f \qquad \text{----(2.21)}$$

where

$$\underset{\sim}{\alpha} = \begin{bmatrix} -z\cdot\frac{4}{a^2}\cdot\frac{\partial^2}{\partial\xi^2} \\ -z\cdot\frac{4}{b^2}\cdot\frac{\partial^2}{\partial\eta^2} \\ -z\cdot\frac{8}{a\cdot b}\cdot\frac{\partial^2}{\partial\xi\partial\eta} \end{bmatrix} \cdot \underset{\sim}{P}\cdot\underset{\sim}{N}^{-1} = \underset{\sim}{B}_b\cdot\underset{\sim}{N}^{-1} \qquad \text{----(2.22)}$$

Hence $\underset{\sim}{\varepsilon} = \underset{\sim}{B}_b\cdot\underset{\sim}{N}^{-1}\cdot f$

where $\underset{\sim}{B}_b$ can be written as:-

$$\underset{\sim}{B}_b = \begin{bmatrix} 0 & 0 & 0 & \frac{-8z}{a^2} & 0 & 0 & \frac{-24z}{a^2}\xi & \frac{-8z}{a^2}\eta & 0 & 0 & \frac{-24z}{a^2}\xi\eta \\ 0 & 0 & 0 & 0 & 0 & \frac{-8z}{b^2} & 0 & 0 & \frac{-8z}{b^2}\xi & \frac{-24z}{b^2}\eta & 0 \\ 0 & 0 & 0 & 0 & \frac{-16z}{ab} & 0 & 0 & \frac{-32z}{a\cdot b}\xi & \frac{-32z}{a\cdot b}\eta & 0 & \frac{-48z}{a\cdot b}\xi^2 \end{bmatrix}$$

$$\begin{bmatrix} \frac{-8z}{a^2}\eta^2 & 0 & \frac{24z}{a^2}\eta^2\xi & \frac{-8z}{a^2}\eta^3 & \frac{-24z}{a^2}\xi\eta^3 \\ \frac{-8z}{b^2}\xi^2 & \frac{-24z}{b^2}\xi\eta & \frac{-8z}{b^2}\xi^3 & \frac{-24z}{b^2}\eta\xi^2 & \frac{-24z}{b^2}\xi\eta\xi^3 \\ \frac{-64z}{a\cdot b}\xi\eta & \frac{-48z}{a\cdot b}\eta^2 & \frac{-96z}{a\cdot b}\xi\eta & \frac{-96z}{a\cdot b}\xi\eta^2 & \frac{-144z}{a\cdot b}\xi\eta\xi^2 \end{bmatrix} \qquad \text{----(2.23)}$$

Hence, the stiffness matrix for the plate bending element can be expressed as:-

$$\underset{\sim}{K_b} = \frac{a \cdot b}{4} \cdot \int_{-t/2}^{t/2} \cdot \int_{-1}^{1} \cdot \int_{-1}^{1} \cdot \underset{\sim}{N}^{-1^t} \cdot \underset{\sim}{B}_b^t \cdot \underset{\sim}{D} \cdot \underset{\sim}{B}_b \cdot \underset{\sim}{N}^{-1} \cdot d\xi \cdot d\eta \cdot dz$$

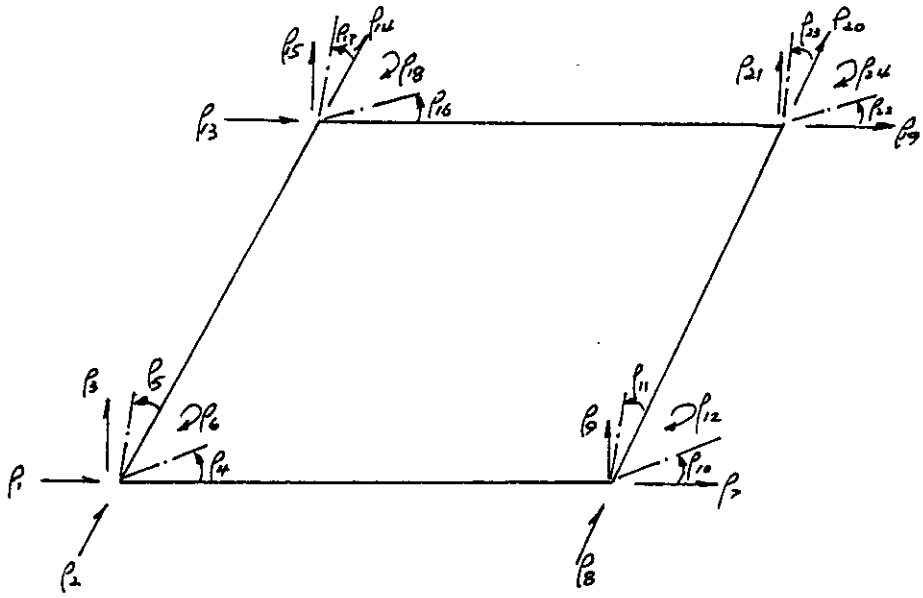
----(2.24)

Since $\underset{\sim}{N}^{-1}$ is independant of $\xi \cdot \eta$: equation (2.24) can be rewritten as:-

$$\underset{\sim}{K_b} = \frac{a \cdot b}{4} \cdot \underset{\sim}{N}^{-1^t} \cdot \left\{ \cdot \int_{-t/2}^{t/2} \cdot \int_{-1}^{1} \cdot \int_{-1}^{1} \cdot \underset{\sim}{B}_b^t \cdot \underset{\sim}{D} \cdot \underset{\sim}{B}_b \cdot d\xi \cdot d\eta \cdot dz \cdot \right\} \underset{\sim}{N}^{-1}$$

----(2.25)

The combined bending and membrane displacement of the plate element is shown below:-

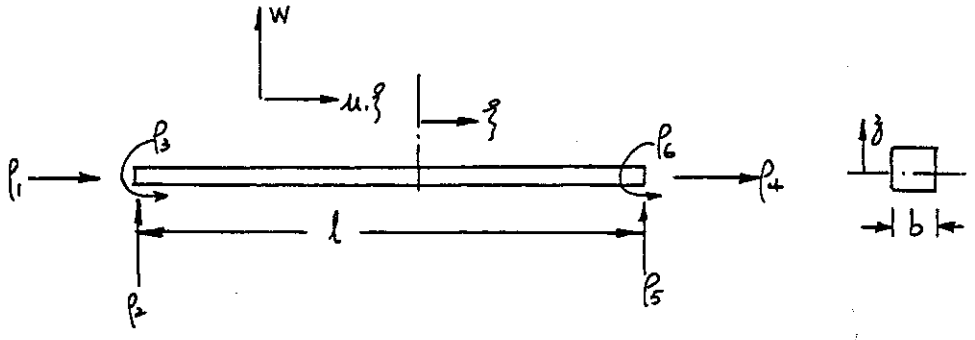


The combined stiffness matrix is just the assemblage of the individual membrane stiffness matrix and bending matrix. Since no coupling is assumed for linear displacement between membrane and bending cases, the assembled stiffness matrix of the element can be represented as:-

$$\underset{\sim}{K_P} = \begin{bmatrix} \underset{\sim}{K_m} & \underset{\sim}{0} \\ \underset{\sim}{0} & \underset{\sim}{K_b} \end{bmatrix} \qquad \text{----(2.26)}$$

2.3 Formulation of the Beam Element Stiffness Matrix

The beam element considered here is a 2 noded element with 3 degrees of freedom per node; (1 in-plane axial displacement, 1 out-of-plane displacement and 1 out-of-plane bending displacement).



Let $\underset{\sim}{U}$ be the generalised displacement of the beam element where:-

$$\underset{\sim}{U} = \begin{bmatrix} u \\ w \end{bmatrix} = \begin{bmatrix} \frac{1}{2}(1-\xi) & 0 & 0 & \frac{1}{2}(1+\xi) & 0 & 0 \\ 0 & \frac{1}{4}(1-\xi)^2(2+\xi) & \frac{l}{8}(1-\xi)^2(1+\xi) & 0 & \frac{1}{4}(1+\xi)^2(2-\xi) & \frac{l}{8}(1+\xi)^2(\xi-1) \end{bmatrix} \cdot \underset{\sim}{p}$$

$$= \underset{\sim}{B} \cdot \underset{\sim}{p} \qquad \text{----(2.27)}$$

where $\underset{\sim}{B}$ is known as the displacement function of the element.

The strain across the thickness of a beam is:-

$$\varepsilon_x = \frac{\partial u}{\partial x} - y \cdot \frac{\partial^2 w}{\partial x^2}$$

where y is the ordinates of thickness and varies between $-t/2$ to $t/2$

Hence, from equation (2.27):-

$$\frac{\partial u}{\partial x} = \frac{2}{l} \cdot \frac{\partial}{\partial \xi} \cdot \left[\frac{1}{2}(1-\xi) \;.\; 0 \;.\; 0 \;.\; \frac{1}{2}(1+\xi) \;.\; 0 \;.\; 0 \right] \cdot \underset{\sim}{f} \qquad \text{----(2.28)}$$

Similarly,

$$\frac{\partial^2 w}{\partial x^2} = \frac{4 \cdot \partial^2}{l^2 \cdot \partial \xi^2} \left[0 \;.\; \frac{1}{4}(1-\xi)^2(2+\xi) \;.\; \frac{l}{8}(1-\xi)^2(1+\xi) \;.\; 0 \;.\; \frac{1}{4}(1+\xi)^2(2-\xi) \;.\; \frac{l}{8}(1+\xi)^2(\xi-1) \right] \cdot \underset{\sim}{f} \qquad \text{----(2.29)}$$

Hence,

$$\varepsilon_x = \left[\frac{1}{l}\frac{\partial(1-\xi)}{\partial \xi} \;.\; \frac{-y}{l^2}\frac{\partial^2((1-\xi)^2(2+\xi))}{\partial \xi^2} \;.\; \frac{-y}{2.l}\frac{\partial^2((1-\xi)^2(1+\xi))}{\partial \xi^2} \;.\; \frac{1}{l}\frac{\partial(1-\xi)}{\partial \xi} \;.\; \frac{-y}{l^2}\frac{\partial^2((1+\xi)^2(2+\xi))}{\partial \xi^2} \;.\; \frac{-y}{2.l}\frac{\partial^2((1+\xi)^2(\xi-1))}{\partial \xi^2} \right] \times \underset{\sim}{f} = \underset{\sim}{\alpha} \cdot \underset{\sim}{f} \qquad \text{----(2.30)}$$

Hence, the stiffness matrix of the beam can be written as:-

$$\underset{\sim}{K_s}' = \frac{b \cdot l}{2} \cdot \int_{-t/2}^{t/2} \cdot \int_{-1}^{1} \cdot \underset{\sim}{\alpha}^t \cdot E \cdot \underset{\sim}{\alpha} \cdot d\xi \cdot d\eta \cdot$$

----(2.31)

2.4 Solving the Equation of Equilibrium

The stiffness matrices derived from the above sections can normally be evaluated using numerical integration schemes. However, as for small displacement linear geometry and linear material analysis, the stiffness matrices do not change at all and as the stiffness matrices depend only on the non-dimensional coordinates ξ, η which again are constant throughout the loading procedure. The stiffness matrices can almost be integrated explicitly. Hence, the element stiffness matrices can firstly be integrated from ξ & η = -1 to 1 and then be stored into the back storage. When solving for the equation of equilibrium, the already integrated stiffness matrices can be called out and be assembled directly into the structural stiffness matrix.

2.5 Linear Static Analysis

2.5.1 Plate Element

In order to study the convergency and the compatibility of the element employed in the analysis, a series of tests were carried out on the plate with different number of elements, boundary conditions and aspect ratios.

Properties of the plate are:- $E = 10^7$ lb/in^2
thickness = 0.1"
width = 10"
and poisson's ratio = 0.3

The plate was divided into 2x2, 4x4 and 6x6 elements respectively. A load was applied at the centre of the plate and the non-dimensional deflection was recorded. Only one quarter of the plate was used in the analysis. The following results are observed:-

i) Simply Supported Edges

The results are shown in Table A of Fig. 1, and the graphs of corresponding deflections versus different numbers of elements employed are shown in Fig. 2. A curve of the theoretical non-dimensional deflection was used to compare with the finite element results. Very good results were obtained. The differences between the finite element values and the theoretical values varied from -1% using 2x2 elements to -0.007% using 6x6 elements for a unit aspect ratio. The differences appeared to be slightly increased as the aspect ratio increased, but converged to well under -1% as the number of elements used are increased to 6x6. The evaluated results were all appeared to be below the plate theory predicted values (25). This is particularly true when the employed displacement function is a 16 term polynomial series.

ii) Clamped Edges

The results are tabulated in Table B of Fig. 1 and the graphs of the corresponding deflection versus different number of elements employed are shown in Fig.3. Again, very good results were obtained from the analysis. The differences between the evaluated results and the theoretical values appeared to be slightly greater than those obtained by using a simply supported plate. However, the difference converges rapidly to around -1% when the plate element number increased to 6 x 6.

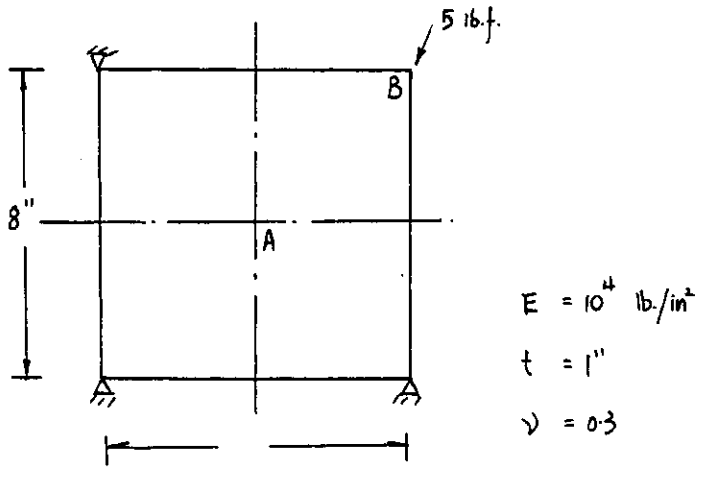
All the results obtained in the analysis can be seen to be slightly less than the theoretical values, and on employing an increasing number of elements in the analysis, the results aproach the exact solution. This shows strongly the conforming characteristic of the element employed here.

Fig. 4 shows the variation of the displacement of a plate with different aspect ratios. A curve of the theoretical values was used to contrast the differences. Again, it can be seen that the difference between the curves increased slightly as the aspect ratio increased. However, such differences are shown to converge when the number of elements employed in the analysis are increased.

iii) Twisting Test

A test was carried out to study the twisting behaviour of the employed element.

A square plate was simply supported at 3 corners and subjected to a vertical load of 5 lbf at the fourth corner as shown in diagram below:-



Results are compared with those obtained in Ref.(25) and are shown in Table C of Fig. 1. Reasonably good results are observed.

2.5.2 Bar Element

Two simple tests on the static deflection of the bar using different number of elements were carried out; one on a simply-supported beam and the other on a cantilever beam. The def lection obtained in the former analysis was 0.349" using 4 elements along the bar (an error of -0.24% compared with the theoretical value of 0.35). In the latter case, the result obtained was 0.553" compared with the theoretical value of 0.5535" (a difference of 0.1%). The results are plotted on Fig. 5a and 5b respectively. Again, they all converged to the exact value as the number of elements employed increased.

3. GEOMETRIC NON-LINEARITY

The non-linear analysis of plate and shells with and without stiffener has been treated by classical methods (26,27), finite difference (28), dynamic relaxation (29), perturbation analysis (30) and by use of Ritz procedures (31). However, as a result of the development of recent computing technology, the finite element method appears to be the most powerful and popular numerical approach. The approach was developed in the early 50s and numerous research works had devoted primarily to problems where the linear type of stress-strain relationship were considered. This type of approach would seem to be quite adequate for problems involving only small deflections. (Problems with deflections comparably small with thickness are normally considered as linear because the strain developed within the structure can generally be assumed to be infinitesimally small. Those descibed in Section 2 are categorised as small deflection problems.) The geometry of the element can then remain basically unchanged during the process of loading. Under this assumption, the displacement of each harmonic depends only on the loading of the same harmonic variation. Furthermore, since there is no coupling between the bending and membrane displacement, the solution of these can virtually be obtained independantly. In practice, as coupling in general occurs between all the harmonics, the above assumption is quite inadequate even though the strains may be very small.

Here, when large deflections are considered, the stresses due to the membrane action, which is normally ignored in small plate bending theory, may reduce the deflection even though the displacement itself is small. On the other hand, when a stability problem is considered, the deflection may increase much more rapidly than that predicted by linear small displacement theory when a certain load is reached. Such behaviour is known as geometric non-linear behaviour.

The pioneering non-linear work on finite element work is due to Turner et al (32). Generally, in the non-linear field, incremental approaches were adopted for tracing the complete load-deflection characteristic of a structure (33,36). The approach involves the geometric stiffness matrix and the updating of coordinates. The updating of coordinates is obtained by following either an Eulerian formulation (moving coordinates) (39,40) in which the construction of the tangential stiffness matrix relied on the updated set of coordinates, or a Lagrangian formulation (fixed coordinates) (35) in which an initial displacement matrix is added to the formulation of the tangential stiffness matrix. The Lagrangian formulation is more economical than the Eulerian formulation and gives a better solution when a small number of elements are employed (36).

However, the incremental approach often leads to an unquantifiable build-up of errors during the process of calculation and, to counter this problem, the Newton-Raphson iteration (37) method is sometimes adopted to rectify these errors. For most instability problems, there is a danger of a lack of convergence to a higher equilibrium state. For this reason, Connor and Brebbia (38) recommended a combination of incremental and iteration techniques which was also used by Murray and Wilson (39,40). Whilst both authors used the same iteration technique, their approaches in formulating the tangential stiffness matrix are somewhat different. Whereas Connor and Brebbia (38) used an initial displacement matrix, Murray and Wilson (39,40) relied on updating the coordinates. Instead of using the Newton-Raphson method which requires that the tangential stiffness matrix be found and then triangulised in each step, we will adopt a modified Newton-Raphson procedure (19) in which the out-of-balance load vector computed at the end of each load increment is applied to the tangential stiffness matrix for iteration.

3.1 Formulation of Large Deflection Equation

The formulation of geometric non-linear stiffness matrices for most elements is obviously well established since there has been many researches contributing to this field in the past two decades. In our case here, we will however look for a unified way to formulate the stiffness matrices for the elements so that it not only includes the geometric non-linearity effect but also is ready to accommodate the material non-linearity effect when needed, since we will be looking into the elasto-plastic behaviour of the structure involved.

The treatment of geometric non-linearity in finite element formulations is to examine the basic non-linear equilibrium equations together with their solution. This would subsequently lead to the general continuum formulation of both the large displacement and the initial stability problem. Throughout the formulation, a Lagrangian system is adopted in which the displacements are referred to its original configuration.

Let's consider at any time t, an equilibrium set of equation is:-

$$\int_S T_i \cdot v_i \cdot dS + \int_V F_i \, v_i \cdot dV = \int_V \sigma_{ij} \cdot v_{ij} \, dV \qquad \text{----(3.1)}$$

where:- T_i are the components of surfaces force per unit of current surface area.

S is the current surfaces of the element.

F_i are the components of the body force per unit of current volume.

V is the current volume of the element.

σ_{ij} is the stress field throughout the element in equilibrium with F_i and T_i.

$V_{ij} = \frac{1}{2}\left(\frac{\partial V_i}{\partial x_j} + \frac{\partial V_j}{\partial x_i}\right)$ is the rate of deformation derived from the velocity field $\underset{\sim}{V}(\underset{\sim}{x})$.

$\underset{\sim}{x}$ are the current coordinates.

In the linear displacement analysis, V_{ij} is equal to $\dot{\varepsilon}_{ij}$, the strain rate.

Equation (3.1) refers to the current set of coordinates. In order to transform equation (3.1) into a set of coordinates referring to its initial frame of reference, the relationship between the initial and current coordinates is:-

$$x_i = X_i + U_i \qquad \text{----(3.2)}$$

where x_i & X_i are the current and initial coordinates respectively.

U_i are the components of the total displacements of the material of a point at time t.

If Lagrangian formulation is to be used, the Green's strain tensor which refers to the set of initial coordinates should be adopted, and this is defined as:-

$$E_{ij} = \tfrac{1}{2}\left(\frac{\partial x_K}{\partial X_i}\cdot\frac{\partial x_K}{\partial X_j} - \delta_{ij}\right) \qquad \text{----(3.3)}$$

where δ_{ij} is the Kronecker Delta

Hence the strain rate:-

$$\dot{E}_{ij} = \tfrac{1}{2}\left(\frac{\partial v_K}{\partial X_i}\cdot\frac{\partial x_K}{\partial X_j} + \frac{\partial x_K}{\partial X_i}\cdot\frac{\partial v_K}{\partial X_j}\right) \qquad \text{----(3.4)}$$

The appropriate stress whose product with $\dot{E}_{ij}$ will give the work done per unit initial volume is the Kirchoff stress S_{ij}. Hence the R.H.S. of equation (3.1) becomes:-

$$\int_v \sigma_{ij}\cdot v_{ij}\cdot dv = \int_{v^\circ} S_{ij}\cdot\dot{E}_{ij}\cdot dv^\circ \qquad \text{----(3.5)}$$

Considering equation (3.2), the general displacement U_i can be represented as:-

$$U_i = A_i^\alpha\cdot\rho_l^\alpha \qquad \text{----(3.6)}$$

where α is the number of nodal freedoms and A_i^α is the component of displacement shape functions.

Hence:-

$$\frac{\partial u_i}{\partial x_j} = \frac{\partial A_i^\alpha}{\partial x_j}\cdot\rho_l^\alpha \qquad \text{----(3.7)}$$

Similarly,

$$v_i = A_i^{\alpha} \cdot \dot{\rho}_{\ell}^{\alpha} \qquad \text{----(3.8)}$$

and

$$\frac{\partial v_i}{\partial X_j} = \frac{\partial A_i^{\alpha}}{\partial X_j} \cdot \dot{\rho}_{\ell}^{\alpha} \qquad \text{----(3.9)}$$

Substitute (3.9) into (3.4); we have:-

$$\dot{E}_{ij} = Sym. \left[\left(\frac{\partial A_i^{\alpha}}{\partial X_j} + \frac{\partial A_K^{\beta}}{\partial X_j} \cdot \rho_{\beta}^{\beta} \cdot \frac{\partial A_K^{\alpha}}{\partial X_i} \right) \cdot \dot{\rho}_{\ell}^{\alpha} \right] \qquad \text{----(3.10)}$$

Substitute (3.10) into (3.5); we have:-

$$\int_{V^o} S_{ij} \dot{E}_{ij} \, dV^o = \left\{ \int_{V^o} S_{ij} \left(\frac{\partial A_i^{\alpha}}{\partial X_j} + \frac{\partial A_K^{\beta}}{\partial X_j} \cdot \rho_{\beta}^{\beta} \cdot \frac{\partial A_K^{\alpha}}{\partial X_i} \right) dV^o \right\} \cdot \dot{\rho}_{\ell}^{\alpha} \qquad \text{----(3.11)}$$

The LHS of equation (3.1) becomes:-

$$\int_S T_i \cdot V_i \, dS + \int_V F_i \, V_i \, dV = \left\{ \int_{S^o} T_i^o \cdot A_i^{\alpha} \cdot dS^o + \int_{V^o} F_i^o \cdot A_i^o \, dV^o \right\} \cdot \dot{\rho}_{\ell}^{\alpha} \qquad \text{---(3.12)}$$

Combining (3.11) & (3.12), it becomes:-

$$\left\{ \int_{S^o} T_i^o \cdot A_i^{\alpha} \cdot dS^o + \int_{V^o} F_i^o \cdot A_i^{\alpha} \cdot dV^o \right\} \dot{\rho}_{\ell}^{\alpha} = \left\{ \int_{V^o} S_{ij} \left(\frac{\partial A_i^{\alpha}}{\partial X_j} + \frac{\partial A_K^{\beta}}{\partial X_j} \cdot \rho_{\beta}^{\beta} \cdot \frac{\partial A_K^{\alpha}}{\partial X_i} \right) dV^o \right\} \dot{\rho}_{\ell}^{\alpha} \qquad \text{----(3.13)}$$

If the 'equivalent' applied forces P_i^α at the nodes are defined in terms of surface and body forces as:-

$$P_i^\alpha = \int_{S^\circ} T_i^\circ \cdot A_i^\alpha \cdot dS^\circ + \int_{V^\circ} F_i^\circ \cdot A_i^\alpha \cdot dA^\circ \qquad \text{----(3.14)}$$

The set of equilibrium equation is:-

$$P_i^\alpha = \int_{V^\circ} S_{ij} \left(\frac{\partial A_i^\alpha}{\partial X_j} + \frac{\partial A_K^\beta}{\partial X_j} \cdot \rho_\beta^\beta \cdot \frac{\partial A_K^\alpha}{\partial X_i} \right) \cdot dV^\circ \qquad \text{----(3.15)}$$

It is apparent that equation (3.15) is a function of the current state of deformation ℓ which means that equation (3.15) will be changing throughout the loading procedure. Two types of non-linearity arise in this equation; the geometric non-linearity and the material non-linearity (since the relationship between S_{ij} and $\dot{E}_{ij}$ can not remain linear when material is above yield). This aspect will be discussed in Chapter 4. In this Chapter, however, we will consider only the geometric non-linear effect.

Consider equation (3.15), the body force increment becomes:-

$$\Delta P_i^\alpha = \left\{ \int_{V^\circ} \Delta S_{ij} \left[\frac{\partial A_i^\alpha}{\partial X_j} + \frac{\partial A_K^\beta}{\partial X_j} \cdot \rho_\beta^\beta \cdot \frac{\partial A_K^\alpha}{\partial X_i} \right] dV^\circ + \int_{V^\circ} S_{ij} \left[\frac{\partial A_K^\beta}{\partial X_j} \cdot \frac{\partial A_K^\alpha}{\partial X_i} \right] dV^\circ \cdot \Delta \rho_\beta^\beta \right\} \qquad \text{----(3.16)}$$

Furthermore, if the linear stress-strain increment in the Lagrangian frame of reference can be related as:-

$$\Delta S_{ij} = D_{ijkl} \cdot \Delta E_{kl} \qquad \text{----(3.17)}$$

$$\therefore \Delta S_{ij} = D_{ijkl} \cdot \left[\frac{\partial A_k^{\alpha}}{\partial X_l} + \frac{\partial A_p^{\alpha}}{\partial X_k} \cdot \frac{\partial A_p^{\beta}}{\partial X_l} \cdot \rho_0^{\beta} \right] \cdot \Delta \rho_m^{\alpha} \qquad \text{----(3.18)}$$

Substitute (3.18) into (3.16), equation becomes:-

$$\Delta P_l^{\alpha} = \left\{ \int_{V^0} \left[\frac{\partial A_i^{\alpha}}{\partial X_j} + \frac{\partial A_k^{\alpha}}{\partial X_i} \cdot \frac{\partial A_k^{\beta}}{\partial X_j} \cdot \rho_0^{\beta} \right] \cdot D_{ijkl} \cdot \left[\frac{\partial A_k^{\alpha}}{\partial X_l} + \frac{\partial A_p^{\alpha}}{\partial X_k} \cdot \frac{\partial A_p^{\beta}}{\partial X_l} \cdot \rho_0^{\beta} \right] dV^0 + \int_{V^0} S_{ij} \left[\frac{\partial A_k^{\beta}}{\partial X_j} \cdot \frac{\partial A_k^{\alpha}}{\partial X_i} \right] \cdot dV^0 \right\} \Delta \rho_0^{\beta} \qquad \text{----(3.19)}$$

Compare (3.1) with the equation 3.19 :-

$$\Delta \underset{\sim}{P} = \underset{\sim}{K_T} \cdot \Delta \underset{\sim}{f}$$

It can be shown that the tangential stiffness of the element is equal to:-

$$\therefore \underset{\sim}{K_T} = \int_{V^0} \left\{ \frac{\partial A_i^{\alpha}}{\partial X_j} + \frac{\partial A_k^{\alpha}}{\partial X_i} \cdot \frac{\partial A_k^{\beta}}{\partial X_j} \cdot \rho_0^{\beta} \right\} \cdot D_{ijkl} \cdot \left\{ \frac{\partial A_k^{\alpha}}{\partial X_l} + \frac{\partial A_p^{\alpha}}{\partial X_k} \cdot \frac{\partial A_p^{\beta}}{\partial X_l} \cdot \rho_0^{\beta} \right\} dV^0 + \int_{V^0} S_{ij} \left\{ \frac{\partial A_k^{\beta}}{\partial X_j} \cdot \frac{\partial A_k^{\alpha}}{\partial X_i} \right\} \cdot dV^0 \qquad \text{----(3.20)}$$

If the term $\frac{\partial A_K^{\alpha}}{\partial x_i} \cdot \frac{\partial A_K^{\beta}}{\partial x_j} \cdot \rho^{\beta}$ is to be ignored in equation (3.20), the deformation rate $v_{ij} = \frac{1}{2}\left(\frac{\partial v_i}{\partial x_j} + \frac{\partial v_j}{\partial x_i}\right)$ employed in formulating the above stiffness matrix is thus reduced to the linear strain rate $\dot{\varepsilon}_{ij} = \frac{1}{2} \cdot \frac{\partial v_i}{\partial x_j}$. Hence, equation (3.20) is reduced to :-

$$\underset{\sim}{K}_T = \int_{V^0} \left[\frac{\partial A_i^{\alpha}}{\partial x_j}\right] \cdot D_{ijkl} \cdot \left[\frac{\partial A_K^{\alpha}}{\partial x_l}\right] \cdot dV^0 + \int_{V^0} S_{ij} \left\{\frac{\partial A_K^{\beta}}{\partial x_j} \cdot \frac{\partial A_K^{\alpha}}{\partial x_i}\right\} dV^0 \qquad \text{----(3.21)}$$

The term $\int_{V^0} \left[\frac{\partial A_i^{\alpha}}{\partial x_j}\right] \cdot D_{ijkl} \cdot \left[\frac{\partial A_K^{\alpha}}{\partial x_l}\right] \cdot dV^0$ is shown to be equivalent to the small displacement stiffness matrix $\underset{\sim}{K}_e$ mentioned in Section 2 while $\int_{V^0} S_{ij} \left\{\frac{\partial A_K^{\beta}}{\partial x_j} \cdot \frac{\partial A_K^{\alpha}}{\partial x_i}\right\} \cdot dV^0$ is equivalent to the geometric stiffness matrix $\underset{\sim}{K}_{\sigma}$

3.1.1 Finite Element Formulation of the Plate Element Stiffness Matrices

Here $\frac{\partial A_i^{\alpha}}{\partial X_j}$ is equivalent to $\underset{\sim}{B}_e$ which can be expressed as:-

$$\frac{\partial A_i^{\alpha}}{\partial X_j} = \left[\begin{array}{c|c} \frac{\partial A_i}{\partial X_0} & -z\cdot\frac{\partial^2 w_i}{\partial X_0^2}\cdot N^{-1} \\ \frac{\partial A_i}{\partial Y_0} & -z\cdot\frac{\partial^2 w_i}{\partial Y_0^2}\cdot N^{-1} \\ \frac{\partial A_i}{\partial Y_0}+\frac{\partial A_i}{\partial X_0} & -2z\cdot\frac{\partial^2 w_i}{\partial X_0\partial Y_0}\cdot N^{-1} \end{array}\right] \qquad \text{----(3.21.a)}$$

From equation 2.10 & 2.23, $\underset{\sim}{B}_e$ =

$$\left[\begin{array}{cccccccc|cccccccc} \frac{\eta-1}{2a} & 0 & \frac{1-\eta}{2a} & 0 & \frac{-(1+\eta)}{2a} & 0 & \frac{1+\eta}{2a} & 0 & 0 & 0 & 0 & -\frac{8z}{a^2} & 0 & 0 & -\frac{24z\xi}{a^2} & -\frac{8z\eta}{a^2} & 0 & 0 \\ 0 & \frac{\xi-1}{2b} & 0 & \frac{-(1+\xi)}{2b} & 0 & \frac{1-\xi}{2b} & 0 & \frac{1+\xi}{2b} & 0 & 0 & 0 & 0 & 0 & -\frac{8z}{b^2} & 0 & 0 & -\frac{8z\xi}{b^2} & -\frac{24z}{b^2}\eta \\ \frac{\xi-1}{2b} & \frac{\eta-1}{2a} & \frac{-(1+\xi)}{2b} & \frac{1-\eta}{2a} & \frac{1-\xi}{2b} & \frac{-(1+\eta)}{2a} & \frac{1+\xi}{2b} & \frac{1+\eta}{2a} & 0 & 0 & 0 & 0 & -\frac{16z}{ab} & 0 & 0 & -\frac{32z}{a\cdot b}\xi & -\frac{32z}{a\cdot b}\eta & 0 \end{array}\right.$$

$$\left.\begin{array}{cccccc} -\frac{24z\xi\eta}{a^2} & -\frac{8z\eta^2}{a^2} & 0 & \frac{24z\eta^2\xi}{a^2} & \frac{-8z\cdot\eta^3}{a^2} & -\frac{24z\xi\eta^3}{a^2} \\ 0 & -\frac{8z\xi^2}{b^2} & -\frac{24z\xi\eta}{b^2} & -\frac{8z\xi^3}{b^2} & -\frac{24z\cdot\eta\xi^2}{b^2} & -\frac{24z\cdot\eta\xi^3}{b^2} \\ -\frac{48z\xi^2}{ab} & -\frac{48z\xi^2\eta}{ab} & -\frac{48z\eta^2}{ab} & -\frac{96z\xi^2\cdot\eta}{ab} & -\frac{96z\xi\eta^2}{ab} & -\frac{144z\cdot\xi^2\eta^2}{a\cdot b} \end{array}\right]$$

$$= \left[\begin{array}{c|c} \underset{3\times8}{B_v} & -z\cdot\underset{3\times16}{B_w} \end{array}\right]$$

Hence for linear displacement:-

$$\underset{\sim}{K}_T = \int_{V^o} \underset{\sim}{B}_e^T \cdot \underset{\sim}{E} \cdot \underset{\sim}{B}_e \cdot dV^o = \int_{V^o} \begin{bmatrix} \underset{\sim}{B}_v^t \\ -j\,\underset{\sim}{B}_w^t \end{bmatrix}_{24\times 3} \underset{3\times 3}{\underset{\sim}{E}} \left[\underset{\sim}{B}_v \;\vdots\; -j\,\underset{\sim}{B}_w \right]_{3\times 24} dV^o$$

$$= \int_{V^o} \left[\begin{array}{c|c} \underset{\sim}{B}_v^t \cdot \underset{\sim}{E} \cdot \underset{\sim}{B}_v & -\underset{\sim}{B}_v^t \cdot \underset{\sim}{E} \cdot j \cdot \underset{\sim}{B}_w \\ \hline -j\,\underset{\sim}{B}_w^t \cdot \underset{\sim}{E} \cdot \underset{\sim}{B}_v & j^2 \cdot \underset{\sim}{B}_w^t \cdot \underset{\sim}{E} \cdot \underset{\sim}{B}_w \end{array}\right]_{24\times 24} dV^o = \left[\begin{array}{c|c} \underset{\sim}{K}_m & \underset{\sim}{K}_{mb} \\ \hline \underset{\sim}{K}_{bm} & \underset{\sim}{K}_b \end{array}\right]_{24\times 24}$$

Here,

$$\underset{\sim}{K}_{mb} = \underset{\sim}{K}_{bm} = -\int_{-t/2}^{t/2} \cdot \int_A \cdot j \cdot \underset{\sim}{B}_w^t \cdot \underset{\sim}{E} \cdot \underset{\sim}{B}_v \cdot dj \cdot dA$$

For linear analysis, because $\underset{\sim}{E}$ is the same across the thickness from $j = -t/2$ to $j = t/2$, therefore

$$-\int_{-t/2}^{t/2} \cdot \int_A \cdot j \cdot \underset{\sim}{B}_w^t \cdot \underset{\sim}{E} \cdot \underset{\sim}{B}_v \cdot dj \cdot dA = \underset{\sim}{0}$$

Hence, $\underset{\sim}{K}_T = \begin{bmatrix} \underset{\sim}{K}_m & \underset{\sim}{0} \\ \underset{\sim}{0} & \underset{\sim}{K}_b \end{bmatrix}_{24\times 24}$ which is exactly the same as that used in equation (2.29), is the stiffness matrix $\underset{\sim}{K}_e$ for small displacement only.

It is obvious now that the term: $\dfrac{\partial A_K^\alpha}{\partial x_i} \cdot \dfrac{\partial A_K^\beta}{\partial x_j} \cdot \rho^\beta$
is purely due to the large displacement geometric non-linearity effect.

Hence, from (3.20):-

$$\int_{V^o}\left[\frac{\partial A_i^{\alpha}}{\partial X_j}+\frac{\partial A_K^{\alpha}}{\partial X_i}\cdot\frac{\partial A_K^{\beta}}{\partial X_j}\cdot\rho_{\beta}^{\beta}\right]\cdot D_{ijkl}\cdot\left[\frac{\partial A_K^{\alpha}}{\partial X_l}+\frac{\partial A_P^{\alpha}}{\partial X_K}\cdot\frac{\partial A_P^{\beta}}{\partial X_l}\cdot\rho_{\beta}^{\beta}\right]\cdot dV^o$$

$$= \underset{\sim}{K}_e + \underset{\sim}{K}_L \qquad \text{----(3.22)}$$

where $\underset{\sim}{K}_L$ is known as the large displacement stiffness matrix. The second term in equation (3.20):- $\int_V S_{ij}\left[\frac{\partial A_K^{\beta}}{\partial X_j}\cdot\frac{\partial A_K^{\alpha}}{\partial X_i}\right]\cdot dV$ is dependent of the stress level and the loading. This term is known as the initial stress matrix or the geometric stiffness matrix $\underset{\sim}{K}_G$. Hence,

$$\underset{\sim}{K}_T = \underset{\sim}{K}_e + \underset{\sim}{K}_L + \underset{\sim}{K}_G \qquad \text{----(3.23)}$$

In finite element analysis, the term $\frac{\partial A_K^{\alpha}}{\partial X_\cdot}\frac{\partial A_K^{\beta}}{\partial X_\cdot}\cdot\rho_{\beta}^{\beta}$ can be expressed as:- (from equation (3.7), we deduced:-)

$$\frac{\partial A_K^{\beta}}{\partial X_i}\cdot\rho_{\beta}^{\beta} = \frac{\partial W}{\partial X_i} \quad \& \quad \frac{\partial A_K^{\alpha}}{\partial X_j} = \frac{\partial \omega_K^{\alpha}}{\partial X_j}\cdot\underset{\sim}{N}^{-1}$$

$$\therefore \quad \underset{\sim}{B}_L = \frac{\partial A_K^{\alpha}}{\partial X_i}\cdot\frac{\partial A_K^{\beta}}{\partial X_j}\cdot\rho_{\beta}^{\beta}$$

$$= \begin{bmatrix} \underset{\sim}{0} & \frac{\partial W}{\partial X_0}\cdot\frac{\partial \omega_i}{\partial X_0}\cdot\underset{\sim}{N}^{-1} \\ \underset{\sim}{0} & \frac{\partial W}{\partial Y_0}\cdot\frac{\partial \omega_i}{\partial Y_0}\cdot\underset{\sim}{N}^{-1} \\ \underset{\sim}{0} & \left[\frac{\partial W}{\partial Y_0}\cdot\frac{\partial \omega_i}{\partial X_0}+\frac{\partial W}{\partial X_0}\cdot\frac{\partial \omega_i}{\partial Y_0}\right]\underset{\sim}{N}^{-1} \end{bmatrix} \qquad \text{----(3.24)}$$

From equation (3.21.a) and (3.24), $\left(\underset{\sim}{B}_e + \underset{\sim}{B}_L \right)^t$ =:-

$$\begin{bmatrix} \dfrac{\partial A_i}{\partial X_o} \\ \dfrac{\partial A_i}{\partial Y_o} \\ \dfrac{\partial A_i}{\partial Y_o} + \dfrac{\partial A_i}{\partial X_o} \\ -z\dfrac{\partial^2 \vartheta_i}{\partial X_o^2}\cdot\underset{\sim}{N}^{-1} + \dfrac{\partial W}{\partial X_o}\cdot\dfrac{\partial \vartheta_i}{\partial X_o}\cdot\underset{\sim}{N}^{-1} \\ -z\dfrac{\partial^2 \vartheta_i}{\partial Y_o^2}\cdot\underset{\sim}{N}^{-1} + \dfrac{\partial W}{\partial Y_o}\cdot\dfrac{\partial \vartheta_i}{\partial Y_o}\cdot\underset{\sim}{N}^{-1} \\ -2z\dfrac{\partial^2 \vartheta_i}{\partial X_o \partial Y_o}\cdot\underset{\sim}{N}^{-1} + \dfrac{\partial W}{\partial Y_o}\dfrac{\partial \vartheta_i}{\partial X_o}\cdot\underset{\sim}{N}^{-1} + \dfrac{\partial W}{\partial X_o}\cdot\dfrac{\partial \vartheta_i}{\partial Y_o}\cdot\underset{\sim}{N}^{-1} \end{bmatrix} \qquad \text{----(3.25)}$$

$$= \begin{bmatrix} \underset{\sim}{B}_v \\ \hline -z\cdot\underset{\sim}{B}_W + \underset{\sim}{B}_Z \end{bmatrix} \qquad \text{----(3.25.a)}$$

Substitute the appropriate displacement shape functions of the plate element into equation (3.25) and let $\dfrac{\partial W}{\partial X_o} = W_1$, $\dfrac{\partial W}{\partial Y_o} = W_2$, we have:-

$$
\left[\begin{array}{cccccccc|cccccccccccc}
\frac{\eta-1}{2a} & 0 & \frac{1-\eta}{2a} & 0 & \frac{-(1+\eta)}{2a} & 0 & \frac{1+\eta}{2a} & 0 & 0 & \frac{2w_1}{a} & 0 & \frac{4w_1\xi}{a}+\frac{-8\xi}{a^2} & \frac{2w_1\eta}{a} & 0 & \frac{6w_1\xi^2}{a}+\frac{-24\xi^2}{a^2} & \frac{4w_1\xi\eta}{a}+\frac{-8\xi\eta}{a^2} & \frac{2w_1\eta^2}{a} & 0 & \frac{6w_1\xi\eta^2}{a}+\frac{-24\xi\eta^2}{a^2} & \frac{4w_1\xi^3}{a}+\frac{-8\xi^3}{a^2} & \frac{6w_1\xi^2\eta}{a}+\frac{-24\xi^2\eta}{a^2} \\
0 & \frac{\xi-1}{2b} & 0 & \frac{-(1+\xi)}{2b} & 0 & \frac{1-\xi}{2b} & 0 & \frac{1+\xi}{2b} & 0 & 0 & \frac{2w_2}{b} & 0 & \frac{2w_2\xi}{b}+\frac{-8\xi}{b^2} & \frac{4w_2\eta}{b}+\frac{-8\eta}{b^2} & 0 & \frac{2w_2\xi^2}{b}+\frac{-8\xi^2}{b^2} & \frac{4w_2\xi\eta}{b}+\frac{-24\xi\eta}{b^2} & \frac{2w_2\eta^2}{b} & \frac{4w_1\xi\eta}{b}+\frac{-8\xi\eta}{b^2} & \frac{6w_1\xi^2\eta}{b}+\frac{-24\xi^2\eta}{b^2} & \frac{4w_1\xi^3}{b}+\frac{-8\xi^3}{b^2} & \frac{6w_1\xi^2\eta}{b}+\frac{-24\xi^2\eta}{b^2} \\
\frac{\xi-1}{2b} & \frac{\eta-1}{2a} & \frac{-(1+\xi)}{2b} & \frac{1-\eta}{2a} & \frac{1-\xi}{2b} & \frac{-(1+\eta)}{2a} & \frac{1+\xi}{2b} & \frac{1+\eta}{2a} & 0 & \frac{2w_1}{a} & \frac{2w_2}{b} & \frac{4w_1\xi}{a}+\frac{2w_2\xi}{b}+\frac{-8\xi}{ab} & \frac{2w_1\eta}{a}+\frac{4w_1\eta}{b}+\frac{-16\xi}{ab} & \frac{6w_2\xi^2}{a}+\frac{-24\xi^2}{ab} & \frac{4w_1\xi^2}{a}+\frac{2w_1\eta}{b}+\frac{4w_1\xi}{b}+\frac{-32\xi\eta}{ab} & \frac{2w_1\eta^2}{a}+\frac{6w_1\xi\eta}{b}+\frac{-24\eta^2}{ab} & \frac{6w_2\xi^2}{a}+\frac{4w_1\xi\eta}{b}+\frac{-48\xi^2\eta}{ab} & \frac{6w_2\xi\eta}{a}+\frac{6w_1\xi^2\eta}{b}+\frac{-48\xi^2\eta}{ab} & \frac{6w_2\xi^2\eta}{a}+\frac{6w_1\xi\eta^2}{b}+\frac{-72\xi^2\eta^2}{ab}
\end{array}\right]^{-1} \qquad \text{---- 3.26}
$$

$$
= \left[\begin{array}{c|c} \underset{\sim}{B_v} & -\gamma\cdot\underset{\sim}{B_w}+\underset{\sim}{B_t} \end{array}\right] \qquad \text{--- 3.26a}
$$

$$
\text{Hence,}\quad \underset{\sim}{K_a}+\underset{\sim}{K_L} = \int_{V^0}\left[\begin{array}{c} \underset{\sim}{B_v}^t \\ \hline -\gamma\underset{\sim}{B_w}^t+\underset{\sim}{B_t}^t \end{array}\right] \underset{\sim}{E} \left[\begin{array}{c|c} \underset{\sim}{B_v} & -\gamma\cdot\underset{\sim}{B_w}+\underset{\sim}{B_t} \end{array}\right] dV \qquad \text{--- 3.27}
$$

$$\underset{\sim}{K}_e + \underset{\sim}{K}_L = \int_{V^o} \left[\begin{array}{c|c} \underset{\sim}{B}_v^t \cdot \underset{\sim}{E} \cdot \underset{\sim}{B}_v & -z \cdot \underset{\sim}{B}_v^t \cdot \underset{\sim}{E} \cdot \underset{\sim}{B}_w + \underset{\sim}{B}_v^t \cdot \underset{\sim}{E} \cdot \underset{\sim}{B}_z \\ \hline -z \underset{\sim}{B}_w^t \cdot \underset{\sim}{E} \cdot \underset{\sim}{B}_v & -z^2 \underset{\sim}{B}_w^t \cdot \underset{\sim}{E} \cdot \underset{\sim}{B}_w + -z \underset{\sim}{B}_w^t \cdot \underset{\sim}{E} \cdot \underset{\sim}{B}_z \\ + & \\ \underset{\sim}{B}_z^t \cdot \underset{\sim}{E} \cdot \underset{\sim}{B}_v & -z \cdot \underset{\sim}{B}_w \cdot \underset{\sim}{E} \cdot \underset{\sim}{B}_z^t + \underset{\sim}{B}_z^t \cdot \underset{\sim}{E} \cdot \underset{\sim}{B}_z \end{array}\right] \cdot dV^o \qquad \text{----(3.28)}$$

$$= \int_A \int_{-t/2}^{t/2} \left[\begin{array}{c|c} \underset{\sim}{B}_v^t \cdot \underset{\sim}{E} \cdot \underset{\sim}{B}_v & -z \cdot \underset{\sim}{B}_v^t \cdot \underset{\sim}{E} \cdot \underset{\sim}{B}_w + \underset{\sim}{B}_v \cdot \underset{\sim}{E} \cdot \underset{\sim}{B}_z \\ \hline -z \underset{\sim}{B}_w^t \cdot \underset{\sim}{E} \cdot \underset{\sim}{B}_v & -z^2 \underset{\sim}{B}_w^t \cdot \underset{\sim}{E} \cdot \underset{\sim}{B}_w + -z \underset{\sim}{B}_w^t \cdot \underset{\sim}{E} \cdot \underset{\sim}{B}_z \\ + & \\ \underset{\sim}{B}_z \cdot \underset{\sim}{E} \cdot \underset{\sim}{B}_v & -z \cdot \underset{\sim}{B}_w \cdot \underset{\sim}{E} \cdot \underset{\sim}{B}_z^t + \underset{\sim}{B}_z^t \cdot \underset{\sim}{E} \cdot \underset{\sim}{B}_z \end{array}\right] dA \cdot dz \,. \qquad \text{----(3.28.a)}$$

For linear problems, $\underset{\sim}{E}$ is uniform across the thickness.
Hence, $\int_{-t/2}^{t/2} \cdot z \cdot E(\sigma) \cdot dz$ becomes zero. However, for most non-linear problems, $E(\sigma)_{z=t/2} \neq E(\sigma)_{z=-t/2}$

Hence $\int_{-t/2}^{t/2} \cdot z \cdot E(\sigma) \cdot dz$ can no longer be obtained explicitly, therefore these terms have to be included.

Consider the geometric stiffness matrix $\underset{\sim}{K}_G$, from (3.23):-

$$\underset{\sim}{K}_G = \int S_{ij} \left[\frac{\partial A_K^\beta}{\partial x_j} \cdot \frac{\partial A_K^\alpha}{\partial x_i} \right] \cdot dV$$

where $\frac{\partial A_K^{\alpha}}{\partial x_i}$ can be expressed in matrix notation as:-

$$\frac{\partial A_K^{\alpha}}{\partial x_i} = \begin{bmatrix} \frac{\partial w_1}{\partial x_0}, \frac{\partial w_2}{\partial x_0}, \frac{\partial w_3}{\partial x_0}, \frac{\partial w_4}{\partial x_0}, \cdots\cdots\cdots \frac{\partial w_{14}}{\partial x_0}, \frac{\partial w_{15}}{\partial x_0}, \frac{\partial w_{16}}{\partial x_0} \\ \frac{\partial w_1}{\partial y_0}, \frac{\partial w_2}{\partial y_0}, \frac{\partial w_3}{\partial y_0}, \frac{\partial w_4}{\partial y_0} \cdots\cdots\cdots \frac{\partial w_{14}}{\partial y_0}, \frac{\partial w_{15}}{\partial y_0}, \frac{\partial w_{16}}{\partial y_0} \end{bmatrix} \cdot \underset{\sim}{N}^{-1} \quad \text{-----(3.29)}$$

$$\& \quad S_{ij} = \begin{bmatrix} S_{11} & S_{12} \\ S_{21} & S_{22} \end{bmatrix} \quad \text{----(3.30)}$$

$$\therefore \underset{\sim}{K}_G = \int_{V_0} \underset{\sim}{N}^{-1t} \begin{bmatrix} \frac{\partial w_1}{\partial x_0}, \frac{\partial w_1}{\partial y_0} \\ \frac{\partial w_2}{\partial x_0}, \frac{\partial w_2}{\partial y_0} \\ \frac{\partial w_3}{\partial x_0}, \frac{\partial w_3}{\partial y_0} \\ \vdots \quad \vdots \\ \frac{\partial w_{14}}{\partial x_0}, \frac{\partial w_{14}}{\partial y_0} \\ \frac{\partial w_{15}}{\partial x_0}, \frac{\partial w_{15}}{\partial y_0} \\ \frac{\partial w_{16}}{\partial x_0}, \frac{\partial w_{16}}{\partial y_0} \end{bmatrix} \times \begin{bmatrix} S_{11} & S_{12} \\ S_{21} & S_{22} \end{bmatrix} \times \begin{bmatrix} \frac{\partial w_1}{\partial x_0}, \frac{\partial w_2}{\partial x_0}, \cdots\cdots \frac{\partial w_{15}}{\partial x_0}, \frac{\partial w_{16}}{\partial x_0} \\ \frac{\partial w_1}{\partial y_0}, \frac{\partial w_2}{\partial y_0} \cdots\cdots \frac{\partial w_{15}}{\partial y_0}, \frac{\partial w_{16}}{\partial y_0} \end{bmatrix} \cdot \underset{\sim}{N}^{-1} \cdot dV$$

----(3.31.a)

$$= \int_{V^e} \left[\begin{array}{c|c} \underset{\sim}{0} & \underset{\sim}{0} \\ \hline \underset{\sim}{0} & \underset{\sim}{N}^{-t} \cdot \underset{\sim}{G} \cdot \underset{\sim}{S} \cdot \underset{\sim}{G} \cdot \underset{\sim}{N}^{-1} \end{array}\right] dV \qquad \text{----(3.31.b)}$$

3.1.2 Finite Element Formulation of the Beam Element

From equation (2.27):-

$$\underset{\sim}{u} = \begin{bmatrix} u \\ w \end{bmatrix} = \begin{bmatrix} \frac{1}{2}(1-\xi) & 0 & 0 & \frac{1}{2}(1+\xi) & 0 & 0 \\ 0 & \frac{1}{4}(1-\xi)^2(2+\xi) & \frac{l}{8}(1-\xi)^2(1+\xi) & 0 & \frac{1}{4}(1-\xi)^2(2+\xi) & \frac{l}{8}(1+\xi)^2(\xi-1) \end{bmatrix} \cdot \underset{\sim}{p}$$

$$\frac{\partial u}{\partial x} = \frac{2}{l}\frac{\partial u}{\partial \xi} = \frac{2}{l} \cdot \begin{bmatrix} -\frac{1}{2} & 0 & 0 & \frac{1}{2} & 0 & 0 \end{bmatrix} \cdot \underset{\sim}{p}$$

$$\frac{\partial w}{\partial x} = \frac{2 \cdot \partial w}{l \cdot \partial \xi} = \frac{2}{l}\left[0 \;,\; \frac{3}{4}(\xi^2-1) \;,\; \frac{l}{8}(3\xi^2-2\xi-1) \;,\; 0 \;,\; \frac{3}{4}(1-\xi^2) \;,\; \frac{l}{8}(3\xi^2+2\xi-1) \right] \cdot \underset{\sim}{p}$$

$$\frac{\partial^2 w}{\partial x^2} = \frac{4 \cdot \partial^2 w}{l^2 \cdot \partial \xi^2} = \frac{4}{l^2}\left[0 \;,\; \frac{3}{2}\xi \;,\; \frac{l}{4}(3\xi-1) \;,\; 0 \;,\; -\frac{3}{2}\xi \;,\; \frac{l}{4}(3\xi+1) \right] \cdot \underset{\sim}{p}$$

$$\Longrightarrow \frac{\partial u}{\partial x} = \frac{\partial u}{\partial x} - z \cdot \frac{\partial^2 w}{\partial x^2} = \left[-\frac{1}{l} \;,\; -\frac{6z}{l^2}\xi \;,\; -\frac{(3\xi-1)}{l}z \;,\; \frac{1}{l} \;,\; \frac{6z}{l^2}\xi \;,\; -\frac{1}{l}(3\xi+1)z \right] \cdot \underset{\sim}{p}$$

Hence, the finite element formulation for $\frac{\partial A_i^{\alpha}}{\partial x_j}$ in (3.20) is:-

$$\frac{\partial A_i^{\alpha}}{\partial x_j} = \frac{1}{\ell}\left[-1 \,,\; \frac{-6\xi\gamma}{\ell} \,,\; -(3\xi-1)\gamma \,,\; 1 \,,\; \frac{6\xi\cdot\gamma}{\ell} \,,\; -(3\xi+1)\gamma \right]^t = \underset{\sim}{B}_0 \qquad ----(3.32)$$

&

$$\frac{\partial A_K^{\alpha}}{\partial x_i} = \frac{2}{\ell}\left[0,\; \frac{3(\xi^2-1)}{4} \,,\; \frac{\ell(3\xi^2-2\xi-1)}{8} \,,\; 0,\; \frac{3(1-\xi^2)}{4},\; \frac{\ell(3\xi^2+2\xi-1)}{8} \right]^t$$

Let $\frac{\partial A_K^{\beta}}{\partial x_j}\cdot\rho_{\beta}^{\beta} = w = \frac{2}{\ell}\left[0 \,.\; \frac{3(\xi^2-1)}{4} \,,\; \frac{\ell(3\xi^2-2\xi-1)}{8} \,,\; 0,\; \frac{3(1-\xi^2)}{4} \,.\; \frac{\ell(3\xi^2+2\xi-1)}{8} \right] \cdot \rho$

Hence $\underset{\sim}{B}_L$ for the beam element is:-

$$\frac{2w}{\ell}\cdot\left[0 \,.\; \frac{3(\xi^2-1)}{4} \,,\; \frac{\ell(3\xi^2-2\xi-1)}{8} \,,\; 0 \,.\; \frac{3(1-\xi^2)}{4} \,,\; \frac{\ell(3\xi^2+2\xi-1)}{8} \right]^t$$

----(3.33)

Hence $\frac{\partial A_i^{\alpha}}{\partial x_j} + \frac{\partial A^{\alpha}}{\partial x_i}\cdot\frac{\partial A_{\alpha}^{\beta}}{\partial x_j}\cdot\rho_{\beta}^{\beta} = \underset{\sim}{B}_e + \underset{\sim}{B}_L$

$$= \left[-\frac{1}{\ell}\cdot\left(\frac{3(\xi^2-1)}{2\ell}\cdot w - \frac{6\xi\gamma}{\ell^2}\right) \,,\; \left(\frac{(3\xi^2-2\xi-1)}{4}\cdot w - \frac{(3\xi-1)}{\ell}\gamma\right)\cdot\frac{1}{\ell} \,.\right.$$

$$\left.\left(\frac{3w(1-\xi^2)}{2\ell} + \frac{6\xi\gamma}{\ell^2}\right) \,,\; \left(\frac{w}{4}(3\xi^2+2\xi-1) - \frac{\gamma}{\ell}(3\xi+1)\right]^t \right. \qquad ----(3.34)$$

Hence

$$\underset{\sim}{K_e} + \underset{\sim}{K_L} = \int_{V^o} \left[\frac{\partial A_i^{\kappa}}{\partial X_j} + \frac{\partial A_{\kappa}^{\alpha}}{\partial X_i} \frac{\partial A_{\kappa}^{\beta}}{\partial X_j} \rho_{\alpha\beta} \right] \cdot D_{ijkl} \cdot \left[\frac{\partial A_{\kappa}^{\kappa}}{\partial X_l} + \frac{\partial A_{\rho}^{\alpha}}{\partial X_{\kappa}} \frac{\partial A_{\rho}^{\beta}}{\partial X_l} \rho_{\alpha\beta} \right] \cdot dV$$

is simply equal to:-

$$\frac{l \cdot b}{2} \cdot \int_{-1}^{1} \cdot \int_{-\frac{y}{2}}^{\frac{y}{2}} \cdot E \cdot \begin{vmatrix} -1/l \\ \frac{3(\xi^2-1)}{2l} \cdot \omega - \frac{6\xi\gamma}{l^2} \\ \frac{(3\xi^2-2\xi-1)}{4}\omega - \frac{(3\xi-1)}{l}\gamma \\ 1/l \\ \frac{3(1-\xi^2)}{2l}\omega + \frac{6\xi\gamma}{l^2} \\ \frac{\omega}{4}(3\xi^2+2\xi-1) - \frac{\gamma(3\xi+1)}{l} \end{vmatrix} \left[-1/l \cdot \left(\frac{3(\xi^2-1)}{2l} \cdot \omega - \frac{6\xi\gamma}{l^2} \right), \left(\frac{(3\xi^2-2\xi-1)}{4}\omega - \frac{(3\xi-1)}{l}\gamma \right), 1/l, \right.$$

$$\left. \left(\frac{3(1-\xi^2)}{2l}\omega + \frac{6\xi\gamma}{l^2} \right), \left(\frac{\omega}{4}(3\xi^2+2\xi-1) - \frac{\gamma(3\xi+1)}{l} \right) \right] d\gamma \cdot d\xi \quad \text{----(3.35)}$$

where b and l are the width and length of the beam respectively. The geometrix stiffness matrix $\underset{\sim}{K_G}$ is just the last term in equation (3.20), where:-

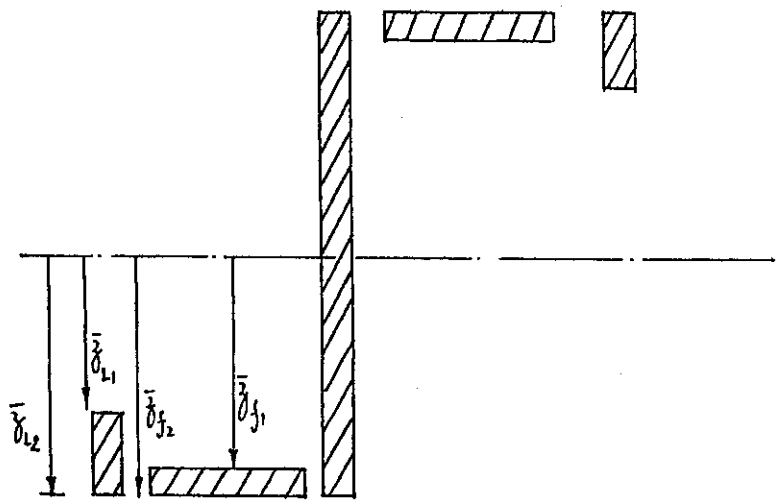
$$\underset{\sim}{K_G} = \int_{V^o} S_{ij} \left[\frac{\partial A_{\kappa}^{\beta}}{\partial X_j} \cdot \frac{\partial A_{\kappa}^{\alpha}}{\partial X_i} \right] \cdot dV^o$$

$$= \frac{4 \cdot l \cdot b}{2l^2} \int_{-\frac{y}{2}}^{\frac{y}{2}} \cdot \int_{-1}^{1} \cdot \begin{vmatrix} 0 \\ \frac{3(\xi^2-1)}{4} \\ \frac{l(3\xi^2-2\xi-1)}{8} \\ 0 \\ \frac{3(1-\xi^2)}{4} \\ \frac{l(3\xi^2+2\xi-1)}{8} \end{vmatrix} S_o \left[0, \frac{3(\xi^2-1)}{4}, \frac{l(3\xi^2-2\xi-1)}{8}, 0, \frac{3(1-\xi^2)}{4}, \frac{l(3\xi^2+2\xi-1)}{8} \right] \cdot d\gamma \cdot d\xi$$

----(3.36)

where $S_o = E \cdot \varepsilon = E \cdot \frac{\partial u}{\partial x} = E\left(\frac{\partial u}{\partial x} - z \cdot \frac{\partial^2 w}{\partial x^2}\right)$

For the Z type stiffener, the tangential stiffness matrices of each individual stiffener component (i.e. 2 lips, 2 flanges, and 1 web) have also to be evaluated with reference to the neutral axis of the stiffener itself:-



The total stiffness matrix for a complete stiffener is the summation of all the stiffness matrices of its components:-

$$\underset{\sim}{K_s} = \sum_{i=1}^{n} \cdot \underset{\sim}{K_c^i}$$

where $\underset{\sim}{K}_s$ is the total stiffener stiffness matrix.

$\underset{\sim}{K}_c^i$ is the ith stiffener component stiffness matrix.

Having obtained the tangential stiffness for the stiffener, the tangential stiffness of the stiffener with reference to the plate deformation is to be transformed using the transformation matrix shown in Appendix 1. Hence, the complete form of the stiffener stiffness matrix is:-

$$\underset{\sim}{K}_T^b = \underset{\sim}{T}_s^t \cdot \left[\underset{\sim}{K}_c + \underset{\sim}{K}_L + \underset{\sim}{K}_G \right] \cdot \underset{\sim}{T}_s$$

$$= \underset{\sim}{T}_s^t \cdot \underset{\sim}{K}_T' \cdot \underset{\sim}{T}_s \qquad \text{----(3.37)}$$

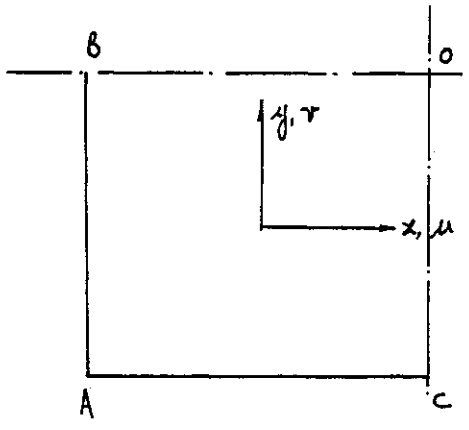
where $\underset{\sim}{T}_s$ is the transformation matrix of the one-sided stiffener described in Appendix 1.

3.2 Large Deflection Static Loading Analysis

The following sections describe and test the large displacement behaviour of the plate elements formulated via equations (3.1) to (3.55).

3.2.1 Non-linear deflection of plate without stiffners

In the finite element large displacement analysis, the in-plane movements of the plate along all edges are restrained. As shown in the diagram below, all the movements in u, v along edges OA, OC and AC are to be suppressed:-



Using only a quarter plate, when the structure is subject to simply-supported boundary conditions, the out-of-plane displacements of all nodes along BA and AC are to be suppressed. In addition, the rotation $\partial w/\partial x$ along BO and $\partial w/\partial y$ along CO are also suppressed.

When the structure is subject to a clamped edge condition, $\partial w/\partial x$ along AB and $\partial w/\partial y$ along AC are also suppressed in addition to those mentioned in the simply-supported boundary condition.

Figure 6 shows the non-dimensional load-deflection curve of the centre plate using 3x3 elements for the finite element modelling. A curve of Levy's (ref. 27) theoretical results on large displacement of plate subject to the same boundary and load conditions is compared with the one obtained by finite element method. Both curves are very close to each other. The result

shows that the large displacement stiffness matrix employed in the present analysis is quite adequate. The linear deflection curves in Figure 6 contrast the difference between linear and non-linear analyses.

Figure 7a shows a set of 9 curves corresponding to the load displacement curves of the 9 nodal points. The plate was simply-supported and was subject to a uniformly distributed pressure. Figure 7b shows the enlargement of the load displacement curve of the centre plate (node 9) with the linear load displacement result as a reference.

Figure 8a shows a set of 9 curves corresponding to the load-displacement curves of the 9 selected nodal points with the same boundary conditions but subject to a central load. Figure 8b shows the enlargement of the load-displacement curve of the centre plate (node 9). Again, with the linear load-displacement result as a reference.

3.3 Numerical Integration of the Tangential Stiffness Matrix

To evaluate the tangential stiffness matrices, we notice that both the matrices $\underset{\sim}{K}_L$ & $\underset{\sim}{K}_G$ are dependent on the current stage of displacements as well as the stress level. We will therefore no longer be able to evaluate these matrices explicitly as those in the small displacement linear geometry cases (see Section 2.4). Here, a numerical integration procedure is sought to enable these matrices to be evaluated at any stage of deformation and stress level.

In general, Gauss Quadrature (19,41,42) using n points is exact if the integral is a polynomial of degree 2n-1 or less. Since the polynomial expression employed in the plate bending displacement function (see equation 2.13) is of sixth order term (x^3y^3), an exact integration of the stiffness matrices will require 4x4 sampling points. However, as we have described in section 2.5, on the convergency test of the element, the behaviour of the plate element has been proved to be conforming, that is, the displacement function employed in the analysis results in overestimating the system stiffness. Thus, by not evaluating the element stiffness matrices exactly during numerical integration, better results can be obtained provided that the error in the numerical integration compensates approximately for the overestimation of the structural stiffness due to the finite element discretization (43,44,45). Hence, the numerical integration of the stiffness matrices can effectively be carried out using 2x2 sampling points.

For a 2 dimensional problem, the integration of the stiffness matrices using 2x2 sampling points can be expressed as:-

$$\underset{\sim}{K}_T = \int_A F(\xi, \eta) \cdot d \cdot A$$

$$= \int_{-1}^{1} \cdot \int_{-1}^{1} \cdot F(\xi, \eta) \cdot d\xi \cdot d\eta = \sum_i \cdot \sum_j \cdot W_i \cdot W_j \cdot F(\xi, \eta) \qquad \text{----(3.38)}$$

where the weightings W_i and W_j are equal to 1 and the sampling points in (ξ, η) are taken as ± 0.57735.

In most non-linear problems, numerical integration of the tangential stiffness matrices should be carried out across the plate thickness (ζ) as well as the plate area (ξ, η) (i.e. in all the 3 volumetric directions) using the Gauss Quadrature methods shown above. However, in the case of elasto-plastic bending, yielding normally starts at the extreme surfaces of the elements. If the Gaussian integration is used in the ζ direction, information at the top and bottom surfaces of the elements will be lost. Here, we will follow the Simpson's integration scheme (i.e. taking 3 sampling points across the plate thickness, one each at the top and bottom surfaces of the element, and a third point in the mid-plane of the element), which gives a better stress representation when yielding first starts.

Such a combined integration scheme will lead to the integration of the tangential stiffness matrices $\underset{\sim}{K}_T$ as:-

$$\underset{\sim}{K}_T = \int_V F(\xi, \eta, \zeta) \cdot dV$$

$$= \int_{-t/2}^{t/2} \cdot \int_A \cdot F(\xi, \eta, \zeta) \cdot dA \cdot d\zeta$$

----(3.39)

From (3.38) equation (3.39) becomes:-

$$\underset{\sim}{K_T} = \sum_{K=0}^{n} \cdot \sum_{i} \cdot \sum_{j} \cdot Z_K \cdot W_i \cdot W_j \cdot f(\xi, \eta, \zeta) \cdot \qquad \text{----(3.40)}$$

where the weightings Z_0, Z_1 and Z_2 are t/6, 4t/6 and t/6 respectively, and the sampling points are taken as -t/2, 0 and t/2 respectively.

3.4 The Incremental Load Procedure

From the principle of Virtual Displacement, we have:-

$$\underset{\sim}{P}_o^t \cdot \underset{\sim}{f} = \int \cdot \underset{\sim}{\varepsilon}^t \cdot \underset{\sim}{\sigma}_o \cdot dv \qquad \text{----(3.41)}$$

where the L.H.S. of equation is the set of external work done and R.H.S. of equation is the internal work done of the system. For an application of an external force δP, the system will respond to this force increment by increasing its internal stress from σ_o to $\delta\sigma_o$. Hence, the new set of equilibrium equation becomes:-

$$(\underset{\sim}{P}_o + \delta\underset{\sim}{P}) \cdot \underset{\sim}{f} = \int_v \cdot \underset{\sim}{\varepsilon}^t \cdot (\underset{\sim}{\sigma}_o + \delta\underset{\sim}{\sigma}) \cdot dv$$

$$= \int_v \underset{\sim}{B}^t \cdot (\underset{\sim}{\sigma}_o + \delta\underset{\sim}{\sigma}) \cdot dv \cdot \underset{\sim}{f}$$

$$\Longrightarrow \underset{\sim}{P}_o + \delta\underset{\sim}{P} = \int_v \underset{\sim}{B}^t (\underset{\sim}{\sigma}_o + \delta\underset{\sim}{\sigma}) \cdot dv \qquad \text{----(3.42)}$$

As

$$\left.\begin{aligned} \underset{\sim}{\sigma}_o &= \underset{\sim}{D} \cdot \underset{\sim}{B} \cdot \underset{\sim}{f} \\ \& \quad \delta\underset{\sim}{\sigma}_o &= \underset{\sim}{D} \cdot \underset{\sim}{B} \cdot \delta\underset{\sim}{f} \end{aligned}\right\} \qquad \text{----(3.43)}$$

Substitute (3.43) into (3.42), we have:-

$$\underset{\sim}{P}_o + \delta\underset{\sim}{P} = \int_v \underset{\sim}{B}^t \cdot \underset{\sim}{D} \cdot \underset{\sim}{B} \cdot dv \cdot \underset{\sim}{f} + \int_v \underset{\sim}{B}^t \cdot \underset{\sim}{D} \cdot \underset{\sim}{B} \cdot dv \cdot \delta\underset{\sim}{f} \qquad \text{----(3.44)}$$

the first term on the R.H.S. of equation (3.44) is obviously equal to $\underset{\sim}{P}_0$. Hence, equation (3.44) becomes:-

$$\delta \underset{\sim}{P} = \int_V \underset{\sim}{B}^t \cdot \underset{\sim}{D} \cdot \underset{\sim}{B} \cdot dv \cdot \delta \underset{\sim}{f} \qquad \text{----(3.45)}$$

which implies that for any applied force increments, the system will respond with a set of displacements. Hence,

$$\Delta \underset{\sim}{F} = \underset{\sim}{K}_T \cdot \Delta \underset{\sim}{f} \qquad \text{----(3.46)}$$

Equation (3.46) will allow a step-by-step solution to the set of incremental force and incremental displacement. Thus, the complete path of applied force and the deformation of the system can be traced by this incremental procedure. This is known as the linearised incremental procedure. The word 'linearised' implies that although the load-displacement curve is non-linear, the step-by-step incremental procedure is piecewise treated as linear, i.e. the tangential stiffness matrix formulated at the beginning of the loading step is regarded as linear throughout the same loading step. Thus,

$$\Delta \underset{\sim}{F}^{ext.} = \underset{\sim}{K}_T(\underset{\sim}{f}_i) \cdot \Delta \underset{\sim}{f} \qquad \text{----(3.47)}$$

In practice, the above assumption is not enough even though the increment is infinitely small. If no precaution is taken against the errors accumulated throughout the whole loading procedure, the load-displacement curve so obtained will be diverted from the real

load-displacement curve. To overcome this problem, the following iteration procedure is required.

Consider an equilibrium set of external and internal force at the beginning of the loading step i :-

$$\underset{\sim}{F}_i^{ext.} = \underset{\sim}{F}_i^{ext.} = \underset{\sim}{K}_T(\rho_i)\cdot\underset{\sim}{\rho}_i \qquad \text{----(3.48)}$$

where $\underset{\sim}{K}_T(\rho_i)$ the tangential stiffness is a function of the displacements at step i.

After the application of the external force $\Delta F^{ext.}$, the system will respond with internal force increment $\Delta F^{int.}$, which can be computed from equation (3.42). In order to have an equilibrium set of forces at the end of the loading step, we must have:-

$$\underset{\sim}{F}_{i+1}^{ext} = \underset{\sim}{F}_{i+1}^{int}$$

If equation (3.48) is true, then we will have:-

$$\underset{\sim}{F}_{i+1}^{ext.} - \Delta\underset{\sim}{F}^{ext.} = \underset{\sim}{F}_{i+1}^{int.} - \Delta\underset{\sim}{F}^{int.} \qquad \text{----(3.49)}$$

Re-arranging (3.49), we have

$$\Delta\underset{\sim}{F}^{ext.} - \left[\underset{\sim}{F}_{i+1}^{ext.} - \underset{\sim}{F}_{i+1}^{int.}\right] = \Delta\underset{\sim}{F}^{int.} = \underset{\sim}{K}_T(\rho_i)\cdot\Delta\underset{\sim}{\rho} \qquad \text{----(3.50)}$$

$$\Longrightarrow \quad \Delta \underset{\sim}{F}^{ext.} - \left[\underset{\sim}{F}_{i+1}^{ext.} - \underset{\sim}{K}_T(\underset{\sim}{\rho}_{i+1}) \cdot \underset{\sim}{\rho}_{i+1} \right] = \underset{\sim}{K}_T(\underset{\sim}{\rho}_i) \cdot \Delta \underset{\sim}{\rho} \qquad \text{----(3.51)}$$

The second term in (3.51) is known as the out-of-balance force:

$$\left[\underset{\sim}{F}_{i+1}^{ext.} - \underset{\sim}{K}_T(\underset{\sim}{\rho}_{i+1}) \cdot \underset{\sim}{\rho}_{i+1} \right] = \Delta \bar{\underset{\sim}{F}}_{i+1}$$

At the beginning of the loading increment, the out-of-balance force $\Delta \bar{\underset{\sim}{F}}_{i+1}$ is not known, and is assumed to be zero, and the tangential stiffness is evaluated based on the displacements at the beginning of the loading procedure. Hence, using equation (3.47), the displacement increments are computed. The total displacements at the end of the loading step is up-dated and so is the total external force where

$$\underset{\sim}{F}_{i+1}^{ext.} = \underset{\sim}{F}_i^{ext.} + \Delta \underset{\sim}{F}_i \qquad \& \qquad \underset{\sim}{\rho}_{i+1} = \underset{\sim}{\rho}_i + \Delta \underset{\sim}{\rho}$$

The out-of-balance force $\Delta \bar{\underset{\sim}{F}}_{i+1}$ is then evaluated based on the up-dated total displacements, $\underset{\sim}{\rho}_{i+1}$. The net force increment is then applied to the system, and a new set of displacements $\Delta \underset{\sim}{\rho}'$ is computed. The operation is repeated until the out-of-balance force $\Delta \bar{\underset{\sim}{F}}_{i+1}$ is practically zero. Chart 1 shows the iteration procedure of the above.

The applied force vector $\Delta \underset{\sim}{F}$ would have its components equal to zero everywhere except at the nodes where external forces are applied. Thus,

$$\Delta \underset{\sim}{F}_{m\times 1} = \begin{bmatrix} \underset{\sim}{0} \\ \hline \Delta f \end{bmatrix}_{l\times 1}^{m\times 1}$$

where l = no. of external force points

n = m+1 = total no. of degrees of freedom of the system.

When the out-of-balance force $\Delta \underset{\sim}{\bar{F}}$ is added on to the incremental force vector, it would be reasonable to expect that the resultant force vector $\Delta \underset{\sim}{F} + \Delta \underset{\sim}{\bar{F}}$ is also expressable in the form of:-

$$\left\{ \Delta \underset{\sim}{F} + \Delta \underset{\sim}{\bar{F}} \right\} = \begin{bmatrix} \underset{\sim}{0} \\ \hline \Delta f \end{bmatrix}_{l\times 1}^{m\times 1}$$

However, if the tangential stiffness matrix, which is evaluated based on total displacement at i+1 step, is directly multiplied by the total displacement f_{i+1}, the resultant vector product may not necessarily be in the same form as that appears in the external load increment vector, i.e.:-

$$\underset{\sim}{K}_T(f_{i+1}) \cdot f_{i+1} \neq \begin{bmatrix} \underset{\sim}{0} \\ \hline f \end{bmatrix}_{l\times 1}^{m\times 1}$$

To overcome this, the tangential stiffness matrix should be partitioned alongside with the total displacement vector before they are multiplied:-

$$\underset{\sim}{P}_{n\times 1} = \begin{bmatrix} \underset{\sim}{0} \\ \hline \underset{\sim}{P} \end{bmatrix}_{m\times 1} = \left[\begin{array}{c|c} \underset{\sim}{K}_{11} & \underset{\sim}{K}_{12} \\ \hline \underset{\sim}{K}_{21} & \underset{\sim}{K}_{22} \end{array}\right] \begin{bmatrix} \underset{\sim}{\delta}_0 \\ \hline \underset{\sim}{\delta}_1 \end{bmatrix} \qquad \text{----(3.52)}$$

$$\Longrightarrow \underset{\sim}{0} = \underset{\sim}{K}_{11} \cdot \underset{\sim}{\delta}_0 + \underset{\sim}{K}_{12} \cdot \underset{\sim}{\delta}_1 \Rightarrow \underset{\sim}{\delta}_0 = -\underset{\sim}{K}_{11}^{-1} \cdot \underset{\sim}{K}_{12} \cdot \underset{\sim}{\delta}_1 \qquad \text{----(3.53)}$$

$$\underset{\sim}{P} = \underset{\sim}{K}_{21} \cdot \underset{\sim}{\delta}_2 + \underset{\sim}{K}_{22} \cdot \underset{\sim}{\delta}_1 \qquad \text{----(3.54)}$$

Substitute (3.53) into (3.54), we have:-

$$\underset{\sim}{P} = \underset{\sim}{K}_{22} \cdot \underset{\sim}{\delta}_1 - \underset{\sim}{K}_{21} \cdot \underset{\sim}{K}_{11}^{-1} \cdot \underset{\sim}{K}_{12} \cdot \underset{\sim}{\delta}_1$$

$$= \left[\underset{\sim}{K}_{22} - \underset{\sim}{K}_{21} \cdot \underset{\sim}{K}_{11}^{-1} \cdot \underset{\sim}{K}_{12} \right] \cdot \underset{\sim}{\delta}_1 \qquad \text{----(3.55)}$$

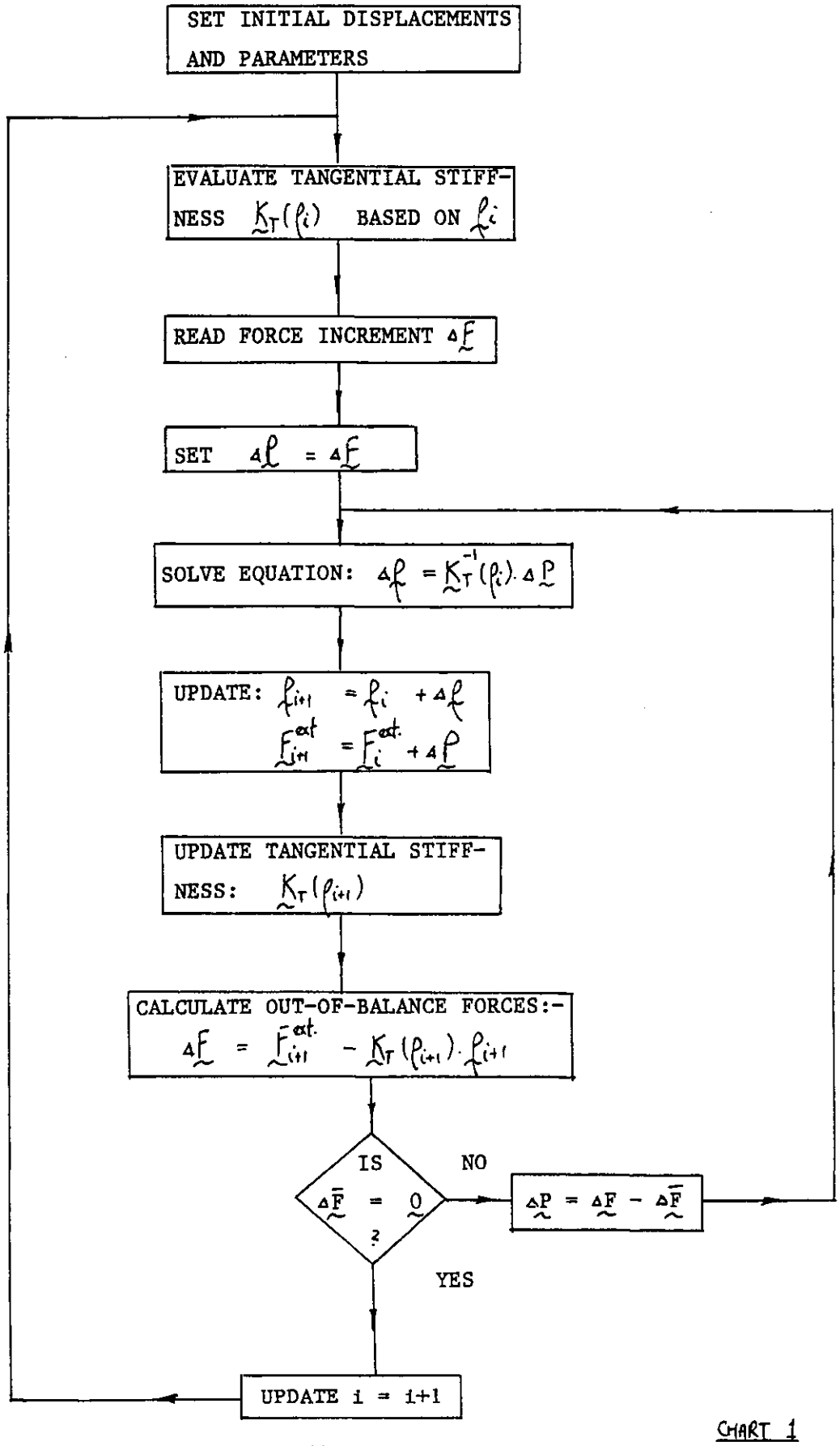

SET INITIAL DISPLACEMENTS AND PARAMETERS
EVALUATE TANGENTIAL STIFFNESS $\underset{\sim}{K}_T(\rho_i)$ BASED ON $\underset{\sim}{\rho}_i$
READ FORCE INCREMENT $\Delta\underset{\sim}{F}$
SET $\Delta\underset{\sim}{\rho} = \Delta\underset{\sim}{F}$
SOLVE EQUATION: $\Delta\underset{\sim}{\rho} = \underset{\sim}{K}_T^{-1}(\rho_i).\Delta\underset{\sim}{P}$
UPDATE: $\underset{\sim}{\rho}_{i+1} = \underset{\sim}{\rho}_i + \Delta\underset{\sim}{\rho}$
$\underset{\sim}{F}_{i+1}^{ext.} = \underset{\sim}{F}_i^{ext.} + \Delta\underset{\sim}{P}$
UPDATE TANGENTIAL STIFFNESS: $\underset{\sim}{K}_T(\rho_{i+1})$
CALCULATE OUT-OF-BALANCE FORCES:-
$\Delta\underset{\sim}{F} = \underset{\sim}{F}_{i+1}^{ext.} - \underset{\sim}{K}_T(\rho_{i+1}).\underset{\sim}{\rho}_{i+1}$
IS $\Delta\bar{\underset{\sim}{F}} = \underset{\sim}{0}$?
NO
$\Delta\underset{\sim}{P} = \Delta\underset{\sim}{F} - \Delta\bar{\underset{\sim}{F}}$
YES
UPDATE i = i+1

CHART 1

4. BUCKLING ANALYSIS

Basically, there are two types of buckling analysis, referred to here as " linear" buckling and "non-linear" buckling. In the linear buckling analysis, the tangential stiffness matrix will just be composed of the small displacement elastic stiffness matrix $\underset{\sim}{K}_e$, which is neither displacement dependent nor coordinate dependent, and the geometric stiffness matrix $\underset{\sim}{K}_G$. (Formulation of these matrices are fully described in section 3). Because of the fact that only $\underset{\sim}{K}_G$ is dependent of the existing stresses, and hence the deformation of the structure, any subsequent initial deformation imposed on the structure will only 'accelerate' the buckling mode of the structure for a given loading. In practice, the above assumption becomes inadequate when the initial displacement or the subsequent deformation of the structure is no longer small comparing with its thickness. The alternative approach will be the "non-linear" buckling analysis which will accommodate for any large displacements occuring in the flat plate or shell type structures. Such an analysis would be much more sensitive to any non-linear behaviour arising due to the material non-linearity or large displacements.Here, the tangential stiffness matrix is evaluated following the procedures described in sections 2 and 3.

4.1 Evaluation of the Buckling Loads

There are normally two ways of evaluating the buckling load of a given structure. One of which is known as the incremental load method, and the other is known as the eigen value type of solution for buckling.

In the incremental load method, the load is increased at the beginning of step and subsequent displacements are incremented and iterated in accordance with the steps and procedures shown in Chart 1 . The total displacements and the existing stresses are

then re-cycled back to formulate the tangential stiffness matrix (equations (3.1) to (3.37)). Hence, the procedures are repeated in order to compute the complete load-displacement curve of the structure. In so doing, two types of loading increments will occur. In the linear buckling analysis, because of the nature of the tangential stiffness matrix, singularity will occur in the matrix at the buckling load level and thus on solving for equation (3.47), an infinite displacement increment will occur. In the non-linear analysis, if only bifurcation structure is considered (i.e. if the plate is considered to be perfectly flat), the resulting load displacement curve will be exactly the same as that obtained in the linear buckling case. If however, an initial displacement is imposed on the structure, or if the structure is of a shell type, the out-of-plane displacements will 'incite' the growing of the large displacement stiffness matrix ($\underset{\sim}{K}_L$ in equatin (3.28)), and on approaching the buckling load (provided that the deflection of the structure is relatively large compared with its thickness), singularity will not occur in the tangential stiffness matrix. Instead, the load- displacement curve will continue with a strain-hardening effect very much similar to that of a large displacement out-of-plane load-displacement curve.

In the eigen-value type of solution for buckling, we assume that during an infinitesimal displacement, the membrane force remains substantially unchanged. The formulation of the geometric stiffness matrix $\underset{\sim}{K}_G$ is based on a known distribution, nevertheless an arbitrary level of membrane stresses. Hence, the membrane stresses are assumed to remain constant so that changing one by a factor λ will change all the others by the same factor throughout all the subsequent load increments. Finally at the point of buckling, the geometric stiffness matrix will become $\lambda \underset{\sim}{K}_G$.

The Finite Element approach is to, first of all, set up the elastic stiffness matrix $\underset{\sim}{K_e}$. Thus, an arbitrary load increment $\Delta \underset{\sim}{P}$ is then applied and the displacement increment is solved via equation (3.46). This incremental displacement together with any initial displacement is then substituted into equations (3.29) to (3.31.b) to formulate the stiffness matrix $\underset{\sim}{K_g}$. The equation of equilibrium states that when buckling occurs, $\underset{\sim}{K_e}$ will be equal and opposite to $\lambda \underset{\sim}{K_g}$. In other words:-

$$\text{Det.} \left\{ \underset{\sim}{K_e} + \lambda \underset{\sim}{K_g} \right\} = 0 \qquad \text{----(4.1)}$$

Hence, we have derived a linear set of eigen-value equations. The eigen-value solution can be obtained by various standard methods (e.g. the Sturm sequence technique or the sub-space iteration method etc.).

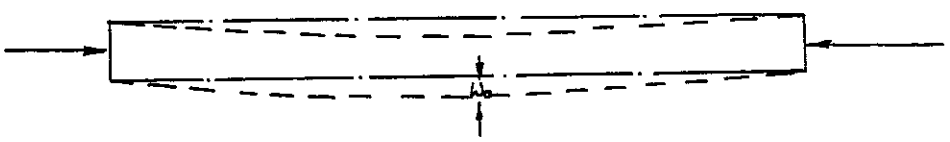
The eigen-value type of solution for buckling does have the disadvantage of its limited applications. The applicability is limited only to small linear buckling analysis. Furthermore, a complete load-displacement curve is not possible to be calculated. However, if only the buckling load levels and their corresponding mode shapes are of interest, the method will serve its purpose.

4.2 Buckling Analysis on the Simple Plate and beam Elements

4.2.1 Linear Buckling of Plate Without Stiffeners using Incremental Load Method.

When subject to an in-plane load, Figure 9 shows that the structure has experienced infinite displacements at the centre plate when the applied stress approaches the theoretical critical stress of the structure. The figure also shows the non-dimensional load displacement curves of four selected nodes (see diagram drawn on Figure 9). During the analysis, the program stopped just before the total applied stress reached the theoretical critical stress of the structure due to singularities formed in the tangential stiffness matrix. From this result, it is evident that the geometric stiffness matrix employed in the analysis is appropriate and that the results generated are very accurate.

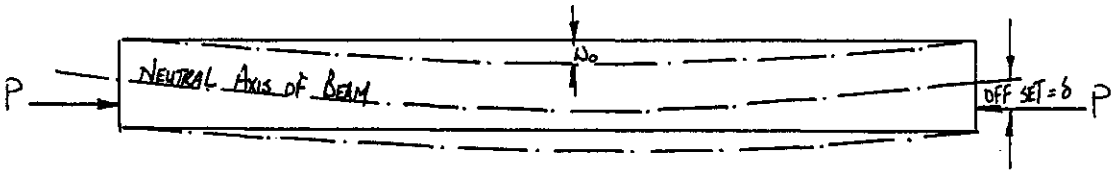
4.2.2 Linear Buckling of the Beam Element with Various Initial Displacements Using Incremental Load Method



A beam made up of 6 elements simulating the stiffeners was subject to an in-plane compressive loading. Figure 10 shows the buckling behaviour of the beam with different initial displacements, w_0. The very top curve on Figure 10 shows the load-deflection behaviour of the beam with very little initial displacements whereas the bottom curve of the figure shows the load-deflection behaviour of the same beam but with a larger initial displacement (12.5% of the beam thickness). Despite the different imposed initial

displacements, the beam buckles at an applied force of 4,800 lbf which coincides with the theoretical critical load of the structure. However, the individual load displacement curves corresponding to the different initial displacements do vary slightly.

4.2.3 Linear Buckling of a Beam with Various Off-sets from its Local Neutral Axis



In finite element analysis, Appendix 1 has already mentioned that instead of representing the movements of the beam by the two end nodes along the stiffener's neutral axis, the movements have to be transformed from the stiffeners neutral axis to either its top or bottom surface (depending on where the stiffener is in contact with the plate). In this way, the coupling between the out-of-plane rotations and the in-plane movements of the stiffener can be fully represented. To show that an off-set stiffener has been properly modelled, the behaviour of the computed load-displacement curve should show some correlation with the off-set positions (δ). Fig. 11 shows the load-displacement curve of the beam subject to uniform compressive load but off-set at different positions. The figure highlights the behaviour of the stiffener when subject to different off-sets which vary from the mid-plane of the plate ($\delta = t/2$) to the local neutral axis of the stiffener ($\delta = 0$). In order to make a direct comparison of the displacement behaviour of the stiffener with $\delta = 0$ to $\delta = t/2$, the stiffener is subject to an initial deflection of 10% of its thickness so that the load-displacement curve when $\delta = 0$ can be visible.

4.2.4 Non-linear Buckling of the Plate Without Stiffeners

It has been shown in Figure 9 that when linear buckling is being considered, the central plate will experience an infinite out-of-plane displacement at the critical load. However, when non-linear buckling is considered, this will no longer be the case. This is because of the nature of the tangential stiffness matrix which, when used in non-linear buckling analysis, will normally consist of the large displacement matrix $\underset{\sim}{K}_L$ in addition to the other two matrices $\underset{\sim}{K}_\alpha$ & $\underset{\sim}{K}_\sigma$. As section 3.2 has already shown that $\underset{\sim}{K}_L$ is proportional to the square of the out-of-plane displacements of the structure, the relatively large deflections at the onset of buckling will increase $\underset{\sim}{K}_L$ to such an extent that it will be able to offset the stiffness loss made by the geometric stiffness matrix $\underset{\sim}{K}_\sigma$. From this point onwards, the structure is in a position to 'regain' stiffness as further compressive load is applied. Thus, at the post-buckling stage, the load-displacement curve will be very similar to that being obtained from the non-linear bending of plate (see Fig. 6). To illustrate this, a plate which has slight imperfections is subject to an in-plane compressive load. Figure 12 shows the load-displacement curves of 4 selected nodes on the plate. Figure 13 merely highlights the behaviour of them at the pre-buckling stage.

However, it should be noticed that whether or not the large displacement stiffness matrix ($\underset{\sim}{K}_L$) is sufficient enough to off set the stiffness loss made by $\underset{\sim}{K}_\sigma$ would depend entirely on the imposed initial displacements. If these initial displacements are not sufficient, the effect of the large displacement stiffness matrix $\underset{\sim}{K}_L$ will be minimal. Hence, on reaching the first critical load, the response will be the same as that expected in the linear buckling analysis (Fig. 9). Figure 14 shows the central deflection of a plate subject to the same compressive loadings, but with different initial imperfections. The first three curves on

Figure 14 represent the plate with initial displacements of less than 1% of the plate thickness. All three curves are seen to stop just before the structure could continue into the post buckling stage due to the presence of singularities in the tangential stiffness matrix. However, when the imposed initial deflections are significant, it enables the last two curves in Figure 14 to continue into the post buckling stage in the manner that has already been discussed above. Figure 15 shows the enlargement of the first three curves of Figure 14 while Figure 15 shows the last two curves of Figure 14. The analysis shows evidently that the structure is very sensitive to the presence of imperfections.

4.3 Buckling of a Stiffened Plate

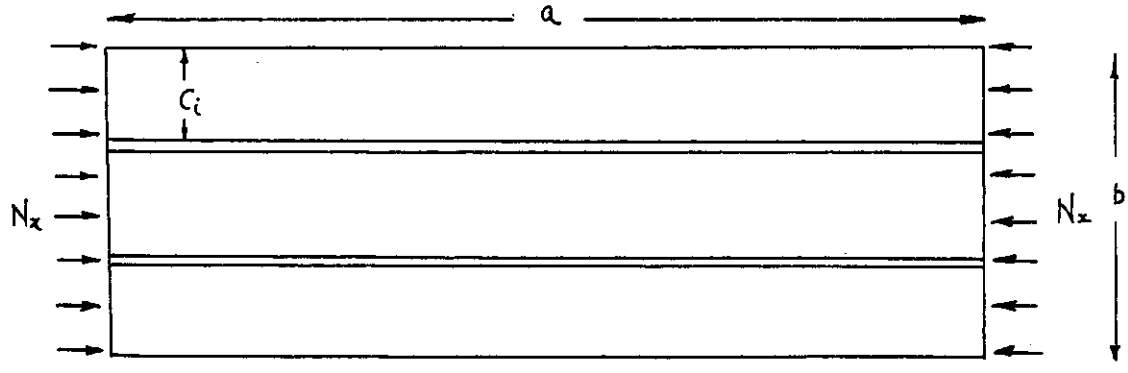
4.3.1 Brief Historical Review

Although various authors had tackled the problem before, Bryan (46) was the first to investigate theoretically the stability of compressed stiffened plate by applying the energy criterion of stability to the solution of a buckling problem. In his paper, he looked into the stability of a plate stiffened by a set of ribs parallel to the direction of applied forces. He also looked into the effect of a second set of stiffeners placing perpendicular to the applied force. He concluded that in order to obtain the greatest strength, the stiffeners must be parallel with the direction of the applied force, and that, to obtain the same strength, they may be then placed twice as far apart as if they were perpendicular to the applied force. Timoshenko (47,48) first considered the problem of minimum rigidity of the stiffeners required to restrict buckling in a stiffened plate. By applying the energy method he obtained approximate solutions for rectangular plates having longitudinal or transverse stiffeners under various loading conditions. He also prepared the first numerical table for the design of stiffened plate. Lokskin in 1935 looked into the

stability problem of longitudinally or transversely stiffened plates by applying the method of integration of differential equations for stiffened plate with initial deflection. He also derived the stability conditions for plates having any number of equidistant stiffeners. Since then, different stability problems of stiffened plates had been analysed in numerous periodicals and in well known monographs by: Timoshenko (49), Timoshenko & Gere (50), Bleich (51), Kollbrunner and Meister (52). Papkovick (53), Savin & Fleishman (54), and Bulson (55). Barbre (56) and Ratzersderfer (57) analysed the problem of minimum stiffener flexural stiffness required for the plate to buckle with no deflection of the stiffeners. Jojic (58) investigated the case of a rectangular plate reinforced by multiple stiffeners. Cox & Riddel (59) discussed in detail plate with one to multiple stiffeners. They investigated the smallest size of stiffeners required to prevent overall buckling of a flat panel before local buckling of plate between stiffeners can occur. The effect of torsional stiffness of the stiffeners is included. Svennernd (60) discussed buckling strength of longitudinally stiffened plate, applying the critical stress method as suggested by Bleich, and found the required strength of stiffeners to resist buckling of the whole plate before local buckling occurs. Since then, a number of papers concerning the analysis of buckling of stiffened plate under different boundary conditions had been appearing in various journals. More recently, Van der Neut (61) investigated the interaction between the local and overall buckling of stiffened plates and Koiter (62) explained analytically the mechanics of the failure of the stiffened panel due to this interactive effect.

4.3.2 Analytical Analysis of Buckling of Stiffened Plate and Study of the Analytical and F.E. Results

There are apparently various methods to evaluate the critical stresses of the stiffened plate of the above mentioned nature with one to multiple stiffeners. Amongst these methods, if one follows the energy method (49) one can derive from it the expression for the critical stress of the following system:-



$$\sigma_{crit} = \frac{\pi^2 \cdot D}{b^2 \cdot t \cdot \beta^2} \cdot \left\{ \frac{(1+\beta^2)^2 + 2\sum_i \gamma_i \sin^2 \frac{\pi c_i}{b}}{\left(1 + 2 \cdot \sum_i \cdot \delta_i \sin^2 \cdot \frac{\pi c_i}{b}\right)} \right\} \qquad \text{----(4.2)}$$

where the parameters are :-

$$\left.\begin{aligned} \beta &= a/b \\ \gamma &= \frac{E \cdot I_i}{b \cdot D} \\ \delta_i &= \frac{P_i}{b \cdot N_x} = \frac{A_i}{b \cdot t} \end{aligned}\right\} \qquad \text{---- (4.3)}$$

and where A_i is the area of the ith stiffener.

Seide & Stein (63) had produced a buckling chart to extrapolate the critical stresses for stiffened plate having 1,2, 3 or more stiffeners situated in the mid-plane of the plate. The chart operates on three different parameters γ , β & δ as defined in equation (4.3).

4.3.2.1 Plate with Stiffeners Located on one Side of the Plate

Timoshenko (49) suggested that the stiffness of a one-sided stiffener could be taken into account by replacing the moment of inertia of the stiffener about its centre of gravity (γ in equation (4.2)) by an effective moment of inertia and using this value in the solution valid for stiffeners with their centre of gravity located in the mid-plane of the plate as that suggested in equation (4.2) and reference (49). However, Seide (64) suggested that if the stiffeners are very large compared to the plate, the attached plate can have very little effect on the bending of each stiffener about an axis passing through the C.G. of the stiffener X-section. On the other hand, stiffeners that are very small compared to the plate would appear to be forced to bend about the mid-plane of the plate. The effective moment of inertia of a given stiffener can therefore vary between the moment of inertia taken about the centre of gravity of the stiffener's X-section and the moment of inertia about the mid-plane of the plate depending on the proportions of the attached plate. Following this agreement, the effective moment of inertia of this stiffeners are derived as (64):-

$$\frac{E \cdot I_{eff.}}{d \cdot D} = \frac{E \cdot I_s}{d \cdot D} + \frac{1}{1 + Z_{n.g} \cdot \frac{A_s}{d \cdot t}} \cdot \frac{E \cdot A_s \cdot \bar{z}^2}{d \cdot D} \qquad \text{---- (4.4)}$$

where I_{eff} is the effective moment of inertia of the stiffener about the mid-plane of the plate.

I_s is the moment of inertia of stiffener about its own C.G.

d is the bay width of plate between two stiffeners.

D & E are the usual bending modulus & Young's modulus of the plate and stiffeners respectively.

$\bar{z}$ is the distance of the C.G. of stiffener from the mid-plane of the attached plate.

$z_{n,q}$ is a constant dependent on the aspect ratio of the stiffened plate bay area.

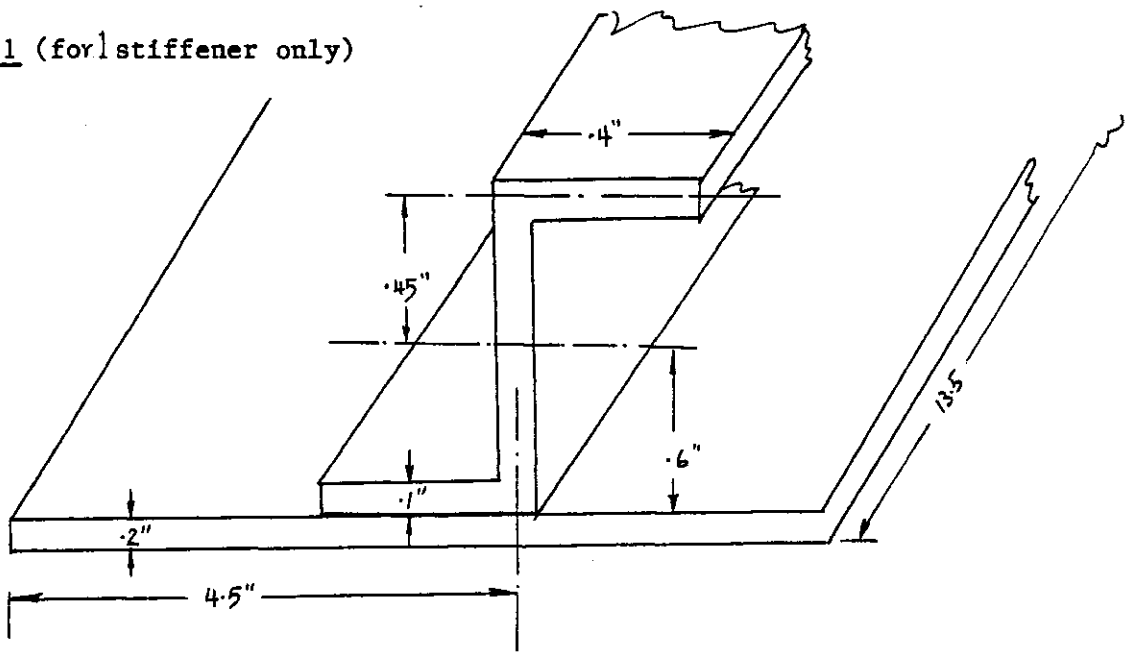
Reference (64) contains charts showing the value of $Z_{n,q}$ for different number of stiffeners and modes of buckling. To calculate the critical stress of the stiffened panel, the value of $Z_{n,q}$ of the corresponding panel is first extrapolated from ref. (64). Hence, the value of the effective moment of inertia of stiffener I_{eff} and the L.H.S. of equation (4.4) can be evaluated. Having obtained that, the buckling chart of ref. (63) is then used to extrapolate the critical stress using the 3 parameters β , γ' & δ as that described in equation (4.3), but with

$$\gamma' = \frac{E \cdot I_{eff}}{d \cdot D}$$

4.3.2.2 Example Study

In order that these analytical results described in ref. 46 can be used to check against our finite element results, three structures with arbitrary dimensions are employed here so that the evaluated terms γ' , β^* & δ would lie within the ranges given by ref. (64). They are shown as follows:-

CASE 1 (for 1 stiffener only)



Analytical Result

$E = 10^7$ lb./in^2 ; $a/d = 13.5"/4.5" = 3$; $D = 7326$

$A_s = (0.4 \times 0.1) \times 2 + 1 \times 0.1 = .18$

$I_s = (0.1 \times 0.1 \times 0.1/12) + (4 \times 1 \times 1/6) + (0.4 \times 1 \times 0.45 \times 0.45 \times 2) = 0.0246$

$$\frac{E \cdot A_s \cdot \bar{z}^2}{d \cdot D} = \frac{10^7 \times 0.18 \times 0.6^2}{4.5 \times 7326} = 19.65 \quad ; \quad \frac{A_s}{d \cdot t} = \frac{0.18}{4.5 \times 2} = 0.2$$

For $Z_{n.g}$, from N.A.C.A. TN 2873 . for $a/d = 3$, $Z_{n.g} = 0.95$

$$\frac{1}{1 + Z_{n.g} \cdot \frac{A_s}{d \cdot t}} = \frac{1}{1 + 0.95 \times .2} = \frac{1}{1.19} \Longrightarrow \frac{1}{1 + Z_{n.g} \cdot \frac{A_s}{d \cdot t}} \times \frac{E \cdot A_s \cdot \bar{z}^2}{d \cdot D} = 16.5$$

$$\frac{E \cdot I_s}{d \cdot D} = 7.46 \; ; \; \frac{E \cdot I_{eff}}{d \cdot D} = 7.46 + 16.5 = 23.96$$

from N.A.C.A. TN 1825 . for 1 stiffener only, $\frac{\sigma_{crit} \cdot d^2 \cdot t}{\pi^2 \cdot D} = 3.1$

$$\therefore \sigma_{crit} = \frac{3.1 \times \pi^2 \times D}{d^2 \cdot t} = \underline{55,344 \text{ lb./in}^2}$$

Finite Element Result

The same model is used in the finite element analysis. Only one half of the plate is used because of symmetry along its length. On employing 4x2 elements across the structure and taking the effect of off-setting the stiffener on one side of the plate into account, the result shows that the structure buckles at an applied stress level of around 54,000 lb/in^2 and that when this stress is reached, it continues into the post-buckling stage, behaving very similarly to those described in section (4.2.4). Fig. 17 shows the force-displacement curves of the 4 selected nodes on the structure. When comparing with the analytical results of ref. (64) remarkably close agreements are observed, and the discrepency between the two sets of results are only 2%.

CASE 2 (2 stiffeners)

Analytical Result

The stiffened plate with 2 stiffeners but the same configurations as that shown in Diagram 2 has been analysed, and the following results are obtained:-

$$\text{for} \quad a/d = 3 \; ; \; D = 7326 \; ; \; A_s = 0.18 \; ; \; I_s = 0.0246 \; ; \; \frac{A_s}{d \cdot t} = \frac{0.18}{4.5 \times 2} = 0.2 \; ;$$

$$Z_{n.q} = 1.19 \ (\text{from N.A.C.A. TN 2873}) \therefore \ \frac{1}{1 + Z_{n.q} \cdot \frac{A_s}{d \cdot t}} = \frac{1}{1 + 1.119 \times 2} = 0.817$$

$$\Longrightarrow \ \frac{1}{1 + Z_{n.q} \frac{A_s}{d \cdot t}} \times \frac{E \cdot A_s \cdot \bar{z}^2}{d \cdot D} = 16.5$$

$$\Longrightarrow \ \frac{E \cdot I_s}{d \cdot D} = 7.46 \; ; \; \frac{E \cdot I_{eff}}{d \cdot D} = 7.46 + 16.5 = 23.96$$

From N.A.C.A. TN 1825, $\frac{\sigma_{crit} \cdot d^2 \cdot t}{\pi^2 \cdot D}$ is found to be 2.5

$$\therefore \ \sigma_{crit} = \frac{2.5 \times \pi^2 \times D}{d^2 \cdot t} = \underline{44,632 \ \text{lb./in.}^2}$$

Finite Element Result

A 6x2 element model was used in this finite element analysis. Taking the effect of off-setting the stiffeners on one side of the plate and also taking the large displacement analysis into account, the result shows that the structure buckles at an applied stress level of around 43,600 lb/in^2. Again, further load increments have enabled the structure to enter into the post-buckling stage. When this result is compared with the analytical results shown above, the two sets of results are so close to each other that the discrepency between them is only 2%. Fig. 18 shows the force-displacement curves of 4 selected nodal points on the structure.

CASE 3 (3 stiffeners)

A stiffened plate with 3 stiffeners has been analysed. Here, the bay width (i.e. space between adjacent stiffeners) of the structure is reduced to half of that being shown in Diagram 2. Following the procedures shown in the previous 2 cases, the theoretical critical stress for this stiffened plate is found to be 85,000 lb/in^2. The Finite Element result gives 84,300 lb./sq.in. The discrepancy between the two sets of results is only 0.8%. Fig. 19 shows the force displacement curves of 4 selected nodal points on the structure.

5. MATERIAL NON-LINEARITY

Non-linear effects due to plasticity have been tackled in a manner similar to the approach used for geometric non-linearities. A tangential elastic-plastic modulus matrix has been developed (65,66) which relates the incremental stresses to the incremental strains. This tangential modulus matrix, which is a function of the current stress levels, may be incorporated in an incremental procedure (19,66) or alternatively a modified Newton-Raphson approach (19,67). Small increments are desirable in elastic-plastic analyses as a consequence of the incremental nature of the flow rules. However, Nayak and Zienkiewicz (67) have used large load increments for the application of the out-of-balance load vector while, for the formulation of this vector, a further sub-division was employed to improve the accuracy of the representation of the flow rate.

A number of authors (68,69) have used the finite element method for the analysis of elastic-plastic plate problem. Ang & Lopez (70) used a discrete modal approach and Belythescho & Velebit (69) used a complementary energy formulation to apply to the problem by assuming sudden plastification of the whole section depth. Similar approximations have been made using finite differences (28). A more exact analysis was performed by Armen et al (71) and Marcal (72) who allow for progressive growth of plasticity through the depth of the plate. Armen et al (71) also traced the elasto-plastic interfaces across the plane of the element while Marcal considered the plastic properties to be constant over each layer. He used the trapesiodal rule with eleven integration stations through the thickness. Crisfield (73) used an area approach based on Llyushin's theory (74) which relates to the six generalised stress resultants that would occur in any shell element. The yield criterion pre-supposes a sudden plastification of the plate section in a manner similar to that frequently assumed for plate bending. However, it was concluded that this area approach is not as accurate as the usual volume approach though it has the advantage of a considerable saving in computer time. As a consequence prior to the derivation of the plasticity formulation using finite element approach, we shall review some of the basic assumptions and material laws that would involve herewith.

5.1 Basic Assumptions and Constitutive Relation for an Elastic-Plastic Material

From equations (3.1) to (3.7) we have derived the general incremental stiffness equations using a constitute relation in the form of equation (3.18). It is the purpose of this chapter to derive the appropriate form of D_{ijkl} in equation (3.18) for a particular material property.

The classical treatment of the elastic material may be written as a function of strain energy such that:

$$S_{ij} = \frac{\partial W}{\partial E_{ij}} \qquad \text{----(5.1)}$$

where $W = W(E_{ij})$

Differentiating equation (5.1), we have:

$$\Delta S_{ij} = \frac{\partial^2 W}{\partial E_{ij} \partial E_{kl}} \cdot \Delta E_{kl} \qquad \text{----(5.2)}$$

Compare equation (5.2) with equation (3.17), we define:-

$$D_{ijkl} = \frac{\partial^2 W}{\partial E_{ij} \partial E_{kl}} \qquad \text{----(5.3)}$$

Equation (5.2) also shows that what we adopt here is very useful in following the strain history through the structure.

Before the formulation of the constitutive matrix D_{ijkl} can be derived, it is necessary to examine the assumptions that are required.

5.1.1 Assumptions

For finite strains, the usual development of the elasto-plastic constitutive relation may be followed provided that we assume a linear decomposition of strain increments into elastic and plastic parts. Although it is not the case in large strain analyses, however, if the strains are infinitesimal, we can assume the recoverable elastic strains are small so that the elastic & plastic strains may be additively decomposed as:-

$$\varepsilon_{ij} = \varepsilon^{e}_{ij} + \varepsilon^{p}_{ij} \qquad \text{----(5.4)}$$

where subscripts e & p refer to the 'elastic' and 'plastic' state respectively. The plastic part of strain is postulated to be incompressible. Hence,

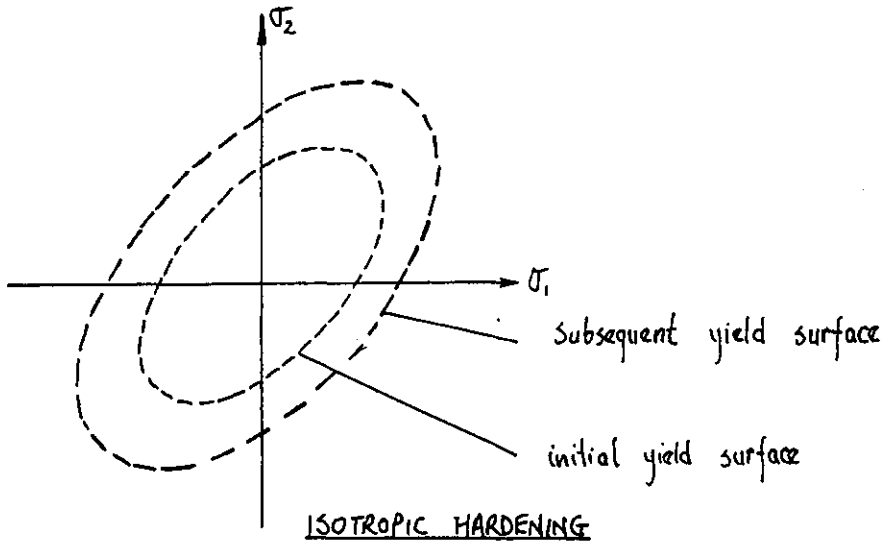
$$\varepsilon^{p}_{ii} = 0 \qquad \text{----(5.5)}$$

The second assumption is that the material has an isotropic hardening effect. This implies a uniform expansion of the initial yield surface. The hardening is measured according to the plastic hypothesis (which is equivalent to work hardening), so the yield criterion for subsequent yielding becomes:-

$$f = \bar{\sigma} - H(\bar{\varepsilon}^{p}) = 0 \qquad \text{----(5.6)}$$

where H is a function of the equivalent plastic strain $\bar{\varepsilon}^{p}$ which is the integral of :.

$$d\bar{\varepsilon}^{p} = \sqrt{\frac{2}{3}} \cdot \left\{ \partial\varepsilon^{p}_{ij} \cdot \partial\varepsilon^{p}_{ij} \right\}^{1/2} \qquad \text{----(5.7)}$$



ISOTROPIC HARDENING

Our third assumption is that there exists a loading function f in 9 dimensional stress space. $f = 0$ at time t constitutes the yield criterion at that time.

$f > 0$ is inadmissable. As it turns out that f is a function of σ_{ij} & ε^p_{ij}, three different loading conditions from a plastic state ($f = 0$) result:-

$$\frac{\partial f}{\partial \sigma_{ij}} \cdot \dot{\sigma}_{ij} < 0 \qquad \text{(during unloading)}$$

$$\frac{\partial f}{\partial \sigma_{ij}} \cdot \dot{\sigma}_{ij} = 0 \qquad \text{(during neutral loading)} \qquad \text{----(5.8)}$$

$$\frac{\partial f}{\partial \sigma_{ij}} \cdot \dot{\sigma}_{ij} > 0 \qquad \text{(during loading)}$$

The dot denotes time differentiation.

Furthermore, the material is assumed to be stable as defined by Drucker (75), which implies that at a regular point of the loading surface, $f = 0$, the vector $d\underset{\sim}{\varepsilon}^p$ is in the direction of the outward normal to the yield surface (in the stress space). This is known as the Normality rule (75) which defines the plastic strain increment as:-

$$d\varepsilon^p_{ij} = d\lambda \cdot \frac{\partial f}{\partial \sigma_{ij}} \qquad \text{----(5.9)}$$

where $d\lambda$ is a non-negative scalar when the material obeys the Von-Mises yield criterion, and the flow rate is equivalent to the Prandtl-Reuss equation. By virtue of equation (5.9) the loading function plays the role of a plastic potential, df remains zero when going from one plastic state to another. Hence:

$$df = \frac{\partial f}{\partial \sigma_{ij}} \cdot d\sigma_{ij} + \frac{\partial f}{\partial \varepsilon^{p}_{ij}} \cdot d\varepsilon^{p}_{ij} = 0 \qquad \text{----(5.10)}$$

The initial yield criterion (Von-Mises) and the loading function are given by:-

$$f_o = \bar{\sigma} - T_o = \bar{\sigma} - \sqrt{3}\,K_o = 0 \qquad \text{----(5.11)}$$

where T_0 is the initial yield stress in uniaxial tension, K_0 is the yield stress in pure shear and $\bar{\sigma}$ is the equivalent stress given by:-

$$\bar{\sigma} = \sqrt{3} \cdot J_2 = \sqrt{\frac{3}{2}} \left\{ \sigma'_{ij} \cdot \sigma'_{ij} \right\}^{1/2} \qquad \text{----(5.12)}$$

in which J_2 is the second deviatoric stress invarient and σ'_{ij} the deviatoric stress components. Areas concerning the behaviour of small strain elasto-plastic rate independant material which correspond with Prandtl-Reuss relations and Von-Mises yield criterion can be found in ref. (76,77).

5.1.2 Formulation of the Constitutive Law

For most material behaviour, the constitutive relation is commonly expressed in terms of true stress and true strain (e.g. the Prandtl-Reuss equation) rather than as a relation between S_{ij} and E_{ij} as that defined in equation (5.2). Therefore, the constitutive relation has to be related between the increments of the true stresses and the Kirchoff stresses. For the incremental stresses at any stage, we will express it in the form of :-

$$\Delta\sigma_{ij} = C_{ijkl} \cdot \Delta e_{kl} \qquad \text{----(5.13)}$$

where $\Delta\sigma_{ij}$ & Δe_{kl} are increments of Eulerian stress and Almensi strains, and C_{ijkl} is derived from the elastic constants and the current position of the yield surface (and work hardening coefficient) for an elastic plastic increment. It is noticed that C_{ijkl} in equation (5.13) is now defined as the relationship between the Eulerian stress increment $\Delta\sigma_{ij}$ & and the Almansi's strain increment Δe_{kl} both of which are a function of current coordinates. However, if a Lagrangian frame of reference is to be adopted, the original frame of reference is to be used throughout the load increments which implies that the Kirchoff stress increment and the Green's strain increment must be employed.

To relate the Green's strain increment to the Almansi's strain increment and also the Kirchoff stress increment to Eulerian stress increment, the following relationships are used:-

$$\Delta e_{mn} = \frac{\partial X_r}{\partial x_m} \cdot \frac{\partial X_s}{\partial x_n} \cdot \Delta E_{rs} \qquad \text{----(5.14)}$$

where Δe_{mn} is the Almansi strain increment & ΔE_{rs} is the Green's strain increment.

$$\Delta S_{ij} = \left| \frac{\partial \underline{x}}{\partial \underline{X}} \right| \cdot \frac{\partial X_i}{\partial x_m} \cdot \frac{\partial X_j}{\partial x_n} \cdot \Delta\sigma_{mn}$$

----(5.15)

Where ΔS_{ij} is the Kirchoff stress increment & $\Delta\sigma_{mn}$ is the Eulerian stress increment.

In the above two equations $\frac{\partial X_i}{\partial x_j}$ refers to the co-ordinates transformation where:-

$$\frac{\partial X_i}{\partial x_j} = (\delta_{ij} + h_{ik}) \cdot T_{kj} \qquad \text{----(5.16)}$$

and in most cases $h_{ij} = h_{ji} \ll 1$ & T_{kj} is an orthogonal rotation. Neglecting the terms of order of h_{ij}, assumming small strain :-

$$\Longrightarrow \left|\frac{\partial \underline{x}}{\partial \underline{X}}\right| \approx 1$$

$$\therefore \quad \Delta S_{ij} = \frac{\partial X_i}{\partial x_m} \cdot \frac{\partial X_j}{\partial x_n} \cdot \Delta \sigma_{mn} \qquad \text{----(5.17)}$$

sub. eqn. 5.17 & eqn. 5.14 into eqn. 5.11; we have,

$$\Delta S_{ij} = \frac{\partial X_i}{\partial x_m} \cdot \frac{\partial X_j}{\partial x_n} \cdot \frac{\partial X_r}{\partial x_K} \cdot \frac{\partial X_s}{\partial x_\ell} \cdot C_{ijk\ell} \cdot \Delta E_{rs} \qquad \text{----(5.18)}$$

The material law C_{ijkl} can now be derived as follow s:-

The true stress and strain increment is composed of the deviatoric and the hydrostatic part:-

$$\left.\begin{aligned} d\sigma &= d\sigma' + d\sigma^H \\ d\varepsilon &= d\varepsilon' + d\varepsilon^H \end{aligned}\right\} \qquad \text{----(5.19)}$$

and,

$$\left.\begin{aligned} d\sigma' &= d\sigma'_e + d\sigma'_p \\ d\varepsilon' &= d\varepsilon'_e + d\varepsilon'_p \end{aligned}\right\} \qquad \text{----(5.20)}$$

$$\left.\begin{aligned} d\sigma^H &= d\sigma^H_e + \cancel{d\sigma^H_p}^{=0} \\ d\varepsilon^H &= d\varepsilon^H_e + \cancel{d\varepsilon^H_p}^{=0} \end{aligned}\right\} \qquad \text{----(5.21)}$$

This is true since $d\sigma_p^H$ & $d\varepsilon_p^H$ is zero during plastic deformation

$$d\varepsilon'^e_{ij} = d\varepsilon^e_{ij} - \tfrac{1}{3}\delta_{ij} d\varepsilon_{ii} \qquad \text{----(5.22)}$$

i.e. $$d\varepsilon^H = \frac{1}{3}\delta_{ij} \cdot \varepsilon_{ii}$$

The elastic component of strain is:-

$$d\varepsilon^e_{ij} = \frac{d\sigma'_{ij}}{2G} + \frac{1}{3K}\delta_{ij}\, d\bar{\sigma}_{ii} \qquad \text{----(5.23)}$$

from (5.20) and (5.23), we have:-

$$d\varepsilon'_{ij} = \frac{d\sigma'_{ij}}{2G} + \frac{1}{3K}\delta_{ij}\, d\bar{\sigma}_{ii} - \frac{1}{3K}\delta_{ij}\, d\bar{\sigma}_{ii} + d\varepsilon'_p$$

$$= \frac{d\sigma'_{ij}}{2G} + d\varepsilon^p_{ij}$$

$$\Rightarrow \quad d\sigma'_{ij} = 2G \cdot d\varepsilon'_{ij} - 2G\, d\varepsilon^p_{ij} \qquad \text{----(5.24)}$$

The equivalent stress is defined as:-

$$\bar{\sigma}^2 = \frac{3}{2}\sigma'_{ij} \cdot \sigma'_{ij} \qquad \text{----(5.25)}$$

On differentiating eqn. 5.25, we have:-

$$\bar{\sigma} \cdot d\bar{\sigma} = \frac{3}{2}\sigma'_{ij}\, d\sigma'_{ij}$$

$$\Rightarrow \quad \sigma'_{ij} \cdot d\sigma'_{ij} = \frac{2}{3}\bar{\sigma} \cdot d\bar{\sigma} \qquad \text{----(5.26)}$$

Let the plastic modulus be H', and

$$H' = \frac{d\bar{\sigma}}{d\bar{\varepsilon}} = \frac{d\bar{\sigma}}{d\bar{\varepsilon}_p} \qquad \text{----(5.27)}$$

Using Prandtl-Reuss theory, the plastic strain increment:-

$$d\varepsilon_{ij}^{P} = \frac{3\,d\bar{\sigma}}{2\cdot H'\cdot\bar{\sigma}}\cdot\sigma_{ij}' = \frac{3\bar{\sigma}\cdot d\bar{\sigma}}{2\cdot H'\cdot\bar{\sigma}^{2}}\cdot\sigma_{ij}' \qquad \text{----(5.28)}$$

The Plastic work increment is:-

$$dW_{P} = \bar{\sigma}\cdot d\bar{\varepsilon}^{P} = \sigma_{ij}'\cdot d\varepsilon_{ij}^{P} \qquad \text{----(5.29)}$$

where $$\bar{\sigma}\cdot d\bar{\varepsilon}^{P} = \frac{\bar{\sigma}\cdot d\bar{\sigma}}{H'} \qquad \text{----(5.30)}$$

from eqn. 5.24, we have

$$\sigma_{ij}'\cdot d\varepsilon_{ij}^{P} = \sigma_{ij}'\left(d\varepsilon_{ij}' - \frac{d\sigma_{ij}'}{2G}\right)$$

$$= \sigma_{ij}'\cdot d\varepsilon_{ij}' - \frac{\sigma_{ij}'\cdot d\sigma_{ij}'}{2G} \qquad \text{----(5.31)}$$

Sub. eqn. 5.26 into 5.31, we get:-

$$\sigma_{ij}'\cdot d\varepsilon_{ij}^{P} = \sigma_{ij}'\cdot d\varepsilon_{ij}' - \frac{\bar{\sigma}\cdot d\bar{\sigma}}{3G} \qquad \text{----(5.32)}$$

Sub. eqn. 5.29 and 5.30 into 5.32, we have:-

$$\frac{\bar{\sigma}\cdot d\bar{\sigma}}{H'} = \sigma_{ij}'\cdot d\varepsilon_{ij}' - \frac{\bar{\sigma}\cdot d\bar{\sigma}}{3G}$$

$$\Longrightarrow \quad \left(\frac{1}{H'} + \frac{1}{3G}\right)\bar{\sigma}\cdot d\bar{\sigma} = \sigma_{ij}'\cdot d\varepsilon_{ij}'$$

$$\Longrightarrow \quad \bar{\sigma}\cdot d\bar{\sigma} = \frac{1}{\left(\frac{1}{H'} + \frac{1}{3G}\right)}\cdot\sigma_{ij}'\cdot d\varepsilon_{ij}' \qquad \text{----(5.33)}$$

Sub. (5.33) into (5.28), we have:-

$$d\varepsilon_{ij}^{P} = \frac{3\,\sigma_{ij}'\cdot\sigma_{kl}'}{2H'\cdot\bar{\sigma}^{2}\left(\frac{1}{H'} + \frac{1}{3G}\right)}\cdot d\varepsilon_{kl}' \qquad \text{----(5.34)}$$

Sub. (5.34) into (5.24), we derive:-

$$d\sigma'_{ij} = 2G \cdot d\varepsilon'_{ij} - \frac{3G \cdot \sigma'_{ij} \cdot \sigma'_{kl}}{H' \cdot \bar{\sigma}^2 \cdot \left(\frac{1}{H'} + \frac{1}{3G}\right)} \cdot d\varepsilon'_{kl} \qquad \text{----(5.35)}$$

From 5.19, $d\sigma_{ij} = d\sigma'_{ij} + d\sigma^H$

Sub. (5.35) into (5.19), we finally arrive:-

$$d\sigma_{ij} = 2G\, d\varepsilon'_{ij} + 3K\, d\varepsilon^H_{ij} - \frac{3G\, \sigma'_{ij} \cdot \sigma'_{kl}}{H' \cdot \bar{\sigma}^2 \cdot \left(\frac{1}{H'} + \frac{1}{3G}\right)} \cdot d\varepsilon'_{kl}$$

$$= 2G\left(\delta_{ik} \cdot \delta_{jl} + \frac{3K}{2G} \cdot \delta_{ij} \cdot \delta_{kl}\right) d\varepsilon_{kl} - \frac{3G\, \sigma'_{ij} \cdot \sigma'_{kl}}{H' \cdot \bar{\sigma}^2 \left(\frac{1}{H'} + \frac{1}{3G}\right)} \cdot d\varepsilon'_{kl}$$

----(5.36)

For plastic loading, $d\varepsilon'_{kl} = d\varepsilon_{kl}$, since the hydrostatic part becomes ineffective during plastic deformation.

$$\therefore\ d\sigma_{ij} = 2G\left\{\delta_{ik} \cdot \delta_{jl} + \frac{\nu}{1-2\nu} \cdot \delta_{ij}\, \delta_{kl} - \frac{3 \cdot \sigma'_{ij} \cdot \sigma'_{kl}}{2H' \bar{\sigma}^2 \left(\frac{1}{H'} + \frac{1}{3G}\right)}\right\} d\varepsilon_{kl}$$

_____for plastic loading

$$d\sigma_{ij} = 2G \cdot \left\{\delta_{ik} \cdot \delta_{jl} + \frac{\nu}{1-2\nu} \cdot \delta_{ij} \cdot \delta_{kl}\right\}$$

_____for elastic loading
& elastic unloading

Hence, the constitutive equation C_{ijkl} for plastic loading is:

$$C_{ijkl} = 2G \cdot \left\{ \delta_{ik} \cdot \delta_{jl} + \frac{\nu}{1-2\nu} \cdot \delta_{ij} \cdot \delta_{kl} - \frac{3\,\sigma'_{ij} \cdot \sigma'_{kl}}{2 \cdot H' \cdot \bar{\sigma}^2 \left(\frac{1}{H'} + \frac{1}{3G}\right)} \right\} \qquad \text{----(5.37)}$$

The constitutive equation C_{ijkl} for elastic loading and elastic unloading is:-

$$C_{ijkl} = 2G \left\{ \delta_{ik} \cdot \delta_{jl} + \frac{\nu}{1-2\nu} \cdot \delta_{ij} \cdot \delta_{kl} \right\} \qquad \text{----(5.38)}$$

When Lagrangian frame of reference is to be employed, the material constitutive law derived above should be pre and post multiplied with the appropriate co-ordinate transformation matrices such that:-

$$D_{ijkl} = \frac{\partial X_i}{\partial x_m} \cdot \frac{\partial X_j}{\partial x_n} \cdot \frac{\partial X_r}{\partial x_k} \cdot \frac{\partial X_s}{\partial x_l} \cdot C_{ijkl} \qquad \text{----(5.38.1)}$$

From eqn. 5.24, the equation can also be expressed as:-

$$d\sigma'_{ij} = E_{ijkl} \cdot (d\varepsilon'_{ij} - d\varepsilon^p_{ij})$$

$$\Rightarrow \quad d\sigma_{ij} = E_{ijkl} \cdot (d\varepsilon_{ij} - d\varepsilon^p_{ij}) \qquad \text{----(5.38.2)}$$

where E_{ijkl} is the usual elastic material constitutive law.

Comparing with equation 5.36, we can therefore express:-

$$d\sigma_{ij} = E_{ijkl} (d\varepsilon_{ij} - d\varepsilon^p_{ij}) = C_{ijkl} \cdot d\varepsilon_{ij} \qquad \text{----(5.39)}$$

5.2 Finite element formulation of material Constitutive equation

If the stress vector can be expressed 3 dimensionally as:-

$$\underset{\sim}{\sigma} = \{ \sigma_x , \sigma_y , \sigma_z , \sqrt{2}\sigma_{xy} , \sqrt{2}\sigma_{yz} , \sqrt{2}\sigma_{xz} \}$$

Taking the mean stress σ_m as $\frac{1}{3}(\sigma_x + \sigma_y + \sigma_z) = \frac{1}{3} \cdot \underset{\sim}{e}_3^t \cdot \underset{\sim}{\sigma}$

where $\underset{\sim}{e}_3 = \{ 1 , 1 , 1 , 0 , 0 , 0 \}$

Then, $\underset{\sim}{\sigma}' = \{ \sigma_x' , \sigma_y' , \sigma_z' , \sqrt{2}\sigma_{xy} , \sqrt{2}\sigma_{yz} , \sqrt{2}\sigma_{xz} \}$

$$= \underset{\sim}{\sigma} - \sigma_m \cdot \underset{\sim}{e}_3$$

$$= \underset{\sim}{\sigma} - \frac{1}{3} \cdot \underset{\sim}{e}_3 \cdot \underset{\sim}{e}_3^t \cdot \underset{\sim}{\sigma}$$

$$= (\underset{\sim}{I} - \frac{1}{3} \cdot \underset{\sim}{e}_3 \cdot \underset{\sim}{e}_3^t) \underset{\sim}{\sigma} \qquad \text{----(5.40.a)}$$

Similarly:

$$\underset{\sim}{\varepsilon}' = \underset{\sim}{\varepsilon} - \varepsilon_m \cdot \underset{\sim}{e}_3 = (\underset{\sim}{I} - \frac{1}{3} \cdot \underset{\sim}{e}_3 \cdot \underset{\sim}{e}_3^t) \cdot \underset{\sim}{\varepsilon}$$

$$\sigma_{ij}' \cdot \sigma_{kl}' = \underset{\sim}{\sigma}' \cdot \underset{\sim}{\sigma}'^t$$

$$\bar{\sigma}^2 = \frac{3}{2} [\underset{\sim}{\sigma}^t \underset{\sim}{\sigma} - 3\sigma_m^2] \qquad \text{----(5.40.b)}$$

$$d\sigma_{ij} = \{ d\sigma_x , d\sigma_y , d\sigma_z , \sqrt{2}\, d\sigma_{xy} , \sqrt{2}\, d\sigma_{yz} , \sqrt{2} \cdot d\sigma_{xz} \} = d\underset{\sim}{\sigma} \qquad \text{----(5.40.c)}$$

$$d\varepsilon_{ij} = \{ d\varepsilon_x , d\varepsilon_y , d\varepsilon_z , \sqrt{2}\, d\varepsilon_{xy} , \sqrt{2} \cdot d\varepsilon_{yz} , \sqrt{2} \cdot d\varepsilon_{xz} \} = d\underset{\sim}{\varepsilon} \qquad \text{----(5.40.d)}$$

From eqn. 5.39, we have:-

$$d\underset{\sim}{\sigma} = \underset{\sim}{C} \cdot d\underset{\sim}{\varepsilon} \qquad \text{----(5.40.e)}$$

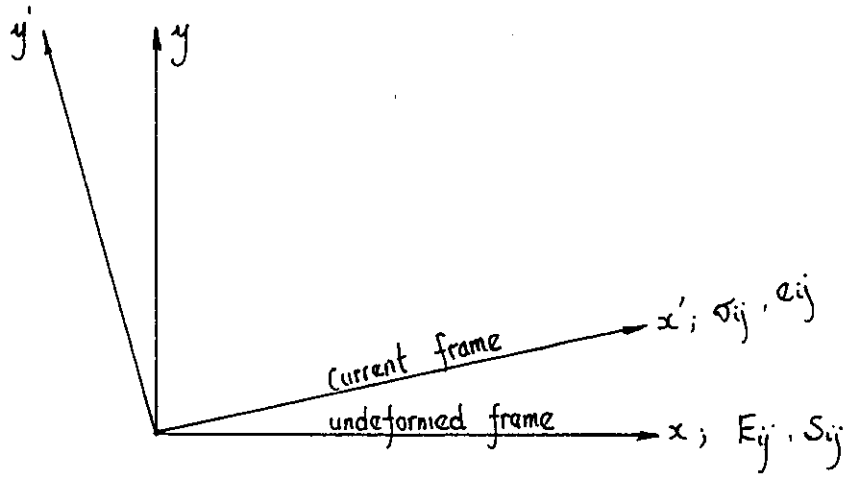
where:-

$$\underset{\sim}{C} = \left\{ \underset{\sim}{E} - \frac{3G \cdot \underset{\sim}{\sigma}' \cdot \underset{\sim}{\sigma}'^{t}}{H' \cdot \bar{\sigma}^2 \cdot \left(\frac{1}{H'} + \frac{1}{3G}\right)} \right\} \qquad \text{----(5.41)}$$

where $\underset{\sim}{E}$ is the usual elastic modulus of material in 3 dimensions, and H' is the plastic modulus of material defined in equation 5.27.

5.3 Transformation of co-ordinate system

Since C_{ijkl} is relating the true stress and strain system and the Constitutive law that we are looking for here D_{ijkl} is relating the second Kirchoff stress and Green's strain in the unde formed frame of reference, it is therefore necessary to transform C_{ijkl} obtained from above to D_{ijkl}.



The xy plane is the Lagrangian frame of reference which refers the corresponding stress and strain to its undeformed co-ordinates. The x'y' plane is the Eulerian frame of reference which refers the corresponding stress and strain to its current co-ordinates.

Let $\underset{\sim}{T}_\sigma$ be the transformation matrix which transform the second Kirchoff stress into the Eulerian stress,

$$\sigma_{ij} = \underset{\sim}{T}_\sigma \cdot S_{ij} \qquad \text{----(5.42)}$$

Let $\underset{\sim}{T}_\varepsilon$ be the transform matrix which transforms the Green's strain to Almensi's strain,

$$\varepsilon_{ij} = \underset{\sim}{T}_\varepsilon \cdot E_{ij} \qquad \text{----(5.43)}$$

The two transformation matrices $\underset{\sim}{T}_\sigma$ and $\underset{\sim}{T}_\varepsilon$ has the properties of orthogonality, where:-

$$\underset{\sim}{T}_\sigma^{-1} = \underset{\sim}{T}_\varepsilon^{t} \qquad \& \qquad \underset{\sim}{T}_\varepsilon^{-1} = \underset{\sim}{T}_\sigma^{t}$$

Hence, from eqn. 2.40,

$$\underset{\sim}{\sigma} = \underset{\sim}{C} \cdot \underset{\sim}{\varepsilon}$$

we have, after substituting eqn. 5.42 and eqn. 5.43 into 5.40:-

$$\underset{\sim}{T}_\sigma \cdot \underset{\sim}{S} = \underset{\sim}{C} \cdot \underset{\sim}{T}_\varepsilon \cdot \underset{\sim}{E}$$

$$\Longrightarrow \qquad \underset{\sim}{S} = \underset{\sim}{T}_\sigma^{-1} \cdot \underset{\sim}{C} \cdot \underset{\sim}{T}_\varepsilon \cdot \underset{\sim}{E}$$

$$= \underset{\sim}{T}_\varepsilon^{t} \cdot \underset{\sim}{C} \cdot \underset{\sim}{T}_\varepsilon \cdot \underset{\sim}{E}$$

Compare with:-

$$\underset{\sim}{S} = \underset{\sim}{D} \cdot \underset{\sim}{E}$$

Hence, we have got:-

$$\underset{\sim}{D} = \underset{\sim}{T}_\varepsilon^{t} \cdot \underset{\sim}{C} \cdot \underset{\sim}{T}_\varepsilon \qquad \text{----(5.44)}$$

5.4 Reduction to Plane Stress

In most thin plate analyses, the stresses in the out-of-plane direction (z-direction) is often assumed to be zero which gives:-

$$\sigma_z = \sigma_{xz} = \sigma_{yz} = 0$$

Also, $$d\sigma_z = d\sigma_{xz} = d\sigma_{yz} = 0 \qquad \text{----(5.45)}$$

and similarly,

$$d\varepsilon_{xy} = d\varepsilon_{yz} = 0 \qquad \text{----(5.46)}$$

therefore, the non-vanishing terms of the original 6x6 Constitutive matrix becomes:-

$$\begin{Bmatrix} d\sigma_{11} \\ d\sigma_{22} \\ d\sigma_{12} \\ d\sigma_{33} \end{Bmatrix} = \begin{bmatrix} C_{1111} & C_{1122} & C_{1112} & C_{1133} \\ C_{2211} & C_{2222} & C_{2212} & C_{2233} \\ C_{1211} & C_{1222} & C_{1212} & C_{1233} \\ C_{3311} & C_{3322} & C_{3312} & C_{3333} \end{bmatrix} \cdot \begin{Bmatrix} d\varepsilon_{11} \\ d\varepsilon_{22} \\ d\varepsilon_{12} \\ d\varepsilon_{33} \end{Bmatrix} \qquad \text{----(5.47)}$$

However, $d\sigma_{33} = d\sigma_z = 0$ while $d\varepsilon_{33}$ is non-zero, therefore $\underset{\sim}{C}$ is condensed to:-

$$\hat{\underset{\sim}{C}} = C_{mn} - \frac{C_{m4}\, C_{4n}}{C_{44}}$$

where m = 1,2,3
& m = 1,2,3

The Constitutive matrix is finally condensed to:-

$$\hat{\underset{\sim}{C}} = \begin{bmatrix} \left\{C_{1111} - C_{1133}\frac{C_{3311}}{C_{3333}}\right\}, & \left\{C_{1122} - C_{1133}\frac{C_{3322}}{C_{3333}}\right\}, & \left\{C_{1112} - C_{1133}\frac{C_{3312}}{C_{3333}}\right\} \\ \left\{C_{2211} - C_{2233}\frac{C_{3311}}{C_{3333}}\right\}, & \left\{C_{2222} - C_{2233}\frac{C_{3322}}{C_{3333}}\right\}, & \left\{C_{2212} - C_{2233}\frac{C_{3312}}{C_{3333}}\right\} \\ \left\{C_{1211} - C_{1233}\frac{C_{3311}}{C_{3333}}\right\}, & \left\{C_{1222} - C_{1233}\frac{C_{3322}}{C_{3333}}\right\}, & \left\{C_{1212} - C_{1233}\frac{C_{3312}}{C_{3333}}\right\} \end{bmatrix} \qquad \text{----(5.48)}$$

Hence, the constitutive matrix for the Lagrangian frame of reference becomes:-

$$\underset{\sim}{D} = \underset{\sim}{\hat{T}}_{\varepsilon}^{t} \cdot \underset{\sim}{\hat{C}} \cdot \underset{\sim}{\hat{T}}_{\varepsilon} \qquad \text{----(5.49)}$$

where the transformation matrix $\underset{\sim}{\hat{T}}_{\varepsilon}$ is now refered to the co-ordinates in 2-dimensional space only.

5.5 Total Strain Increment

If the displacement can be expressed as:-

$$\underset{\sim}{U} = \{ u, \; v, \; w \}$$

then, the total strain can be written as:-

$$\underset{\sim}{\varepsilon} = \begin{Bmatrix} \varepsilon_x \\ \varepsilon_y \\ \varepsilon_{xy} \end{Bmatrix} = \begin{Bmatrix} \frac{\partial u}{\partial x} \\ \frac{\partial v}{\partial y} \\ \frac{\partial v}{\partial x} + \frac{\partial u}{\partial y} \end{Bmatrix} + \begin{Bmatrix} \frac{1}{2}\left(\frac{\partial w}{\partial x}\right)^2 \\ \frac{1}{2}\left(\frac{\partial w}{\partial y}\right)^2 \\ \left(\frac{\partial w}{\partial x}\right)\left(\frac{\partial w}{\partial y}\right) \end{Bmatrix} + \begin{Bmatrix} -z\frac{\partial^2 w}{\partial x^2} \\ -z\frac{\partial^2 w}{\partial y^2} \\ -2z\frac{\partial^2 w}{\partial x \partial y} \end{Bmatrix}$$

and the total str ain increment becomes:-

$$\Delta\underset{\sim}{\varepsilon} = \begin{Bmatrix} \Delta\varepsilon_x \\ \Delta\varepsilon_y \\ \Delta\varepsilon_{xy} \end{Bmatrix} = \begin{Bmatrix} \frac{\partial \Delta u}{\partial x} \\ \frac{\partial \Delta v}{\partial y} \\ \frac{\partial \Delta u}{\partial y} + \frac{\partial \Delta v}{\partial x} \end{Bmatrix} + \begin{Bmatrix} \frac{1}{2}\left(\frac{\partial \Delta w}{\partial x}\right)^2 \\ \frac{1}{2}\left(\frac{\partial \Delta w}{\partial y}\right)^2 \\ \left(\frac{\partial \Delta w}{\partial x}\right)\left(\frac{\partial w}{\partial y}\right) \end{Bmatrix} + \begin{Bmatrix} \frac{\partial w}{\partial x} \cdot \frac{\partial \Delta w}{\partial x} \\ \frac{\partial w}{\partial y} \cdot \frac{\partial \Delta w}{\partial y} \\ \frac{\partial \Delta w}{\partial y} \cdot \frac{\partial w}{\partial y} + \frac{\partial \Delta w}{\partial x} \cdot \frac{\partial w}{\partial x} \end{Bmatrix} + \begin{Bmatrix} -z\frac{\partial^2 \Delta w}{\partial x^2} \\ -z\frac{\partial^2 \Delta w}{\partial y^2} \\ -2z\frac{\partial^2 \Delta w}{\partial x \partial y} \end{Bmatrix}$$

From eqn. 3.25 and 3.25.a, the above total strain increment can be written as:-

$$\Delta\underset{\sim}{\varepsilon} = \underset{\sim}{B}_v \cdot \Delta f + \underset{\sim}{B}_z \cdot \Delta f - z \cdot \underset{\sim}{B}_w \cdot \Delta f + \begin{bmatrix} \frac{\partial \Delta w}{\partial x} & 0 \\ 0 & \frac{\partial \Delta w}{\partial y} \\ \frac{\partial \Delta w}{\partial x} & \frac{\partial \Delta w}{\partial y} \end{bmatrix} \begin{bmatrix} \frac{\partial w}{\partial x} \\ \frac{\partial w}{\partial y} \end{bmatrix}$$

$$= \underset{\sim}{B}_v \cdot \Delta f + \underset{\sim}{B}_z \cdot \Delta f - z \cdot \underset{\sim}{B}_w \cdot \Delta f + \underset{\sim}{T}_3 \cdot \Delta \underset{\sim}{S}$$

5.6 Plastic Strain Increment Evaluation

From eqn. 5.39, we have:-

$$d\underset{\sim}{\sigma} = \underset{\sim}{E} \cdot (d\underset{\sim}{\varepsilon} - d\underset{\sim}{\varepsilon}^p) = \hat{\underset{\sim}{C}} \cdot d\underset{\sim}{\varepsilon}$$

where $d\underset{\sim}{\varepsilon}$ is the total strain increment and $d\underset{\sim}{\varepsilon}^p$ is the plastic strain increment.

R-arranging eqn. 5.39, we have:-

$$\underset{\sim}{E} \cdot d\underset{\sim}{\varepsilon} - \underset{\sim}{E} \cdot d\underset{\sim}{\varepsilon}^p = \hat{\underset{\sim}{C}} \cdot d\underset{\sim}{\varepsilon}$$

$$\Longrightarrow \quad \underset{\sim}{E} \cdot d\underset{\sim}{\varepsilon}^p = (\underset{\sim}{E} - \hat{\underset{\sim}{C}}) \cdot d\underset{\sim}{\varepsilon}$$

$$\Longrightarrow \quad d\underset{\sim}{\varepsilon}^p = \underset{\sim}{A} \cdot d\underset{\sim}{\varepsilon} = (\underset{\sim}{I} - \underset{\sim}{E}^{-1} \cdot \hat{\underset{\sim}{C}}) \cdot d\underset{\sim}{\varepsilon} \qquad \text{----(5.50)}$$

where $\underset{\sim}{I}$ is a unit matrix, $\underset{\sim}{E}$ is the usual elastic modulus matrix and it can be expressed as:-

$$\underset{\sim}{E} = \frac{E}{1-\nu^2}\begin{bmatrix} 1 & \nu & 0 \\ \nu & 1 & 0 \\ 0 & 0 & \frac{1-\nu}{2} \end{bmatrix}$$

$\underset{\sim}{\hat{C}}$ is the condensed Constitutive matrix for plastic loading (see equation 5.48). $\underset{\sim}{A}$ is therefore not necessarily a symmetrical matrix even though $\underset{\sim}{E}^{-1}$ and $\underset{\sim}{C}$ are.

If the plastic strain increment history is to be recorded, $\underset{\sim}{A}$ has to be evaluated throughout the whole process of loading for all integration points when using the Finite Element procedure.

5.7 Evaluation of Plasticity Within a Loading Step

The tangency condition df = 0 mentioned at the beginning of this Chapter should ensure that the resultant stresses remain on the yield surface. However, owing to the finite nature of the load increments, δf will not necessary be zero (see eqn.5.10). To avoid the accumulation of this error, the stress resultants are adjusted by moving them normal to the yield surface until f=1 where f is the yield function which if governed by the Von-Mises yield criterion, would be expressed as:-

For a plate element:- $$f = \frac{(\sigma_x^2 + \sigma_y^2 - \sigma_x\sigma_y + 3\sigma_{xy}^2)^{1/2}}{\sigma_{yield.}} \qquad ----(5.51)$$

Now, let f_{i+1} be the elastic value of the yield function at the end of the $(i+1)^{th}$ increment and where $f_{i-1} < 1$ at any stationary point through the depth of the element.

Let f_i be the plastic value at the end of the increment and $f_i > 1$

The strain increments to cause the stresses that just reach the yield surface can be approximated as 'x' times the total strain increments where,

$$x = \frac{1 - f_{i-1}}{f_i - f_{i-1}} \qquad \text{----(5.52)}$$

So, the first approximated stresses at the end of the ith increment is:-

$$\underset{\sim}{\sigma}_{i,1} = \underset{\sim}{\sigma}_{i-1} + \underset{\sim}{D} \cdot d\underset{\sim}{\varepsilon}_t \qquad \text{----(5.53)}$$

where i, 1 is the first trial at step i.

With $f_i > 1$ (from eqn. 5.51), then, equation 5.53 can be used to estimate the stresses to reach the yield surface $\underset{\sim}{\sigma}_{i,e}$ where

$$\underset{\sim}{\sigma}_{i,e} = (1 - x) \cdot \underset{\sim}{\sigma}_{i-1} + x \cdot \underset{\sim}{\sigma}_{i,1} \qquad \text{----(5.54)}$$

A second estimate of the stresses at the end of the increment is given by:-

$$\underset{\sim}{\sigma}_{i,e} = \underset{\sim}{\sigma}_{i,e} + (1 - x) \cdot \underset{\sim}{D}(\underset{\sim}{\sigma}_{i,e}) \cdot d\underset{\sim}{\varepsilon}_t \qquad \text{----(5.55)}$$

Note that the constitutive matrix $\underset{\sim}{D}$ is now a function of the estimated stresses $\underset{\sim}{\sigma}_{i,e}$.

5.8 Method of Solution

In most elastic analysis, equations 3.1 to 3.37 can be applied to formulate the tangential stiffness matrix. In elasto-plastic analysis, these equations still hold provided that the material Constitutive matrix employed follows those described in equations 5.1 to 5.49. Basically, the analogy for solving the incremental displacements can follow the steps and procedures shown in equations 3.38 to 3.56 whether the problem is an elastic one or an elasto-plastic one.

In elastic analysis, the Constitutive matrix $\underset{\sim}{D}$ can normally be made constant throughout the whole loading procedure. Hence, the stress levels (see equation 3.30) can easily be obtained by multiplying the elastic modulus $\underset{\sim}{E}$ by the current strain level which is in turn a linear function of the current deformation of the structure.

In elasto-plastic analysis however, the Constitutive matrix $\underset{\sim}{D}$ is a function of the current stress level which if plasticity occurs, will no longer be a linear function of the current deformation of the structure at all. Therefore, an up-to-date record of the current stress levels is strictly required in this case. There are apparently two ways of evaluating the stress levels of a stationary point at any loading stage; one is to accumulate the total stress increments which is known as the incremental stress approach, and the other one is to accumulate the total plastic strain increments which is known as the incremental strain approach. Both approaches will produce the same result, so, the choice is rather of personal one.

5.8.1 Incremental Stress Approach

The approach is to accumulate all the stress increments throughout the subsequent loading/unloading history, especially when yielding has occurred. The stress increment at a stationary point can be evaluated as:-

$$d\underset{\sim}{\sigma} = \underset{\sim}{E} \cdot d\underset{\sim}{\varepsilon}^{t} \qquad \text{------- for elastic loading \& elastic unloading}$$

$$d\underset{\sim}{\sigma} = \underset{\sim}{C} \cdot d\underset{\sim}{\varepsilon}^t \qquad \text{------ for plastic loading}$$

where $d\underset{\sim}{\varepsilon}^t$ is the total strain increment, and matrices $\underset{\sim}{E}$ and $\underset{\sim}{C}$ are the Constitutive law of the material described in equations 5.38 and 5.37 respectively.

Thus, the total stress level at load step i is calculated as:-

$$\underset{\sim}{\sigma}_i = \underset{\sim}{\sigma}_{i-1} + d\underset{\sim}{\sigma}$$

Where $\underset{\sim}{\sigma}_{i-1}$ is the total stress level recorded in the previous load step.

The procedure is relatively simple and does not require any further explanation. However, it should be noticed that if prior to the load increment, the stress $\underset{\sim}{\sigma}_{i-1}$ of a particular stationary point is below yield and that $\underset{\sim}{\sigma}_i$ is greater than yield after the load increment, then the iteration procedures described in Section 5.7 has to be used in order to compute the correct stress increment $d\underset{\sim}{\sigma}_{i,n}$ before it is being accumulated. The disadvantage of this approach is that the incremental stresses are continuously required to update the present total stress level even in the plastic unloading stage.

5.8.2 Incremental Strain Approach

An alternative way to evaluate the stress level at any stage is to accumulate the plastic strain increments rather than to accumulate the stress increments at the stationary points where yieldings have been exceeded.

Referring to equation 5.39, the stress at any stage can be shown as:-

$$\underset{\sim}{\sigma} = \underset{\sim}{E} \cdot \underset{\sim}{\varepsilon}^e \qquad \text{----(5.56)}$$

where $\underset{\sim}{\varepsilon}^e$ is the total elastic strain evaluated, and

$$\underset{\sim}{\varepsilon}^e = \underset{\sim}{\varepsilon}^t - \underset{\sim}{\varepsilon}^p$$

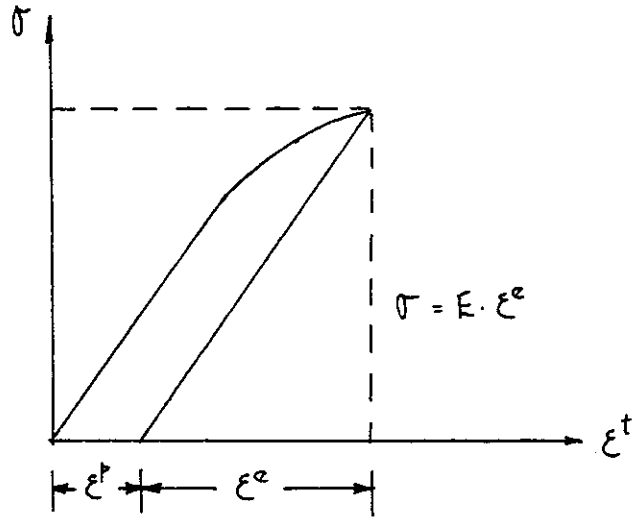
where $\underset{\sim}{\varepsilon}^t$ is the total strain evaluated directly from the present displacement level:- $\underset{\sim}{\varepsilon}^t = \underset{\sim}{B}\, \underset{\sim}{f}$

and $\underset{\sim}{\delta}$ is the displacement function described in equation 3.26

$\underset{\sim}{\varepsilon}^p$ is known as the total plastic strain increments accumulated throughout the whole loading procedures:-

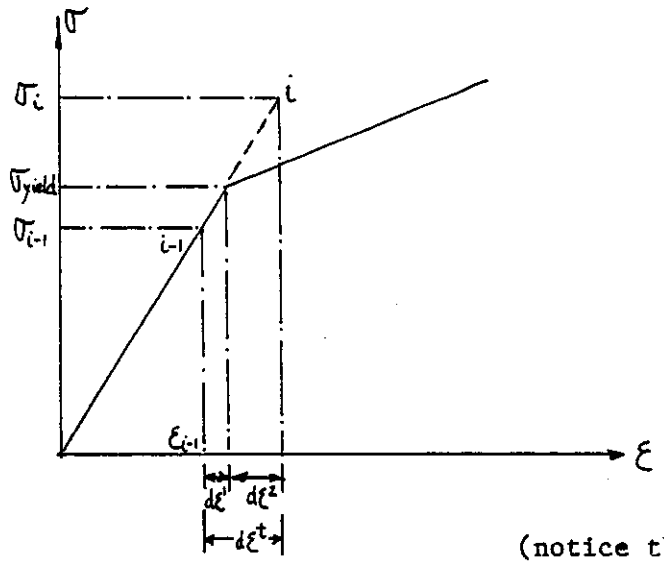
$$\underset{\sim}{\varepsilon}_i^p = \underset{\sim}{\varepsilon}_{i-1}^p + d\underset{\sim}{\varepsilon}^p$$

Hence, if the plastic strain history is recorded, the total elastic, and hence the up-to-date, stress level can be obtained without any difficulties at all.



The evaluation of the plastic strain increment for any stationary point during each loading step can easily be evaluated by using equation 5.50. If before the load increment, the stress at a particular stationary point is below the yield surface, while after the load increment, the stress is above the yield surface, then the elastic strain increment up to the yield surface can be calculated as:-

$$d\underset{\sim}{\varepsilon}' = \frac{1 - f_{i-1}}{f_i - f_{i-1}} \cdot d\varepsilon^t \qquad \text{----(5.57)}$$



(notice that the suffice 1 and 2 refer to stages 1 and 2)

where:

$d\varepsilon^1$ is the true elastic strain increment up to the yield surface only,

$d\varepsilon^t$ is the 'evaluated' total elastic strain increment using the elastic Constitutive matrix $\underset{\sim}{E}$,

$d\varepsilon^2$ is the combined elastic and plastic strain increments.

To obtain the plastic strain participation $d\underset{\sim}{\varepsilon}^p$, we have:-

$$d\underset{\sim}{\varepsilon}^p = \underset{\sim}{A} \cdot d\underset{\sim}{\varepsilon}^2 \qquad \text{----(5.58)}$$

where:

$$\underset{\sim}{A} = \left(\underset{\sim}{I} - \underset{\sim}{E}^{-1} \cdot \underset{\sim}{D}^1(\underset{\sim}{\sigma}^1) \right)$$

and where:

$\underset{\sim}{E}^{-1}$ is the usual inverse elastic Constitutive matrix,

$\underset{\sim}{D}'(\underset{\sim}{\sigma}')$ is evaluated as a function of the maximum stress level just below the yield surface $\underset{\sim}{\sigma}'$

and $\underset{\sim}{\sigma}'$ is equal to $\underset{\sim}{E}(\underset{\sim}{\varepsilon}_{i-1} + d\underset{\sim}{\varepsilon}')$.

Having obtained the plastic strain increment participation, the total plastic strain can now be updated, and the stress level at the end of that loading step can easily be evaluated as:-

$$\underset{\sim}{\sigma}_i = \underset{\sim}{E} \cdot (\underset{\sim}{\varepsilon}^t_{i-1} - \underset{\sim}{\varepsilon}^p) \qquad \text{----(5.59)}$$

Any subsequent stress level on further loadings can then be calculated as:-

$$\underset{\sim}{\sigma}_n = \underset{\sim}{E} \cdot (\underset{\sim}{\varepsilon}^t_{n-1} - \underset{\sim}{\varepsilon}^p_{n-1})$$

where $\underset{\sim}{\varepsilon}^p_{n-1}$ is the accumulated plastic strain increment

$$\underset{\sim}{\varepsilon}^p_{n-1} = \underset{\sim}{\varepsilon}^p_{n-2} + d\underset{\sim}{\varepsilon}^p_{n-1}$$

5.9 Criterion for elastic unloading

This section concerns the detection of a plastic unloading when (or after) a stationary point has reached the yield surface. This is absolutely necessary especially in the elasto-plastic dynamic buckling analysis where plastic unloading often takes place in regardless of the present states of external applied load.

From equation 5.26, we have

$$d\bar{\sigma} = \tfrac{3}{2} \cdot \frac{\sigma'_{ij}}{\bar{\sigma}} \cdot d\sigma'_{ij}$$

$$= \left\{ \frac{3\sigma'_x}{2\bar{\sigma}}, \frac{3\sigma'_y}{2\bar{\sigma}}, \frac{3\sigma'_z}{2\bar{\sigma}}, \frac{3\sigma_{xy}}{\bar{\sigma}}, \frac{3\sigma_{yz}}{\bar{\sigma}}, \frac{3\sigma_{xz}}{\bar{\sigma}} \right\} \begin{bmatrix} d\sigma_x \\ d\sigma_y \\ d\sigma_z \\ d\sigma_{xy} \\ d\sigma_{yz} \\ d\sigma_{xz} \end{bmatrix} \qquad \text{----(5.60)}$$

$$= \underset{\sim}{H}^t \cdot d\underset{\sim}{\sigma} \qquad \text{----(5.61)}$$

From equation 5.30, we have

$$H' = \frac{d\bar{\sigma}}{d\bar{\varepsilon}^p} \quad \Longrightarrow \quad d\bar{\sigma} = H' \cdot d\bar{\varepsilon}^p \qquad \text{----(5.62)}$$

Substitute equation 5.62 into 5.61, we have

$$\underset{\sim}{A}^t \cdot d\underset{\sim}{\sigma} = \cdot H' \cdot d\bar{\varepsilon}^p \qquad \text{----(5.63)}$$

The Prandtl-Reuss relation states that

$$d\underset{\sim}{\varepsilon}^p = \underset{\sim}{A} \cdot d\bar{\varepsilon}^p \qquad \text{----(5.64)}$$

and equation 5.38.2 states that:-

$$d\underset{\sim}{\sigma} = \underset{\sim}{E} \cdot \left\{ d\underset{\sim}{\varepsilon} - d\underset{\sim}{\varepsilon}^p \right\}$$

Substitute equation 5.64 into equation 5.38.2, and then pre-multiply both sides by $\underset{\sim}{A}^t$, we have:-

$$\cdot H' \cdot d\bar{\varepsilon}^p = \underset{\sim}{A}^t \cdot \underset{\sim}{E} \cdot \left\{ d\underset{\sim}{\varepsilon} - \underset{\sim}{A} \cdot d\bar{\varepsilon}^p \right\}$$

$$\Longrightarrow \quad \underset{\sim}{A}^t \cdot \underset{\sim}{E} \cdot \underset{\sim}{A} \cdot d\bar{\varepsilon}^p + H' \cdot d\bar{\varepsilon}^p = \underset{\sim}{A}^t \cdot \underset{\sim}{E} \cdot d\underset{\sim}{\varepsilon}$$

$$\Longrightarrow \quad d\bar{\varepsilon}^p = \frac{\underset{\sim}{A}^t \cdot \underset{\sim}{E}}{H' + \underset{\sim}{A}^t \cdot \underset{\sim}{E} \cdot \underset{\sim}{A}} \cdot d\underset{\sim}{\varepsilon}$$

$$= \underset{\sim}{B} \cdot d\underset{\sim}{\varepsilon} \qquad \text{----(5.65)}$$

It is obvious that if $d\bar{\varepsilon}^p < 0$ in a load step, plastic unloading is indicated. When this happens, $d\bar{\varepsilon}^p$ is set to zero, and in the next load step, the tangential stiffness matrix is formulated based on the elastic modulus $\underset{\sim}{E}$. If isotropic hardening is assumed, plastic

action is resumed only if $\bar{\sigma}$ exceeds its previous maximum value.

5.10 Convergence

In the elastic range, the incremental and iterative approach described in Chart 1 can be used to converge to the exact solution quite easily. In the plastic range, however, apart from the fact that errors are bound to exist owing to the finite size of the load increments and hence a much smaller load step has to be used once the yield surface is reached, there is also a need to keep check on the maximum deflection evaluated within the structure so that the errors evaluated would not be accumulated.

Nayak and Zienkiewicz (67) and Brebbia and Connor (38) used the Euclidean norm, $n=(f^t f)^{\frac{1}{2}}$ as a basis for determining convergence. They applied iterations until the Euclidean norm of iterative deflection changes was of the order of 1% of the Euclidean norm of the total deflections. However, for most instability problems, the maximum out-of-plane deflection has been adopted as the basis for determining convergence. Iteration is applied until the maximum iterative deflection, w, is within a few percentage of the maximum total deflection. After the onset of plasticity, since the flow rules are related to the load increment, a convergence restriction is placed on the incremental deflection. Here, the maximum iterative deflection (see Chart 1) must be less than say 10% of the maximum incremental deflection. The overall total deflection restriction is also applied.

5.11 MATERIAL NON-LINEARITY ANALYSIS

During the elasto-plastic analysis, the relationship between the stress increments and the elastic and plastic strain increments depends entirely on the Constitutive law for the material concerned.

Equation 5.41 of section 5.2 has already shown that this constitutive matrix $\underset{\sim}{C}$ is a function of the plastic modulus of the material which implies that the stress-strian relationship chosen for the material is particular important.

Throughout this analysis, the material is assumed to be an alluminium alloy with a stress-strain relationship expressible by a modified Ramberg-Osgood formula giving the plastic-strain :-

$$\varepsilon_p = \frac{1.1 \times Y_o}{m \cdot E} \cdot \left\{ \left(\frac{\sigma}{1.1 \times Y_o} \right)^m - \left(\frac{1}{1.1 \times Y_o} \right)^m \right\} \qquad \text{----(5.66)}$$

Where Y_o is the yield stress level and is taken as 33,000 p.s.i.

m is the material characteristic and is taken as 10.

The inverse of the plastic modulus is thus:-

$$\frac{1}{E_p} = \frac{d\varepsilon_p}{d\sigma} = \frac{1}{E} \left(\frac{\sigma}{1.1 \times Y_o} \right)^{m-1} \qquad \text{----(5.67)}$$

This plastic modulus E_p is calculated based on the current stress level at the corresponding stationary points and then substituted back into the Constitutive matrix $\underset{\sim}{C}$ in equation 5.41 when formulating for the tangential stiffness matrix $\underset{\sim}{K_T}$ during each loading step.

5.11.1 Elasto-Plastic Loading/Unloading of Plate

A plate was subject to a simple tensile test so that the non-linear stress-strain curves computed from using the finite element program can be studied. Incremental load method was used in the analysis and the tangential stiffness matrices at various loading steps were formulated following the steps and procedures laid down in section 3 and section 5. The plastic modulus of the material was evaluated using equation 5.67 during each loading step. Before yielding occurred, the applied load increments were relatively large. Near to the point of yielding, very small load increments were applied so that the structure could get round the 'elbow' of the stress-strain curve. After that, relatively large load increments were

resumed. Fig.20 shows the plotting of the stress-strain curve of a typical plate element. It can be seen that the curve is almost identical to that obtained by equation 5.66.

Another test was carried out. This time, the plate was first subject to tensile loading until it had exceeded the yield stress. When that happened, the structure was unloaded until it had reached a much lower stress level, loading then resumed again until it had exceeded the previous maximum load level. Fig.21a to Fig.21c shows the stress strain curves of the structure under such loading/unloading sequence.

6. DYNAMIC LOADING ANALYSIS

When the application of the loading is rapid and severe, the contribution of the acceleration-dependent inertia forces and the velocity-dependent damping forces is quite significant and can no longer be negligible as in the case of static load analysis. In order to take these forces into account, the equation of equilibrium has to be considered rather differently. In finite element transient dynamic analysis, there are various ways of computing for the dynamic response of a system. The varieties of solution methods were generated not only because of their acadamic interest, but generally due to the nature of the problem involved. To perform the dynamic analysis, the basic equations of motion can be written as:-

$$\underset{\sim}{m}\cdot\ddot{\underset{\sim}{x}} + \underset{\sim}{c}\cdot\dot{\underset{\sim}{x}} + \underset{\sim}{k}\cdot\underset{\sim}{x} = \underset{\sim}{f} \qquad \text{----(6.1)}$$

where:

$\underset{\sim}{m}$, $\underset{\sim}{c}$, $\underset{\sim}{k}$ are the mass, damping and stiffness matrices respectively,

$\underset{\sim}{f}$ is the external applied load vector,

$\underset{\sim}{x}$, $\dot{\underset{\sim}{x}}$ and $\ddot{\underset{\sim}{x}}$ are the displacement, velocity and acceleration vectors of the finite element assemblage.

6.1 Modal Superposition Scheme

To solve equation 6.1, if the involved structure can be assumed to be linear throughout the entire loading history, that is that their dynamic resisting forces could be related to the acceleration, velocity or displacement vector by means of linear influence coefficients, then it is possible to compute the vibration modes and frequencies for the structure and to evaluate the response in terms of the modal co-ordinates. This procedure is sometimes known as the modal superposition method. Details of the scheme can be found from many references (41).

Because of the change in geometry when local buckling commences, the fundamental eigen modes of the structure also change quite drastically. It is therefore not possible to use the modal superposition method to compute the structural response throughout the entire loading period.

To illustrate this, the first 6 natural modes of a stiffened panel are computed at t = 0 (i.e. before loading is applied):-

$$ {}_i\phi_{t=0} \qquad \text{where } i = 1 \ldots 6 \qquad \text{----(6.2)} $$

The first 6 eigen modes at various time steps ($t = t_1, t_2 \cdots t_n$) are then computed using a step-by-step integration method, which will be described further along the chapter. Hence, we have

$$ {}_i\phi_{t=t_n} \qquad \text{where: } i = 1, 2, \cdots 6 \quad t_n = t_1, t_2 \cdots t_n \qquad \text{----(6.3)} $$

If changes in the eigen modes are not significant, we should expect that the product of the transpose of the first 6 eigen vectors at t = 0 and those at t = tn be equal to unity, i.e.:-

$$ {}_i\phi^T_{t=0} \times {}_j\phi_{t=t_n} = 1 \qquad \text{for } i = j \qquad \text{----(6.4)} $$

However, Fig. 22 and Fig. 23 show that this is not so because of the occurrence of the unstable eigen modes. Fig. 22 shows the change in the eigen modes at various time steps. Here, the applied load is equal to the local buckling load of the panel. It can be shown from this figure that the best correlation between the $t = t_o$ modes and the $t = t_n$ modes is only the 6th mode. Similarly, Fig. 23 shows that the modal correlation of the structure when the applied load is equal to 1.5 times the local buckling load of the panel. Again, only mode 1 has experienced close correlation at most of the time steps.

It is in this aspect that a numerical step-by-step integration method is sought to compute the response of the structure.

6.2 Numerical time integration schemes

Various time integration schemes have been developed and widely used (e.g. Wilson-θ method and Houbolt method etc.). Details of these can be found from refs. (80-87). Of various integration schemes, only the Newmark-β method and the Central Difference method with diagonal mass matrix and Central Difference method with consistent mass matrix are being examined here merely to compare and hence choose the most suitable and computationally economical scheme for our present problem.

6.2.1 Newmark-β method

The above method is one of the most widely used implicit integrating methods. The governing equations are:-

$$\dot{\underset{\sim}{U}}_{t+\Delta t} = \dot{\underset{\sim}{U}}_t + \frac{\Delta t}{2}\left(\ddot{\underset{\sim}{U}}_t + \ddot{\underset{\sim}{U}}_{t+\Delta t}\right) \qquad \text{----(6.5)}$$

$$\underset{\sim}{U}_{t+\Delta t} = \underset{\sim}{U}_t + \Delta t\,\dot{\underset{\sim}{U}}_t + \Delta t^2\left[\left(\tfrac{1}{2}-\beta\right)\ddot{\underset{\sim}{U}}_t + \beta\,\ddot{\underset{\sim}{U}}_{t+\Delta t}\right] \qquad \text{----(6.6)}$$

For $\beta = \frac{1}{4}$, the formula corresponds to the assumption of a constant acceleration between t and t+Δt. The associated velocity is piecewise linear (ref.86). The value also provides the response with unconditional stability. For β = 1/6, the above formula corresponds to a piecewise linear acceleration within each time interval. In linear analysis, in the absence of damping, the combination of equation 6.1, equation 6.5 and 6.6 gives:-

$$\left(\beta\Delta t^2\,\underset{\sim}{K} + \underset{\sim}{M}\right)\underset{\sim}{U}_{t+\Delta t} = \beta\Delta t^2\,\underset{\sim}{F}^{ext}_{t+\Delta t} + \left[\underset{\sim}{U}_t + \Delta t\,\dot{\underset{\sim}{U}}_t + \left(\tfrac{1}{2}-\beta\right)\Delta t^2\,\ddot{\underset{\sim}{U}}_t\right]\underset{\sim}{M} \qquad \text{----(6.7)}$$

where $\underset{\sim}{F}^{ext.}_{t+\Delta t}$ is the external applied load at time $t+\Delta t$. In non-linear analysis, where the increment displacement is required at each time step to obtain the internal nodal forces, the above equation is written as:-

$$\left(\beta\Delta t^2\,\underset{\sim}{K} + \underset{\sim}{M}\right)\Delta\underset{\sim}{U}_{t+\Delta t} = \beta\Delta t^2\,\underset{\sim}{F}^{ext.}_{t+\Delta t} - \Sigma\Delta\underset{\sim}{F}^{int.}_t\,\beta\Delta t^2 + \left[\Delta t\,\dot{\underset{\sim}{U}}_t + \left(\tfrac{1}{2}-\beta\right)\Delta t^2\,\ddot{\underset{\sim}{U}}_t\right]\underset{\sim}{M} \qquad \text{----(6.8)}$$

where

$$\Sigma \Delta \underset{\sim}{F}^{int} = \Sigma \underset{\sim}{K} \cdot \Delta \underset{\sim}{U} \qquad \text{----(6.9)}$$

On examining the Newmark-β method, the displacements found by Equation 6.8 and the accelerations found from these displacements by Equation 6.6, will not satisfy the equation of motion at time $t+\Delta t$ One can derive from the above equations the nodal error forces by:-

$$\underset{\sim}{F}^{error} = \underset{\sim}{F}^{ext.} - \underset{\sim}{F}^{int} - \underset{\sim}{M}\ddot{\underset{\sim}{U}} \qquad \text{----(6.10)}$$

These nodal error forces represent the error in the solution procedure, unless steps are taken to control their growth, otherwise the solution so obtained will become meaningless (86).

6.2.2 Central Difference Method

The Central Difference method can be shown to be equivalent to the Newmark-β method with $\beta = 0$. The governing equations used are:-

$$\dot{\underset{\sim}{U}}_{t+\frac{\Delta t}{2}} = \dot{\underset{\sim}{U}}_{t-\frac{\Delta t}{2}} + \Delta t \cdot \ddot{\underset{\sim}{U}}_t \qquad \text{----(6.11)}$$

$$\underset{\sim}{U}_{t+\Delta t} = \underset{\sim}{U}_t + \Delta t \cdot \dot{\underset{\sim}{U}}_{t+\frac{\Delta t}{2}} \qquad \text{----(6.12)}$$

and assuming that:- $$\dot{\underset{\sim}{U}}_{t+\frac{\Delta t}{2}} = \dot{\underset{\sim}{U}}_t + \frac{1}{2} \Delta t \cdot \ddot{\underset{\sim}{U}}_t \qquad \text{----(6.13)}$$

from equation (6.11), we have:-

$$\dot{\underset{\sim}{U}}_{t+\frac{3\Delta t}{2}} = \dot{\underset{\sim}{U}}_{t+\frac{\Delta t}{2}} + \Delta t \cdot \ddot{\underset{\sim}{U}}_{t+\Delta t} \qquad \text{----(6.14)}$$

From equation (6.13), if we proceed the whole equation from $t+\frac{\Delta t}{2}$ to $t+\frac{3\Delta t}{2}$ and t to $t+\Delta t$; we will have:-

$$\dot{\underset{\sim}{U}}_{t+\frac{3\Delta t}{2}} = \dot{\underset{\sim}{U}}_{t+\Delta t} + \frac{1}{2} \cdot \Delta t \cdot \ddot{\underset{\sim}{U}}_{t+\Delta t} \qquad \text{----(6.15)}$$

The R.H.S. of equation (6.15) is then substituted into the L.H.S. of equation (6.14), and the L.H.S. of (6.13) into the R.H.S. of (6.14), we will get:-

$$\dot{\underset{\sim}{U}}_{t+\Delta t} + \tfrac{1}{2}\cdot\Delta t\cdot\ddot{\underset{\sim}{U}}_{t+\Delta t} = \dot{\underset{\sim}{U}}_{t} + \tfrac{1}{2}\Delta t\cdot\ddot{\underset{\sim}{U}}_{t} + \Delta t\cdot\ddot{\underset{\sim}{U}}_{t+\Delta t} \qquad \text{----(6.16)}$$

$$\Rightarrow \dot{\underset{\sim}{U}}_{t+\Delta t} = \dot{\underset{\sim}{U}}_{t} + \tfrac{1}{2}\cdot\Delta t\cdot\left(\ddot{\underset{\sim}{U}}_{t} + \ddot{\underset{\sim}{U}}_{t+\Delta t}\right) \qquad \text{----(6.17)}$$

from equation 6·12 & 6·17, we have:-

$$\Delta\dot{\underset{\sim}{U}} = \dot{\underset{\sim}{U}}_{t+\Delta t} - \dot{\underset{\sim}{U}}_{t} = \tfrac{1}{2}\Delta t\cdot\left(\ddot{\underset{\sim}{U}}_{t} + \ddot{\underset{\sim}{U}}_{t+\Delta t}\right)$$
$$= \tfrac{1}{2}\Delta t\cdot\Delta\ddot{\underset{\sim}{U}}_{t}^{t+\Delta t} + \Delta t\cdot\ddot{\underset{\sim}{U}}_{t} \qquad \text{----(6.18)}$$

$$\Delta\underset{\sim}{U} = \underset{\sim}{U}_{t+\Delta t} - \underset{\sim}{U}_{t} = \Delta t\cdot\dot{\underset{\sim}{U}}_{t+\frac{\Delta t}{2}} \qquad \text{----(6.19)}$$

$$\Delta\ddot{\underset{\sim}{U}} = \ddot{\underset{\sim}{U}}_{t+\Delta t} - \ddot{\underset{\sim}{U}}_{t} \qquad \text{----(6.20)}$$

If equation (6.1) can further be written as:-

$$\underset{\sim}{F}_{t+\Delta t}^{ext} = \underset{\sim}{F}_{t+\Delta t}^{int} + \underset{\sim}{F}_{t+\Delta t}^{inert.} + \underset{\sim}{F}_{t+\Delta t}^{damp.} \qquad \text{----(6.21)}$$

where $\underset{\sim}{F}_{t+\Delta t}^{ext.}$ is the external force at time step t + Δt

$\underset{\sim}{F}_{t+\Delta t}^{inert.} = \underset{\sim}{M}\cdot\ddot{\underset{\sim}{x}}_{t+\Delta t}$ is the inertia force at time step t + Δ t

$\underset{\sim}{F}_{t+\Delta t}^{damp.} = \underset{\sim}{C}\cdot\dot{\underset{\sim}{x}}_{t+\Delta t}$ is the damping force at time step t + Δ t

$\underset{\sim}{F}^{int.}_{t+\Delta t}$ is the total internal force at time step $t + \Delta t$, and is evaluated as the summation of all the incremental internal forces up to time $t + \Delta t$, hence:-

$$\underset{\sim}{F}^{int.}_{t+\Delta t} = \sum_{t=0}^{t=t} \underset{\sim}{\Delta F}^{int.} + \underset{\sim}{K} \cdot \Delta \underset{\sim}{x}^{t+\Delta t}_{t} \qquad \text{----(6.22)}$$

at time $t=t+\Delta t$, the equation of motion is:-

$$\underset{\sim}{M} \cdot \ddot{\underset{\sim}{x}}_{t+\Delta t} = \underset{\sim}{F}^{ext}_{t+\Delta t} - \left\{ \sum_{t=0}^{t=t} \Delta \underset{\sim}{F}^{int.} + K \cdot \Delta \underset{\sim}{x}^{t+\Delta t}_{t} \right\} - \underset{\sim}{C} \cdot \dot{\underset{\sim}{x}}_{t+\Delta t} \qquad \text{----(6.23)}$$

at $t = t$

$$\underset{\sim}{M} \cdot \ddot{\underset{\sim}{x}}_{t} = \underset{\sim}{F}^{ext.}_{t} - \left\{ \sum_{t=0}^{t=t-\Delta t} \Delta \underset{\sim}{F}^{int.} + \underset{\sim}{K} \cdot \Delta \underset{\sim}{x}^{t}_{t-\Delta t} \right\} - \underset{\sim}{C} \cdot \dot{\underset{\sim}{x}}_{t} \qquad \text{----(6.24)}$$

equation (6.23) - (6.24); we have:-

$$\underset{\sim}{M}(\ddot{\underset{\sim}{x}}_{t+\Delta t} - \ddot{\underset{\sim}{x}}_{t}) = (\underset{\sim}{F}^{ext.}_{t+\Delta t} - \underset{\sim}{F}^{ext.}_{t}) - \left\{ \sum_{t=0}^{t=t} \Delta \underset{\sim}{F}^{int.} - \left(\sum_{t=0}^{t=t-\Delta t} \Delta \underset{\sim}{F}^{int.} + \underset{\sim}{K} \cdot \Delta \underset{\sim}{x}^{t}_{t-\Delta t} \right) + \underset{\sim}{K} \cdot \Delta \underset{\sim}{x}^{t+\Delta t}_{t} \right\} - \underset{\sim}{C}(\dot{\underset{\sim}{x}}_{t+\Delta t} - \dot{\underset{\sim}{x}}_{t}) \qquad \text{----(6.25)}$$

$$\Rightarrow \underset{\sim}{M} \Delta \ddot{\underset{\sim}{x}}^{t+\Delta t}_{t} = \Delta \underset{\sim}{F}^{ext.}_{t}{}^{t+\Delta t} - \underset{\sim}{K} \Delta \underset{\sim}{x}^{t+\Delta t}_{t} - \underset{\sim}{C} \cdot \Delta \dot{\underset{\sim}{x}}^{t+\Delta t}_{t} \qquad \text{----((6.26)}$$

From equation (6.18), we have

$$\Delta \dot{\underset{\sim}{x}}^{t+\Delta t}_{t} = \frac{1}{2} \Delta t \cdot \Delta \ddot{\underset{\sim}{x}}^{t+\Delta t}_{t} + \Delta t \, \ddot{\underset{\sim}{x}}_{t}$$

Substitute this equation into eqn. 6.26, we have:-

$$\underset{\sim}{M} \cdot \Delta \ddot{\underset{\sim}{x}}^{t+\Delta t}_{t} = \Delta \underset{\sim}{F}^{ext.}_{t}{}^{t+\Delta t} - \underset{\sim}{K} \cdot \Delta \underset{\sim}{x}^{t+\Delta t}_{t} - \underset{\sim}{C} \left(\tfrac{1}{2} \Delta t \cdot \Delta \ddot{\underset{\sim}{x}}^{t+\Delta t}_{t} \right) - \Delta t \cdot \underset{\sim}{C} \cdot \ddot{\underset{\sim}{x}}_{t} \qquad \text{----(6.27)}$$

Re-arranging (6.27), we have :-

$$\left(\underset{\sim}{M} + \frac{\Delta t}{2} \cdot \underset{\sim}{C} \right) \cdot \Delta \ddot{\underset{\sim}{x}}^{t+\Delta t}_{t} = \Delta \underset{\sim}{F}^{ext.}_{t}{}^{t+\Delta t} - \underset{\sim}{K} \Delta \underset{\sim}{x}^{t+\Delta t}_{t} - \Delta t \cdot \underset{\sim}{C} \cdot \ddot{\underset{\sim}{x}}_{t} \qquad \text{----(6.28)}$$

$$\Rightarrow \Delta \ddot{\underset{\sim}{x}}^{t+\Delta t} = \left(\underset{\sim}{M} + \frac{\Delta t}{2} \cdot \underset{\sim}{C} \right)^{-1} \cdot \left\{ \Delta \underset{\sim}{F}^{ext.}_{t}{}^{t+\Delta t} - \underset{\sim}{K} \Delta \underset{\sim}{x}^{t+\Delta t}_{t} - \Delta t \cdot \underset{\sim}{C} \cdot \ddot{\underset{\sim}{x}}_{t} \right\} \qquad \text{----(6.29)}$$

In using the Central Difference scheme, two very important points need to be considered:-

a) The conditional stability of the Central Difference scheme

This can normally be overcome by taking a very small time step (by trial and error). However, if the integration of the equation of motion involves the solution of a large set of linear algebra at each time step, especially when non-linearities are included, the computing time spent could be quite immense. It is therefore necessary to evaluate the maximum time step size which will provide a numerical stability. This time step is evaluated by considering equation (6.1), with the absence of damping and external applied forces:-

$$\underset{\sim}{M}\cdot\ddot{\underset{\sim}{U}}_t + \underset{\sim}{K}\cdot\underset{\sim}{U}_t = \underset{\sim}{0}$$

$$\Rightarrow \quad \ddot{\underset{\sim}{U}}_t = -\underset{\sim}{M}^{-1}\cdot\underset{\sim}{K}\cdot\underset{\sim}{U}_t \qquad \text{----(6.30)}$$

Substituting equation (6.30) into equations (6.11) to (6.13) and following the algebraic manipulation (79) we derive:-

$$\Delta t^2\cdot\underset{\sim}{M}^{-1}\cdot\underset{\sim}{K}\cdot\underset{\sim}{U}_t + \underset{\sim}{U}_{t+\Delta t} - 2\underset{\sim}{U}_t + \underset{\sim}{U}_{t-\Delta t} = \underset{\sim}{0} \qquad \text{----(6.31)}$$

Substitute $\underset{\sim}{M}^{-1}\cdot\underset{\sim}{K}$ by the system eigenvalue λ and $\underset{\sim}{U}_t$ by $\underset{\sim}{U}\cdot e^{\beta\cdot n\cdot\Delta t}$, we obtain:-

$$\Delta t^2\cdot\lambda + e^{\beta\cdot\Delta t} - 2 + e^{-\beta\Delta t} = 0 \qquad \text{----(6.32)}$$

Since equation (6.32) is bounded for all time, $\left| e^{\beta\Delta t} \right|$ must be less than 1, thus equation (6.32) becomes:-

$$\Delta t^2\cdot\lambda \leq 4$$

$$\Rightarrow \quad \Delta t \leq \frac{2}{\sqrt{\lambda_{max.}}} \qquad \text{----(6.33)}$$

where $\lambda_{max.}$ is the maximum eigenvalue of the finite element which provides the strictest condition. In linear analysis, coupling does not exist between bending and membrane behaviour. The time step* is governed by either the maximum bending eigenvalue or the maximum membrane eigenvalue depending on what type of solution is required. However, in most large displacement analysis, the membrane and bending displacements are in general coupled. Therefore, the time step chosen should strictly be governed by the smallest values between the two:-

$$\Delta t^* \propto \left\{ \frac{1}{\sqrt{\lambda^{max.}_{bending}}} ; \frac{1}{\sqrt{\lambda^{max.}_{membrane}}} \right\} \qquad ----(6.34)$$

When large displacement takes place however, the maximum eigenvalue of the system is generally increased, thus the required time step size should also have to be reduced in order to avoid any numerical instability. In most non-linear analyses, it would therefore be necessary to keep checking on the current maximum eigen value of the structure so that a correct time step size can be used throughout the entire loading history without having to upset the numerical stability.

---

*In practice, however, Δt used in the program is only about 80% of the time step size evaluated in equation (6.33) to allow for a reasonable margin.

b) Lumping of the Mass Matrix

As mentioned above, the convenience of using the Central Difference scheme is that when a diagonal mass matrix is employed, and in the absence of damping, the nodal accelerations in equation (6.29) can be solved recursively without going through the triangulization of a banded matrix as in the case of the implicit method. If however, a consistent mass matrix is employed in the Central Difference scheme, the advantage of such a scheme will be obscured since the solution procedure also involves the triangulization of a banded mass matrix, and needs to go through a much smaller time step than that used in the Newmark-β method. Here, the lumping of the mass matrix is carried out directly from the well known consistent mass matrix (details of the formulation of the consistent mass matrix can be obtained from refs. (19 and 88)). The lumping procedure follows the one suggested by Kay (79) in his investigation on the stability of the lumped mass matrix in Central Difference integrating technique. It can be concluded that the lumped mass matrix is evaluated as:-

$$M^d_{ii} = \sum_j^k M^c_{ij} \qquad \text{----(6.35)}$$

where M^d_{ii} is the lumped mass of the i th degree of freedom of the element, and $\underset{\sim}{M}^c$ is the usual consistent mass matrix; k is the number of couplings of the same displacement harmonic between one node and the other nodes within the element. The method also suggests multiplying the rotation terms by a rotational gradient α, which can be adjusted to match the maximum frequencies obtained from both the diagonal mass and the consistent mass matrices. Details of this can again be consulted through refs. (79 and 89).

When plasticity occurs, the maximum eigenvalue of the system ${}^p\lambda_{max}$. (whether by using a Diagonal Mass Matrix or by using a Consistent Mass Matrix) will be different from its elastic value ${}^e\lambda_{max}$. However, we can make further assumption here that during plastic deformation, the ratio of the maximum eigen value obtained by using a Diagonal Mass Matrix and that by using a Consistent Mass Matrix should almost be the same as that in the elastic case, i.e.:-

$$\frac{{}^{P}\lambda^{D}_{max.}}{{}^{P}\lambda^{C}_{max.}} \doteqdot \frac{{}^{e}\lambda^{D}_{max.}}{{}^{e}\lambda^{C}_{max.}} \qquad \text{----(6.36)}$$

So the rotational scalar α can remain almost unchanged throughout the whole loading history regardless the state of plasticity. The above assumption does not seem to be unreasonable since in most instability problems, the change in material mass is hardly significant and that their mass matrices should remain reasonably constant.

6.3 Treatment of the Non-diagonal Damping Matrix When Using a Lumped Mass Matrix

Equation (6.29) shows that in the event of the presence of damping, a Central Difference integrating scheme will still not benefit from the employment of a lumped mass matrix if a non-diagonal damping matrix is used since the L.H.S. of that equation would still contain a non-diagonal matrix term. In general, the damping matrix $\underset{\sim}{C}$ can not be constructed from element damping matrices, such as the mass and the stiffness matrices of the element assemblage, and its purpose is to approximate the overall energy dissipation during the system response. Hence, in general, the damping matrix $\underset{\sim}{C}$ is a full matrix (41) and is a function of the element mass matrix, stiffness matrix, critical dampings and also the fundamental frequencies of the system. $\underset{\sim}{C}$ is therefore expressed as (41):-

$$\underset{\sim}{C} = \alpha \cdot \underset{\sim}{M} + \beta \cdot \underset{\sim}{K} \qquad \text{----(6.37)}$$

where α & β are the constants to be determined from the two given damping ratios that correspond to the two unequal frequencies of vibration of the system. It was also shown in reference (41) that the evaluation of the two constants α & β can be expressed as:-

$$\begin{aligned} \alpha + \beta \omega_1^2 &= 2\omega_1 \xi_1 \\ \alpha + \beta \omega_2^2 &= 2\omega_2 \cdot \xi_2 \end{aligned} \qquad \text{----(6.38)}$$

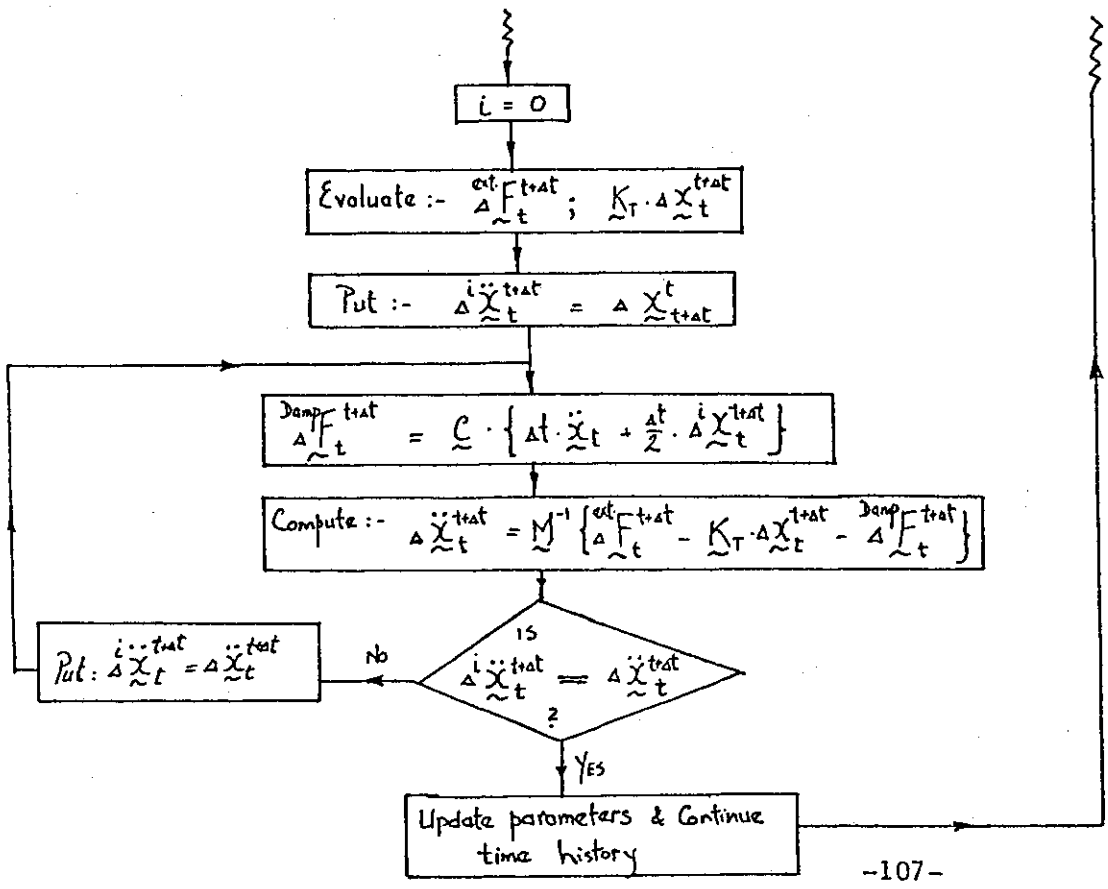
and ξ_1 & ξ_2 are the two critical damping ratios for the corresponding frequencies. Normally, the first two frequencies are employed.

Having evaluated the damping matrix $\underset{\sim}{C}$ (equation (6.37) & equation (6.29)) can now be re-arranged as:-

$$\underset{\sim}{M}\cdot\Delta\ddot{\underset{\sim}{X}}_t^{t+\Delta t} = {}^{ext.}\Delta\underset{\sim}{F}_t^{t+\Delta t} - \underset{\sim}{K}\cdot\Delta\underset{\sim}{X}_t^{t+\Delta t} - \underset{\sim}{C}\left(\Delta t\cdot\ddot{\underset{\sim}{X}}_t + \frac{\Delta t}{2}\cdot\Delta\ddot{\underset{\sim}{X}}_t^{t+\Delta t}\right)$$

----(6.39)

The term $\underset{\sim}{C}\cdot\ddot{\underset{\sim}{X}}_{t+\Delta t}$ on the LHS of equation (6.28) is now moved to the RHS of equation (6.39). This is desirable as it would keep the LHS of equation (6.39) as a function of the Diagonal Mass matrix only so that the solution procedure can be done on element by element level. However, such arrangement would leave the RHS of equation (6.39) with the acceleration term $\Delta\ddot{\underset{\sim}{X}}_t^{t+\Delta t}$ which is not known at the beginning of the solution procedure. In order to solve equation (6.39) the solution procedure has to be carried out iteratively until the accelerations $\Delta\ddot{\underset{\sim}{X}}_t^{t+\Delta t}$ evaluated from any two successive iterations converge. The iteration procedure taken in the Central difference integration scheme with damping included can be shown as :-



6.4 Evaluation of the maximum eigen value of the system

It has been shown in the previous paragraphs that the maximum eigen value of the system during the analysis is strictly needed when employing the Central Difference integration scheme. This maximum eigen value serves two purposes prior to the running of the dynamic program; one is to obtain the rotational inertia scalar α employed in the lumped mass formulation, and the other is to evaluate a correct time step size in order to fulfill the numerical stability requirement. Because of the non-linearities involved, this eigen value will no longer be constant throughout the dynamic analysis and therefore it has also to be evaluated at regular time intervals.

The eigen value extraction algorithm can normally follow the formulations described in Ref. (79). However, since it is the highest eigen value that we are interested in, an alternative scheme known as the Direct Power method can be employed. The iteration procedure is described as follows:-

$$\underset{\sim}{M} \cdot \underset{\sim}{\omega}_n = \underset{\sim}{K} \cdot \underset{\sim}{U}_{n-1} \qquad \text{----(6.40)}$$

$$\underset{\sim}{U}_n = \frac{1}{C_n} \cdot \underset{\sim}{\omega}_n \qquad \text{----(6.41)}$$

where $\underset{\sim}{U}_{n-1}$ is the trial vector. Here, the sweeping of the previous eiven vectors is not required since it is only the highest eigen value that we are interested in. It can be shown that the maximum eigen value $\lambda_{max.}$ converges to $1/C_n$ where C_n is the element of $\underset{\sim}{\omega}_n$ with the largest absolute value. To start the iteration, the trial vector $\underset{\sim}{U}_{n-1}$ can be set to a unit vector and $\underset{\sim}{\omega}_n$ can be evaluated as:-

$$\underset{\sim}{\omega}_n = \underset{\sim}{M}^{-1} \cdot \underset{\sim}{K} \cdot \underset{\sim}{U}_{n-1} \qquad \text{----(6.42)}$$

Here, the advantage of using a diagonal mass matrix is more obvious because this would mean that the evaluation of the highest eigenvalue of the system can virtually be obtained on an element level.

6.5 Solution Procedure

Prior to the running of the dynamic loading program, a separate program has to be run. This separate program assembles the structural stiffness matrix and the mass matrix to evaluate the fundamental frequencies as well as the maximum frequency. As has been mentioned before, the fundamental frequencies are used to formulate the damping matrix $\underset{\sim}{C}$ of the system, while the maximum frequency is used to evaluate the rotational inertia scalar α as well as the suitable critical time step size.
In order to evaluate the change in mode shapes and eigen values of the system during loading, the same program (hereafter known as the pre-process program) can be used to perform eigen value and eigen vector extractions. This operation is particularly useful when studying the effect of the change of eigen mode shapes of the system with reference to the change of structural geometry and material properties(see for instance Section 6.1).

The reason for the above eigen value extraction procedures (for the lowest eigen modes) to be performed separately is that such operation would require the inverse of the full stiffness matrix $\underset{\sim}{K}^{-1}$, and if the inversion is to be carried out in the main dynamic program during the analysis stage, enormous amount of memory core would inevitably be required. In order to save the unnecessary computer storage (after all, this is the main reason for choosing a Central Difference integration scheme), the stiffness matrix and the mass matrix at various loading stages are recorded and stored out of core. On completing the main dynamic program, the pre-process program will then be recalled to perform the eigen value analysis using the pre-recorded stiffness and mass matrices as that in the case of Section 6.1.

While it is reasonable to assume that the rotational inertia scalar α would not have any significant change throughout the stages of loading (see section 6.3), the fundamental frequencies ω_1 & ω_2 will change quite considerably once buckling is approached. However, we will make a further assumption here that the formulation of the damping matrix C based on the values of λ_1 & λ_2 (i.e. ω_1 & ω_2), would have very little effect on the

equilibrium state of the system and therefore the choice of λ_1 & λ_2 is purely arbitrary. Hence, by keeping the terms ω_1 & ω_2 at any loading stage equal to the structure's undeformed basic frequencies ω_1° & ω_2°, we are adjusting the critical values ξ_1 & ξ_2 at the corresponding loading stage so that equation (6.38) can remain constant. This does not seem to be unreasonable since, in our present analysis, external dampings are only applied after unloading has been completed.

The Direct Power method is included in the main dynamic program (because it does not take up large computer storage, see section 6.4) to keep check on the change of the maximum eigen value so that a suitable time step size can be used. This is strictly required especially when the geometry and the material of the structure has changed.

During the entire loading stage, some 5,000 to 6,000 time steps are required as the time step size is very small due to the numerical stability requirement. It was noticed that if the applied load is not severe and that it has not exceeded 60% of the critical stress of the structure, the updating of the tangential stiffness matrix can be done once every 30 to 40 time steps without causing any unnecessary divergence to the structural response. However, once it has exceeded so, the updating of the tangential stiffness matrix will have to be carried out on every single time step. This is particularly important as the consequence of failing to do this will lead to divergent responses and results will be very similar to that which occurred in the numerical unstable case (see Section 7.2.1.4).

To ensure convergency even after the onset of plasticity, the program also checks on the norm of the out-of-plane deflection increment $\Delta x = (\Delta f^t \cdot \Delta f)^{1/2}$. The load increment will be re-iterated once the maximum incremental displacement Δx exceeds 2% of the Euclidean norm of the total deflection ($x = (f^t \cdot f)^{1/2}$, see section 5.10).

The criterion that governs the plastic unloading once the stationary point has entered the yield surface has already been described in section 5.9. This is strictly required for all the dynamic buckling analysis since the loading and unloading condition of a stationary point is completely independent of the external loading/unloading condition.

Chart 2 contains a flow chart of the computational procedures.

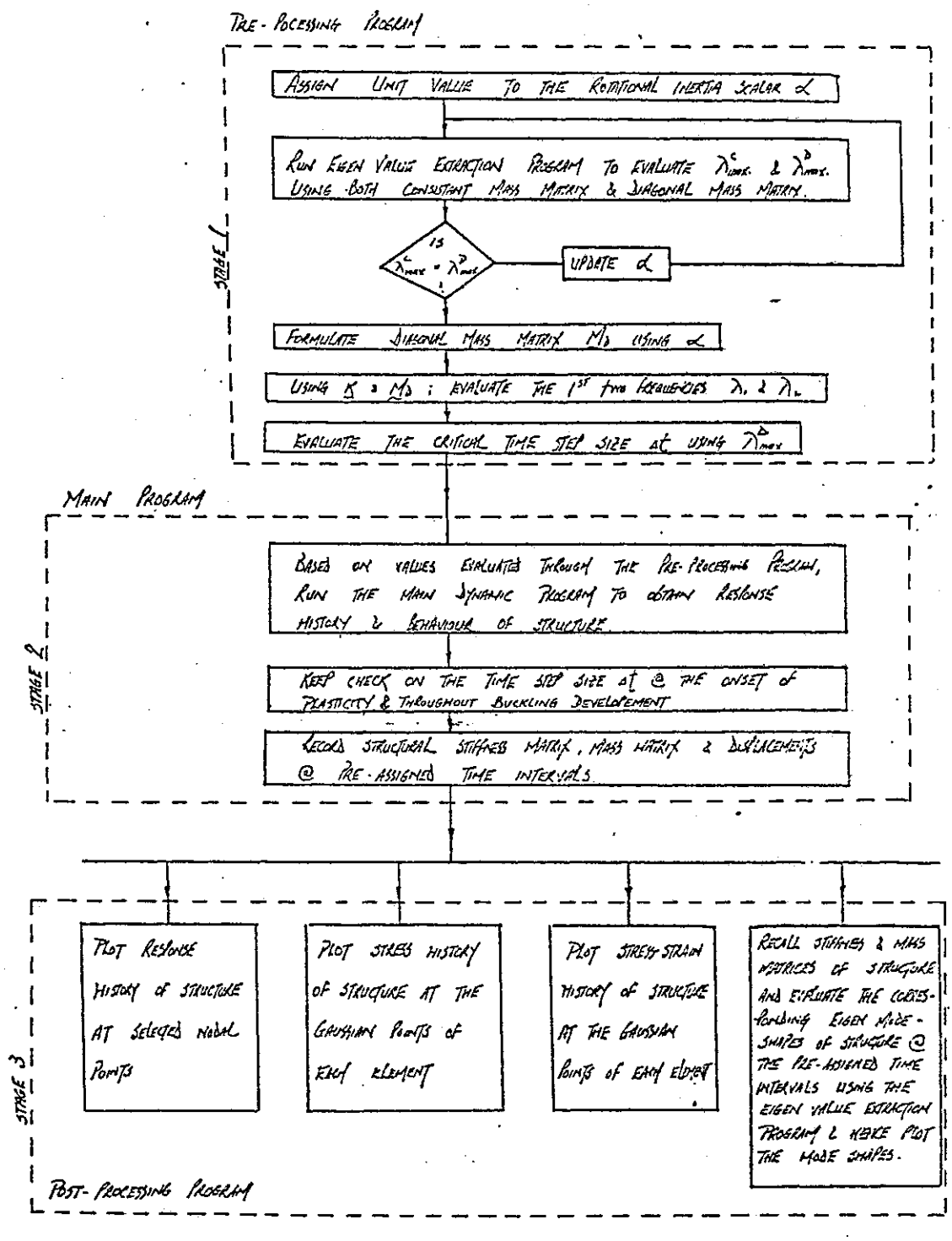

PRE-PROCESSING PROGRAM
ASSIGN UNIT VALUE TO THE ROTATIONAL INERTIA SCALAR α
RUN EIGEN VALUE EXTRACTION PROGRAM TO EVALUATE λ^c_max & λ^D_max USING BOTH CONSISTANT MASS MATRIX & DIAGONAL MASS MATRIX.
IS λ^c_max = λ^D_max ?
UPDATE α
FORMULATE DIAGONAL MASS MATRIX M_D USING α
USING K & M_D ; EVALUATE THE 1ST TWO FREQUENCIES λ1 & λ2
EVALUATE THE CRITICAL TIME STEP SIZE Δt USING λ^D_max
STAGE 1
MAIN PROGRAM
BASED ON VALUES EVALUATED THROUGH THE PRE-PROCESSING PROGRAM, RUN THE MAIN DYNAMIC PROGRAM TO OBTAIN RESPONSE HISTORY & BEHAVIOUR OF STRUCTURE.
KEEP CHECK ON THE TIME STEP SIZE Δt @ THE ONSET OF PLASTICITY & THROUGHOUT BUCKLING DEVELOPEMENT
RECORD STRUCTURAL STIFFNESS MATRIX, MASS MATRIX & DISPLACEMENTS @ PRE-ASSIGNED TIME INTERVALS
STAGE 2
PLOT RESPONSE HISTORY OF STRUCTURE AT SELECTED NODAL POINTS
PLOT STRESS HISTORY OF STRUCTURE AT THE GAUSSIAN POINTS OF EACH ELEMENT
PLOT STRESS-STRAIN HISTORY OF STRUCTURE AT THE GAUSSIAN POINTS OF EACH ELEMENT
RECALL STIFFNESS & MASS MATRICES OF STRUCTURE AND EVALUATE THE CORRESPONDING EIGEN MODE-SHAPES OF STRUCTURE @ THE PRE-ASSIGNED TIME INTERVALS USING THE EIGEN VALUE EXTRACTION PROGRAM & HENCE PLOT THE MODE SHAPES.
STAGE 3
POST-PROCESSING PROGRAM

CHART 2

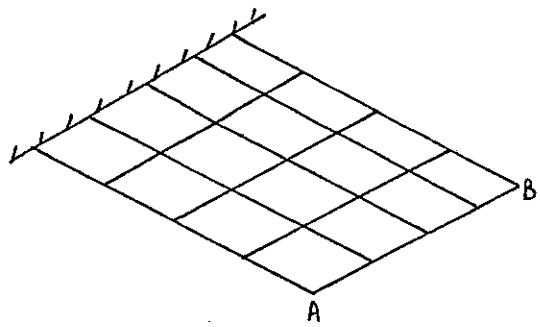
6.6 Dynamic Response Analysis Test (Comparison between the Newmark-β & Central Difference Methods

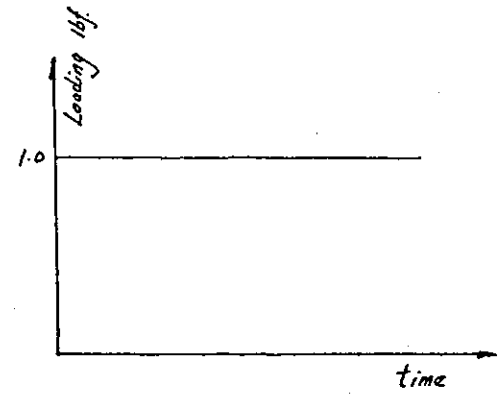
The structure employed in the test is a plate element with one end built-in and the properties of the plate are:-

$E = 10{,}000\ lb/in^2$ thickness = 0.1 in.

Poisson's ratio = 0.3 length of plate = 10 in.

width of plate = 2.5 in.





The variation of the frequencies of the system with different rotational gradient α is shown in Fig. 24. In that analysis, a rotational gradient of 1.45 is found to give exactly the same maximum frequency using the diagonal mass system as that obtained using the consistent mass matrix. The membrane mass matrix employed in this element contains no rotational terms and therefore is independent of the imposed rotational gradient α. The critical time step evaluated from the system is 0.00012 sec. for membrane response, and 0.0003 sec. for bending respose. On applying $\alpha = 1.45$ to the rotational terms on the diagonal mass matrix, the critical time evaluated from the membrane analysis was unchanged. However, in the linear bending response analysis, the critical time was found to be slightly less than the predicted value of 0.0003 sec. and is, in fact, reduced to 0.00028 sec. to

obtain numerical stability (about 90% of the predicted value). When non-linearity was included in the analysis, the time step employed in both bending and membrane analysis was reduced to 0.00012 sec. before numerical instability occurred.

Figs 25a and b show the linear dynamic response of points A and B in the system shown in the above diagram, using the Central Difference diagonal mass matrix method. Fig. 25a shows the displacement variation with time of that system. The maximum amplitude obtained was 0.6182 in. and the minimum obtained was 0.00035 in. The static deflection line is drawn to contrast the results and it was found that the evaluated displacements fluctuate between $\pm$ 0.31 in. from the static deflection line. The time taken for the system to complete one cycle was 0.61 sec. This agrees well with the theoretical maximum period of the structure using the diagonal mass matrix (see Tables in Fig. 24). The result exhibits a very slight artificial damping. The critical time step was found to be 0·00028 sec. to provide numerical stability. An attempt was also made to use a time step of 0.0003 sec. and was found that the result diverged after 250 time steps. The total number of time steps used in this analysis was 5,000 and the computing time used on the CDC 6500 was 86 sec. The velocities and accelerations are shown in Graph 8b and 8c respecively.

Figs. 26a and b show the linear dynamic response of points A and B for the same system, this time using the Newmark-β method with $\beta = 1/4$. Fig. 26a shows the displacement variation of the points with time. The maximum amplitude evaluatd was 0.6187 in., and the minimum 0.000057 in. The static deflection line is drawn to contrast the result and again it can be seen that the line is the mean of the fluctuating displacements. The time step used in this program was deliberately lower (0.00028 sec.) so that the results can be compared with those obtained using the Central Difference method. On using very large time steps of 0.002 sec. (Fig. 30a) and 0.02 sec. (Fig. 30b), the integration scheme also shows its

unconditional stability. The time taken to complete one cycle was found to be 0.5871 sec. which, when compared with the theoretical value of 0.591 sec., shows excellent agreement. The scheme also shows a very slight artificial damping. The total time step used in this analysis was 5,000 with a step size of 0.00028 sec. Total computing time used by the CDC 6500 was 478 sec. which is nearly 6 times longer than that used by the Central Difference diagonal mass method.

An analysis was carried out using the Central Difference integration scheme with a consistent mass matrix. The algorithm also required a critical time step of 0.00028 sec. A curve of the response is plotted on Fig. 27a. The results are exactly the same as those obtained using the Newmark-β method with $\beta = 1/4$. Displacement curves obtained by the above two methods are shown for comparison on Fig. 27a and are identical. Displacement curves obtained by the Central difference diagonal mass and consistent mass matrix are also plotted on Fig. 27b. Here, they show a frequency change, but the displacement amplitudes are unchanged. The frequency change is caused by the change of the lowest eigenvalue when lumping the mass matrix. As can be seen from the tables in Fig. 24, the lowest eigenvalues for the diagonal and consistent mass matrix were 106.6 and 112.9 respectively. There is also a slight difference in the highest eigen-values obtained by using the two Mass Matrices (see Fig.24).

Figs 29a and 29b show the displacement and velocity responses obtained using the Central Difference diagonal mass matrix and Newmark-β method with $\beta = 1/4$. In Fig. 29a the displacement curves obtained by the two methods do not exhibit any difference in magnitude and, in fact, where very slight artificial damping occurs, they both appeared to have the same damping. The frequency change occurring in this comparison appears to be the same as that in Fig. 27b. This is because the Newmark-β method with $\beta = 0$ is virtually the same algorithm as the Central Difference method using the consistent mass matrix. Fig. 29b shows the comparison between the velocity responses between the two algorithms, again they are very much alike except that a slight frequency change has occurred.

An analysis was carried out using an amplified rotation gradient α_a In this analysis, α_a was deliberately set to be equal to 7 (i.e. when lumping the mass matrix, the lumped rotation terms from the consistent mass matrix were multiplied by a factor of 5). On examining the maximum eigenvalue using such a lumped mass matrix, the maximum eigenvalue was found to be equal to 2.1×10^7. The corresponding critical time would be 0.00045 sec.; using 90% of the evaluated critical time would give a critical time step of 0.0004 sec. The displacement and velocity responses of the above analysis were plotted in Figs. 28a & 28b and were compared with those obtained in Fig. 25a and Fig. 25b.. Surprisingly, no significant differences were found except for a slight phase shift in the velocity and acceleration response curves.

Figs. 30a and b show the comparison of the displacement response using the Central Difference diagonal mass method and Newmark β method with $\beta = 1/4$. The time steps used were 0.00028 sec. and 0.002 sec. respectively. Fig. 30a shows that at a time step of 0.002 sec. (8 times the critical time), the Newmark β method exhibits the same response as that obtained using a time step of 0.00028 sec.

But when the time step size was increased to 0.02 sec. (80 times the critical time), the algorithm results in a very large phase shift (see Fig. 30b). [Notice that the displacement obtained by Newmark-β method at the end of the second cycle in Fig. 30a is lagging the displacement obtained by the Central Difference method, and the one on Fig. 30b is leading].

Membrane analyses using both Central Difference diagonal mass and Newmark-β methods were also carried out. The system is the same as the one used in the bending analysis, but the applied loads on points A and B are in-plane compressive loads. The static deflection obtained using the finite element analysis was 0.361 in. for both points. Figs. 31a to 31d show the dynamic responses of the system using the above described method under such loadings. As there is no rotational inertia in the membrane mass matrix, the critical time step followed strictly from the maximum eigenvalue obtained using the consistent mass matrix (0.00012 sec. Fig. 24). Again the lumping of the mass matrix causes a periodic time difference. Fig. 31a shows the frequency change between the two algorithms. The theoretical analysis shown in Fig. 24 gives the Newmark-β scheme a periodic time of 0.0221 sec. and the Central Difference Scheme a periodic time of 0.0221 sec.. On completing 5 cycles, the former method would take 0.107 sec. and the latter 0.1105 sec. On examining the displacement curves on Fig. 31a, the total time taken for the Newmark-β method to compute 5 cycles was found to be 0.105 sec., and that for the Central Difference diagonal mass method was 0.109 sec. The results show the great reliability and accuracy of the integration algorithm contained in this program. Figs. 31a and 31b show the membrane velocity and acceleration responses of the system using both methods, and again it is obvious that the results did not exhibit any significant difference.

Fig. 32a shows the displacement responses using the Central Difference diagonal mass method with and without the geometric nonlinearity effects respectively. For such small loading, the effects of the geometric non-linearity did not appear to have any significant contribution. No phase shifting occurred but the displacement magnitude using the nonlinear analysis was seen to be slightly less than that using the linear analysis. The time step used was only 0.00012 sec. which is the membrane critical time step. (When geometric non-linearity is considered, the coupling between the membrane and bending displacements requires the critical time step to follow the minimum obtained between the two analyses). The total computing time taken during the 5,000 integration steps was 1471 sec. on the CDC 6500. Much of this time was spent on forming the geometric stiffness matrix which was updated every 10 time steps.

Figs. 32 to 32c show the nonlinear displacement response with damping present. The critical time step was again 0.00012 sec. The damping ratios used were 10% and 20% respectively, and the first two lowest frequencies were chosen to obtain the constants α and β when evaluating the damping matrix $\underset{\sim}{C}$ using Equations (6.37) and (6.38). The displacement converges to the predicted static deflection when damping is included. Similarly, graphs 32b and 32c also show the velocity and acceleration of the system being damped down to static values (i.e. zero velocities and accelerations).

7. FULL ANALYSIS (STATIC AND DYNAMIC LOADING) ON THE B.A.C. DESIGNED STIFFENED PANEL

Sections 2 to 6 have shown in detail the necessary formulations and procedures involved in producing a mathematical tool to investigate an elasto-plastic dynamic buckling problem (primarily for a stiffened panel) using Finite Element approach. To this extent, a package based on the above formulations has also been written to compute the response of a stiffened plate when it is subject to either static or dynamic loadings. Details and the user's manual of this package are shown in Ref. (90). The package has, during the stage by stage analyses, been able to show great accuracies and close agreements with some existing results when it is performed on some simple model testings (Sections 2 to 6). However, since the ultimate purpose of the present analysis is to investigate the non-linear buckling behaviour and hence the collapse dynamic loading of a B.A.C. designed stiffened panel, it is therefore necessary to examine here the behaviour of this structure by applying the load both statically and dynamically. In this chapter, we will also predict the magnitude of a dynamic applied load which will cause the overall collapse of the above mentioned structure.

The configuration of the B.A.C. designed stiffened panel is shown in Diagram A below:-

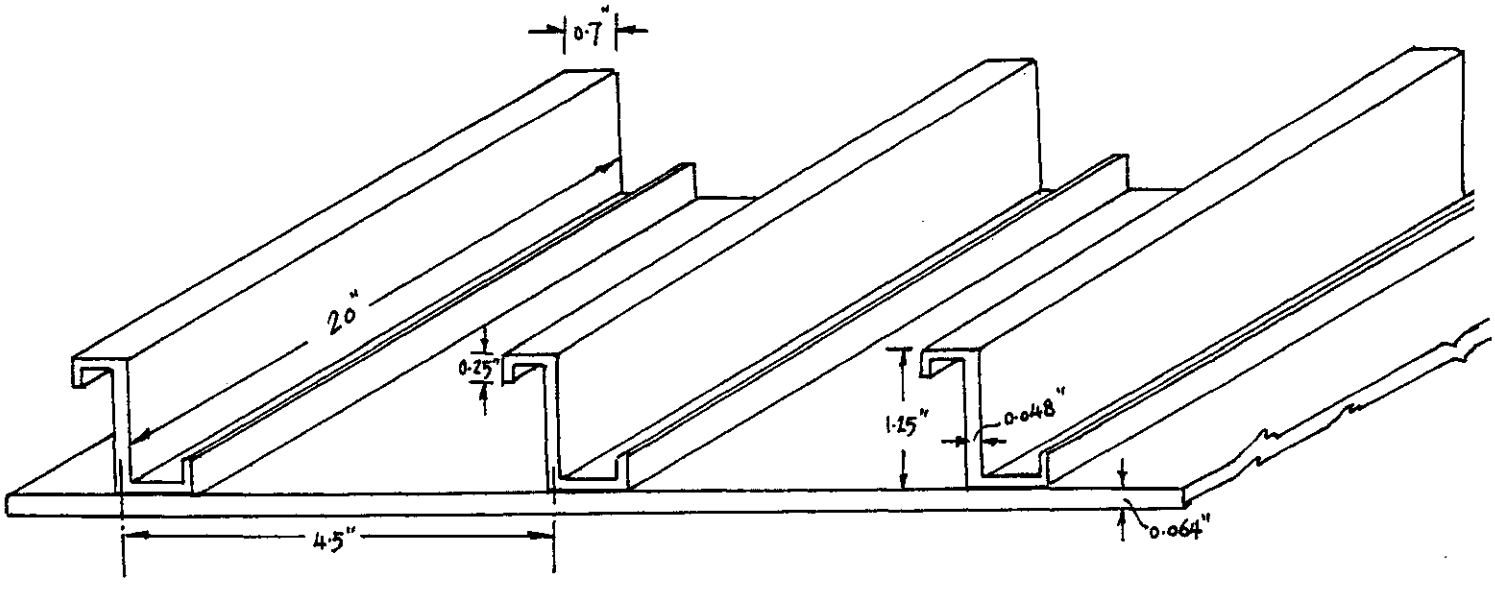


DIAGRAM A

The loading configuration is given by B.A.C. and is shown in Diagram B as:-

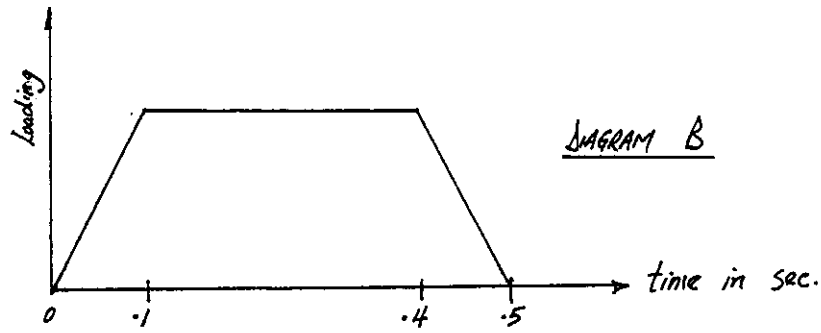


DIAGRAM B

The nodal positioning and the corresponding Gaussian Points for each of the elements are shown in Diagram C below.

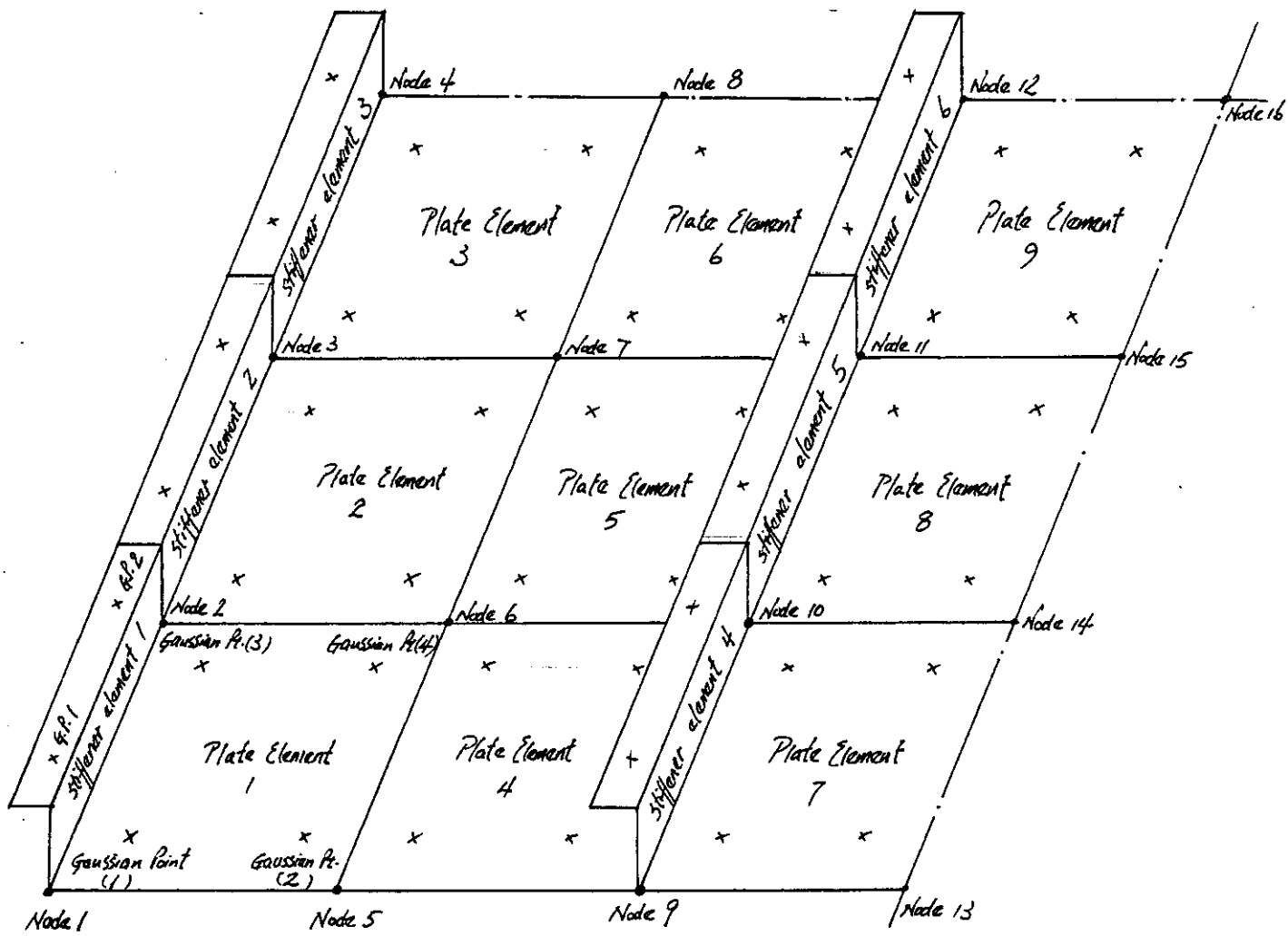
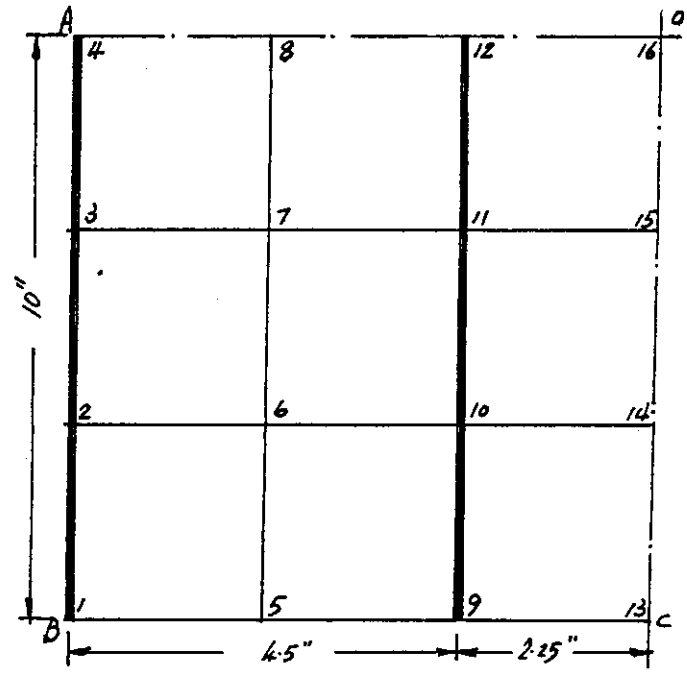


DIAGRAM C

The static local and overall buckling behaviour of the above mentioned stiffened panel have also been analysed using the Engineering Data Sheets. The calculation of which is shown in Appendix 2. These results are then used to check against the Finite Element results computed by the package. The following sections describe in detail the stage-by-stage analysis.

7.1 Static Buckling of the Stiffened Plate with B.A.C. design Criterion

In finite element analysis, the above structure is modelled as below:-



Lines of symmetry along OA & OC
Simply-supported @ edges AB & BC

Only one quarter of the plate is used because of the lines of symmetry on edge AO and OC . Bearing in mind the assumptions we have made in Section 1, we further assume that the structure is simply-supported along edge AB and BC, the following boundary conditions are imposed:-

Rotation dw/dy along OA and rotation dw/dx along edge OB are to be restrained.

Out-of-plane movements, w, along edges AB and BC are also restrained.

In-plane movements in Y-direction along OA together with in-plane movements in X-direction along OC are suppressed.

The uniformly distributed compressive edge loading is modelled in terms of a set of nodal forces ($F = \sigma \cdot b \cdot t$) applied on nodes 1, 5, 9 and 13 in the ratio of 1, 2, 2 and 1 respectively. In addition to these, another set of nodal forces is also applied to the nodes where the stiffeners are attached to. These forces, which are the product of the applied stress and the cross-sectional area of the stiffener ($F = \sigma \cdot A_s$), have to be transformed from the stiffener's local axis to the mid-plane of the plate before they are applied to the corresponding nodes. Details of the transformation procedures can be found in Appendix 1. Details of the model is shown in Diagram C.

The finite element analysis of the above model produces the following results:-

7.1.1 Elastic non-linear buckling of the stiffend plate

a) Incremental Load Method

The structure buckles at an applied stress level of around 8,400 lb/in^2. Comparing with the theoretical critical stress of 8,700 lb/in^2 which is evaluated by using the Engineering Data Sheet (Appendix 2), the finite element result is some 4% below the theoretical value. The discrepancy is mainly due to the absence of the torsional rotation terms when modelling the stiffeners. Nevertheless. this discrepancy level is still acceptable and it is quite evident that had this been included in the model, the result would be much closer to the theoretical value.

Fig. 33 shows the nodal load-displacement curves of the structure. It is noticed that local plate buckling takes place when the applied stress reaches 8,400 lb/in^2. Further load increments have enabled the plate elements to continue into their post-buckling state with their load displacement curves behaving very similar to that described in the previous section. The figure also shows that the buckling mode shape of the structure is identical to that shown in Fig. 34a (Fig. 34a is in fact plotted to illustrate the eigen value results which will be described in the next section).

b)Eigen-value Solution for Buckling

The buckling behaviour of a structure can alternatively be obtained by using an eigen value type of solution. However, in this section, the eigen value solution is used as an independent check on the results obtained from the incremental load method.

In this analysis, not only the buckling loads at various buckling levels are evaluated, the corresponding buckling modes are also plotted by using a 3-dimensional plotting package. The mode shapes

are expressed in terms of the evaluated eigen-vectors. Only transverse displacements are illustrated. The internal displacements of the plate elements are interpolated from the nodal values to give better definition.

The twelve buckling modes are plotted on Fig. 18a to Fig. 18l by using this 3-dimensional plotting package. Their corresponding critical stresses are tabulated as below:-

λi =	λ_1	λ_2	λ_3	λ_4	λ_5	λ_6	λ_7	λ_8	λ_9	λ_{10}	λ_{11}	λ_{12}
σ_{crit} (lb./in^2)	8,047	9,107	10,651	10,743	14,773	15,247	15,600	17,967	18,337	19,602	28,994	32,915

where λi represents the critical stress in the ith buckling mode.

All the above critical stresses are evaluated based on the configuration of the deformed structure at an applied stress level of 1,000 lb/in^2. The above shows that the first critical stress is 8,047 lb/in^2 which is very close to that obtained by the incremental load method. Fig. 34a also shows that the buckling wave length of the structure is about $\frac{1}{3}$ of the plate length, which agrees with the results found previously. At the line which represents the stiffener, it remains almost straight. This indicates that only local plate buckling has occurred and that the stiffener has not buckled yet. Mode 2 to Mode 10 (Fig. 34b to Fig. 34j) show the different buckling modes of the structure. In all those 10 cases, the stiffener has not buckled at all even though slight bending may be present. Fig. 18k shows the 11th mode of buckling which corresponds to an applied stress of 28,994 ln/in^2. In this figure, significant bending is found on the line which represents the stiffener. This shows evidently that the stiffener has buckled at this stress level. The result agrees very well with that obtained by using Engineering Data Sheet (σ_{crit} = 28,222 lb/in^2 for a perfect stringer without any load shedding, see Appendix 2). Also in that section, we have mentioned that the

stiffener would then be buckled at a slightly lower stress level (22,890 lb/in^2, see Appendix 2) due to the fact that some loads would have been shedded into the near-by stiffener during the post-buckling of the plate elements. However, our present eigen-value analysis is based on the deformation of the structure at an initial perturbation of 1,000 lb/in, and therefore it will not take into account any load shedding that would otherwise incur from the local plate buckling.

Both results, which are derived from the incremental load method and the eigen-value solution method, demonstrate the correlation between the finite element method and the analytical method.

7.1.2 Elasto-Plastic Buckling of the Stiffened Plate

The same stiffened plate as that described in section 7 is used. Incremental load method is employed and uniformly distributed edge loadings are applied until the applied stress has reached 16,800 lb/in^2. Fig. 35 shows the load-displacement behaviour of 9 selected nodes of the structure. On examining Fig. 35, the following results are observed:-

Prior to the local buckling of the plate element, the structure behaves exactly the same as that described in section 7.1.2 (b). After the structure has entered into the post-buckling stage, the deflections of all the elements are largely dominated by the non-linear large displacement effect. Due to the formation of the buckling waves, some nodal points in the plate elements are deflected in an opposite direction during the post-buckling stage (noticeably nodes 6, 14 and 15 and all the nodes where the stiffener is attached). The nodal deflections shown in Fig. 35

also suggest that when the applied stress has reached 10,000 lb/in^2, the wave length is about $\frac{2}{3}$ of the plate length in contrast with the wave length of $\frac{1}{3}$ of the plate length when the first critical stress is reached. This agrees very well with Fig. 34b which shows the 2nd buckling mode shape of the structure (σ_2 = 9,107 lb/in^2).

The stress-strain curves of some of the plate elements which have exceeded yielding are shown in Figs. 36a to 36d. The elements to which these curves correspond are drawn on the top of each figure. The following table lists the state of plasticity, the applied stress level at which plasticity was first detected and the maximum equivalent stress at the corresponding Gaussian points:-

Element No.	Figure No.	Maximum Equivalent stress recorded at top or bottom surfaces of the following Gaussian points at an applied stress level of 16,480 lb/sq.in.				State of Plasticity	Applied stress level @ 1st yield
		G.P.1	G.P.2	G.P.3	G.P.4		
1	22a	31,500	32,000	33,100	26,500	Yes	16,480
2	22b	30,000	26,000	32,000	31,000	No	/
3	22c	24,100	29,500	17,500	18,500	No	/
4	22d	30,500	30,000	38,500	34,000	Yes	14,080
5	22e	18,500	30,000	30,000	26,000	No	/
6	22f	16,000	30,800	25,000	26,000	No	/
7	22g	38,500	34,000	18,000	37,500	Yes	14,080
8	22h	30,000	29,200	29,000	32,000	No	/
9	22i	25,500	34,000	22,000	24,000	Yes	16,480

The above table shows that plasticity had taken place on elements 4 and 7 when the applied stress level reached 14,080 lb/in^2. The corresponding loading per unit width of the structure at the 14,080 lb/in^2 and 16,480 lb/in^2 applied stress levels are 1425.64 lb and 1680.21 lb respectively.

The stresses shown in the above table only highlight the maximum equivalent stresses at either surface of the corresponding plate elements. The equivalent stresses at the mid-plane of these plate elements are shown in the following table:-

Element No.	Equivalent stresses recorded at the mid-plane of the plate at the following Gaussian points when applied stress level reached 16,480 lb/sq.in.				State of Plast-icity
	G.P.1	G.P.2	G.P.3	G.P.4	
1	20,365	10,671	18,979	9,719	No
2	17,786	8,129	20,770	16,966	No
3	16,311	10,644	18,119	11,538	No
4	14,630	16,775	12,394	22,374	No
5	6,952	18,841	16,923	21,664	No
6	9,052	19,226	17,698	18,839	No
7	12,268	10,130	23,206	17,178	No
8	19,576	10,882	22,062	18,563	No
9	19,916	11,000	18,515	15,190	No

No plasticity was detected across the mid-plane of the plate.

7.2 Dynamic Loading Analysis

The model employed throughout the dynamic analysis is the one used in the static loading analysis (Diagram C in section 7), configuration of which has already been described in Appendix 2. The purpose of the present analysis is to study:-

1) The response of the structure at different loading magnitudes.

2) The behaviour of the structure due to the presence of plasticity.

3) The overall behaviour of the structure when a stress level, which, when applied statically, would cause the structure to begin to yield, is applied dynamically along the edge of the structure.

4) The final deformation of the structure after plasticity has taken place.

The first part of this analysis examines the elastic response of the stiffened plate where only non-linearities due to geometry changes are included. Also in one of the analyses, the stiffness matrix of the structure is updated only once every 40 time steps to see if so doing would affect the response behaviour of the structure to any significant extent (updating the stiffness matrix once every time step would be extremely expensive especially when the whole loading procedure involves something like 5,000 time steps).

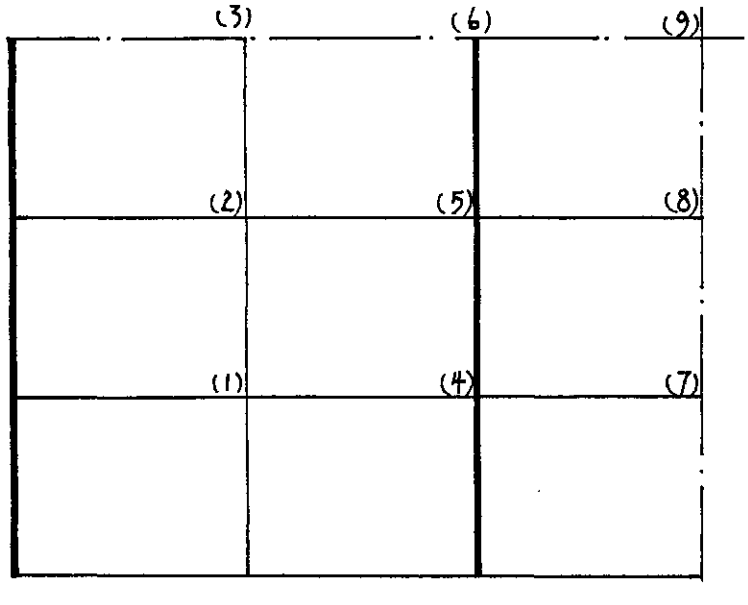
The second part of the analysis examines the elasto-plastic behaviour of the structure.

While running the dynamic program, the results are recorded at a regular interval regardless of the state of response. Therefore it is likely that some relevant information may be missing out. This will be explained in detail when we examine the results.

The following paragraphs explain the presentation of the results:-

1) <u>The out-of-plane displacement history of the 9 selected nodes on the stiffened plate</u>

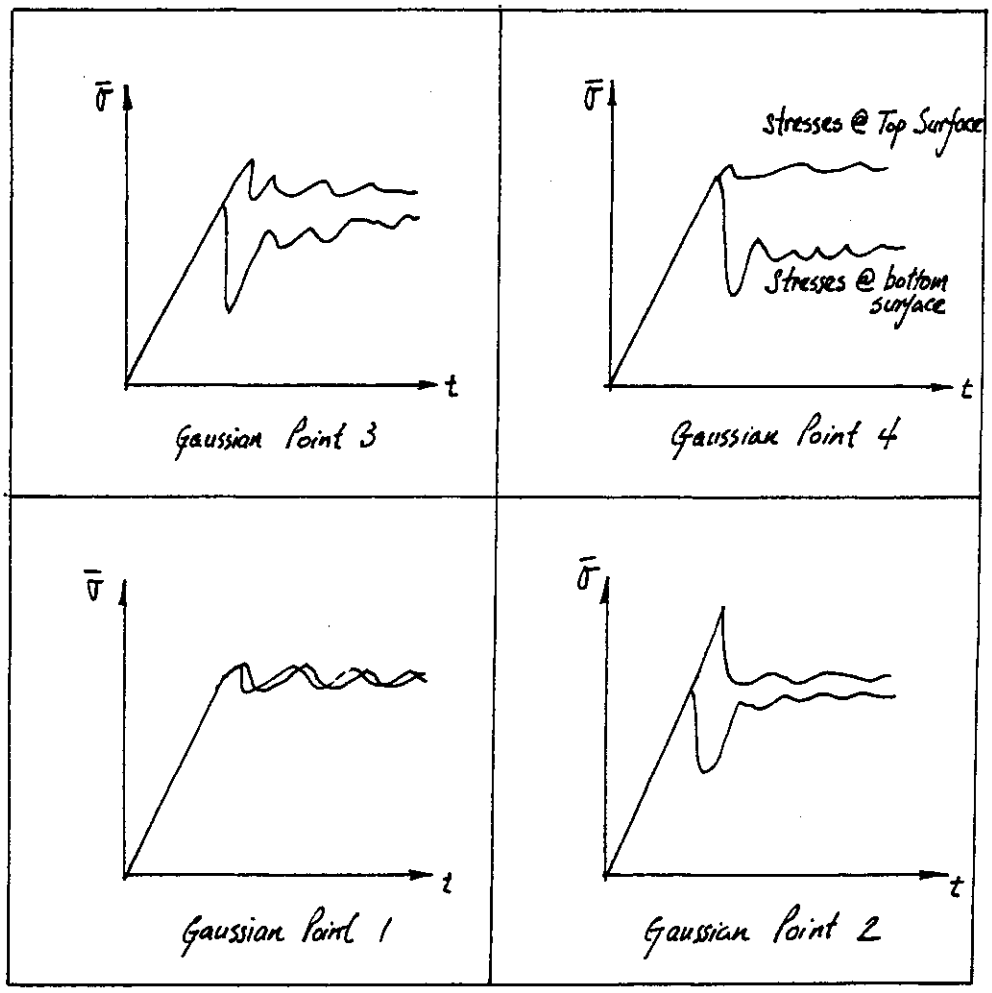
These 9 nodes are shown in the following diagram:-



Out-of-plane displacements at the supported edges are ignored.

2) Stress history of the plate elements (equivalent stresses)

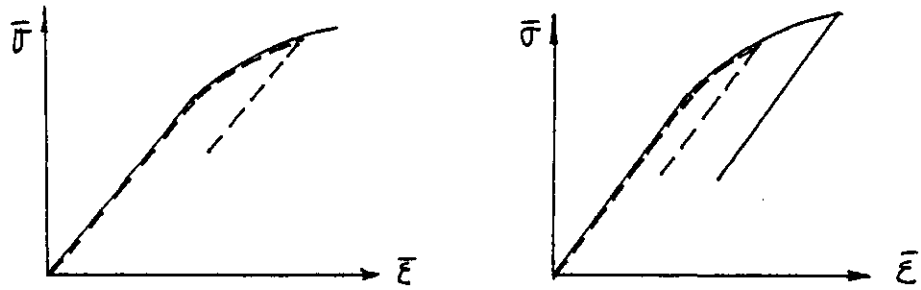
The stress history in each plate element is plotted out in a set of 4 frames. Each frame consists of 2 curves; each representing the stress history of the top and bottom surfaces of the corresponding Gaussian point. Thus, they are presented in the following manner:-



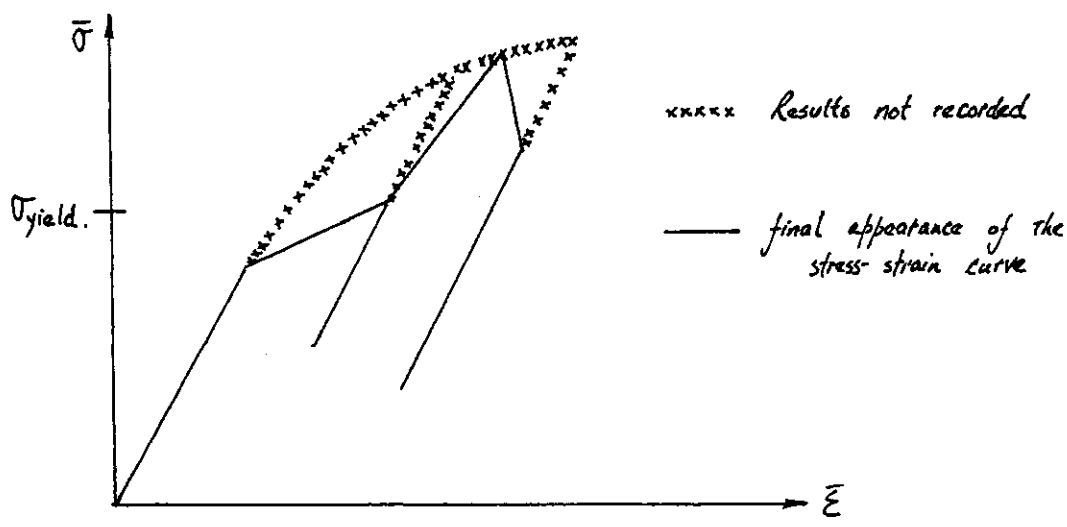
Not all peak stresses will be shown because of the extended time intervals between successive points on the graphs. Therefore the stress history graphs will fail to denote whether or not the element has reached the yield stress level, especially in the marginal cases.

3) The stress-strain curves of the plate elements

These curves are plotted out in the same format as that described in paragraph 2 except that during most of the elastic response, only one curve will appear in the corresponding frame. This is because despite the fact that the actual stress levels at the top and bottom plate may not be the same, nevertheless their stress-strain ratios should remain unchanged. Therefore, the two stress-strain curves will overlap each other in most of the time except when one surface is in its elastic unloading, or, when the two surfaces follow different elastic unloading paths as shown in diagrams below:-



The results are plotted only once every 40 time steps. This explains the 'odd' appearance often found in the stress-strain curves as illustrated in the following diagram:-



(Note that the stress-strain curves are only plotted in the second part of the analysis where the elasto-plastic behaviour of the structure is studied.)

4) The stress history and the stress-strain curves of the stiffener elements

The format of these is similar to those mentioned in paragraphs 2 and 3 except that only 2 frames appear in each plot. This is because there are only 2 Gaussian points within each stiffener element.

5) The displacement mode shapes of the structure at various loading/unloading stages

The plates are assumed to have uniform base grids and hence the in-plane displacements of the elements are ignored. When running the dynamic program, the nodal out-of-plane displacements and rotations of the required modes are stored out of core. After the program is finished, a 3-D plotting package is then used to retrieve the stored information. To enable a finer display, extra grids and hence extra out-of-plane displacements are interpolated within each element (see section 7.1.2(b)). Before plotting commences, the nodal out-of-plane displacements are normalised. The effect of this is to normalise the maximum out-of-plane deformation to the same value.

6) The direct stress history curves of the plate element in X and Y directions

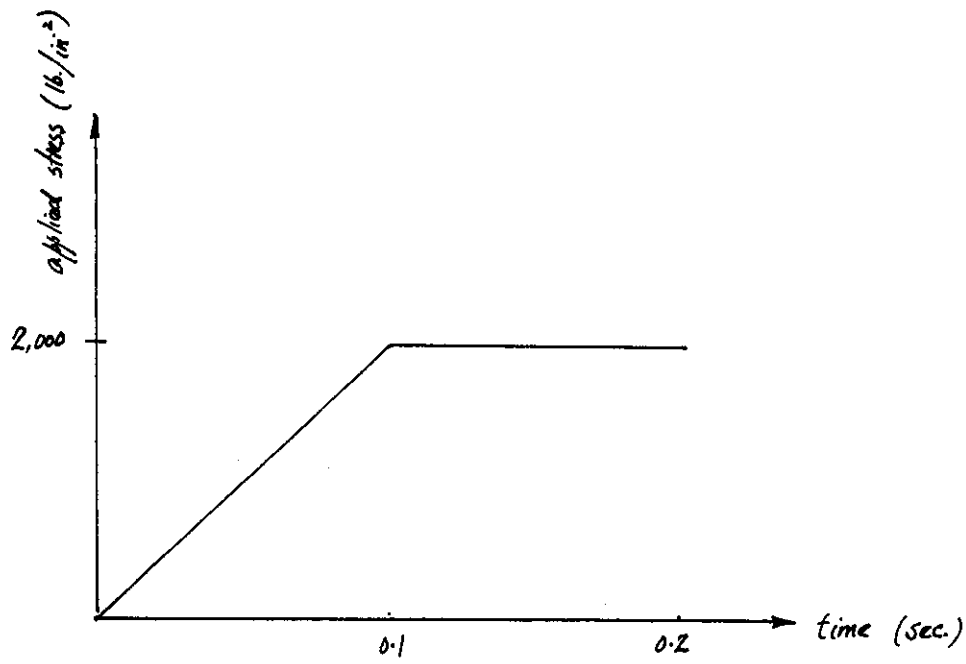
The formats of these curves are exactly the same as those described in paragraph 2 except that for each plate element, there will be two plots; one shows the direct stresses in the direction of the applied load (Y-direction) while the other shows the direct

stresses in the direction perpendicular to the applied load (X-direction).

7.2.1 Elastic responses of the stiffened plate subject to dynamic loading

In the following analysis, the material yield stress level is deliberately raised to about 10 times the otherwise true material yield stress level so that plasticity would not take place even though the structure might have exceeded the yield stress level. The following paragraphs summarise the behaviour of the structure when subject to different loading magnitudes.

7.2.1.1 Total applied stress level = 2,000 lb/sq.in.



The response histories of the 9 selected nodes are shown in Fig. 37a. Throughout the loading period, all the nodal displacements vary linearly with the applied load. After the loading has reached the maximum, the displacements are seen to oscillate constantly along a mean displacement level. Fig. 37a also shows that, throughout the entire loading period, the structure is oscillating with a frequency equal to the structure's own natural frequency which is approximately 16 HZ. (Ref. (91)).

The applied stress level in the analysis is still relatively low. Although slight bending stresses might have been present, there is no sign that the structure has suffered from buckling at all. The stresses within the structure are very close, if not exactly equal, to the applied stresses. Fig. 37b shows the typical stress history of one of the elements. It can be seen from this figure that the stress history curves at the top and bottom surfaces of the plates are overlapping with each other indicating that no significant bending stresses have taken place.

Fig. 38 shows the typical stress history of the stiffener elements. Again, these curves show that no significant bending has taken place in these stiffeners.

Fig. 39 shows the displacement mode shapes of the structure at some random intervals throughout the entire loading history. Disp.1 to Disp.3 in this figure shows the deformation of the structure during the early stage of loading. The final deformation of the structure is shown in Disp.4 and onwards. It can be seen from this figure that the structure is quite stable at this load level.

7.2.1.2Total applied stress level = 8,000 lb/sq.in.

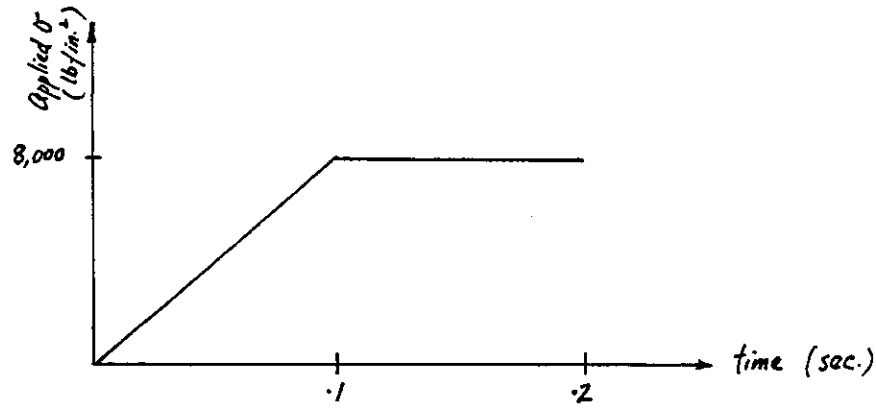


Fig. 40a shows the displacement histories of the structure. It can be seen from this figure that all the nodal deflections have experienced a sudden 'peak' at around 0.16 sec. This indicates that the structure has already suffered from buckling (this buckling may not necessarily be the overall buckling, and indeed, as in this case, it was only a local plate buckling).
Before local buckling occurs, the structure behaves very much the same as that found in the previous case. After local buckling has occurred, the mode shape of the structure is identical to the 1st buckling mode found in the static analysis (Fig. 34). Fig. 40a also shows that the response of the structure is dominated by a frequency which is equal to its fundamental natural frequency.

Fig. 40b shows the typical histories of a plate element. Prior to the occurrence of local plate buckling, the stresses at the top and bottom surfaces of the plate elements are so close to each other that their stress curves can hardly be distinguished at all. Soon after local plate buckling has occurred, the bending stresses in the two extreme surfaces become quite significant. The wide 'gap' that appears between the two stress curves indicates the level of these bending stresses.

Slight divergency has been detected from some stress-history curves as well as the response curves. This could have been caused by the lack of updating the stiffness matrix in every time step (currently, it is updated only once every 40 time steps). We will re-examine this in more detail further along the chapter.

Fig. 40c shows the typical stress history curves of a stiffener element. Again, the figure shows that significant bending has taken place in the stiffeners when local buckling of the near-by plate elements occurs.

Fig. 41 shows the displacement mode shapes of the structure at some random intervals throughout the whole loading history. Disp.1 to Disp.4 shows the deformation of the structure at the very early stage of loading while Disp.5 to Disp.12 shows the deformation of the structure prior to the local plate buckling. Disp.13 to Disp.14 shows the step-by-step deformation of the structure when local plate buckling takes place. These two modes were recorded at 0.13 sec. and 0.16 sec. respectively. These coincide with the occurrence of the sudden 'peak' found in the displacement history curves mentioned at the beginning of this section. Deformations of the structure in the post-buckling period are shown in Disp. 15 to Disp. 26. It can be seen from these pictures that the structural responses are dominated by the 1st local buckling mode.

7.2.1.3 Total applied stress level= 10,000 lb/sq. in.

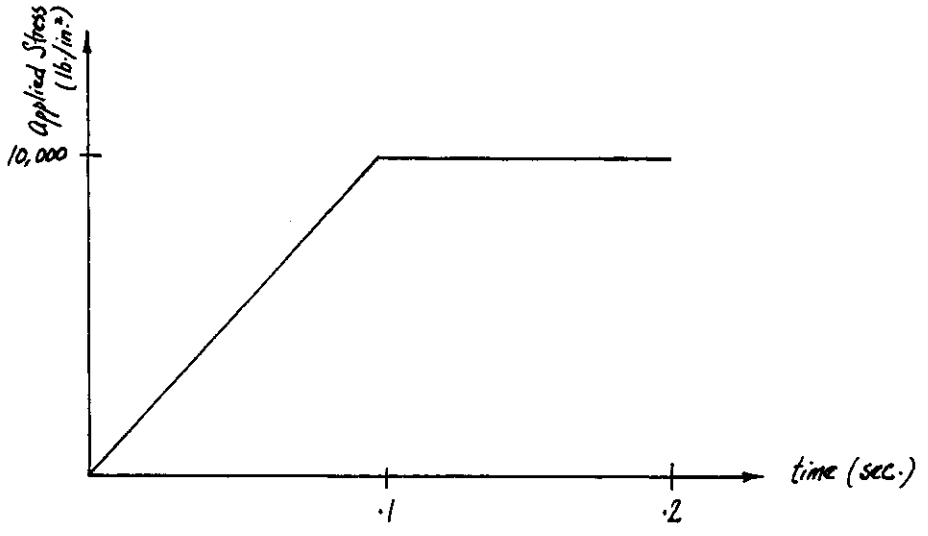


Fig. 42a shows the displacement history of the structure. It is noticed that all the displacements are peaking at 0.12 sec. This shows that local plate buckling has taken place slightly earlier than the previous loading case. It is also noticed that the responses at most nodes are largely dominated by the structure's first natural frequency even though some higher frequencies are also present.

Fig. 42b shows the typical stress history of a plate element. Bending stresses are noticed in most elements. Equivalent stresses at the top and bottom surfaces are found to be varying between 12,000 and 24,000 lb/in^2 in most plate elements except elements 4 and 7 where stresses at some stationary points are found to be as high as 32,000 lb/in^2. These stationary points are situated very near to both the stiffener and the loading edge. Therefore, the relatively high stresses are caused by the following two factors:-

i) the building up of shear stresses between the plate and the nearby stiffener;

ii) the inertia effect of the plate element when the load is applied dynamically.

Despite their relatively high stress level (32,000 lb/in^2 on one occasion), no stresses have exceeded the material yield stress level.

Fig. 42c shows a typical stress history of the stiffener elements. It can be seen from this figure that large bending stresses may have been formed after local plate buckling has occurred.

In the above 3 figures, they all show a substantial level of divergency. This could, as we have explained before, be caused by the structural stiffness matrix not being updated frequently enough during the running of the dynamic program.

Fig. 43 shows the sequence of the displacement mode shapes of the structure throughout the entire loading history. Disp.11 and Disp.12 show the mode shape changes when local plate buckling occurs (at 0.12 sec.). Before loading is removed, Disp.13 and onwards show that the structure remains in the same buckling mode.

7.2.1.4 Importance of updating the stiffness matrix more frequently

Results in the previous loading case have already shown that the tangential stiffness matrix should be updated in every time step despite the expensive running cost. To substantiate this fact, a separate analysis has been carried out with the structure's tangential stiffness matrix updated only once every 40 time steps. Loading is applied to the structure until it has reached its maximum level. Unloading then takes place immediately until the structure is completely free of any external load. No permanent deformation should have occurred because of our purely elastic assumption.

Fig. 44a shows its displacement responses. It is noticed that when unloading has completed, most nodal points are left with a 'residual displacement' which should not have occurred anyway. Fig. 44b shows the typical stress history curves of a plate element. Again, on completion of the unloading, 'residual stresses' are also found in most stationary points.

The above analysis has clearly demonstrated the significance of the accumulated numerical errors due to a second level of numerical instability. This secondary numerical instability becomes very sensitive especially when buckling occurs. It is therefore essential that during this period, the structural tangential stiffness matrix should be updated more frequently so that the growth of these numerical errors can be avoided. It is due to this reason that in all future analyses, the structure's tangential stiffness matrix will be updated once in every single time step.

7.2.1.5 Total applied stress level = 12,000 lb./ sq. in.

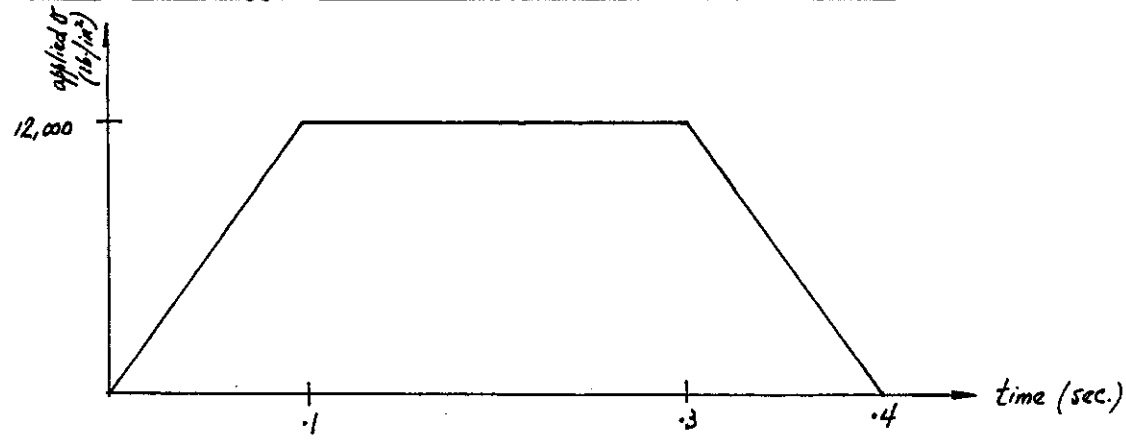


Fig. 45a shows the response history of the structure. Some sign changes are noticed in some of the nodal deflections during the constant loading stage. However, these changes agree with those found in the static loading analysis (see Fig.35). It can also be noticed in this figure that all the nodal displacements are 'peaking' at approximately 0.1 sec. On unloading the structure, it is found that the 'residual displacements' described in the previous loading case have disappeared completely here. This again shows the important phenomenon which has been described in the previous section. Slight oscillations are found throughout the no loading period, this is due to the absence of the external damping.

Figs. 45b and 45c show the stress history curves of plate elements 4 and 7 respectively. The stresses in the other plate elements are generally low. However, some areas in the above two elements have experienced stresses which are above the material yield stress level. These are found at Gaussian Point 2 of element 4 and Gaussian Point 1 of element 7. Again, no 'residual stresses' are found at any of the stationary points when the structure is completely removed from the external load.

Fig. 45d shows the typical stress history curves of a stiffener element. Stresses in other stiffener elements are still relatively low and they are still well below the yield stress level.

Figs. 45e, 45f, 45g and 45h show the direct stress histories of elements 4 and 7 in both X and Y directions. It is noticed that at the 2 Gaussian Points where their equivalent stresses are found to have exceeded the 32,000 lb/in^2 level, their direct stresses in the direction of the applied load are only about 24,000 lb/in^2. Thus, it is evident that significant amount of shear stresses must have been developed there.

The displacement modes for this loading case are exactly the same as those that wil be described in section 7.2.2.2, and will not be shown in here.

7.2.1.6 Short discussion on the elastic dynamic buckling results

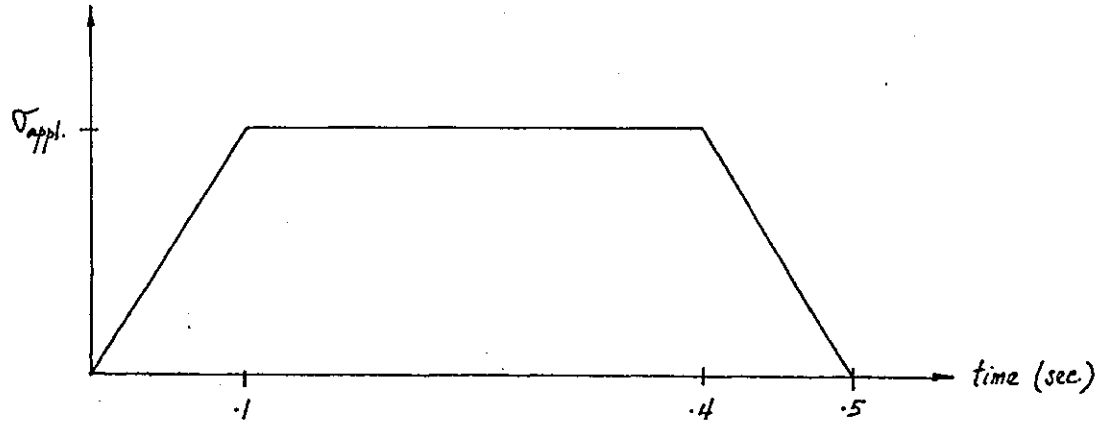
The results in the above 4 loading cases have shown that when loading is applied dynamically, the structure will generally suffer from a higher stress level than it would have been if loading was applied statically. At an applied stress level of 8,000 lb/in^2, the structure has clearly suffered from local buckling. There is no question that one can achieve the same result even with a slightly lower applied stress level.

At an applied stress level of 12,000 lb/in^2, some parts of the structure have exceeded the material yield stress level. The analyses also show that failing to update the structure's tangential stiffness matrix at every time step, especially when buckling begins, will lead to the growth of a secondary numerical instability which will eventually lead to a meaningless result.

7.2.2 Elasto-plastic responses of the stiffened plate when subject to dynamic loading

In all the analyses shown as follows, the material yield stress is set to 33,000 lb/in^2.. The initial time step size used in each analysis is 0.0009 sec., and is subjected to constant changes throughout that analysis depending on the significance of the influences of the material and geometry changes in the structure(see section 6.2) .

The given loading configuration is shown in the following diagram:-



However, during the analyses, unloading often takes place sooner than 0.4 sec. This is because in most cases, the stresses within the structure often die down to a lower level once they have reached their peak levels. These peak stresses normally take place at

the very early stage of the constant loading period. Therefore keeping the constant loading for too long a period will certainly not aggravate the response of the system, but to add extra cost to the running of the dynamic program. Therefore, in all the analyses as follows, unloading will begin at roughly 0.1 sec. after the stresses have reached their peak levels.

External damping which amounts to about 10% of the critical damping ratio is then applied to the structure immediately after unloading has completed. This is to damp out any unnecessary oscillations during the load-free period so that the permanent deformation of the structure due to the formation of plasticity can be studied.

Results are recorded once every 40 time steps prior to the completion of unloading, and they are recorded only once every 100 time steps thereafter.

7.2.2.1 Uniform tensile stress = 33,000 lb/sq.in. (this test is to investigate the program's capability of handling the dynamic plasticity

The structure is subject to a dynamic tensile load which is applied in 0.01 sec. To simulate the tensile loading condition, the structure is built-in along its half length line.

Fig. 46 shows the in-plane displacement response of the structure. This figure shows that in-plane displacements in all nodal points continue to grow even when the applied load has ceased. This continues for a short while until they have over-shot the equilibrium position. From 0.018 sec. to 0.04 sec., the structure behaves very much as a spring oscillating about its equilibrium position. During this period, more and more stationary points within the structure have exceeded the yield stress level.Finally,

when every stationary points have exceeded the yield stress level, the nodal displacements become unstable.

Fig. 47 shows the stress-strain curves in one of the plate elements. It can be seen that the structure has at one stage exceeded the 41,000 lb/in^2 level before elastic unloading takes place.

The above figure has clearly demonstrated the capability of the program in determining the internal plastic loading/elastic unloading which is completely independent of any external loading criteria.

7.2.2.2 Total applied stress level = 12,000 lb/sq.in.

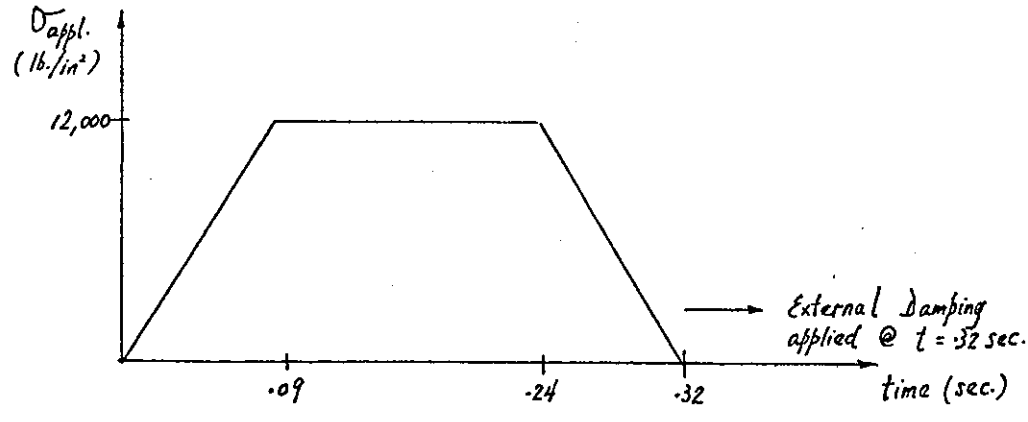


Fig. 48a shows the response history of the structure. Prior to the onset of plasticity, the structure behaves almost the same as it has been in the previous loading case (section 7.2.1.4) where plasticity is prevented. After the onset of the local plate buckling, the maximum eigen value of the stucture rises by about 8-10% which means that the time step size has to be reduced by the same proportion to 0.0008 sec. in order to satisfy the numerical instability requirement. When comparing Fig. 48a with Fig. 45a we would notice that the presence of plasticity has changed some of the nodal response amplitudes. Nodes 1, 4 and 7 are where these changes can be distinguished. Some deformation mode changes during the

constant loading period are also observed. The application of external damping at the end of unloading has resulted in all the nodal oscillations being damped out. Most of the nodes in the plate elements are left with a permanent deformation which varies between 0.004" and 0.001". This indicates the presence of plastic strains within the system. However, the level of permanent deformation is still relatively small comparing with the plate thickness (about 16% of the plate thickness). While most of the plate elements have suffered from permanent deformation, yet, no evidence of permanent deformation is found in any of the stiffener elements. Obviously this is due to the fact that no plasticity has taken place in any of the stiffener elements.

Fig. 48b and Fig. 48c show the equivalent stress-history curves of elements 4 and 7 respectively. Although some peak stresses may have been missed out due to the way that the data is recorded (see beginning of section 7.2), the stress responses on both figures are almost identical to Figs. 45b and 45c. This somehow indicates that the effect of plasticity is insignificant to the response of the structure under this load magnitude. Stresses at the other plate elements vary between 8,000 lb/in^2 and 24,000 lb/in^2 and they are not shown in here. Stresses at all stationary points have died down to a slightly lower level once they have reached their peaks.

Figs. 49a and 49b show the stress-strain curves of the plate elements. Where necessary, some dotted lines are introduced onto these curves to retrace the missing data so that a true stress-strain curve can be reproduced.

Stresses in the stiffener elements are unaffected by the presence of plasticity found in the plate elements. Fig. 50 shows that the stresses in stiffener element 4 is almost identical to those shown in Fig.45d.

In Fig. 51 there is a series of pictures showing the sequence of deformation of the structure throughout the whole loading history. Picture 1 to Picture 11 show the step-by-step deformation of the structure prior to the local plate buckling. Picture 12 to Picture 13 show the deformation of the structure during the local plate buckling. Picture 14 to Picture 78 show the deformation of the structure throughout the rest of the loading history. At the end of the loading period, the presence of the external damping has reduced most of the nodal oscillations (e.g. Pictures 92 to 99). The final deformation of the structure is shown in Picture 99. Some local oscillations are amplified in most of these pictures, this is due to the built-in normalising effect when using the 3-dimensional plotting package.

7.2.2.3 Total applied stress = 14,500 lb/sq.in.

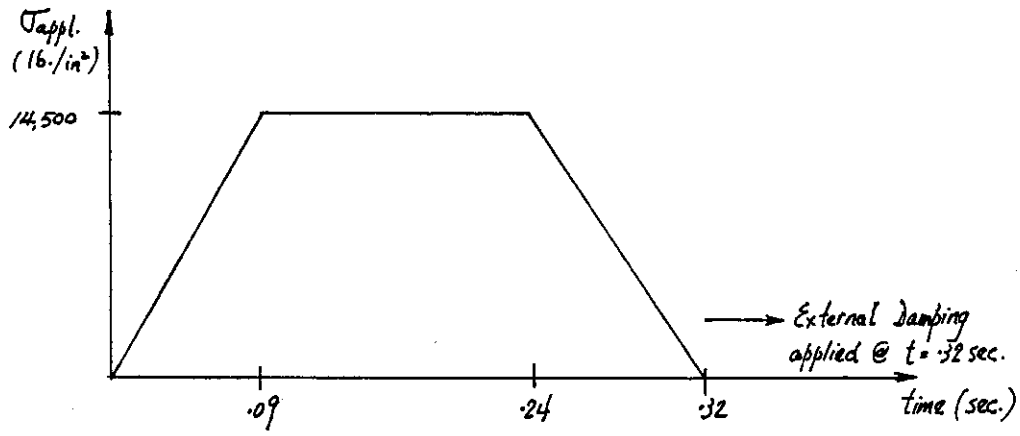


Fig. 52a shows the response of the structure.

Fig. 52b to Fig. 52g show the equivalent stress histories of the plate elements while Fig. 53a to Fig. 53f show their corresponding stress-strain curves. Where necessary, some dotted lines have been inserted onto these curves so that their complete stress-strain paths can be illustrated. Large parts of the plate elements are noticed to have exceeded the material yield stress level.

Fig. 54a shows the stress histories of stiffener elements 4 while Fig. 54b show their stress-strain

curves. Here, we have noticed that stiffener element 4 has exceeded the material yield stress level.

The following paragraphs examine the behaviour of the individual elements within the structure:-

Plate Elements

Element 1 (Fig. 52b & Fig. 53a)

Fig. 52b shows that Gaussian Point 2 has twice entered into the plastic region. It happens first at 0.1 sec. and then followed by an elastic unloading. Elastic loading then occurs shortly afterwards until it exceeds its previous maximum stress level of 33,500 lb/in^2 before it enters into plastic loading again at 0.12 sec. The following two diagrams explain the stress-strain behaviour in this Gaussian Point:-

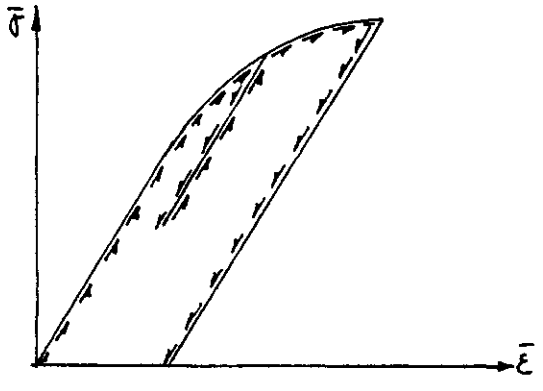


Diagram of the true stress-strain curve which has twice entered into plastic loading

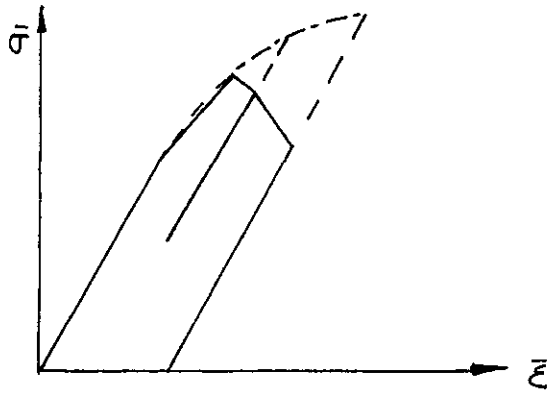


Diagram of the plotted stress-strain curve with some results missed out during recording

Stress in the other Gaussian Points are still quite high even though they haven't yet exceeded the yield level.

Element 2

Most stresses are peaking within the first 0.04 sec. during the constant loading period except at Gaussian Point 4 where the stresses are peaking at a much later stage. However, no stresses have exceeded the material yield stress level.

Element 3

The stresses are generally lower than those in element 2. Although most stresses are peaking at a much later stage, they have not reached the material yield level at all. Generally speaking, they behave very much the same as those in element 2.

Element 4 (Fig. 52c & Fig. 53b)

Two Gaussian Points (2 and 4) have exceeded the yield stress level. In particular, both top and bottom surfaces of Gaussian Point 2 have exceeded the yield stress level. It is worth noting that during the previous loading case (12,000 lb/in^2), the same stationary point has also experienced yield. The present loading, which is some 20% higher than the previous one, causes the growth of plasticity at this Gaussian Point to even further until finally, a plastic hinge is formed. Stresses in the rest of the element are generally higher than those found in Elements 2 and 3.

Element 5

Stresses in this element are very similar to those obtained in Elements 2 and 3 which have already been described above.

Element 6 (Fig. 52d & Fig. 53c)

Yielding has occurred at Gaussian Points 3 and 4 at around 0.11 sec. Soon after that, the stress behaviours of all the Gaussian Points are similar to those in elements 2 and 3.

Element 7 (Fig. 52e & Fig. 53d)

Yielding occurs in Gaussian Points 3 and 1. Whilst the former experiences very slight yielding, the latter has twice entered into the plastic region. These are occurred at 0.09 sec. and 0.13 sec. respectively. Plastic strain which were amounted to about 0.25% is found at Gaussian Point 1 and is by far the largest plastic strain increment found in all the plate elements.

Element 8 (Fig. 52f & 53e)

Yielding occurs at Gaussian Point 2. Again, plastic loadings have occurred twice; one at 0.095 sec. and the other at 0.13 sec. Even then, plastic strain is still relatively small (0.02%) when compared with that obtained in the previous element.

Element 9 (Fig. 52g & 53f)

Yielding occurs at Gaussian Point 3 at 0.095 sec. Stresses in the rest of the element are behaving not much different from those in elements 2 and 3.

Stiffener Element

It is noticed that plasticity has been developed in element 4. These stresses are also above the crippling stress level (Appendix 2) of the stiffener flange (Fig 54a & 54b). Stresses in the rest of the stiffener elements though below the crippling stress level,

are still relatively high when they are compared with those obtained in the previous loading case (12,000 lb/in^2).

While the overall response of the structure can be found in Fig. 52a, the stage-by-stage response of the structure throughout the loading history are examined as below:-

The responses in the plate elements prior to the local plate buckling are similar to those obtained in the previous loading case. However, as the amount of plasticity grows, their responses at the early stage of post-buckling are quite different (see Fig. 52a). In that, not only their amplitudes have changed, but its mode of buckling also experiences significant changes. At the later stage of the constant-loading period, some mode shape changes still exist. But they are not as severe as those appeared in the previous loading case.

In the same figure, we also notice that, throughout the constant-loading period, the responses in all the stiffener elements are no longer constant as they have been previously. In fact, they decrease rather linearly with the increase of time. This can be explained as follows:-

As plasticity accumulates within the plate elements, this will act as a damping mechanism which absorbs most of the energy during plastic deformation. And as no further external work is applied to the structure during the constant-loading period, less and less energy is being transmitted into the stiffeners.

On examining the out-of-plane deflections of the stiffener elements, they are found to vary non-linearly with the applied load level. And indeed, if we further examine the out-of-plane deflections of the stiffener elements when the applied load level reached 16,500

lb/in^2 (this will be covered in section 7.2.2.4), it has become obvious that the overall buckling is about to occur when the applied load reaches 14,500 lb/in^2.

The following table lists the maximum deflections of the central stiffener (node 6) and their corresponding applied load level:-

Applied stress level (lb/in^2)	2,000	8,000	10,000	12,000	14,500	16,500
Max. deflection of Central stiffener (in.)	0.0001	0.007	0.012	0.018	0.035	0.045

The above data, together with the maximum out of plane deflection of the central stiffener when applied stress level reaches 24,000 lb/in^2, are plotted out in Fig. 55 which shows evidently that the present loading is very close to the stiffener's buckling load.

As usual, external damping is applied to the structure after unloading has been completed. Fig. 52a shows that the plate elements are left with a permanent deformation of between 0.005" and 0.015" (8-20% of the plate thickness) while the stiffeners have suffered from a permanent deflection of between 0.005" and 0.01".

Because of the comparatively large deflections caused by the present loading, the maximum eigen-value of the structure was found to have risen by 30% just before loading has completed. This would mean that the time size employed in the numerical integration had to be reduced to 0.0006 sec. All these were done automatically within the program.

In Fig. 56, there are series of pictures showing periodically the deformation of the structure throughout the loading history. Since the deformations of the structure prior to the local plate buckling are exactly the same as those in the previous loading case, they can be found in Picture 1 to 12 of Fig. 51. However, Picture 13 to Picture 55 of Fig. 56 show some of the deformation during the constant-loading and unloading period. We notice from these pictures that at the line where the stiffener is attached to (see Fig. 56 for location), it remains reasonably straight, which indicates that no buckling has yet taken place in the stiffener. Otherwise, the line will appear in a wave form similar to those representing the plate elements. This agrees very well with the curve shown in Fig. 55 which indicates that overall buckling has not yet reached. When unloading has completed, the final deformation(Picture 93 to Picture 105 of Fig. 56.) indicates the presence of the plastic deformation occurring at both the plate and stiffener elements. When comparing these pictures with Fig. 51 the present loading has certainly caused a higher level of permanent deformation

At the elements where plasticity has occurred, their direct stresses in either directions need not exceed the yield stress level even though its equivalent stress does (see for example Fig. 52a & 57a(b). However, such situation would suggest that the corresponding shear stress contributes largely to the formation of the yield stresses. The following table summarises the stresses and hence calculates the correspondng shear stresses:-

Element No.	Gauss Point	Max. stress in X-dirn. (lb/sq.in)	Max. stress in Y-dirn. (lb/sq.in)	Max. equiv stress (lb/sq.in)	Max. shear stress (lb/sq.in)
1	2	-22,000	-31,000	33,900	11,346
4	*2	8,000	24,000	34,000	15,362
	*2	- 9,000	-25,000	38,500	18,268
	*4	-12,000	-28,000	34,500	14,317
6	3	-12,000	-32,000	35,000	12,124
	*4	- 4,000	-25,000	34,000	14,317
7	*1	- 8,000	-26,000	40,000	18,876
	*3	-10,000	-25,000	33,500	14,688
8	2	- 8,000	-32,500	33,900	9,814
9	*3	- 7,000	-24,000	34.500	15.633

For instance, to calculate the shear stress of element 1; from equation (5.25):-

$$\sigma_{xy} = \tfrac{1}{3} (\bar{\sigma}^2 + \sigma_x \cdot \sigma_y - \sigma_x^2 - \sigma_y^2)$$

Hence, $\sigma_{xy} = (33{,}900^2 + 31{,}000 \times 22{,}000 - 31{,}000^2 - 22{,}000^2)$

$= \underline{11{,}346 \text{ lb/sq.in.}}$

The '*' sign in the above table indicates that the corresponding Gaussian Points are situated near to the location of the stiffeners. It is noticed that where this sign appears, the corresponding shear stresses are relatively high. In contrast, their direct stresses in the direction of the applied load are comparatively low. This indicates that the shear stresses at these Gaussian Points have contributed quite significantly to the formation of plasticity. Conversely, where the Gaussian Points are further away from the stiffener (e.g. elements 1, 6 & 8 in the above table), plasticity is mainly caused by the excessive direct stresses and the shear stress would have a very minor contribution. On examining the buckling mode shapes plotted in Fig. 56, these Gaussian Points (those without a '*' sign

in the above table), are locating at the peaks of the buckling waves, and these points are expected to be suffered from very high local bending stresses anyway. It is therefore not surprising that they would be above the yield level.

7.2.2.4 Total applied stress level - 16,500 lb/sq.in

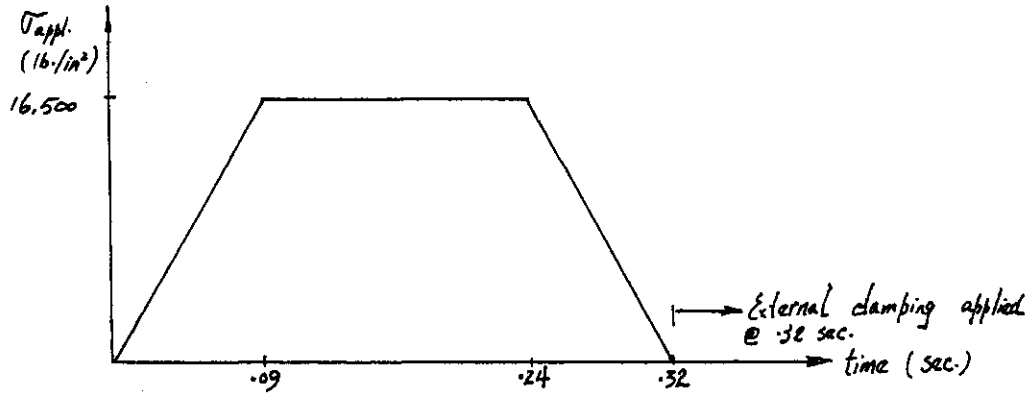


Fig. 58 shows the response of the structure. The peak out-of-plane deflection at the central stiffener element is found to be 0.045 in. As we have mentioned in the previous section (section 7.2.2.3), the stiffener has under this present load level, entered into its post-buckling stage (see Fig. 55). The permanent deformations shown in Fig. 58 are also comparatively larger than those shown in the previous loading case. The following table summarises the nodal permanent deflection , under each different load level (i.e. 12,000 lb/in^2, 14,500 lb/in^2 and 16,500 lb/in^2).

Applied stress level	Permanent deflection at each node. (inch)								
	Node 6	Node 7	Node 8	Node 10	Node 11	Node 12	Node 14	Node 15	Node 16
12,000 lb./in².	0.003	0.0035	0.005	0	0	0	0.001	-0.008	-0.007
14,500 lb./in².	-0.002	-0.0055	-0.01	-0.0015	-0.0035	-0.0045	-0.006	0.001	0.002
16,500 lb./in².	0.02	0.01	0.0076	0.004	0.008	0.008	-0.007	0.018	0.021

The graphs of the figures shown in the above table are shown on Figs 59a to 59c. Fig. 60shows the percentage of the maximum permanent deflections on some selected nodes.

Fig. 61a to Fig. 61i show the stress-strain curves of plate elements 1 to 9. It is noticed from these figures that the residual plastic strains occurred in those plate elements are relatively larger than those found in the previous loading case (which is quite obvious).

Fig. 62a to Fig. 62c show the stress-strain curves of the central stiffener elements (elements 4 to 6). Under the present loading, plasticity has occurred not only in element 4, but also in elements 5 and 6. The stresses in these elements are above the crippling stress level of the stiffener flanges.

7.2.2.5 Total applied stress level = 24,000 lb/sq.in.

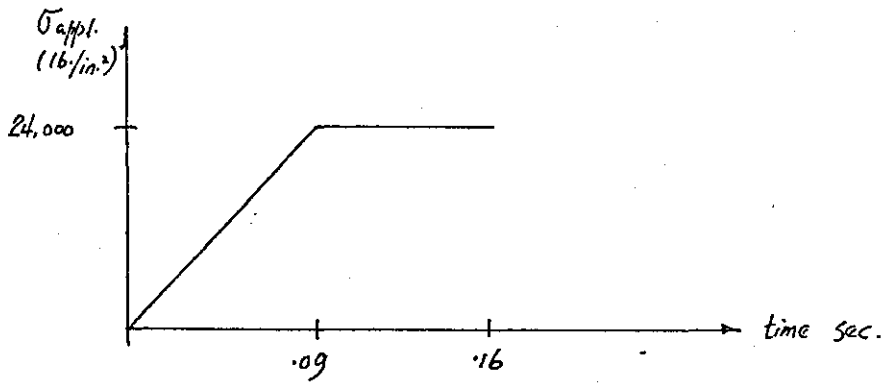


Fig. 63 shows the nodal response curves. It is noticed that the maximum out-of-plane deflection of the central stiffener is 0.072 in. which is also plotted and shown on Fig. 55.

Fig. 64a to Fig. 64c merely show the plastic deformation found in some of the plate elements. A few plastic hinges can be observed in these elements.

Fig. 65a to 65c show the stress-strain curves of the central stiffener elements (stiffener elements 4 to 6). Again, plasticity has occurred in most elements.

7.3 Discussions

From the above analyses, it is clear that the overall buckling would occur when the applied stress reaches between 14,500 lb./in^2. and 16,500 lb./in^2.. At the 14,500 lb./in^2. applied stress level, some stiffener elements are found to have reached the crippling stress level of the stiffener flange. These two factors have strongly indicated that when such load level is reached, the stiffened panel is likely to suffer from an overall collapse.

8. CONCLUSION

The modelling of the problem using finite elements has been proved from the above analyses, to be quite accurate. The finite element package which has been developed especially to investigate the present program can also be used for other purposes such as impact loading, heat transient analysis etc. with only minor modifications. When comparing the results computed from this finite element package with some existing results, very close agreements are observed. When there is not any existing results to be contrast with (e.g. the elasto-plastic dynamic buckling part of the analysis) the stage-by-stage results exhibit a high degree of coherence between them. The mathematical modelling of the geometric non-linearities and the material non-linearities are particularly successful. For instance, for a given structure, the static loading results generated from the finite element package give a critical stress which is quite close to that obtained from the Engineering Data Sheet. The error between the two sets of results is only about 4%. This error is mainly caused by employing a stiffener which has not been modelled to accommodate its torsional stiffness. When another stiffened structure was analysed by using a stiffener in which the torsional stiffness is comparatively small (e.g. section 4.3.2), the results are very close to that obtained by Seide (Ref. 64) (see section 4.3.2). The results could equally be improved by employing a finer model (e.g. a 6x6 element model).

The modelling of the offset stiffener by employing a transformation matrix is seen to be quite appropriate. In that, the structure with 1, 2 & 3 stiffeners located both at the mid-plane of the plate and on one side of the plate have been thoroughly tested and the computed results are very close to those obtained in Ref. 64. The present package is strictly limited to the using of Z section type

stiffeners which is the main drawback. This is because when we modelled the stiffener, the plasticity terms were calculated explicitly to allow for a 'Z' x-sectional area only. Although it is possible that the stiffener could alternatively be modelled with plate elements, however, this would involve extra nodal points which are quite unnecessary. In any case, the running cost of such program would be extremely expensive especially when a complete response history requires something like 5,000 time steps.

The large displacement analyses also produce very good results. It has been shown that when a plate is subject to excessive bending, the computed load-displacement relationships are very close to those obtained by Timoshenko & Levy (Fig. 6 & 7). The formulation in all the large displacement analyses employs a Lagrangian frame of reference which refers the co-ordinates in the structure to its initially undeformed shape. In our present analysis, the Lagrangian formulation has already been proved to be computationally very efficient especially when the direction of the applied load remains almost constant throughout the whole response history.

We have shown in Section 6 that because of the rapid changes in the fundamental eigen-modes of the structure when local buckling occurs, a modal superposition approach would not be appropriate.We have also proved in section 6 that close agreements between the results obtained from a Central Difference Scheme coupling with a Diagonal Mass Matrix and those obtained from a Newmark-β method can be achieved by adjusting the rotational inertia terms in the Diagonal Mass Matrix, so that the fundamental Eigen value evaluated from the two separate schemes can be matched. Thus, our choice for a Central Difference scheme coupling with a Diagonal Mass Matrix lies mainly on its relatively small storage requirements. The Central Difference Scheme has also shown to be computationally more efficient than the Newmark-β integration scheme in which the

triangulisation of a fully banded matrix is required in every time step. It might be argued that the Newmark-β scheme can afford to employ a larger time size (and hence fewer integration steps) because of its unconditional stable characteristic. However, our present analysis shows that the large geometric and material changes often occur in such a short period that even a Newmark-β method would require a very short time-step in order to capture any energy changes during the plastic deformation. Therefore, the small time size employed in the Central Difference Scheme is not too disadvantageous. We have also mentioned that the maximum Eigen value of the structure has to be continuously evaluated during some period of the analysis, especially when plastic deformation occurs, in order to keep the time size within the numerical stability limit. The evaluation of the maximum Eigen value employs a technique known as the Direct Power Method in which the triangulisation of a mass matrix is required. Thus, it can be seen that the adoption of a diagonal mass matrix is particularly advantageous.

The plots shown in this report give a very clear illustration of the response behaviour of the structure during both the static and dynamic analyses. The 3-dimensional plottings give a clear insight into the mode changes as the buckling develops. It also helps one to study the level of permanent deformation of the structure after plasticity has taken place.

In the static load analysis, both the incremental load method and the Eigen value method give very good results, and when these are compared with the results obtained from the Engineering Data Sheets, very close agreements are obtained. For a given structure, the incremental load method predicts a local plate buckling stress of 8,400 lb./in.^{2} while the eigen value analysis of the disturbed system (actually at a configuration when load = 1,000 lb./in.^{2}) shows a first Eigen mode at 8047 lb./in.^{2} However, when the load

is applied dynamically, the result shows that it is this Eigen mode which grows exponentially.

The Eigen value analysis predicts an overall collapse stress of 28,996 lb./in.^{2} This agrees very well with those obtained from the Engineering Data Sheets which, if load sheddings between the plate and the stiffeners during local plate buckling are ignored, give a stress of 29,766 lb./in. If the load sheddings between the plate and nearby stiffeners are taken into consideration, the Engineering Data Sheet predicts an overall buckling stress of 22,890 lb./in. However, if the loading is applied dynamically onto the structure, Fig. 55 indicates that overall buckling will occur when the applied stress reaches around 15,500 lb./in.

Elasto-plastic analysis shows that yielding begins when a uniform stress of 14,080 lb./in.^{2} is applied statically onto the structure. When the applied stress reaches 16,480 lb./in.^{2}, more plate areas have yielded but yet no plasticity has been found in any of the stiffeners. However, when loading is applied dynamically the following changes are observed:-

1) When the applied stress reached 12,000 lb./in.^{2}, yielding begins in the plate (in the same area where yielding begins when applied stress in excess of 14,000 lb./in.^{2} was applied statically.)

2) When the applied stress reaches 14,500 lb./in.^{2}, many plate elements have yielded. A plastic hinge has also been found in one of the plate elements.

3) The stiffener has also suffered from plastic deformation which exceeds the crippling stress of the stiffener flange when the applied stress reaches 14,500 lb./in.^{2} The dynamic load deflection curve of the stiffener shown in Fig. 55 indicates that overall

buckling stress of the structure will occur when the applied stress reaches 15,500 lb./in.^{2} (approximately).

The results show that the wave-length of the permanent deformation found in the structure when it is subject to excessive loadings agrees with that found in service by B.A.C. The exact magnitude of load and the type of loading when the heavy landing took place is not known. However, from Fig. 55, it can be seen that when the applied stress reaches between 14,500 lb./in^2. and 15,500 lb./in^2., the structure is very likely to collapse.

For a ramp type of loading, the time taken for the local buckling and local plasticity to occur depends on the loading magnitude (Sect. 7.2) It has been suggested that the occurrence of these could be avoided if the applied loads were removed quick enough (Ref. 18). Our analysis shows that when the applied stress reaches 14,500 lb./in., local skin buckling takes place at 0.083 sec. Thus, for a loading duration of 0.1 sec., local bucklings are likely to occur even if the loads are removed immediately after they have reached their maximum level. The relatively long constant-load period (0.4 sec.) is not seen to aggravate the stress behaviour of the structure. In fact, all the stresses have 'died down' to a slightly lower level at the latter part of that period.

REFERENCES

1. BLOCK, D.C. & CARD, M.F. 'Buckling of eccentrically stiffened orthotopic cylinder.' N.A.C.A. TN2960 Aug.1965.

2. MCELMAN, J.A. & MIKULAS, M.M.'Static and dynamic effects of eccentric stiffening of plates and cylindrical shells.' A.I.A.A. Jnl. Vol.4, May 1966, p.p.887-894.

3. STUHLMAN, C. & DELUZIO, A. 'Influence of stiffener eccentricity and end moment on stability of cylinder in compression.' A.I.A.A. Jnl. Vol.4, May 1966. p.p.872-877.

4. HUTCHINSON, J.W. 'Elastic post-buckling behaviour of stiffened and barrelled cylindrical shell.' Jnl. Appl. Mechs. Vol.36, No.4, Trans. ASME, Vol.91, Series E, Dec.1969. p.p.784-790.

5. SINGER, J. & BARUCH, M. 'On the stability of eccentrically stiffened cylindrical shells under axial compression.' Int. Jnl. Solids & Struct., Vol.3, July 1967, p.p.445-470

6. FOK, W.C., RHODES, J. & WALKER, A.C. 'Local buckling of outstands in stiffened plates.' Aero Quarterly, 1976, p.277.

7. KOITER, W.T. 6An alternative to the interaction between local and overall buckling in stiffened plates.' Proc. Int. Union of Theoretical & Appl. Maths. on Buckling of structures. Berlin, Germany, 1974.

8. MURRAY, N.W. 'Buckling of stiffened panels loaded axially and in bending.' Struct. Eng. Vol.51, 1973.

9. TULK, J.D. & WALKER, A.C. 'Model studies of the elastic buckling of a stiffened plate.' Jnl. of Strain Analy. Vol.2,1976.

10. TULK, J.D. & THOMPSON, J.M.T. 'An experimental study of imperfection sensitivity in interactive buckling of stiffened plates.' Proc. of Int. Union of Theoretical & App. Maths Symposium on Buckling of Struct. Berlin, Germany, 1974

11. COHEN, G.A. 'Computer analysis of imperfection sensitivity of ring-stiffened orthotropic shells of revolution. A.I.A.A. Jnl. Vol.9, June 1971, p.p.1032-1039.

12. SINGER, J. & HAFTKA, R. 'Buckling of discretely ring-stiffened cylindrical shells.' Israel Jnl. of Technology, Vol.6, 1968, p.p. 125-137.

13. PETERSON, J.P. 'Buckling of stiffened cylinders in axial compression and bending.' N.A.S.A. TN D-5561, Dec. 1969.

14. WELLER, T. & SINGER, J. 'Recent experimental studies on buckling of integrally stiffened cylindrical shells under axial compression. TAE Report No. 100, Feb. 1970, Haifa, Israel.

15. SINGER, J. & ARBOCZ, J. 'Buckling of imperfect stiffened cylindrical shells under axial compression.' A.I.A.A. Jnl. Vol.9 Jan. 1971, p.p.68-75.

16. ROTH, R.S. & KLOSNER, J.M. 'Nonlinear respomse of cylindrical shells subjected to dynamic axial loads.' A.I.A.A. Jnl. Vol.2, Oct. 1964, p.p.1788-1794.

17. DONNELL, L.H. 'A new theory for buckling of twin cylinders under axial compression and bending.' Trans. ASME, Vol.56, Nov. 1934, p.p.795-806.

18. TAUB, J. 'Impact buckling of thin bars in elastic range for any end condition.' Tech. Memo. N.A.C.A. No.749.

19. ZIENKIEWICZ, O.C. 'Finite Element Method in Engineering.' McGraw-Hill, 1971.

20. IRON, B.M.R. 'Inadequacy of nodal connection in a stiffness solution for plate bending.' AIAA Jnl. Vol.3, No.5, 1965.

21. COOK, R.D. 'Concepts and Applications in Finite Element Analysis.' Wiley, 1974.

22. FADDEEVA, V.N. 'Computer Method of Linear Algebra.' N.Y. 1959

23. NOBLE, B. 'Applied Linear Algebra.' Prentice Hall, N.Y. 1969.

24. CRANDALL, S.H. 'Engineering Analysis.' McGraw-Hill, N.Y. 1959.

25. CLOUGH, R.W. & TOCHER, J.L. 'Finite Element stiffness matrices gor analysis of plate bending.' Proc. Conf. on Matrix Methods in Struct. Mechs., AFFOL-TR-66-80, Dayton, Ohio, 1965.

26. LAU, W.W. 'An interim progress report on the investigation into collapse of fuselage panels under dynamic loading.' Internal Report, Dept. of Aeronautics, Imperial College, June 1979.

27. LEVY, S. 'Bending of rectangular plates with large deflection.' N.A.C.A. TN 846, 1942.

28. YAMAKI, N. 'Post-buckling behaviour of rectangular plates with small initial curvature loaded in edge compression.' J. of Appl. Mechs. 26, Sept. 1959, p.p. 407-414.

29. BHAUMIK, A.K. & HANLEY, J.T. 'Elasto-plastic plate analysis by Finite Difference.' J. of Struct. Div. Proc. ASCE, Oct. 1967, p.p. 279-294.

30. RUSHTON, K.R. 'Large deflection of plate with unsupported edges.' J. of Strain Analysis, Vol.7 No.1, 1972, p.p. 44-53

31. THOMPSON, V.M.T. & WALKER, A.C. 'A non-linear perturbation analysis of discrete structural system.' Int. J. of Solids & Struct. 4, 1968, p.p.757-767.

32. GRAVES-SMITH, T.H. 'The effect of initial imperfections on the strength of thin walled box columns.' Int. J. of Mech. Science, Vol. 13, 1971, p.p. 911-925.

33. TURNER, M.J. & MARTIN, H.C. 'Large deflection of structures subject to heating and external loads.' J. of Aerospace Science , Vol. 27, Feb. 1960.

34. ARGYRIS, J.H. 'Recent advance in Matrix Method of Structural analysis.' Pergaman Press, 1964.

35. ARGYRIS, J.H. 'Continua & Discontinua.' Proc. Conf. Matrix Method in Struct. Mech., Air Force Inst. of Tech., Wright Patterson Air Force Base, Ohio, Oct. 1973.

36. MALLET, R.H. & MARCAL, P.V. 'Finite Element analysis of non-linear structures.' J. of Struct. Div. Proc. ASCE, Vol.94, No. S.T.9, Sept. 1968, p.p. 2081-2105.

37. MARCAL, P.v. 'Finite Element analysis of combined problems of non-linear material and geometric behaviour.' Proc. ASME. Conf. on Computational Approach in App. Mech. June, 1969.

38. ODEN, J.T. 'Numerical formulation of non-linear elastic problems.' J. of Struct. Div. Proc. ASCE. Vol. 93, No. S.T.3, Paper 5290, June 1967.

39. BREBBIA, C. & CONNOR, J. 'Geometrically non-linear finite element analysis.' J. of Eng. Mech. Proc. ASCE. Paper 6519, April. 1969.

40. MURRAY, D.W. & WILSON, E.L. 'Finite element large deflection analysis of plate.' J. of Eng. Mech. Div. Vol. 95, E.M.1, Feb. 1969, p.p. 143-165

41. SCHIED, F. 'Numerical Analysis.' Secaum Series, McGraw-Hill, 1968.

42. KOPAL, Z. 'Numerical Analysis.' 2nd ed. Chapman & Hall, 1968.

43. COWPER, G.R. 'Gaussian Quadrature formulas for triangles.' Int. J. Num. Meth. Eng. 7, p.405-408, 1973.

44. FRIED, I. 'Numerical Integration inthe Finite Element Method.' Comp. Struct. 4, p.921-932, 1974.

45. HELLEN, T.K. 'Effective Quadrature rules for quadratic solid isoparametric finite elements.' Int. J. Num. Meth. Eng. 4, 597-600, 1972.

46. BRYAN, G.H. 'On the stability of a plane plate under thrust in its own plane.' London Math. Soc. Proc. 22, 54-67.

47. TIMOSHENKO, S. 'Stability of rectangular plates with stiffeners.' Memoirs of thr Institute Engineers of Ways & Communications, S. Petersburgh 89(1915) 23.

48. TIMOSHENKO, S. 'On the stabilities of the stiffened plates.' Du Eisenbau, 12 (1921), 147-163.

49. TIMOSHENKO, S. 'Theory of Elastic Stability.' McGraw-Hill, N.Y., 1935.

50. TIMOSHENKO, S. 'Theory of Elastic Stability.' 2nd. ed. McGraw-Hill, N.Y. 1961.

51. BLEICH, F. 'Buckling strength of metal structure.' McGraw-Hill, N.Y. ,1952.

52. KOLLBRUNNER, C.F. & MEISTER, F. Ausbeulen, Springer-Verlag, Berlin, 1958.

53. PAPKOVICH, P.F. 'Theory of Elasticity.' Leningrag-Moscow, 1939.

54. SAVIN, G.N. & FLEISHMAN, N.P. 'Rib-reinforced plate & shells.' U.S. Dept. of Commerce, Clearing House for Federal Scientific & Tech. Information, Springfield, Vc.

55. BERLSON, P.S. 'The stability of flat plate.' American Elsevier Publishing Co. Inc. N.Y. 1969.

56. BARBRE, R. 'Stability of rectangular plates under Longitudinal or Transveral stiffeners under uniform compression.' N.A.C.A. TM. No. 904-939.

57. ROZERSDORFER, J. 'Rectangular plates with stiffeners.' Aircraft Engineering, Vol. XIV, No.163, Sept. 1942, p.p. 260-263.

58. JOJIC, K.V. 'The buckling of stiffened rectangular plate.' Proc. of the Faculty of Mech. Eng. Univ. of Belgrade (1955-1956) p.p.115-187.

59. COX, H.L. & RIDDEL, J.R. 'Buckling of longitudenally stiffened flat panel.' The Aeronautical Quarterly, Nov.1949, p.p.225-244.

60. SVENNERUD, A. 'Buckling strength of stiffened panels with application on the longitudenal strength of ship.' European Ship Building No. 6 (1953), 132-134.

61. VAN DER NEUT, A. 'The interaction of local buckling and column failure of thin-walled Compression Members, Proc. XII, Int. Conf. App. Mech. Stanford, N.Y. Springer, 1968.

62. KOITER, W.T. & KUIKEN, G.D.C. 'The interaction between local buckling and overall buckling on the behaviour og build-up Column.' Rpt. No.447, Lab. of Eng. Mech. Delft, May 1971.

63. BULSON, P.S. 'The stability of flat plate.' America Elsevier Co. Inc. N.y. 1969.

64. SEIDE, P. & STEIN, M. 'Compressive buckling of S-S plate with longitudenal stiffeners.' N.A.C.A. TN 1825.

65. MARCAL, P.V. & KING, I.P. 'Elasto-plastic analysis of two dimensional stress system by Finite Element Method.' Int. J. of Mech. Sci. Vol.9 No.3, 1967, p.p.143-155.

66. MARCAL, P.V. 'Finite Element analysis with material non-linearities---theory and practice.' Recent Advance in Matrix Method of Struct. Analy. & Design. Alabama Press, 1971, p.p.257-282.

67. NAYAK, G.C. & ZIENKIEWICZ, O.C. 'Elasto-plastic stress analysis, a generalisation for various constitutive relationships including strain softening.' Int. J. of Num. Meth. in Eng. Vol.5, 1972, p.p.113-135.

68. MARCAL, P.V. & MALLET, R.H. 'Elasto-plastic analysis of plate by Finite Element Method.' Proc. ASME. Dec. 1968.

69. BELYTSCHKO, T. & VELEBIT, M. 'Finite element method for elasto-plastic plate.' J. of Eng. Mechs. Div. Proc. ASCE. EM1, Feb. 1972,p.p.227-242.

70. ANG, A.H.S. & LOPEZ, L.A. 'Discrete model analysis of elastic-plastic plates.' J. of Eng. Mechs. Div. Proc. ASCE., Vol.94, E.M.1, Feb. 1968, p.p.271-293.

71. ARMEN, H. ; PIFKO, A.B. & LEVINE, H.S. 'Plasticity, Chapt. 8 of Finite Element Tech. in Struct. Mechanics.' Tottenham & Brebbia, Southhampton Univ. Eng. 1970.

72. Marcal, P.V. & Pilgrim, W.R. 'A stiffness method for elastic-plastic shells of revolution.' J. of Strain Analysis, Vol.1, No.4, 1966, p.p.339-350.

73. CRISFIELD, M.A. 'Large deflection elasto-plastic buckling analysis of plates using finite elements.' T.R.R.L. Rpt. LR593.

74. ILYUSHIN, A.A. 'The elasto-plastic stability of plate.' N.A.C.A. TM. 1188 Dec. 1947.

75. NAGHDI, P.M. 'Stress-strain relation in plasticity & thermoplasticity Plasticity.' Proc. of 2nd Symp. on Naval Struct. Mech. Pergamon Press, 1960.

76. HILL, R. 'The mathematical theory of plasticity.' Oxford Univ. Press, 1950.

77. PRAGER, W. & HODGE, P.G. 'Theory of perfectly Plastic Solids.' Dover Publication, N.Y. 1951.

78. HURTY, W.C. & RUBINSTIEN, N.F. 'Dynamic of Structure.' Prentice-Hall, 1974.

79. KEY, S.W. & BEISINGER, Z.E. 'The transient dynamic of thin shells by finite element method.' Proc. 3rd Conf. on Matrix Method in Struct. Mech. AFFDL-TR-71-160, Dayton, Ohio, 1971.

80. NICKELL, R.E. 'On stability of approximation operators in problems of structural dynamics.' Jnl. of Solid & Structures, No.7, 1971, p.p. 301-319.

81. JOHNSON, D.E. 'A proof of the stability of the Houbolt method.' AIAA Jnl. Vol.4, 1966

82. JOHNSON, D.E. 'Dynamic response of a cylindrical shell : Two numerical method.' AIAA. Jnl. Vol.3, 1966.

83. ODEN, J.T. & FROST, R.B. 'Convergency accuracy and stability of finite element approx. for a class of non-linear hyperbolic equation.' Jnl. Numerical Methods in Eng., 1973.

84. BELYTSCHKO, T. & SCHOCBERLE, D.F. 'On the unconditional stability of an implicit algoritnm for non-linear structural dynamics. Jnl. Appl. Mech. Vol.42, 1975.

85. WILSON, E.L. & BATHE, K.J. 'Non-linear dynamic analysis of complex structures.' Jnl. Earth. Eng. & Struct. Dynamics. Vol.1, 1973.

86. BELYTSCHKO, T. 'A survey of Numerical Methods and computer programs for dynamic structural analysis.' Jnl. of NUclear Eng. & Design, 37, 1976.

87. WEEKS, G. 'Temporal operators for non-linear structural dynamic problems.' ASCE? Eng. Mech. Div. EM5, Oct. 1972.

88. BREBBIA, C.A. & CONNOR, J.J. 'Foundations of the finite element technique.' Butterworth, 1973.

89. CLOUGH, R.W. ' Analysis of structural vibrations and dynamic response.' Japan/U.S. Seminar on Matrix Methods of Structural analysis & design, Tokyo, Aug. 1969.

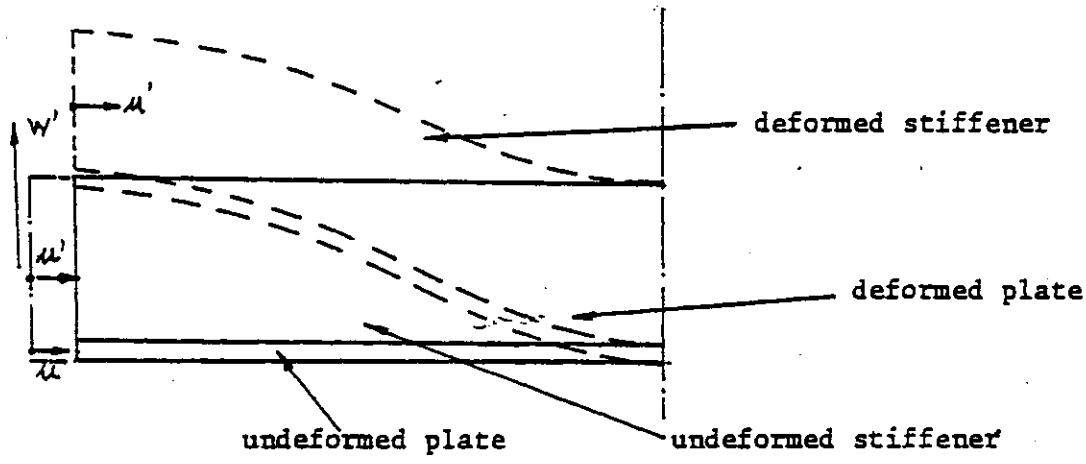
90. LAU, W.W. 'Workshop Manual for the Dynamic Buckling Package.' To be submitted to B.A.C.

91. Lau, W.W. 'A Final report on the investigation into the collapse of fuselage panel under dynamic loading.' Internal Report, Dept. of Aeronautics, Imperial College, Oct. 1981.

APPENDIX I

Eqn. 3.37 in Section 3.3.2 shows the formulation of the beam element stiffness matrix. When this stiffness matrix is assembled onto the plate element stiffness matrix for a complete stiffened panel, the stiffness is expected to behave as if it was built in the mid-plane of the plate. However, when the stiffener is built on one side of the plate, the stiffness matrix of the stiffener has to be transformed in accordingly so that the displacement behaviour of the assembled structure can remain compatible.

The diagram shows below describes the deformation of the stiffened plate when bendings take place:-



WITH ZERO ROTATION @ THE NODES

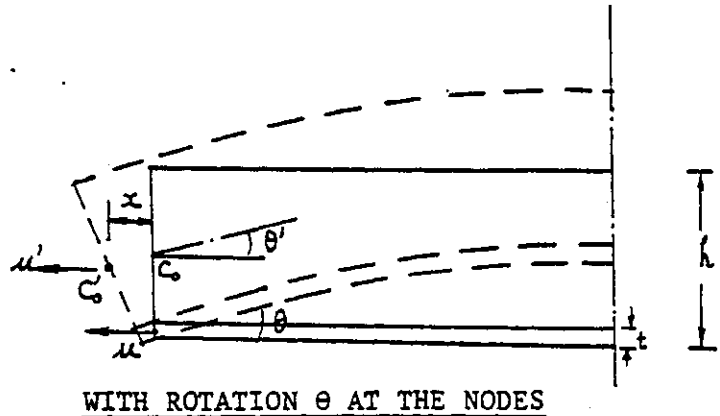
where u is the inplane displacement of the plate

u' is the inplane displacement of the stiffener

w is the out-of-plane displacement of the plate

w' is the out-of-plane displacement of the stiffener

and
$$\left.\begin{aligned} u' &= U + x \\ w' &= w \end{aligned}\right\} \text{-----(A.1.1)}$$



WITH ROTATION θ AT THE NODES

Let C_o' and C_o be the positions of the centre of the X-sectional area of the stiffener before and after bending of the structure has taken place respectively. The displacement between these two positions can be shown as:-

$$x = \frac{-(h+t)}{2} \times \theta \qquad \text{------A.1.2}$$

Hence $$u' = \frac{-(h+t)}{2} \cdot \theta + u \qquad \text{------A.1.3}$$

combining A.1.1 and A.1.3, we have

$$\left.\begin{aligned} u' &= u - \frac{-(h+t)}{2} \cdot \theta \\ w' &= w \\ \theta' &= \theta \end{aligned}\right\} \qquad \text{------A.1.4}$$

where suffix ' refers to the local system of the stiffener while those without suffix ' will refer to the global system of the stiffener.

Thus:-

$$\begin{bmatrix} u_1' \\ w_1' \\ \theta_1' \end{bmatrix} = \begin{bmatrix} 1 & 0 & \frac{-(h+t)}{2} \\ 0 & 1 & 0 \\ 0 & 0 & 1 \end{bmatrix} \cdot \begin{bmatrix} u_1 \\ w_1 \\ \theta_1 \end{bmatrix} \qquad \text{------A.1.5}$$

and for the complete beam element:-

$$\begin{bmatrix} u_1' \\ w_1' \\ \theta_1' \\ u_2' \\ w_2' \\ \theta_2' \end{bmatrix} = \begin{bmatrix} 1 & 0 & \frac{(h+t)}{2} & 0 & 0 & 0 \\ 0 & 1 & 0 & 0 & 0 & 0 \\ 0 & 0 & 1 & 0 & 0 & 0 \\ 0 & 0 & 0 & 1 & 0 & \frac{(h+t)}{2} \\ 0 & 0 & 0 & 0 & 1 & 0 \\ 0 & 0 & 0 & 0 & 0 & 1 \end{bmatrix} \cdot \begin{bmatrix} u_1 \\ w_1 \\ \theta_1 \\ u_2 \\ w_2 \\ \theta_2 \end{bmatrix} = \underset{\sim}{T_s} \cdot \underset{\sim}{U} \qquad \text{---A.1.6}$$

$$\therefore \quad \underset{\sim}{U_s} = \underset{\sim}{T_s} \cdot \underset{\sim}{U} \qquad \text{------A.1.7}$$

where $\underset{\sim}{T_s}$ is the transformation matrix to transform the displacement of the local coordinates of the stiffener to the global coordinate of the system and suffix S refers to the stiffener.

From the equilibrium of work

$$\underset{\sim}{F_s'} = \underset{\sim}{K_s'} \cdot \underset{\sim}{U_s} \qquad \text{------A.1.8.}$$

Substitute A.1.7 into A.1.8, we have:-

$$\underset{\sim}{F}'_s = \underset{\sim}{K}'_s \underset{\sim}{T}_s \cdot \underset{\sim}{u}$$

Post-multiply the equation by $\underset{\sim}{T}_s^t$: we have:-

$$\underset{\sim}{T}_s^t \cdot \underset{\sim}{F}'_s = \underset{\sim}{T}_s^t \cdot \underset{\sim}{K}'_s \underset{\sim}{T}_s \cdot \underset{\sim}{u} \qquad \text{A.1.9}$$

where $\underset{\sim}{T}_s^t \underset{\sim}{K}'_s \cdot \underset{\sim}{T}_s$ is the stiffness matrix of the stiffener with respect to the global system of the structure.

$$\therefore \underset{\sim}{K}_s = \underset{\sim}{T}_s^t \cdot \underset{\sim}{K}'_s \cdot \underset{\sim}{T}_s \qquad \text{A.1.10}$$

and $\underset{\sim}{T}_s^t \cdot \underset{\sim}{F}'_s$ is the external nodal force of the stiffener with respect to the global system.

Hence, when a global system of external force should be applied to the stiffener in the form of:-

$$\underset{\sim}{F}'_s = \underset{\sim}{T}_s \cdot \underset{\sim}{F}_s \qquad \text{A.1.11}$$

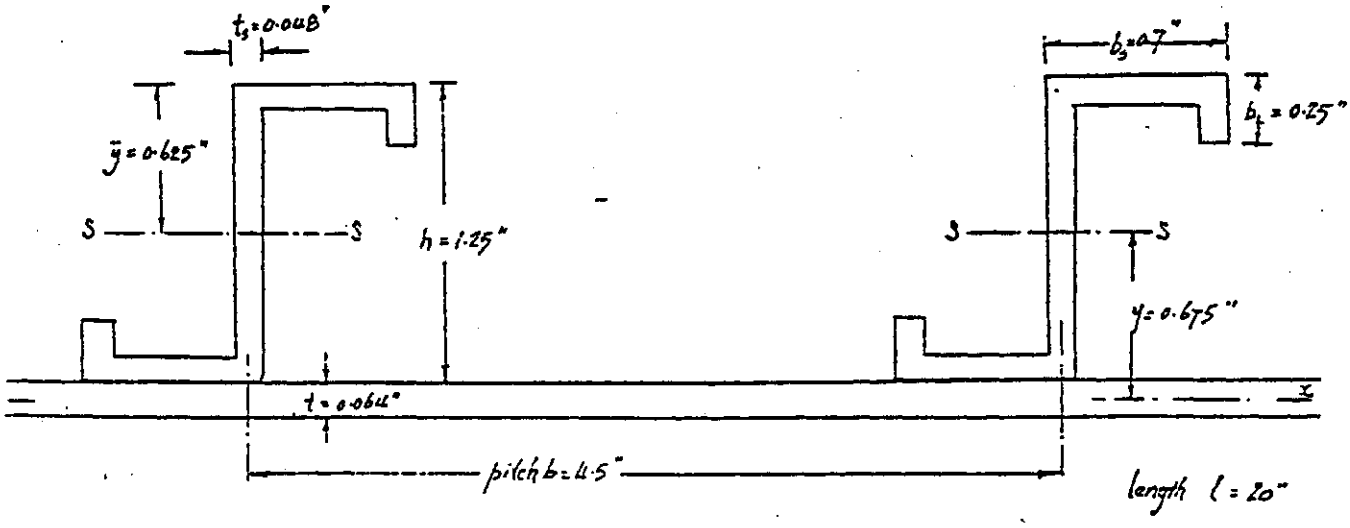
where $\underset{\sim}{F}'_s$ is the model applied force to the stiffener
$\underset{\sim}{F}_s$ is the global applied force to the system
$\underset{\sim}{T}_s$ is the transformation matrix due to the on set of the one sided stiffener.

APPENDIX 2

Buckling Analysis of the Given Stiffened Plate using Engineering Data Sheet

Having derived the appropriate formulation of the analysis using the finite element approach, we will wish to demonstrate the accuracy and efficiency of the technique by analysing the structure (both for the stiffened and unstiffened plate) subject to different loading conditions and boundary conditions, and then compare the results with some already existing results. By so doing, the parameters of the tested structure is normally bounded by the parameters which are already employed in these existing analyses. In examining the structure which is being investigated, the governing parameters (e.g. stiffener area to plate thickness ratio, pitch dimension, Dt/EI ratio etc.) is found to be beyond the ranges covered by those existing results. Therefore the only way to obtain a reasonably accurate result that can otherwise be used as a cross-check on the present finite element results is to evaluate the buckling information based on the given structural parameters using the Engineering Data Sheet upon which the design criteria of that partiuclar structure was based.

The following diagram illustrates the cross section of the fuselage between any two stiffeners. The basic assumptions used in the finite element modelling have already been described in the previous report in Ref [1], and will still be applied to the present analysis.



Material properties

E = Young's modulus for $L_7 2$ = 10^7 LB/IN^2

E_t = Tangential modulus for $L_7 2$

σ_n = Stress @ $E_t = \frac{1}{2}E$

$\sigma_{0.1}$ = Stress @ 0.1% proof = 15 x 2240 LB/IN^2

m = Material characteristic for $L_7 2$ = 10

= Poison's ratio = .3

$\epsilon_{.1}$ = Strain @ 0.1% proof = 0.01

A_s = Area of stringer = .14198 in^2

I_s = 2nd moment of inertia of stringer = <u>0.0348 in^4</u>

I_x = 2nd moment of inertia of stringer about the plate centre line = $.14198 \times .657^2 + .0348$ = <u>.0961 in^4</u>

$\frac{I_x}{I_s} = \frac{.0961}{.0348} =$ <u>2.761</u>

radius of gyration $k = (\frac{I_s}{A_s})^{\frac{1}{2}} = (\frac{.0348}{.14198})^{\frac{1}{2}} =$ <u>0.496 in</u>

$e = \frac{k^2}{\bar{y}} = \frac{.246}{.625} =$ <u>0.393</u> ; e = eccentricity = <u>0.005"</u>

$\frac{e}{c} = \frac{.005}{.393} =$ <u>.01</u> ; $\frac{b_s}{h} = \frac{.7}{1.25} =$ <u>0.56</u> ; $\frac{h}{b} = \frac{1.25}{4.5} = 0.277$

$\frac{t_s}{t} = \frac{.048}{.064} =$ <u>0.75</u>

A_{sk} = Area of skin = 4.5 x 0.64 = <u>0.288 in^2</u>

A. 1 Material properties of L_72

Stress @ .1% proof is 15 x 2440 LB/IN^2 = 33600LB/IN^2
for material characteristin of m = 10;
from E.D.S. (hereafter; E.D.S. would stand for Engineering Data Sheet) 76016:-

$$\sigma_n = \sigma_{0.1} \left(\frac{m.\ \varepsilon_{.1}\ .E}{\sigma_{.1}}\right)^{\frac{1}{m-1}}$$

$$= 33600 \times \left(\frac{10 \times .001 \times 10^7}{33600}\right)^{-1/9}$$

Hence σ_n = 29766 LB/IN^2

Notations

γ_o = elastic edge rotational restrain coefficient

σ_b = local buckling stress of a plate component

σ_0 = elastic buckling stress of a simply-supported plate under uniaxial compression

σ_s = buckling stress of stringer

σ_{edge} = edge stress @ failure of stiffened plate

σ_{ave} = average stress carried by skin when overall buckling occurs

σ_c = crippling stress

$(\sigma_b)e$; $(\sigma_b)f$ = local buckling stress of skin and flange elements.

A. 2 Evaluation of Local Buckling Stress of the Skin

For local buckling stress of the skin with Z type of stringer sitting on one side of the skin is derived from E.D.S. 71014 (02.01.35):-

$$@\ \frac{b_s}{h} = \frac{.7}{1.25} = 0.56 \quad ; \quad \frac{h}{b} = \frac{1.25}{4.5} = 0.277;$$

$$\frac{t_s}{t} = \frac{.048}{.064} = .75$$

from E.D.S. 71014 : K = 4.5

from E.D.S. 72012: $(\sigma_b)e = K \times E \times (\frac{t}{b})^2 = 4.5 \times 10^7 \times (\frac{0.064}{4.5})^2$

$= \underline{9,100\ lb./in^2}$

The above value assumes that there is no laterial restrain acting. However, a small amount of restrain will be provided by frames and can be estimated in 72019, where:-

$$\nu_0 = \frac{A_{SK}}{t.1} = \frac{4.5 \times t}{20 \times t} = \underline{0.225}$$

from E.D.S. 72019;

$$\sigma_0 = \frac{\pi^2 \cdot E}{3(1-\nu^2)} (\frac{t}{b})^2 = \underline{7312\ LB/IN^2}$$

$$\therefore \frac{(\sigma_b)e}{\sigma_0} = \frac{9100}{7312} = \underline{1.244}$$

From Fig 3 of E.D.S. 72019 when $\frac{(\sigma_b)e}{\sigma_0} = 1.233$ & $\nu_o = 0$

μ is found to be 4.5

and @ $\nu_o = 0.255$, $\mu = 4.5$; the corrected $\frac{(\sigma_b)e}{\sigma_0}$ is $\underline{1.2}$

Hence, the corrected value of local buckling stress of the skin

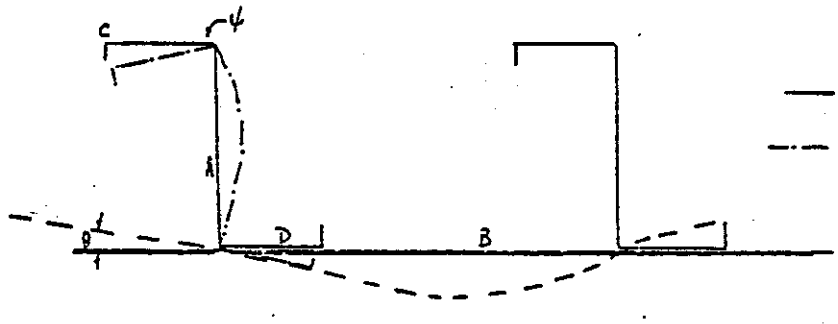
= 7312 x 1.2

= <u>8774 LB/IN^2</u> = σ_b

A. 3 Calculation of the Buckled Half Wave Length

To calculate the buckled wave length of the panel, the procedure set out in E.D.S. 72012 is to be followed:-

from above paragraph $(\sigma_b)x = \sigma_x =$ <u>9100 LB/IN^2</u>



— Deformed shape of the stiffened panel

--- Undeformed shape of the stiffened panel

For C = D, the following calculations are obtained :-

	FLATS	A	B	C.
	Width : b	1.25	4.5	.7 .
	thickness : t	.028	.064	.028
	$E't^2/3b^2$ =	340.08	213.38	526.63
σ_o =	$\eta^2 . E . t^4/3 . b^2$	53308	7312	169990
σ_x/σ_o =	$9100/\sigma_o$	0.17	1.244	0.0535

λ	$\frac{\sigma_x}{\sigma_o}$ = .17			$\frac{\sigma_x}{\sigma_o}$ = 1.244		$\frac{\sigma_x}{\sigma_o}$ = .0535		A_1	A_2	A_3	C_1	$\frac{1}{2}(A_1+A_2)\cdot C_1$	$A_2 \cdot A_3$	$\frac{1}{2}(A_2+A_3)\cdot C_1 + A_1 \cdot A_3$	$\frac{1}{2}(A_1+A_2)\cdot C_1 + A_3$	$\frac{\frac{1}{2}(A_1+A_2)C_1 + A_1 A_3}{\frac{1}{2}(A_1+A_2)\cdot C_1}$	$C_1 \cdot \frac{\frac{1}{2}(A_1+A_2)C_1 + A_2 A_3}{\frac{1}{2}(A_2+A_3)\cdot C_1}$	2.B	$\frac{\Sigma(A_1 B_1 X_1 + A_2 B_2)}{(B_1 C_1' \frac{1}{2}(A_1+A_2)\cdot C_1} = \frac{T}{\theta}$
	$\frac{b'}{\lambda}$	A_2'	A_3'	$\frac{b}{h}$	B_2'	$\frac{b}{h}$	C_1'												
2.	.625	.75	1.57	2.25	2.5	.35	.25	255	533	533	131	51850	113915	181755	525	3.57	4.88	1066	1554
2.5	.5	.65	1.53	1.8	1.0	.28	.15	221	520	213	79	27365	110920	138135	449	3.20	3.79	426	825
3	.416	.61	1.5	1.5	-.5	.233	.1	207	510	-106.7	53	18837	165370	174327	411	3.03	3.55	.23	142
3.5	.327	.6	1.5	1.28	-.95	.2	.07	204	510	-202.7	37	13157	164340	117177	394	2.97	3.33	-.205	-.72
4	.312	.57	1.5	1.115	-.95	.17	.06	193	510	-202.7	32	11107	156730	109537	363	2.86	3.17	-.205	-.88

A. 4 The Panel Failing Load in Overall Buckling

From E.D.S. 72012:-

The buckling stress of the perfect stringer along about an axis parallel to the plane of the skin is (from 01.01.01):-

for: $\frac{l}{k} \cdot \left[\frac{\sigma_n}{E}\right]^{\frac{1}{2}} = \frac{20}{.496} \times \left(\frac{29766}{10^7}\right)^{\frac{1}{2}} = 2.194$

& $\frac{e}{c} = .01 \quad ; \quad m = 10$

Sheet 01.01.01 shows that $\frac{\sigma_s}{\sigma_n} = 1 \quad \therefore \sigma_s = \sigma_n = \underline{29766 \text{ LB/IN}^2}$

The panel skin buckles @ a stress level well below that of a stringer, therefore, it is necessary to determine the condition where load shedded by the buckled skin into the stringer cause failure of the stringer and further determines the removing load carried by the skin. To calculate the failing stress of the stringer due to the shredded load from the buckled skin :- (E.D.S. 02.01.17) for:-

$\frac{I_x}{I_s} = 2.761 \quad : \quad \frac{A_s}{bt} = 0.493 \quad : \quad \sigma_s = 29766 \quad : \quad \sigma_b = 8712$

Approximation	σ_{edge}	σ_b/σ_{edge}	σ_{edge}/σ_s	σ_{edge}
1st : σ_s	29,766	.292	.79	23,515
2nd	23,515	.37	.77	22,913
3rd	22,913	.38	.769	22.890

Hence, the failing stress of the stringer = 22890 LB/IN^2
= σ_{edge}

An estimated average stresses acting on the skin when the panel suffers overall buckling can be made by means of the lower figure of E.D.S. 02.01.23 where:-

$$\frac{\sigma_{edge}}{\sigma_b} = \frac{22890}{8712} = 2.627$$

$$\nu_0 = .225$$

from 02.01.23 ;

$$\frac{\sigma_{ave}}{\sigma_{edge}} = 0.68$$

$$\therefore \quad \sigma_{av} = 0.68 \times 22890 = \underline{15566 \text{ LB/IN}^2}$$

A. 5 Crippling Stress of Z Section Stringers (see E.D.S. 78020)

For a given value of t_{d/t_h} and low values of d/h, the web is primarily responsible for buckling and requires some restraint from the flange in order to delay the buckling until the load is cracked for which the cross section as a whole becomes unstable.

Consider the stiffener of the following dimension:-

h = 1.25 in	$E = 10^7$ LB/IN^2
d = 0.7 in	$\nu = 0.3$
t_d = 0.048 in	m = 10
t_h = 0.048 in	σ_n = 29766 LB/IN^2 = f_n
C_2 = Material yield stress = 33,600 LB/IN^2	

$$\frac{d}{h} = 0.56 \qquad \frac{t_d}{t_n} = 1$$

from fig. 1 $K = 2.2$

$$\therefore \quad f_{be} = K.E.(t_{n/h})^2 = 2.2 \times 10^7 \times (\frac{0.048}{1.25})^2$$

$$= 32,440 \text{ LB/IN}^2$$

$$\frac{f_{be}}{f_n} = \frac{32,440}{29,766} = 1.0898$$

From fig. 3 @ m = 10 $\eta = 0.87$

Thus:- $f_b = \eta . f_{be} = 0.87 \times 32,440 = 28,222 \text{ LB/IN}^2$

$\therefore$ the crippling stress $f_c = (C_2 \cdot f_b)^{\frac{1}{2}}$

$= (33,600 \times 28,222)^{\frac{1}{2}}$

$= \underline{30,794 \text{ LB/IN}^2}$

A. 6 Conclusion of the Analytical Results based on the Engineering Data Sheet

1) The local buckling stresses of the skin = $\underline{8744 \text{ LB/IN}^2}$

2) The stringer failing stress when the overall buckling occurs = $\underline{22890 \text{ LB/IN}^2}$

3) The crippling stress of the stringer flange is $\underline{30,794 \text{ LB/IN}^2}$

4) When overall buckling occurs, the skin will carry an average stress of $\underline{15566 \text{ LB/IN}^2}$

5) At the time of collapse, the applied load per unit length of the panel is:-

$(22890 \times .14198 + 15566 \times .288)/4.5 = \underline{1718 \text{ LB/IN}}$

OUT-OF-PLANE DEFLECTION OF THE PLATE USING F.E. IDEALIZATION

SIMPLY-SUPPORTED		2 × 2 ELEMENT		4 × 4 ELEMENT		6 × 6 ELEMENT	
ASPECT RATIO	THEORETICAL VALUE: β_s	F.E. ANALY. β	% DIFF.	F.E. ANALY. β	% DIFF.	F.E. ANALY. β	% DIFF.
1.0	11.60	11.478	-1.0	11.5677	-0.28	11.591	-0.07
1.2	13.53	13.402	-0.9	13.52	-0.07	13.525	-0.037
1.4	14.84	14.664	-1.18	14.80	-0.27	14.83	-0.06
1.6	15.70	15.44	-1.65	15.60	-0.64	15.67	-0.19
1.8	16.20	15.91	-1.79	16.07	-0.80	16.17	-0.18
2.0	16.51	16.21	-1.79	16.33	-1.09	16.42	-0.64

TABLE A

CLAMPED EDGES		2 × 2 ELEMENT		4 × 4 ELEMENT		6 × 6 ELEMENT	
ASPECT RATIO	THEORETICAL VALUE: β_c	F.E. ANALY. β	% DIFF.	F.E. ANALY. β	% DIFF.	F.E. ANALY. β	% DIFF.
1.0	5.60	5.30	-5.3	5.484	-2.07	5.57	-0.54
1.2	6.47	6.05	-6.47	6.316	-2.37	6.42	-0.77
1.4	6.91	6.30	-8.84	6.72	-2.76	6.83	-1.16
1.6	7.12	6.29	-11.52	6.866	-3.5	7.02	-1.4
1.8	7.20	6.017	-16.43	6.883	-4.4	7.12	-1.1
2.0	7.22	5.97	-17.24	6.830	-5.28	7.12	-1.4

TABLE B

	THEORETICAL VALUE	F.E. RESULT	% DIFF.
DEFLECTION AT A (in.)	0.0624	0.06244	0.06
DEFLECTION AT B (in.)	0.2496	0.25256	1.18

TABLE C

where: $\beta = \dfrac{W \times 10^3 \times D}{P \cdot b}$

$D = \dfrac{E \times h^3}{12(1-\nu^2)}$

FIG 1.

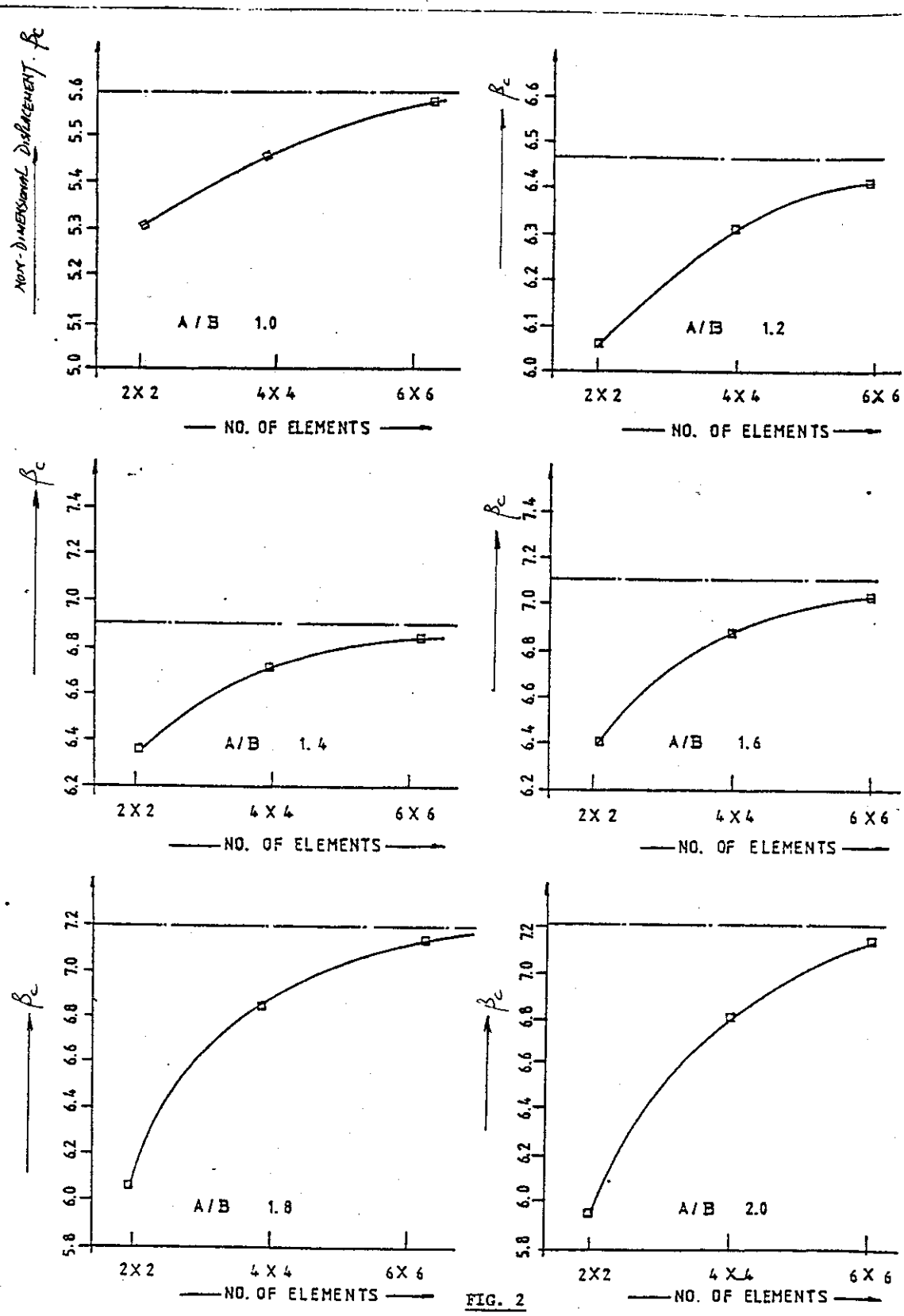

NON-DIMENSIONAL DISPLACEMENT β_c
A/B 1.0
A/B 1.2
A/B 1.4
A/B 1.6
A/B 1.8
A/B 2.0
2X2
4X4
6X6
NO. OF ELEMENTS

FIG. 2

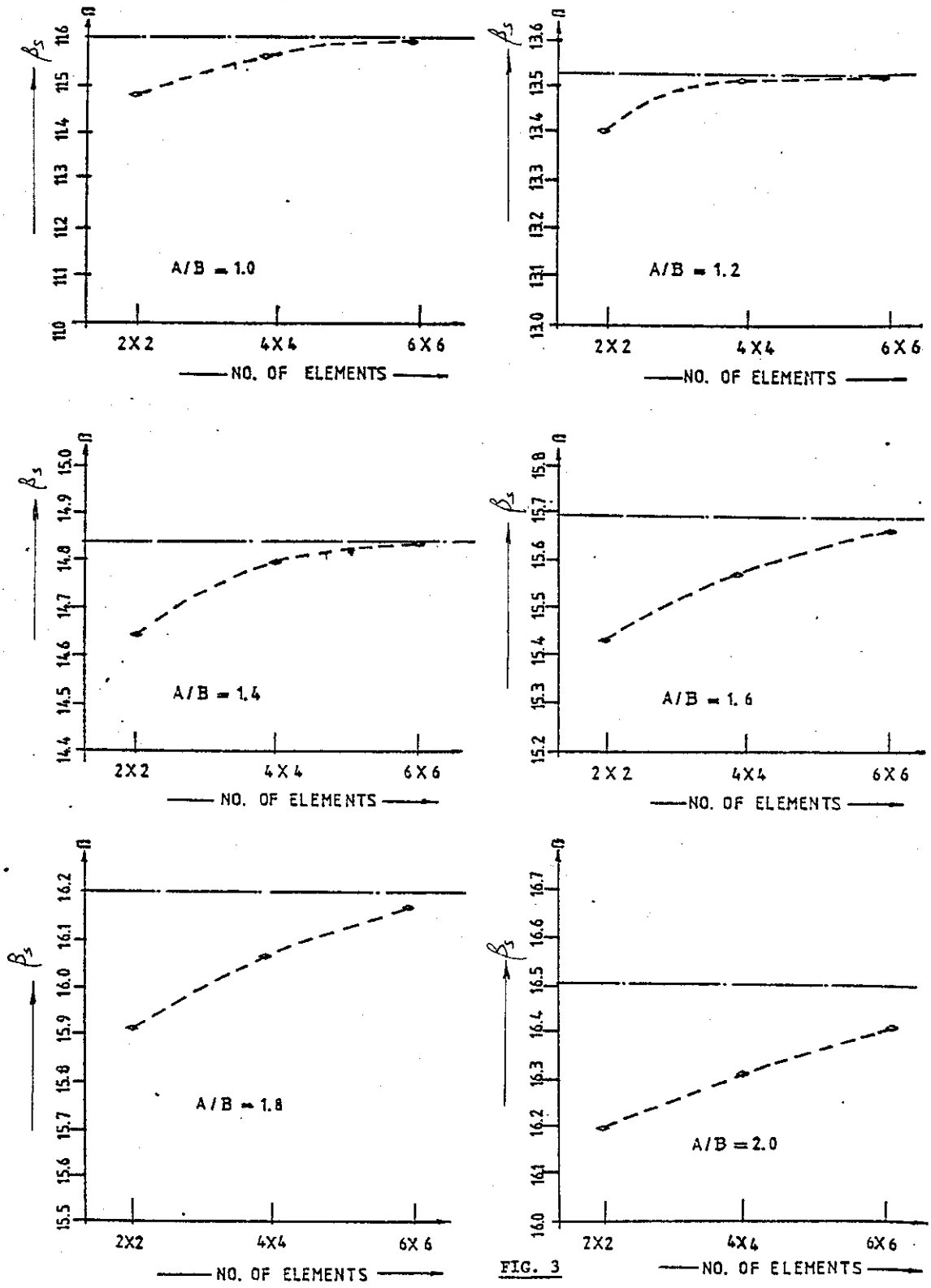
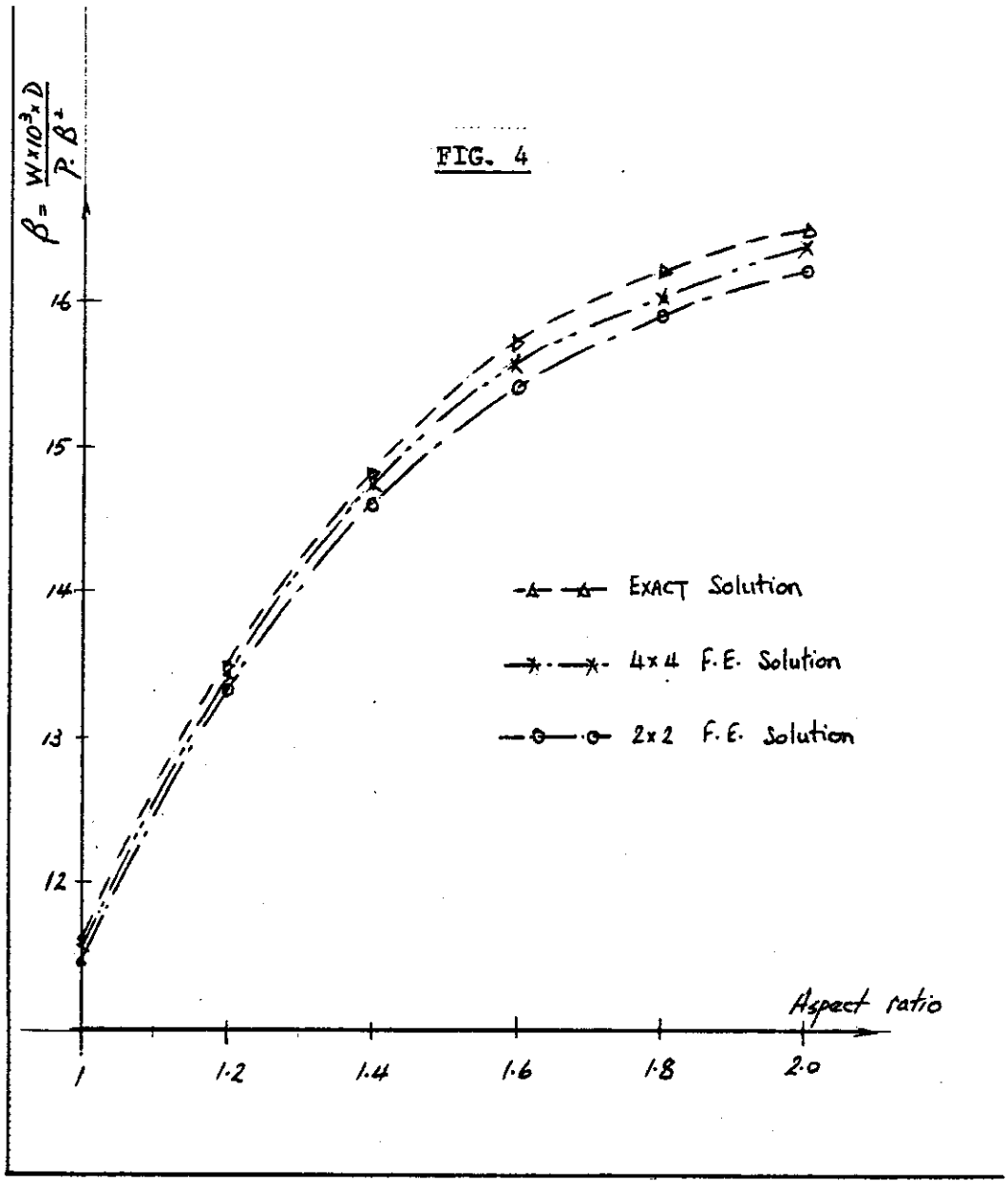

β_s
A/B = 1.0
A/B = 1.2
A/B = 1.4
A/B = 1.6
A/B = 1.8
A/B = 2.0
2X2
4X4
6X6
NO. OF ELEMENTS

FIG. 3

FIG. 4


$\beta = \frac{W \times 10^3 \times D}{P \cdot B^2}$
16
15
14
13
12
Aspect ratio
1
1·2
1·4
1·6
1·8
2·0
EXACT Solution
4×4 F.E. Solution
2×2 F.E. Solution

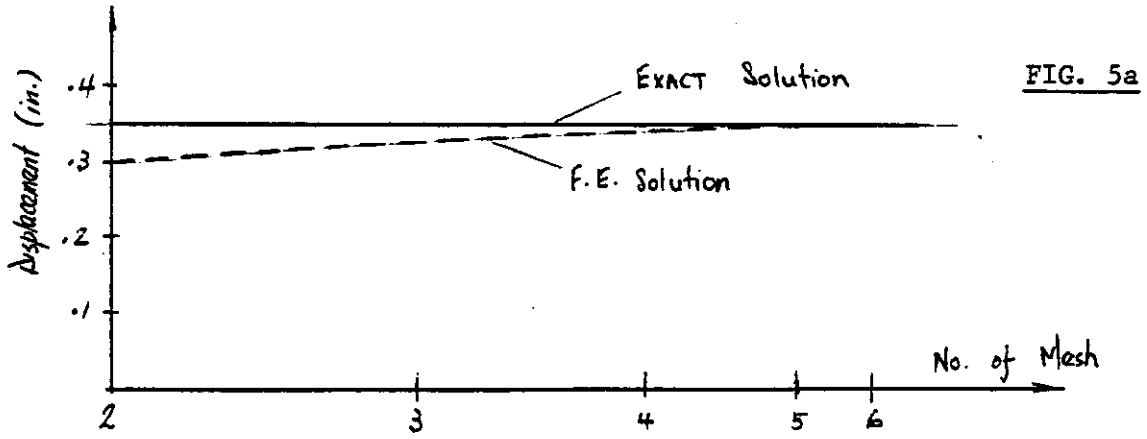
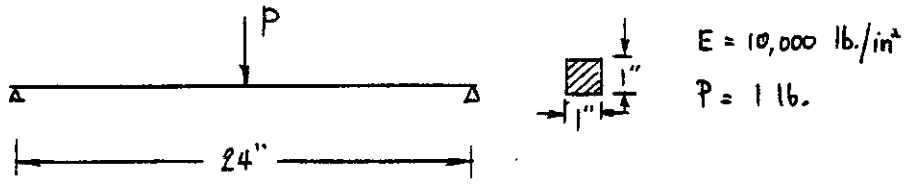

Displacement (in.)
·4
·3
·2
·1
EXACT Solution
F.E. Solution
No. of Mesh
2
3
4
5
6

FIG. 5a


P
24"
1"
1"
E = 10,000 lb./in²
P = 1 lb.

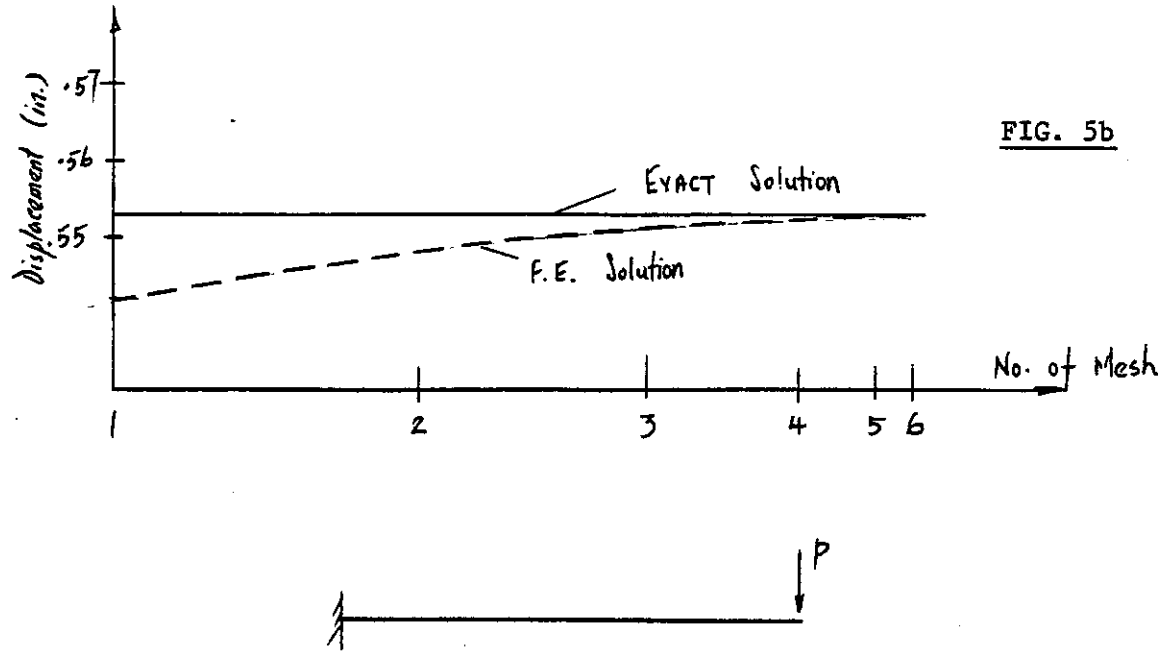

Displacement (in.)
.57
.56
.55
Exact Solution
F.E. Solution
No. of Mesh
1
2
3
4
5
6
P

FIG. 5b

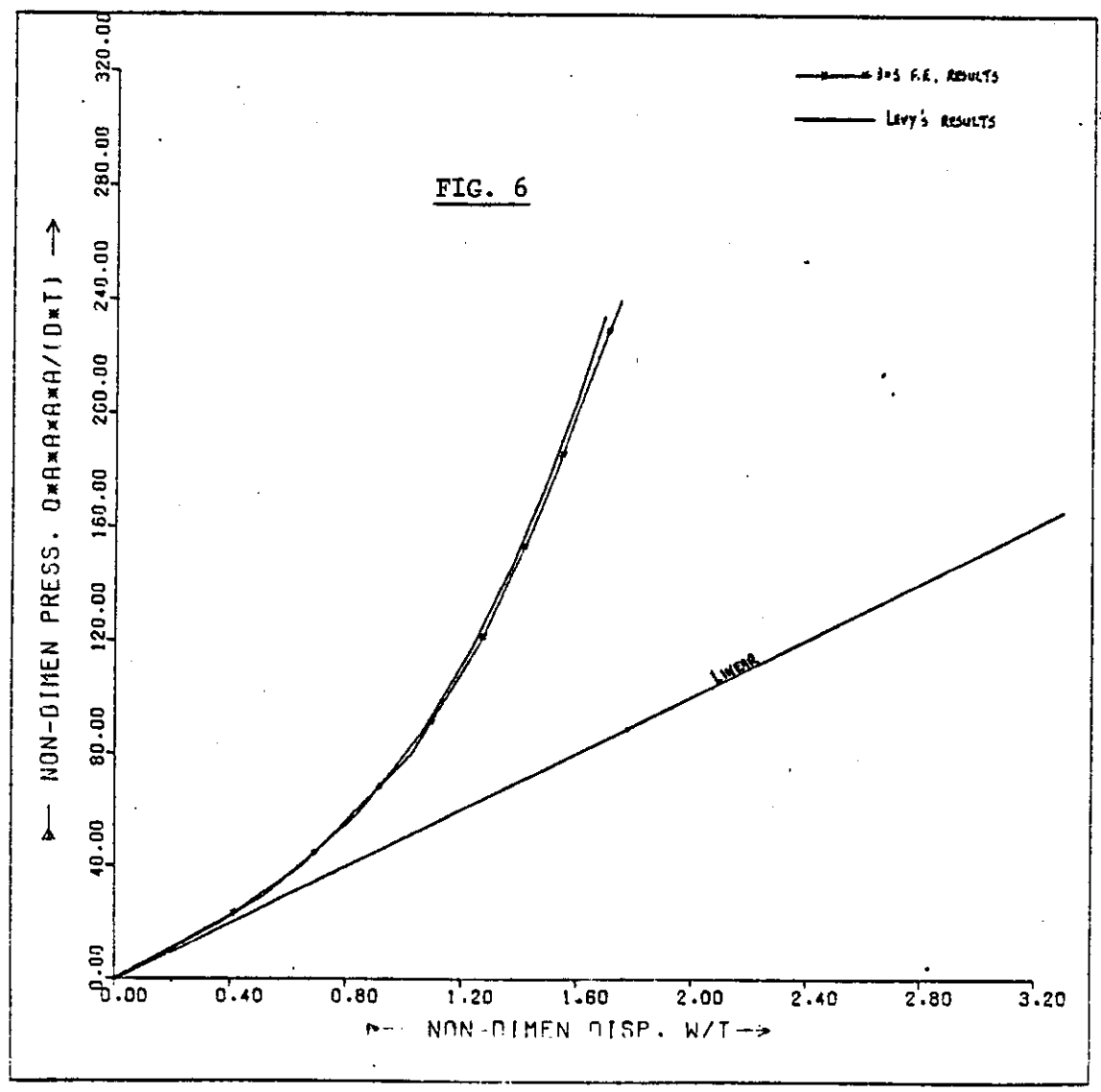

3*3 F.E. RESULTS
LEVY'S RESULTS
NON-DIMEN PRESS. Q*A*A*A*A/(D*T)
0.00
40.00
80.00
120.00
160.00
200.00
240.00
280.00
320.00
LINEAR
0.00
0.40
0.80
1.20
1.60
2.00
2.40
2.80
3.20
NON-DIMEN DISP. W/T

FIG. 6

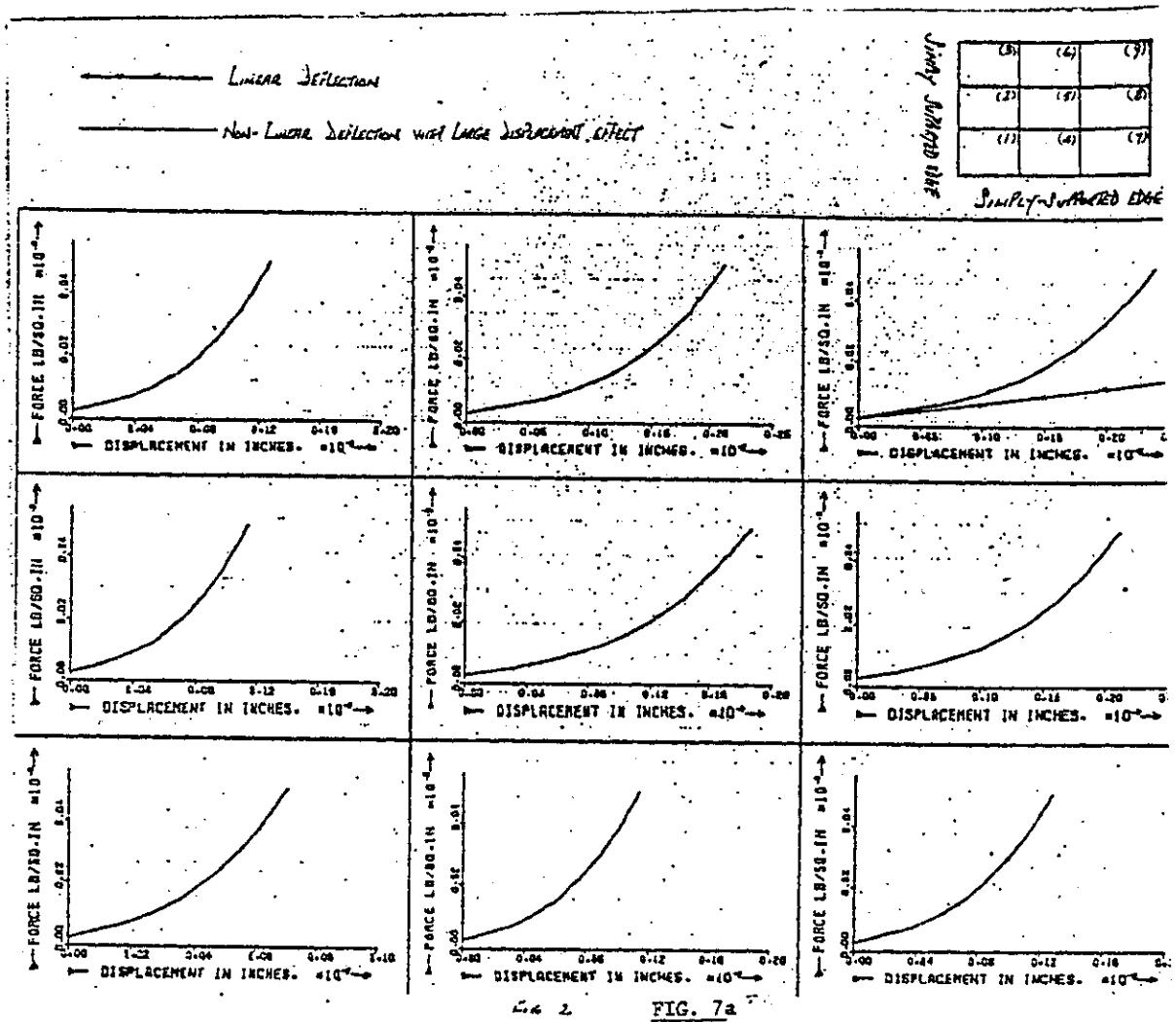

Linear Deflection
Non-Linear Deflection with Large Displacement Effect
Simply-Supported Edge
FORCE LB/SQ.IN
DISPLACEMENT IN INCHES.

FIG. 7a

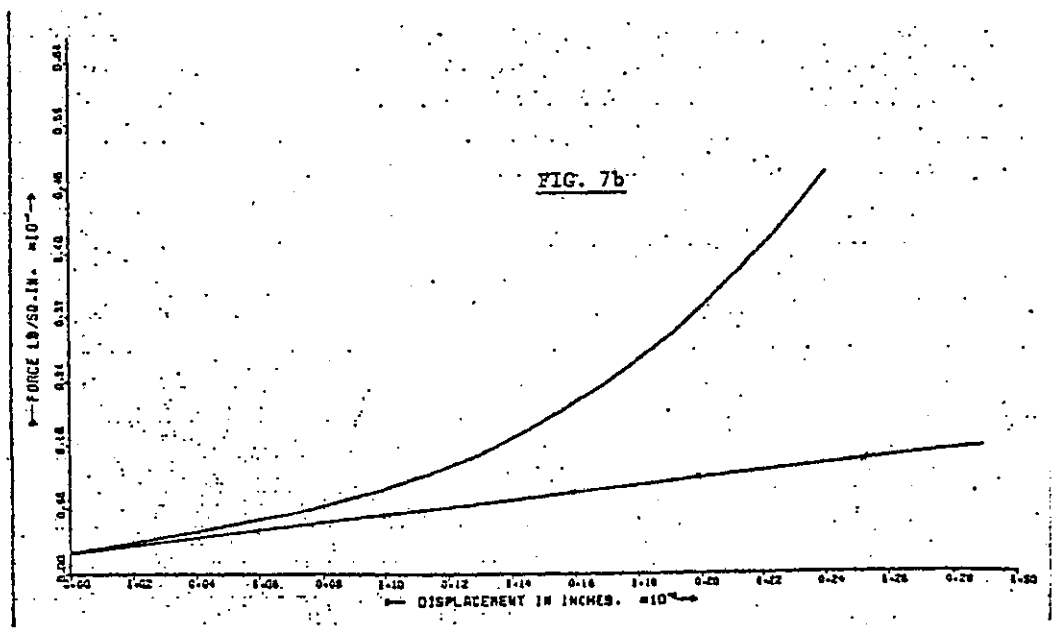

FORCE LB/SQ.IN.
DISPLACEMENT IN INCHES.

FIG. 7b

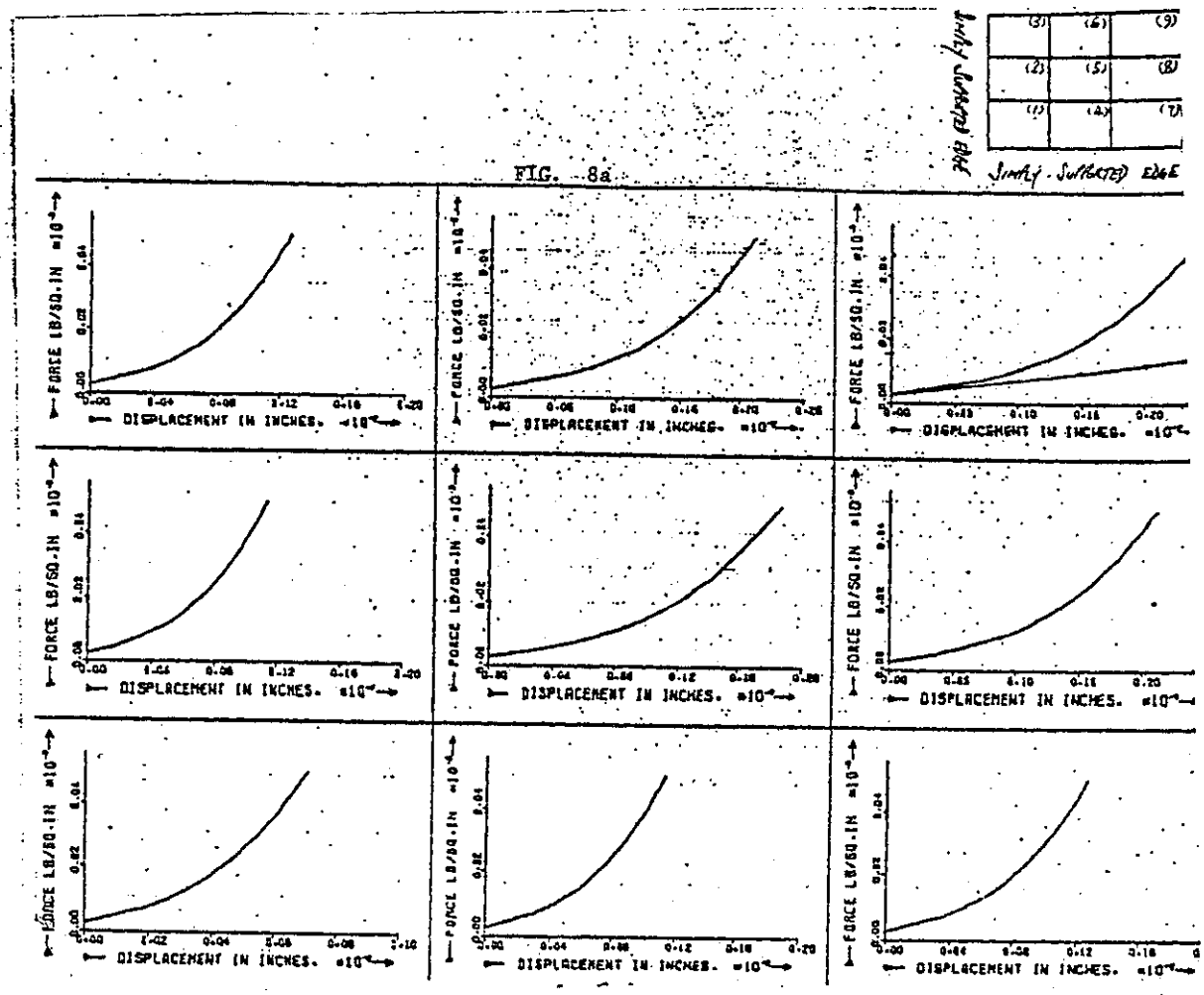

FORCE LB/SQ.IN. ×10⁻³
DISPLACEMENT IN INCHES. ×10⁻³

FIG. 8a

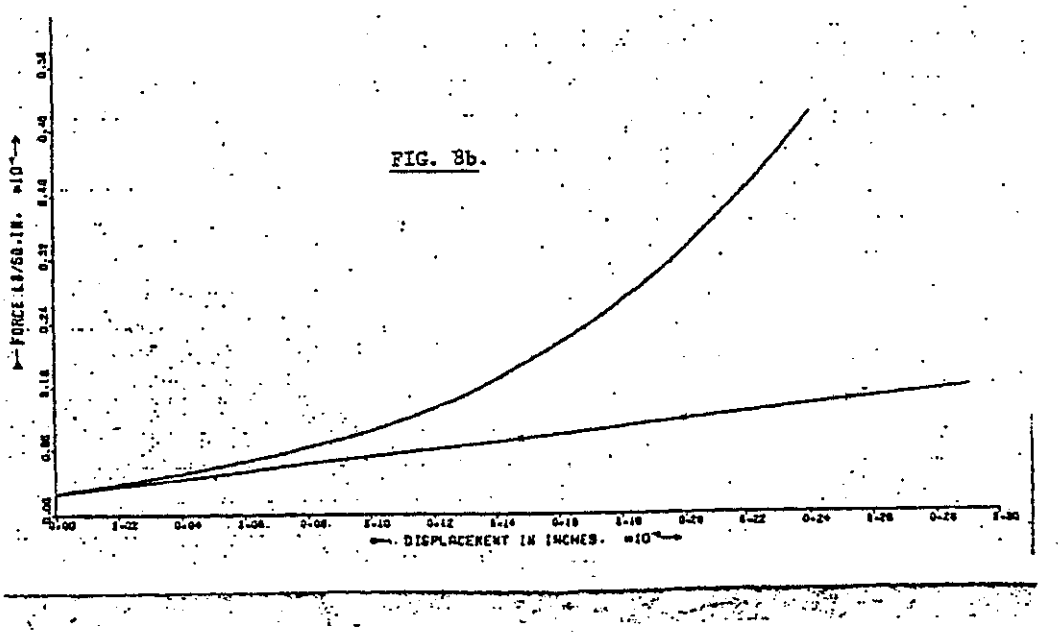

FORCE LB/SQ.IN. ×10⁻³
DISPLACEMENT IN INCHES. ×10⁻³

FIG. 8b.

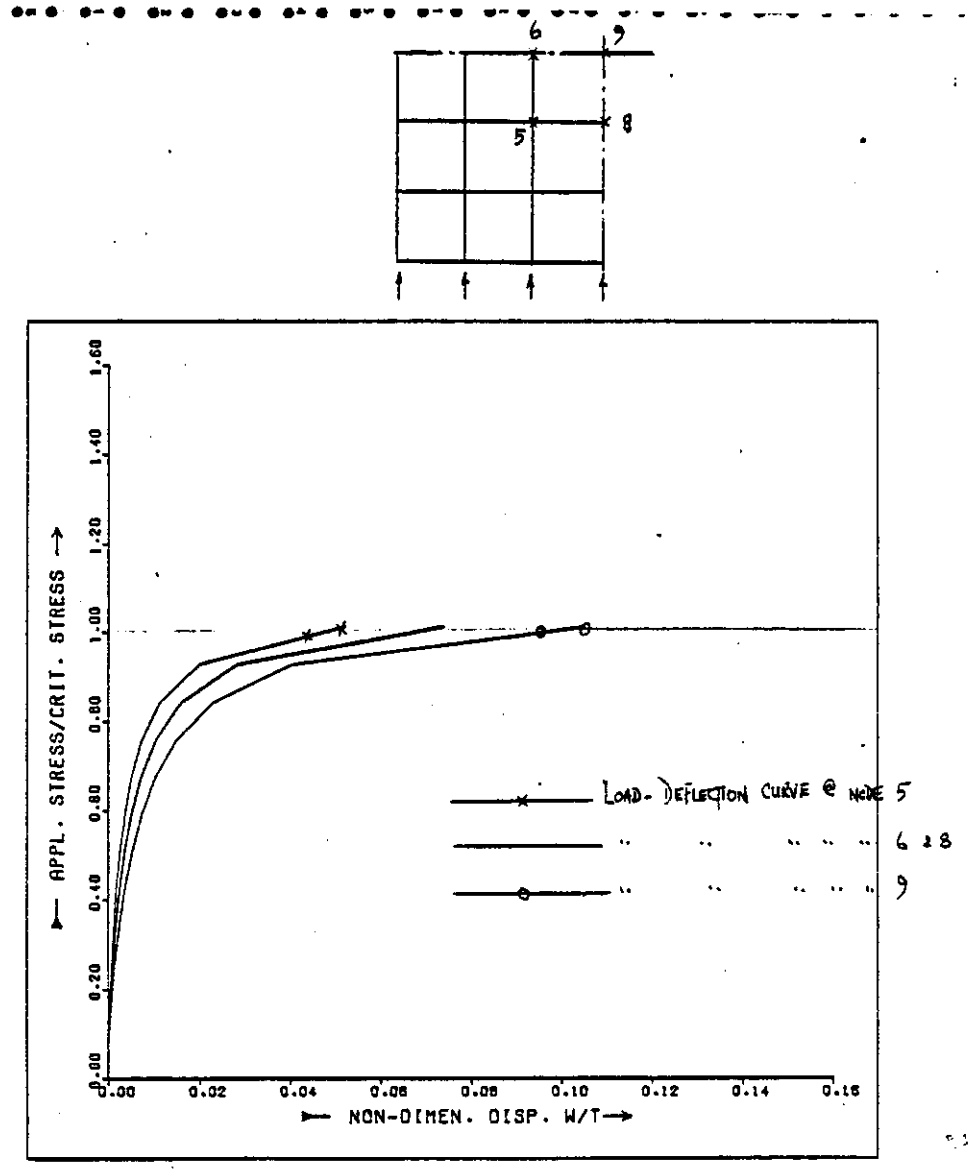

6
9
8
5
APPL. STRESS/CRIT. STRESS →
0.00
0.20
0.40
0.60
0.80
1.00
1.20
1.40
1.60
0.00
0.02
0.04
0.06
0.08
0.10
0.12
0.14
0.16
NON-DIMEN. DISP. W/T
LOAD-DEFLECTION CURVE @ NODE 5
" " " " " 6 & 8
" " " " " 9

FIG. 9

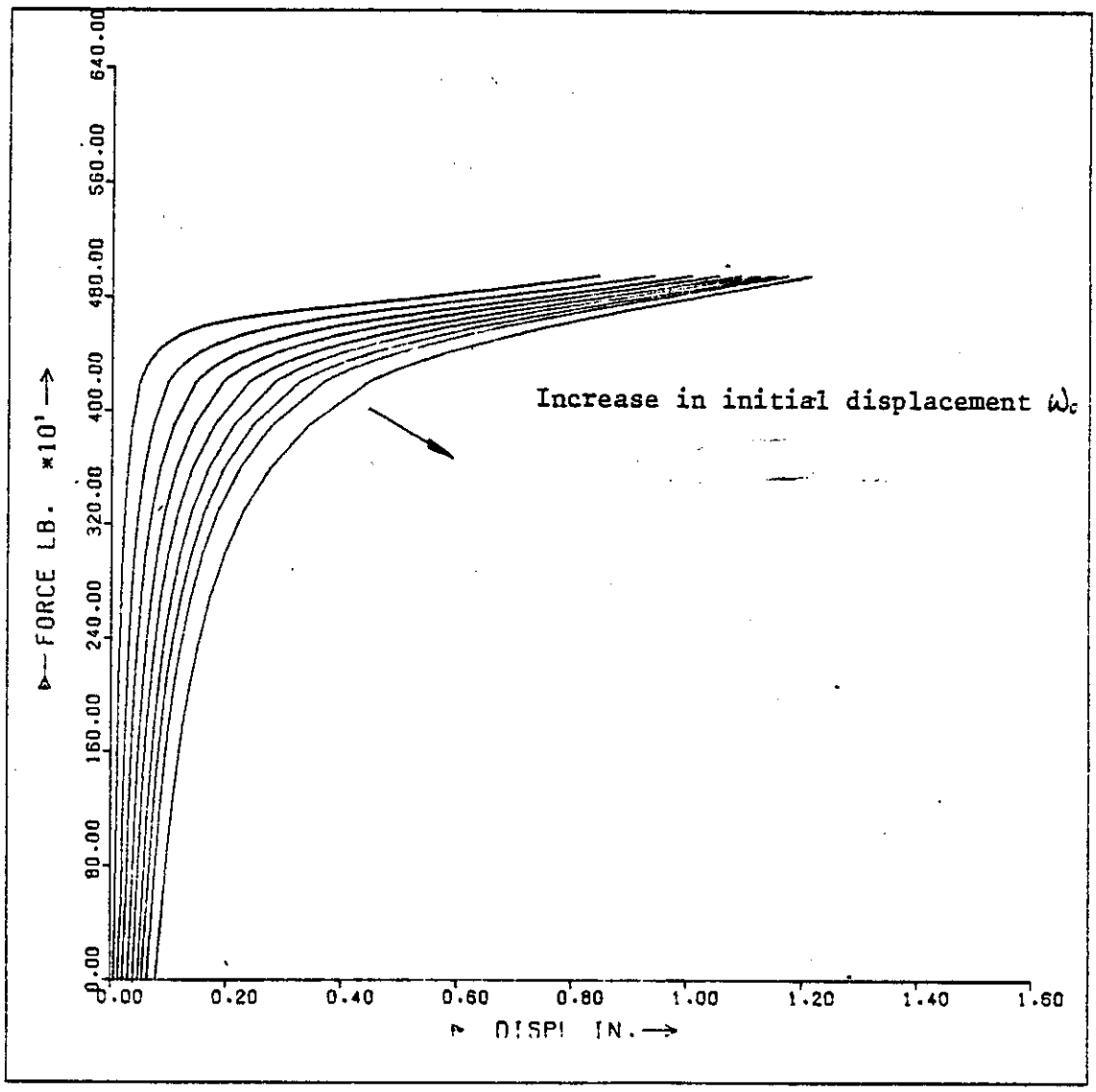

640.00
560.00
480.00
400.00
320.00
240.00
160.00
80.00
0.00
FORCE LB. *10' →
0.00
0.20
0.40
0.60
0.80
1.00
1.20
1.40
1.60
DISPL IN. →
Increase in initial displacement ω_c

FIG. 10

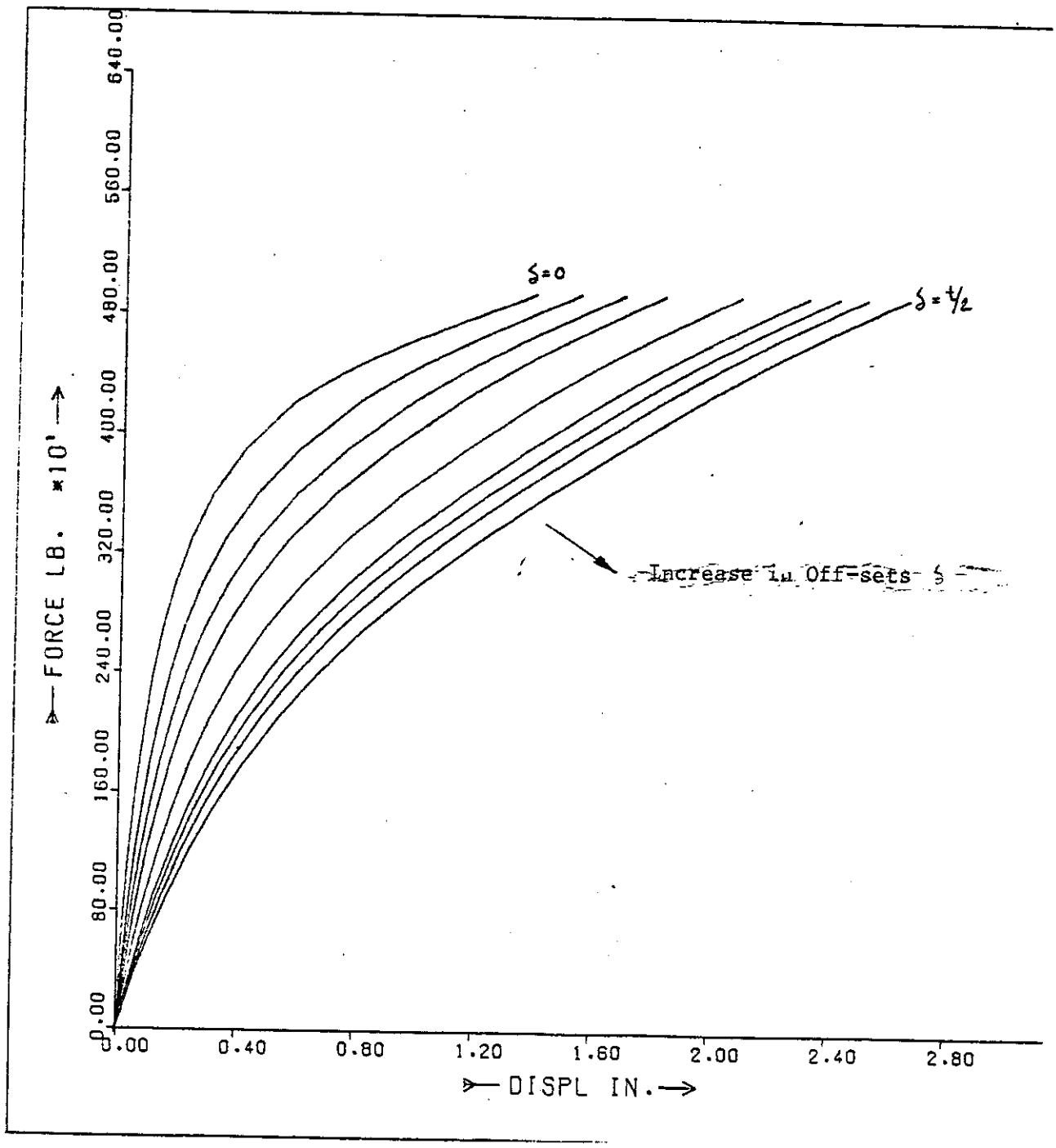
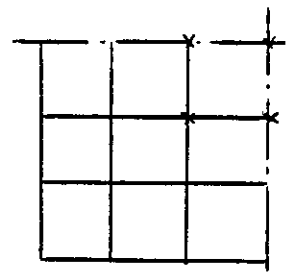


FIG. 11 Non-linear buckling of beam with different Off-sets



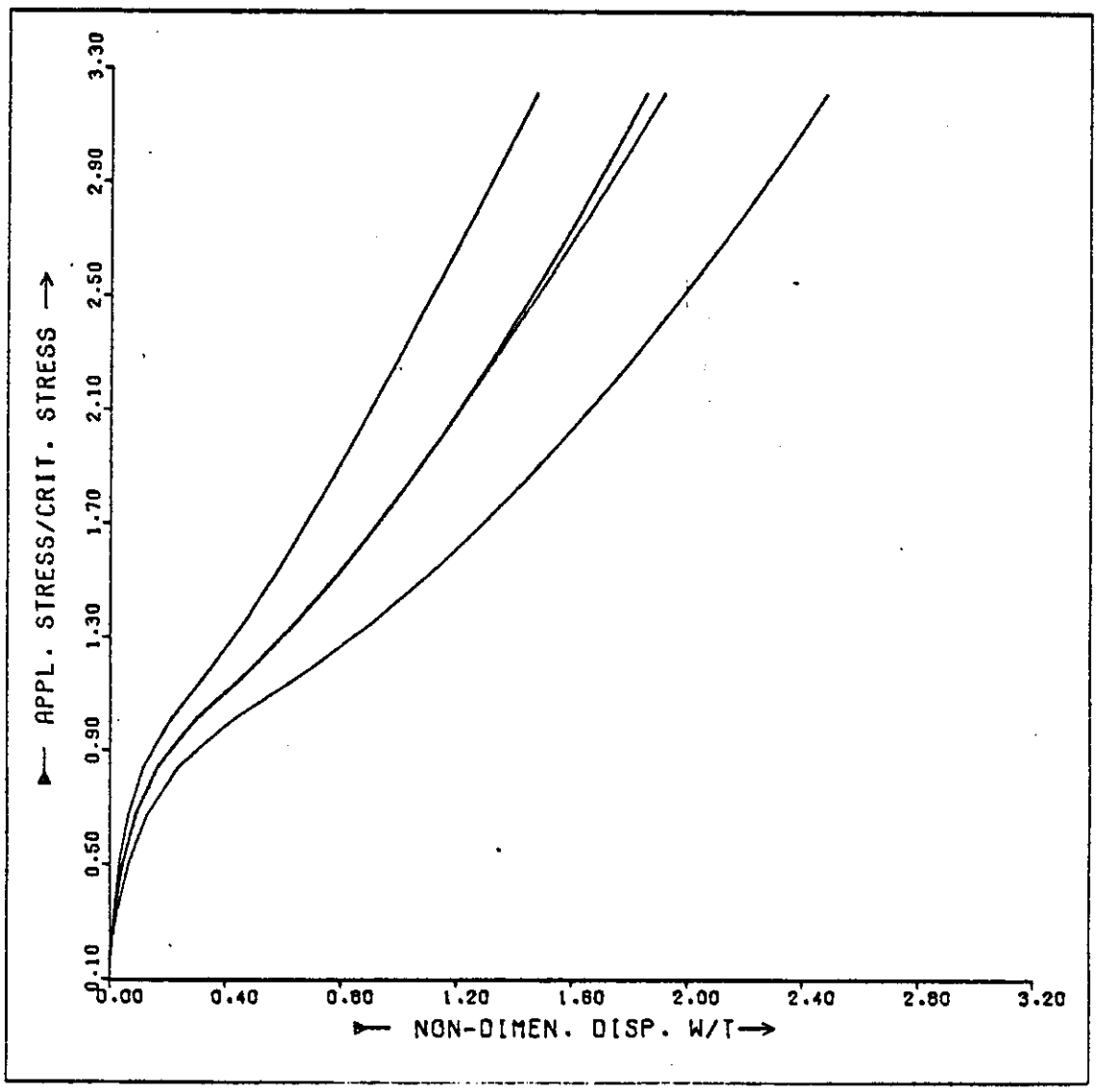


FIG. 12 Non-linear buckling of plate

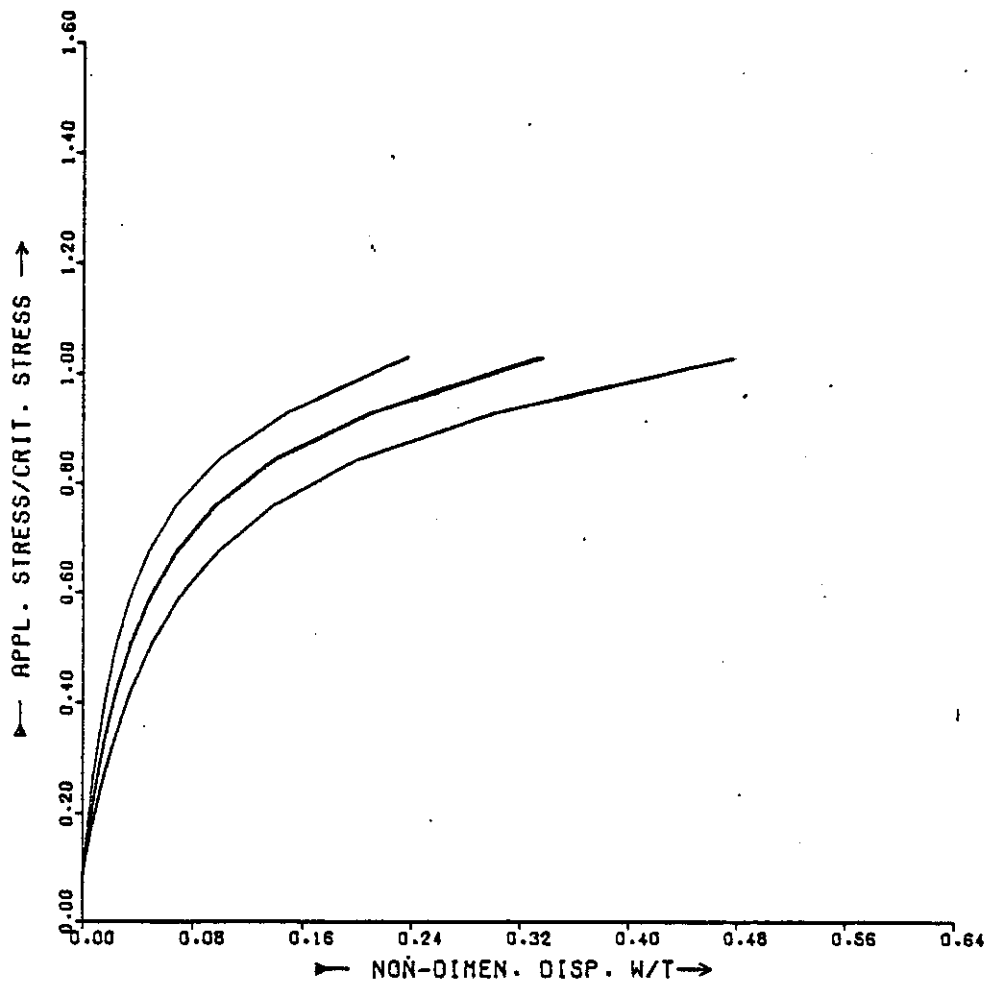


FIG. 13 Load-Displacement curves prior to local buckling of plate

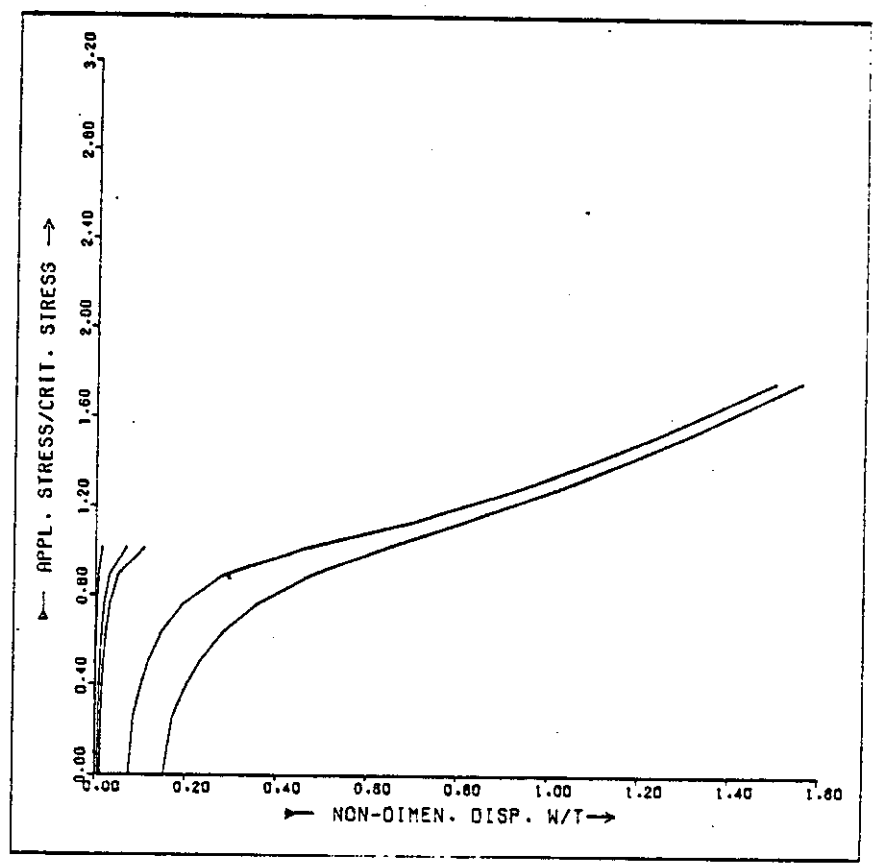


FIG. 14 Non-linear Buckling of plate with various initial Imperfections

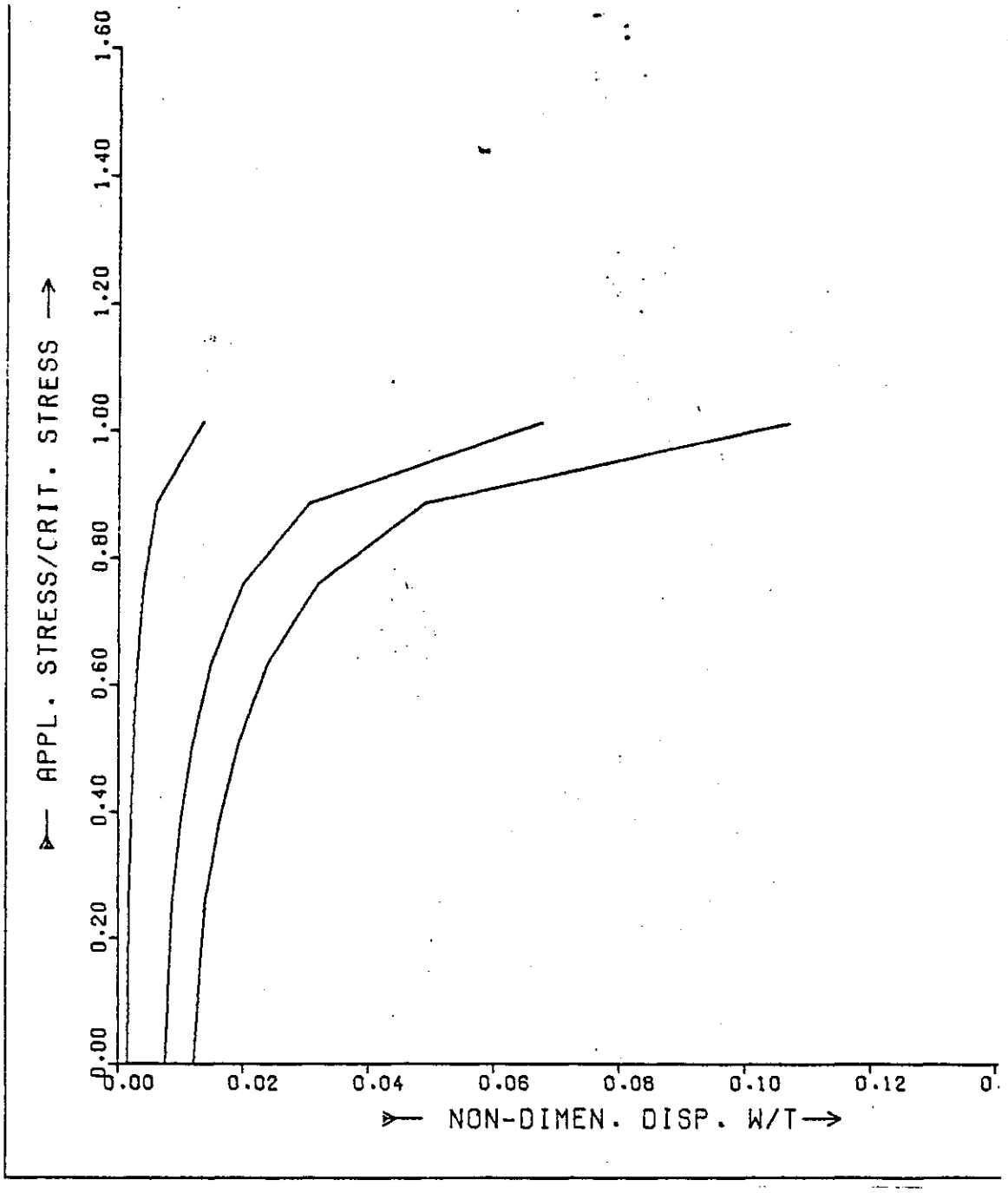


FIG. 15 Non-linear buckling of plate with initial displacements less than 1% of plate thickness

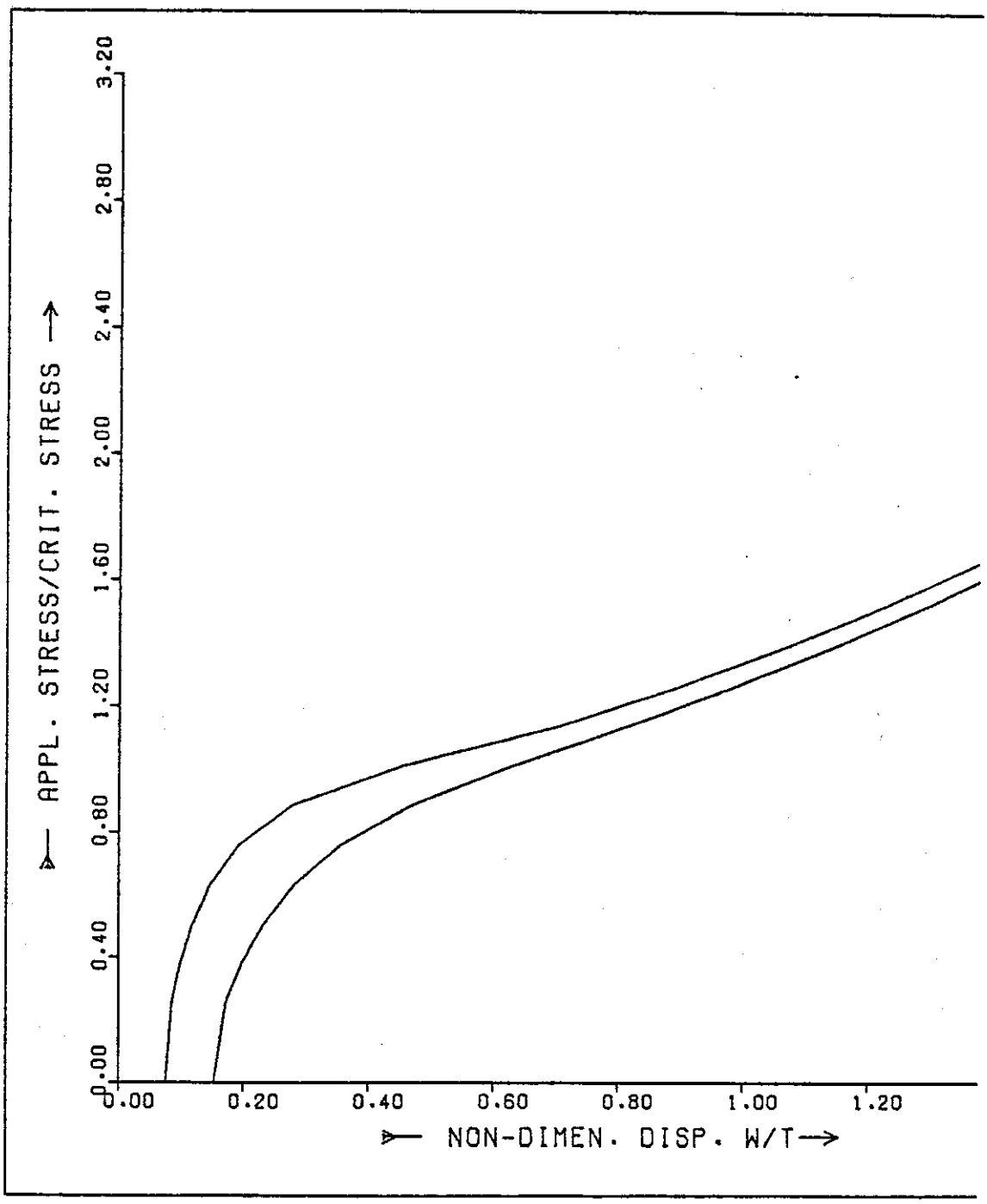
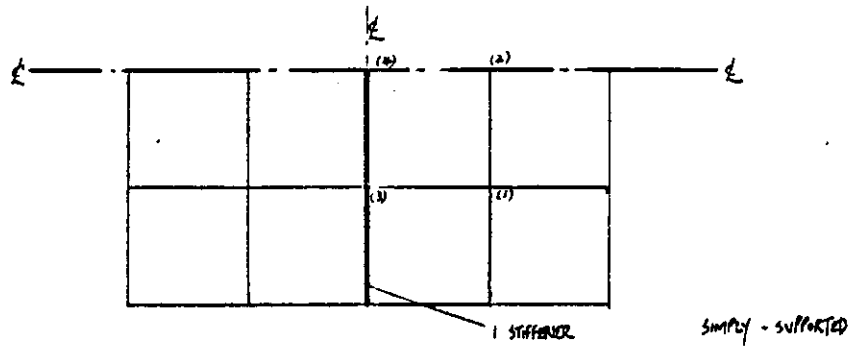


FIG. 16 Non-linear buckling of plate with large initial imperfections



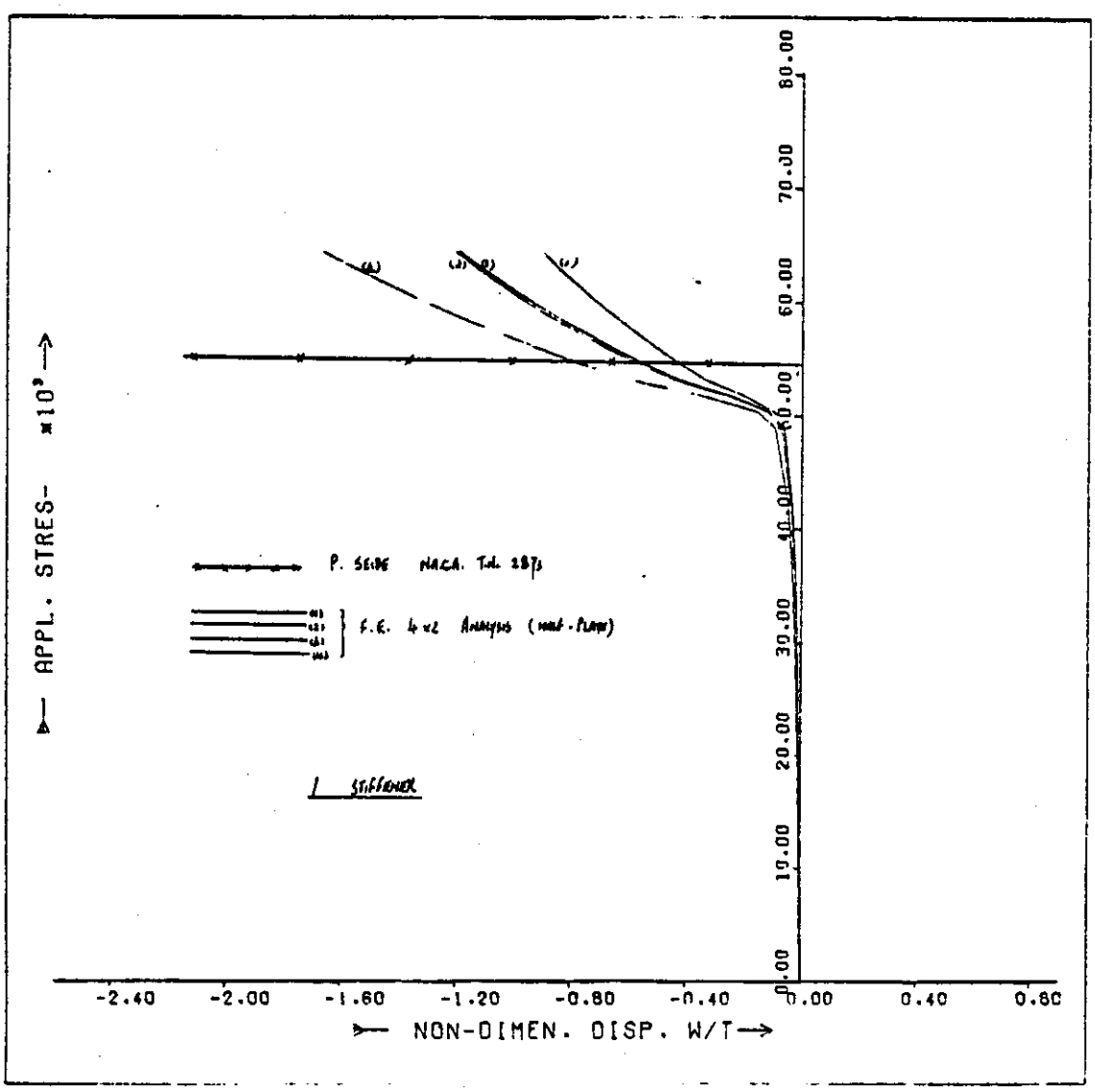


FIG. 17 Non-linear buckling of plate with 1 stiffener

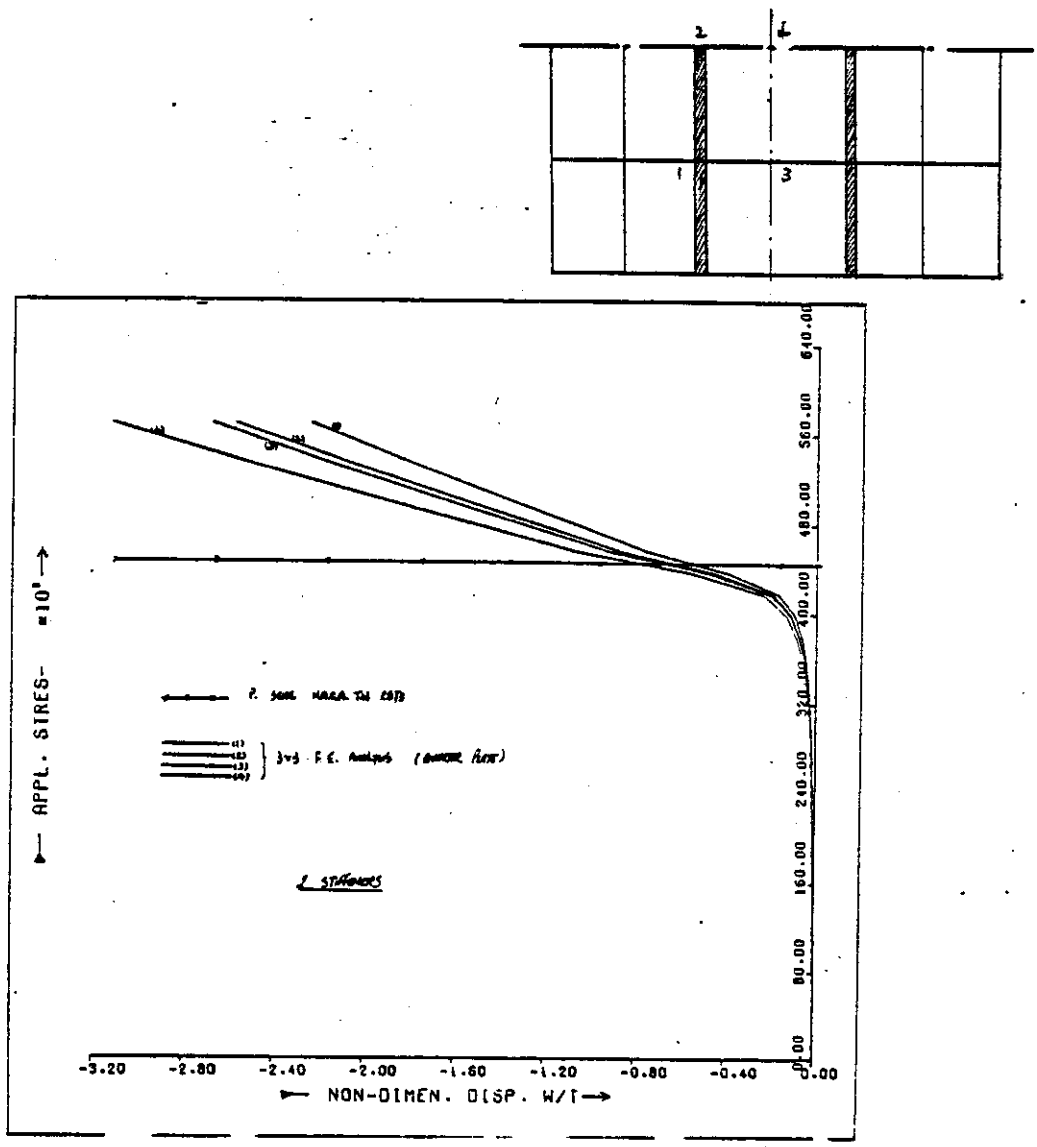


FIG. 18 Non-linear buckling of plate with 2 stiffeners

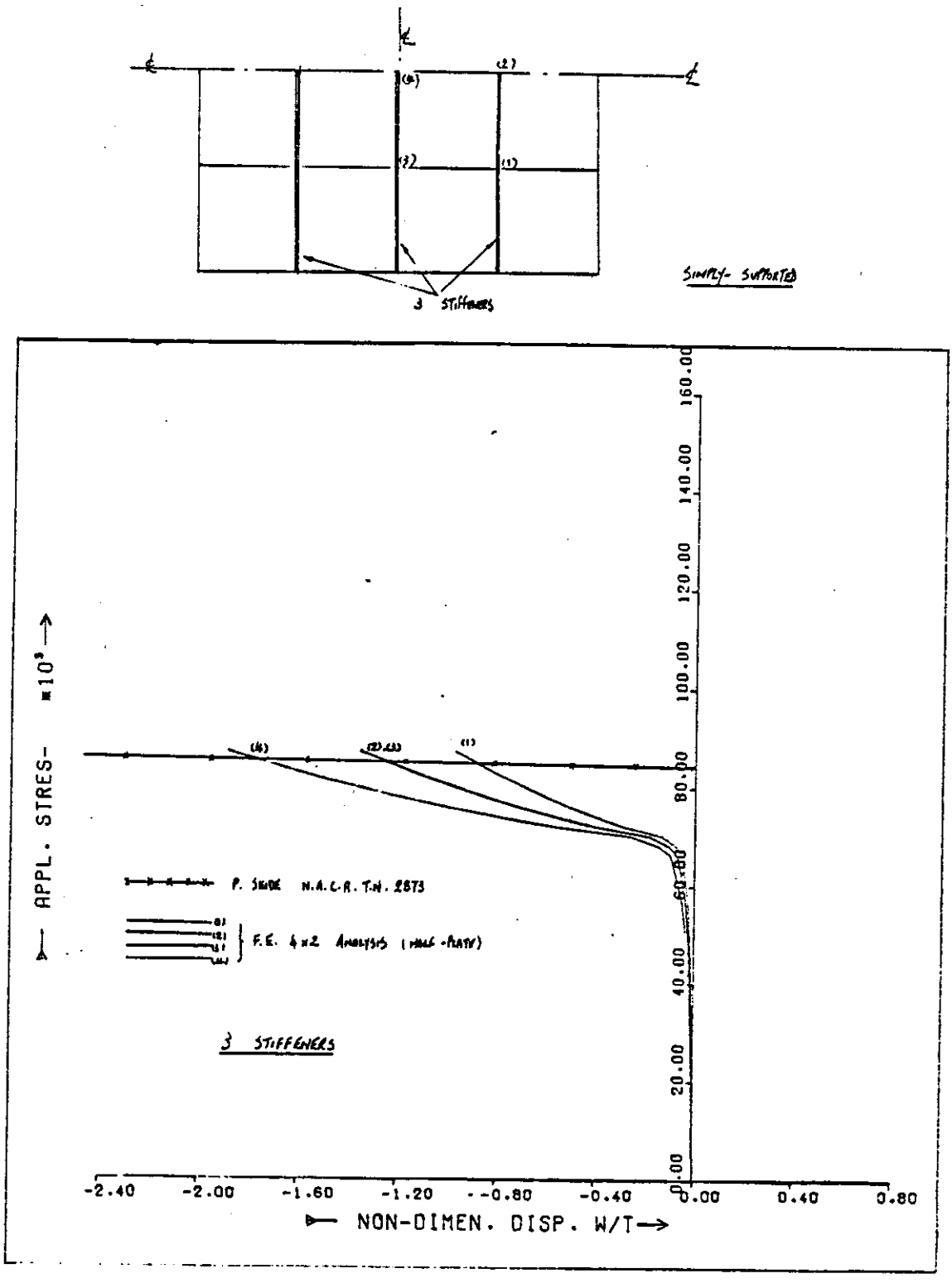


FIG. 19 Non-linear buckling of plate with 3 stiffeners

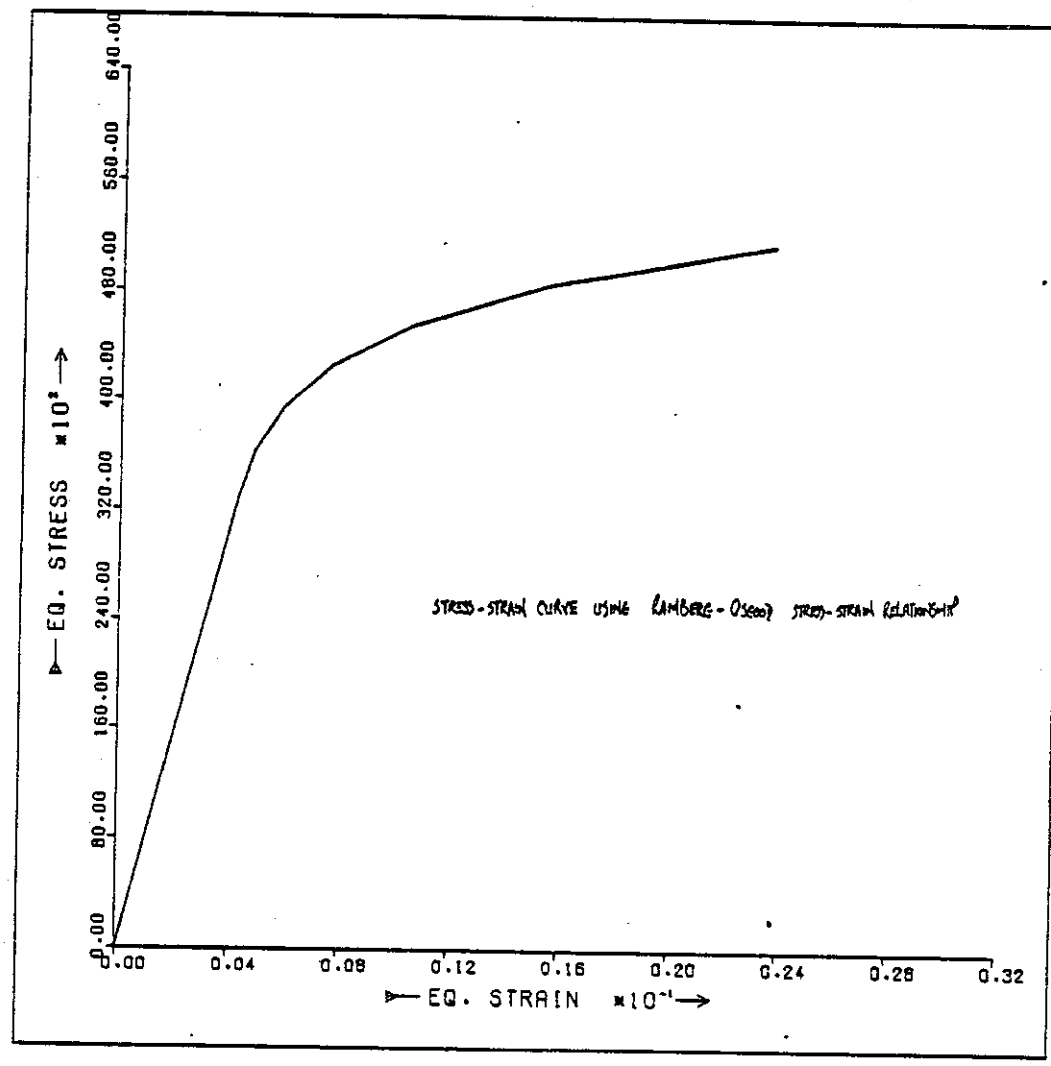

640.00
560.00
480.00
400.00
320.00
240.00
160.00
80.00
0.00
EQ. STRESS ×10³
0.00
0.04
0.08
0.12
0.16
0.20
0.24
0.28
0.32
EQ. STRAIN ×10⁻¹
STRESS-STRAIN CURVE USING RAMBERG-OSGOOD STRESS-STRAIN RELATIONSHIP

FIG. 20

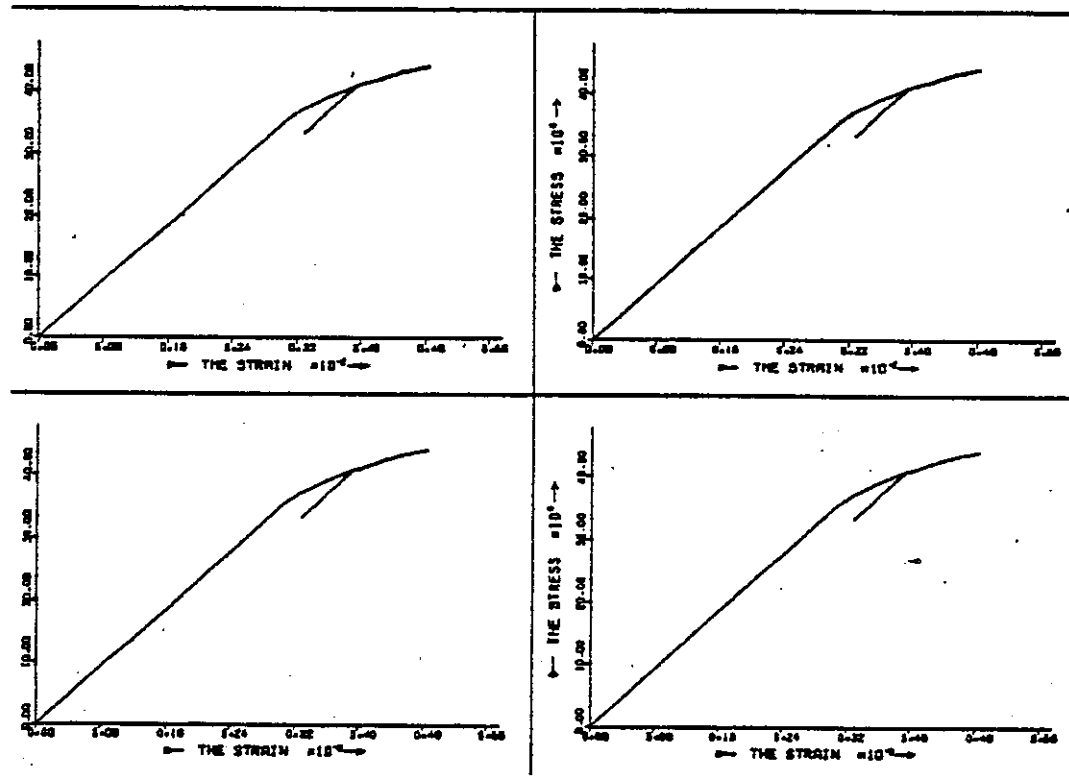


FIG. 21a Stress/Strain curves of plate element 1 (Tensile loading/unloading

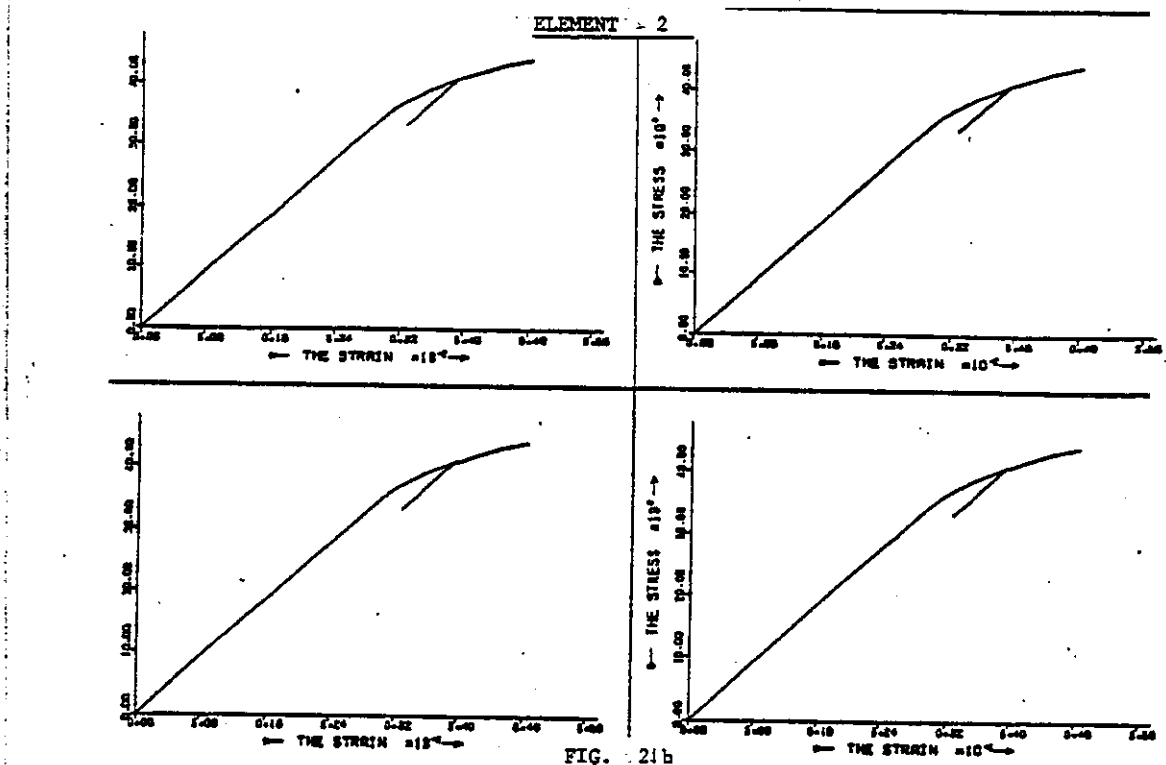


FIG. 21b

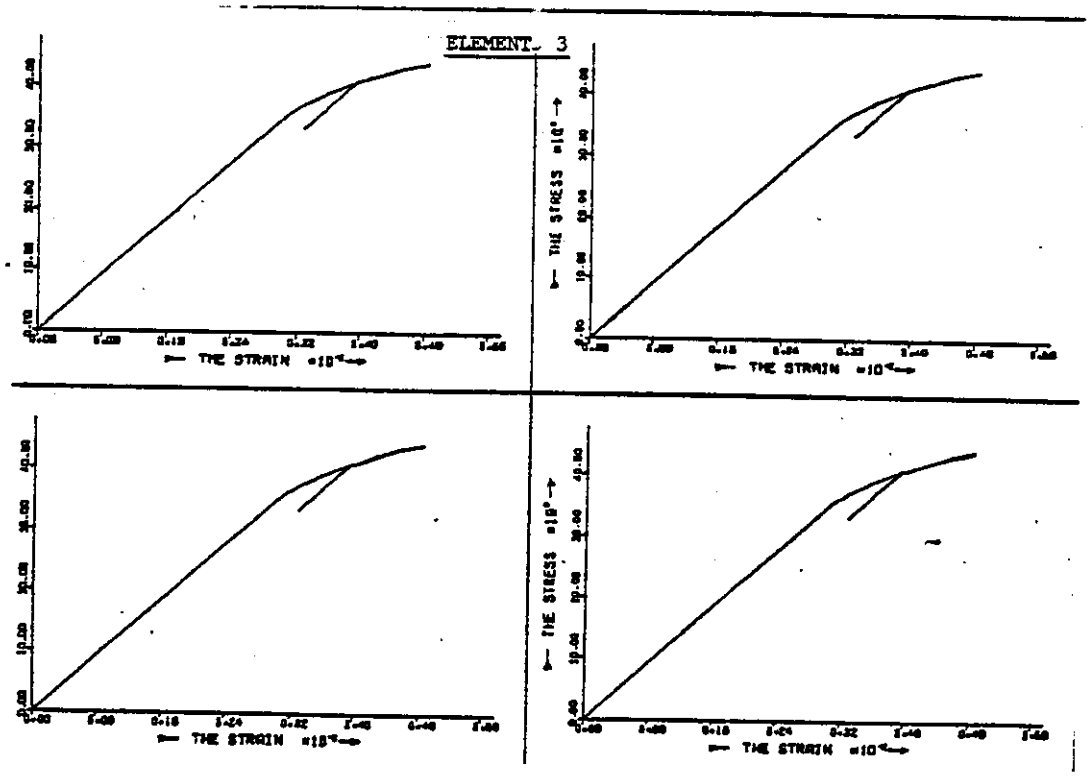


FIG. 21c

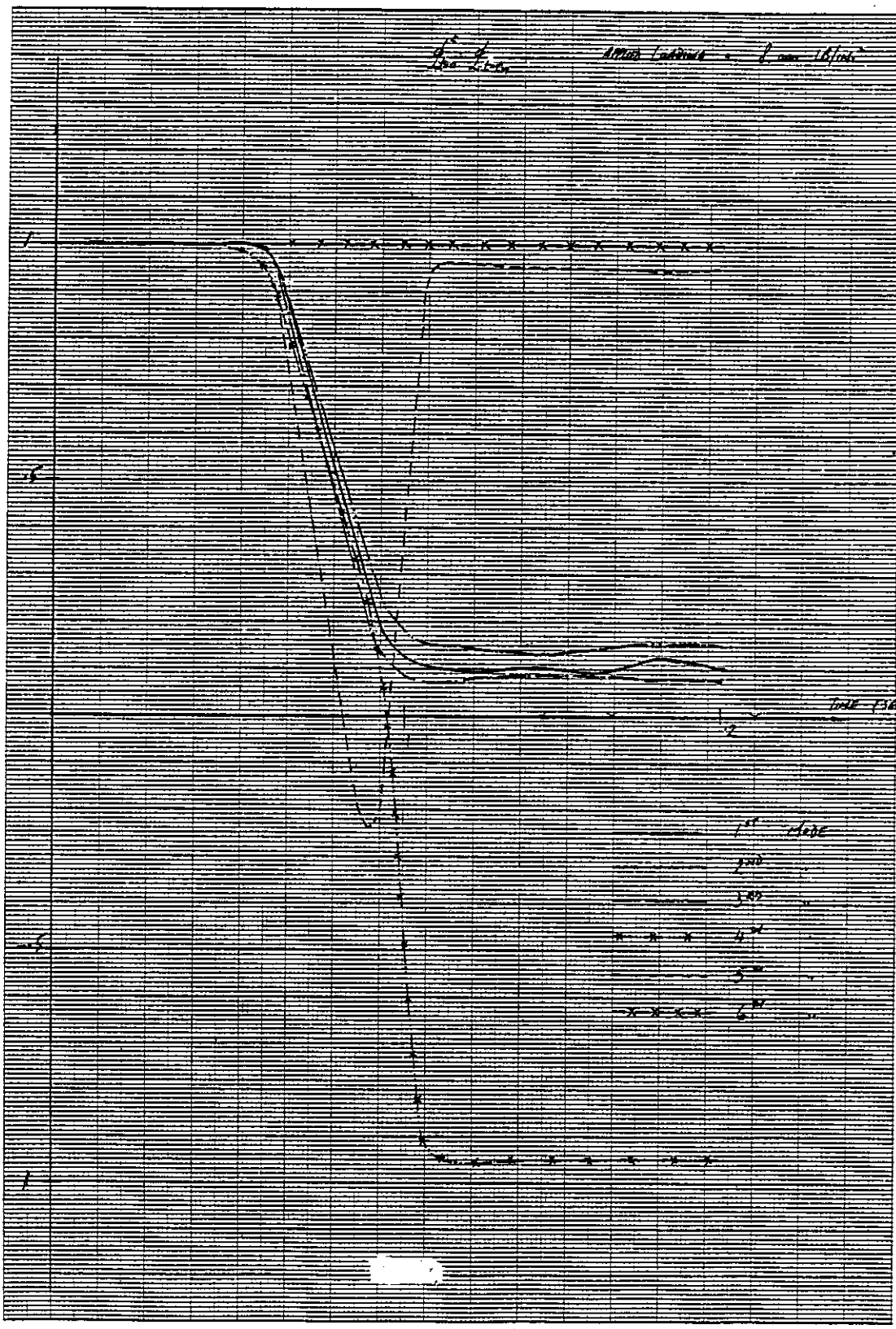


FIG. 22

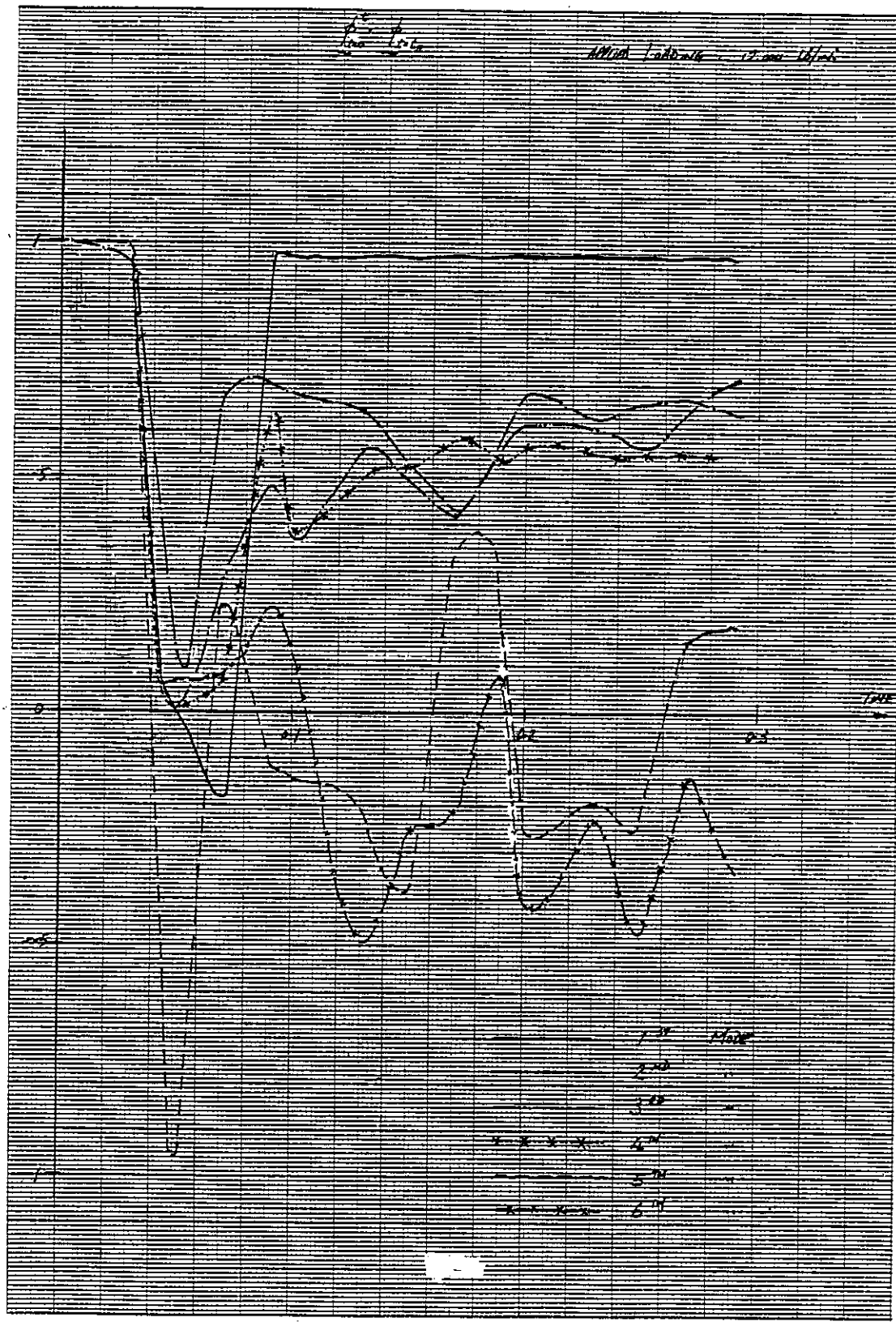


FIG. 23

EIGEN VALUES OF THE SYSTEM USING DIAGONAL MASS MATRIX

		ROTATIONAL GRADIENT α				
		1·75	1·65	1·55	1·45	1·35
Membrane response analysis	Min. Eigen Value	81161·6	81161·6	81161·6	81161·6	81161·6
	Max. Eigen Value	$·6698 \times 10^8$	$·6698 \times 10^8$	$·6698 \times 10^8$	$·6698 \times 10^8$	$·6698 \times 10^8$
Bending response analysis	Min. Eigen Value	106·7	106·69	106·67	106·65	106·62
	Max. Eigen Value	$·5326 \times 10^8$	$·5255 \times 10^8$	$·4723 \times 10^8$	$·4424 \times 10^8$	$·4023 \times 10^8$

EIGEN VALUES OF THE SYSTEM USING CONSISTENT MASS MATRIX

Membrane response analysis	Min. Eigen Value	84711·69
	Max. Eigen Value	$·246 \times 10^9$
Bending response analysis	Min. Eigen Value	112·95
	Max. Eigen Value	$·4414 \times 10^8$

The critical time step is determined by the Max^{m} Eigen value which for the membrane case is $2/\sqrt{·269 \times 10^9} = 0.00012$ sec. The critical time step for the bending case is $2/\sqrt{·441 \times 10^8} = 0.0003$ sec.

PERIODIC TIME

	Using Consistant Mass Matrix	Using Diagonal Mass Matrix
Membrane case	0·0215 sec.	0·0221 sec
Bending case	0·591 sec.	0·608 sec

FIG. 24

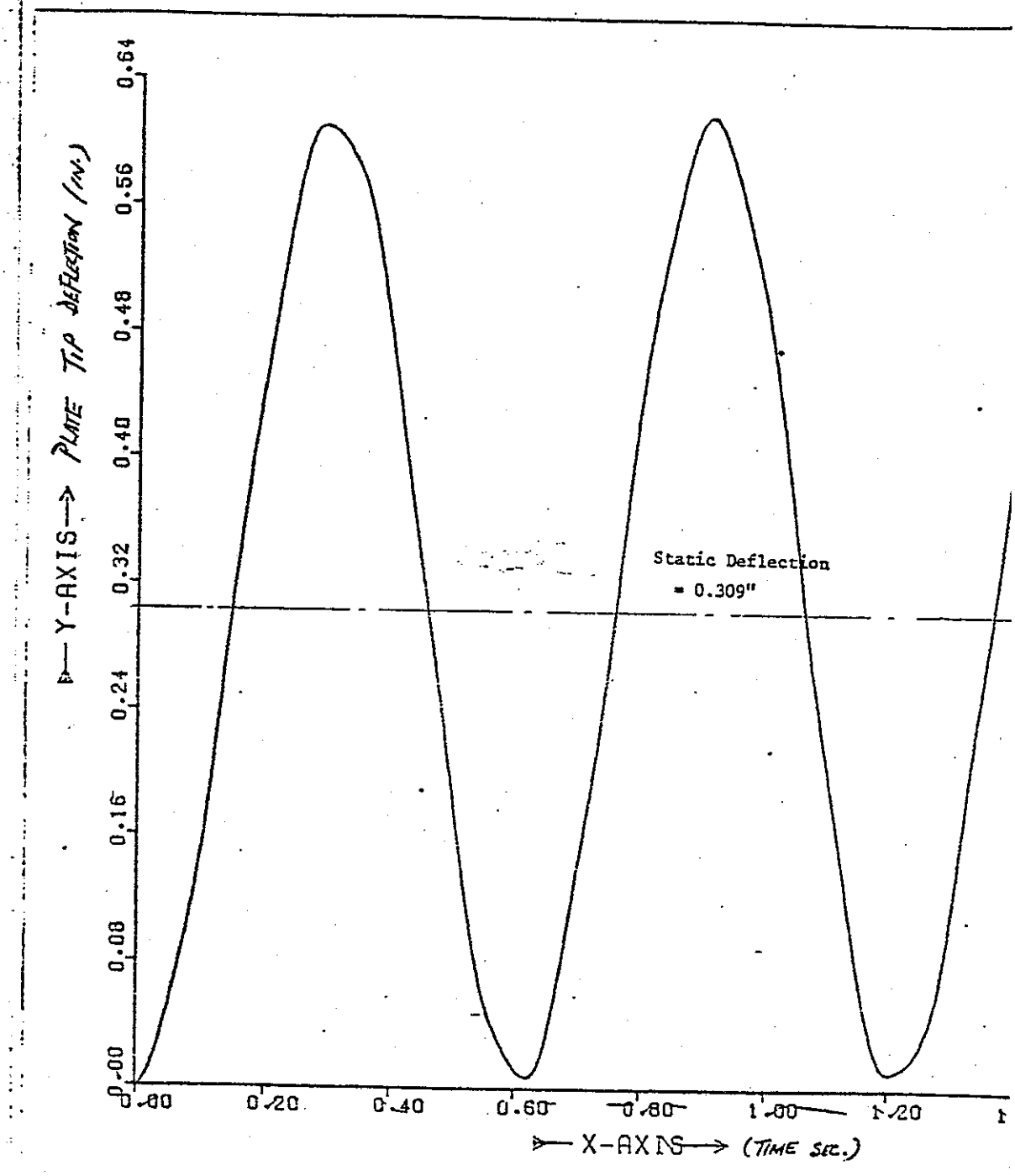


FIG. 25a Displacement response using Central Difference & Lumped Mass Method
Time step size = 0.00028 sec.

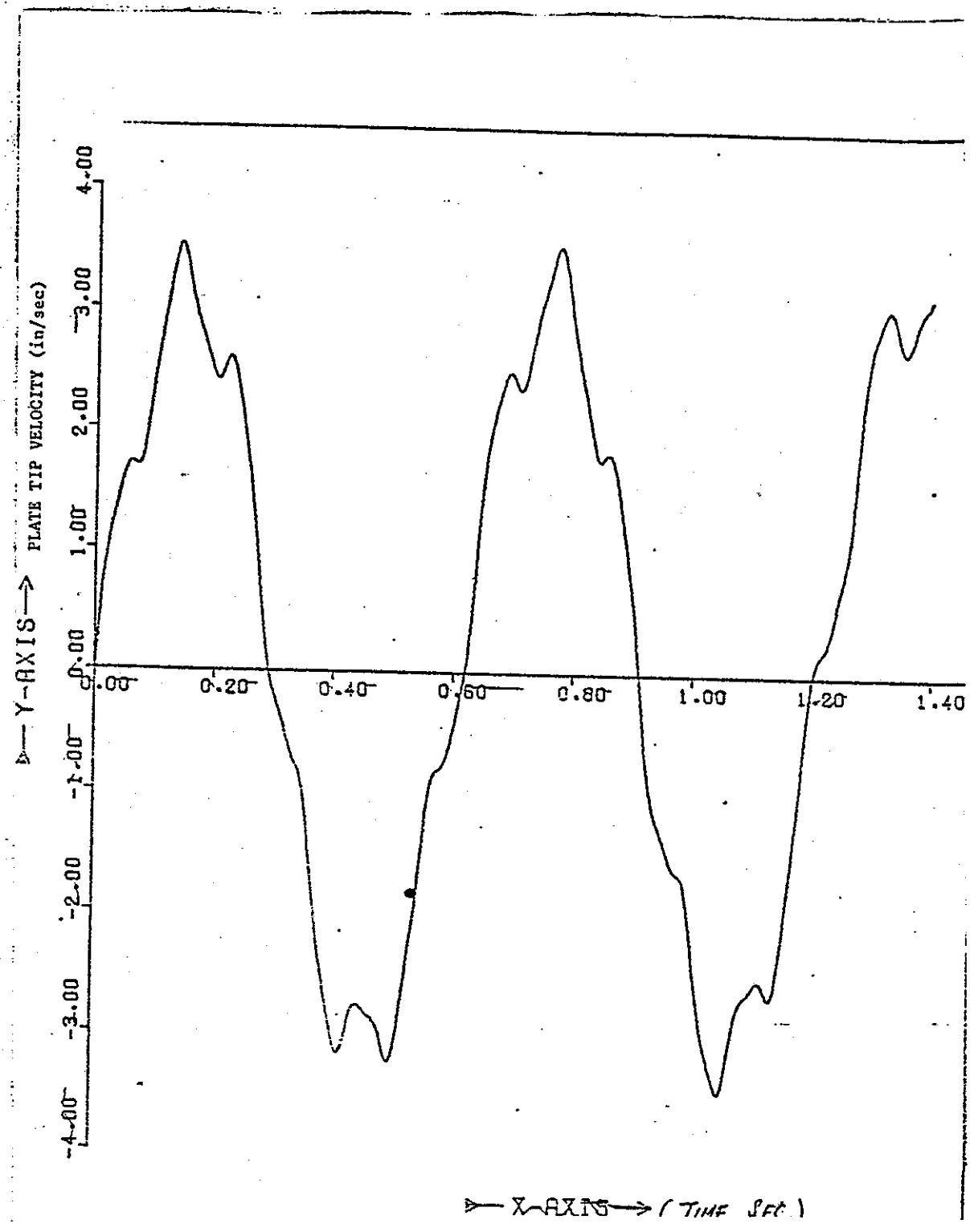

Y-AXIS → PLATE TIP VELOCITY (in/sec)
4.00
3.00
2.00
1.00
0.00
-1.00
-2.00
-3.00
-4.00
0.00
0.20
0.40
0.60
0.80
1.00
1.20
1.40
X-AXIS → (TIME SEC)

FIG. 25b

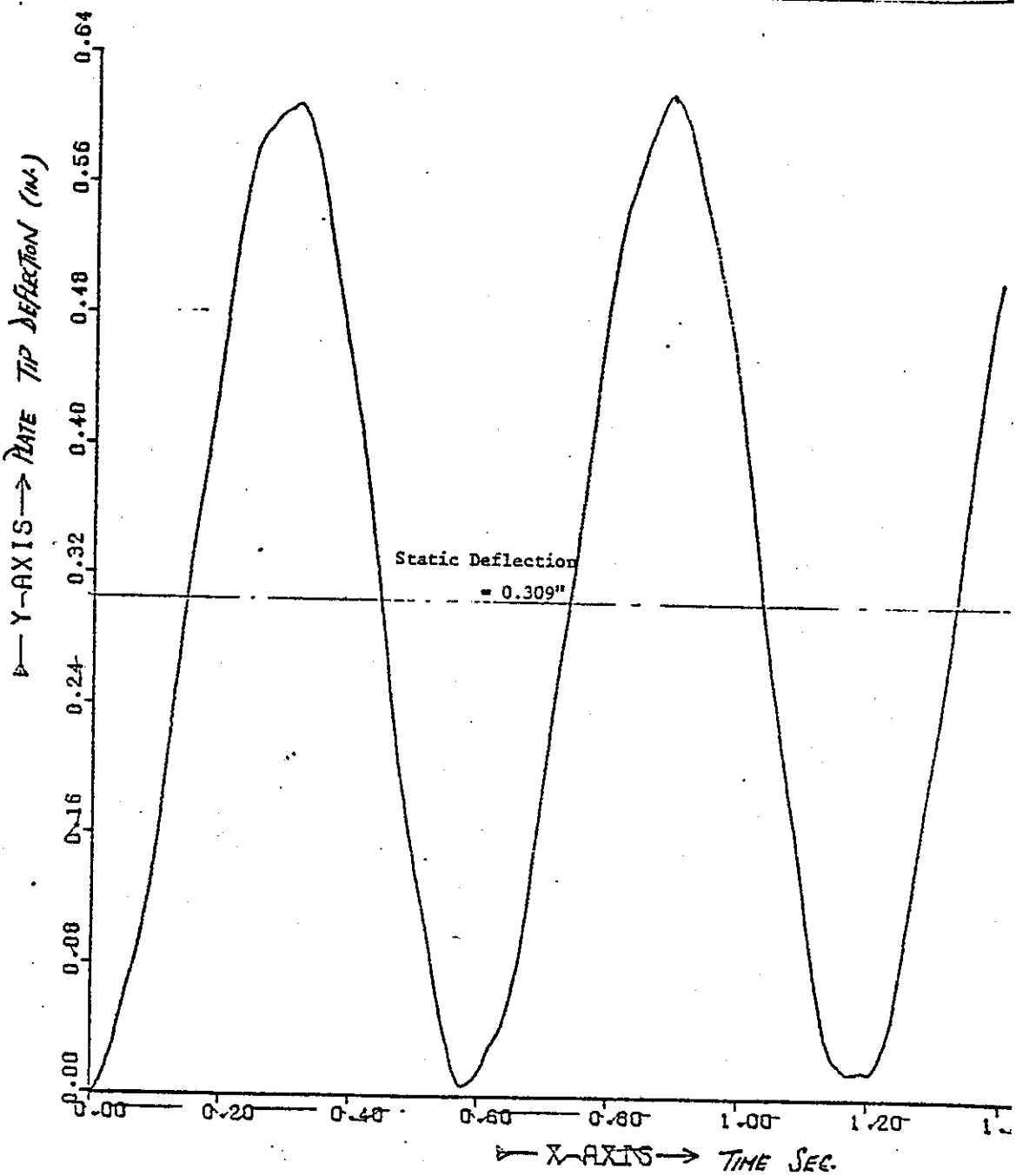


FIG. 26a Displacement response using Newmark-β Method
Time step size = 0.00028 sec. $\beta = 1/4$

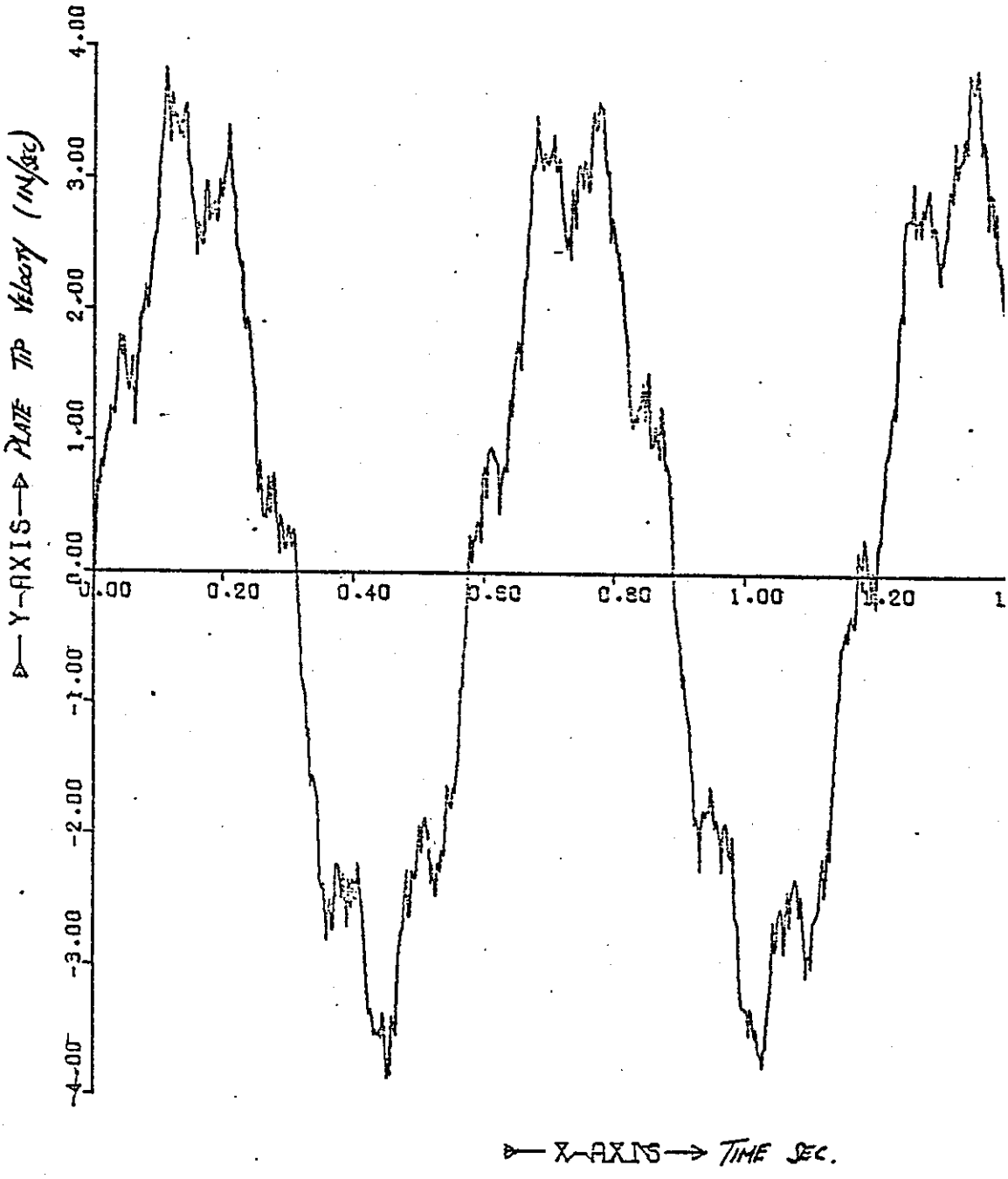


FIG. 26b Velocity response using Newmark-β Method

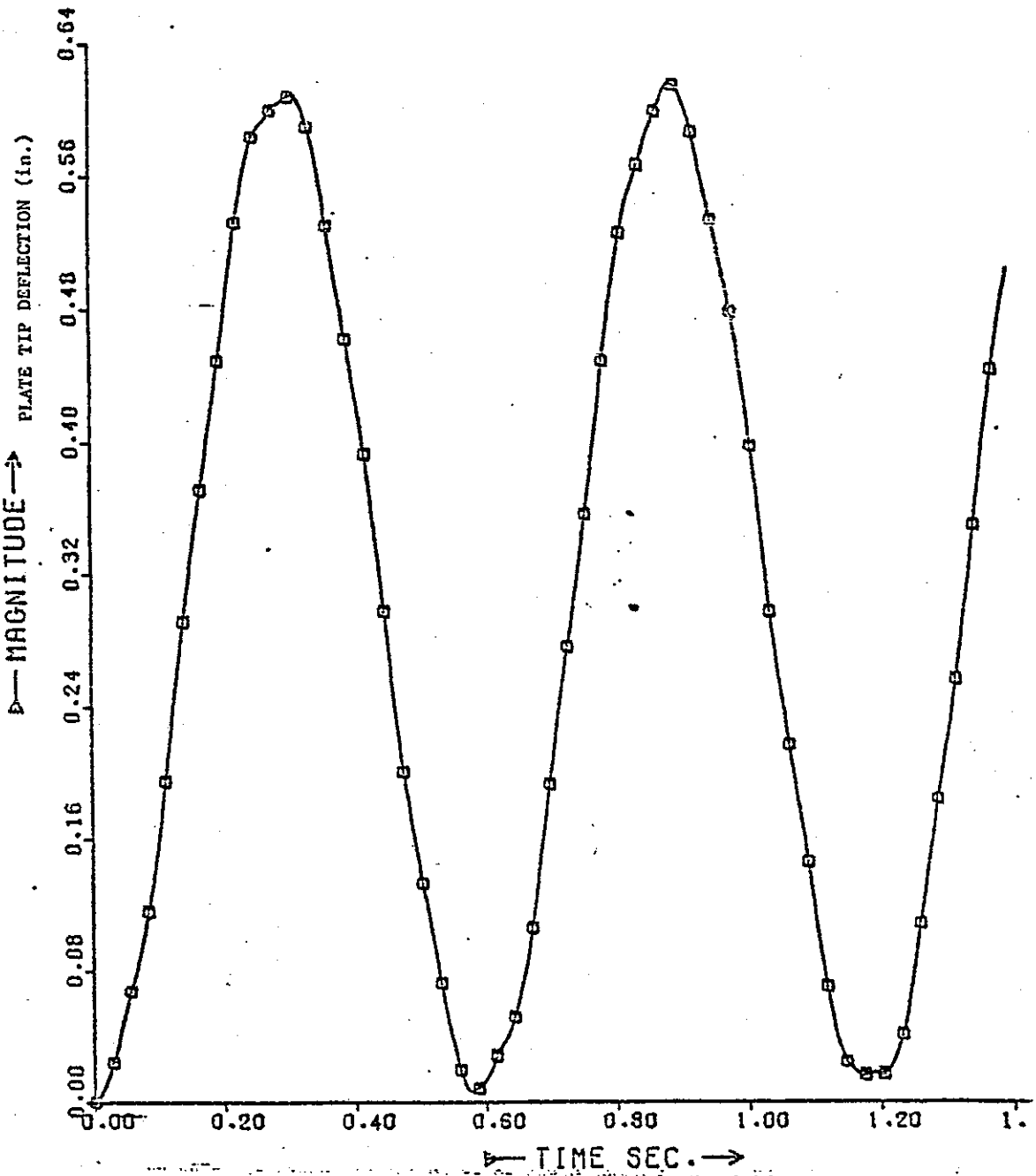


FIG. 27a Comparision of displacement responses using Newmark-β Method and Central Difference Consistent Mass Matrix Method

Key:- o —— Central Difference (Consistent Mass Matrix)

□ —— Newmark-β Method

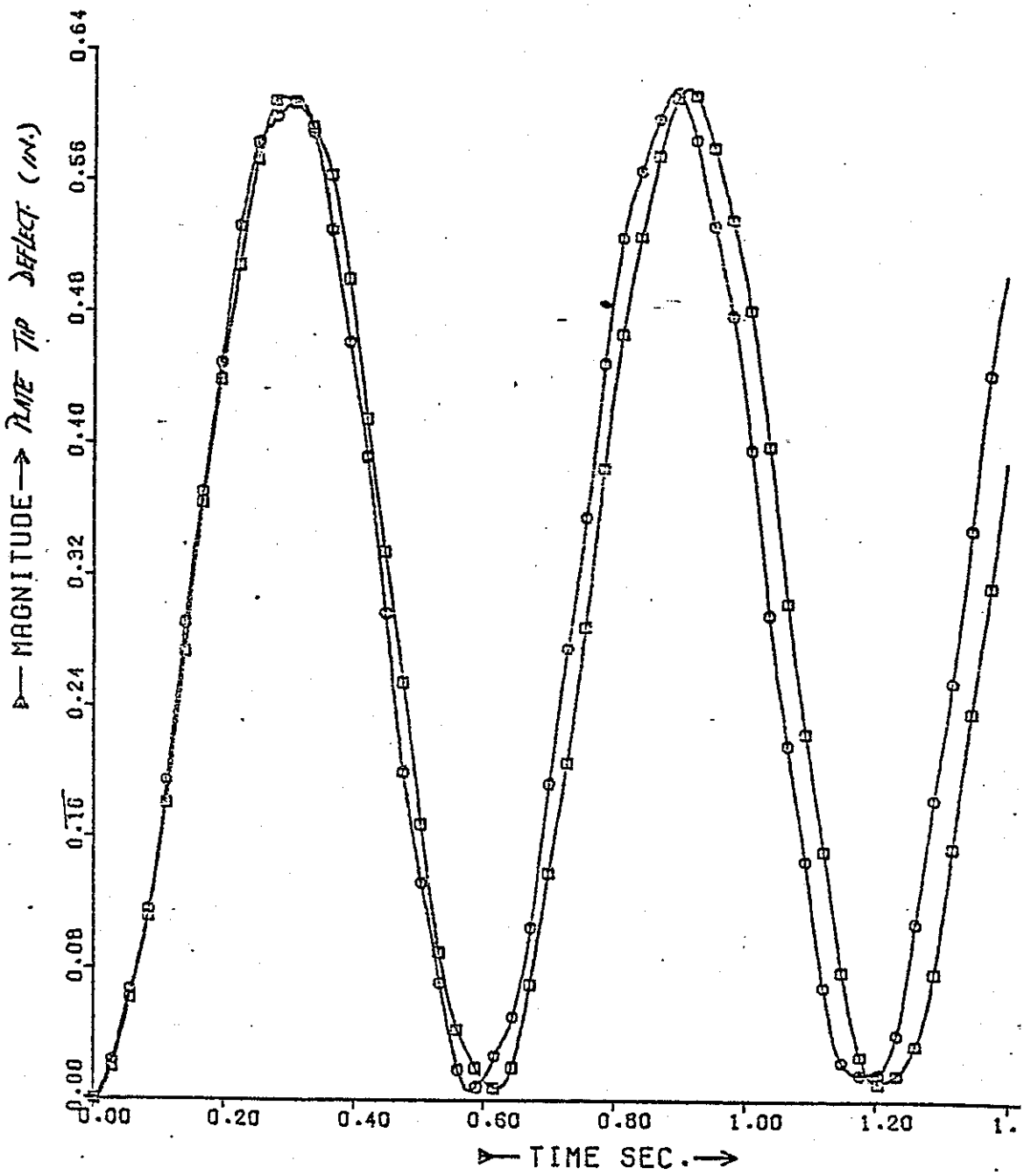


FIG. 27b Comparision of displacement responses using Central Difference Method with Diagonal Mass Matrix and that with Consistent Mass Matrix

Key:- O —— Consistent Mass Matrix

□ —— Diagonal Mass Matrix

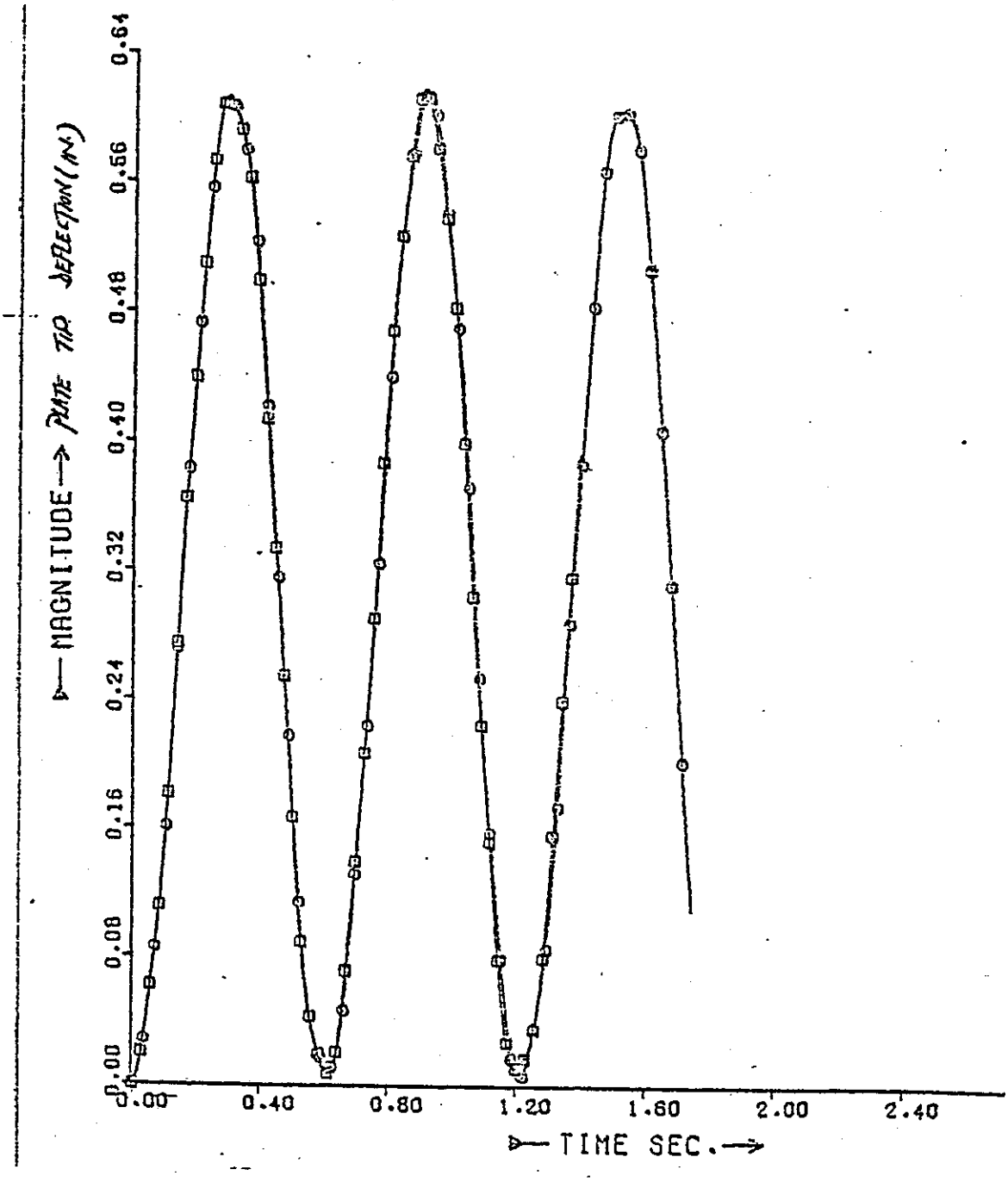


FIG. 28a Comparision on displacement responses using Central Difference Diagonal Mass Matrix Method but with different rotational gradients

Key;- □ —— with mass lumping to match the max. eigen value of system (Δt=.00028 sec.)

O —— same as □ , but with the rotational terms amplified to 5 times its normal values (Δt=.0004 sec.)

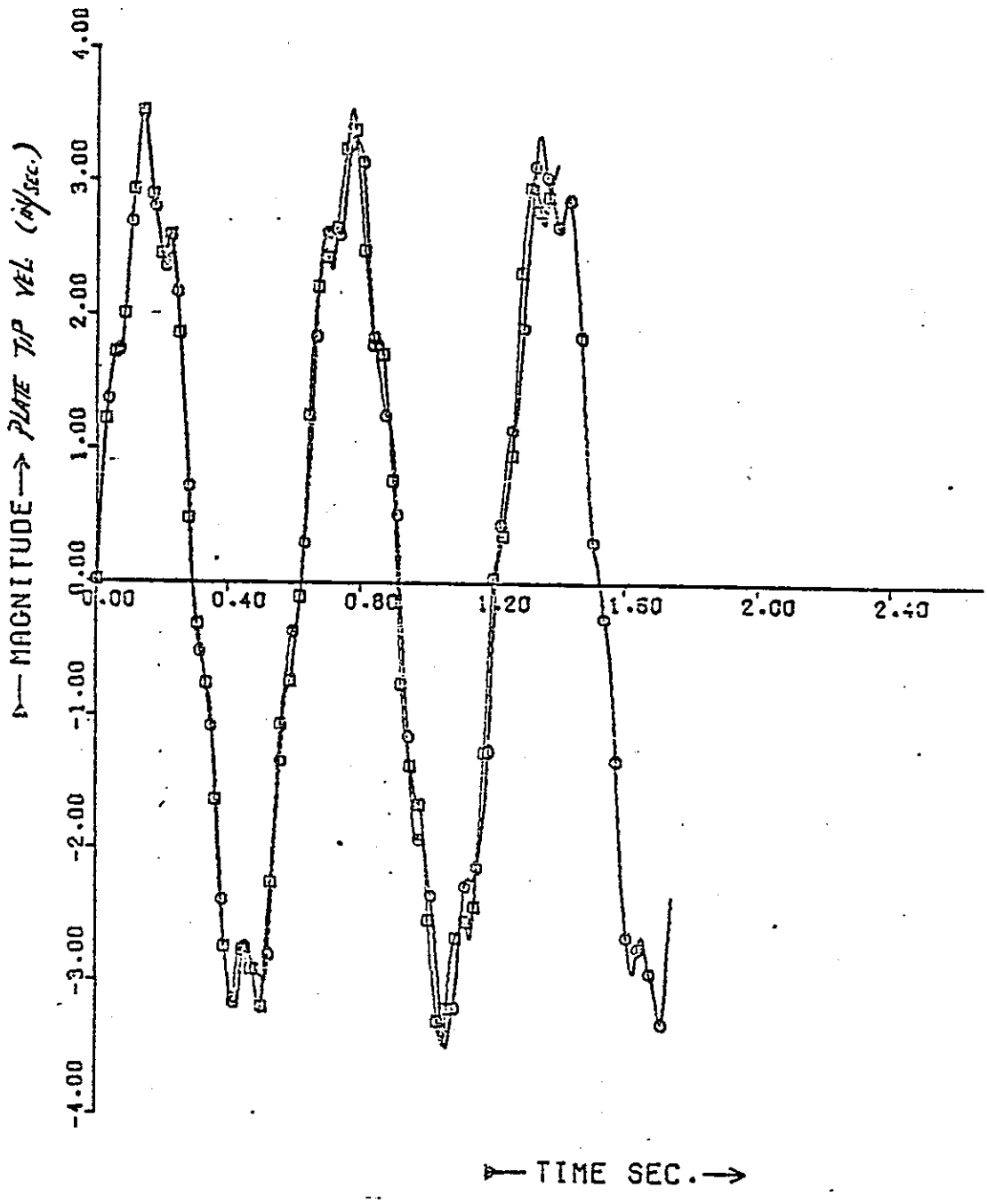


FIG. 28b Comparision on the velocity responses

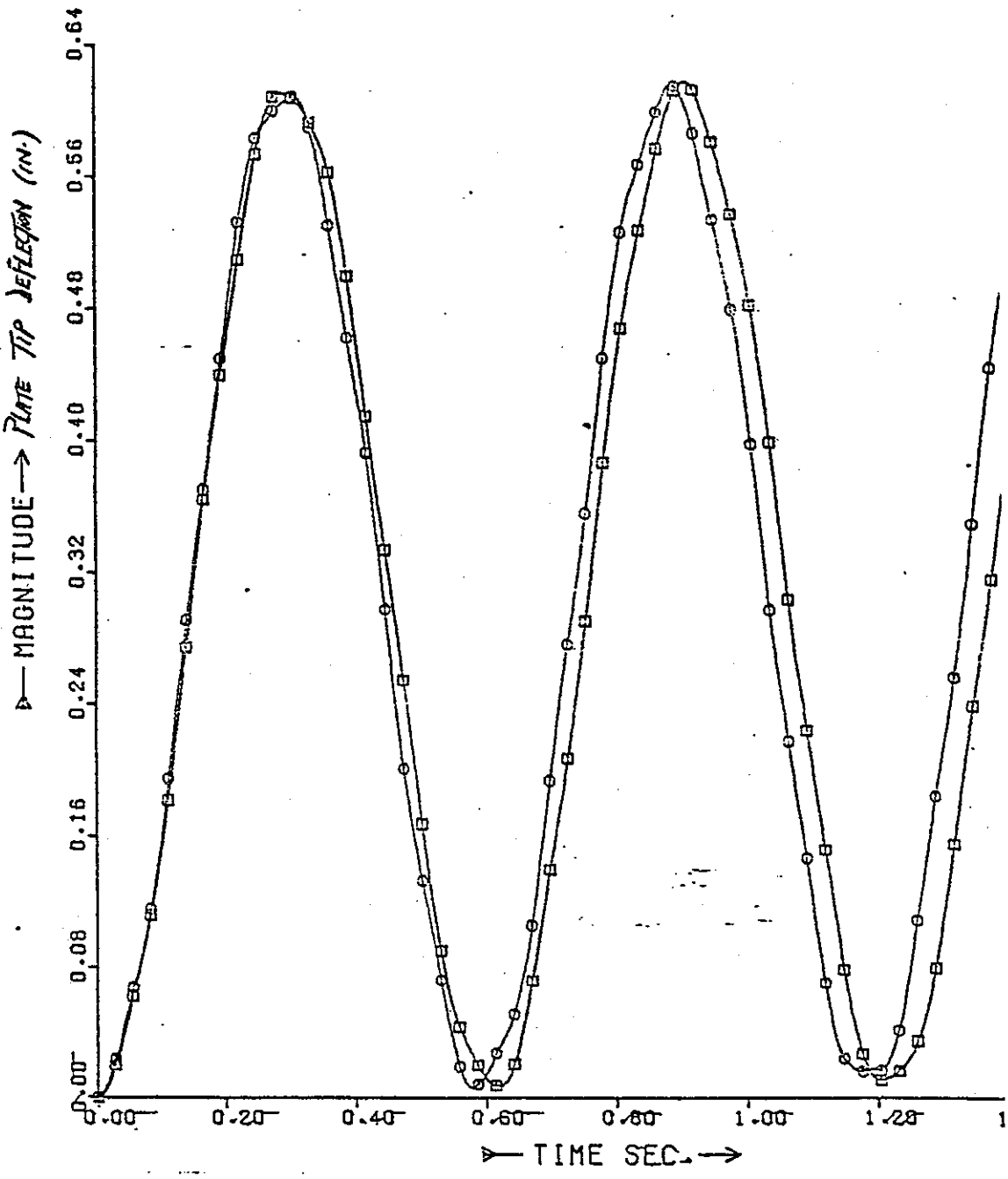


FIG. 29a Comparision on displacement responses using Central Difference Diagonal Mass Method and Newmark-β Method (Δt= .00028 sec.)

Key:- □ —— Central Difference Method

O —— Newmark-β Method

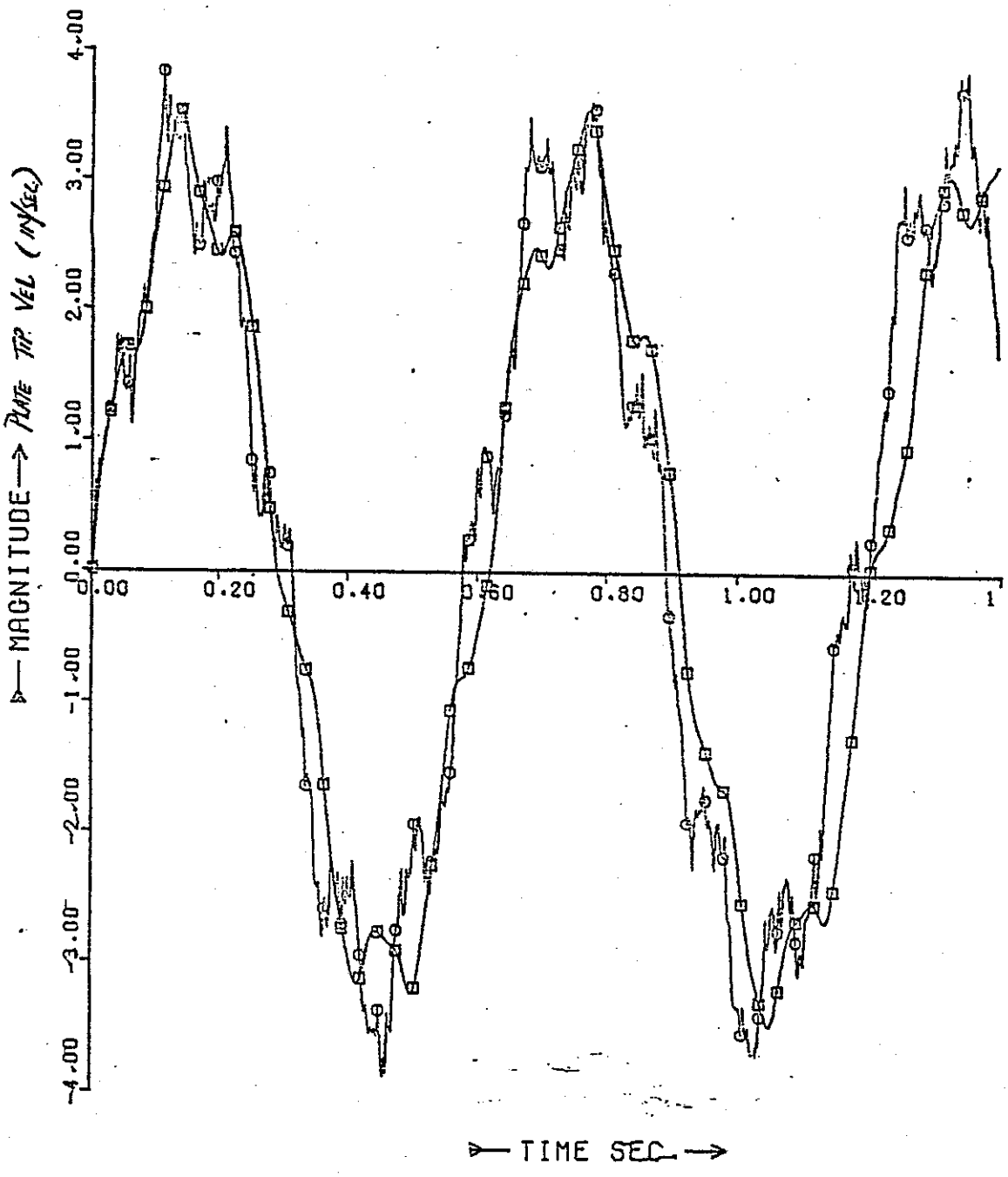


FIG. 29b Comparision on velocity responses

KEY:- O —— Central Difference Method

□ —— Newmark-β Method

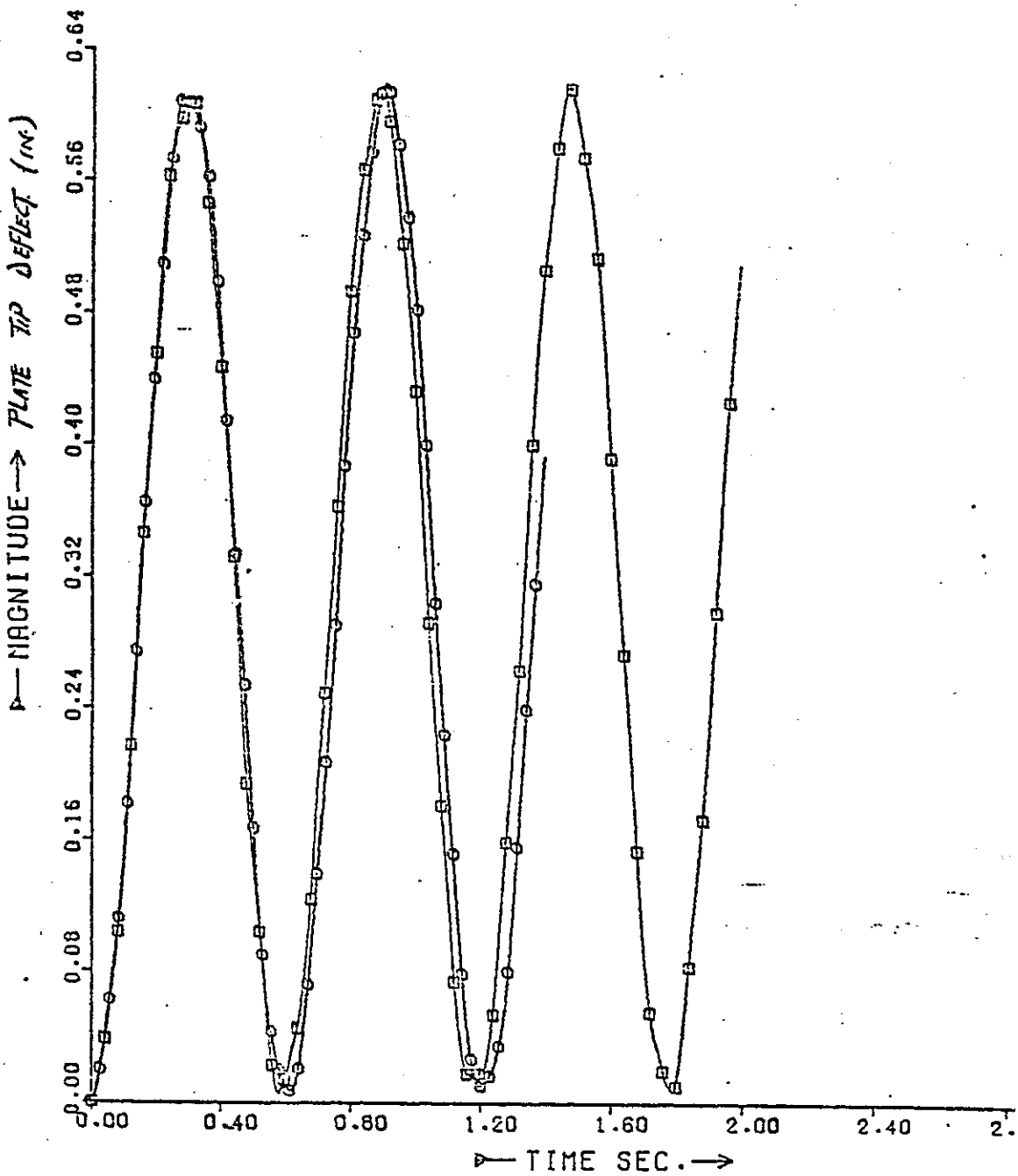


FIG. 30a Comparision on Displacement responses using Central Difference Diagonal Mass Method with Δt=.00028 sec. and that using Newmark-β Method with t=.002 sec.

Key:- O —— Central Difference Method

□ —— Newmark-β Method

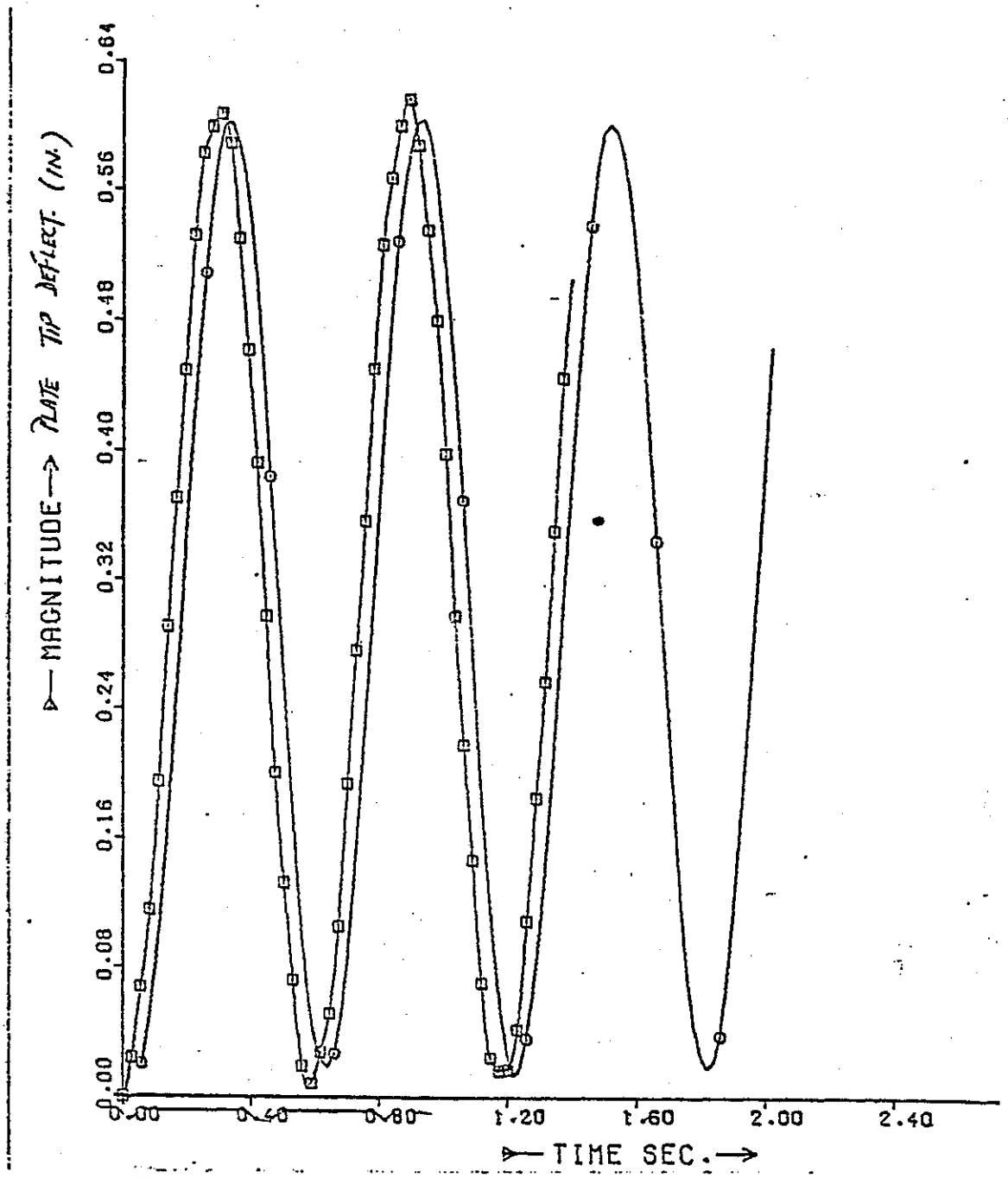


FIG. 305 Comparision on displacement responses using Central Difference Diagonal Mass Matrix Method with Δt=.00028 sec. and that using Newmark-β Method with Δt=.02 sec.

Key:- O —— Central Difference Method

□ —— Newmark-β Method

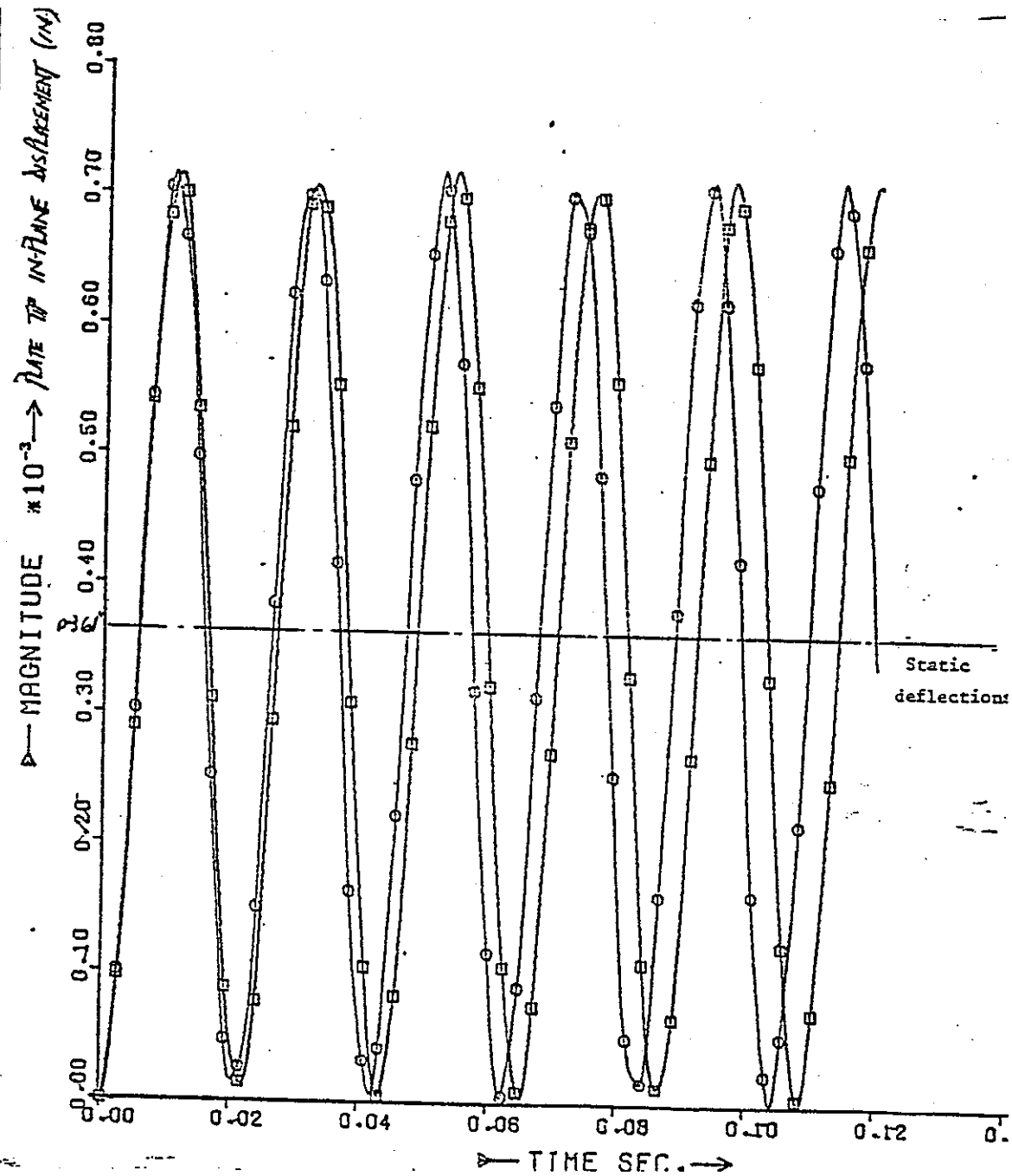


FIG. 31a Membrane displacement analysis using Central Difference Diagonal Mass Matrix and salso using Newmark-β Method (Δt=.00012 sec.)

Key:- □ —— Central Difference Method

○ —— Newmark-β Method

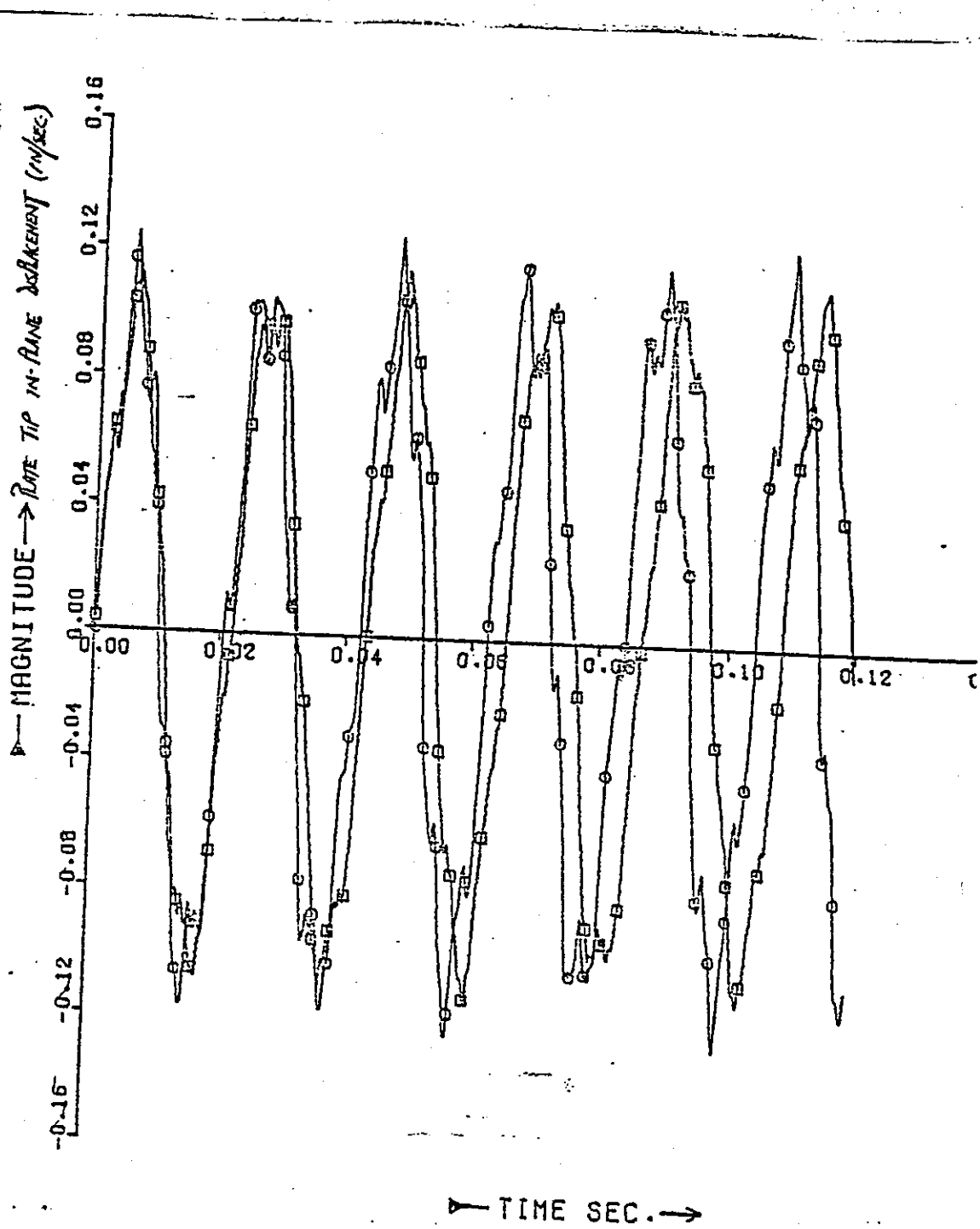


FIG. 31b Membrane velocity responses

Key:- —— Central Difference Method

—— Newmark- Method

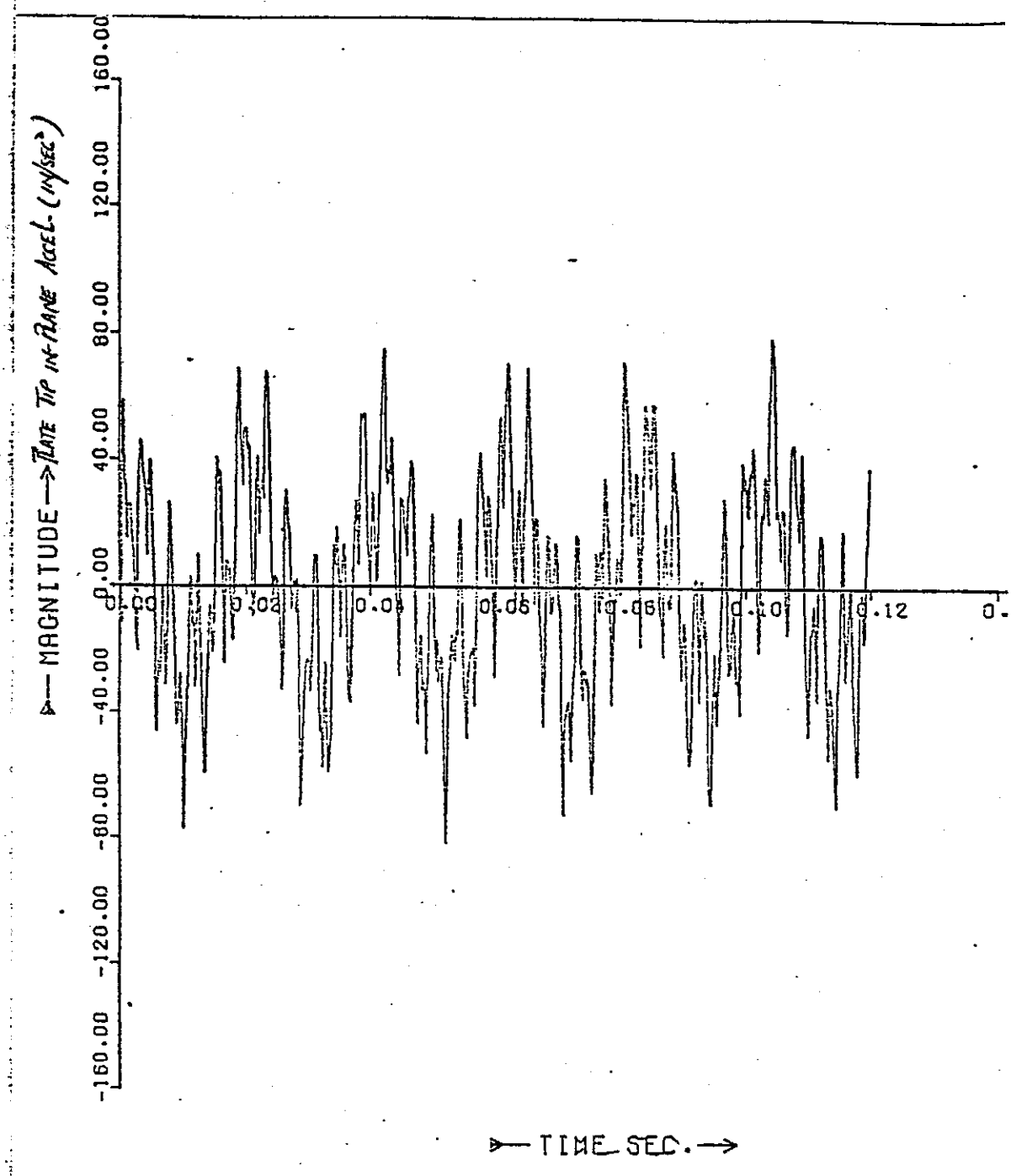


FIG. 31c Membrane acceleration responses (Central Difference Method)

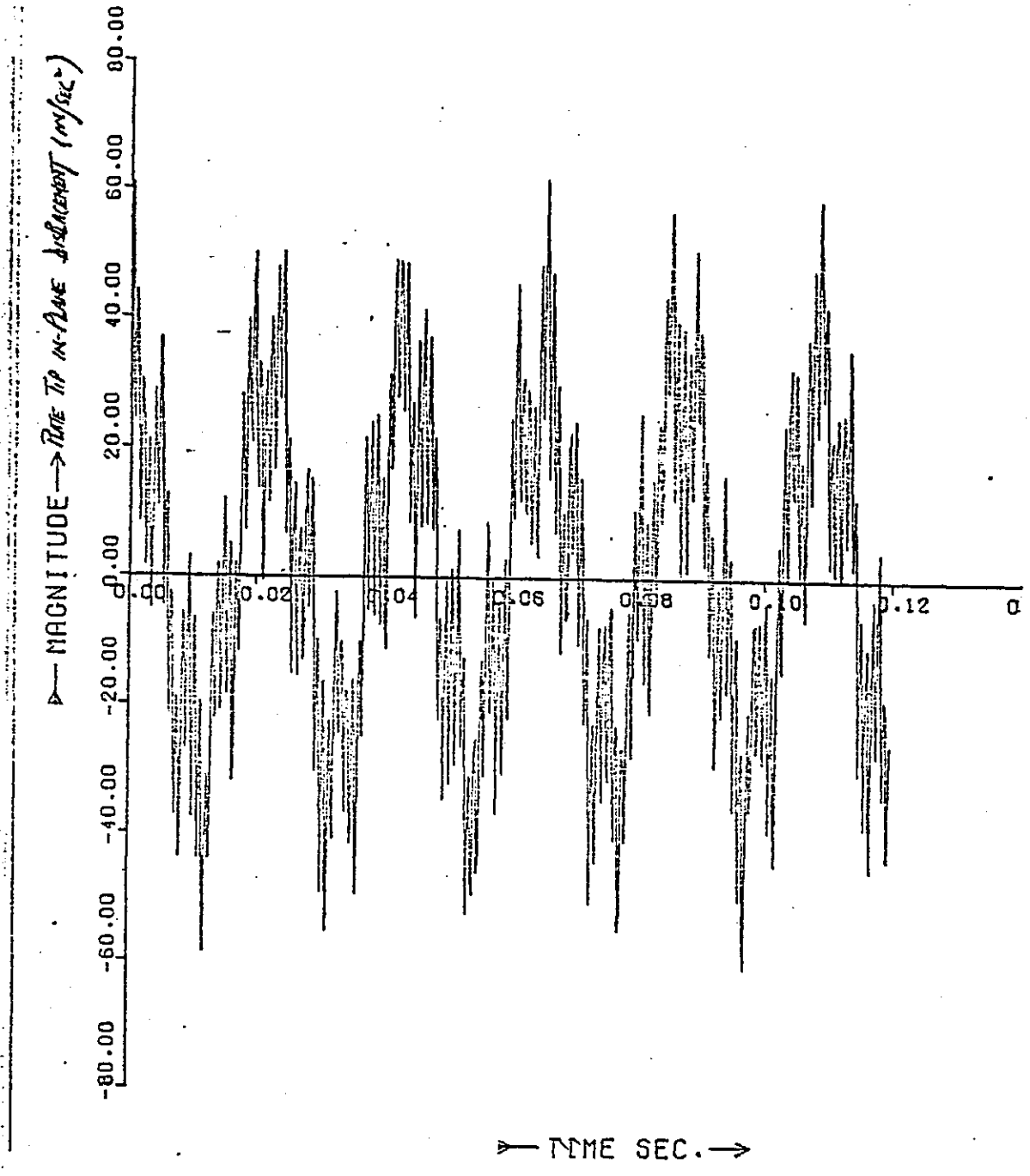


FIG. 31d Membrane acceleration responses (Newmark-β Method)

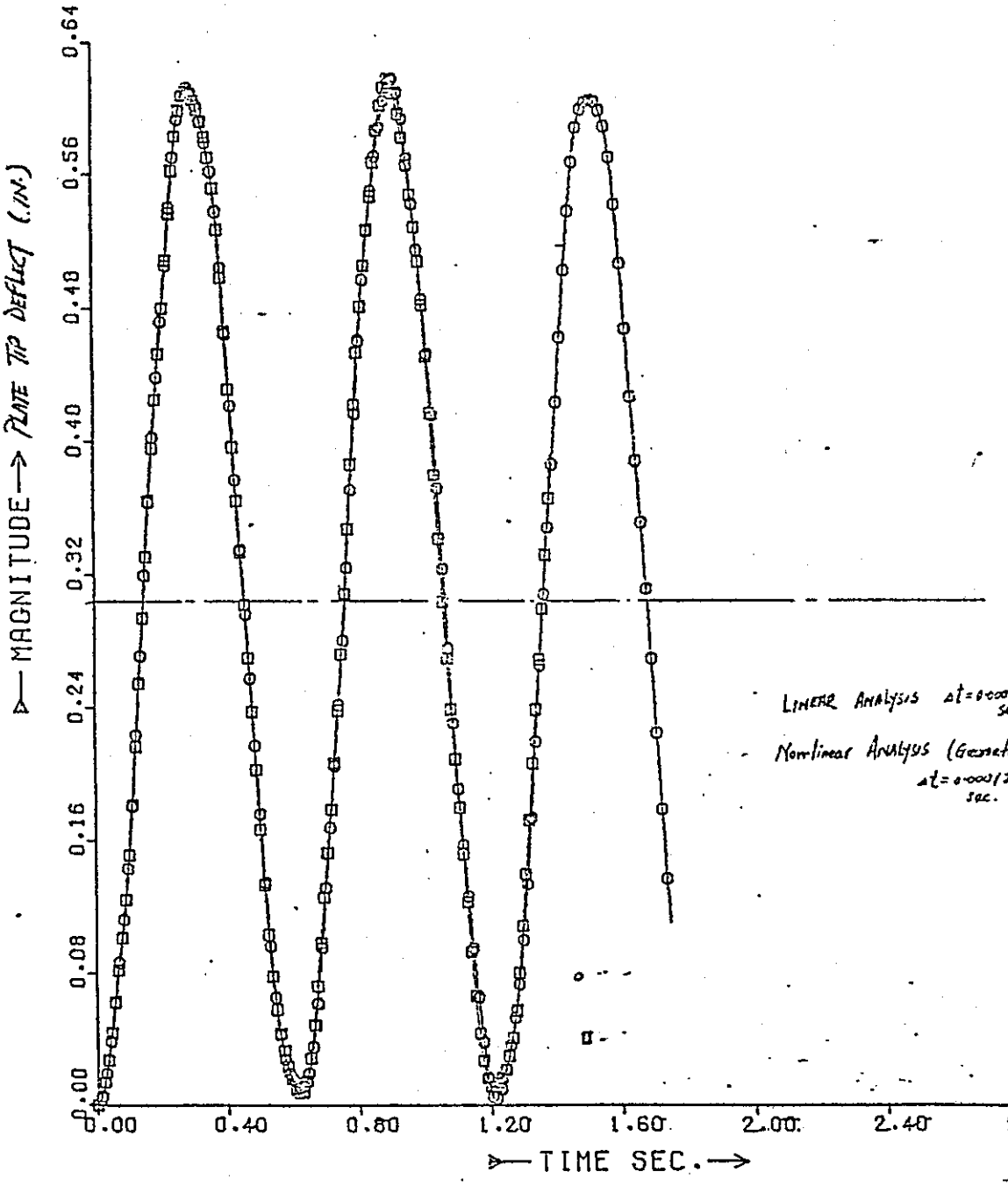


FIG. 32a Displacement responses using Central Difference Lumped Mass Metho

Key:- —— bending and membrane displacements uncoupled (t=.00028 sec.)
—— bending and membrane displacements coupled (t=.00012 sec.).

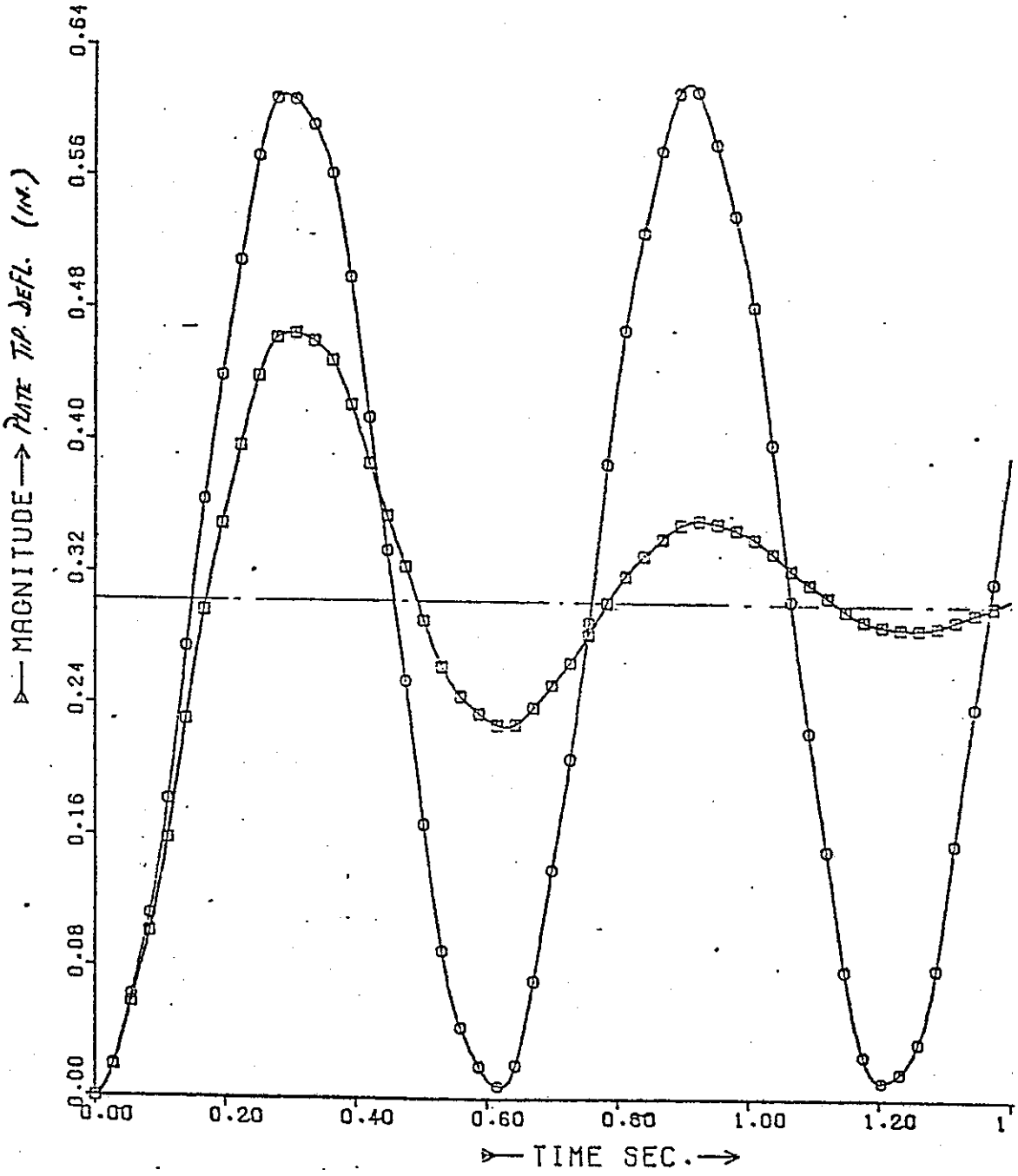


FIG. 32b Displacement responses (with geometric non-linearity) using Central Difference Diagonal Mass Matrix Method

Key:- O —— without damping
□ —— with damping

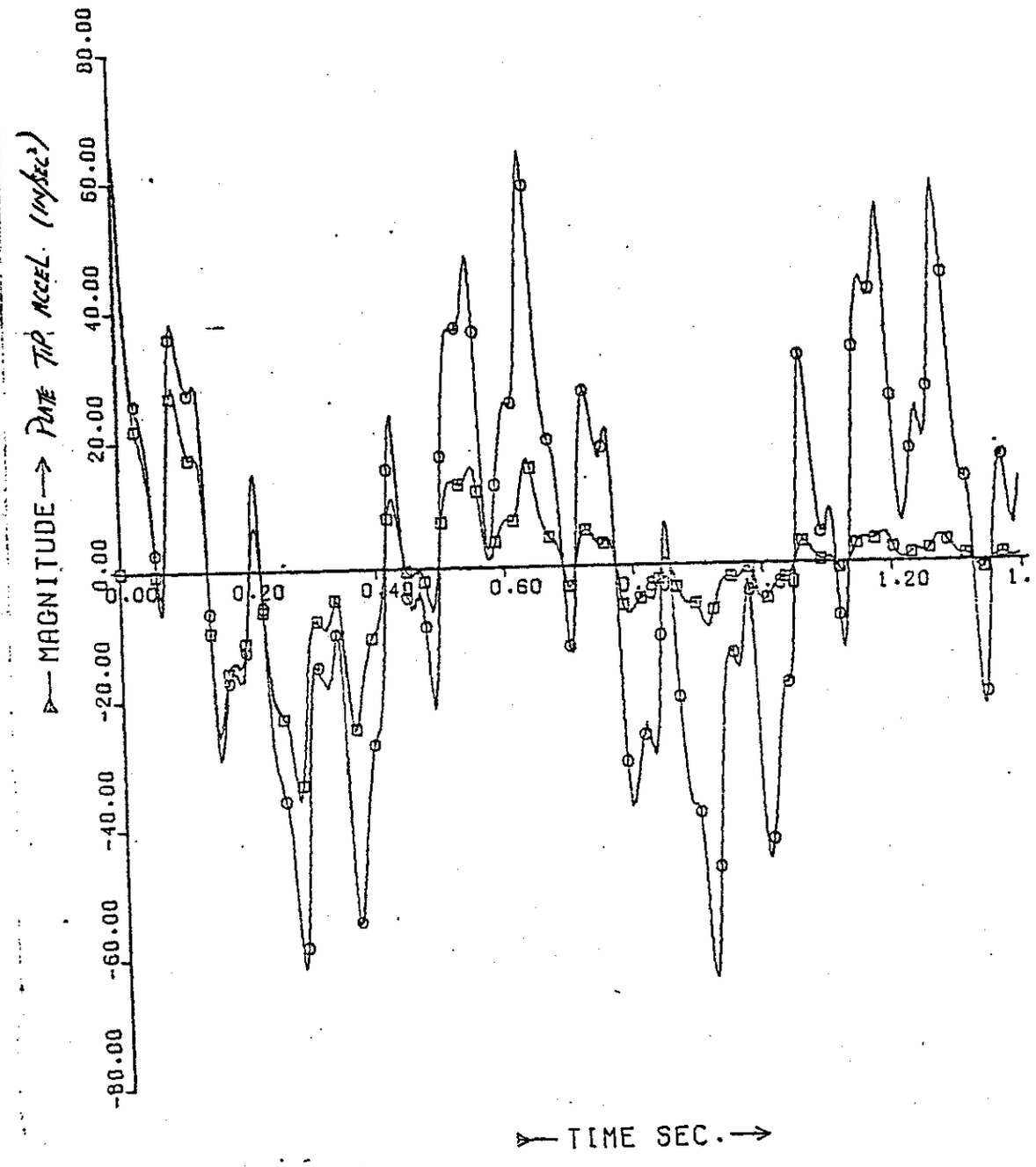


FIG. 32C Acceleration responses

Linear Buckling of stiffened plate

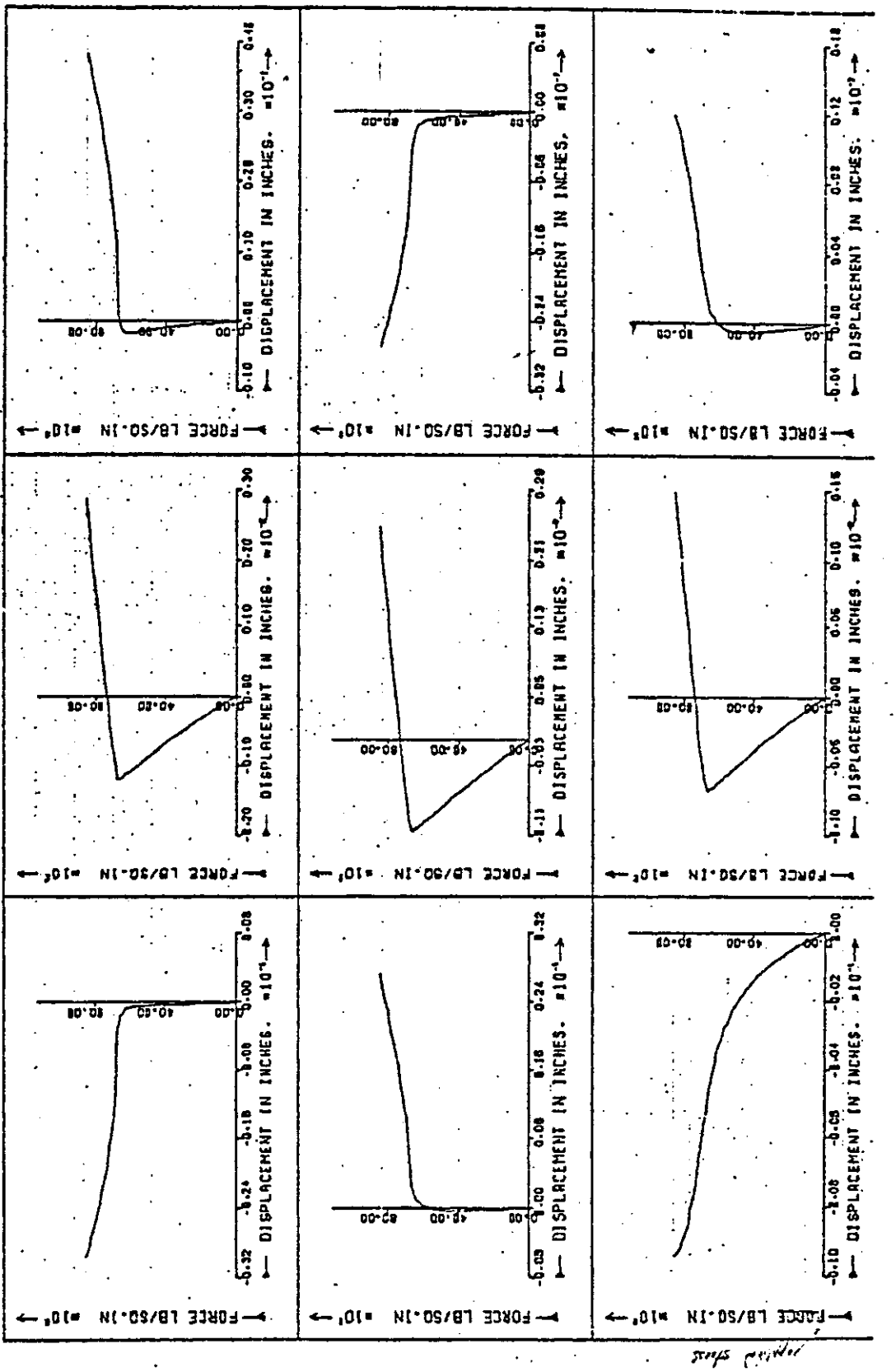
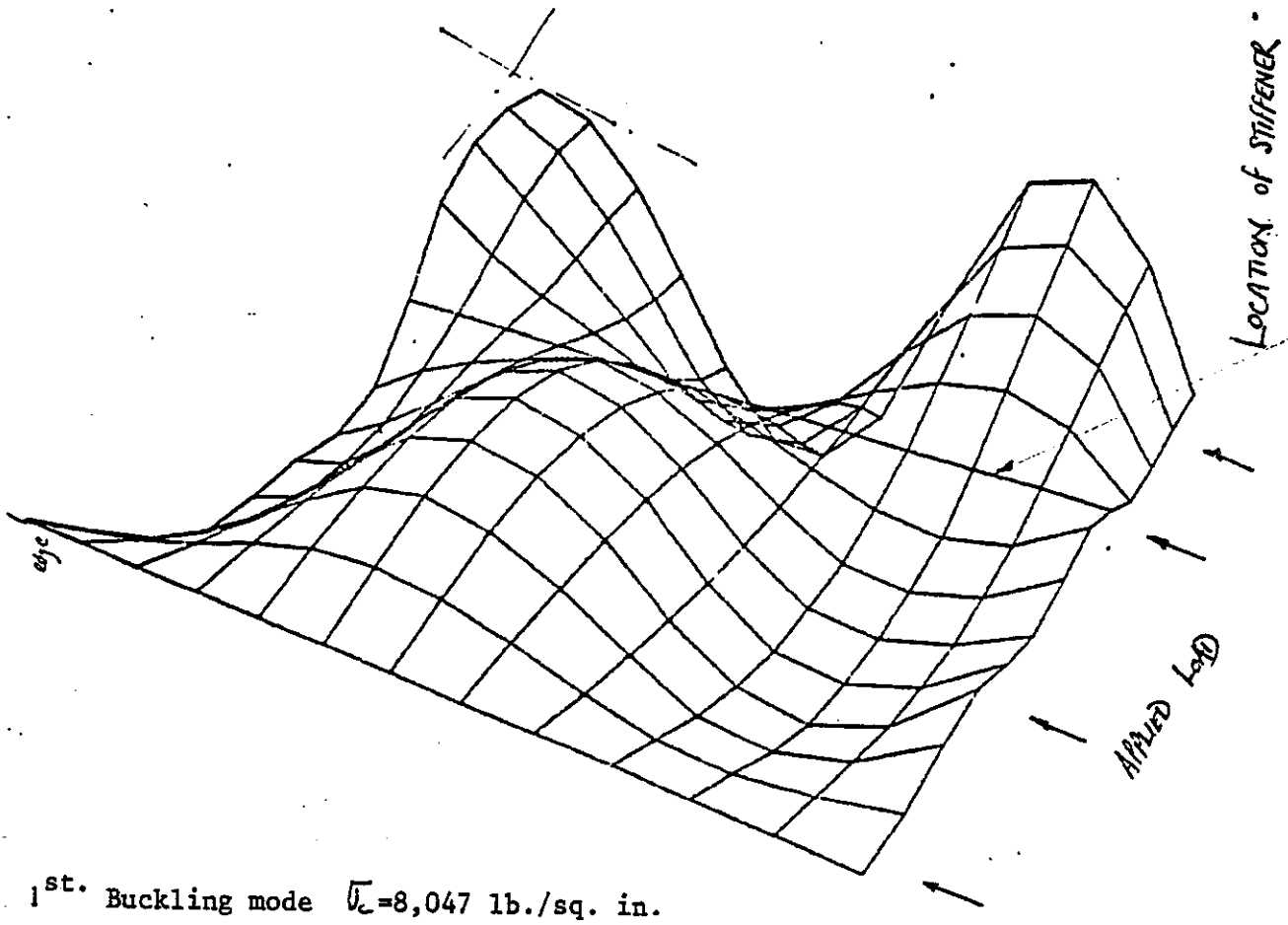
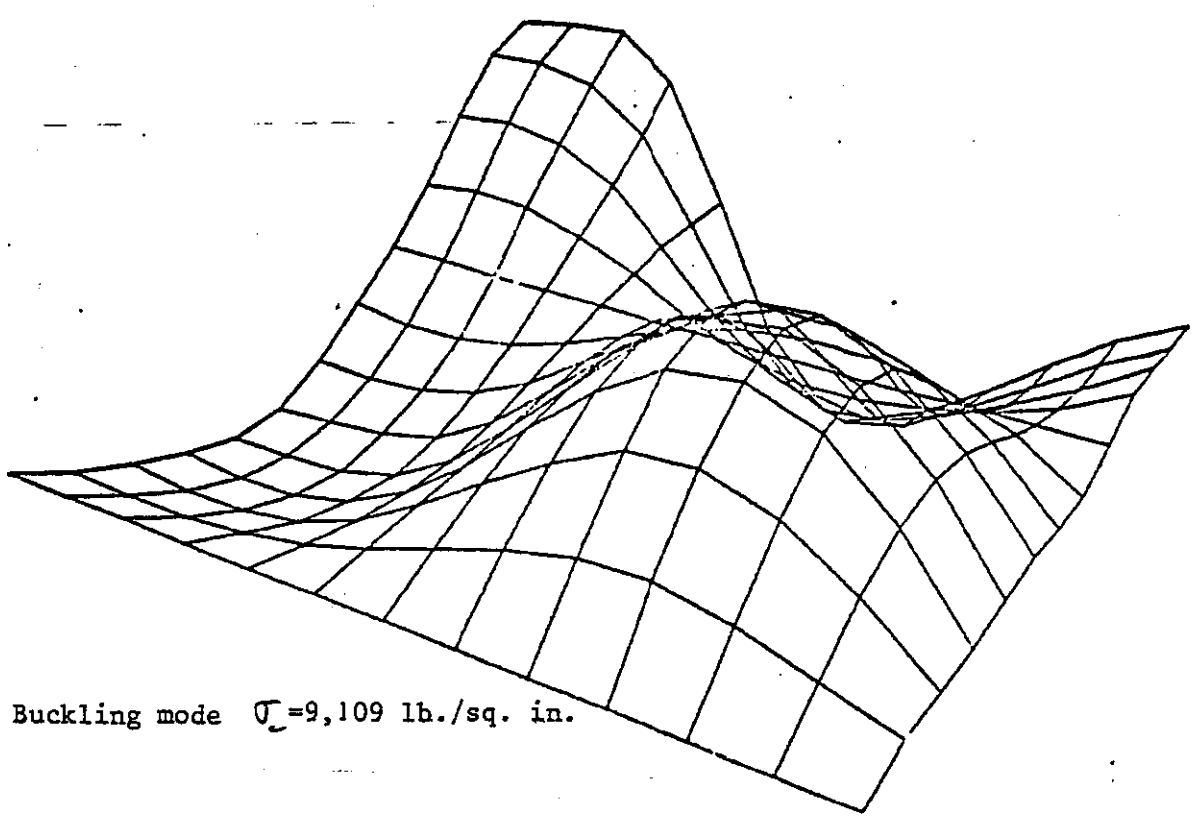


FIG. 33



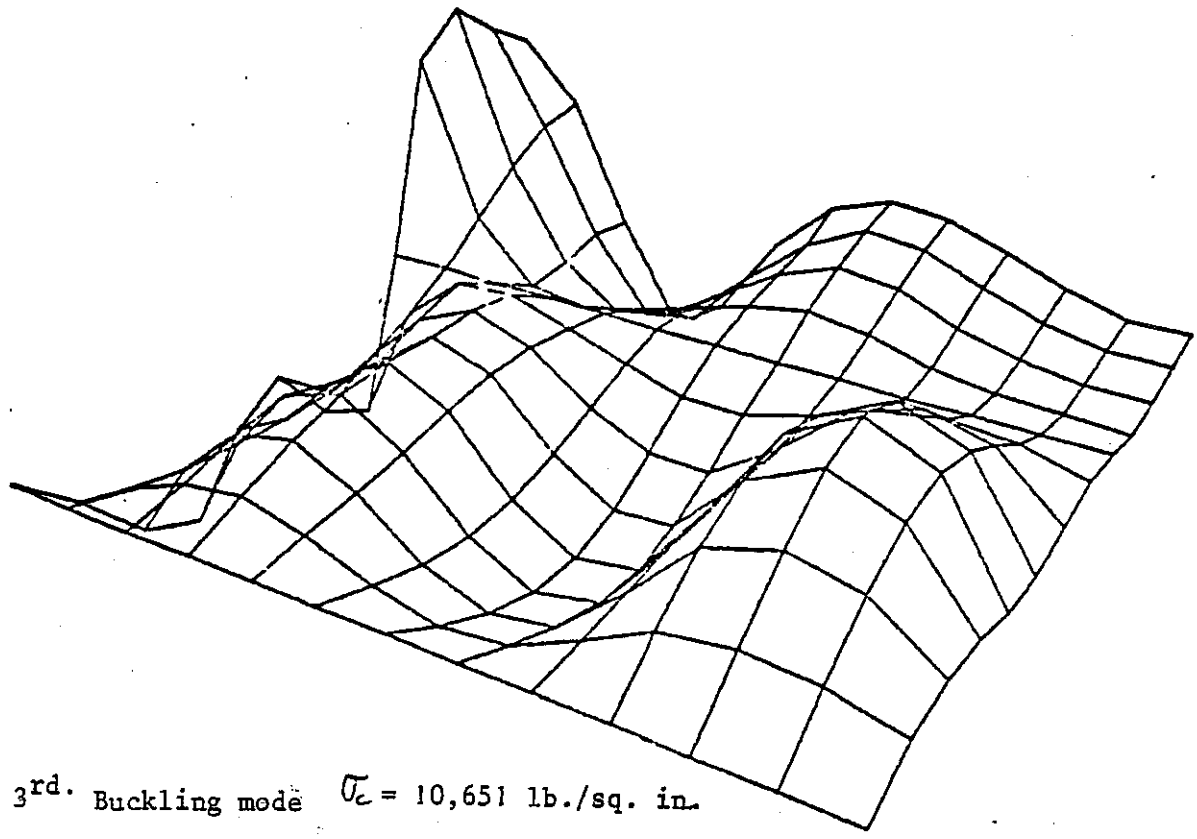
1st. Buckling mode σ_c=8,047 lb./sq. in.

FIG. 34a



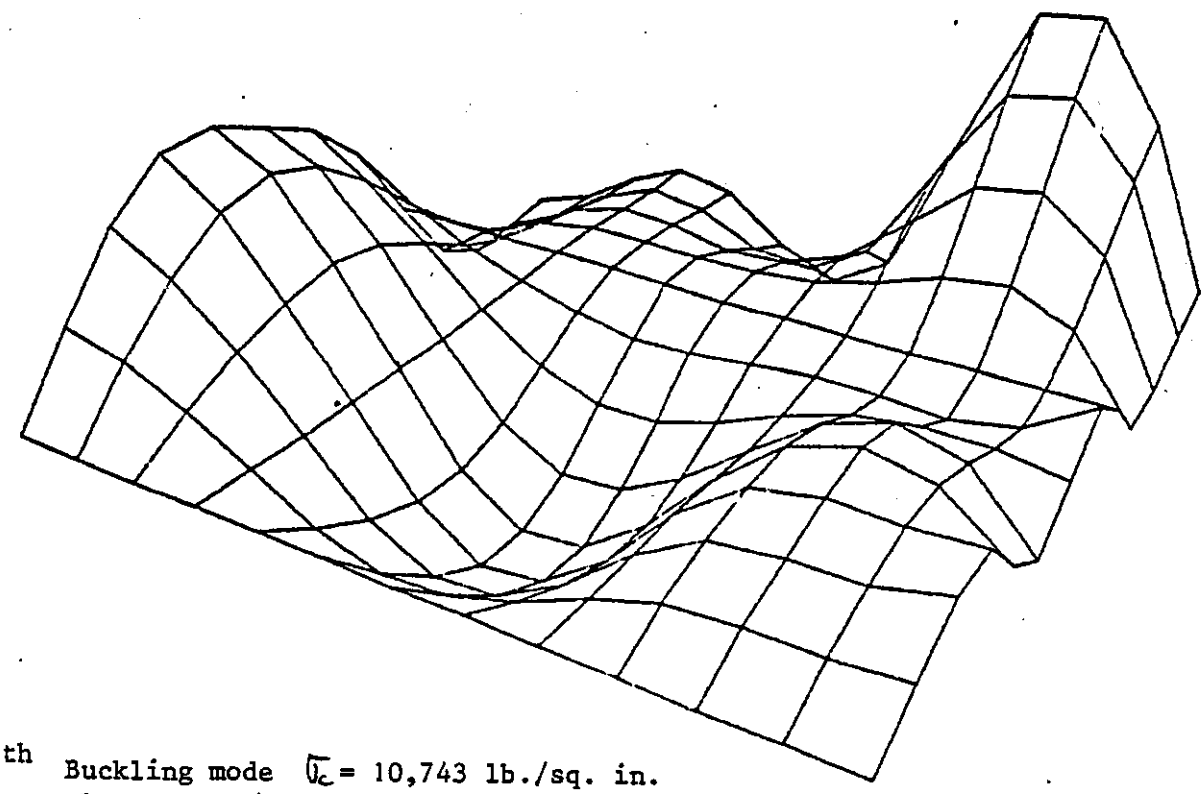
2nd. Buckling mode σ_c=9,109 lb./sq. in.

FIG. 34b



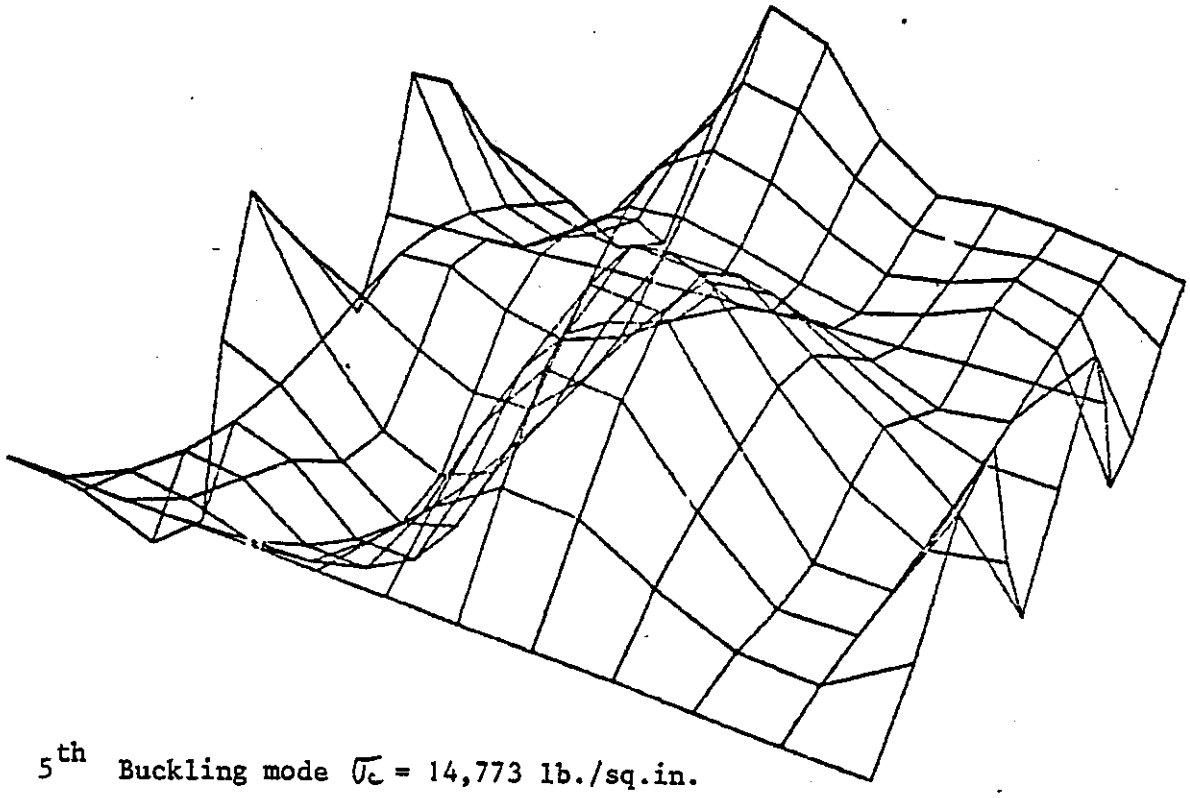
3rd. Buckling mode σ_c = 10,651 lb./sq. in.

FIG. 34c



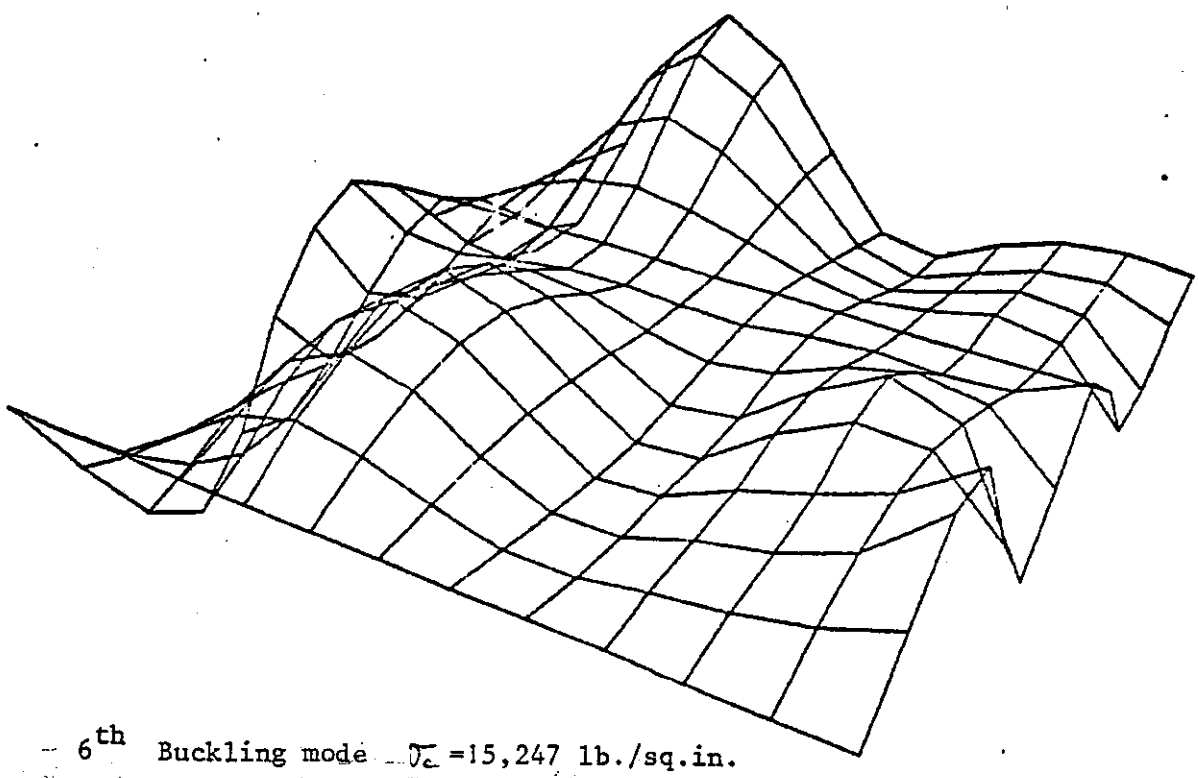
4th Buckling mode σ_c = 10,743 lb./sq. in.

FIG. 34d



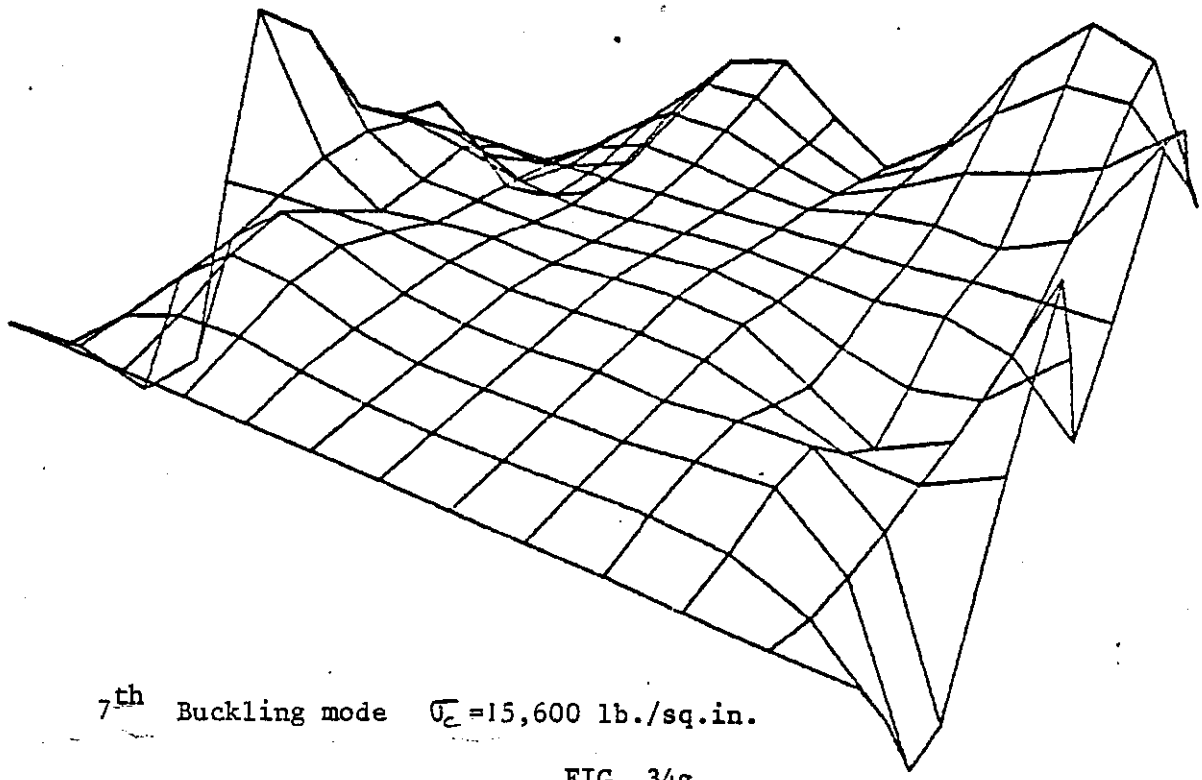
5th Buckling mode σ_c = 14,773 lb./sq.in.

FIG. 34e



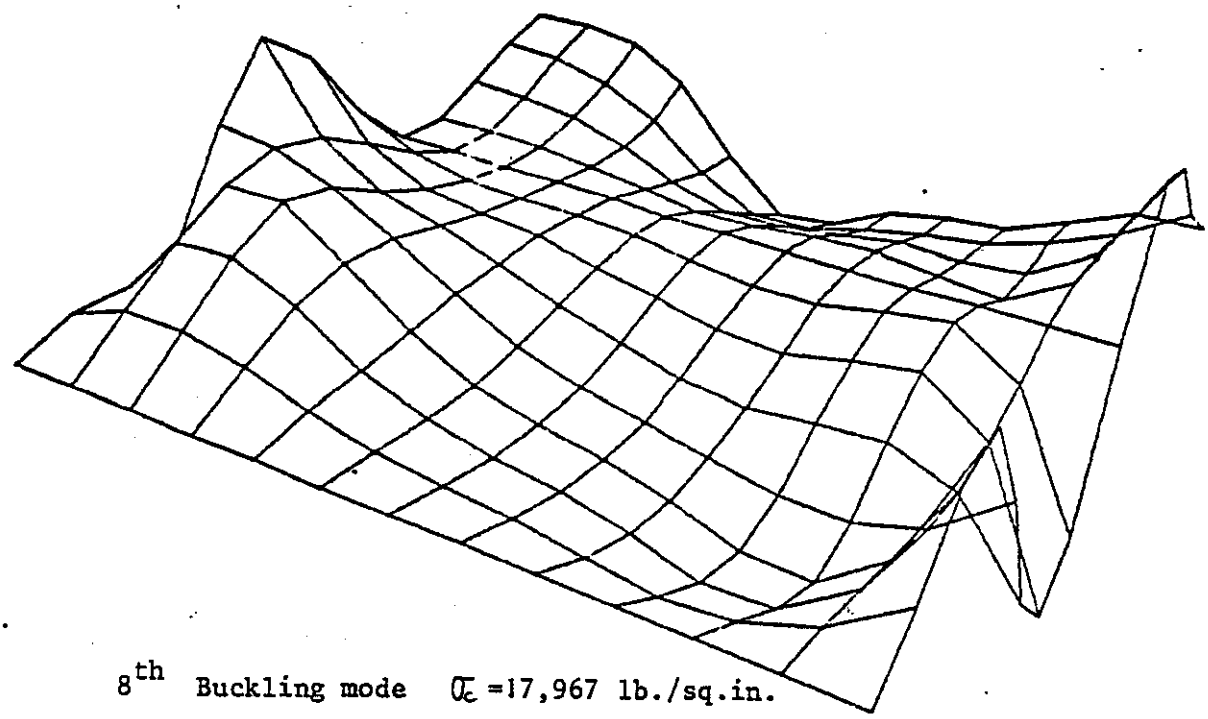
6th Buckling mode σ_c =15,247 lb./sq.in.

FIG. 34f



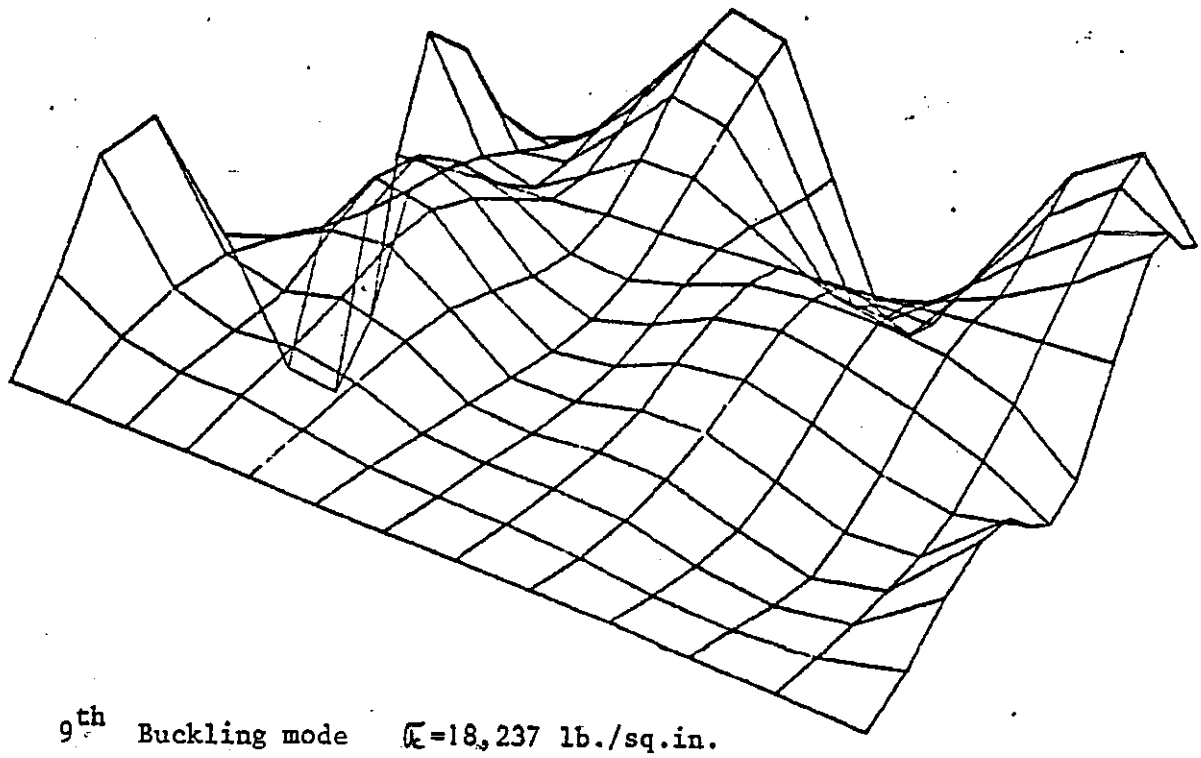
7th Buckling mode σ_c =15,600 lb./sq.in.

FIG. 34g



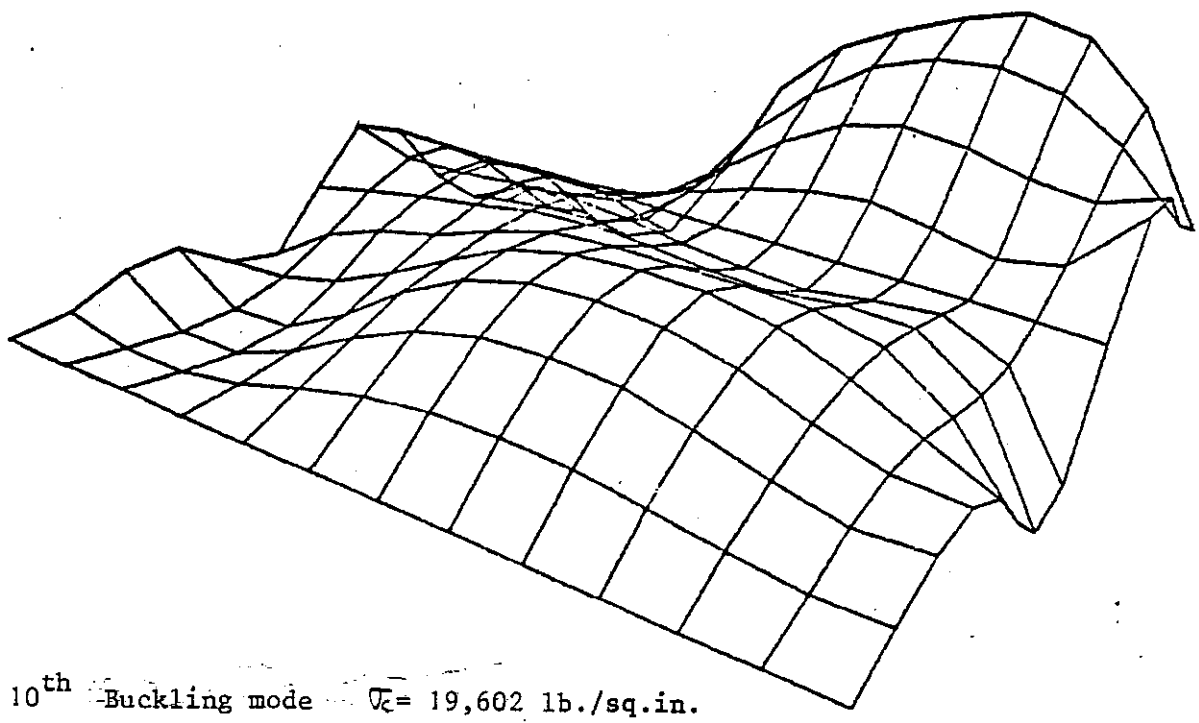
8th Buckling mode σ_c =17,967 lb./sq.in.

FIG. 34h



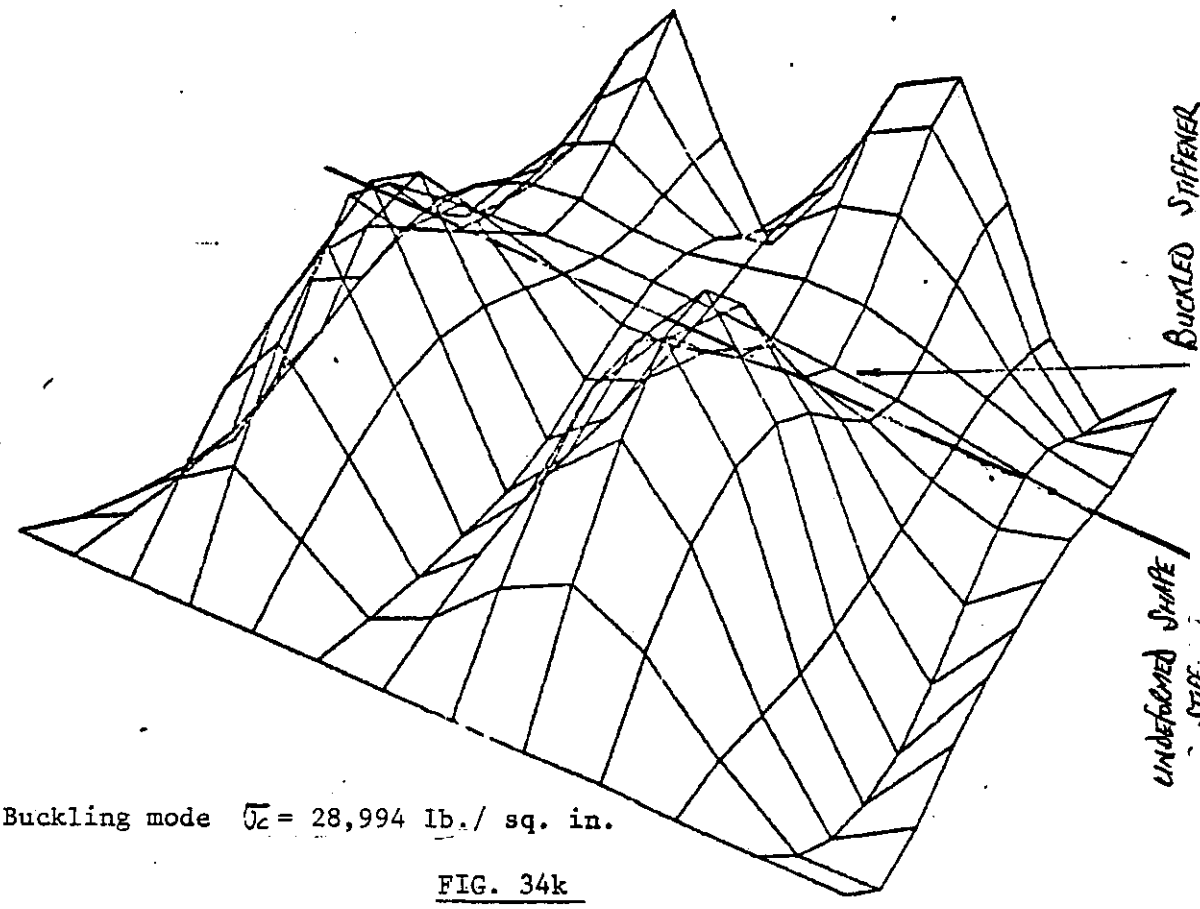
9th Buckling mode $\bar{\sigma}_c$=18,237 lb./sq.in.

FIG. 34i



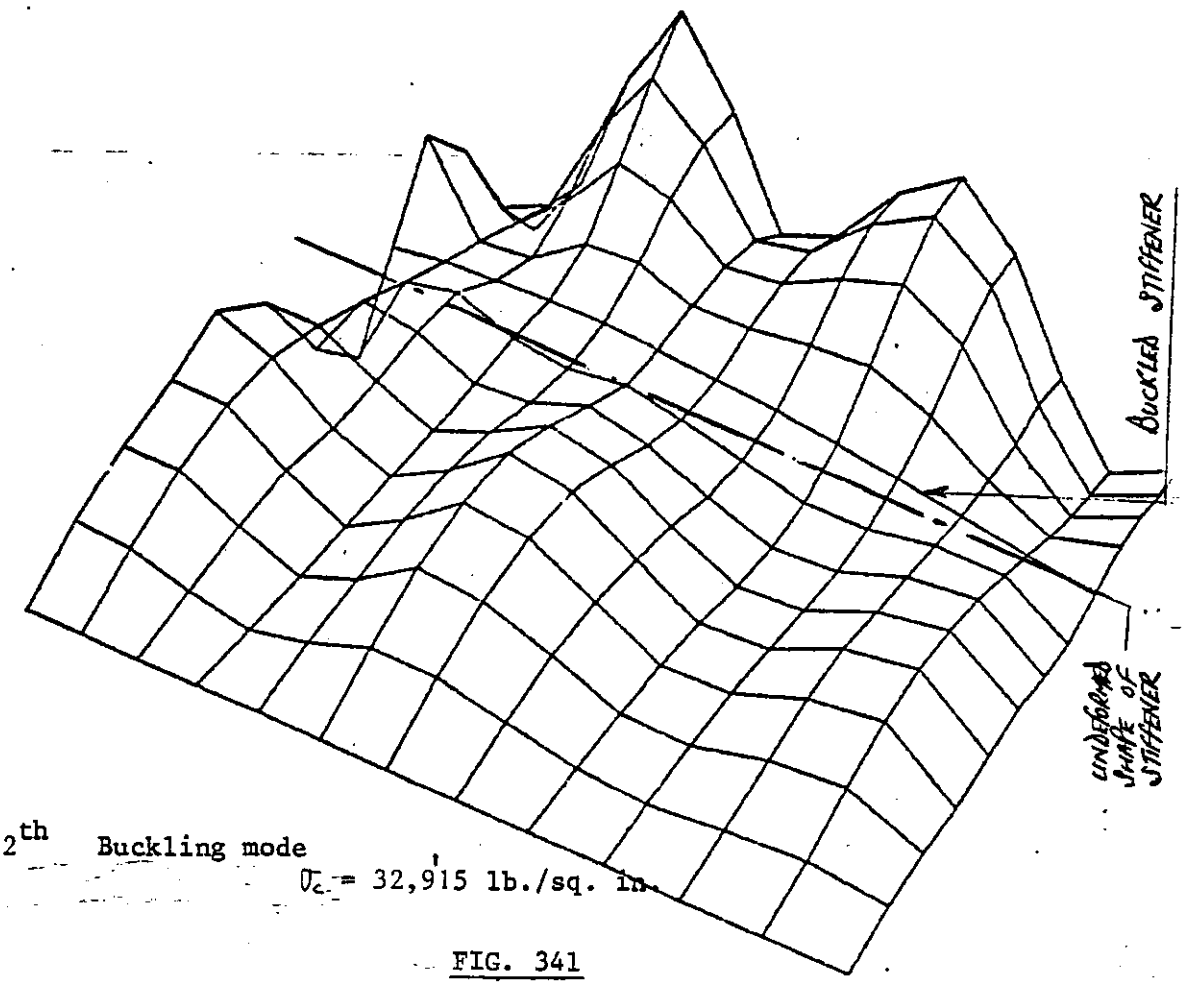
10th Buckling mode $\bar{\sigma}_c$= 19,602 lb./sq.in.

FIG. 34j



11th Buckling mode σ_c = 28,994 lb./ sq. in.

FIG. 34k



12th Buckling mode
σ_c = 32,915 lb./sq. in.

FIG. 341

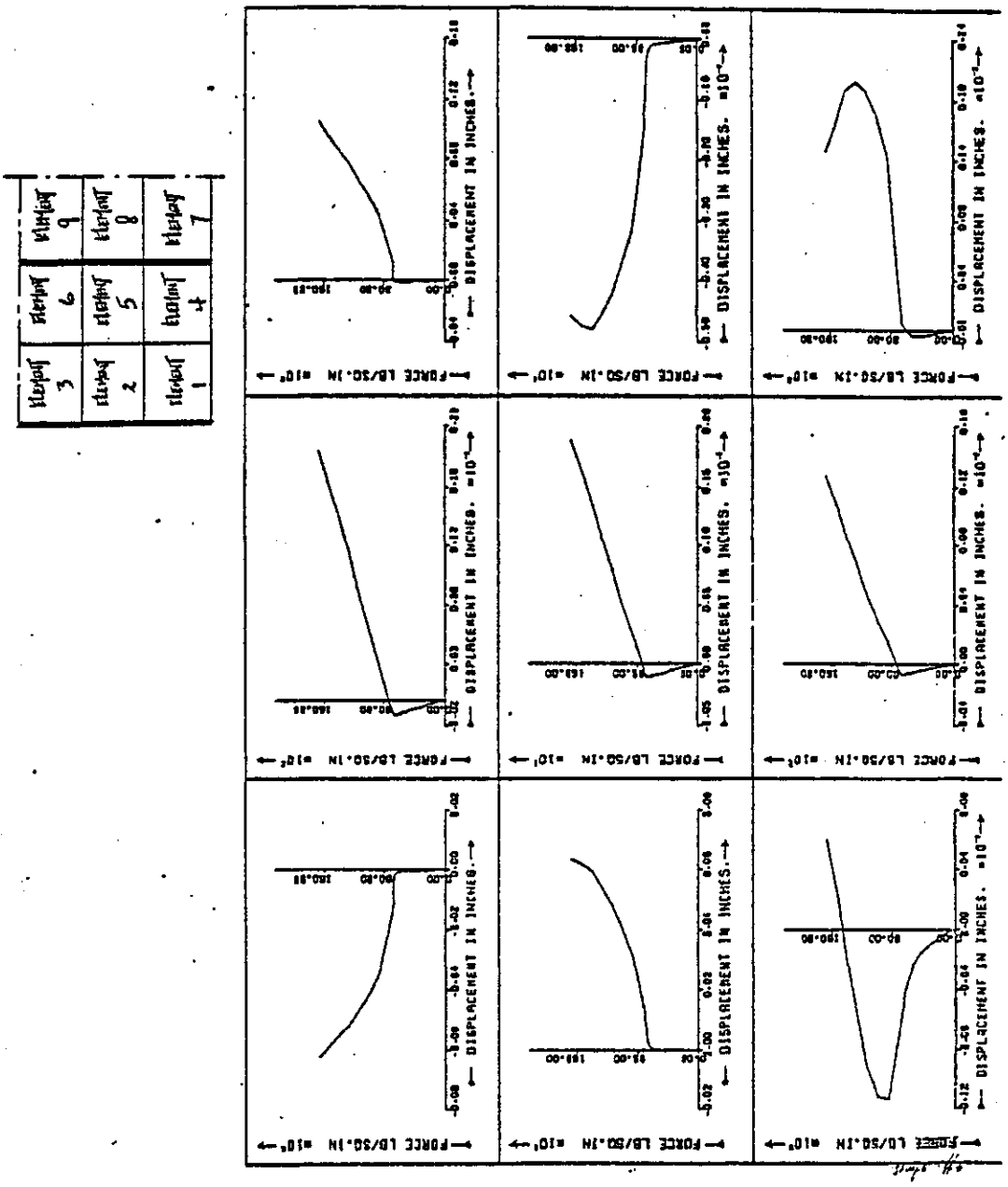


FIG. 35 Elastio-Plastic static buckling of stiffened plate
Load-Displacement curves

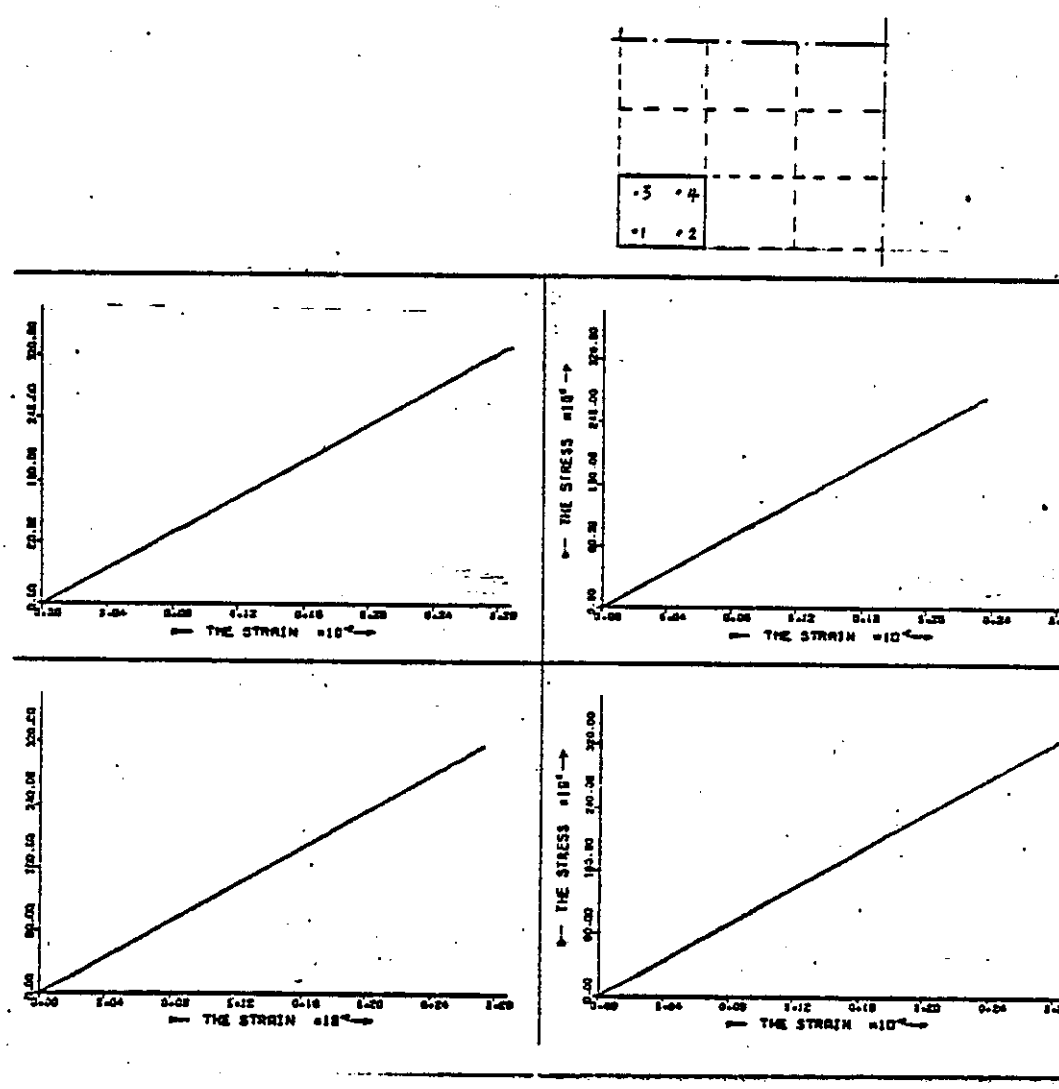


FIG. 36a Elasto-Plastic buckling of stiffened plate
Stress-Strain curves of element 1

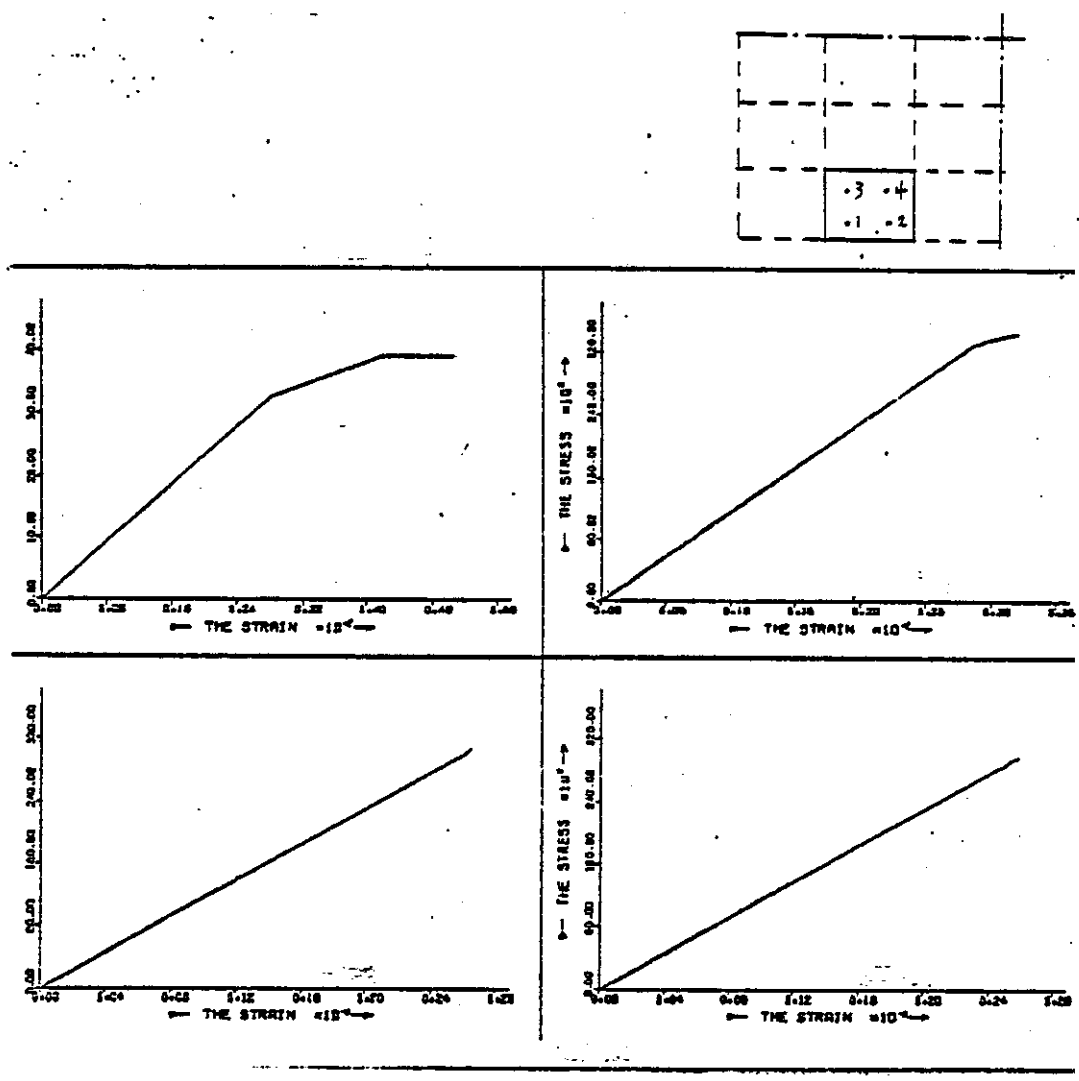


FIG. 36b Elasto-Plastic static buckling of stiffened plate — Stress-Strain curves of element 4

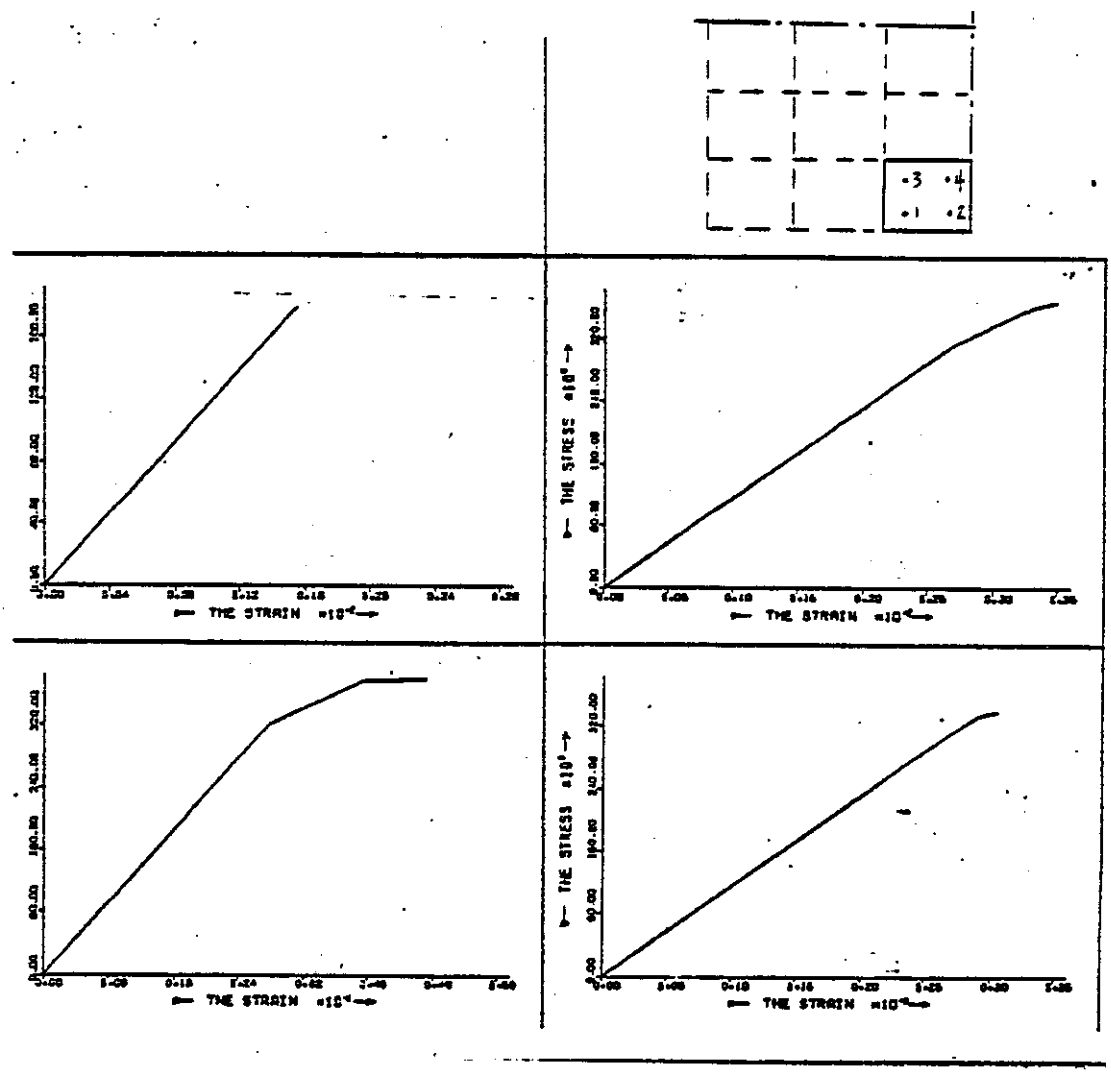


FIG. 36c Elasto-Plastic static buckling of stiffened plate
Stress-Strain curves of element 7

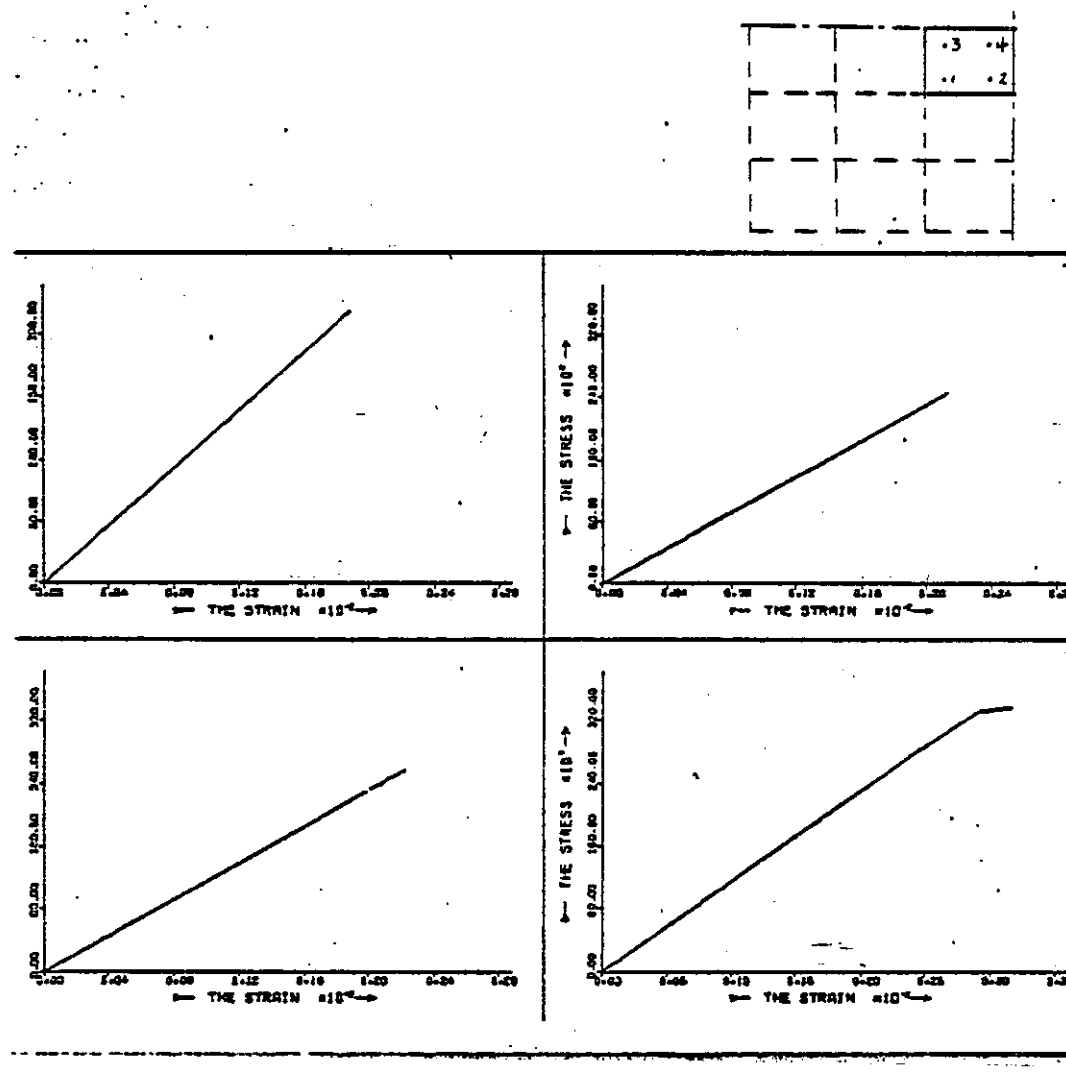
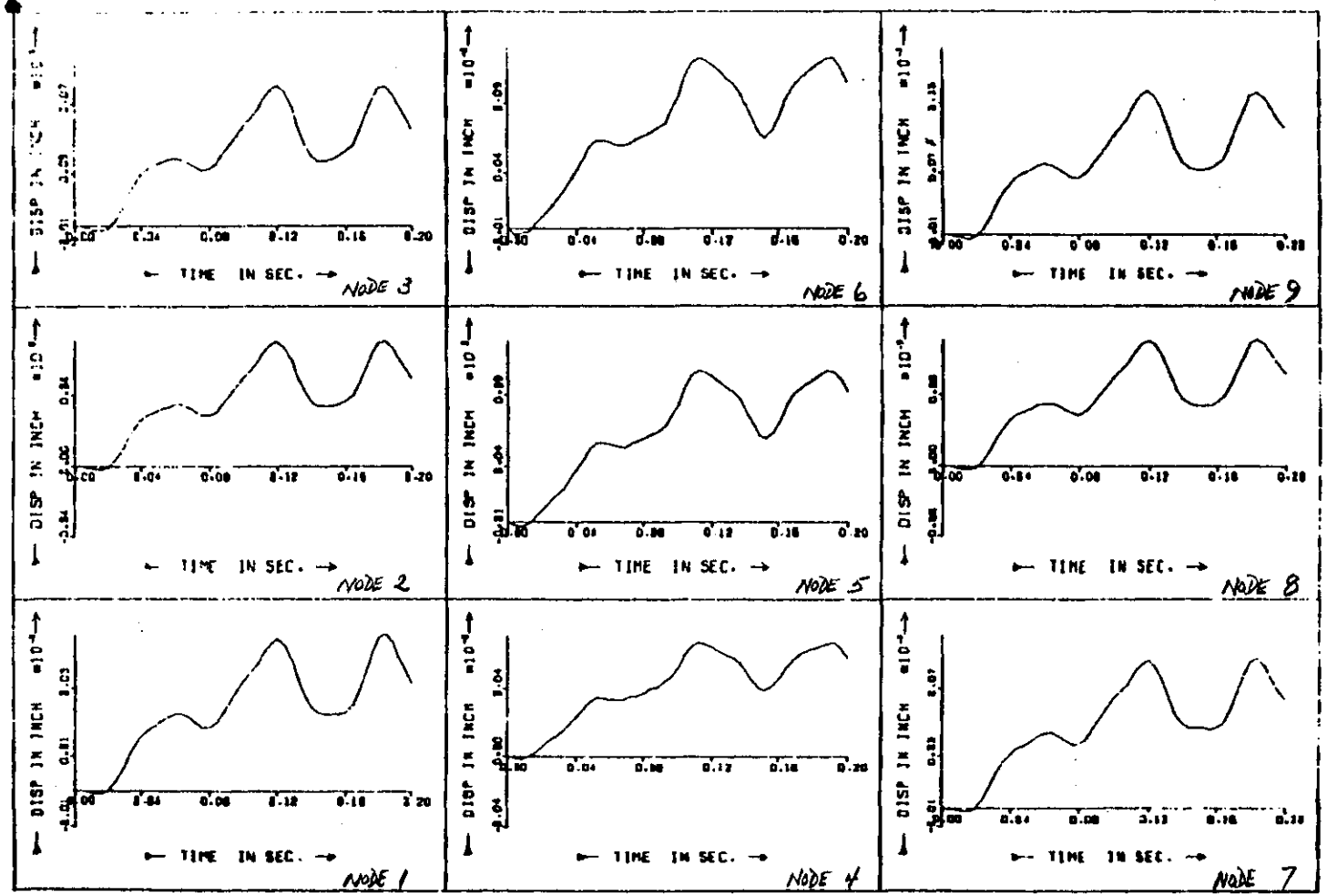


FIG. 36d Elasto-Plastic static buckling of stiffened plate
Stress-Strain curves of element 9

DISPLACEMENT RESPONSE AT ELEMENT 1 TO 9 AT APPLIED STRESS OF 2,000 LB./SQ.IN.



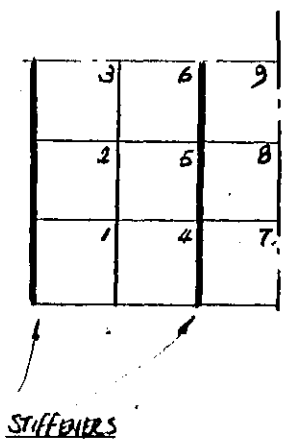


FIG. 37a

STRESS AT PLATE ELEMENT 1

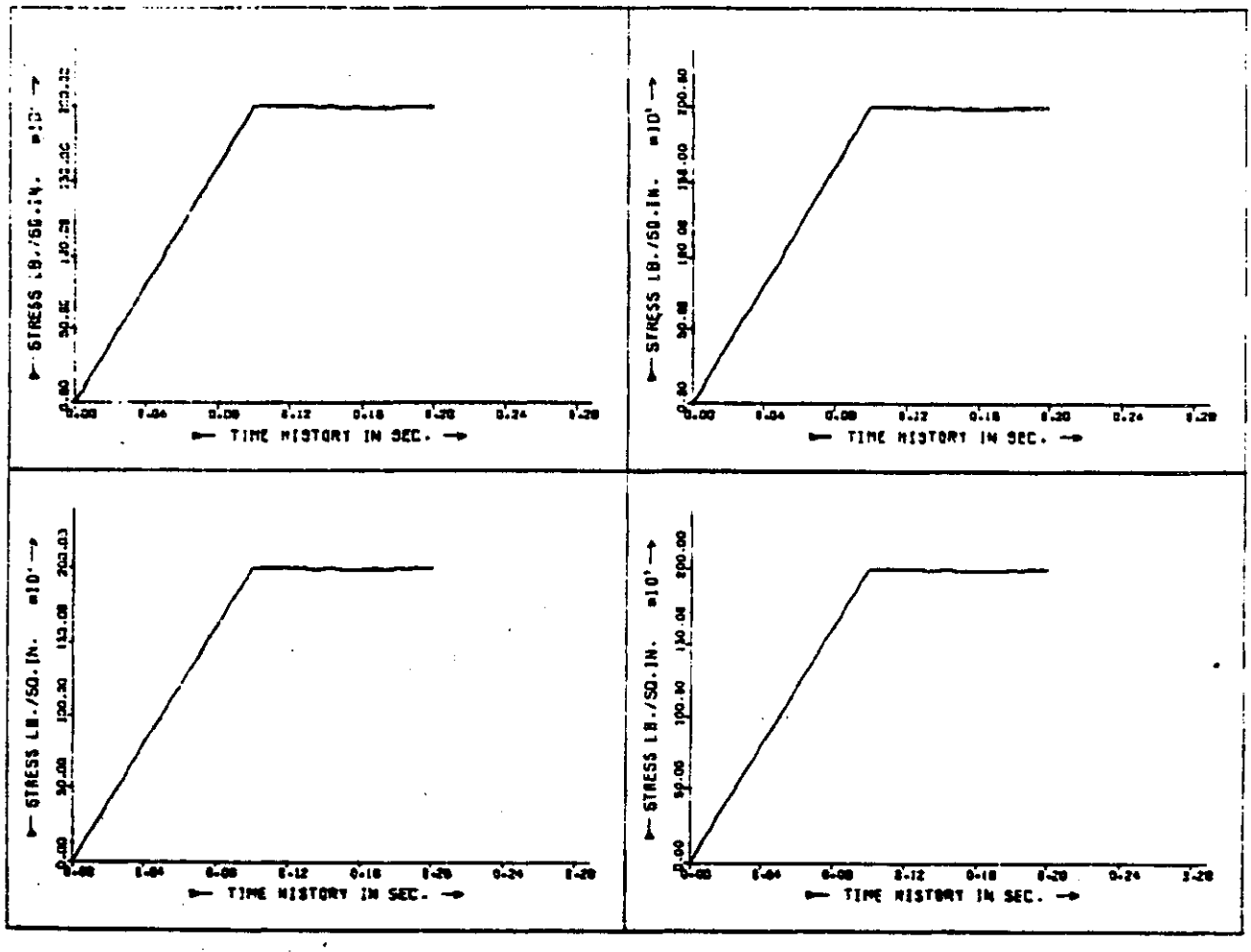


FIG. 37b

STRESS AT BAR ELEMENT 2

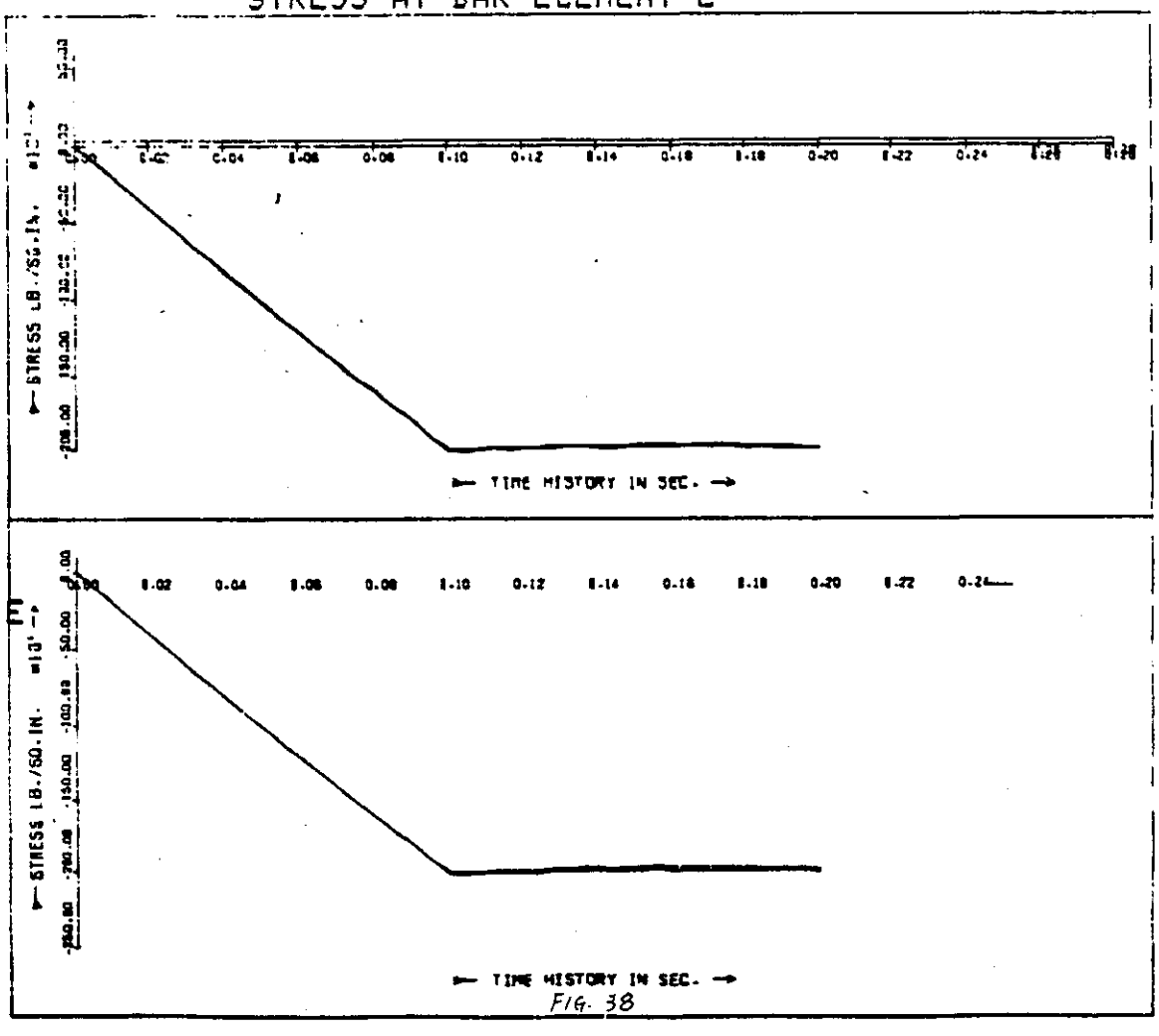


FIG. 38

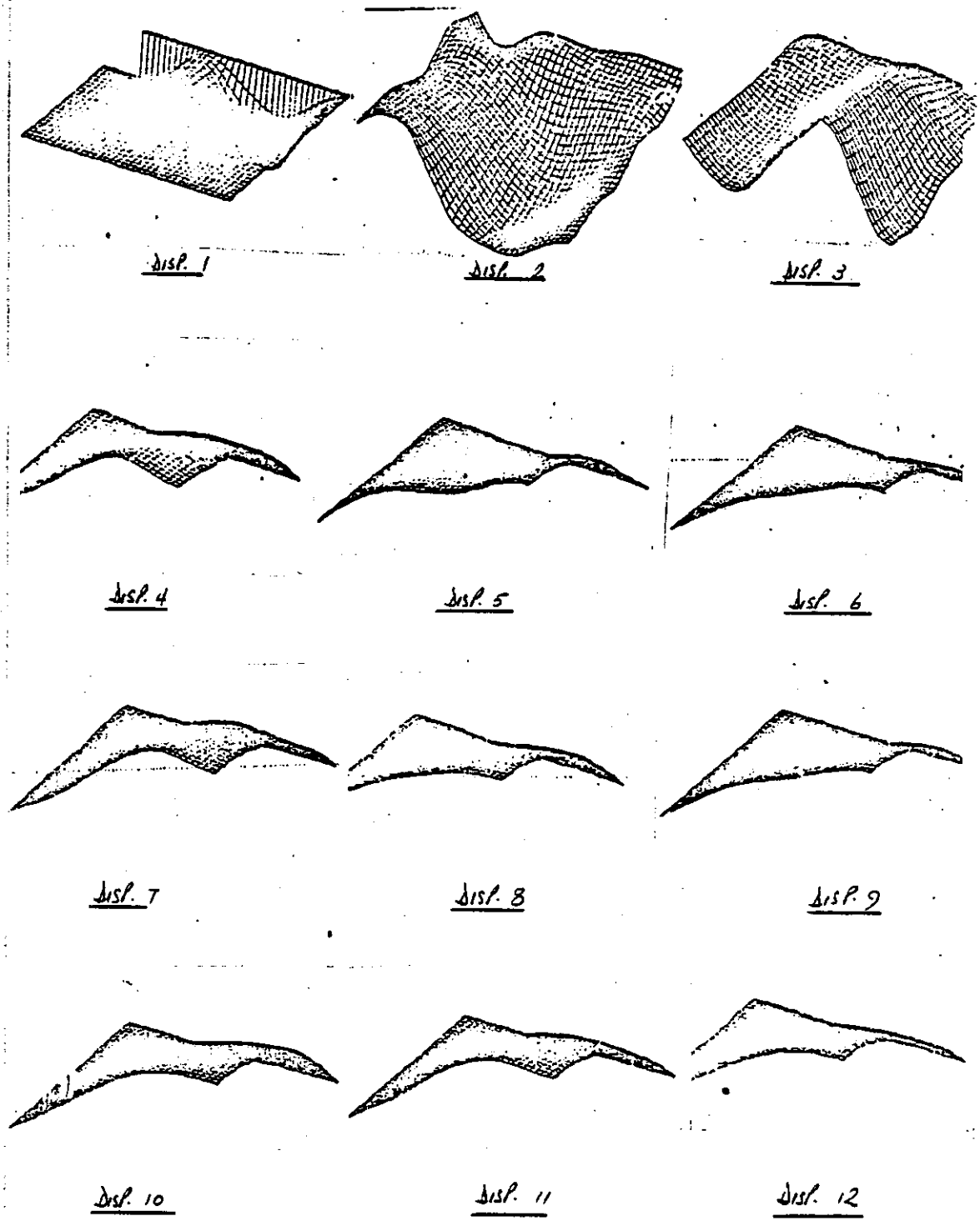


FIG. 39 Sequence of deformation modes of stiffened plate (appl. stress = 2,000 lb./in.^{2}

DISPLACEMENT RESPONSE AT ELEMENT 1 TO 9 AT APPLIED STRESS OF 8,000 LB./SQ.IN.

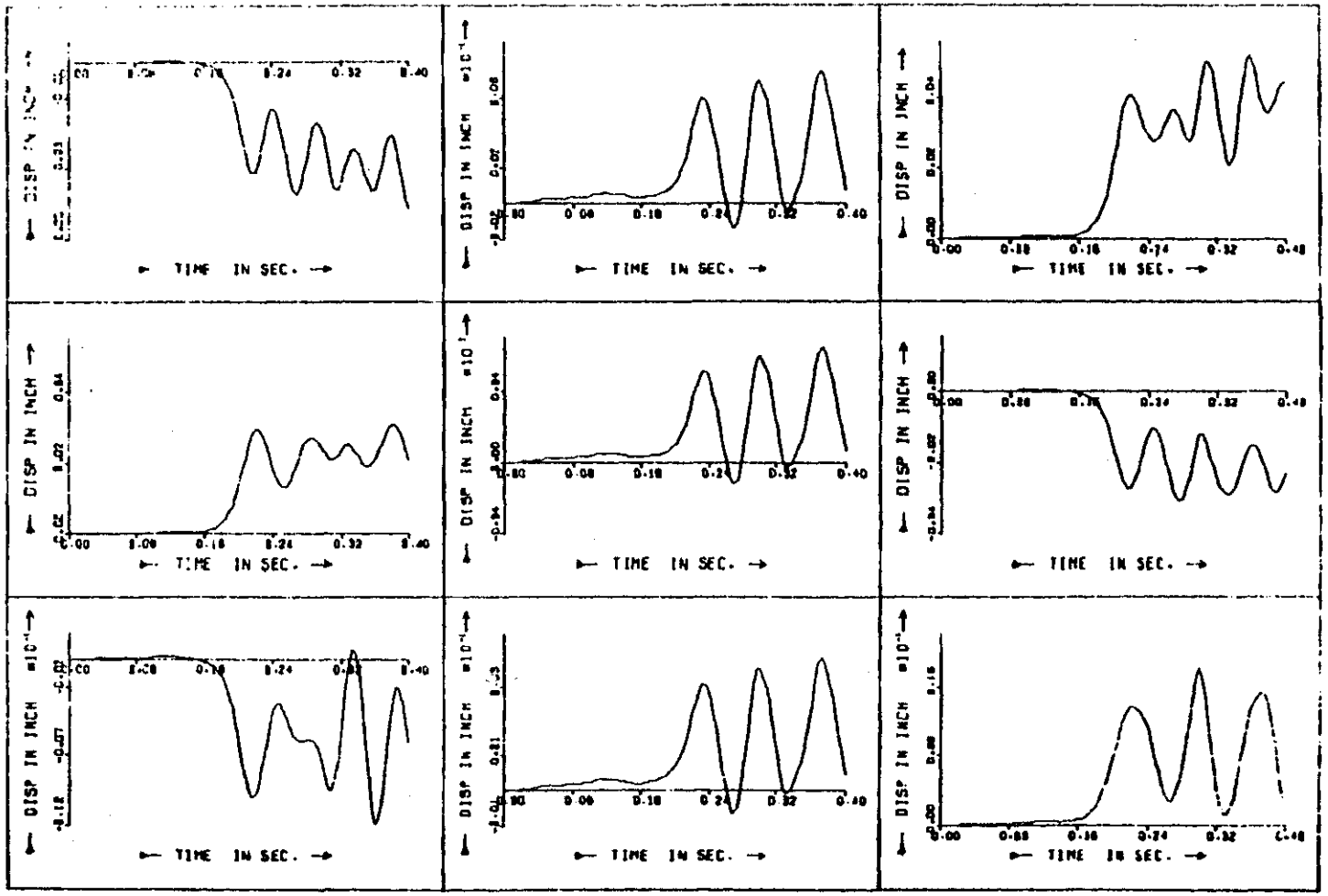


FIG. 40a

STRESS AT PLATE ELEMENT 1

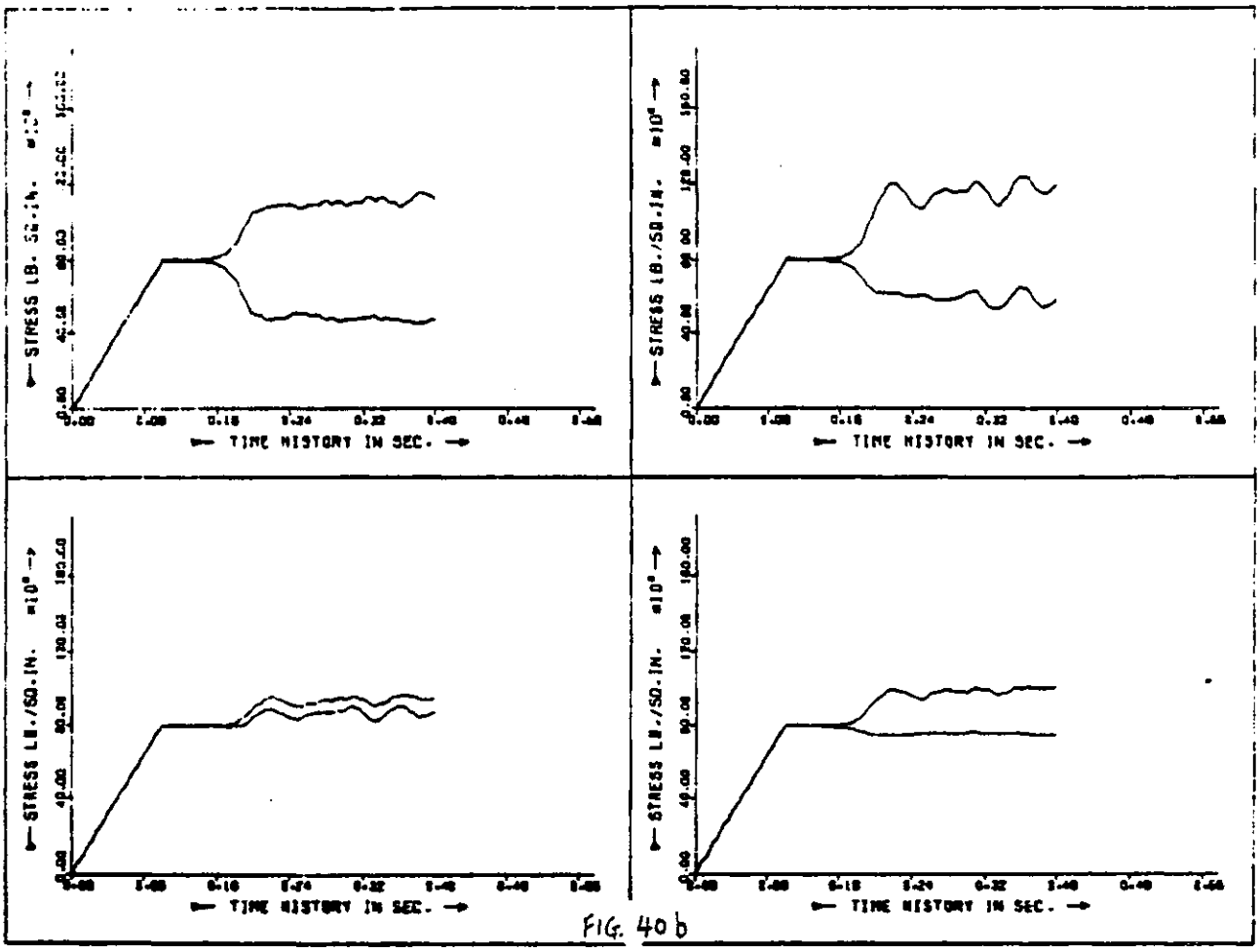


FIG. 40 b

STRESS AT BAR ELEMENT 4

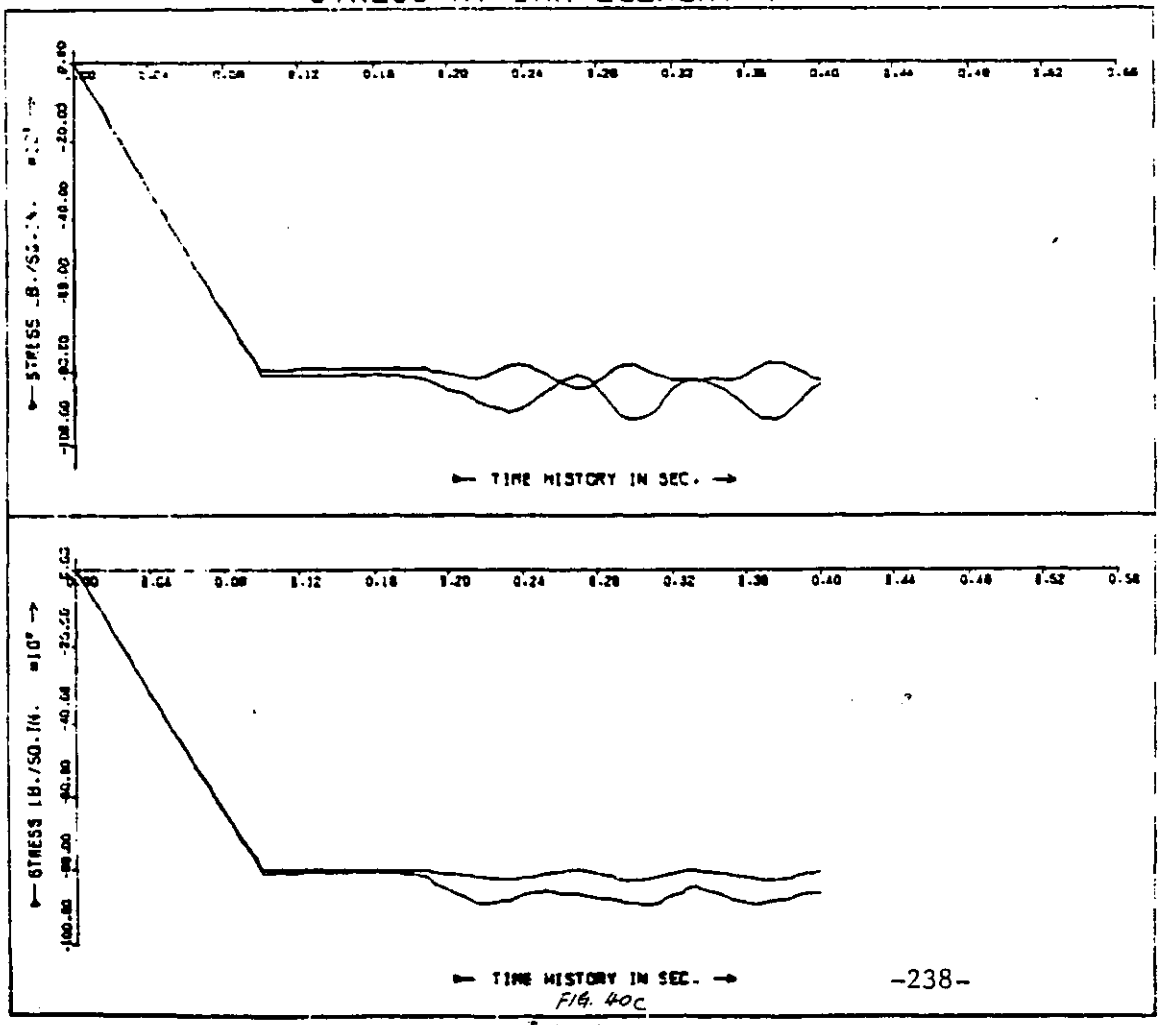


FIG. 40c

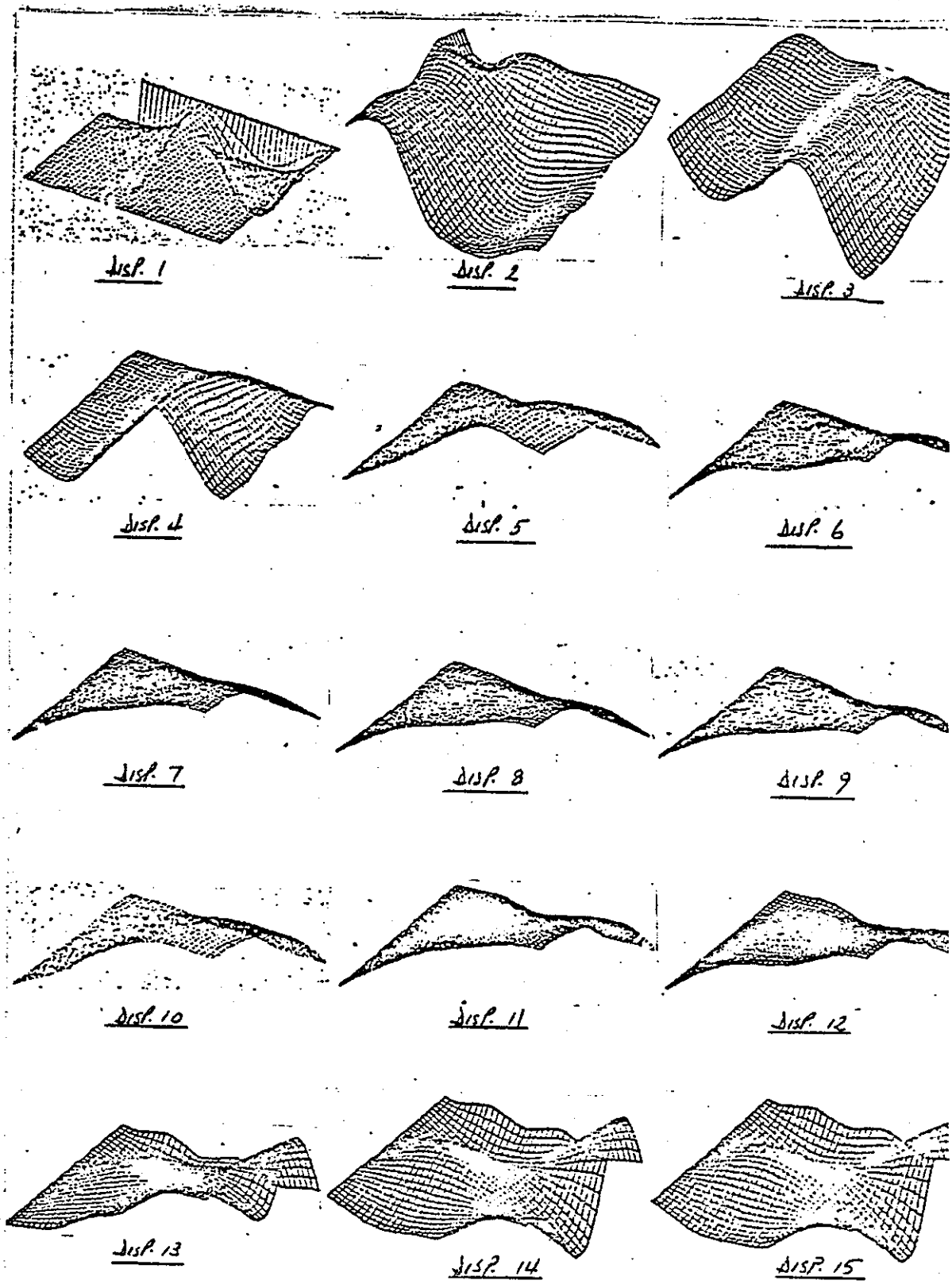
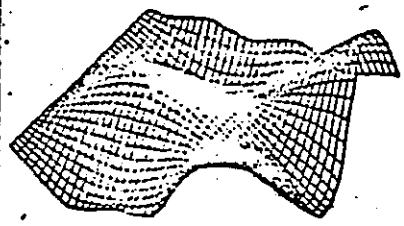
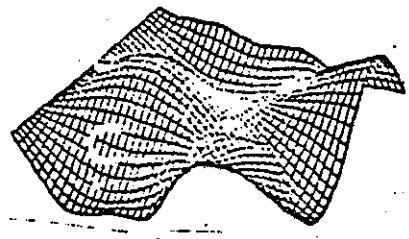


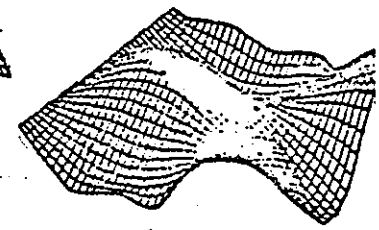
FIG. 41 Sequence of deformation modes of stiffened plate (appl. stress = 8,000 lb./in.^{2})



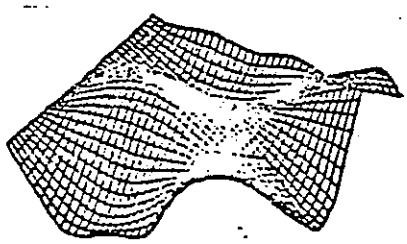
Disp. 16



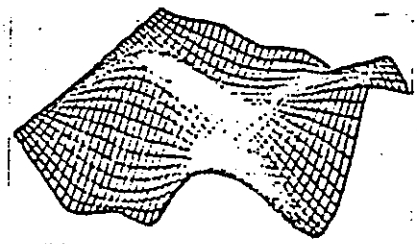
Disp. 17



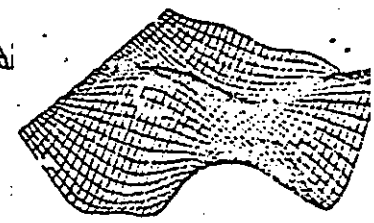
Disp. 18.



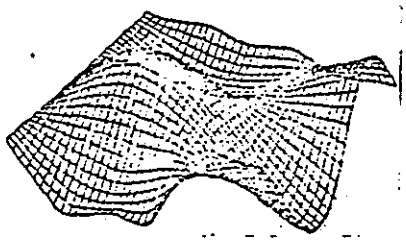
Disp. 19



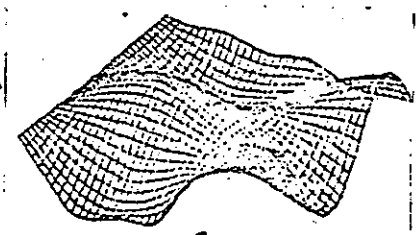
Disp. 20



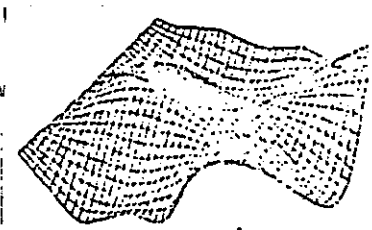
Disp. 21



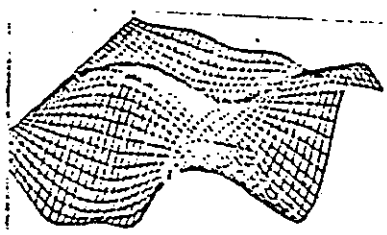
Disp. 22



Disp. 23



Disp. 24



Disp. 25

FIG. 41 (continue)

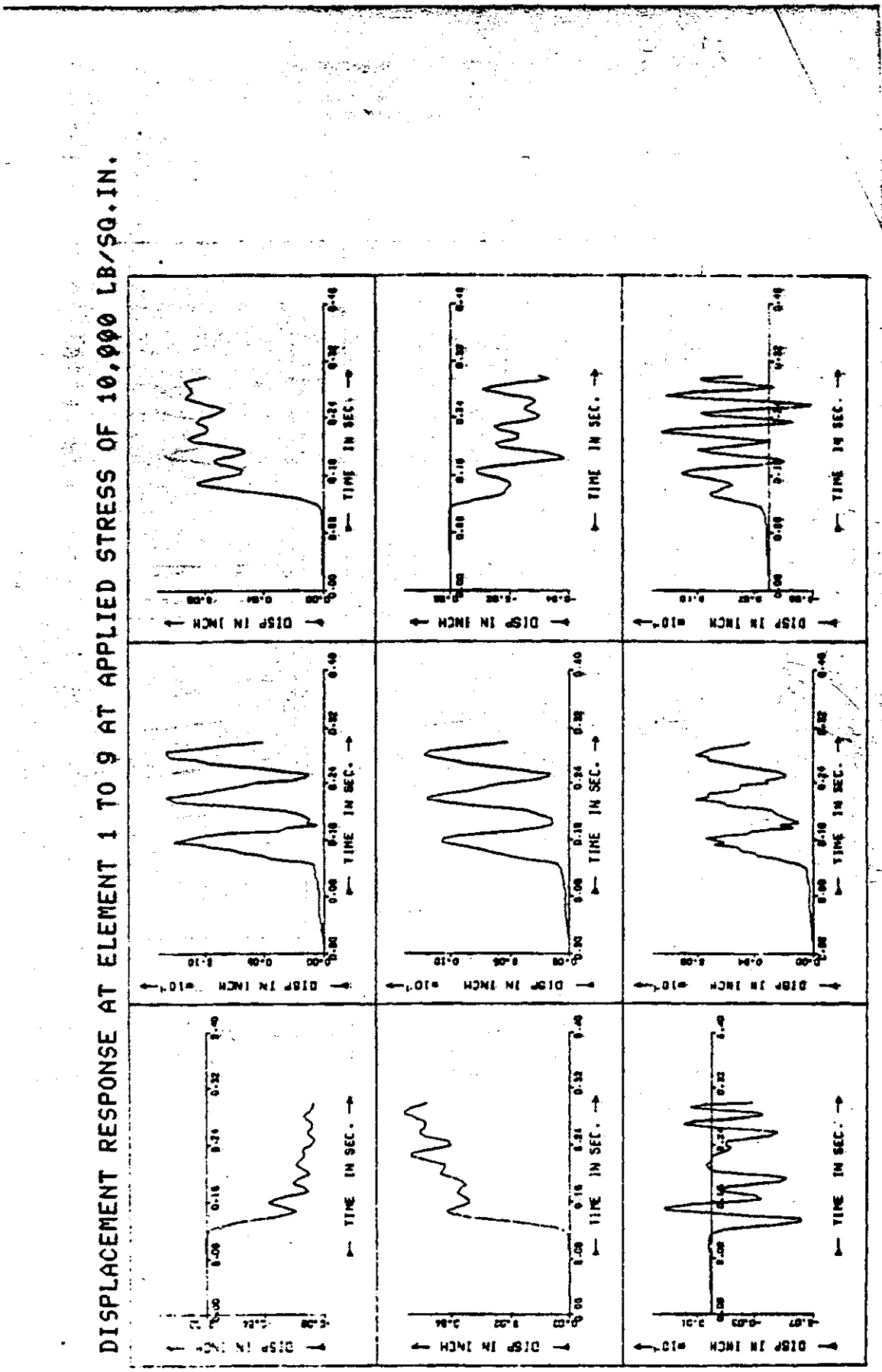

DISPLACEMENT RESPONSE AT ELEMENT 1 TO 9 AT APPLIED STRESS OF 10,000 LB/SQ.IN.
DISP IN INCH
TIME IN SEC.

FIG. 42

STRESS AT PLATE ELEMENT 7

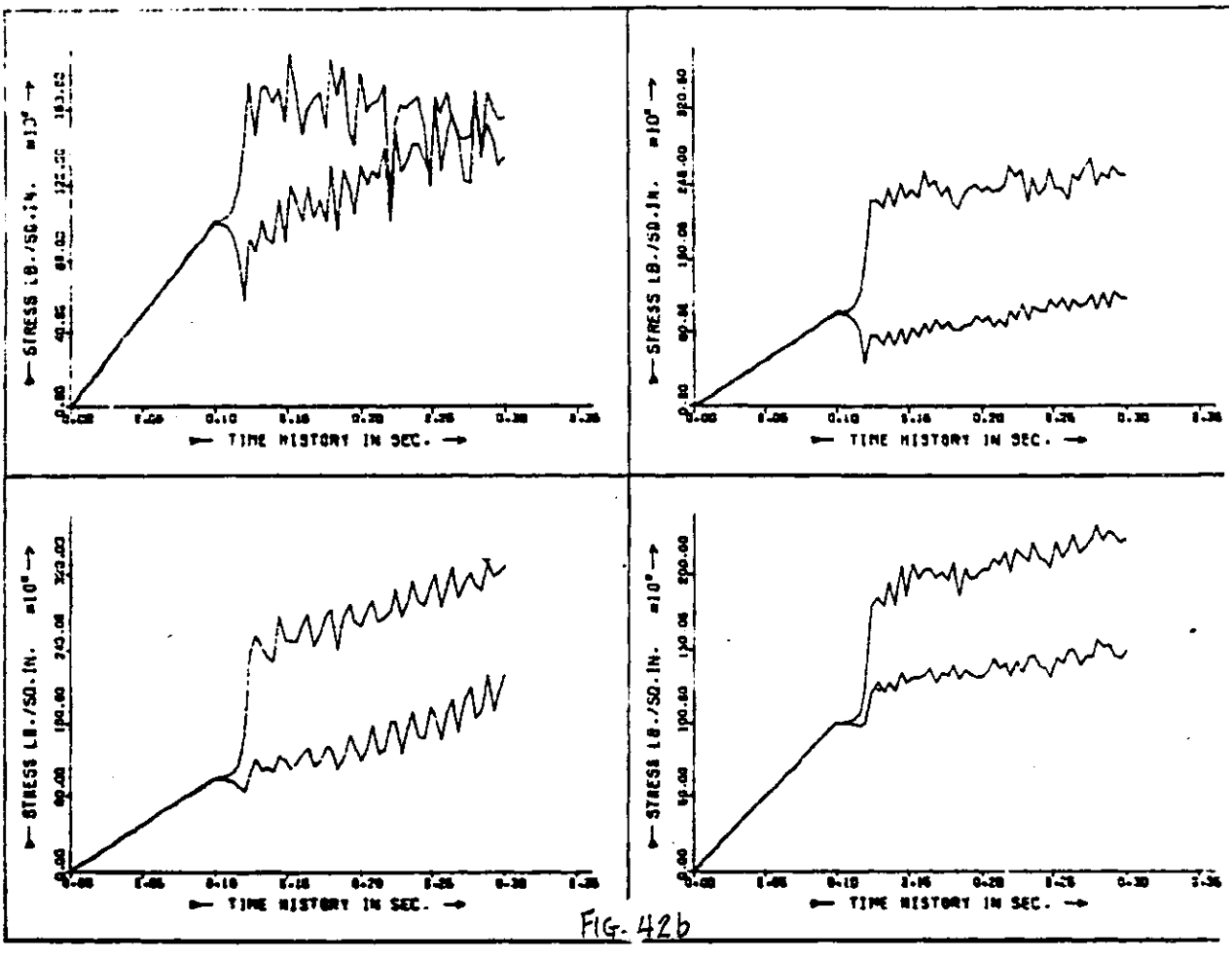


FIG. 42b

STRESS AT BAR ELEMENT 4

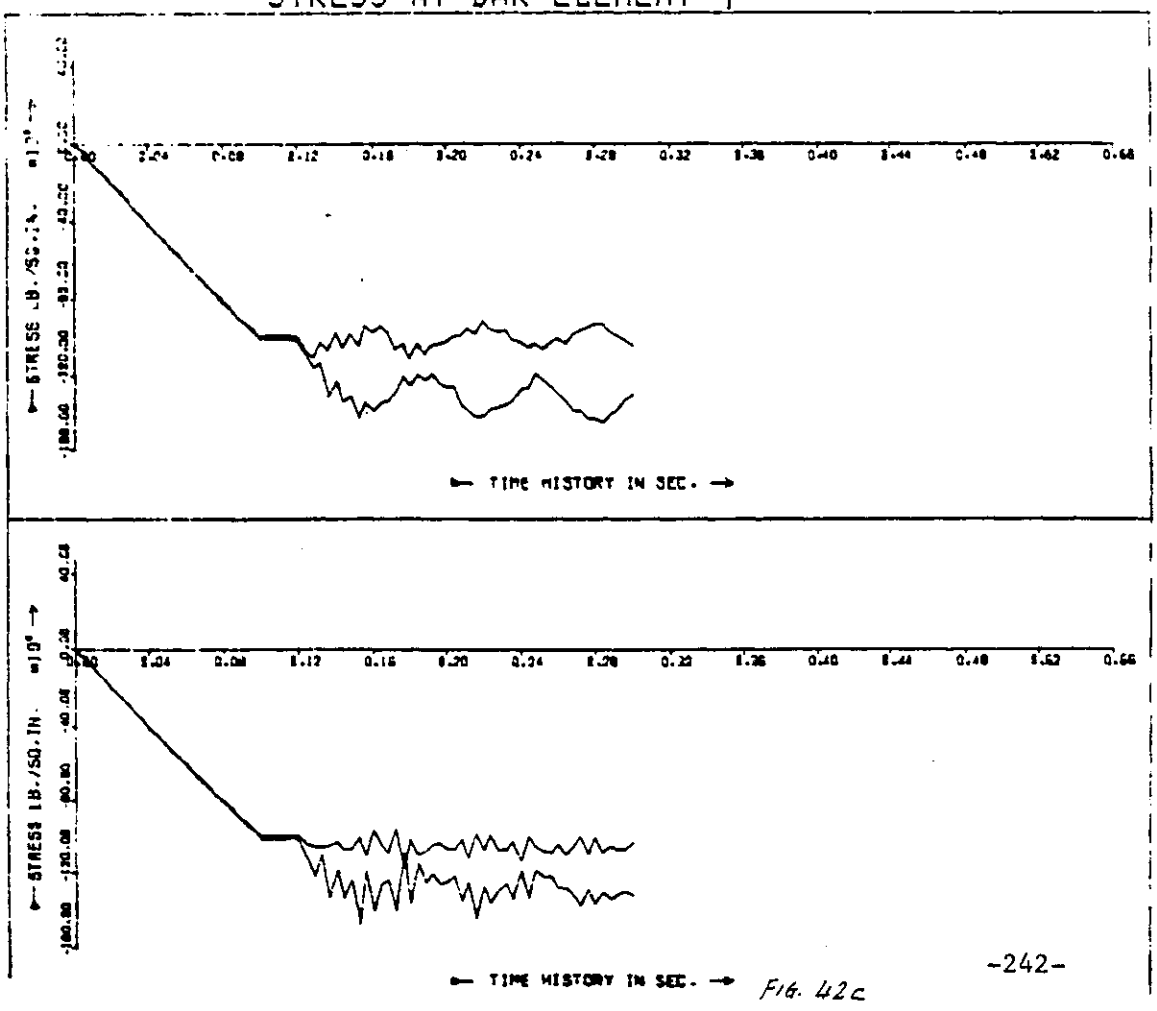


FIG. 42c

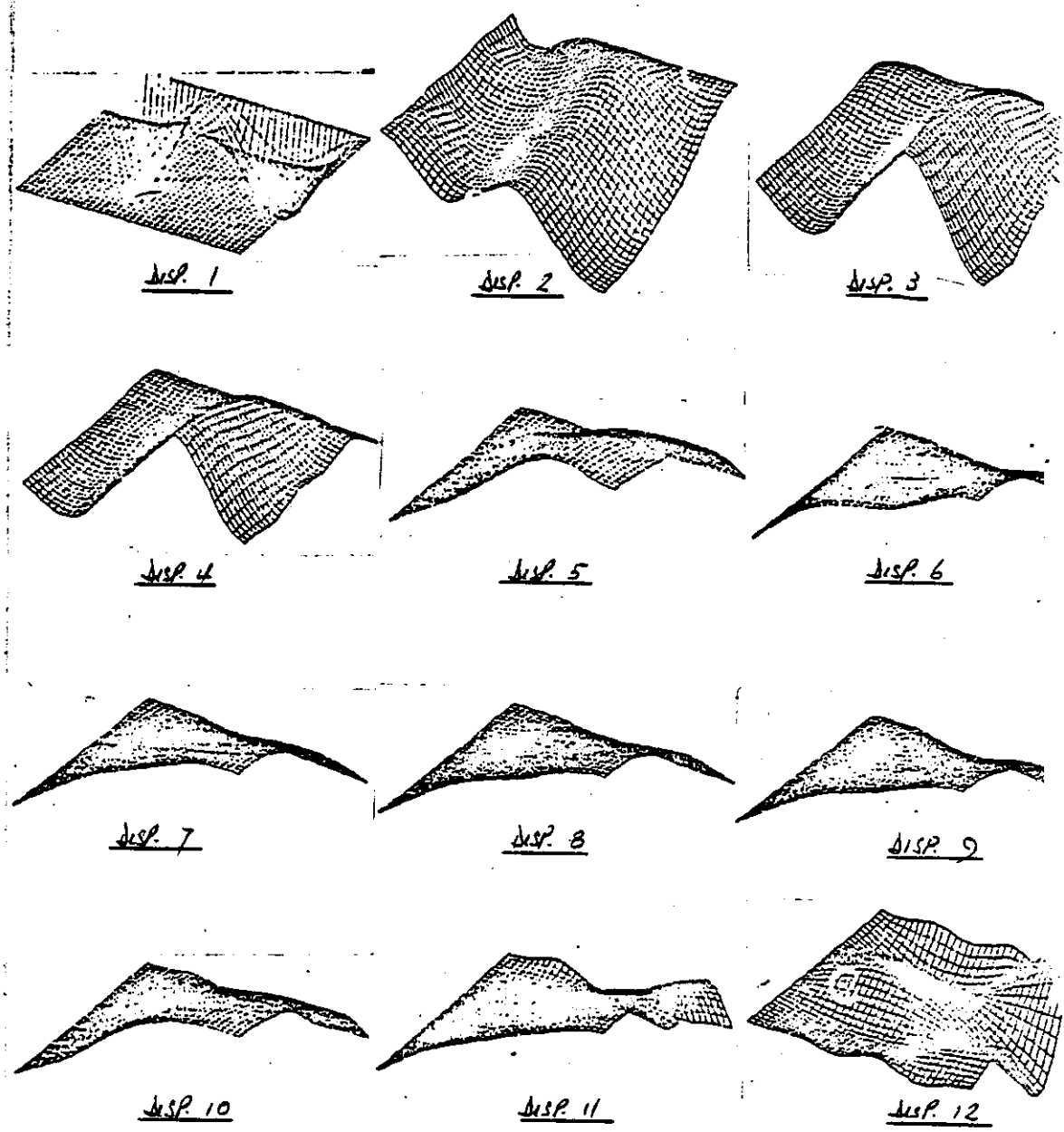
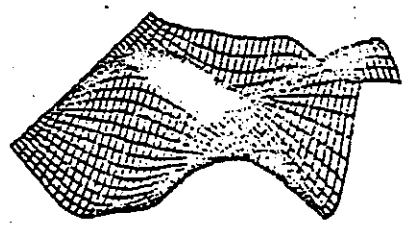
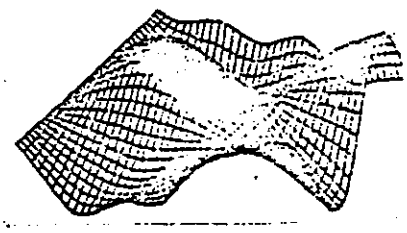


FIG. 43 Sequence of deformation modes of stiffened plate (appl. stress = 10,000 lb



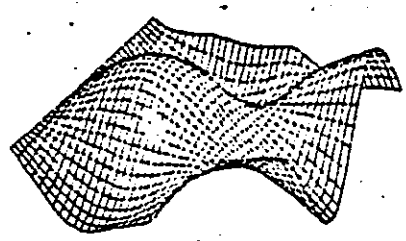
Disp. 13



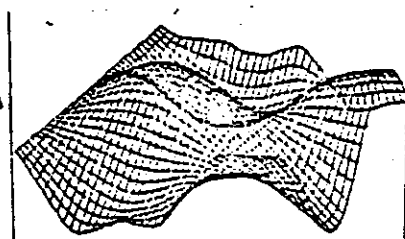
Disp. 14



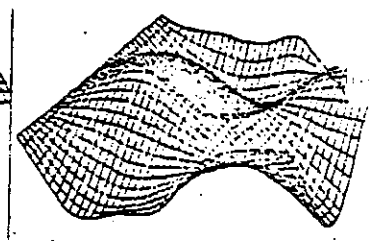
Disp. 15



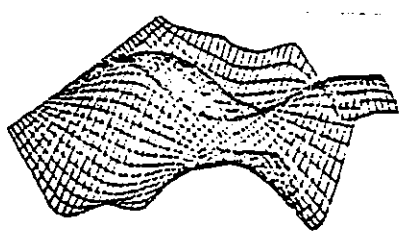
Disp. 16



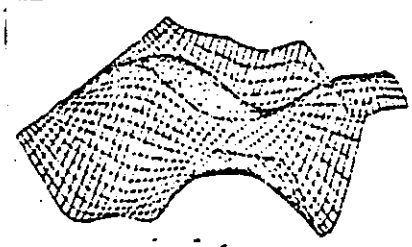
Disp. 17



Disp. 18



Disp. 19



Disp. 20

FIG. 43 (continue)

FIG. 44a Displacement curves of structure showing numerical divergency effect

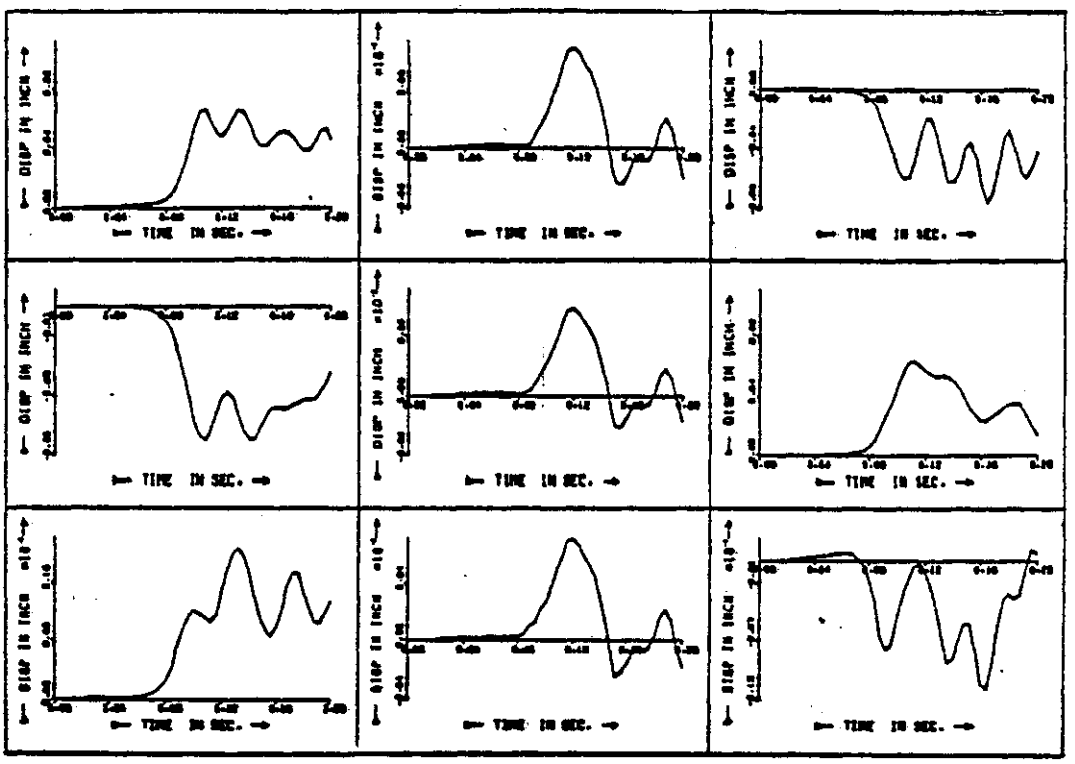
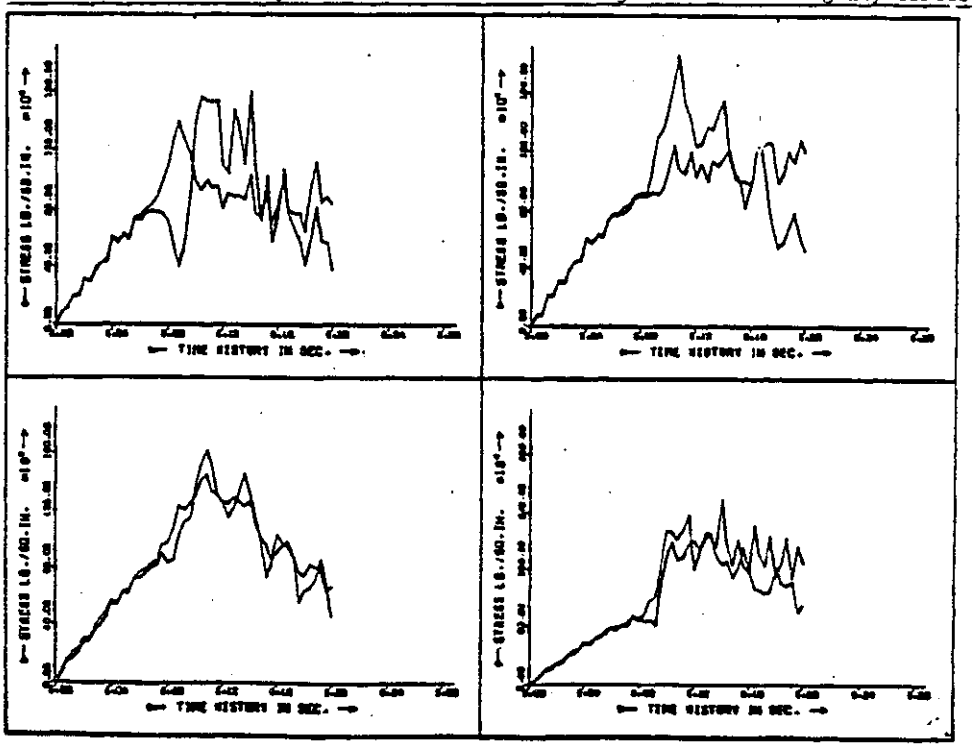


FIG. 44b Stress history curves of structure showing numerical divergency effect



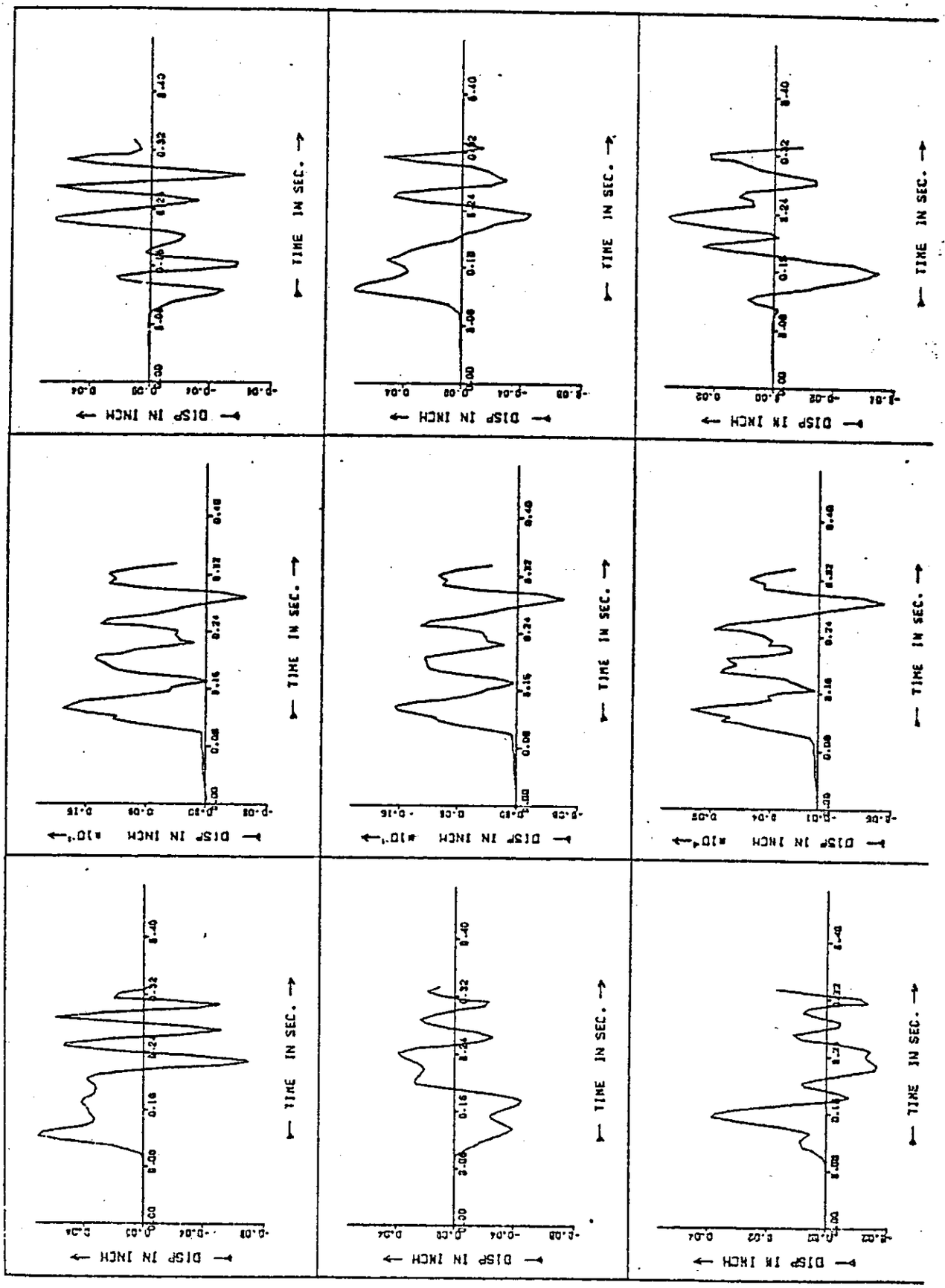


FIG. 45a Nodal displacement curves (appl. stress = 12,000 lb./sq.in.

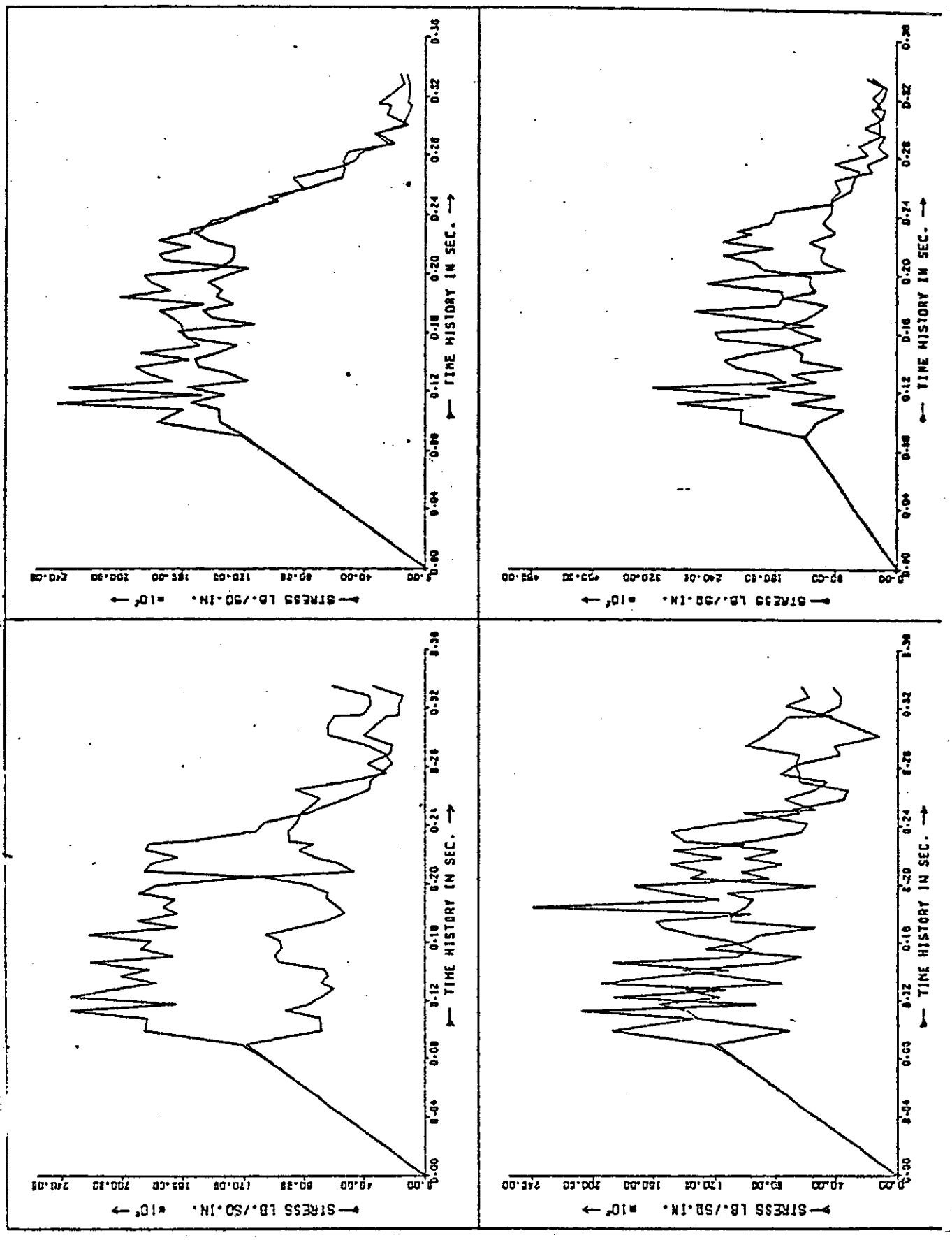


FIG. 45b Gaussian Stresses (equivalent) at element 4

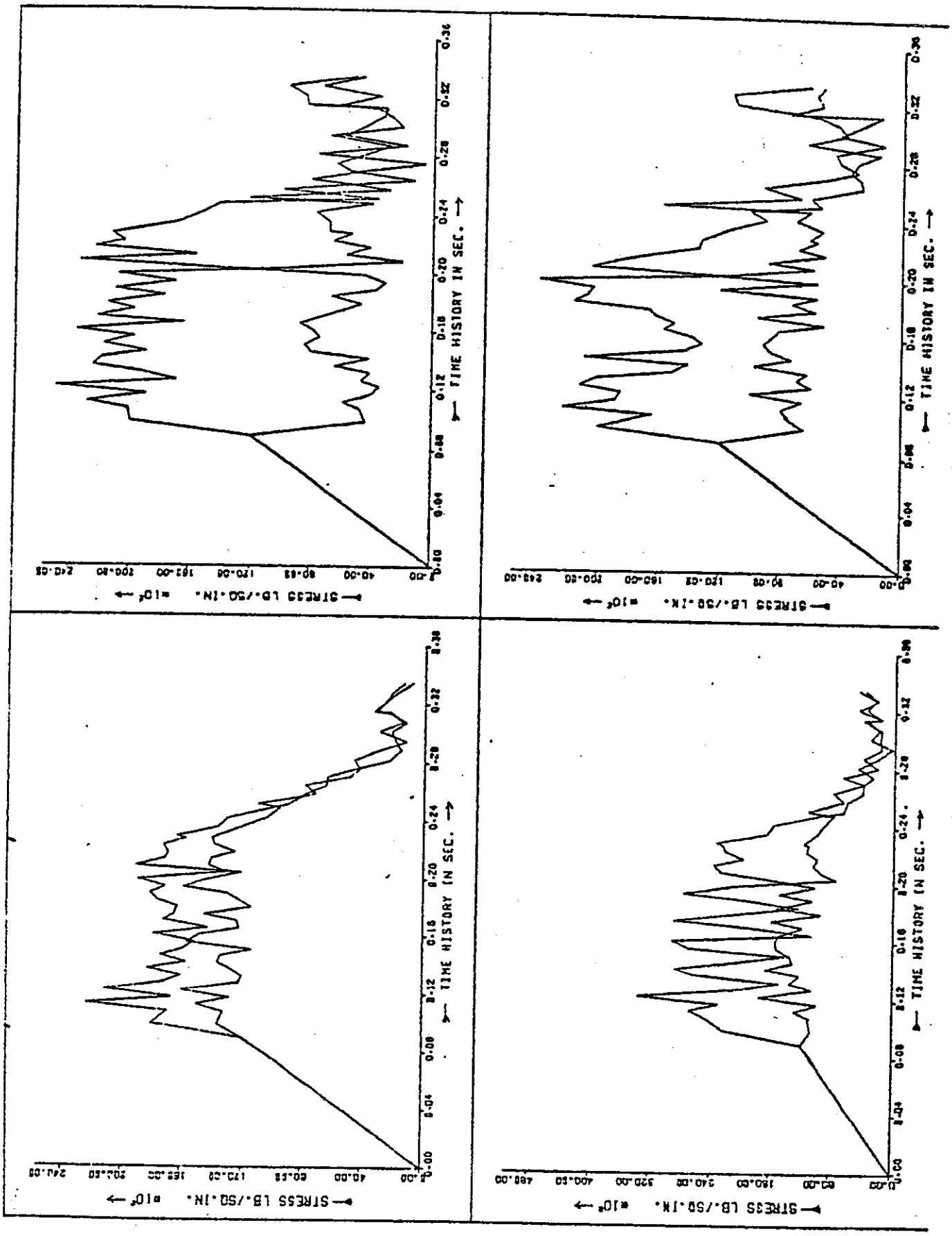


FIG. 45c Gaussian stresses (equivalent) at element 7

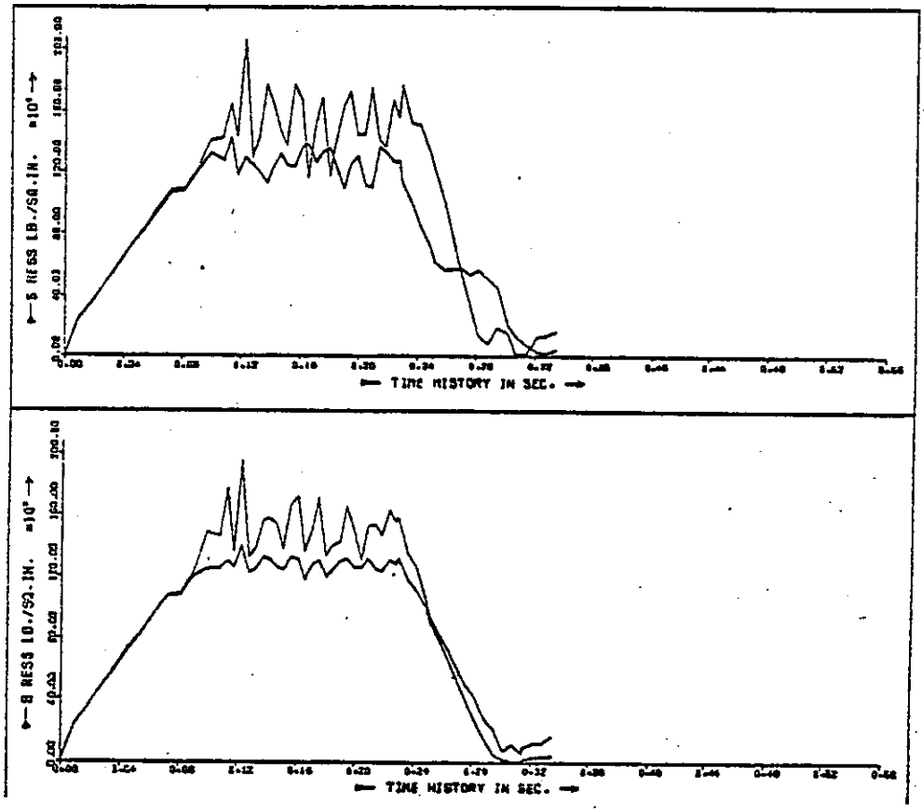


FIG. 45d Stresses at stiffener element 4

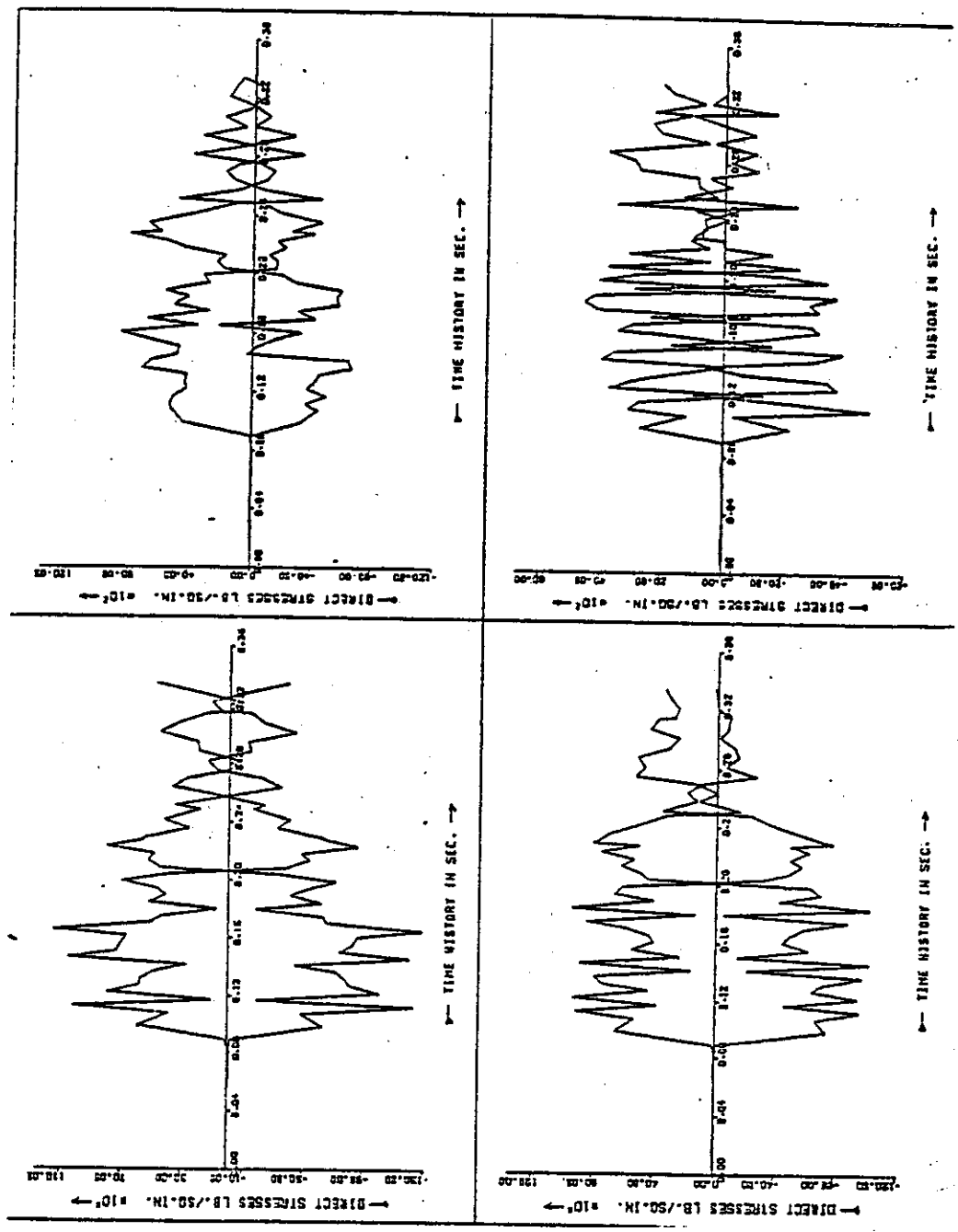


FIG. 45e Gaussian Stresses (direct stresses in X-direction) at element 4

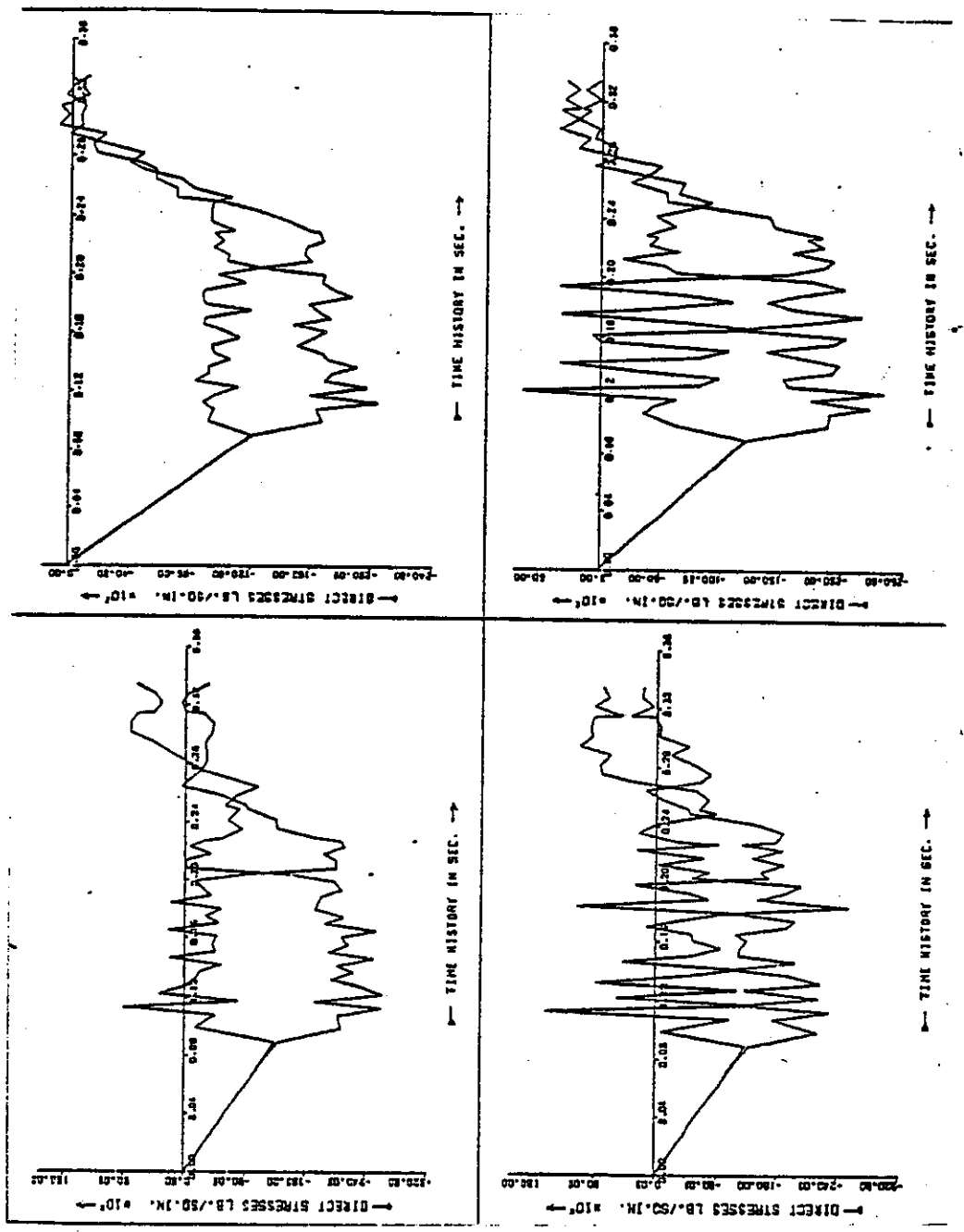


FIG. 45f Gaussian Stresses (direct stresses in Y-direction) at element 4

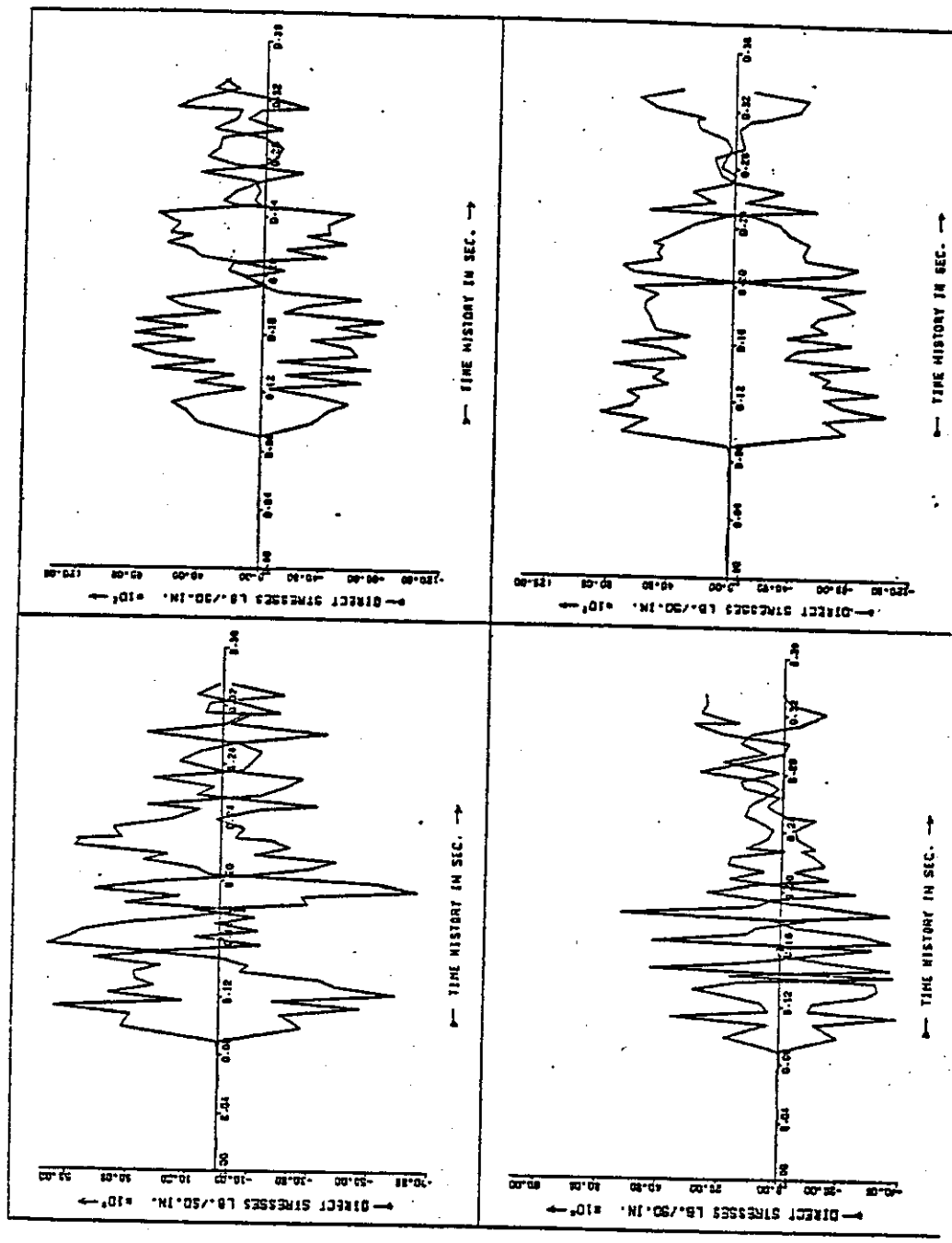


FIG. 45g Gaussian Stresses (direct stresses in X-direction) at element 7

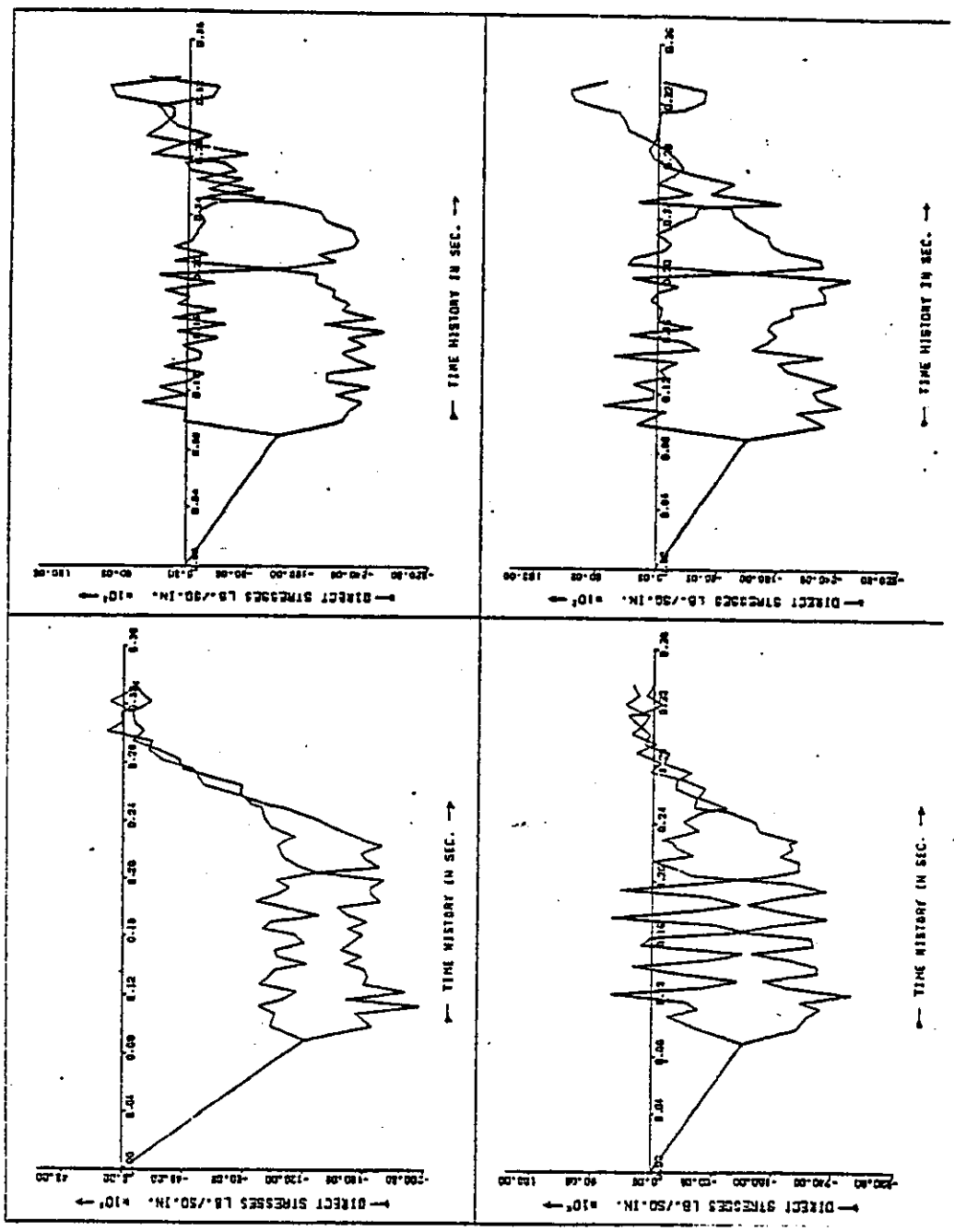


FIG. 45h Gaussian Stresses (direct stresses in Y-direction) at element 7

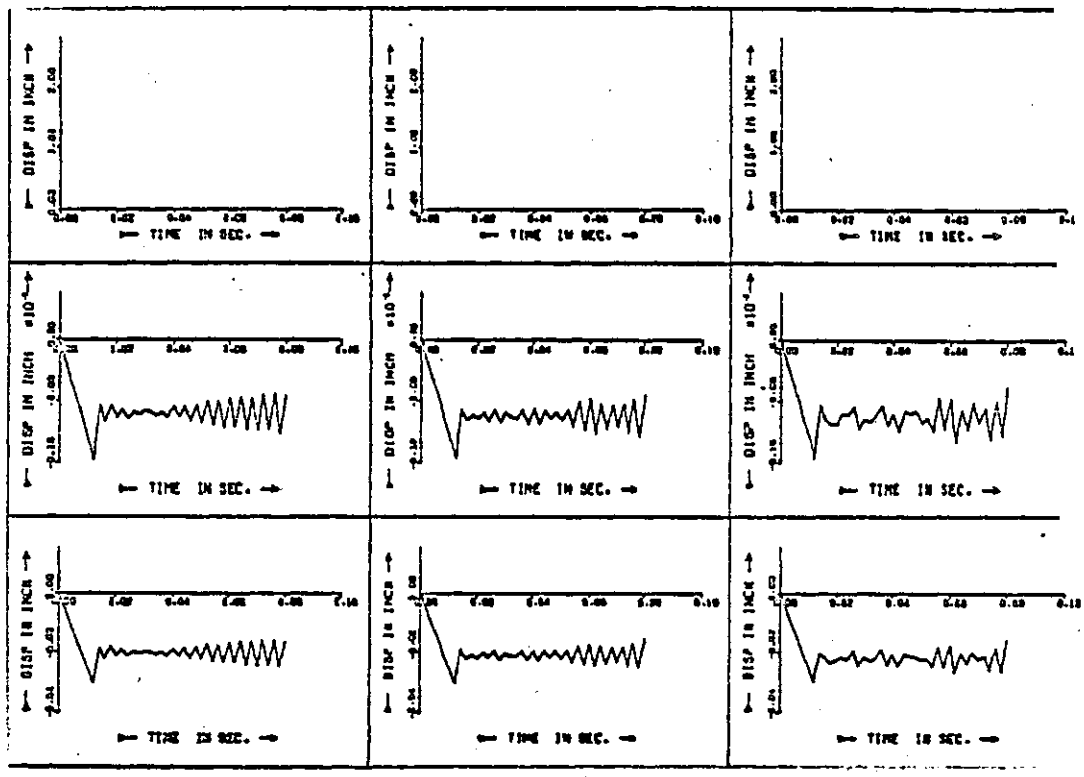


FIG. 46

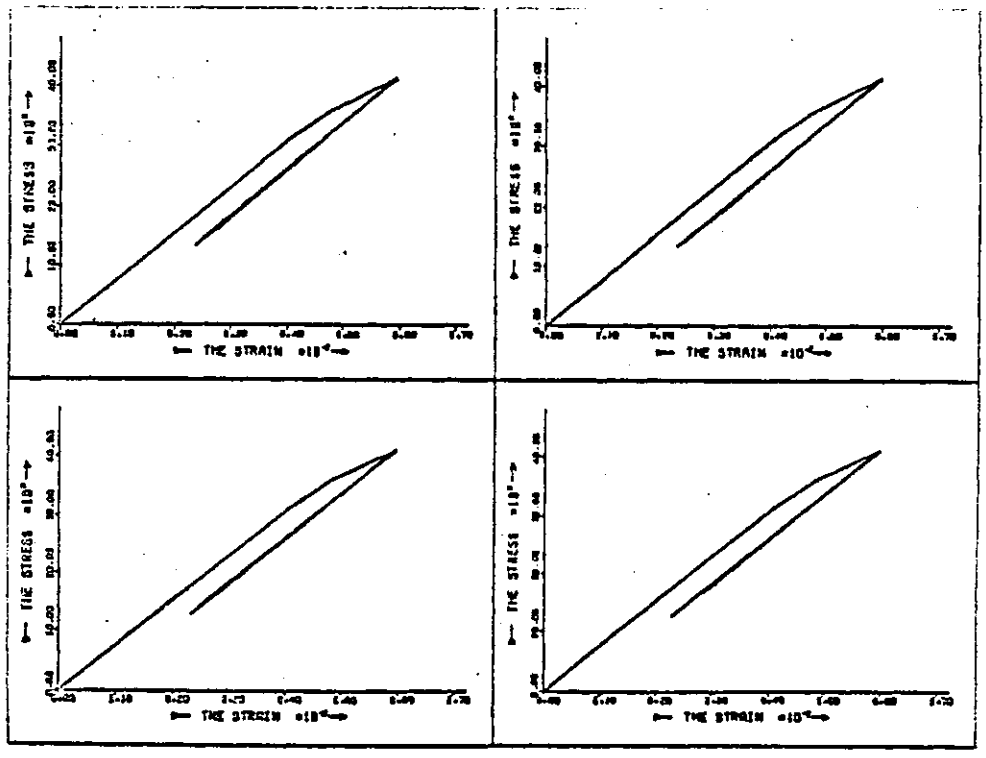


FIG. 47

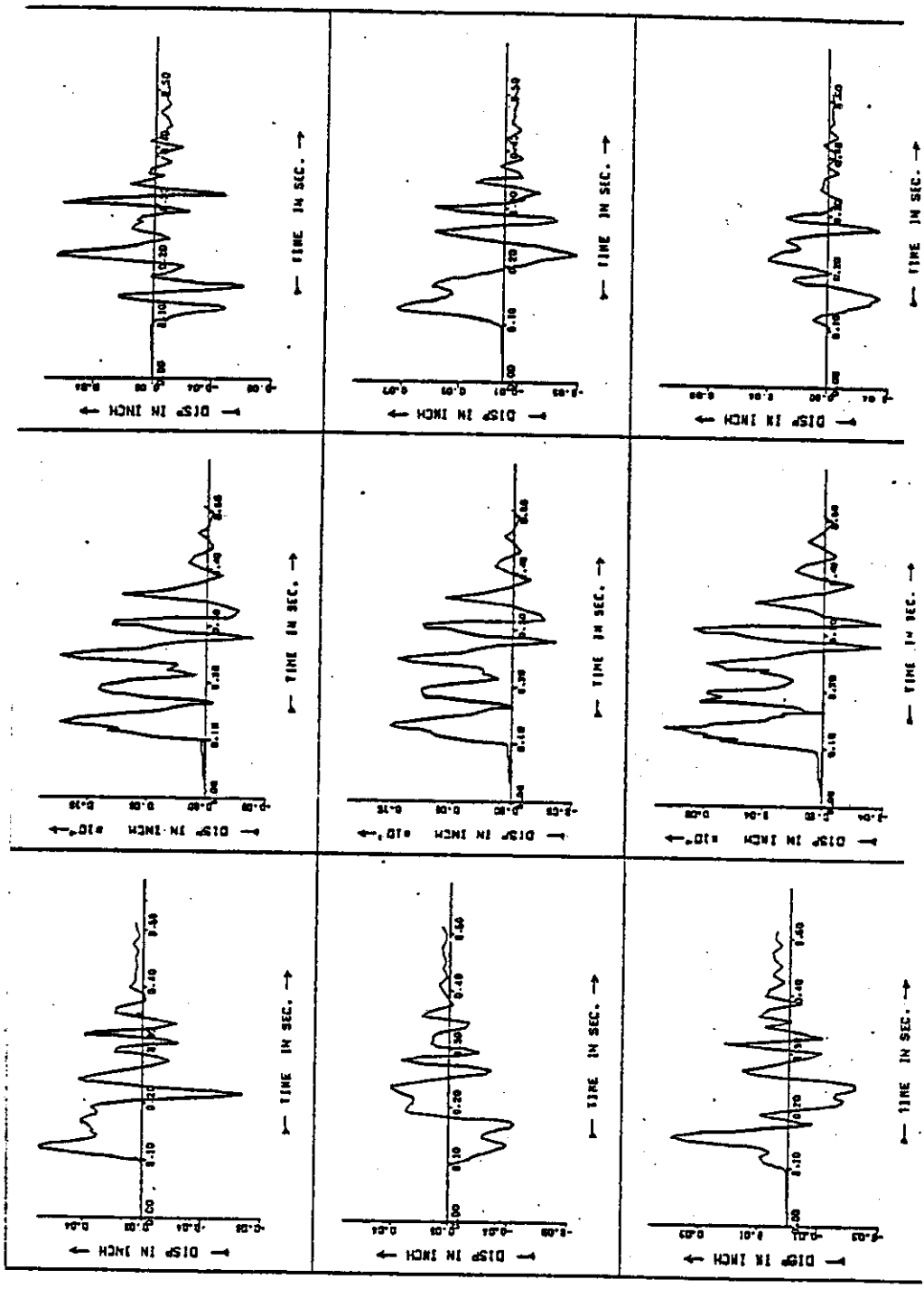


FIG. 48a Nodal Displacement curves (appl. stress = 12,000 lb./sq.in.) with plastic deformation

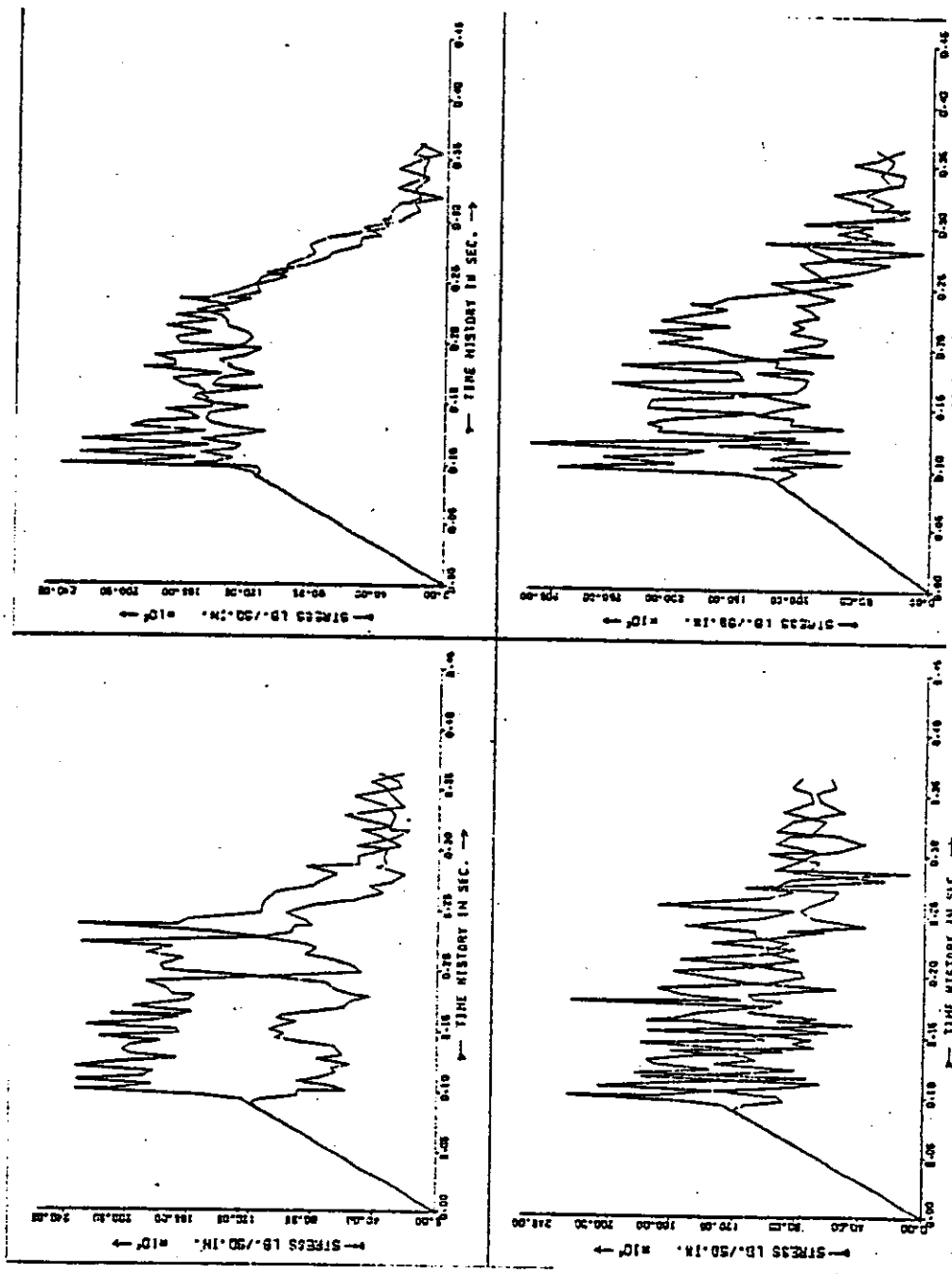


Fig. 48b Gaussian Stresses (equivalent) at element 4

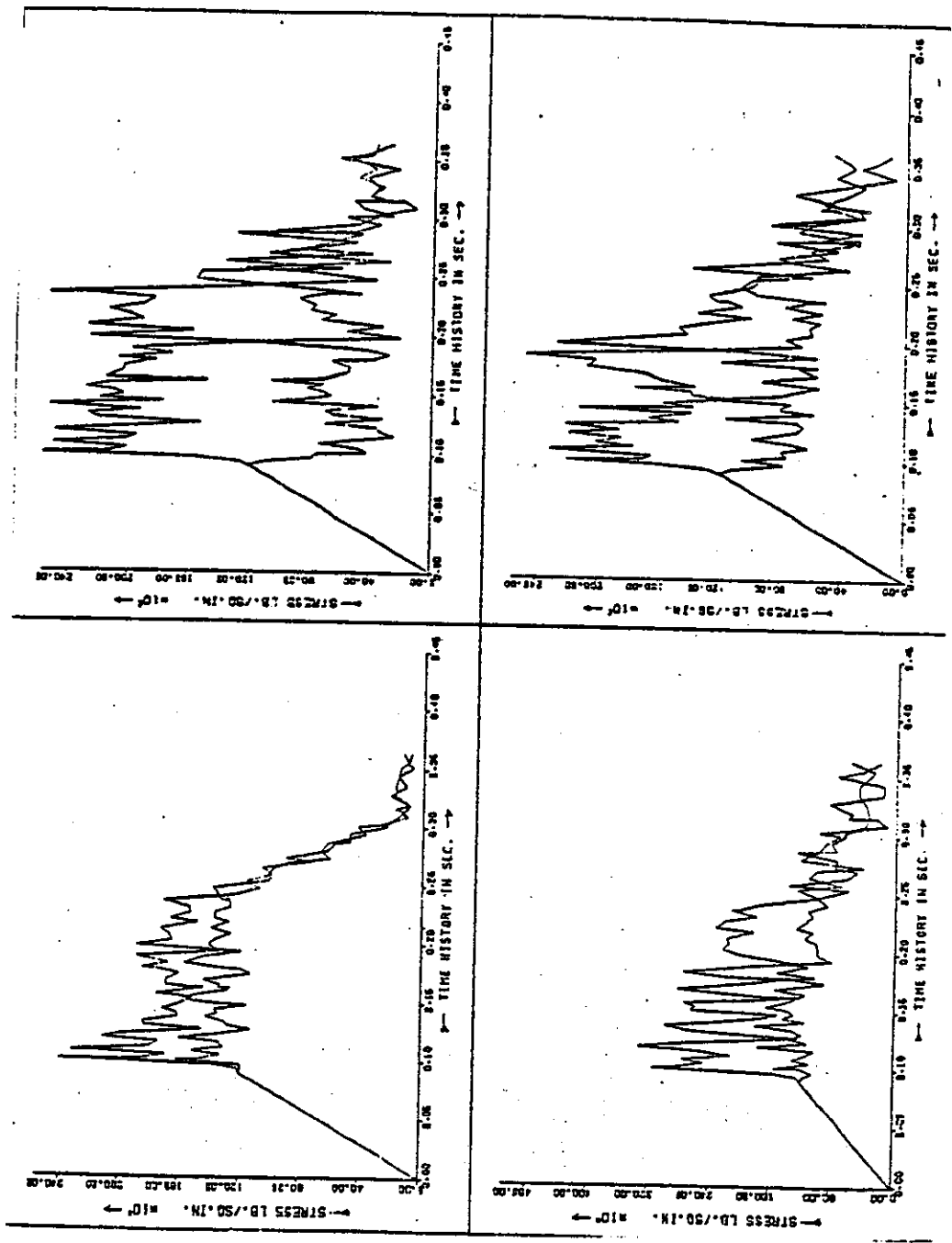


FIG. 48c Gaussian Stresses (equivalent) at element 7

FIG. 49a Stress-Strain curves of element 4

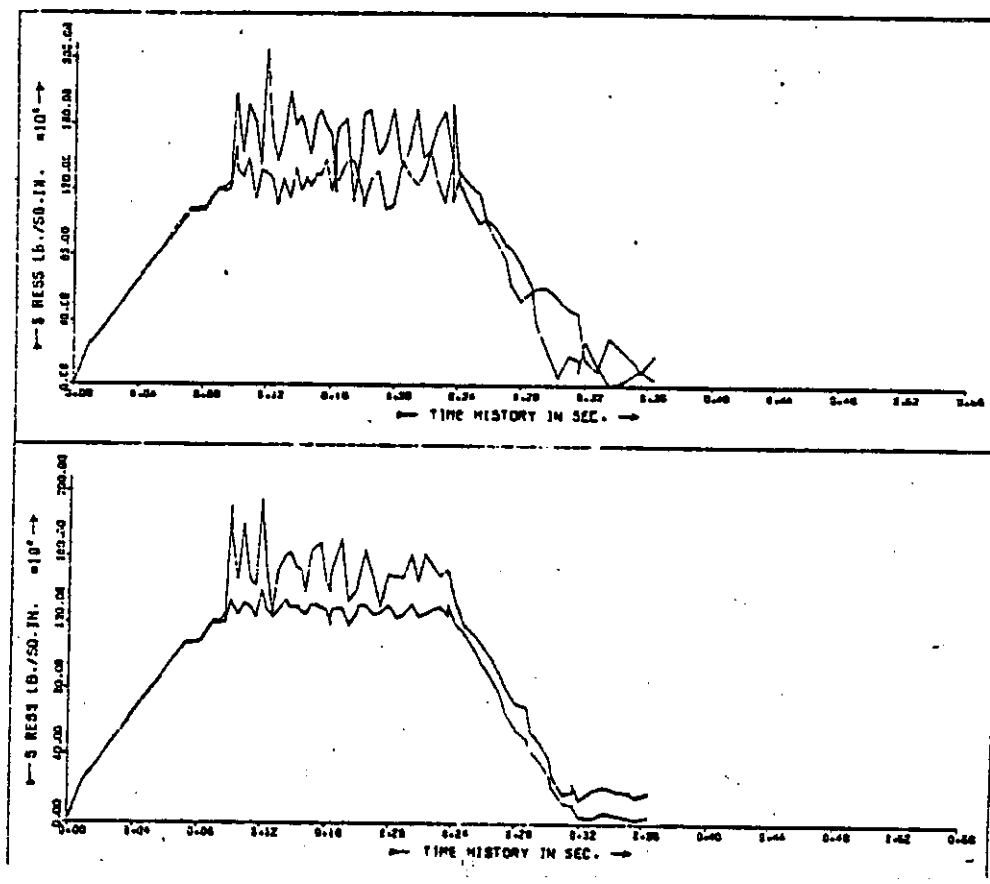


FIG. 50 Stresses at stiffener element 4

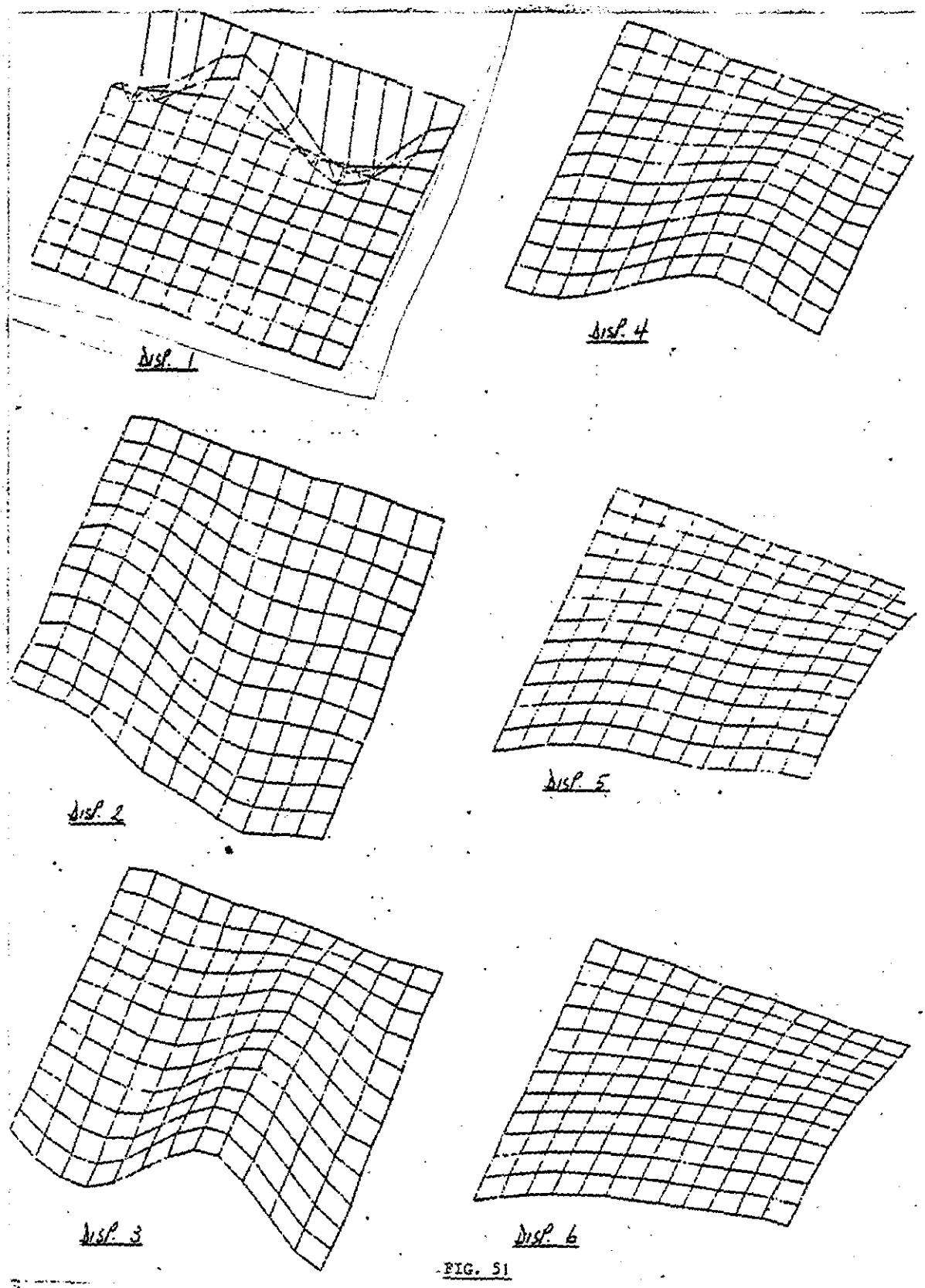


FIG. 51

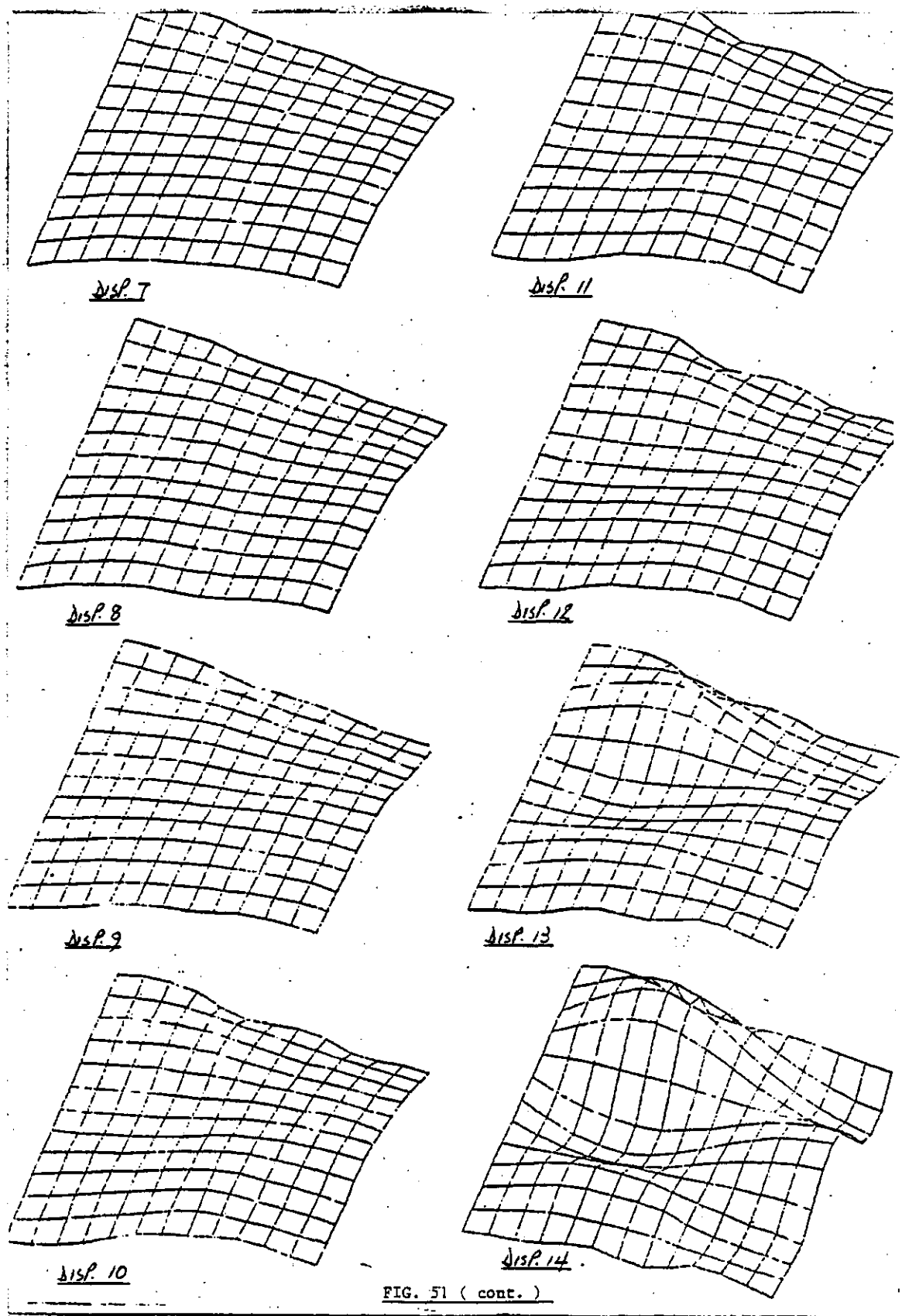


FIG. 51 (cont.)

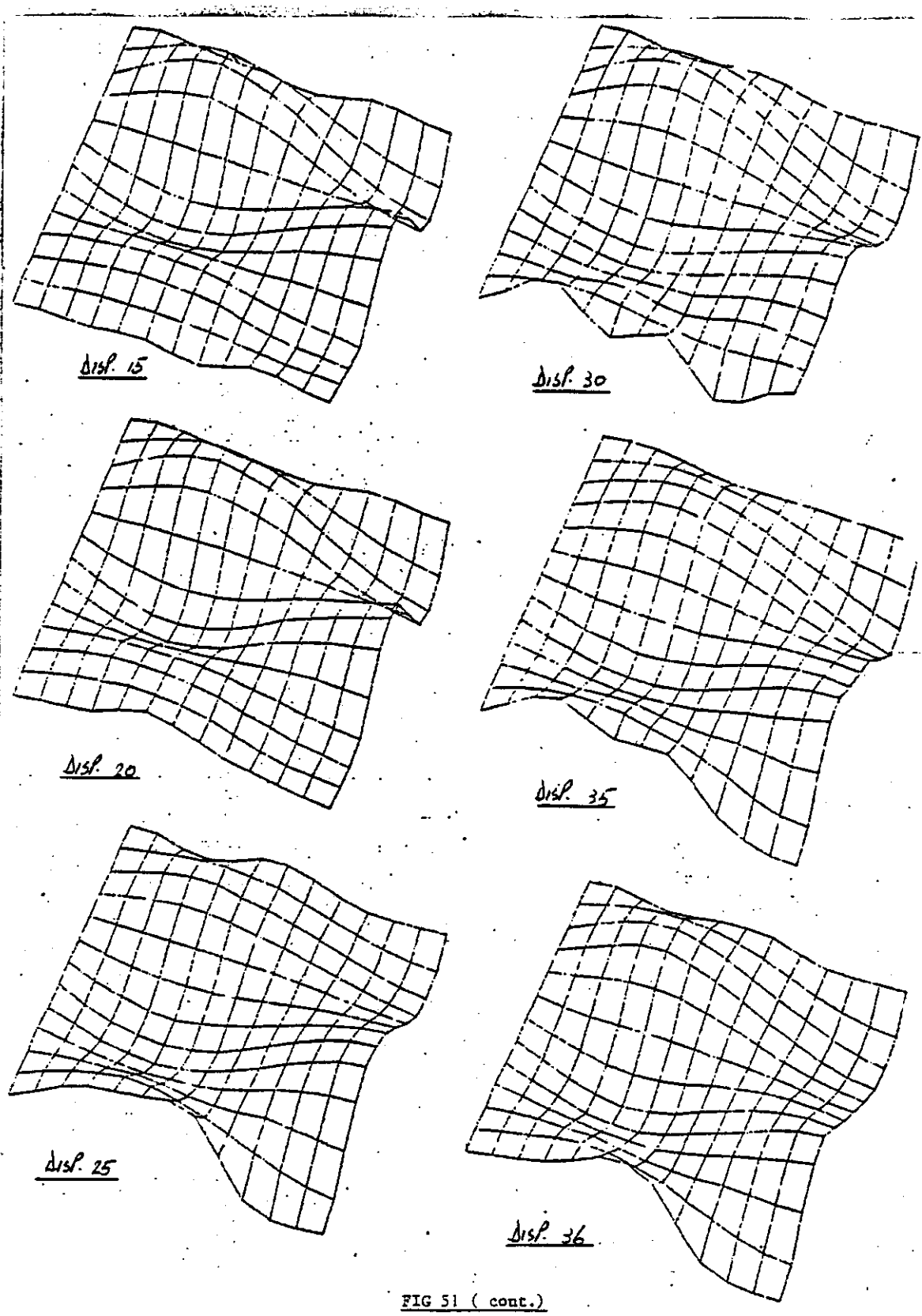
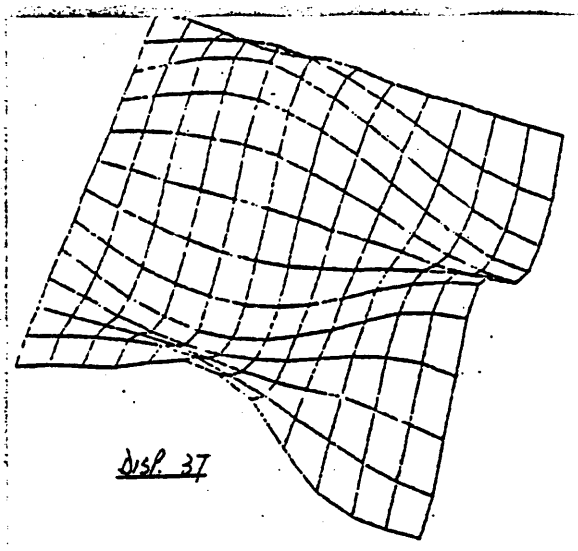
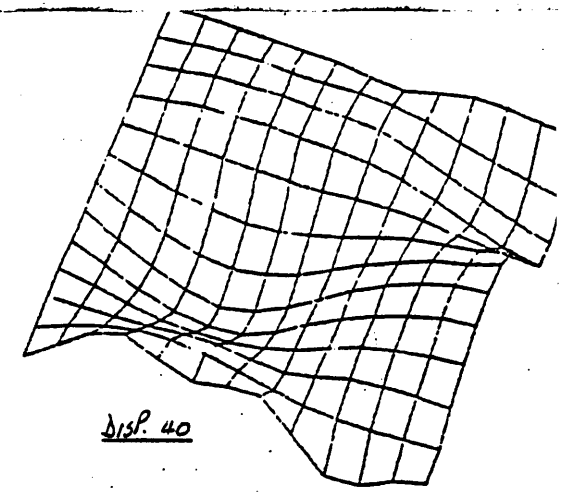


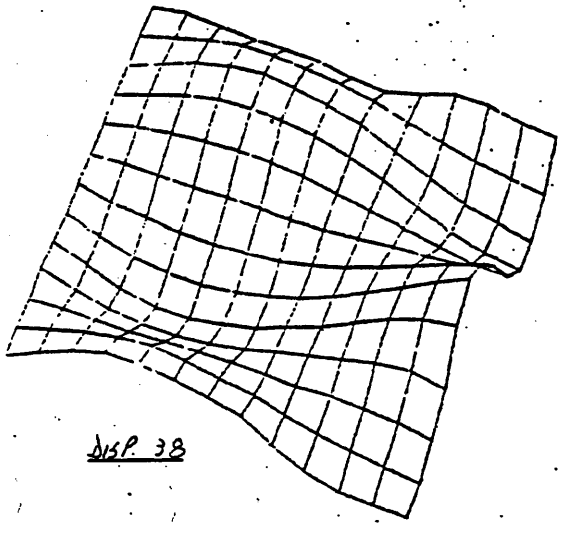
FIG 51 (cont.)



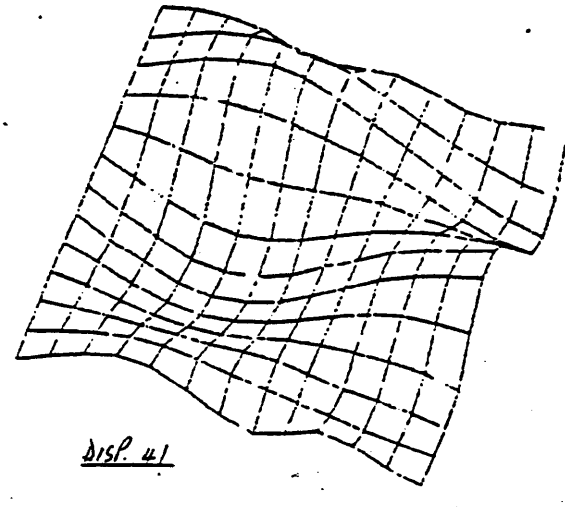
Disp. 37



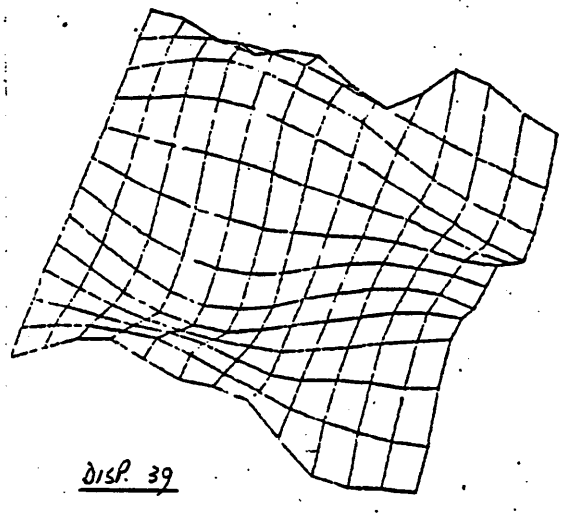
Disp. 40



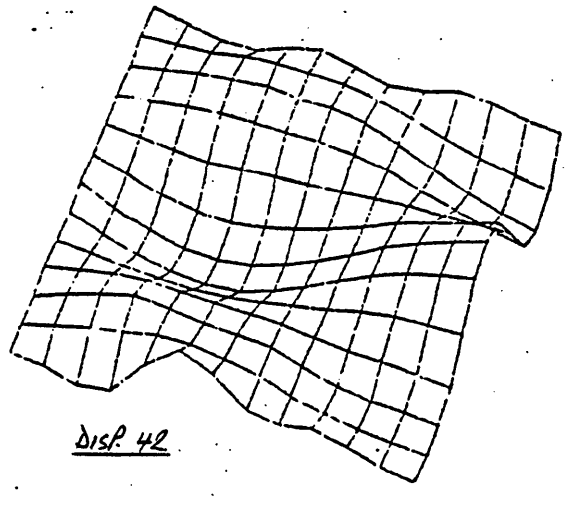
Disp. 38



Disp. 41

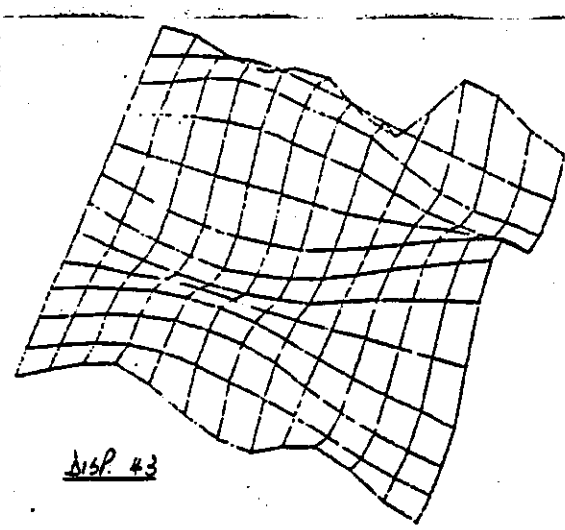


Disp. 39

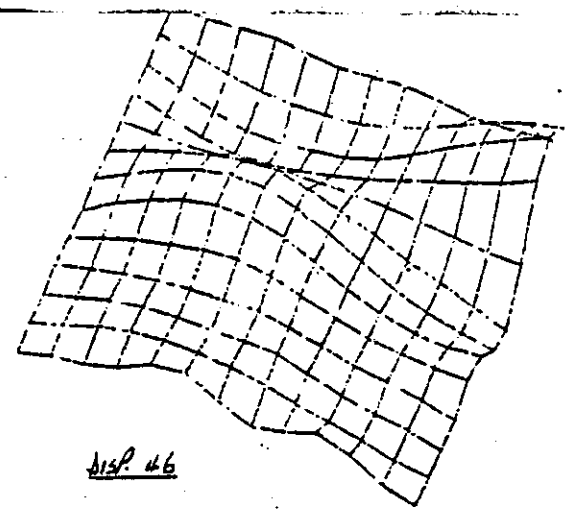


Disp. 42

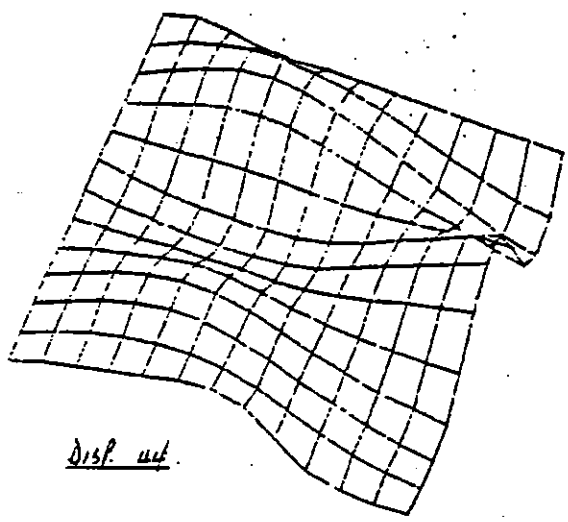
FIG: 51 (cont.)



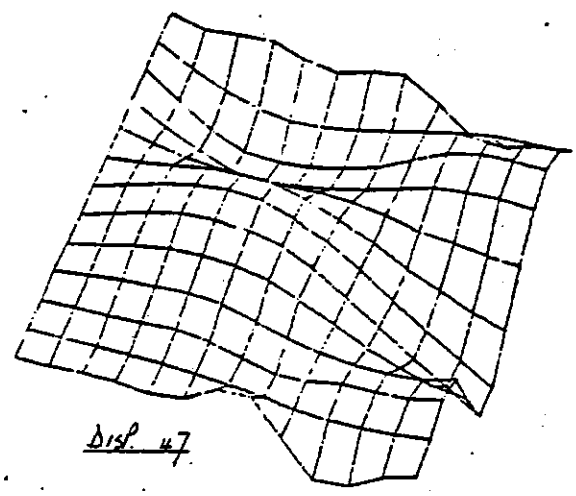
Disp. 43



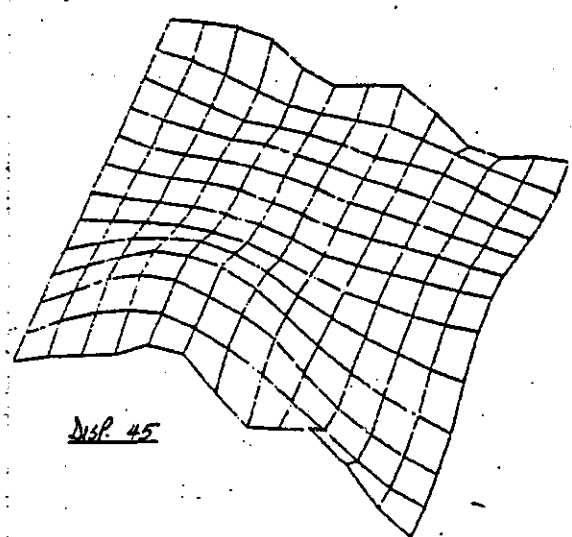
Disp. 46



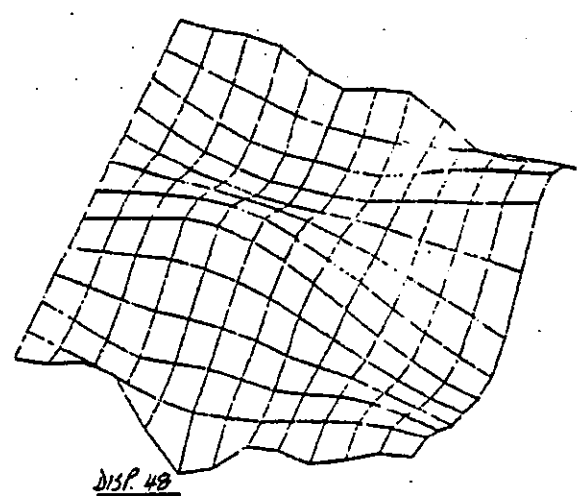
Disp. 44



Disp. 47

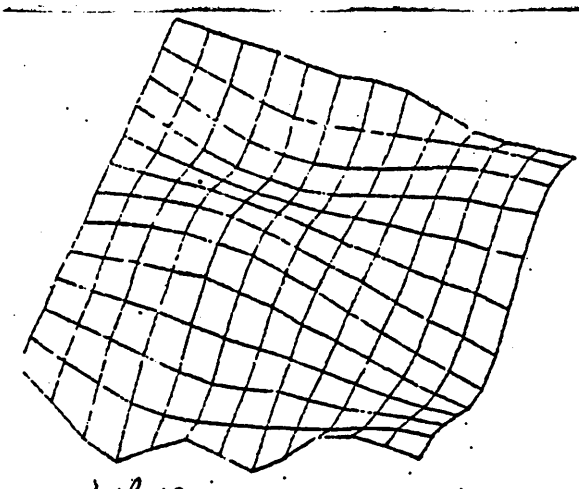


Disp. 45

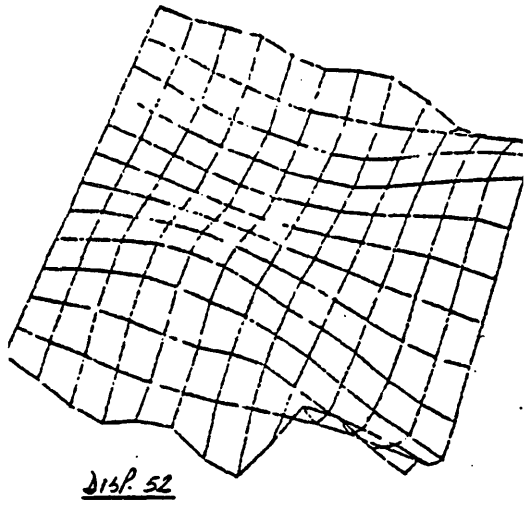


Disp. 48

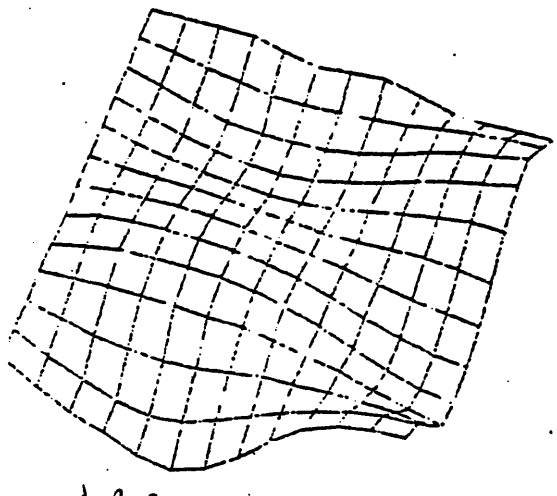
FIG. 51 (cont.)



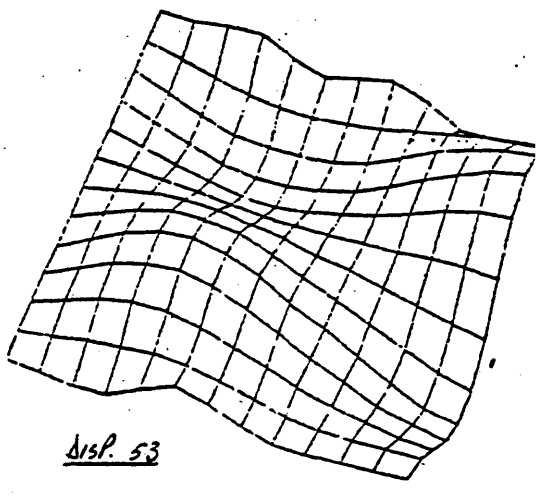
Disp. 49



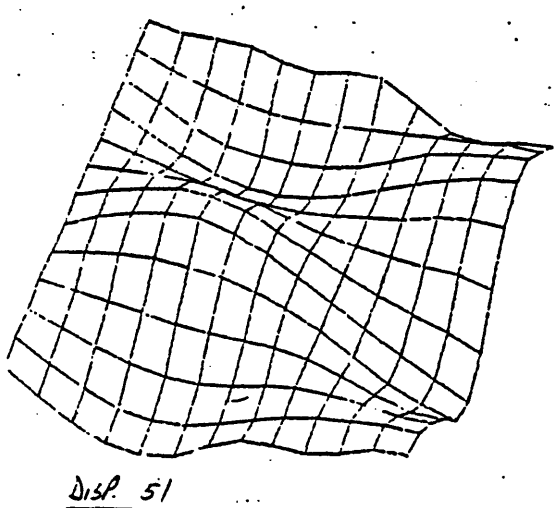
Disp. 52



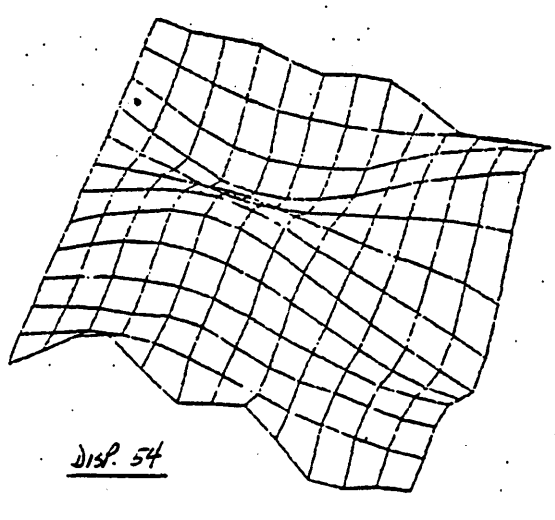
Disp. 50



Disp. 53

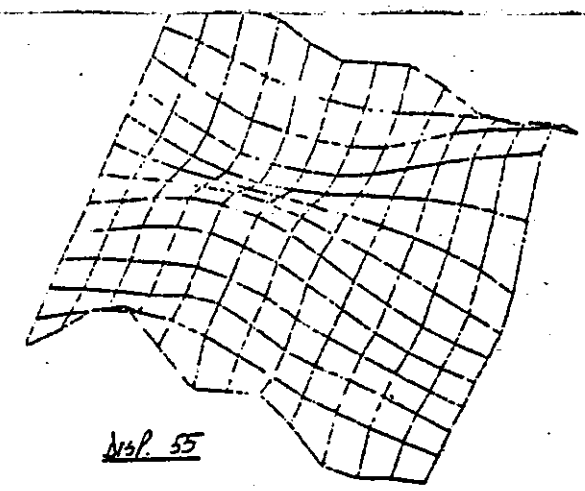


Disp. 51

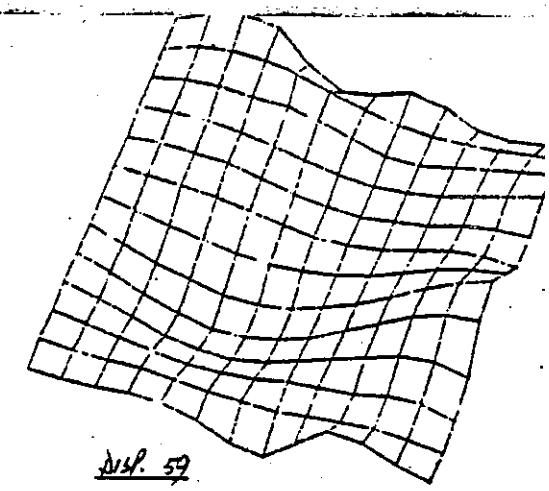


Disp. 54

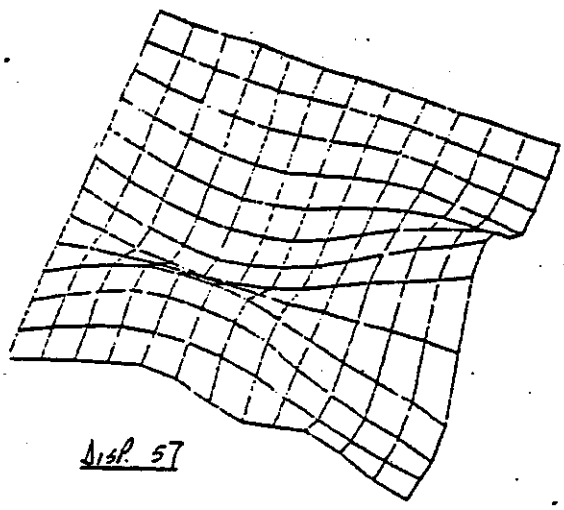
FIG. 51 (cont.)



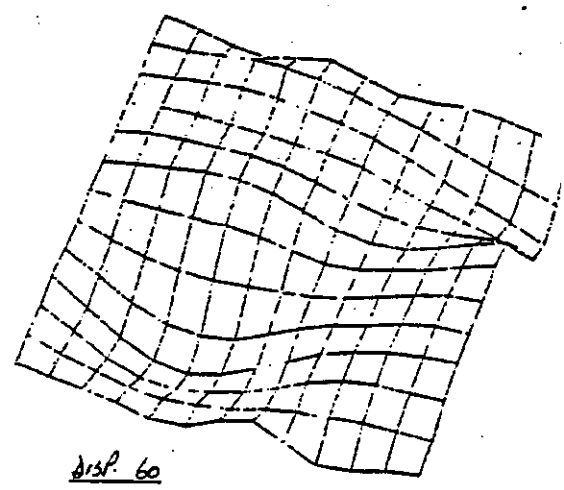
Disp. 55



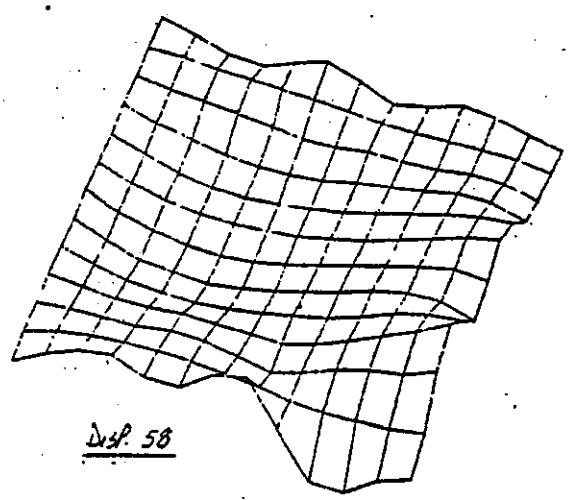
Disp. 59



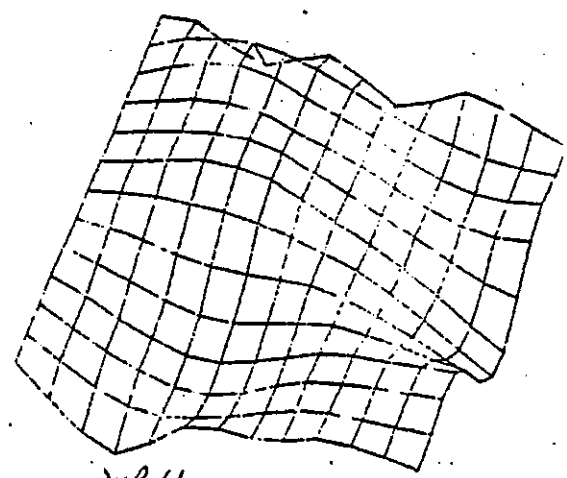
Disp. 57



Disp. 60

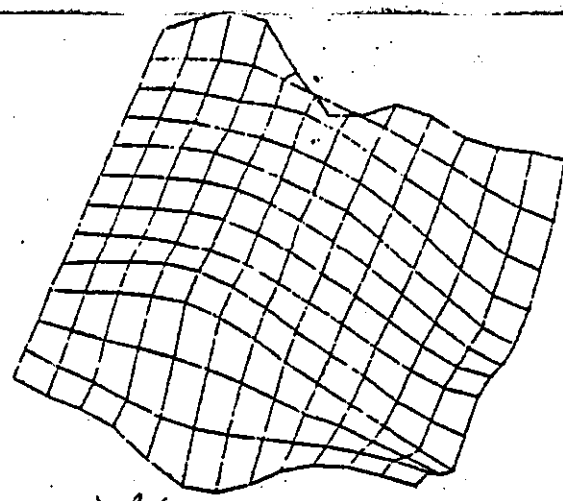


Disp. 58

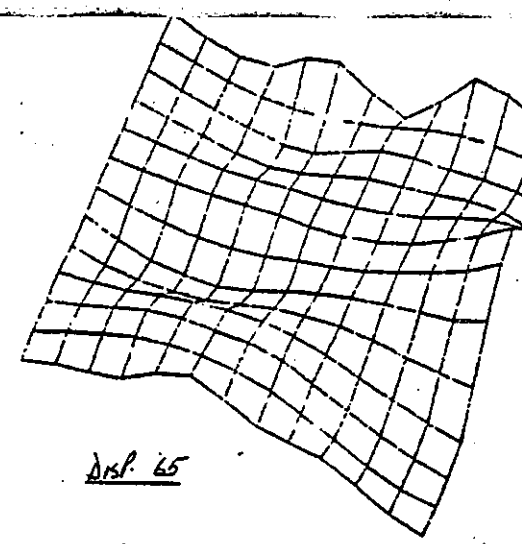


Disp. 61

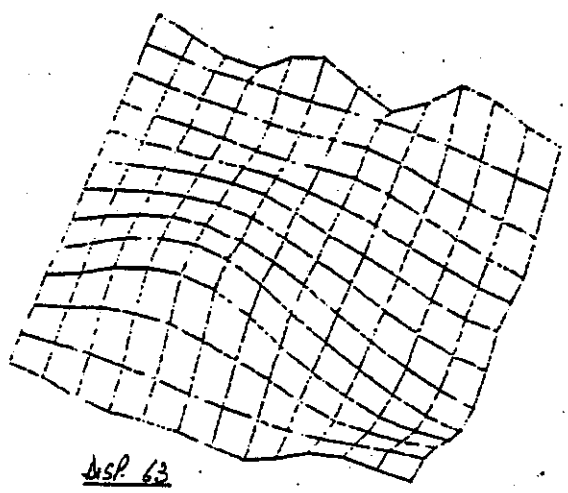
FIG. 51 (cont.)



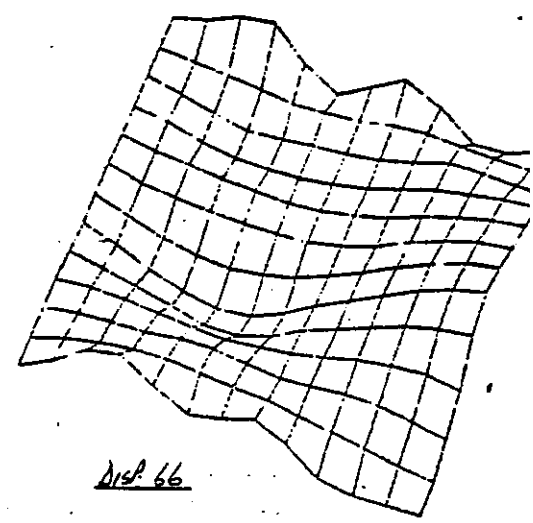
Displ. 62



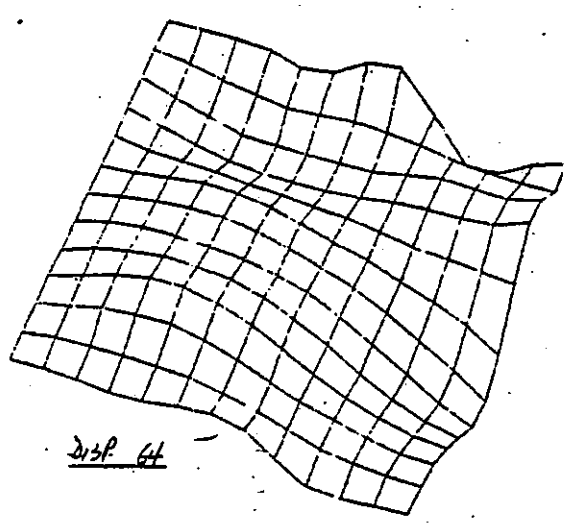
Displ. 65



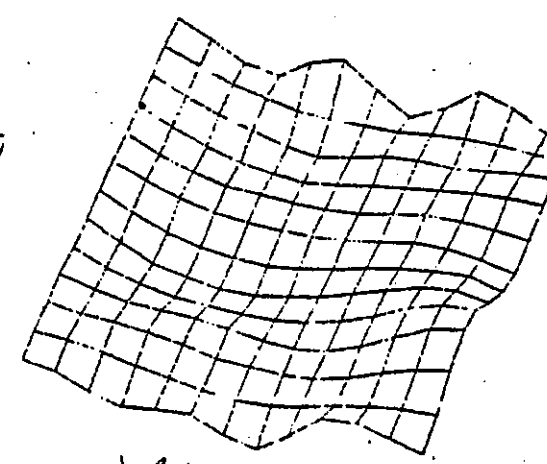
Displ. 63



Displ. 66

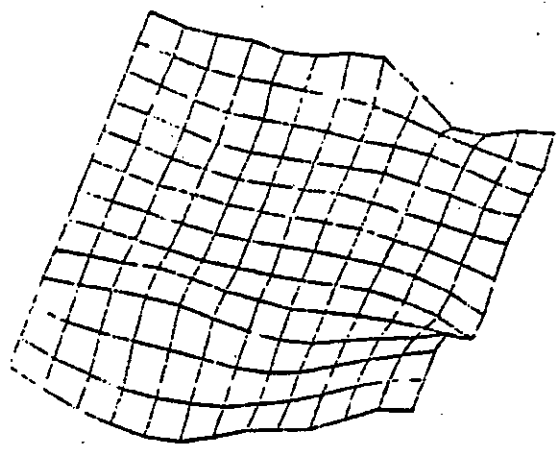


Displ. 64

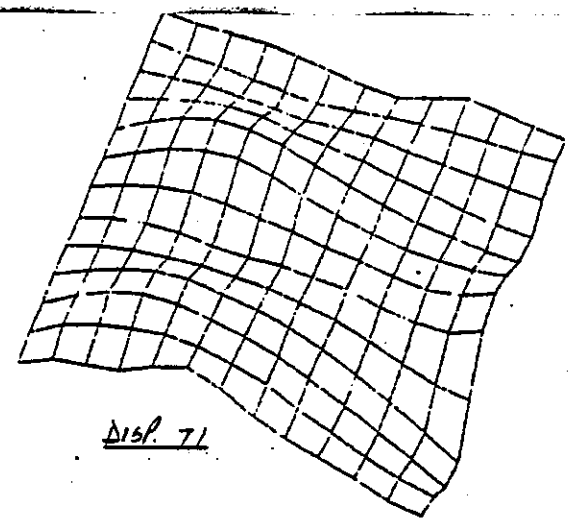


Displ. 67

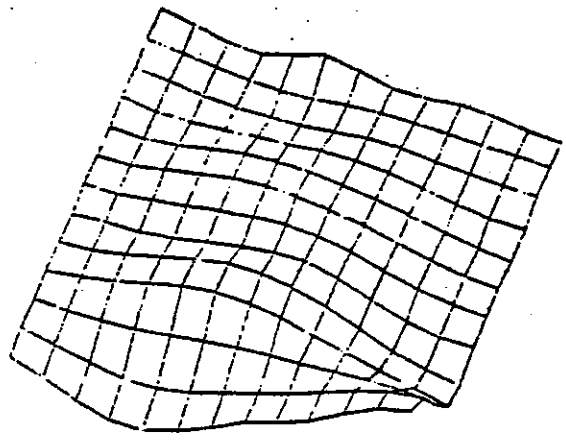
FIG. 51 (cont.)



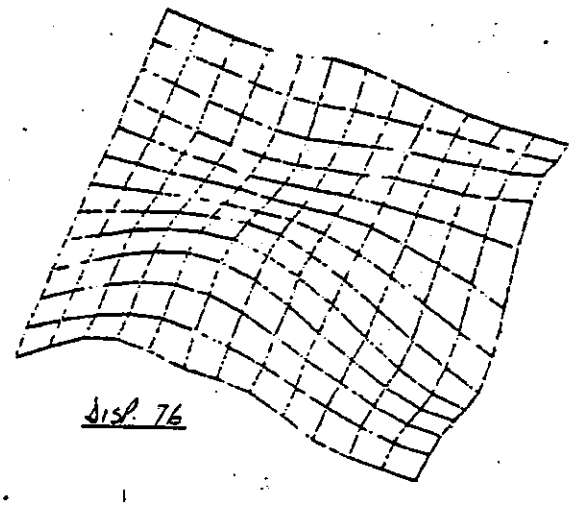
Disp. 68



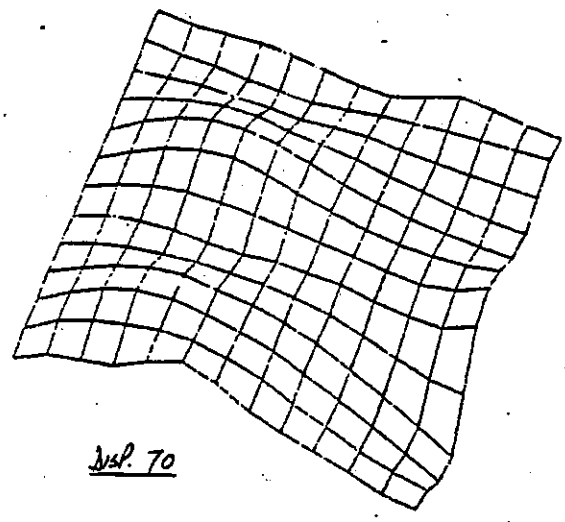
Disp. 71



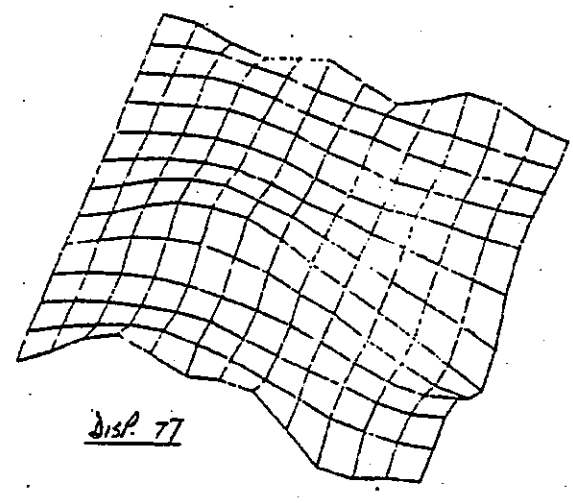
Disp. 69



Disp. 76

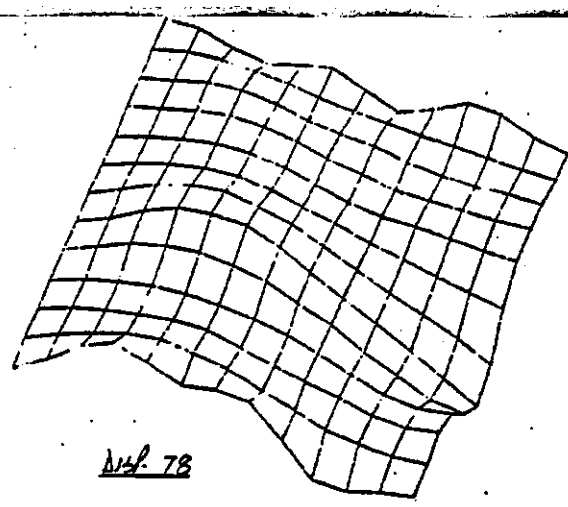


Disp. 70

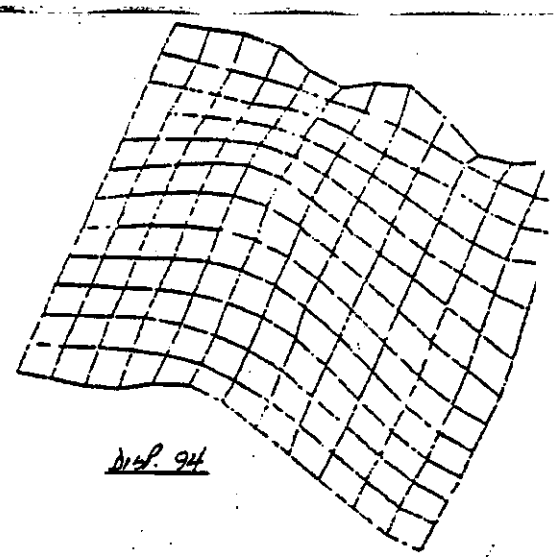


Disp. 77

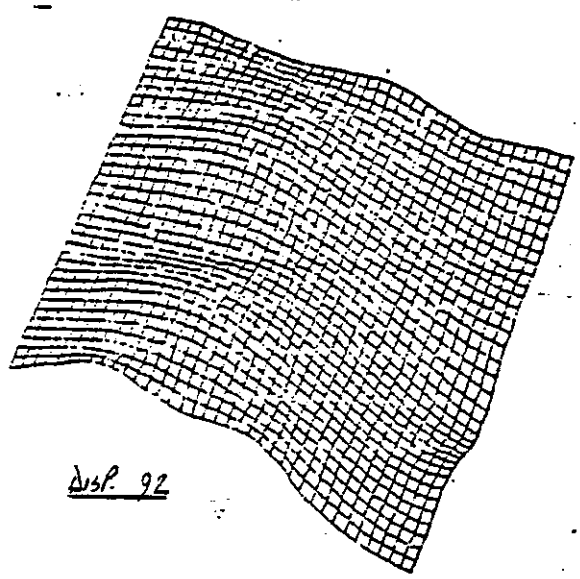
FIG. 51 (cont.)



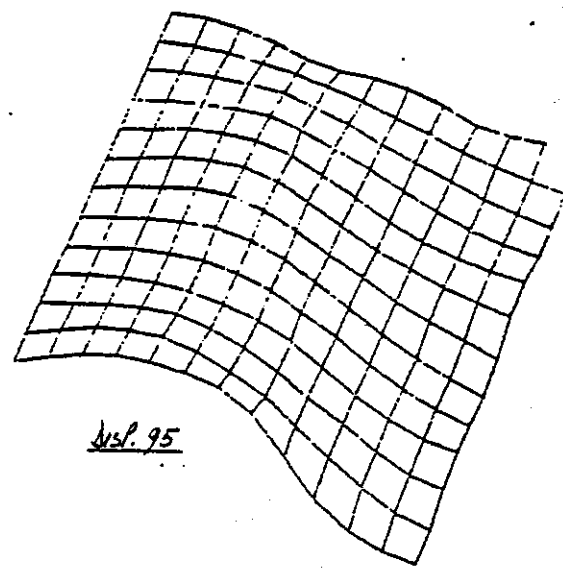
Displ. 78



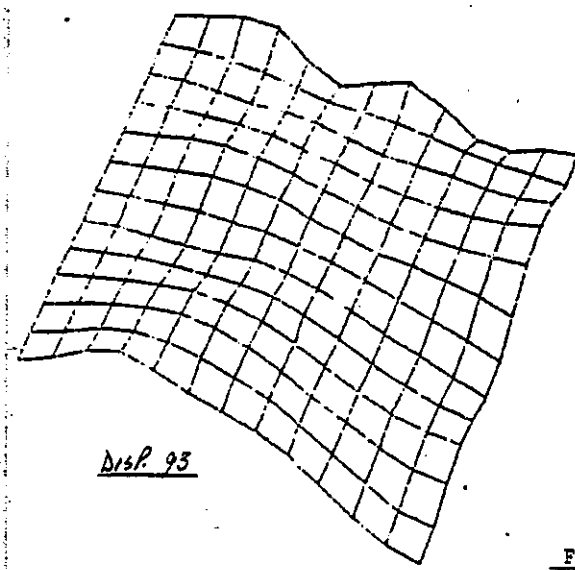
Displ. 94



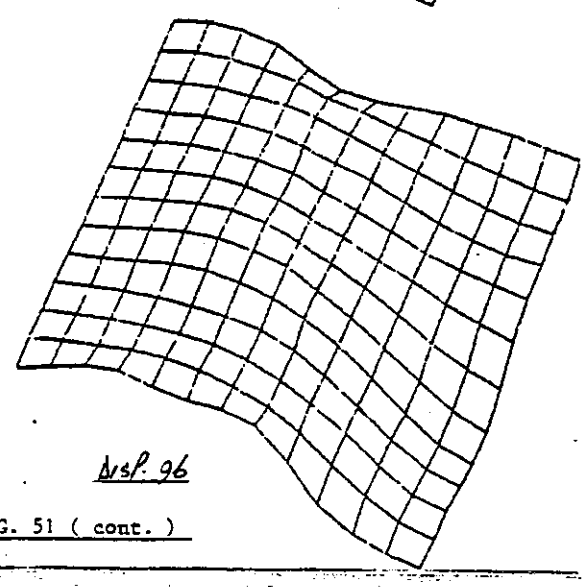
Displ. 92



Displ. 95



Displ. 93



Displ. 96

FIG. 51 (cont.)

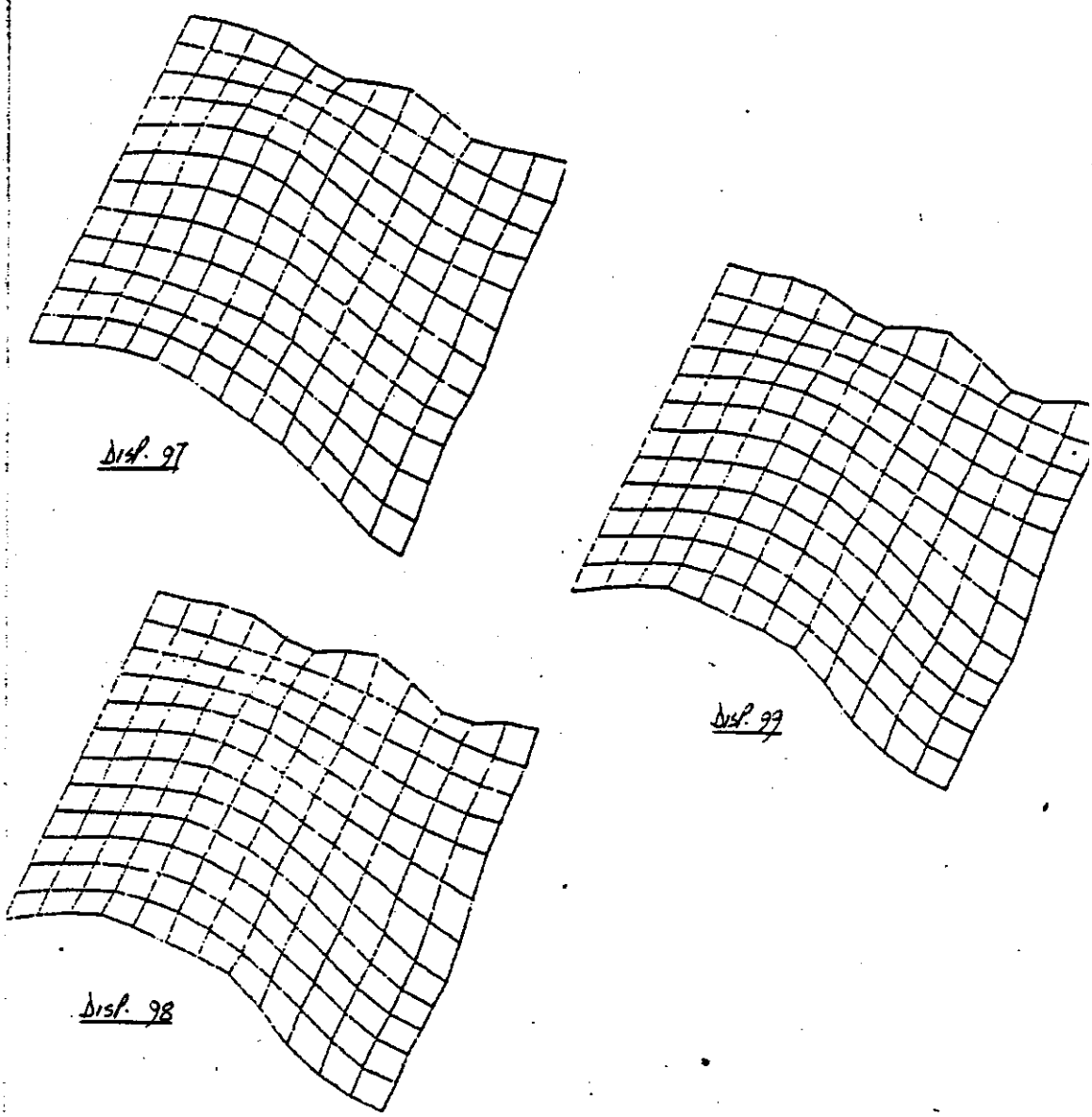


FIG. 51 (cont.)

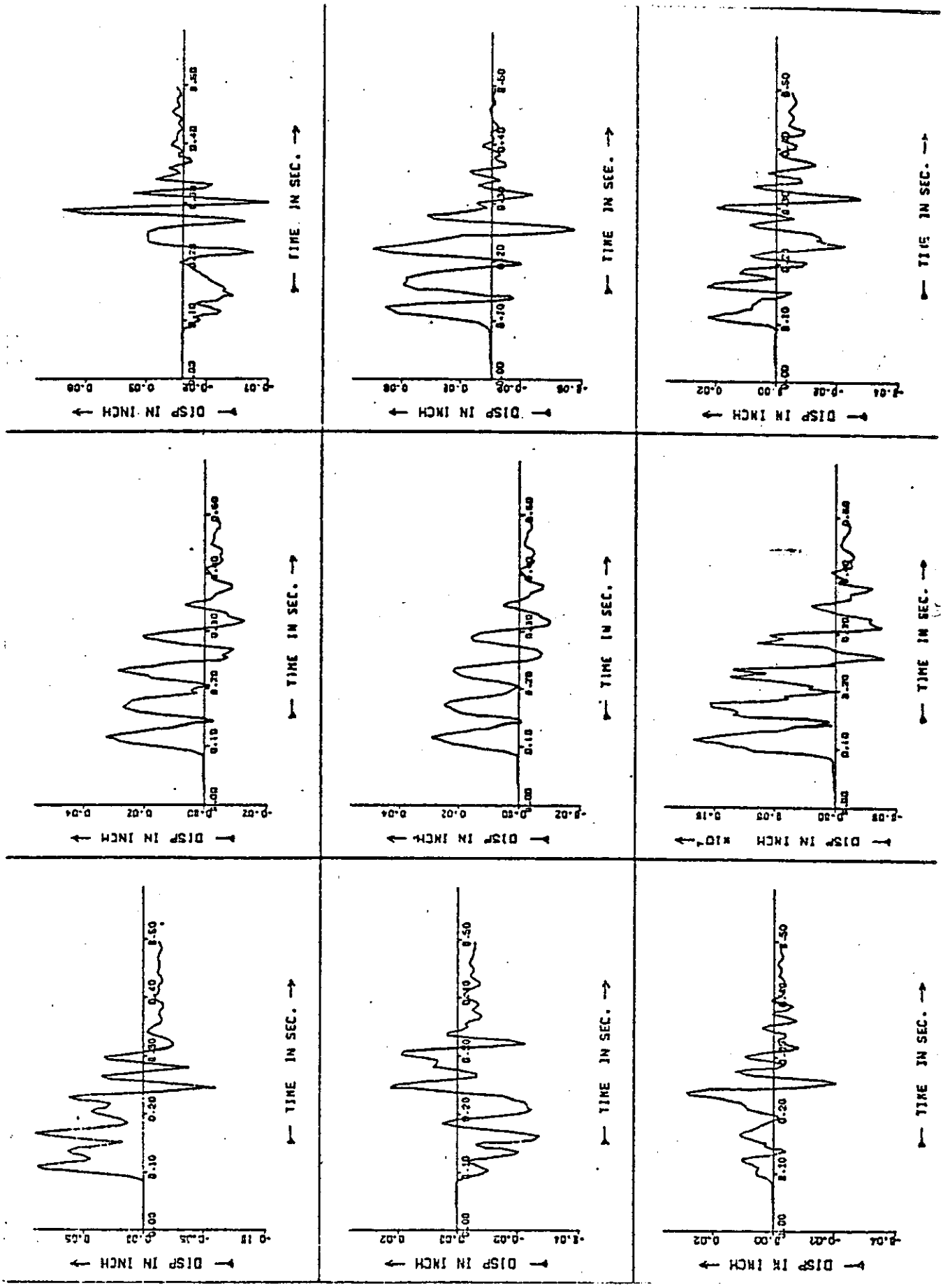


FIG. 52a Nodal Displacement curves (appl. stress = 14,500 lb./sq.in.)

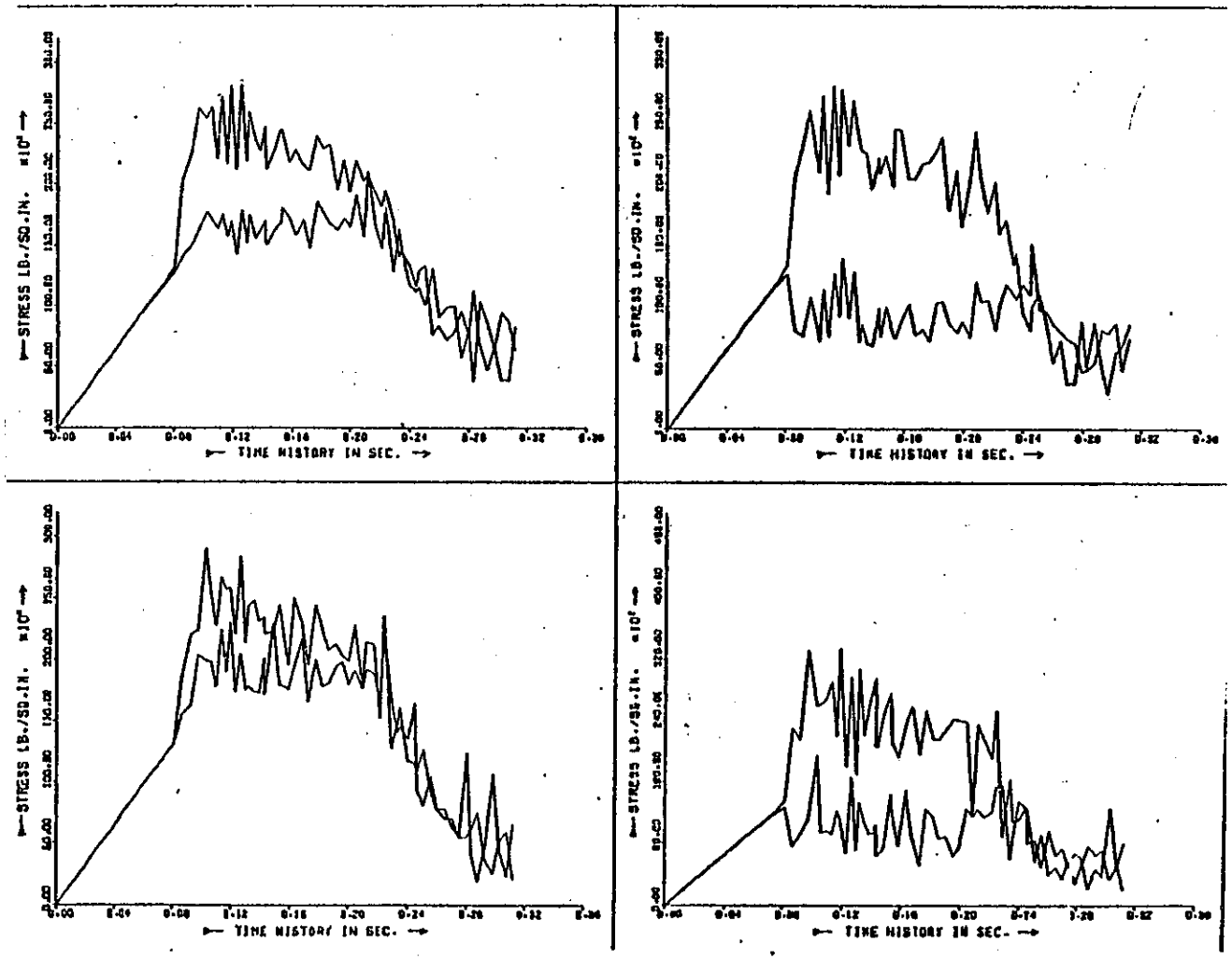


FIG. 52b Gaussian Stresses (equivalent stresses) at element 1

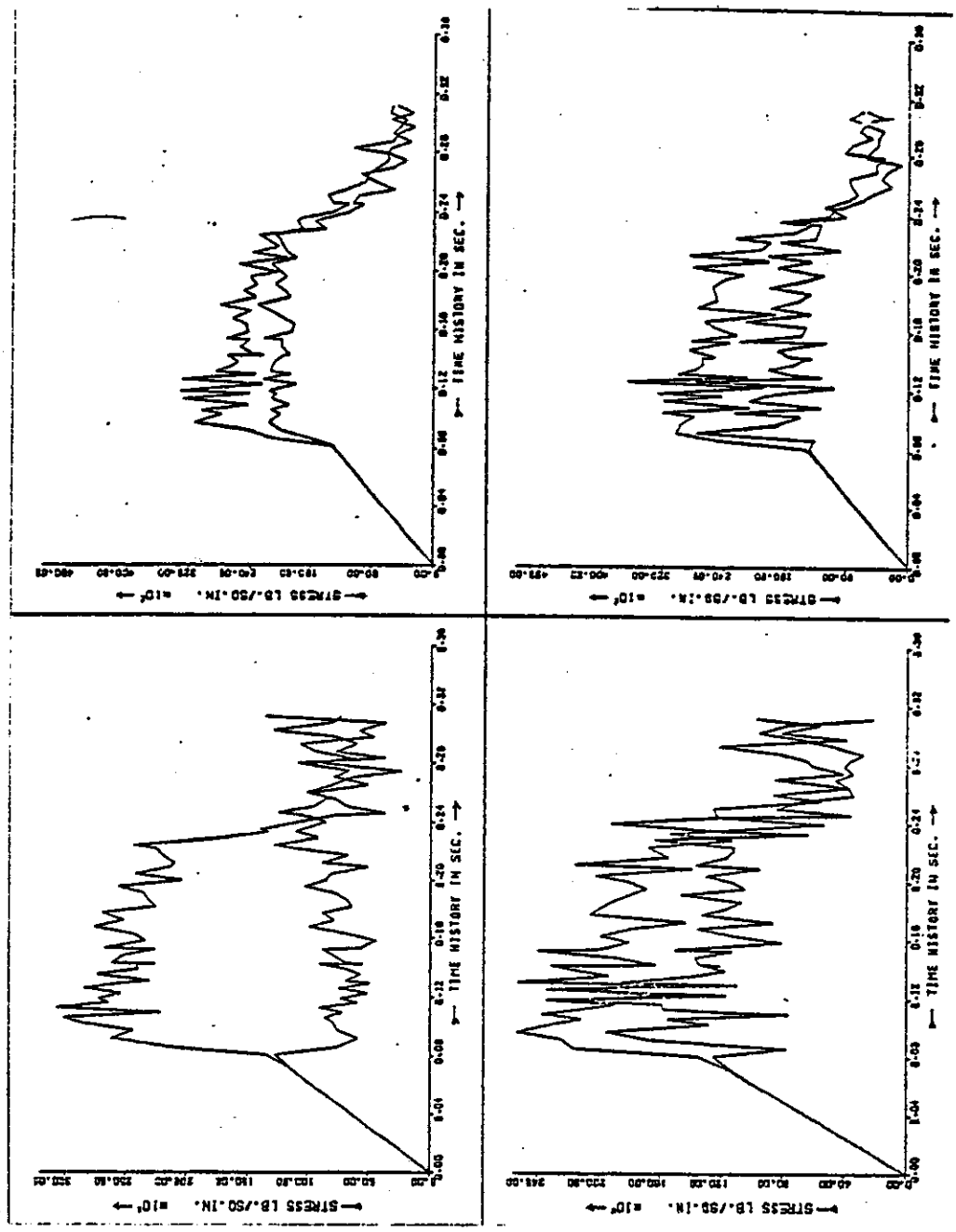


FIG. 52c Gaussian Stresses (equivalent stresses) at element 4

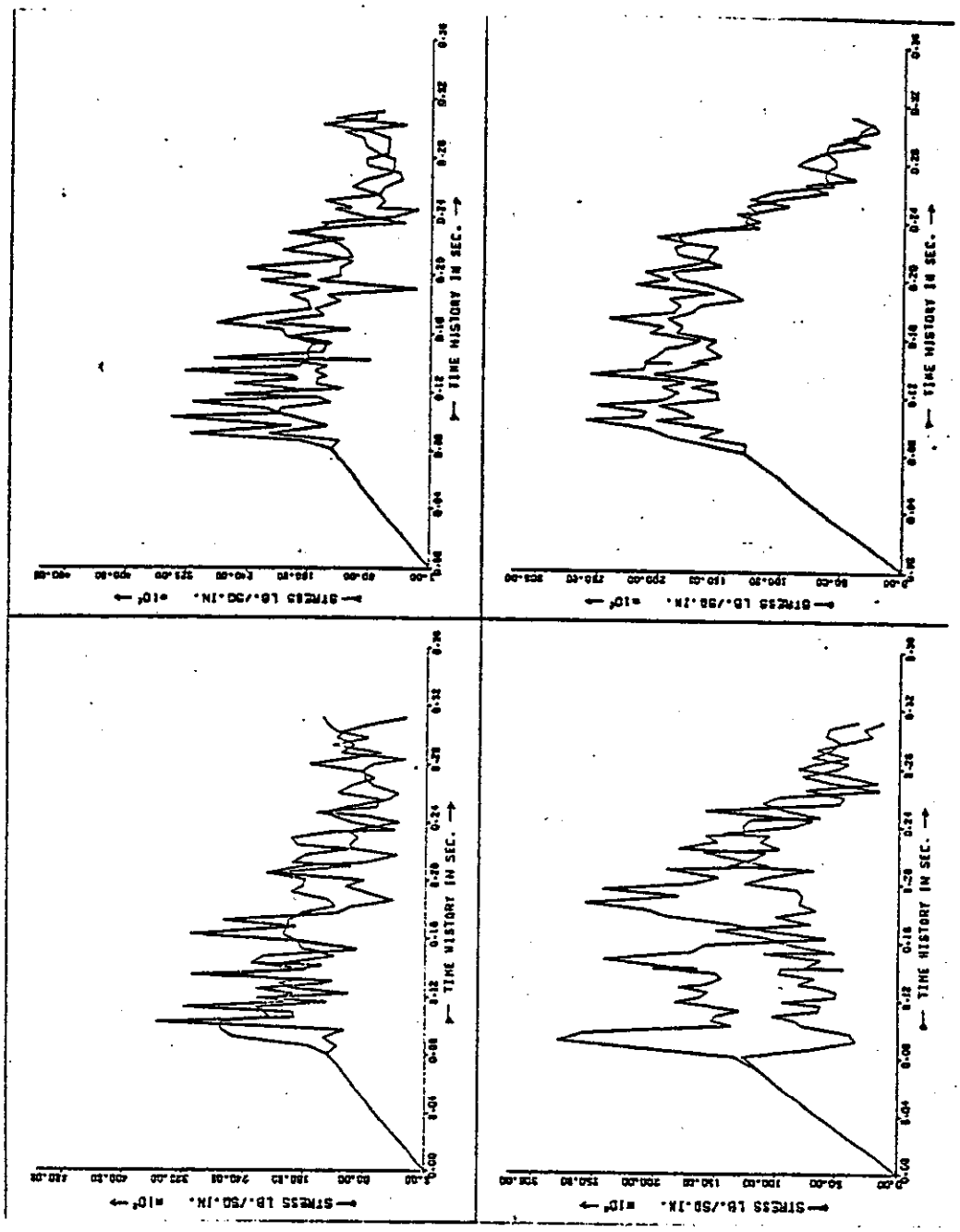


FIG. 52d Gaussian stresses (equivalent stresses) at element 6

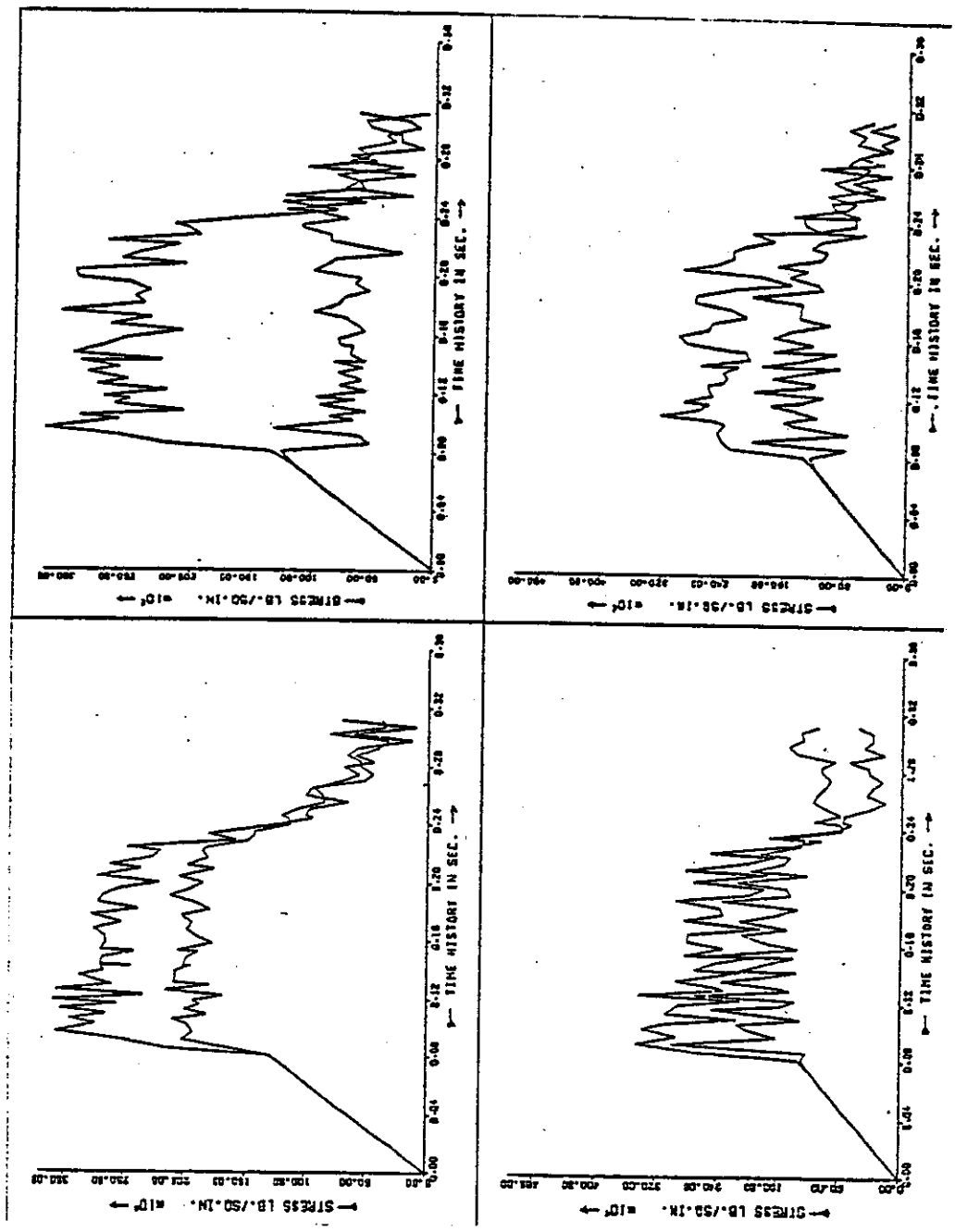


FIG. 52e Gaussian stresses (equivalent stresses) at element 7

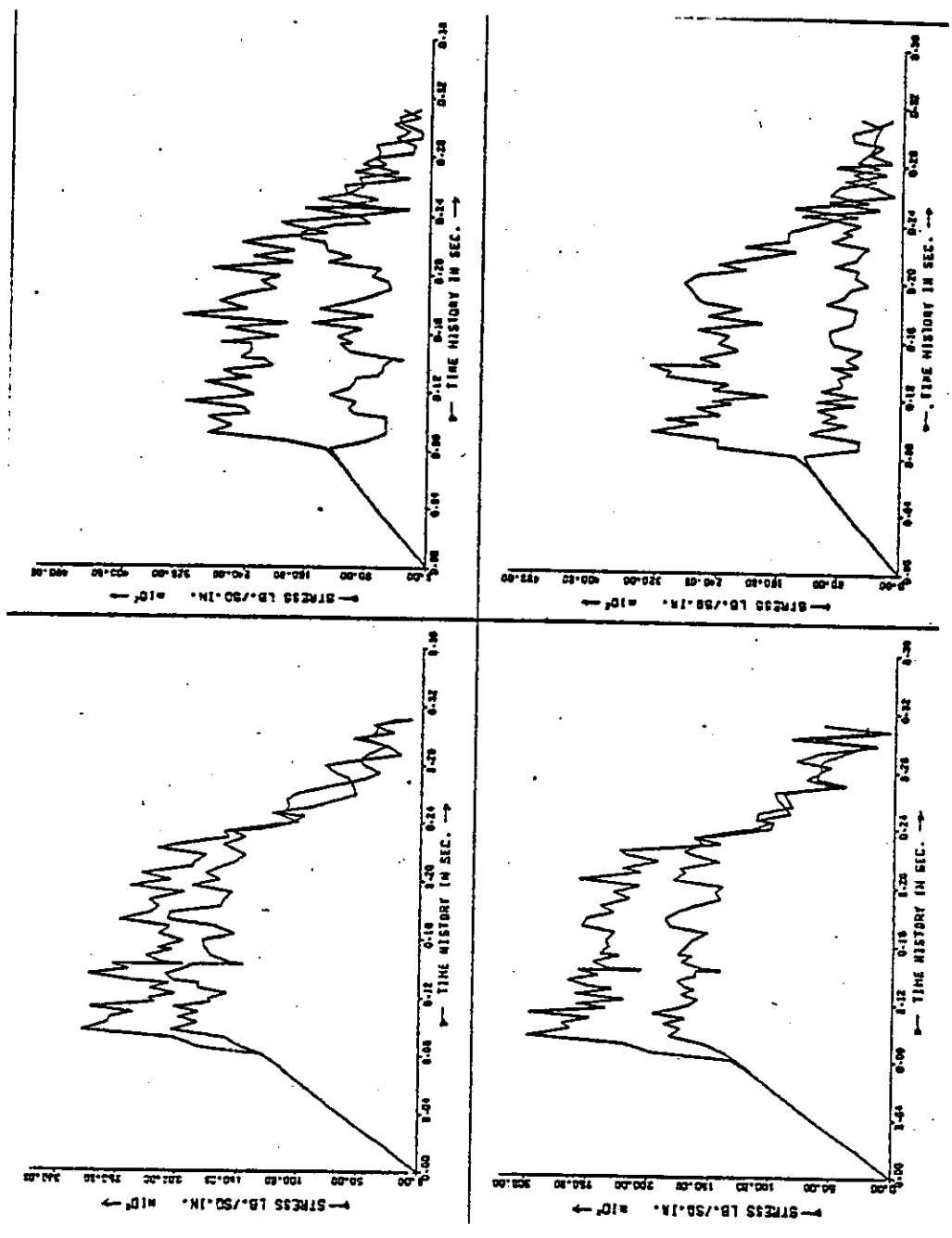


FIG.52f Gaussian stresses (équivalent stresses) at element 8

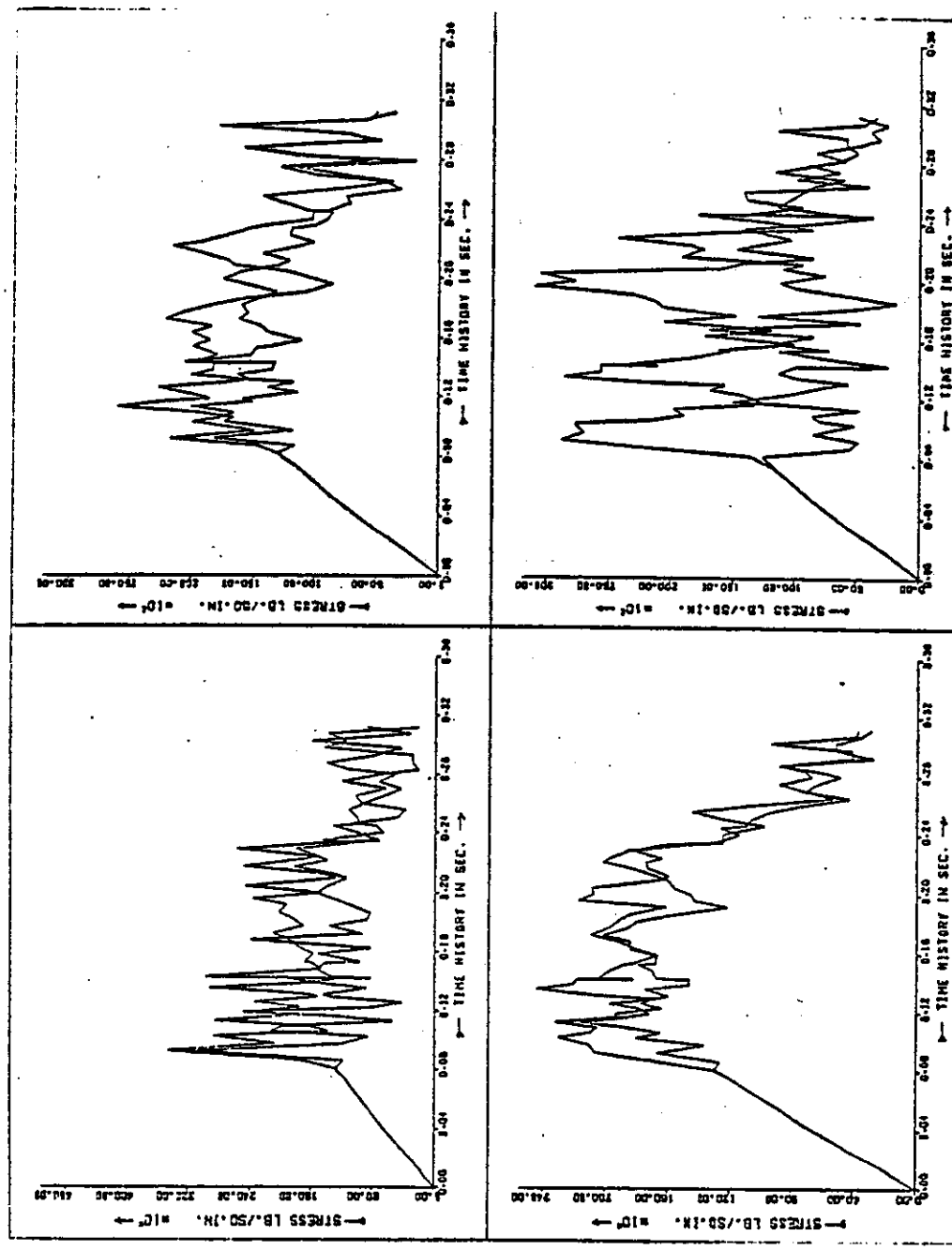


FIG. 529 Gaussian stresses (equivalent stresses) at element 9

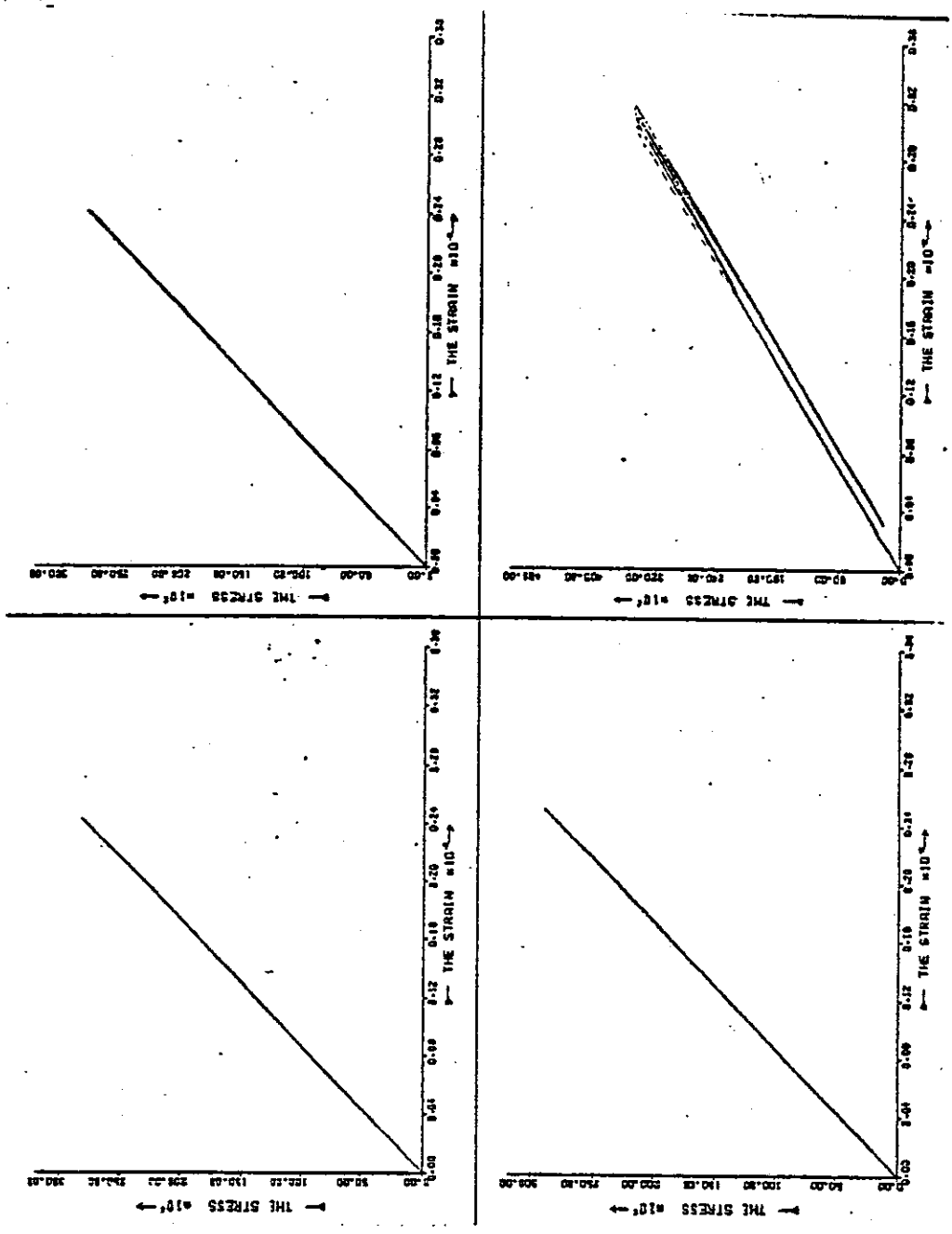


FIG. 53a Stress-Strain curves of element 1

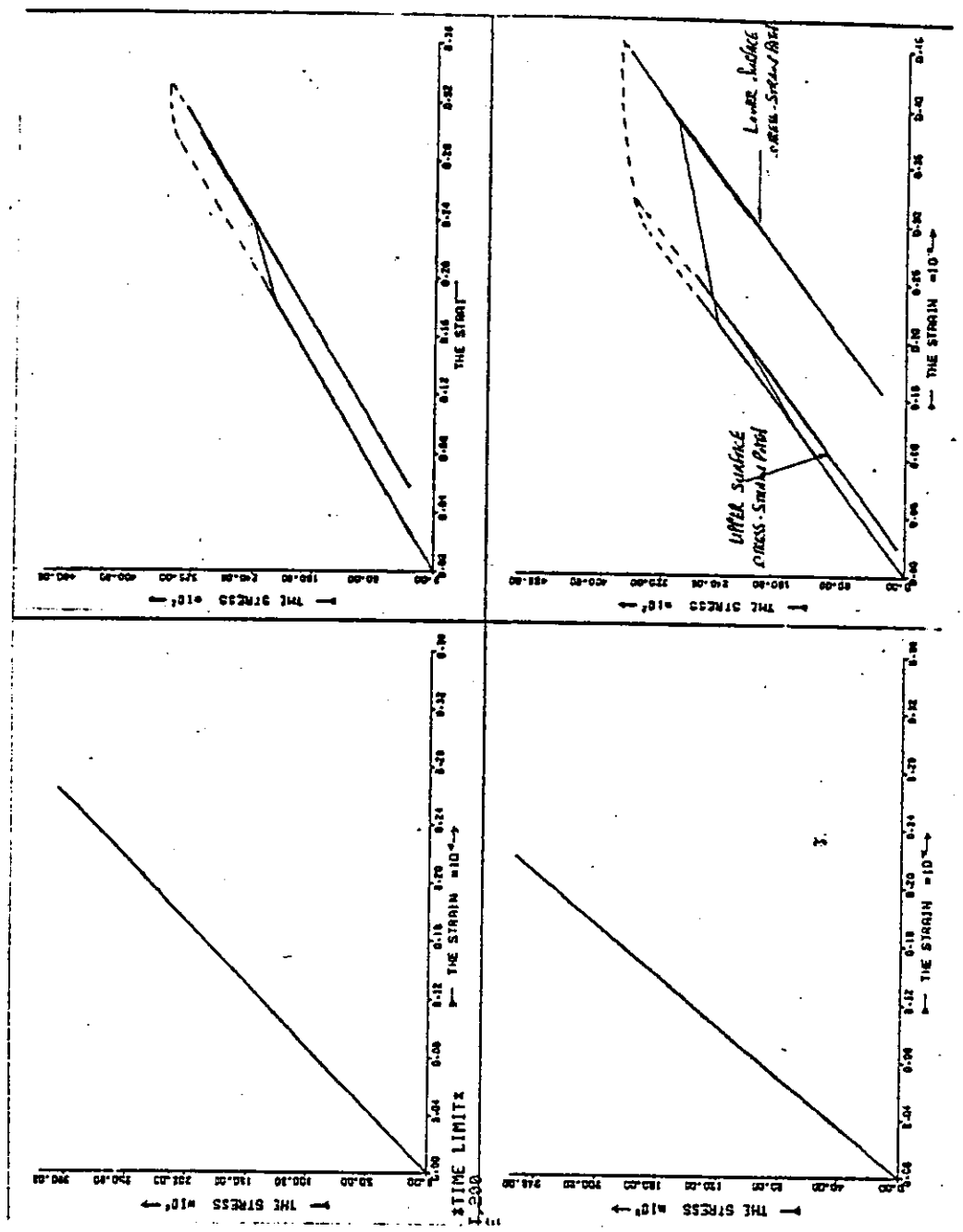


FIG. 53b Stress-Strain curves of element 4

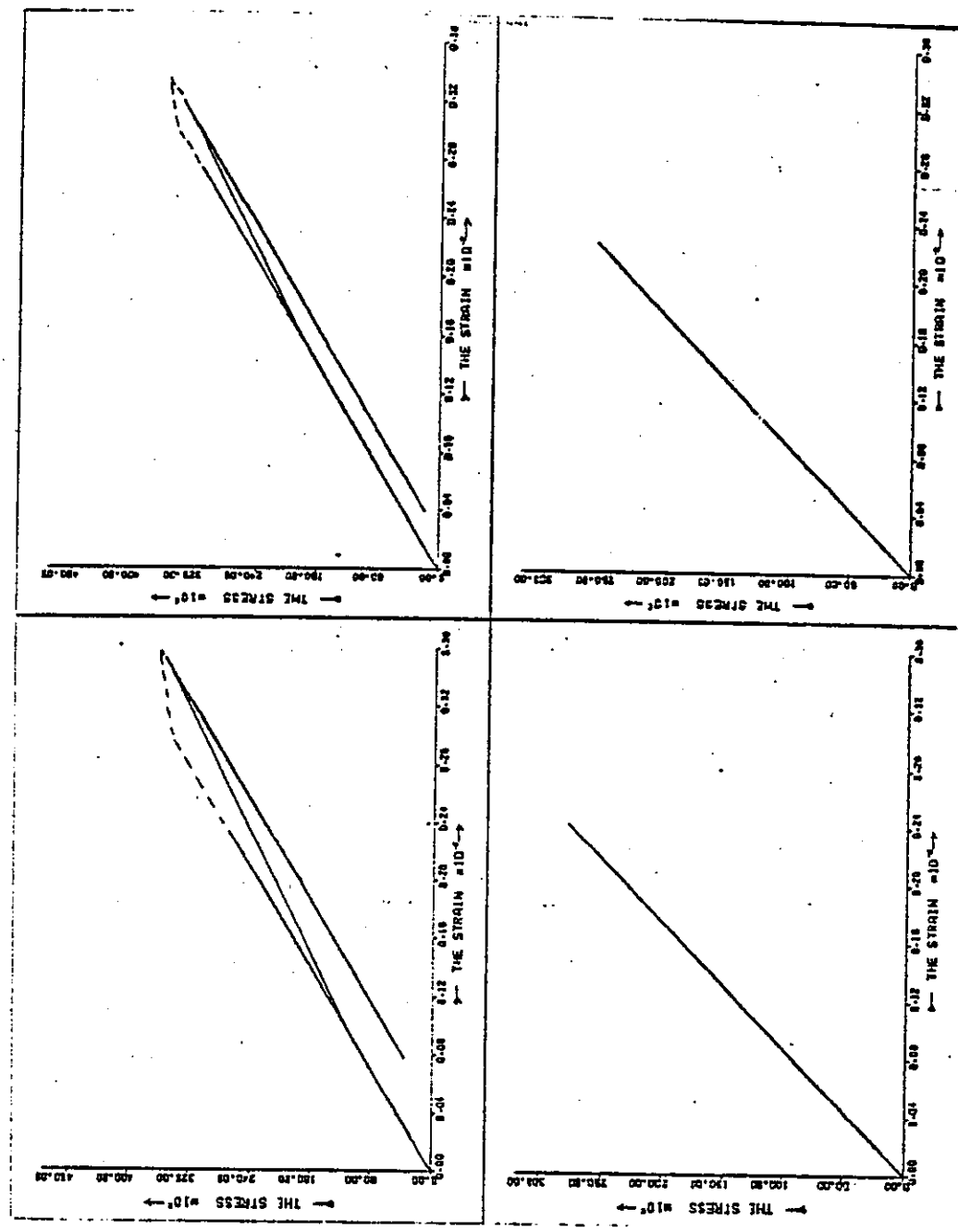


FIG. 53c Stress-Strain curves of element 6

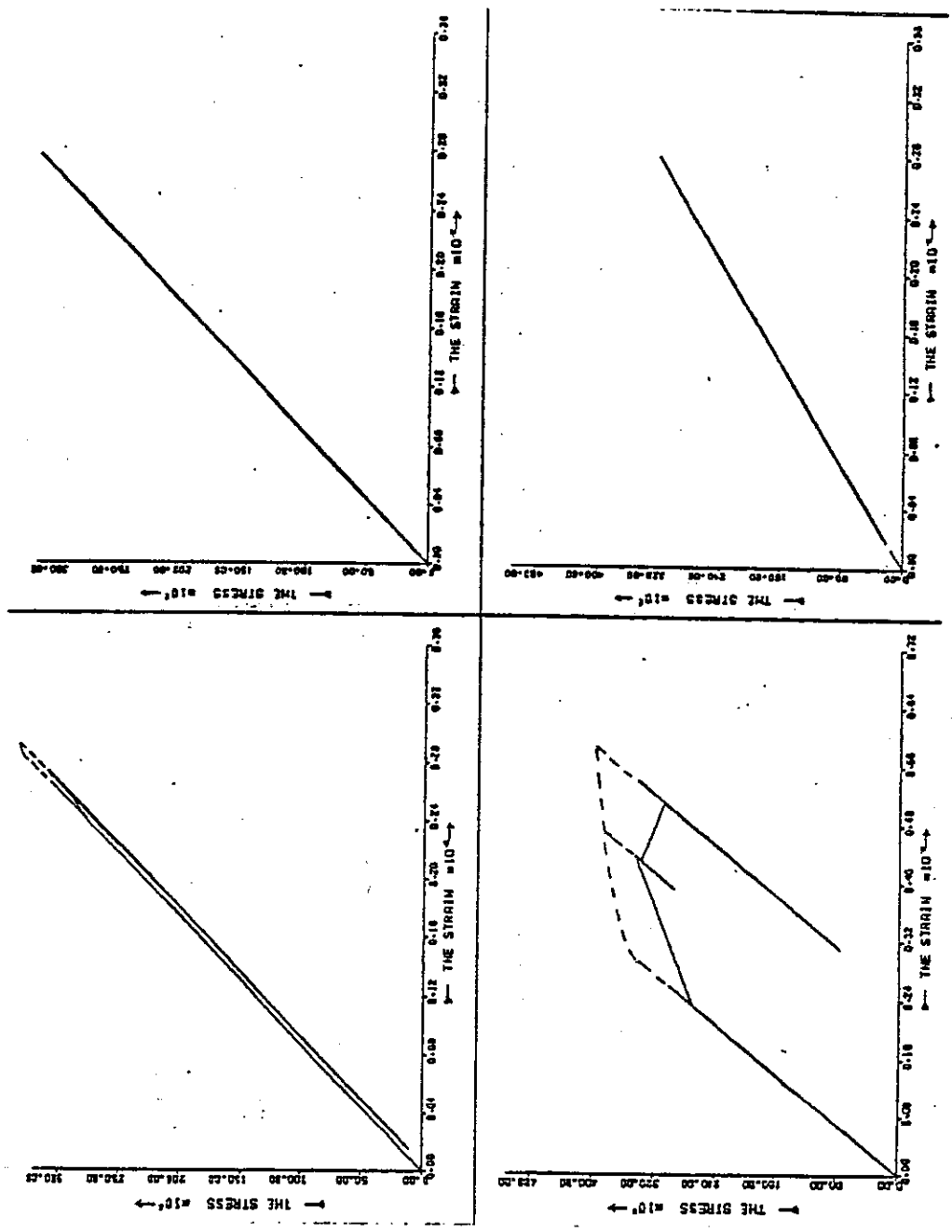


FIG. 53d Stress-Strain curves of element 7

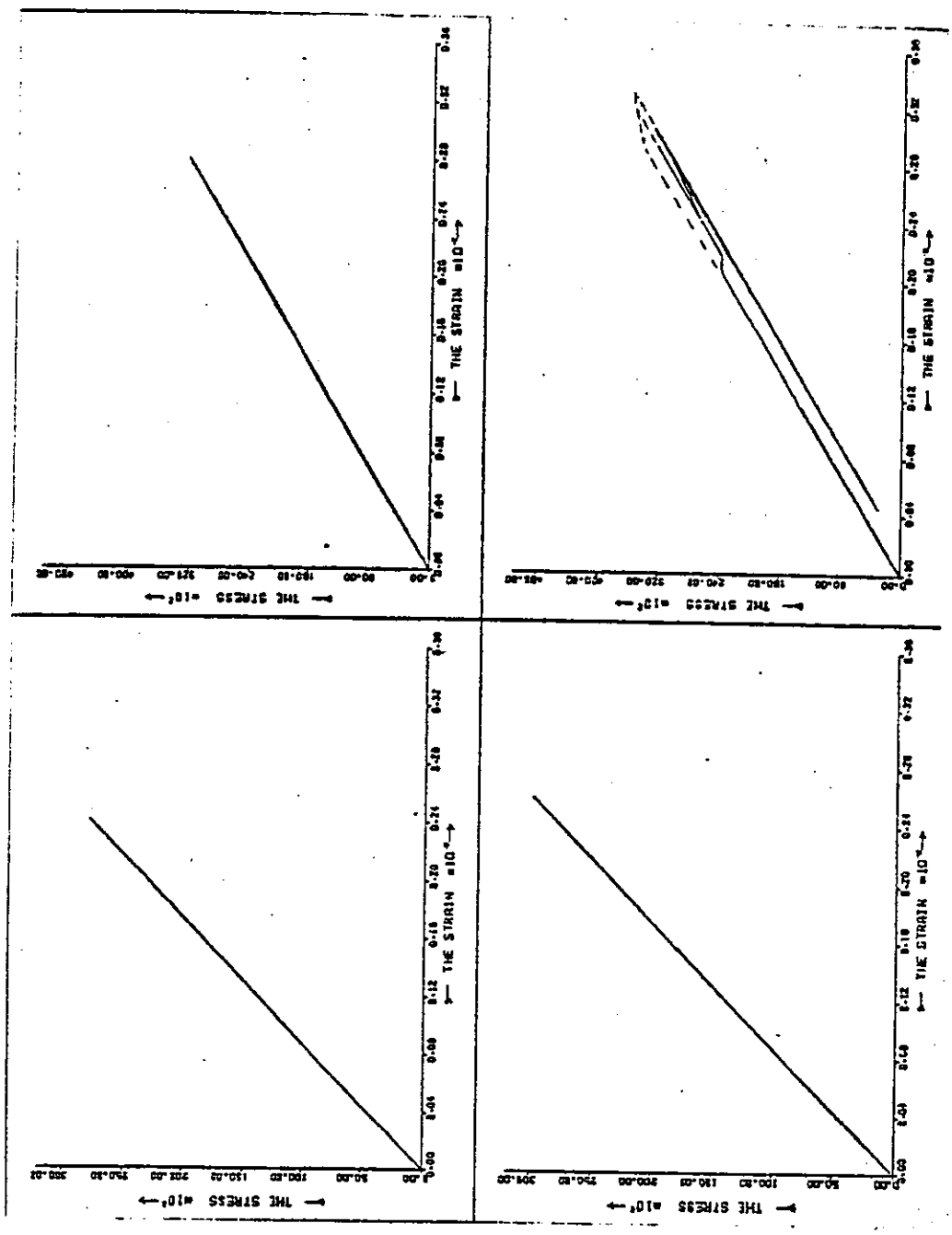


FIG. 53e Stress-Strain curves of element 8

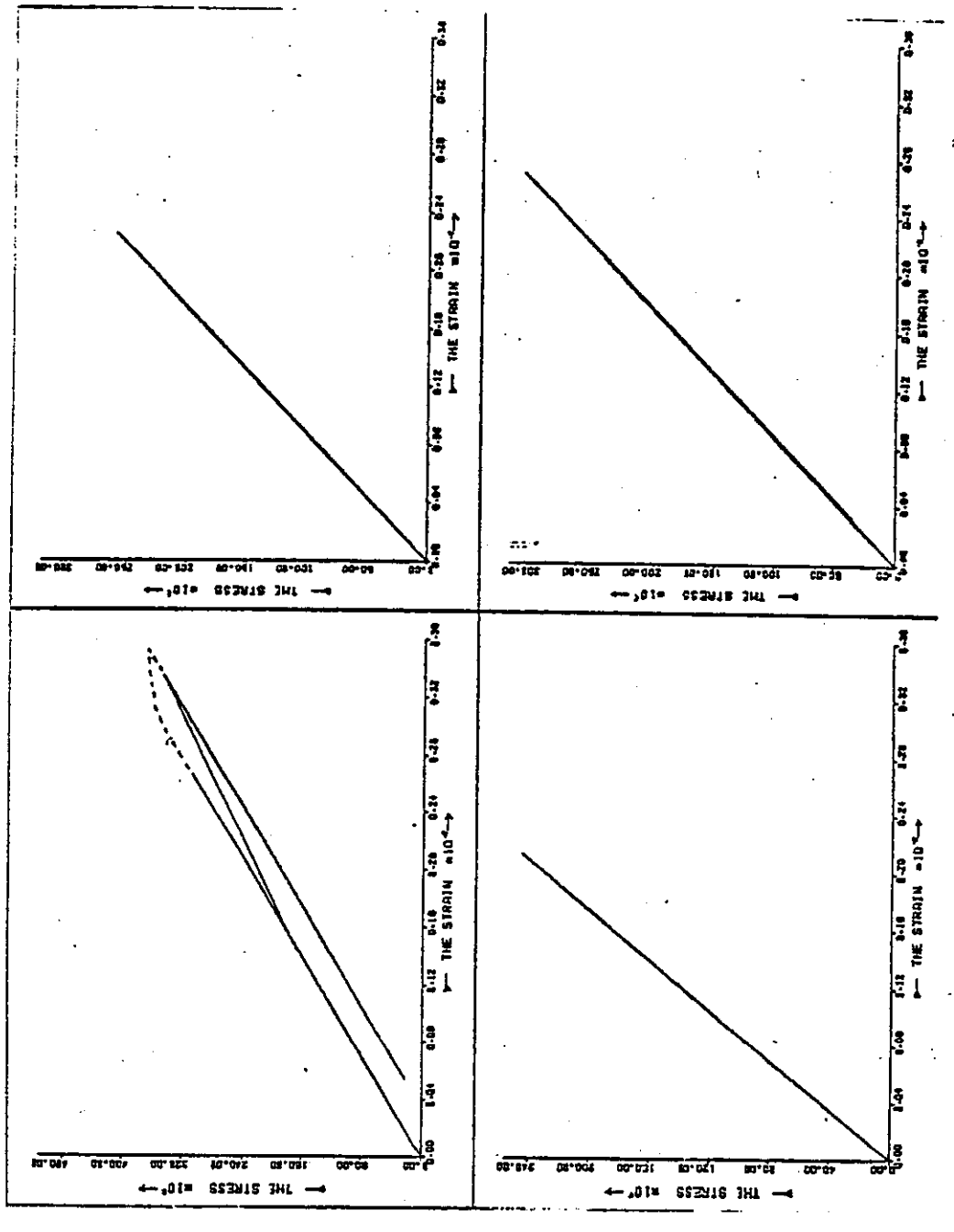


FIG. 53f Stress-Strain curves of element 9

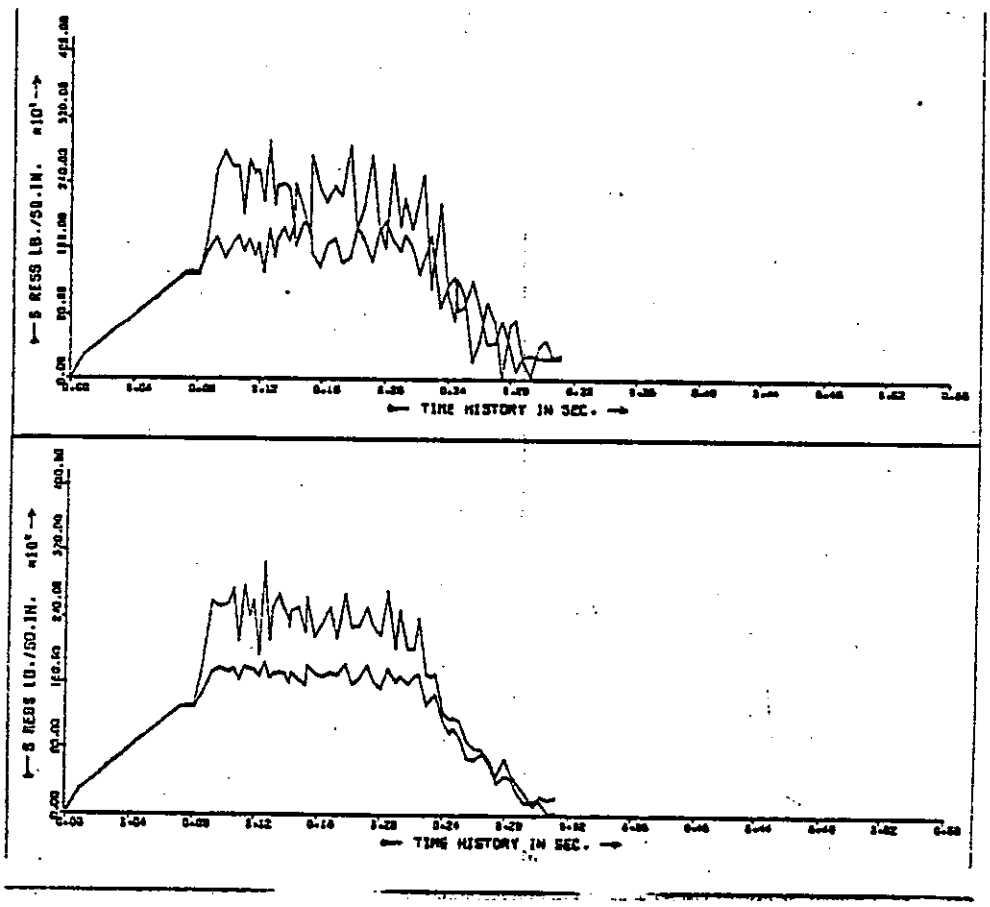


FIG. 54a Gaussian stresses at stiffener element 4

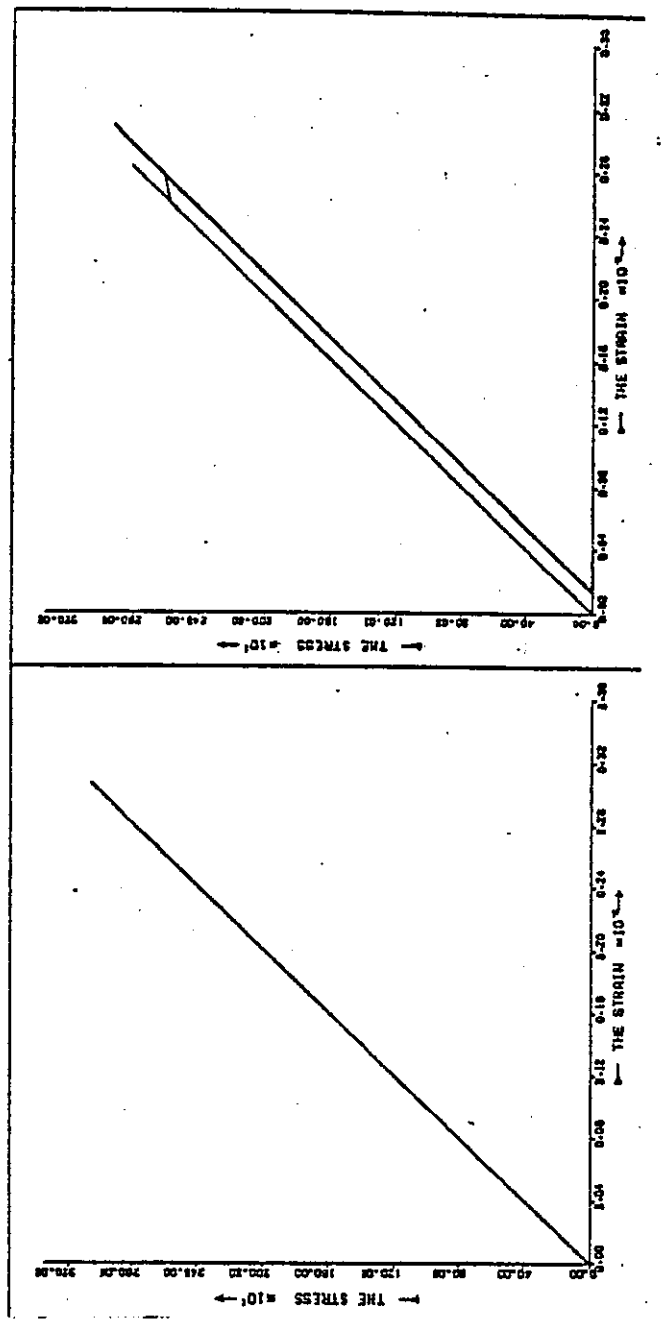


FIG. 54b Stress-Strain curves of stiffener element 4

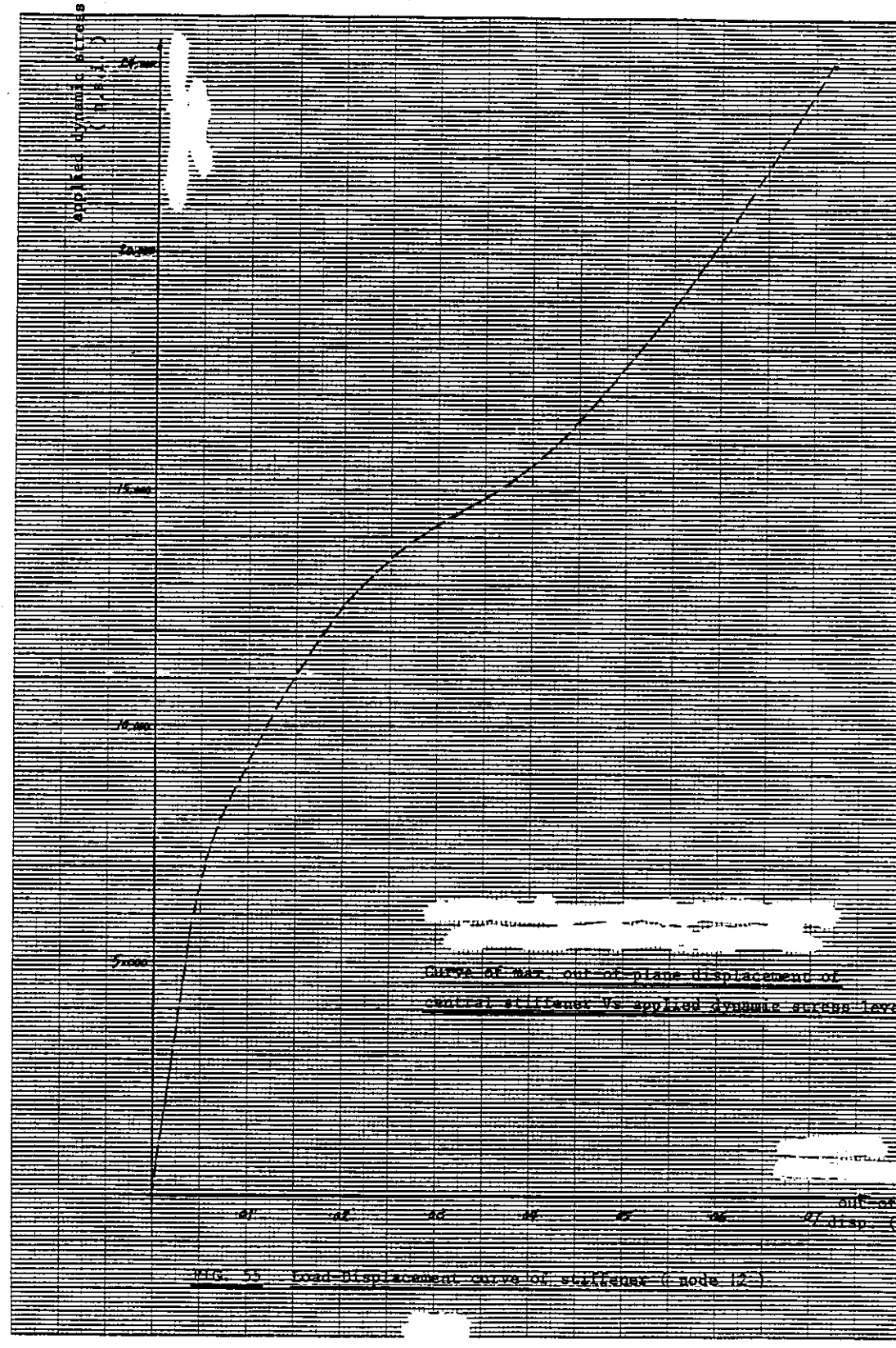


FIG. 55 Load-Displacement curve of stiffener (node 12)

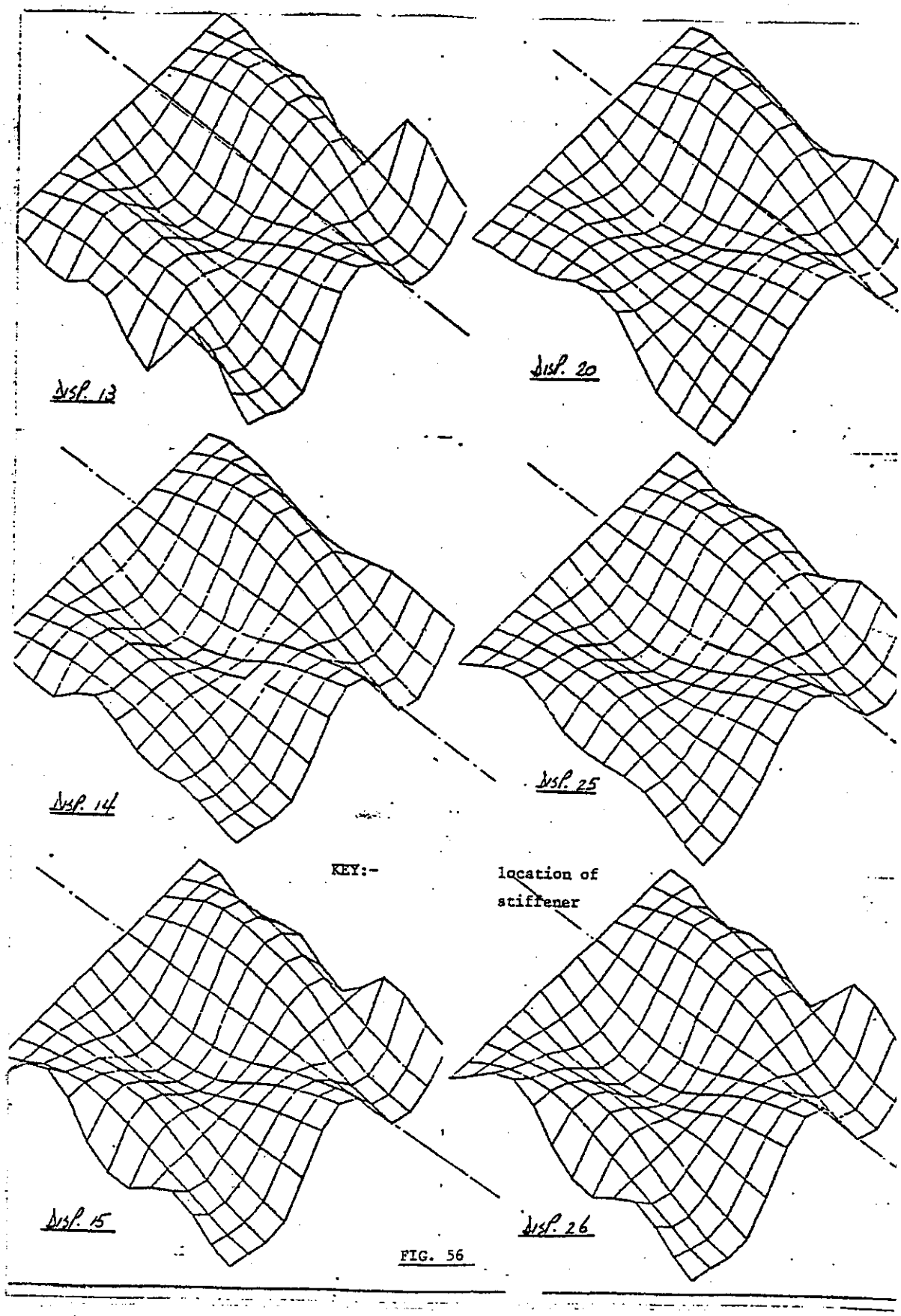
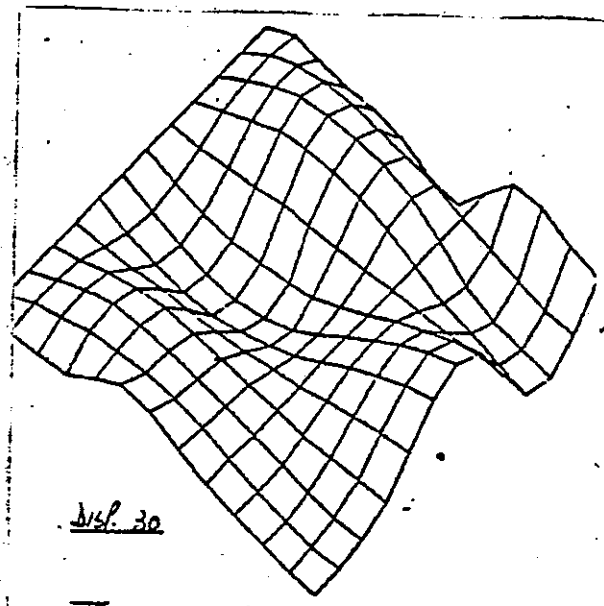
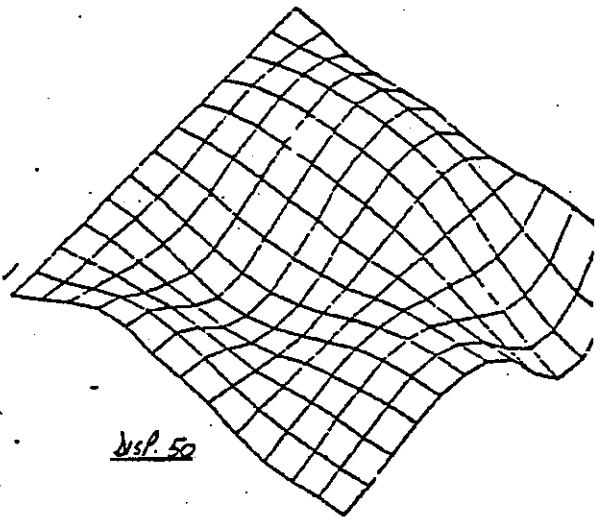

Disp. 13
Disp. 20
Disp. 14
Disp. 25
KEY:-
location of stiffener
Disp. 15
Disp. 26

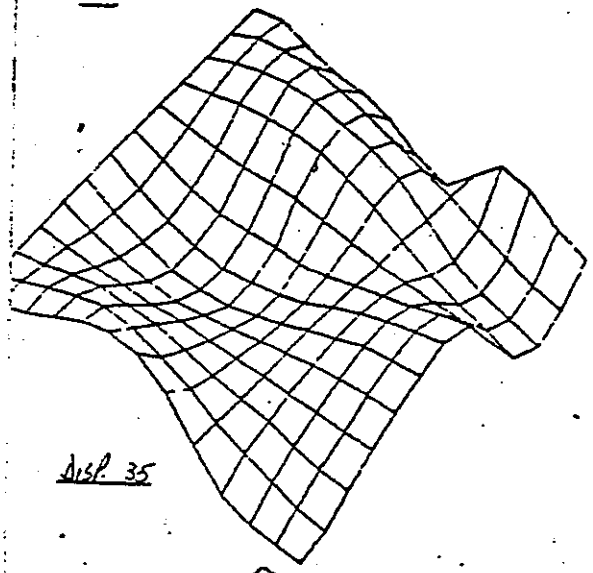
FIG. 56



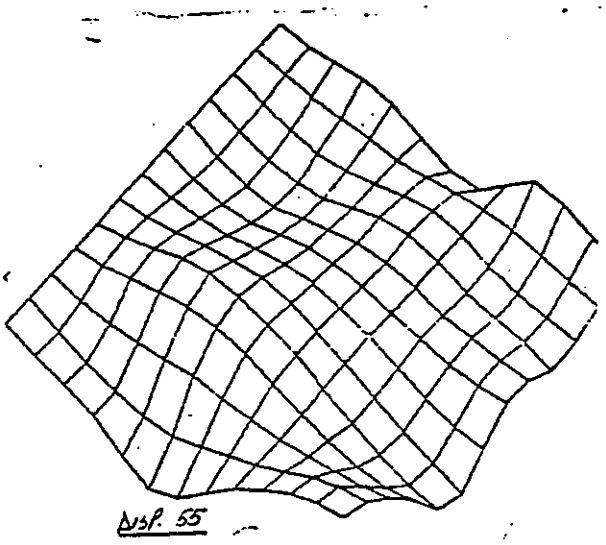
Displ. 30



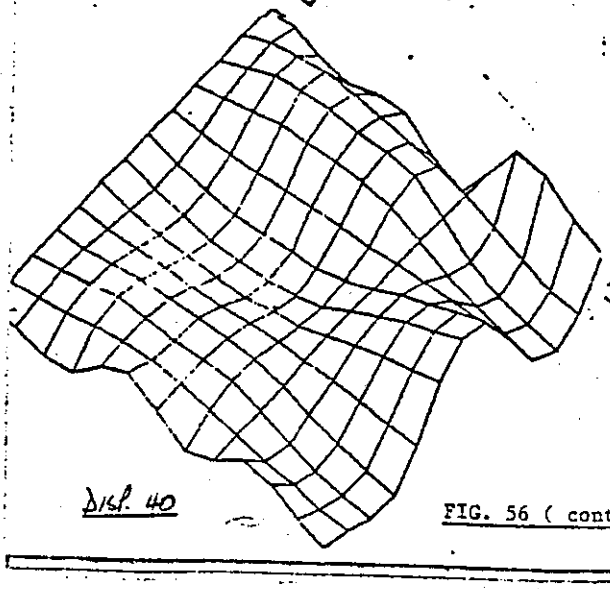
Displ. 50



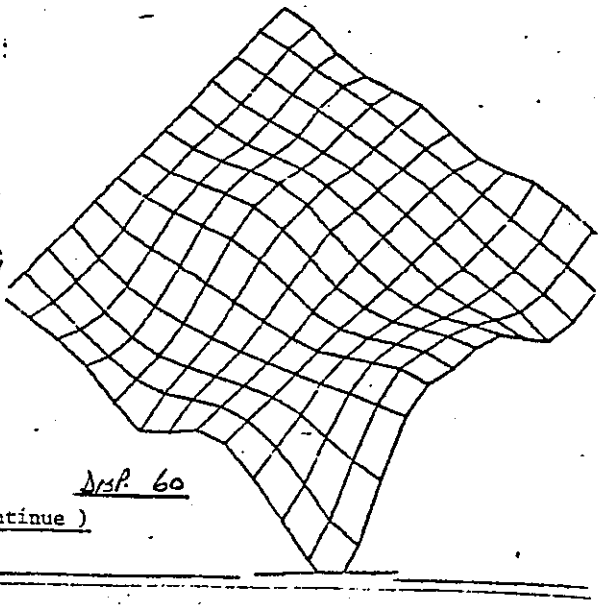
Displ. 35



Displ. 55



Displ. 40



Displ. 60

FIG. 56 (continue)

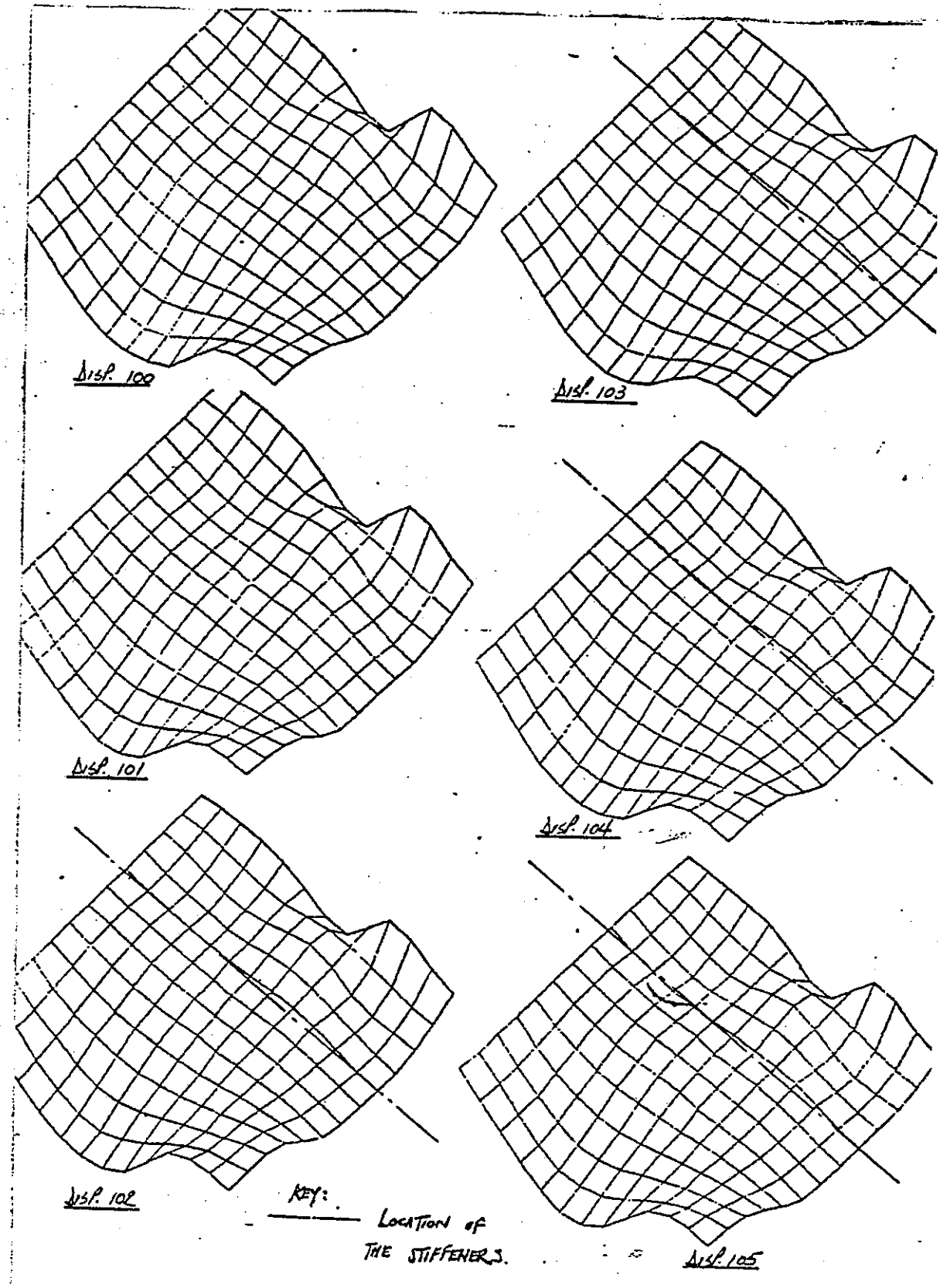

Disp. 100
Disp. 103
Disp. 101
Disp. 104
Disp. 102
Disp. 105
KEY:
LOCATION OF THE STIFFENERS.

FIG. 56 (cont.)

FIG. 57a Gaussian stresses (direct stresses in X-direction) at element 8

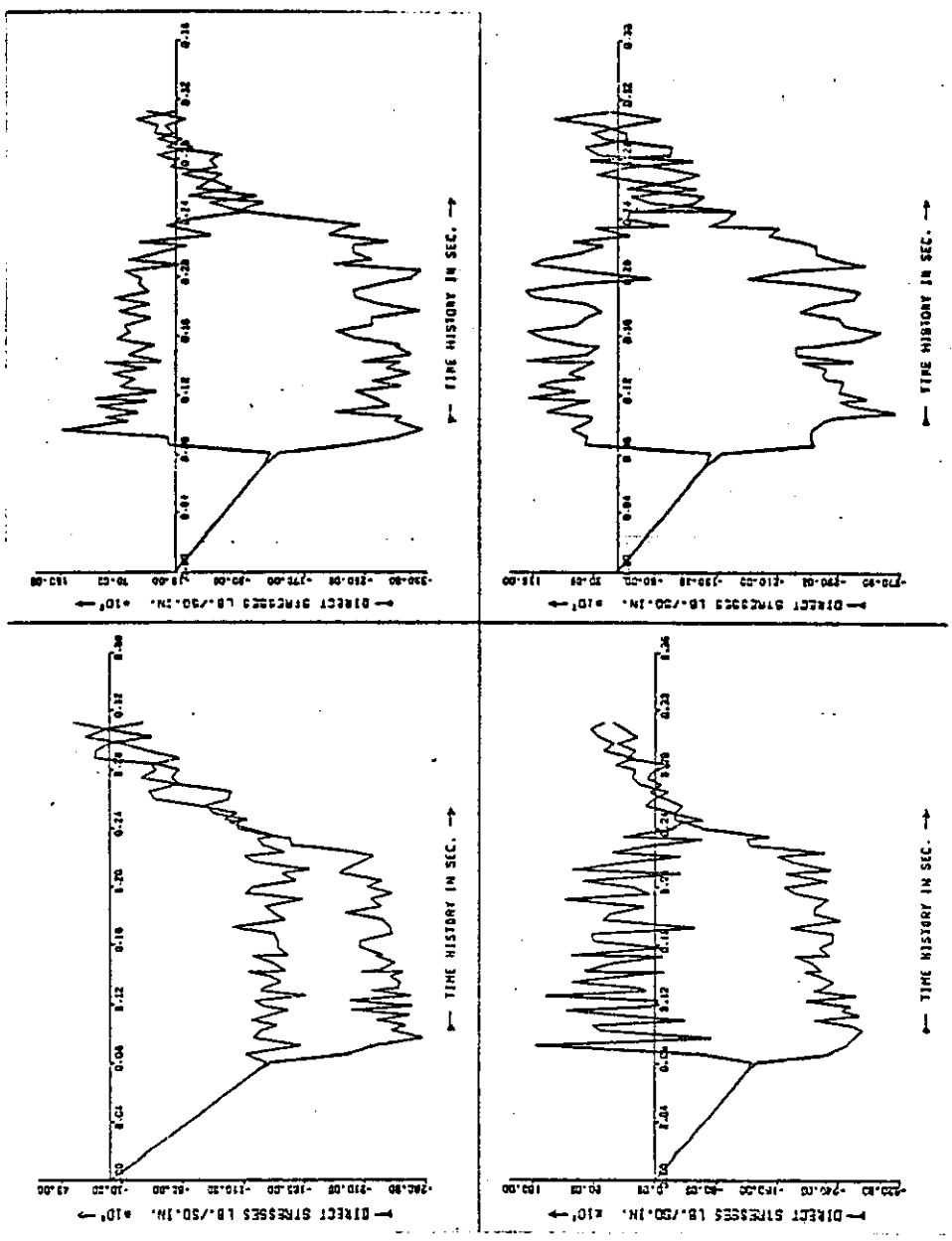


FIG. 57b Gaussian stresses (direct stresses in Y-direction) at element 7

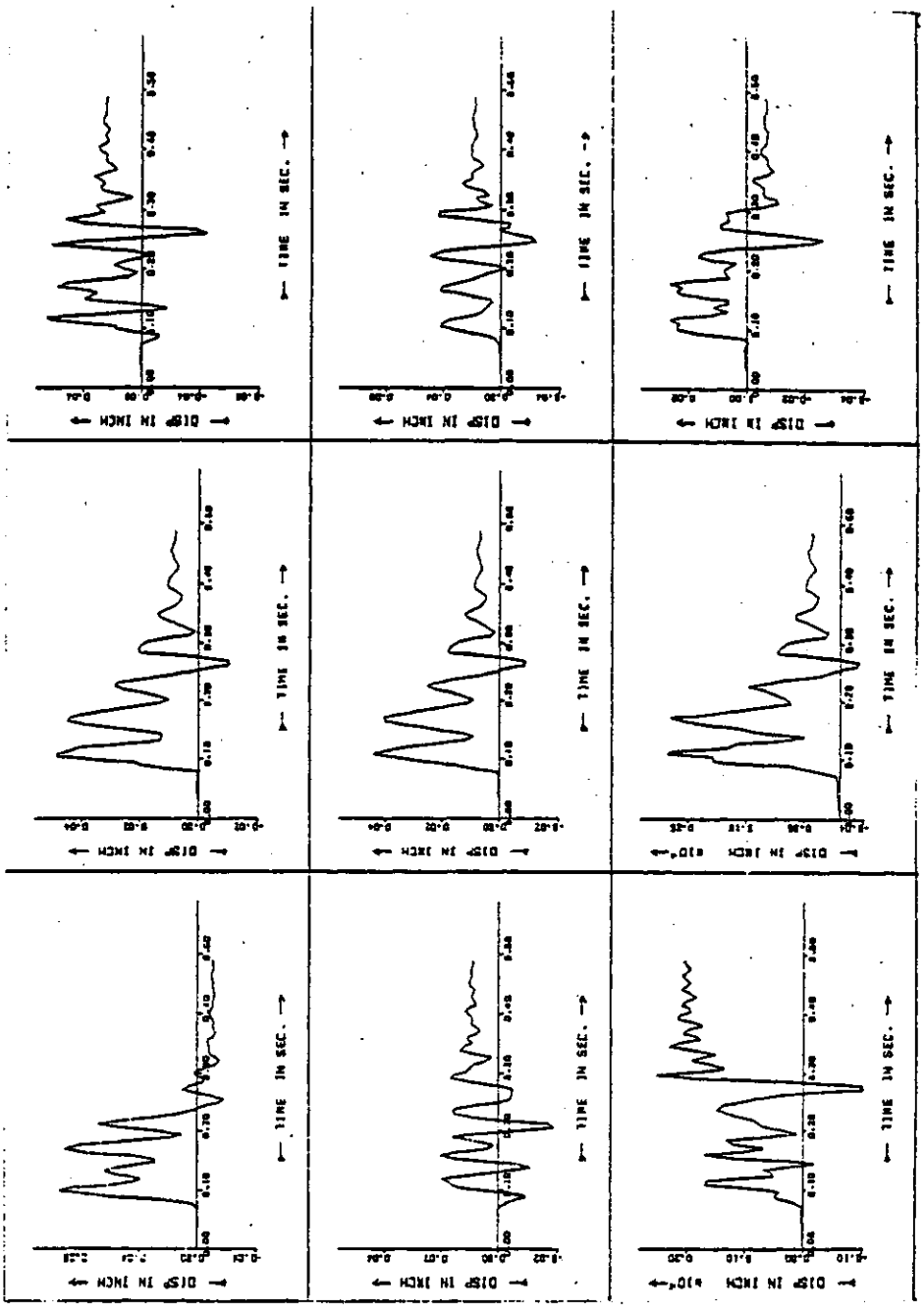


FIG. 58 Nodal displacement curves (applied stress = 16,500 p.s.i.)

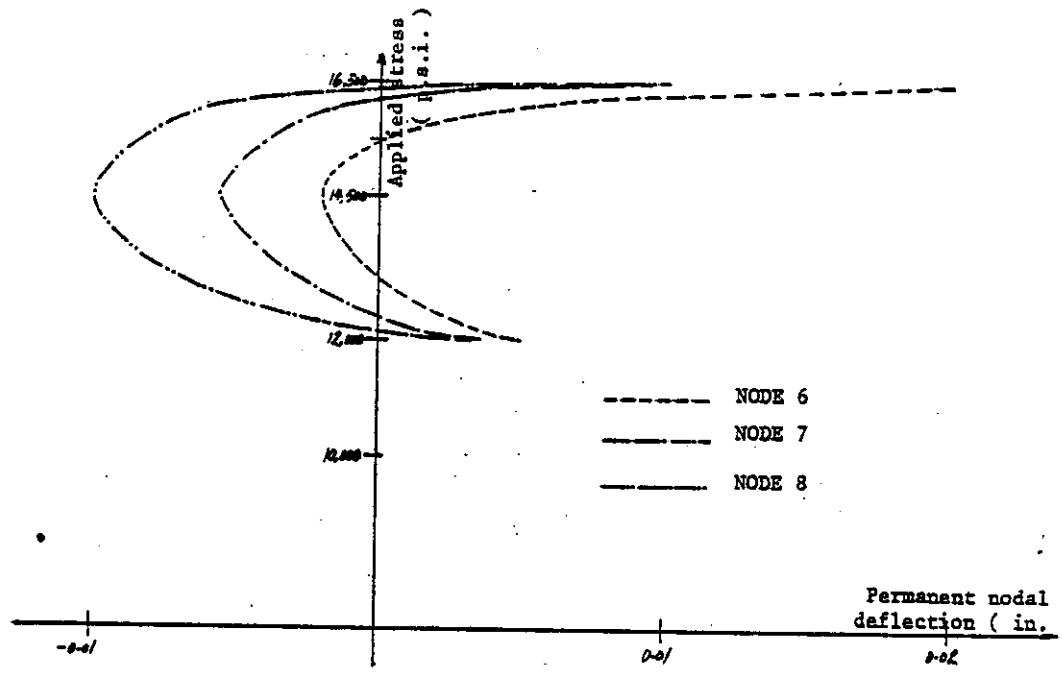


FIG. 59a

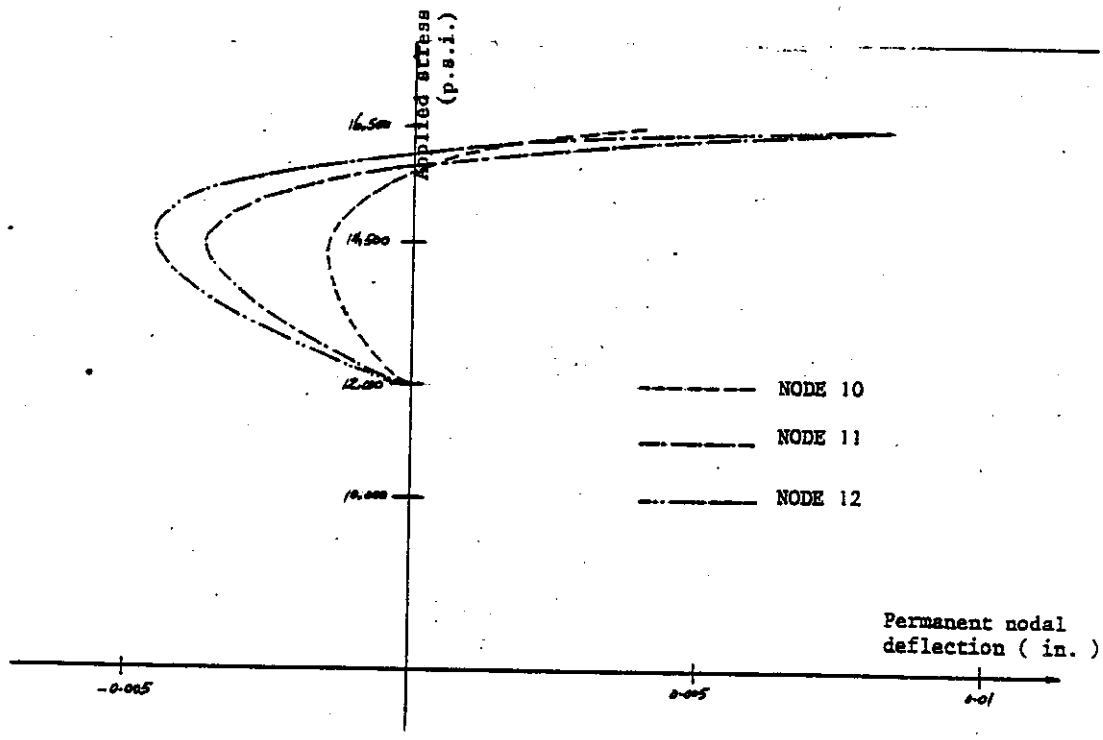


FIG. 59b

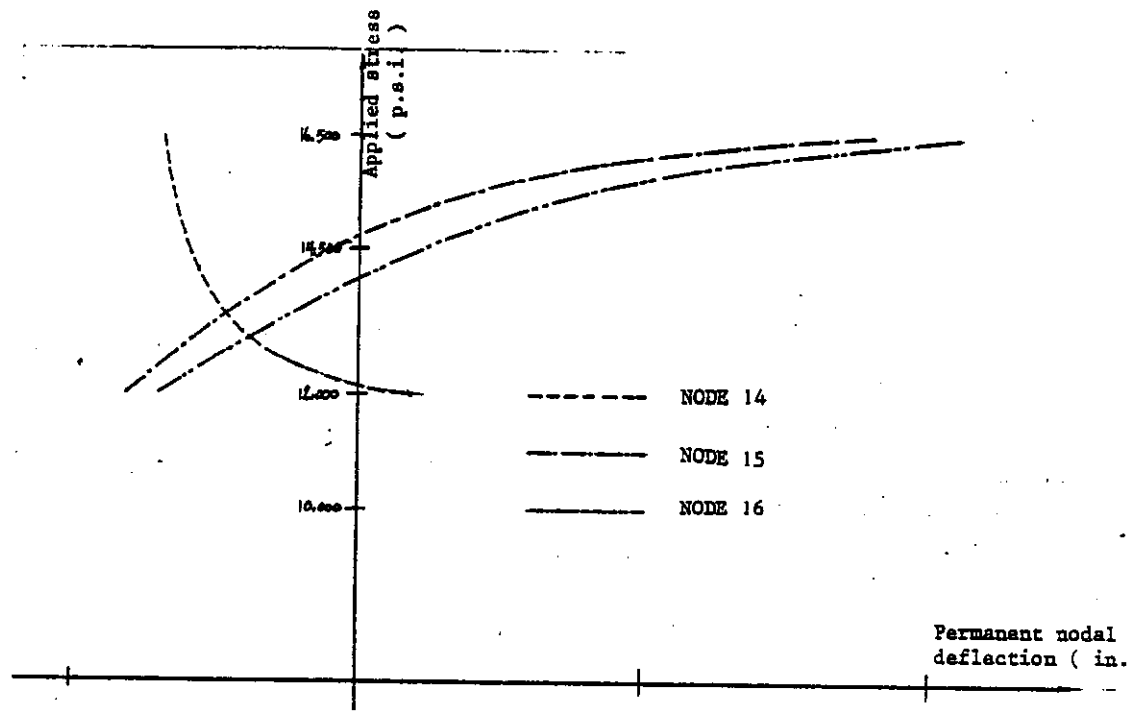


FIG. 59c

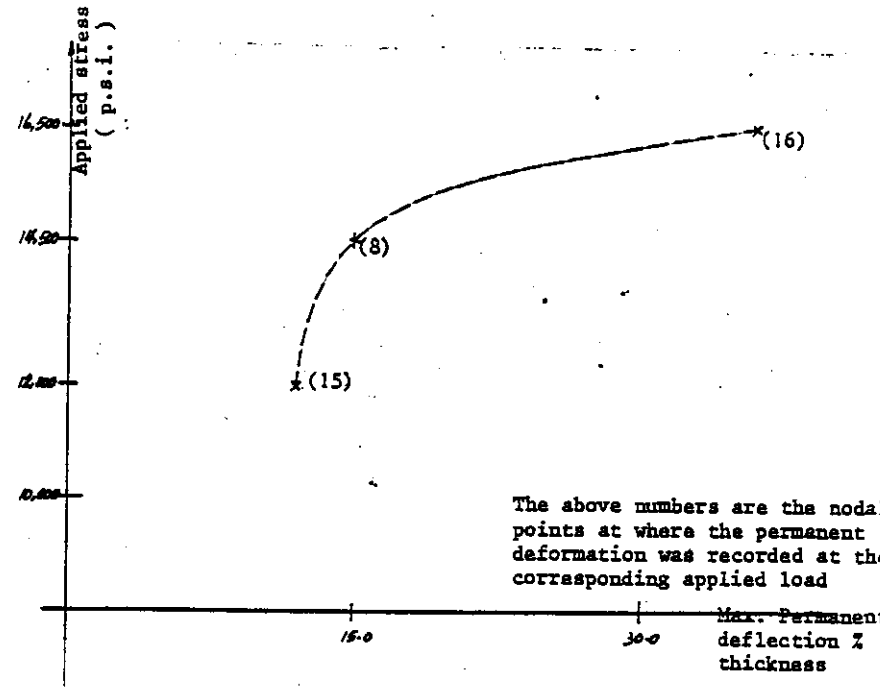


FIG. 60

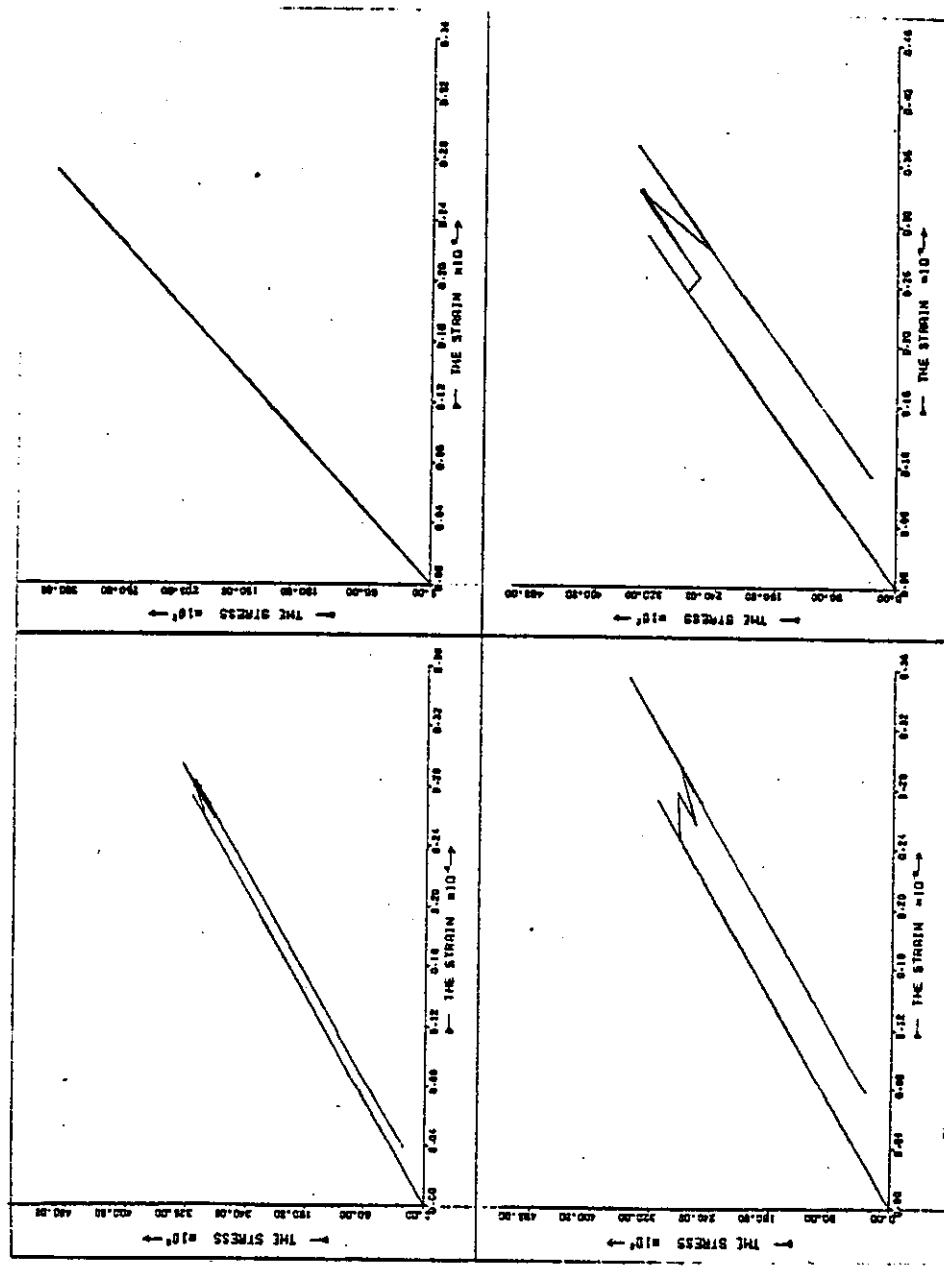


FIG. 61a Stress-Strain curves of element 1 (appl. stress = 16,500 p.s.i.

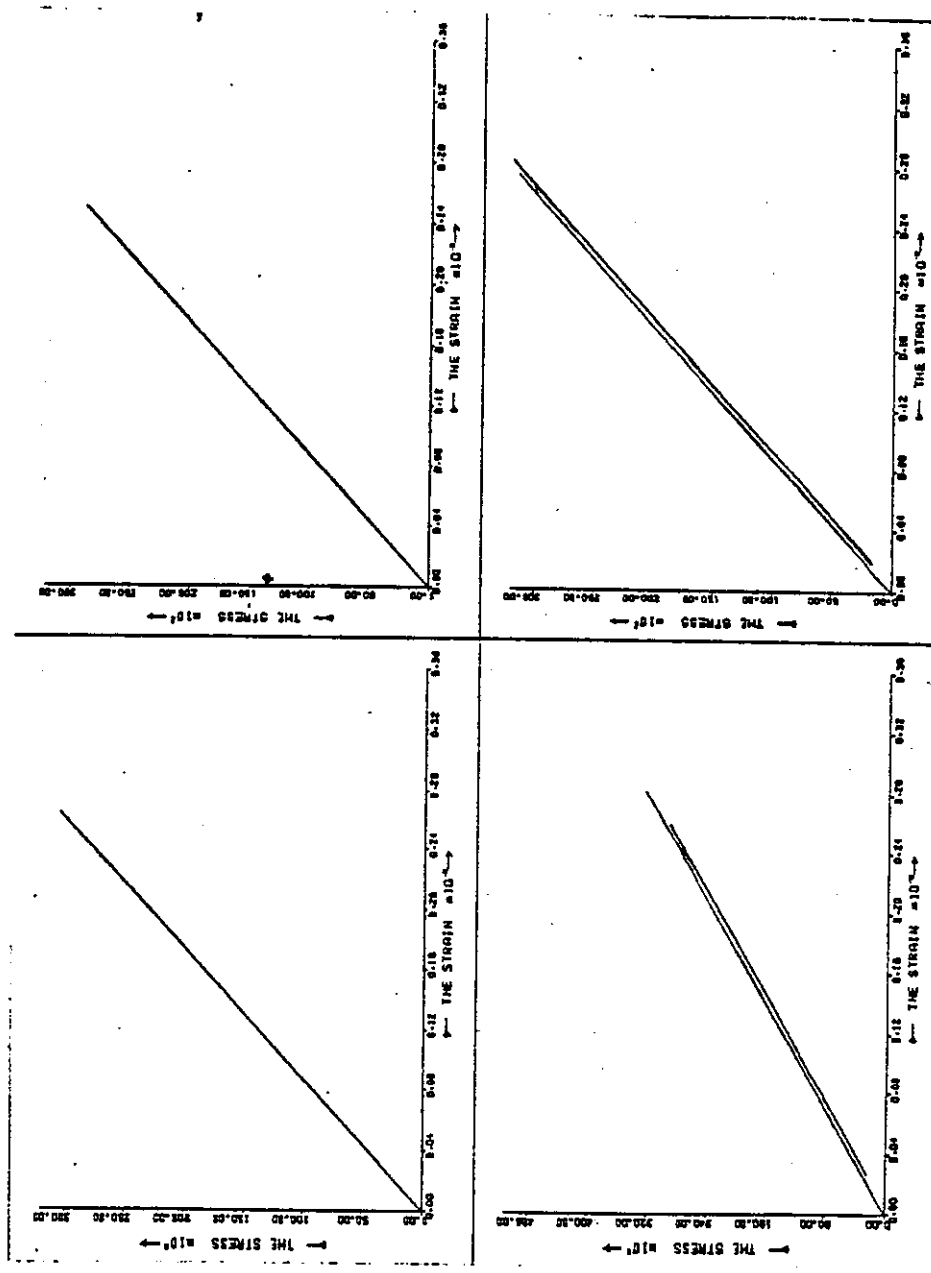


FIG. 61B Stress-Strain curves of element 2 (appl. stress = 16,500 p.s.i.)

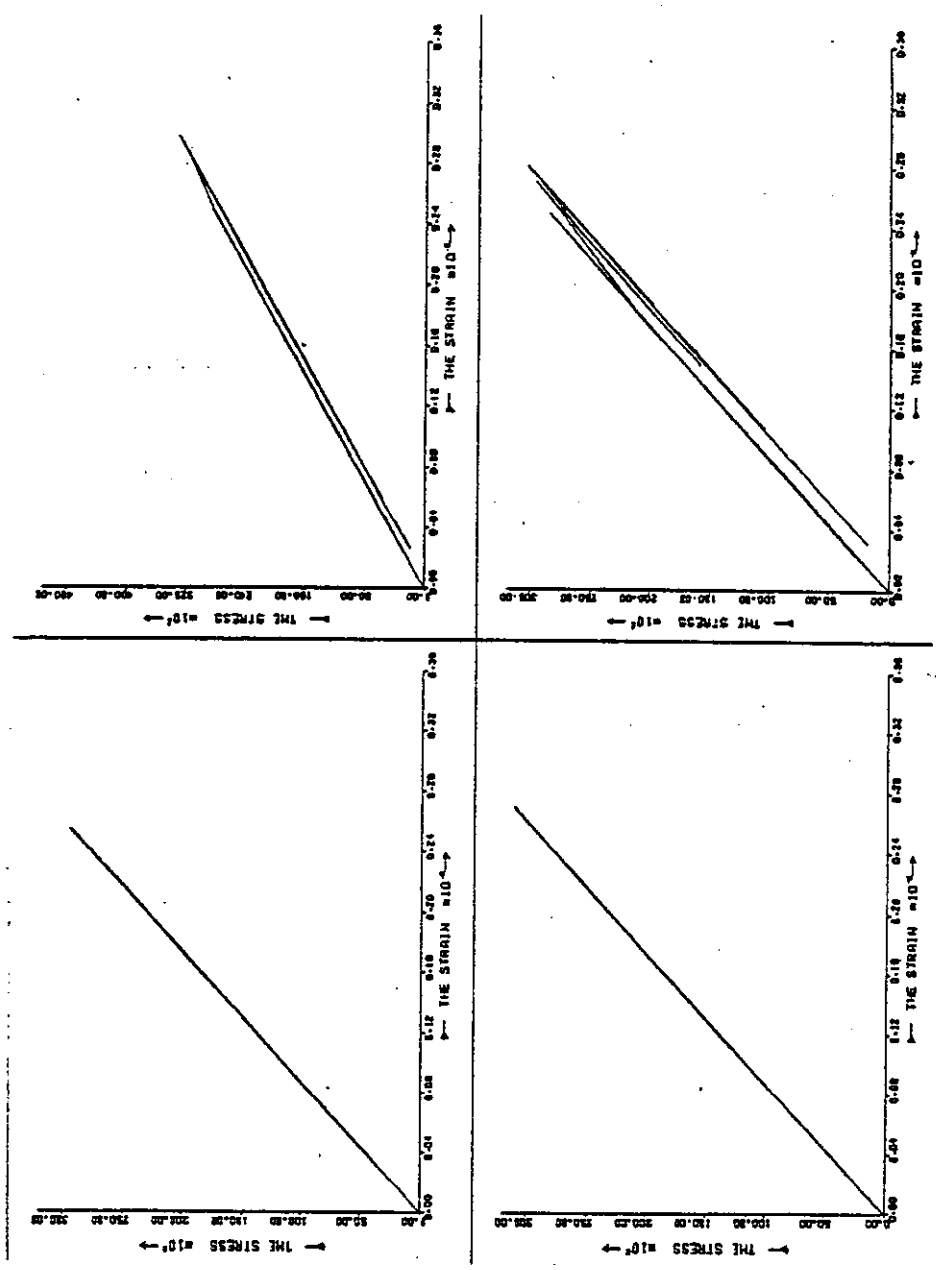


FIG. 61c Stress-Strain curves of element 3 (appl. stress = 16,500 p.s.i.)

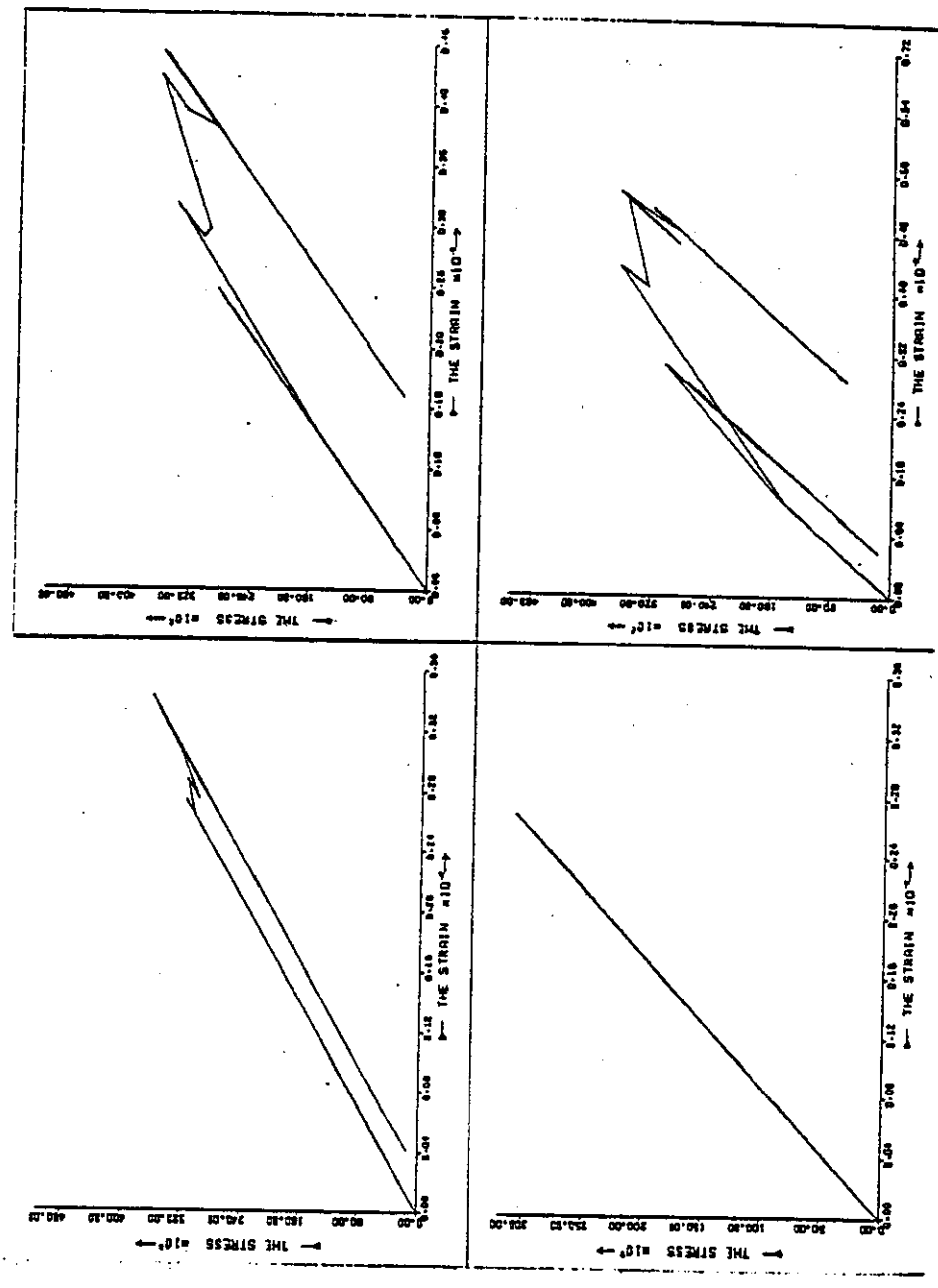


FIG. 61d Stress-Strain curves of element 4 (appl. stress = 16,500 p.s.i.)

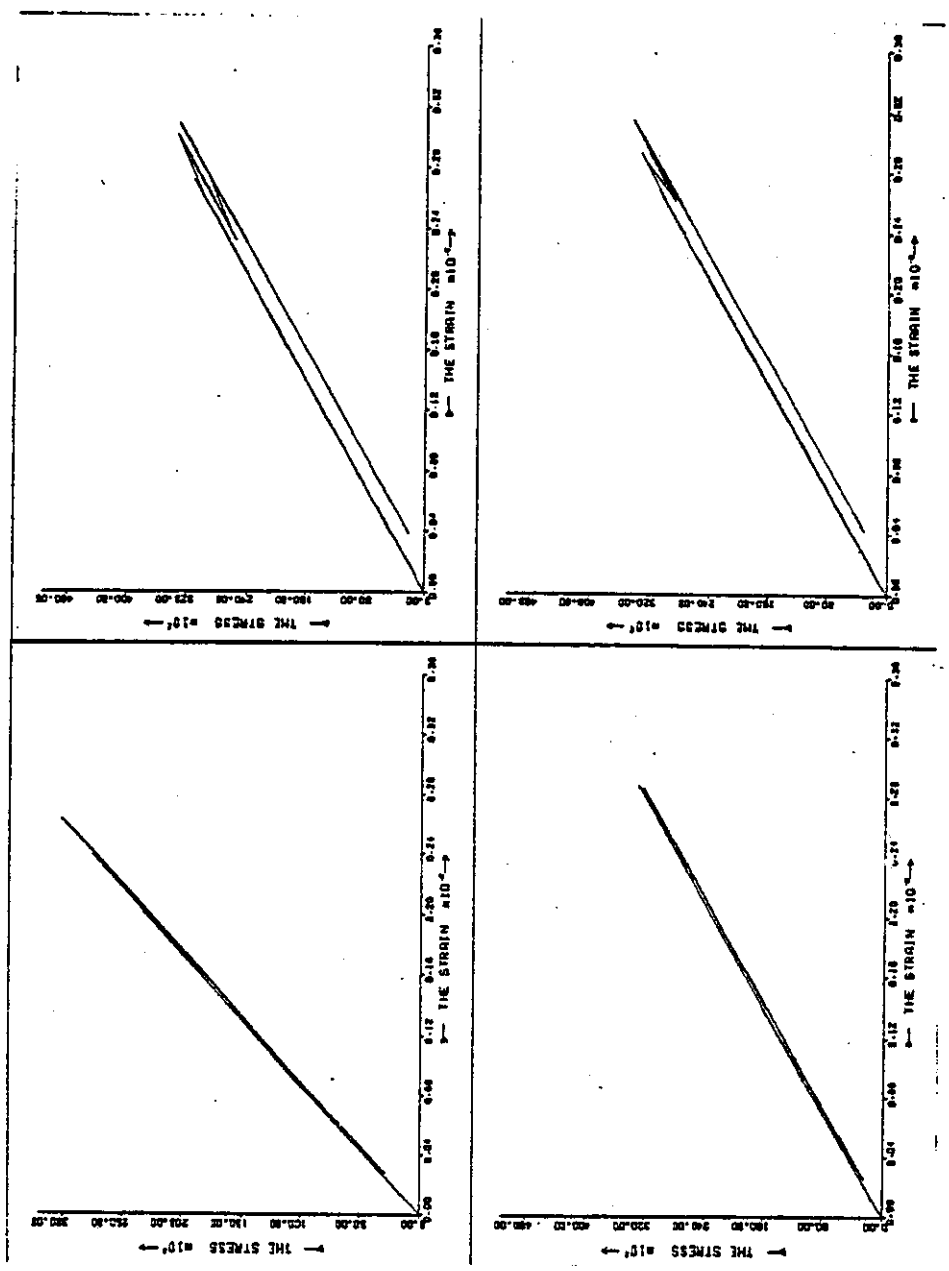


FIG. 61e Stress-Strain curves of element 5 (appl. stress = 16,500 p.s.i.)

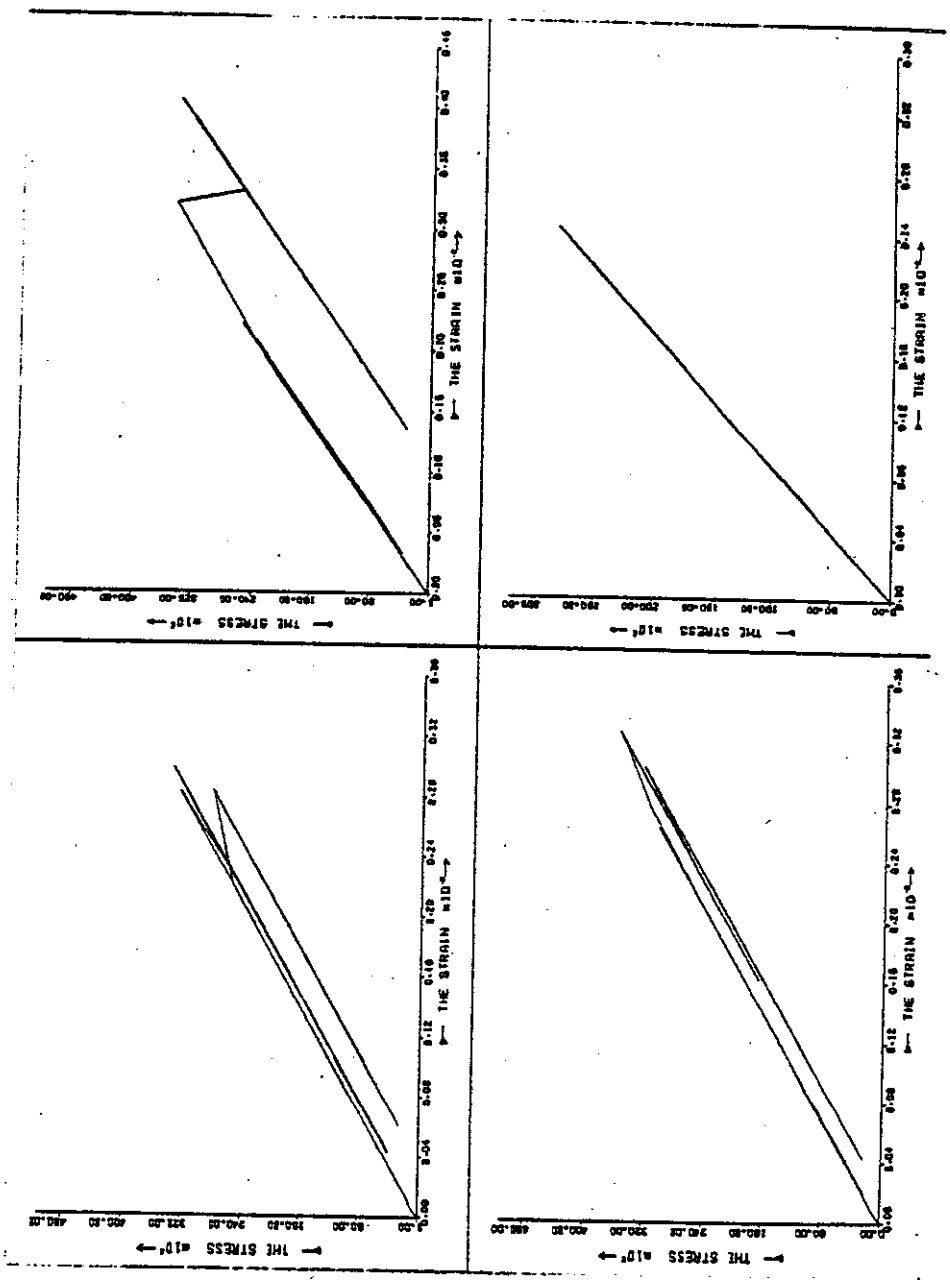


FIG. 61f Stress-Strain curves of element 6 (appl. stress = 16,500 p.s.i.)

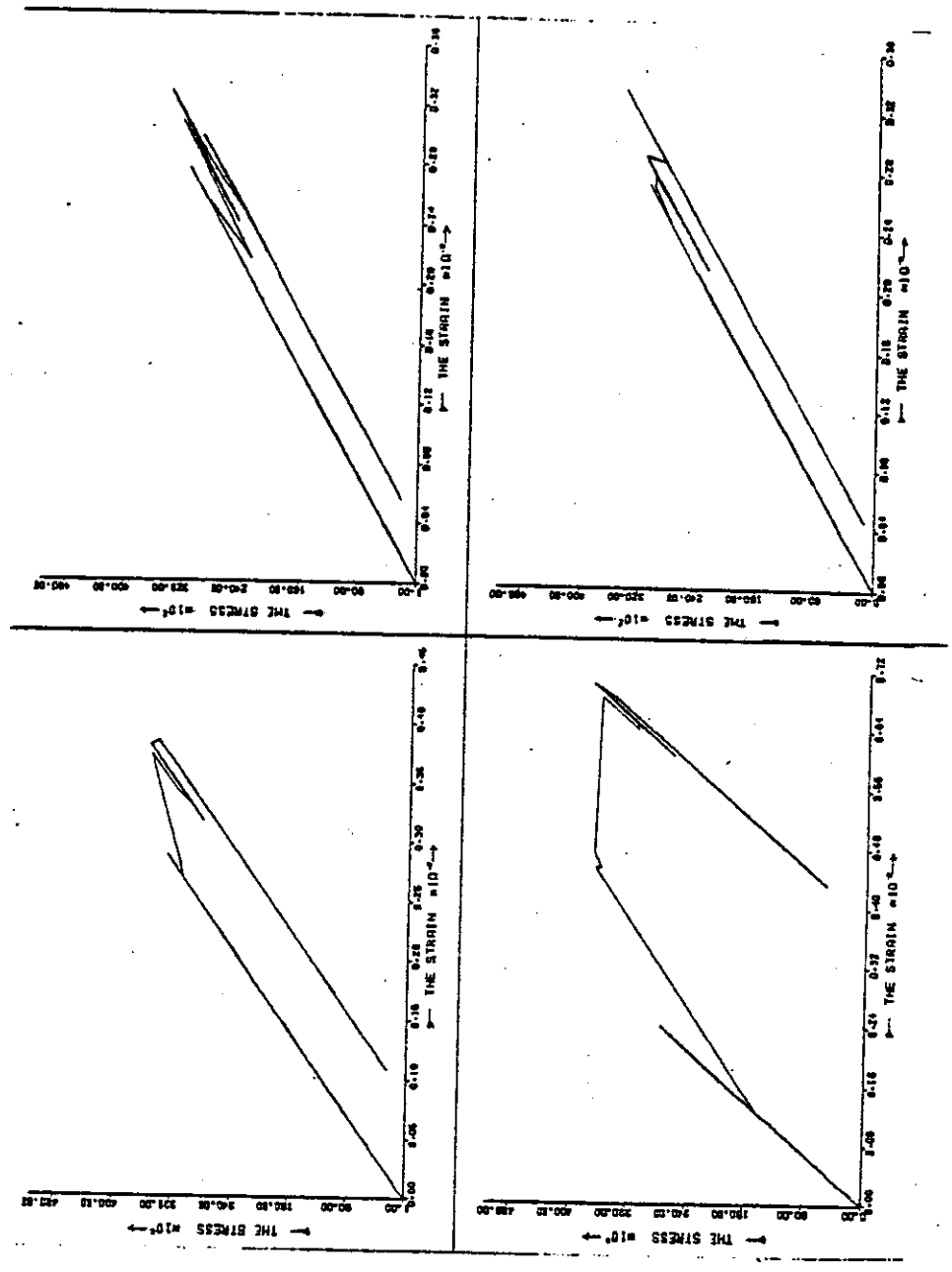


FIG. 61g Stress-Strain curves of element 7 (appl. stress= 16,500 p.s.i.)

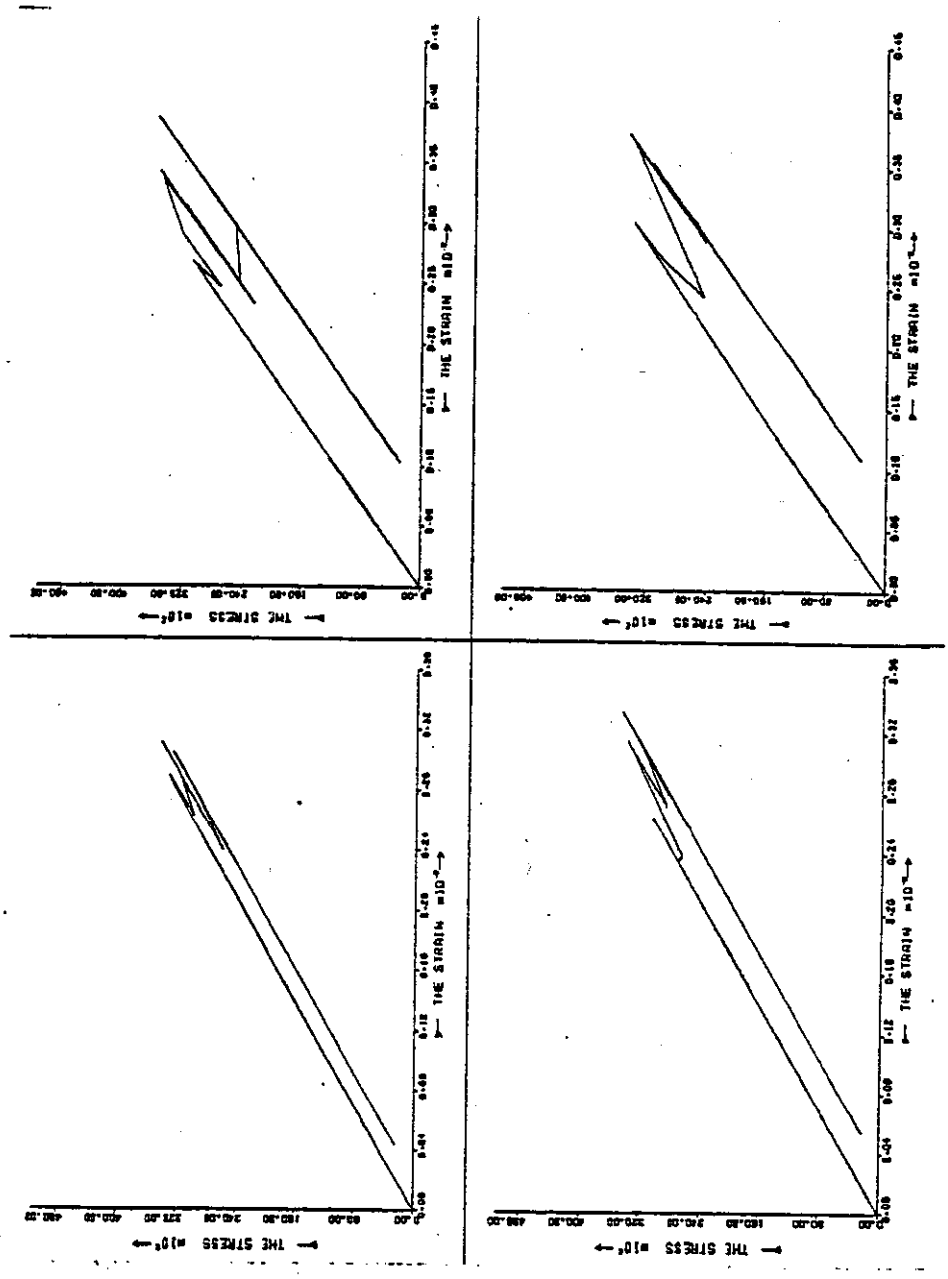


FIG. 61h Stress-Strain curves of element 8 (appl. stress = 16,500 p.s.i.)

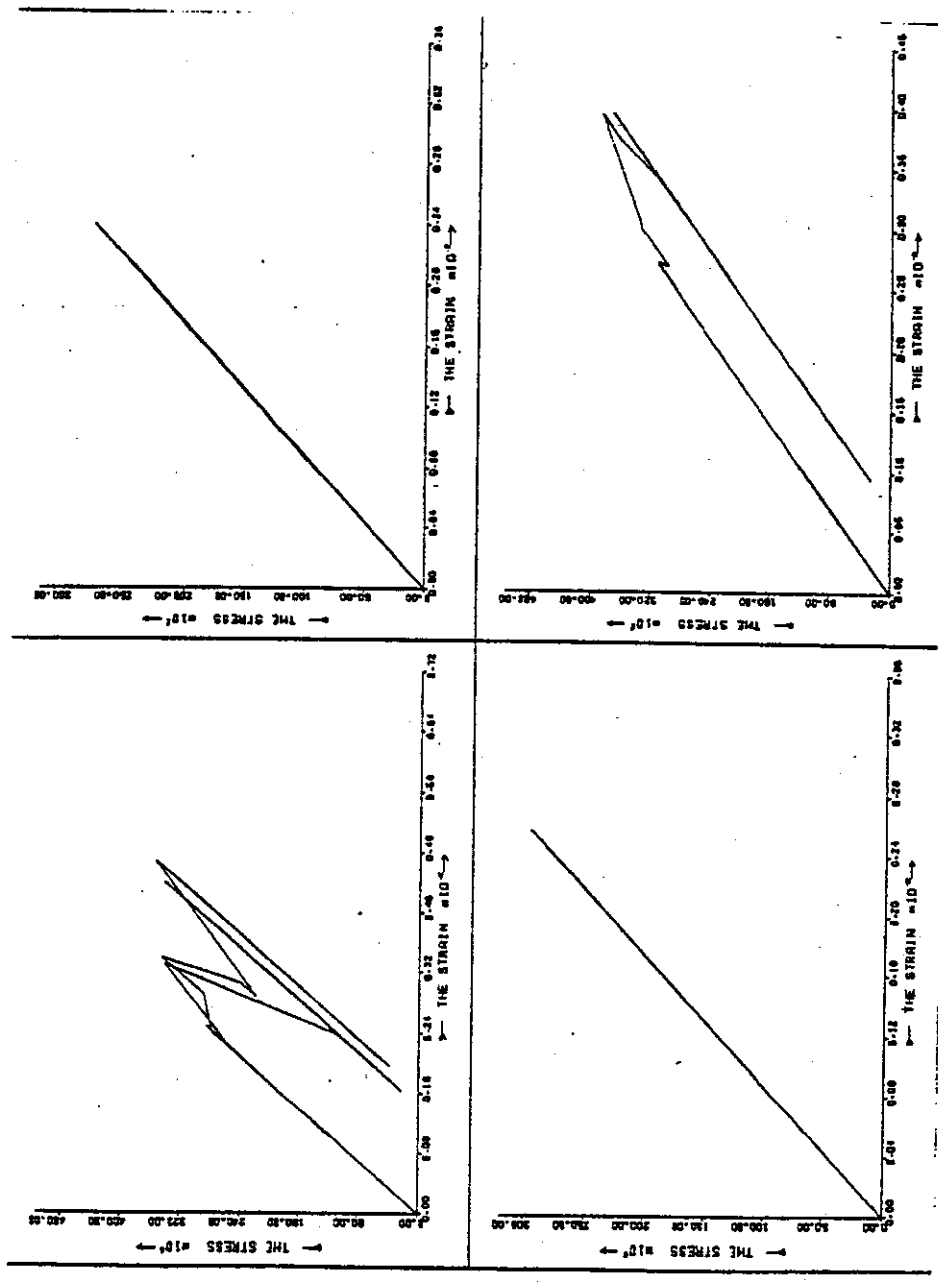


FIG. 61i Stress-Strain curves of element 9 (appl. stress = 16,500 p.s.i.)

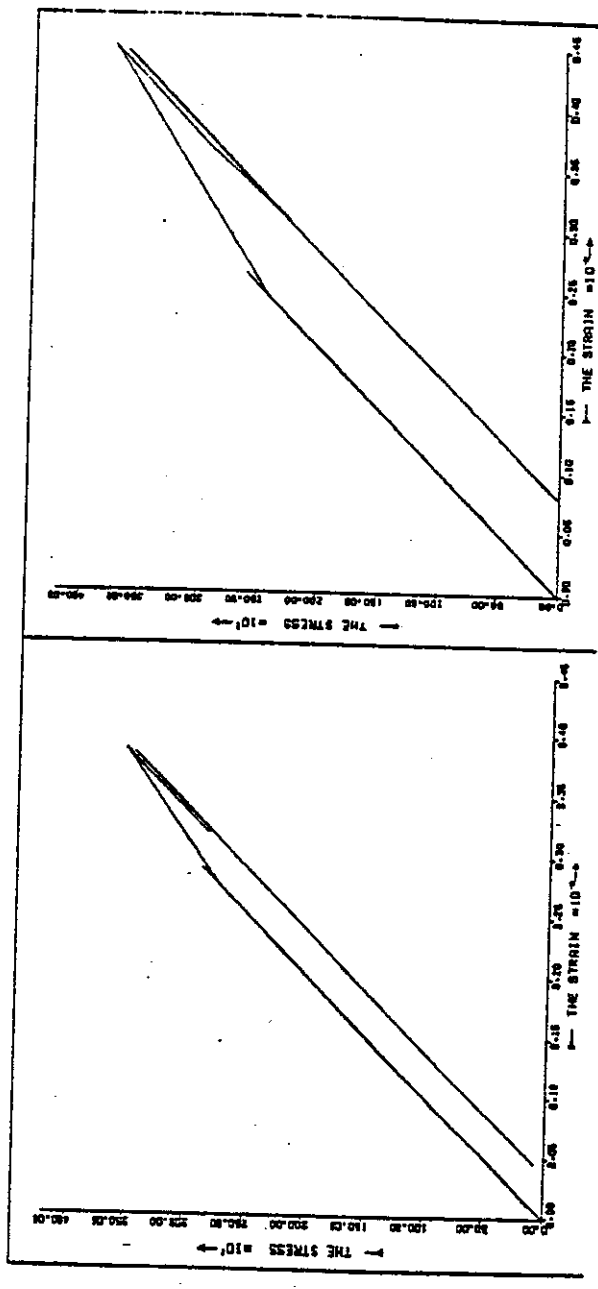


FIG. 62a Stress-Strain curves of stiffener element 4 (appl. stress = 16,500 p.s.i.

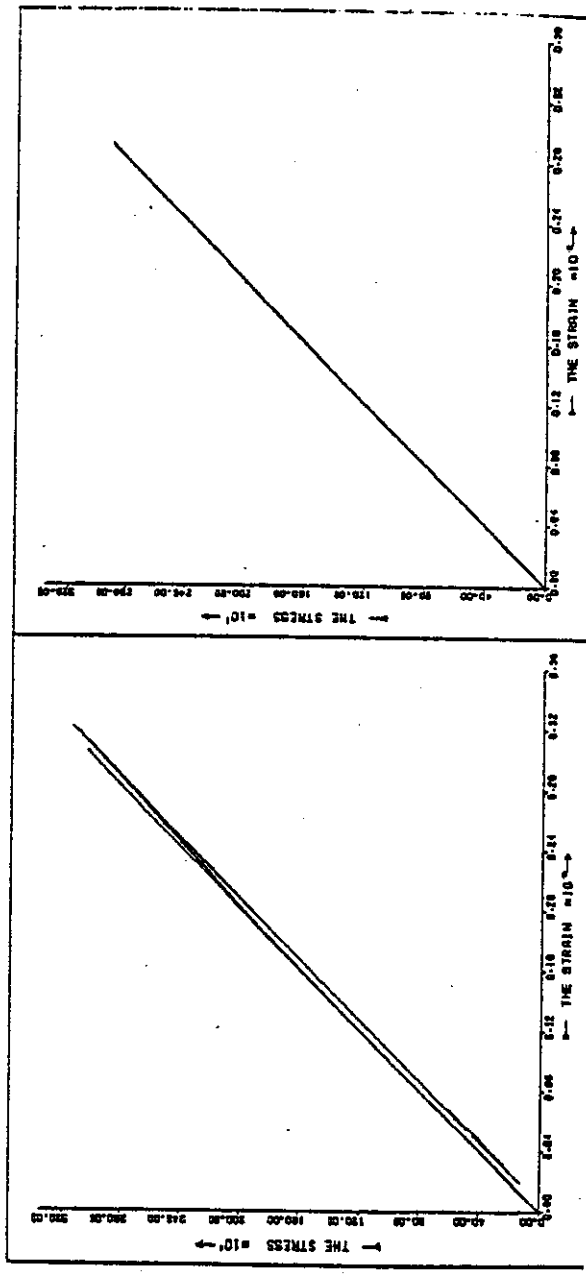


FIG. 62b Stress-Strain curves of stiffener element 5 (appl. stress = 16,500 p.s.i.)

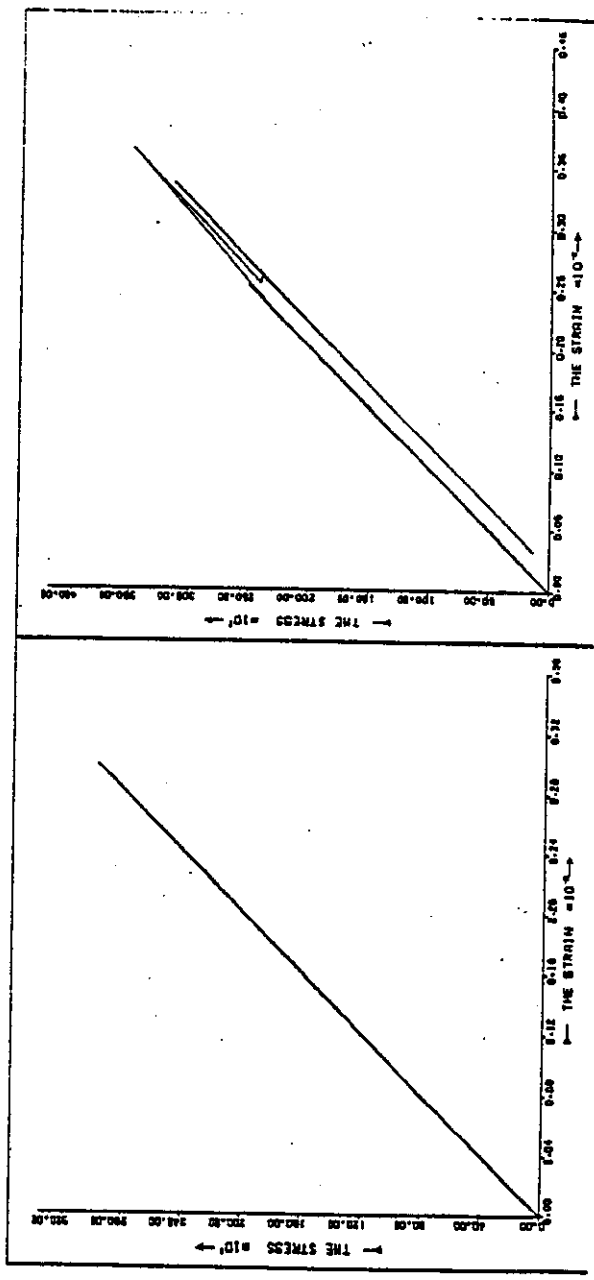


FIG. 62c Stress-Strain curves of stiffener element 6 (appl. stress = 16,500 p.s.i.

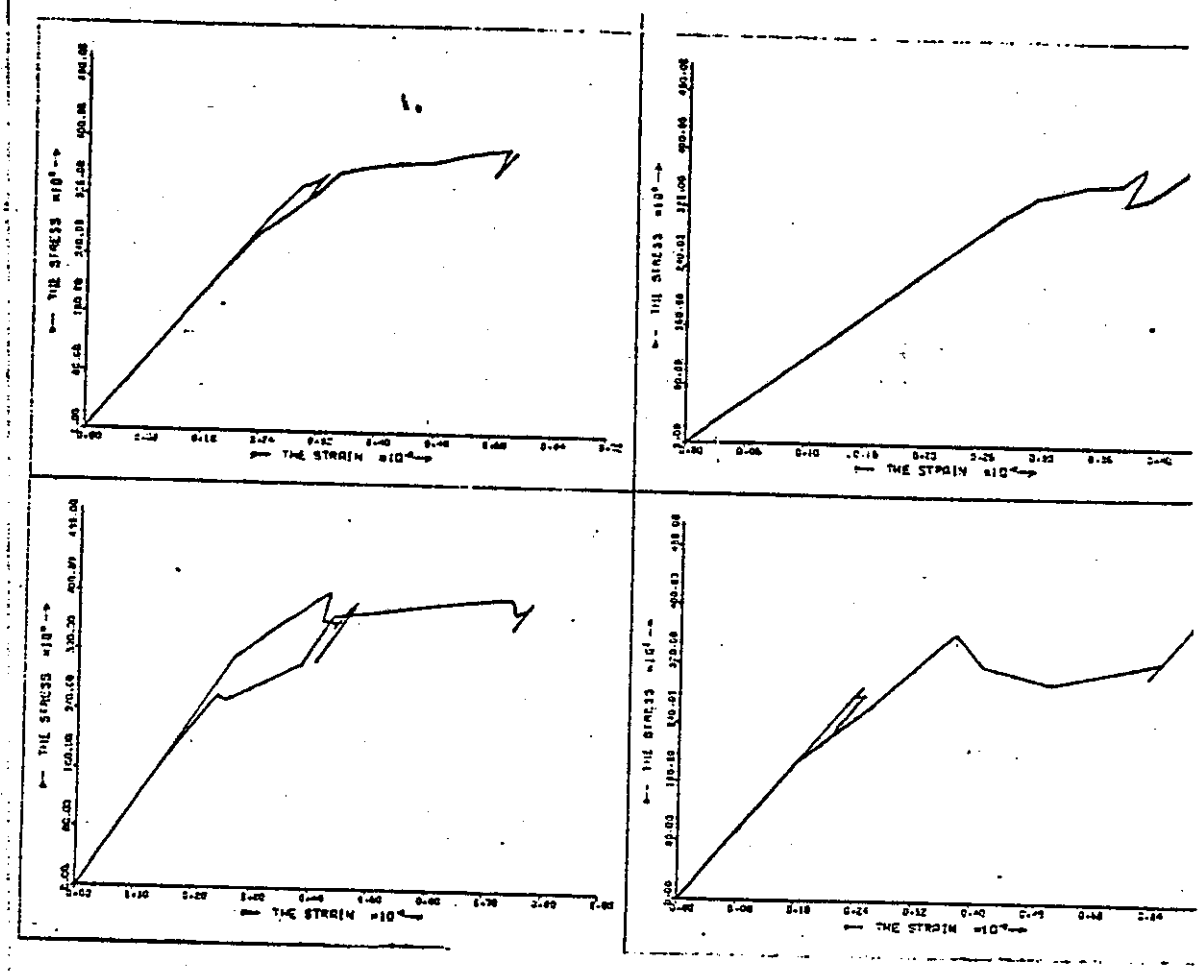


FIG. 64a Stress-Strain curves of element 1 (appl. stress = 24,000 p.s.i.)

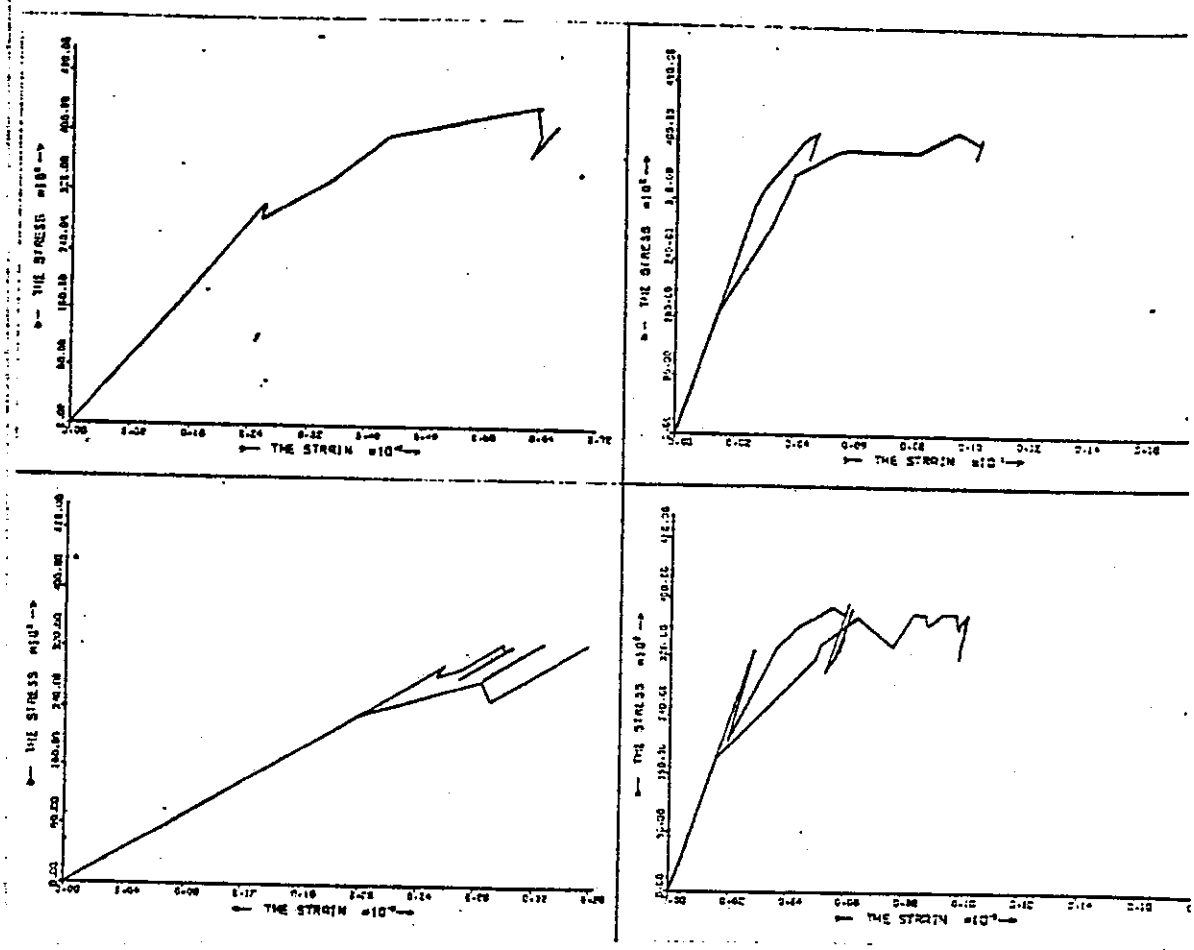


FIG. 64 b Stress-Strain curves of element 4 (appl. stress = 24,000 p.s.i.

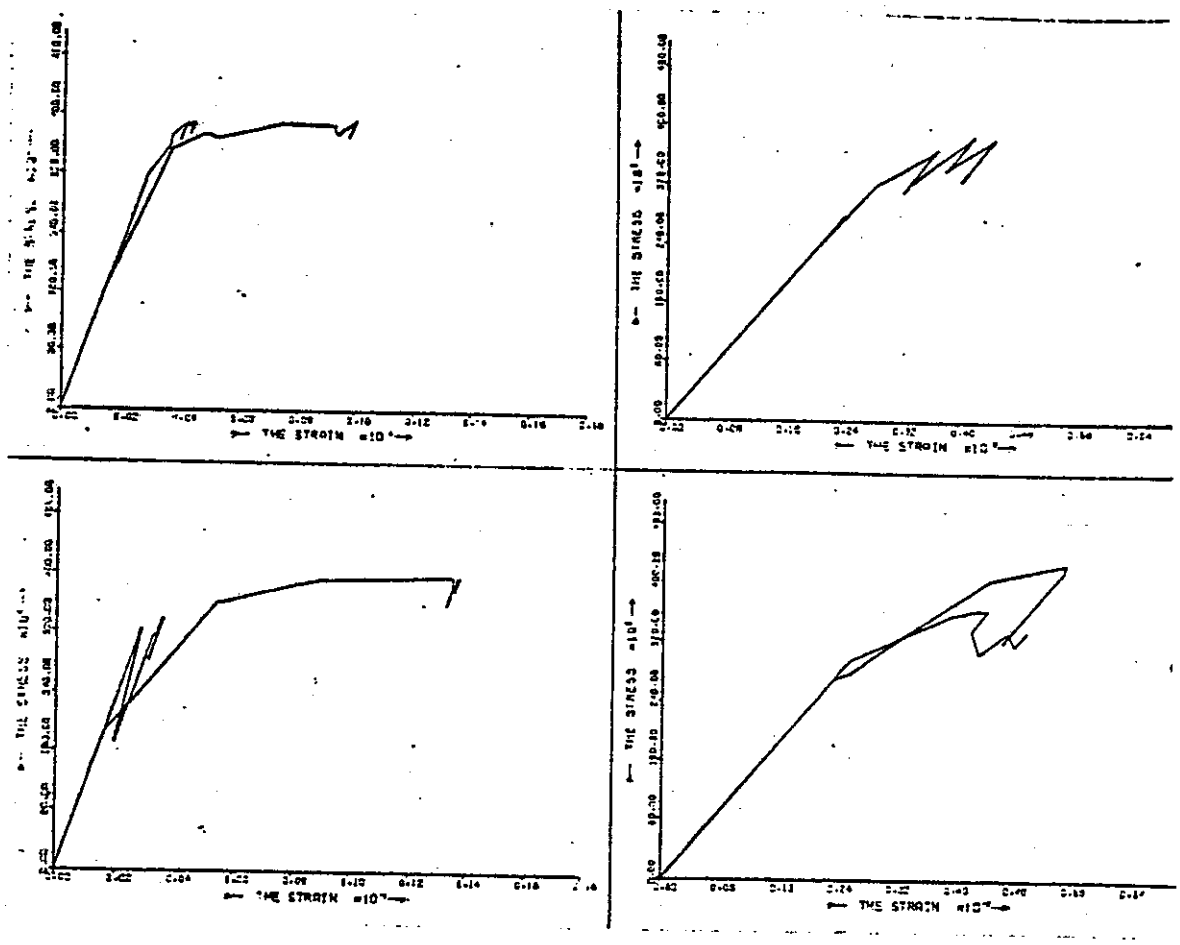


FIG. 64c Stress-Strain curves of element 7 (appl. stress = 24000 p.s.i.)

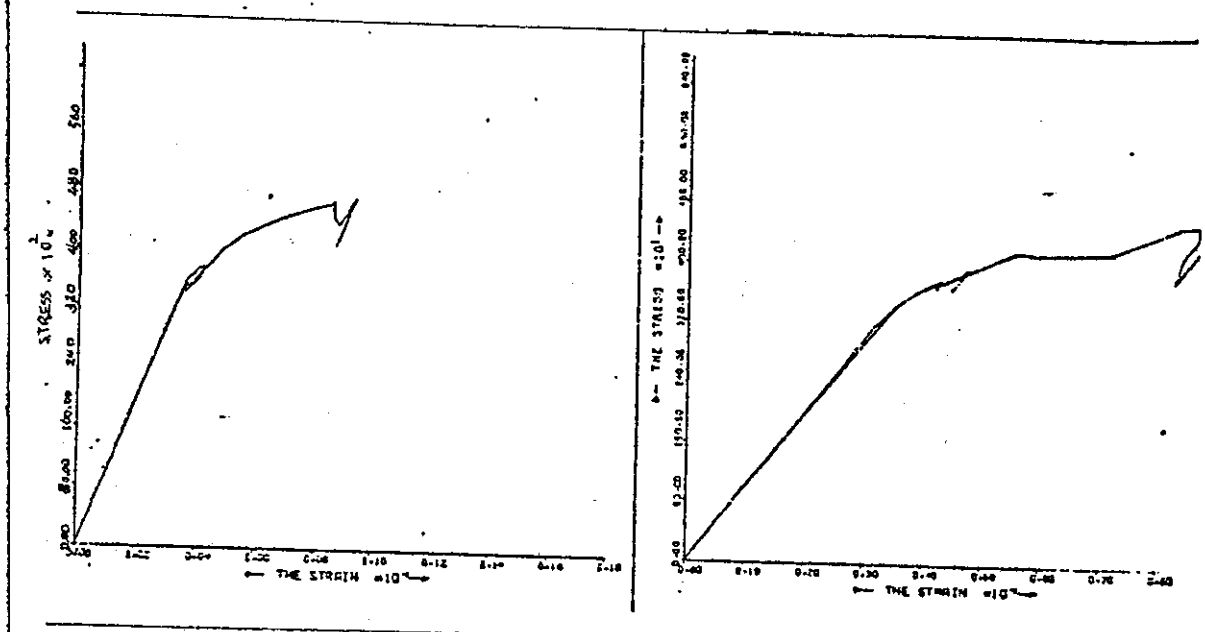


FIG. 65a Stress-Strain curves of stiffener element 4 ($\sigma_{appl.}$ = 24000 p.s.i.)

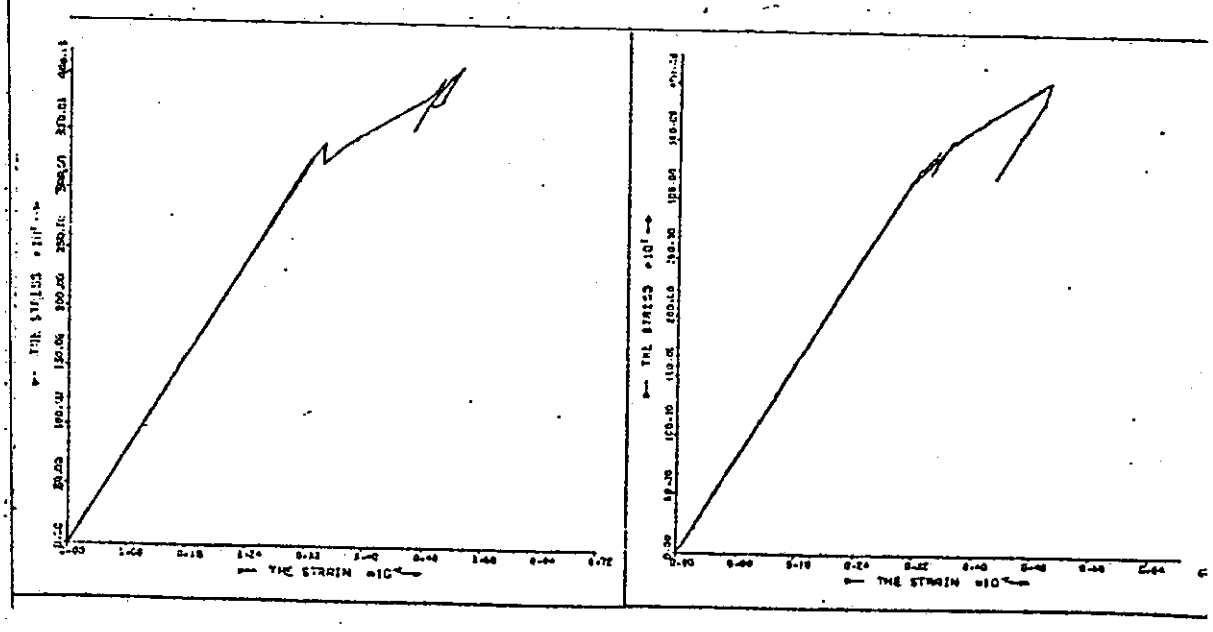


FIG. 65b Stress-Strain curves of stiffener element 5 ($\sigma_{appl.}$ = 24000 p.s.i.)

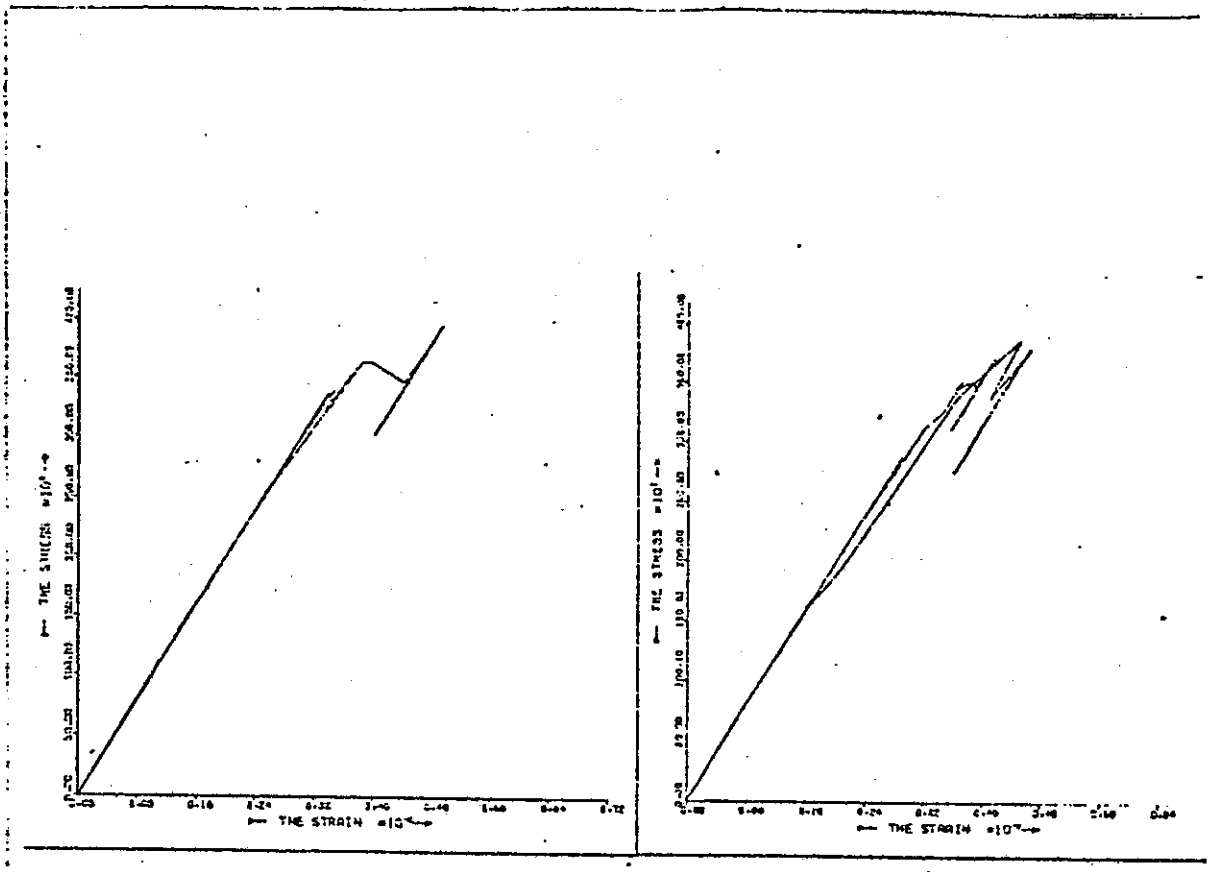


FIG. 65c Stress-Strain curves of stiffener element 6 (= 24000 p.s.i.)